BNL-NCS-51245 - Vol. I of II
DOE/NDC-21/L
NEANDC(US)-208/L
INDC(USA)-84/L

SYMPOSIUM ON NEUTRON CROSS-SECTIONS FROM 10 TO 50 MEV

HELD AT
BROOKHAVEN NATIONAL LABORATORY
UPTON, NEW YORK 11973
May 12-14, 1980

Edited by
M.R. BHAT AND S. PEARLSTEIN

JOINTLY SPONSORED
BY THE OFFICE OF FUSION ENERGY
AND THE DIVISION OF HIGH ENERGY
AND NUCLEAR PHYSICS OF THE
UNITED STATES DEPARTMENT OF ENERGY

July 1980

INFORMATION ANALYSIS CENTER REPORT

NATIONAL NUCLEAR DATA CENTER
BROOKHAVEN NATIONAL LABORATORY
UPTON, NEW YORK 11973

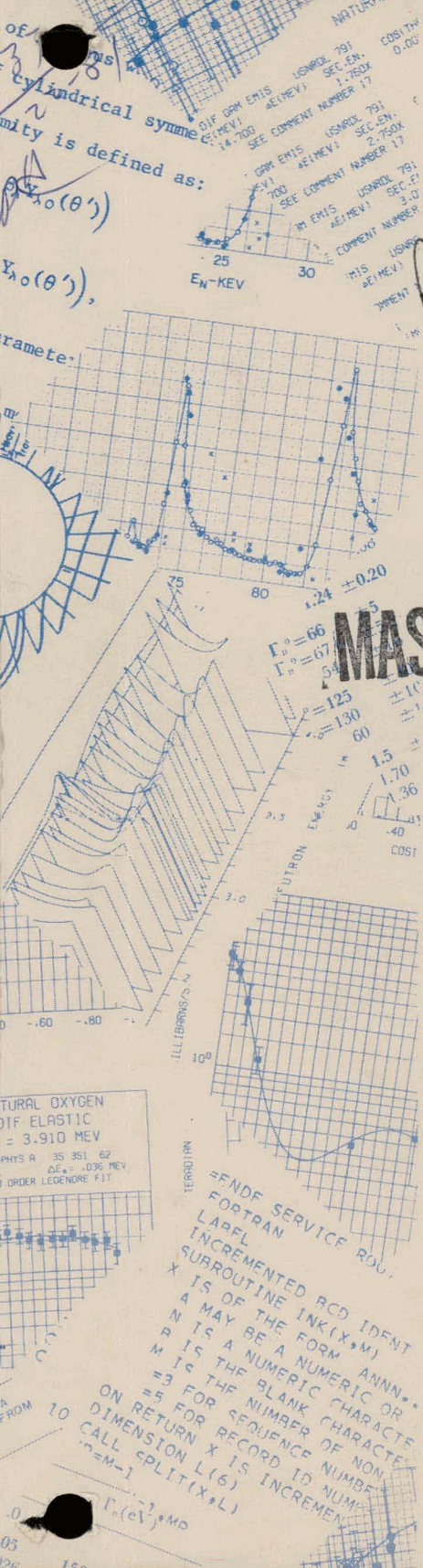

DISCLAIMER

BNL-NCS-51245 - Vol. I of II
DOE/NDC-21/L
NEANDC(US)-208/L
INDC(USA)-84/L
UC-34c
(Physics-Nuclear - TIC-4500)
CONF-800551--(Vol. 1)

SYMPOSIUM ON NEUTRON CROSS-SECTIONS FROM 10 TO 50 MEV

HELD AT
BROOKHAVEN NATIONAL LABORATORY
UPTON, NEW YORK 11973
May 12-14, 1980

Edited by
M.R. BHAT AND S. PEARLSTEIN

July 1980

JOINTLY SPONSORED BY THE OFFICE OF FUSION ENERGY AND THE DIVISION OF HIGH ENERGY AND NUCLEAR PHYSICS OF THE UNITED STATES DEPARTMENT OF ENERGY

NATIONAL NUCLEAR DATA CENTER

BROOKHAVEN NATIONAL LABORATORY
ASSOCIATED UNIVERSITIES, INC.

UNDER CONTRACT NO. DE-AC02-76CH00016 WITH THE

UNITED STATES DEPARTMENT OF ENERGY

DISCLAIMER

Printed in the United States of America
Available from
National Technical Information Service
U.S. Department of Commerce
5285 Port Royal Road
Springfield, VA 22161
Price: Printed Copy $14.00; Microfiche $3.00

TABLE OF CONTENTS

*Not presented orally.

PROLOGUE

This Symposium was organized under the auspices of the Office of Fusion Energy and the Division of High Energy and Nuclear Physics of the U.S. Department of Energy to consider in detail the present state of neutron cross sections from 10 to 50 MeV. A similar Symposium was held at Brookhaven in May 1977 and it was felt that advances made since then should be reviewed and the state of knowledge of the field assessed in view of the immediate needs of the Fusion Materials Irradiation Test (FMIT) Facility under construction at Hanford.

With these objectives in mind, the Symposium was divided into five sessions dealing with the following subjects:

1. Introductory Remarks discussing the recommendations of the 1977 Symposium and the progress made since then.
2. Intense High Neutron Sources And Their Characteristics.
3. Differential Data Including Dosimetry Reactions.
4. Fusion Materials Irradiation Test (FMIT) Facility Related Problems-Shielding And Materials Damage Studies.
5. Nuclear Model Codes And Data Evaluation.

The general format of the Symposium was the same as the last one. Each session opened with one or more review papers which summarized that present status of the subject of the session. The review papers were followed by contributed papers reporting on the advances made in the different laboratories. Each session had a

workshop which provided a specific set of recommendations for future work in the field that could give valuable guidance to the sponsors.

We would like to thank many of our colleagues who gave valuable suggestions and recommendations regarding the organization of this meeting. We also are happy to note an increased participation by our colleagues from abroad as shown in the number of contributed papers as well as those who attended the meeting. We also gratefully acknowledge the cooperation received from the Symposium sponsors, participants and authors which has made possible the prompt publication of the Proceedings of the Symposium. Finally, our grateful thanks are due to Ben Magurno who took care of many details of the meeting and Mary Rizzi and her secretarial staff whose efficient help was essential to the success of the meeting.

June 27, 1980 M.R. Bhat and S. Pearlstein

LIST OF ATTENDEES

R.G. Alsmiller, Jr., ORNL
E.D. Arthur, LASL
G.S. Bauer, KFA
Z.W. Bell, ORNL
M.R. Bhat, BNL
C.D. Bowman, NBS
D. Brenner, LASL
J.C. Browne, LASL
T.W. Burrows, BNL
A.D. Carlson, NBS
J.M. Carpenter, ANL
L.L. Carter, HEDL
R.E. Chrien, BNL
S. Cierjacks, KFK
J.J. Coyne, NBS
R.Y. Cusson, Duke U.
G.F. Dell, BNL
P.J. Dimbylow, NRPB
M. Divadeenam, BNL
D.G. Doran, HEDL
C.L. Dunford, BNL
M.W. Fanelli, BNL
H. Farrar IV, RI
A.T.G. Ferguson, AERE, Harwell
R.W. Finlay, Ohio U.
J.S. Fraser, CRNL
J. Frehaut, BRC
C.Y. Fu, ORNL
R.C. Fuller, BNL
D.G. Gardner, LLL
M.A. Gardner, LLL
A.N. Goland, BNL
R. Gold, HEDL
P. Grand, BNL
L. Green, WF
L.R. Greenwood, ANL
H. Gruppelaar, ECN
M.W. Guinan, LLL
R.C. Haight, LLL
L.F. Hansen, LLL
D.W. Heikkinen, LLL
M. Hillman, BNL
N.E. Holden, BNL
R.J. Howerton, LLL
D.L. Johnson, HEDL
R.G. Johnson, NBS
C. Kalbach, Duke U.
W. Kato, BNL
R.R. Kinsey, BNL
D.W. Kneff, RI
H.J.C. Kouts, BNL
J.J. Kukkonen, BNL
R.J. Labauve, LASL
D.C. Larson, ORNL
O.W. Lazareth, Jr., BNL
J.R. Lemley, BNL
B.R. Leonard, Jr., BNW
P.W. Lisowski, LASL
M.A. Lone, CRNL
B.A. Magurno, BNL
F.M. Mann, HEDL
J.C. McDonald, Mem. Sloan-Kett.
V.L. McLane, BNL
S. Moore, BNL
S.F. Mughabghab, BNL
D.W. Muir, LASL
D.R. Nethaway, LLL
C. Nordborg, NEADB, Saclay
B.D. Pate, U. BC
S. Pearlstein, BNL
R.W. Peelle, ORNL
L.K. Peker, BNL
F.G.J. Perey, ORNL
C. Philis, BRC
T.W. Phillips, LLL
H.G. Priesmeyer, U. Kiel
A. Prince, BNL
S.M. Qaim, KFA
G. Randers-Pehrson, Ohio U.
P. Rose, BNL
G.J. Russell, LASL
U. Salmi, Hebrew U.
F.M. Scheffel, BNL
R.E. Schenter, HEDL
A.B. Smith, ANL
J.R. Stehn, BNL
M.L. Stelts, BNL
L. Stewart, ORNL

LIST OF ATTENDEES (cont.)

B. Strohmaier, IRK
T.S. Subramanian, LBL
H. Takahashi, BNL
S. Tanaka, JAERI
J.K. Tuli, BNL
H. Vonach, IRK
R.L. Walter, Duke U.
P.G. Young, LASL

WORKSHOP REPORTS

Session Chairman: S. Pearlstein, BNL

THIS PAGE

WAS INTENTIONALLY

LEFT BLANK

INTENSE HIGH ENERGY NEUTRON SOURCES AND THEIR CHARACTERISTICS

C.D. Bowman, NBS - Chairperson

R.G. Alsmiller Jr., ORNL
T.W. Burrows, BNL
S. Cierjacks, KFK
R. Gold, HEDL
D. Heikkinen, LLL
R.G. Johnson, NBS
J.J. Kukkonen, BNL
M.A. Lone, CRNL
R. Peelle, ORNL
G.J. Russell, LASL
G.S. Bauer, KFA
J.M. Carpenter, ANL
J.S. Fraser, CRNL
L. Greenwood, ANL
D.L. Johnson, HEDL
D.W. Kneff, RI
B.R. Leonard, BNWL
S. Pearlstein, BNL
H.G. Priesmeyer, KIG
H. Takahashi, BNL

I. Introduction

Since the first symposium in this series on May 3-5,1977, the use of high energy neutrons has continued to increase. The use of accelerators to simulate high energy neutron damage for fusion reactors has grown, the fusion-fission hybrid and the accelerator breeder continue to be considered, encouraging results have been obtained for cancer therapy using high energy neutrons, and concern for personnel radiation safety have reemphasized the need for better measurements of this type for high energy neutrons. However the strongest driving force continues to be the concern for damage to fusion reactor materials.

The construction of the FMIT facility is well underway. Source characteristics and dosimetry methods for this accelerator have been actively studied using the Davis cyclotron and the RTNS-II source. A number of 14 MeV neutron sources around the world have been directed toward the fusion data measurements.

Since 1977, the worldwide interest in powerful spallation sources for condensed matter studies has steadily increased, bringing increased needs for shielding data and for improved personnel dosimetry. These accelerators also make available intense high energy neutron beams and fields suitable for other studies such as materials damage studies for fusion reactors.

II. Progress on 1977 Recommendation

One measure of progress in this field is a review of recommendations made in 1977 all of which related to the fusion materials damage program. Perhaps the strongest recommendation at that time was the need for parallel pursuit of passive dosimetry and dosimetry based on calculational methods. Since that time active dosimetry has also been added to these two. We have seen in this meeting dramatic progress in passive dosimetry, a substantial level of activity in active dosimetry, and a small level of activity following the calculational approach.

The recommendation regarding d+t neutron beams and fields for reference standards purposes has been pursued, but not sufficiently aggressively - perhaps because the desirable characteristics of the fields have not been defined clearly.

Progress has been made in satisfying the request for more measurements on the d+Li systems. The low energy component of the spectrum has apparently been accurately measured, but a complete characterization of the thin target 4π yield and angular distribution over the full energy range has not been completed.

Perhaps for this reason the recommendation for use of a calibrated d+Li source for integral tests of activation cross sections has not yet been very well followed.

The 1977 workshop recommended the development of a small accurately calibrated neutron detector with an efficiency of 1% which could be calibrated to an accuracy of 2-4% from 0.3 to 30 MeV and from 4-8% from 30-50 MeV. No progress seems to have been made in designing such a detector or in promoting its universal use for interrelating the measurements from different facilities.

Finally the list closed with the recommendation that the required measurements and calculations be given the same priority as accelerator construction in order that useful measurements can be made as soon as the facility becomes operational. A firm commitment is required to keep this portion of the program from falling behind.

III. Present Status

For neutron dosimetry the detailed understanding of neutron irradiation experiments requires an accurate characterization of the neutron source environment for each experiment. This is particularly true of fusion materials test environments, which typically have steep flux and (in some cases) energy spectrum gradients as a function of irradiation position. This characterization is presently being performed using a combination of active, passive, and calculational dosimetry. The passive dosimetry technique, based in particular on foil activation and

helium accumulation measurements, is a proven technique, and can be applied to all neutron source facilities used for fusion materials testing. While a large number of passive dosimetry materials are presently used, future routine dosimetry for a given neutron field will use a smaller, optimized reaction set.

Future dosimetry development requires pursuit along all three lines (passive, active, and calculational). Calculational dosimetry probably cannot, by itself, provide an adequate characterization of the neutron environment, because of changes in beam conditions, and because of perturbing or heterogeneity effects produced by the irradiation samples. Calculations are nevertheless required as input to spectral unfolding codes used to interpret passive dosimetry results. Finally, active dosimetry is required for beam diagnostics, to optimize the neutron source operating conditions, and to determine the flux-time history of each irradiation.

Many of the recent experiments using modest sized Be(d,n) and Li(d,n) neutron sources have been in support of FMIT development. These experiments have included cross section measurements for the engineering design of FMIT, as well as dosimetry development and damage analysis studies. This type of neutron source will still be needed after FMIT becomes operational. FMIT will be dedicated to long-term (several month) materials irradiations for fusion studies, and will not be readily available for, and is not designed for, basic physics experiments. These unfulfilled basic physics needs will include cross section measurements, some of

which will undoubtedly be defined as a result of FMIT experiments. Cyclotron-type neutron sources are well-suited to such measurements, and can provide Be(d,n) and Li(d,n) benchmark neutron fields.

It should be pointed out that FMIT will not, by itself, satisfy all of the needs for fusion materials irradiations, primarily due to flux and space limitations. In fact, only a small percentage of proposed materials studies will actually be performed at FMIT. Fission reactors and T(d,n), Be(d,n), spallation source and other Li(d,n) sources will still be needed for materials irradiations as well as for other studies. Work should thus continue in support of these alternate facilities.

Some areas that might be anticipated are as follows: (1) Updates in cross sections for neutron dosimetry and testing of new dosimeters will probably be necessary to improve characterization of irradiation experiments. (2) Measurement may be needed of some activation cross sections which affect radiation dose levels but which were not expected to be important before FMIT operation. (3) Measurements may be needed of gamma radiation fields and spectra and their effects within samples similar to those in FMIT. (4) Measurements which test data and methods to predict neutron flux-spectra deep within bulk samples of materials used in the FMIT facility may be added.

It should be noted that there are some differences between d+Be and d+Li sources. One area where this is true is activation reactions with very high thresholds which may occur with d+Li

neutrons but less so or not at all with d+Be neutrons. For example, the reaction N-14(n,x)Be-7 has a threshold of approximately 30 MeV and can occur in FMIT (35 MeV d+Li) but much less so with similar energy deuterons on beryllium. This reaction has significance for FMIT where air is in the accelerator vault and nitrogen is the test cell atmosphere. Furthermore, one would not expect to be able to calculate the cross section for this reaction very well.

Suitable neutron sources and measurement methods also must be developed for medical programs such as cancer therapy with fast neutrons. Extensive cross section data are needed for tissue material and Na, Ca, P, S, K, I, and Ar for a variety of reactions with a nominal accuracy of 10% and with neutron energies extending to 100 MeV. Monoenergetic sources probably are best suited for these measurements and special care in beam purity and background conditions will probably be necessary for these experiments. Cancer therapy requires detailed neutron transport calculations for each patient to prescribe the proper treatment program. Accurate source characterization is clearly necessary to provide the source term for this irradiation. A specific need is for cross section and thick target yields for the p+Be source for beams up to 70 MeV incident energy.

The rapidly increasing interest in intense spallation sources will have a major impact on neutron measurements and applications. There is a large and increasing demand for slow neutron sources to be used in condensed matter research, biology, chemistry and

fundamental neutron physics. This is exemplified by the oversubscription of existing user-oriented high-flux sources (150% at ILL-Grenoble). The sources with low-duty cycle time structure provide more efficient utilization of the neutrons produced than those which may be said to be continuous. This time structure can be designed in since these are accelerator-driven devices. The spallation sources have advantages over reactors in that they do not involve the use of fissile material and heat dissipation is simpler because of the comparatively efficient mechanism of neutron production. Pulsed spallation neutron sources which are now available or under construction provide effective fluxes of thermal neutrons competitive with those of high flux reactors and have the prospect for producing orders of magnitude greater fluxes than reactors. The uniquely high effective epithermal neutron flux already available is opening up new areas for study.

With respect to fast neutron radiation effects facilities, spallation sources designed for fast neutron radiation effects studies produce a continuous spectrum very similar to that of fast reactors. Of course, there is no prominent 14 MeV component. The high energy tail which extends up to the accelerated particle energy contains a small fraction of all the neutrons but so far as is known, this does not provide either a disadvantage or significant advantage in these applications.

A significant advantage for temperature control in accelerators compared with reactor sources follows from the low nuclear (gamma ray) heating. Another advantage over the reactor

is that the passive target enables much greater flexibility in experiment design. The high flux region is large (10x10x10 cubic centimeters) and flux and spectrum gradients correspondingly low so that large samples can be investigated. This class of applications usually depends only on the time-average value of the flux. The time structure may be useful in some applications.

Nuclear data are required for the design of facilities of many kinds. Spallation sources provide neutrons in a continuous spectrum extending to energies of order 1 Gev and may be used to generate these data with the proper pulse structure mode of operation. The sources may be tailored to provide good time structure for time-of-flight energy analysis even out to energies of several hundred MeV. Thus, the spallation sources extend by an order of magnitude the range of energies accessible by more conventional charged particle reactions.

The broad energy spectrum available with intense spallation neutron sources will be of interest in nuclear physics, radiotherapy studies, and material damage studies. Of interest to nuclear physics is the possibility of producing higher thermal neutron fluxes than are now available from reactors. These would permit improved fundamental experiments such as those on parity violation in (n,p) and (n,d) systems and on the neutron magnetic moment and lifetime. The epithermal neutrons from an intense spallation source could be used for resonant (n,gamma) studies and in investigations of the capture reaction mechanism, giant dipole resonance and nuclear level densities. An intense spallation

neutron source will also produce large fluxes of mesons and neutrinos of interest to medium energy physics. Large fluxes of moderated fast neutrons would also be available for nuclear physics studies.

These sources themselves require further data, particularly for the higher power next generation sources now under study and for any future accelerater breeder based on the spallation reaction. Present data on neutron yields, energy deposition and transport, total and angular neutron cross sections, fission and evaporation product distributions (including light gases) are not adequate for design of advanced facilities. Computational methods suffer from the drawback that underlying processes are not yet well enough understood. An example is the competition between evaporation and high energy nucleon induced fission.

In summary, an array of powerful new neutron generation facilities will probably become available during the 1980's with a major increase in capability for neutron studies. A major effort for accurately characterizing these sources for maximum usefulness will be required.

IV. Recommendations

1. For irradiation dosimetry a trial spectrum derived by calculational methods is indispensible in interpreting results from passive dosimetry. Continual improvements and extensions in the transport cross section libraries for transport codes are vital. Refinements in the three dimensional transport calculation

of neutron flux maps within test modules are desirable. Sensitivity studies of these flux maps to nuclear data must be made.

2. Thin target data for protons and deuterons on Li and Be for energies up to 100 MeV over the full angular range and energy range of neutron emission should be measured. Thin target yields are also needed for precise definition of neutron flux-spectra at positions very close to a source such as in the FMIT facility. Some work has already been done to infer thin target data from available thick target d+Li data and this information is being used in transport calculations to answer design questions in the FMIT facility. For calculational dosimetry in the FMIT facility, improved accuracy will be needed and therefore, specific thin target measurements are needed.

3. Neutron fields for the d+t and/or t+d 14 MeV sources should be established by comparing results obtained by the associated particle and proton recoil techniques. Efforts should be taken to carefully establish the neutron energy of the d+t source to avoid effects of energy uncertainty.

4. Greater effort in active beam position and distribution measurements should be made for all types of high energy neutron sources.

5. Computer codes for calculation of neutron detector efficiency should be tested experimentally for the purpose of achieving an accuracy of 2 to 4% from 0.5 to 30 MeV and to 10% from 30 to 600 MeV. This will require experimental determination

of the detector efficiency of a suitable detector, with associated particle technique, to the above mentioned accuracy.

6. The characteristic of a reference standard d+t 14 Mev neutron field or beam must be defined more carefully so that progress can be made in the establishment and use of such a field.

7. The feasibility of using a 6-Li + d converter for producing fast neutrons in a reactor core for fusion material damage studies should be investigated.

8. Other sources for fusion irradiation will continue to be required after the FMIT is operational for a number of purposes. Plans should be made to continue support for these less intense sources.

9. Spallation sources should be used for studies of cross-sections important for neutrons transport and build-up in the thick shielding required for future more intense accelerator sources.

10. Materials damage arising from the thermal cycling peculiar to spallation sources can and should be studied for future larger spallation sources.

11. Improved measurements of high energy absolute neutron yields and spectra are required for spallation source design. Present experiments suggest a large discrepancy (factor of two) with calculations.

12. Thick target yields for charged particle neutron production as a function of angle and energy should be included in the National Nuclear Data Center bibliography.

13. A firm commitment should be made to assure that passive, active, and calculational dosimetry methods are in place as soon as the FMIT accelerator becomes operational.

14. For the next conference the neutron energy range of interest should be extended to 1 GeV.

DIFFERENTIAL DATA INCLUDING DOSIMETRY REACTIONS

F.G. Perey, ORNL - Chairperson

Z.W. Bell, ORNL
M.R. Bhat, BNL
J.C. Browne, LASL
A.D. Carlson, NBS
R.W. Finlay, OHIO U.
J. Frehaut, BRC
R.C. Haight, LLL
D.L. Johnson, HEDL
D.C. Larson, ORNL
P.W. Lisowski, LASL
V.L. McLane, BNL
A.B. Smith, ANL
T.S. Subramanian, LBL
H. Vonach, IRK
R.L. Walter, DUKE U.

I. Introduction

Two broad review papers were presented assessing the status of differential data measurements, one by Alan Smith and the other by John Browne. We also had four or five specific papers in our plenary session which described programs at several laboratories to address the problems of providing differential data in the region of 10 to 50 MeV. We therefore felt in the working group that an additional summary was not required of us.

In 1977 the emphasis for the needs was strongly in the region below 15 MeV. Our workshop at the time, however, chose to address mostly the needs in the energy region above 15 MeV. At this meeting we hardly heard about the needs in the energy region below 15 MeV. Because of the construction of the Fusion Materials Irradiation Test (FMIT) Facility, the region of maximum importance has moved up for 10 to 15 MeV, where it used to be, to energies around 25 MeV. We were shown that for some shielding problems the higher energy region around 50 MeV was very important. The problems associated with the design and

operation of FMIT so much dominated the conference that some of us in the workshop wondered if the overall needs for data above 10 MeV were given a proper perspective at the meeting. We did not hear much about medical needs. They may not have changed much since the last meeting, but the fact that no one thought it necessary to reiterate them this week should not make us forget them. We also failed to hear about the needs for data for the Engineering Test Facility (ETF). We should also presume that there does not yet exist a sharply focused set of needs for ETF, but that very likely the broad recommendations reviewed in 1977 are still applicable today for future fusion devices where the most important energy region is in the range of 10 to 15 MeV.

Several speakers at this meeting commented upon the fact that a surprising amount of progress has been made in the differential data area since 1977. This was discussed also in the workshop, but several points were stressed that are worth noting in our report. The progress has been far from uniform. Little significant work has been done on the dosimetry cross sections about 10 MeV. At least none were reported at the meeting. Our recommendations of the last meeting seem to have had little effects in this area. Much of the work reported at this meeting on differential data above 10 MeV was largely the result of ongoing programs or were the consequence of our ability to exploit techniques well in hand; such as for total cross sections. We did not recommend last time that new

facilities be built to solve the differential data problem above 10 MeV. We felt then that we did have a number of facilities which could not provide all the needed data but could be exploited efficiently to acquire some data which if used in connection with theoretical calculations could possibly go a long way toward meeting the needs. We think that the output of differential data since 1977 has shown that we were at least partially correct. We also saw how data and theory can be coupled effectively with each other. We also saw at this conference that reliance on theory only may be very misguided since large differences than many anticipated were found between predictions used in designs and subsequently acquired data. We think that the art of assessing credible uncertainties in model calculations needs to be very much improved before we can bridge important data gaps by model calculations.

The most important point that the working group thought it should make at this stage was: we feel far less confident at this meeting than we did in 1977 about our ability to rise to the challenge of the data needs. The vitality of the data measuring community as demonstrated by our output since 1977 is more representative of the past than the present and will not likely be seen again unless some current trends are reversed. It is unfortunately an easily documentable fact that there has been, in the last few years, a general erosion of our capabilities in the differential data measurement area. We feel

that the technical capabilities that we had three years ago are still largely there and in some areas have improved. However, our ability to exploit them, for financial reasons mostly, has decreased. Our facilities are underused and understaffed. The prospects for the future do not appear bright to most. Losses of highly skilled staff have been significant and cannot be easily made up overnight. We see in the not too distant future a maturing of the Fusion Energy Program to the stage of designing, building, and operating devices where neutronic problems will become increasingly important, giving rise to specific data needs hard to anticipate accurately now. The history of the development of the data needs for FMIT and our ability to perceive them should, we think, serve as a lesson for those who think that the experience in the fission area is not too relevant. We do not know yet, and probably will not know for some time, the price we have to pay or the cost we incurred, if any, for having had to generate data overnight. In the case of FMIT we were able to react to some degree, but many in the workshop felt that we will be less able to do so in the future if the current trends are not soon reversed. Some people in the workshop felt strongly that, although they fully agree with the above options, the workshop report was not the appropriate place to express them. Others felt equally strongly that we would be less than responsible if we did not make our opinions known here.

We reviewed the recommendations we made last time and found that they were still essentially valid today. This is in large part due to the fact that the recommendations dealt with broad approaches. Our experience in the intervening three years seems to confirm them to be useful and worth reiterating again with a few changes in emphasis. Some comments will be added mostly in areas where recommendations were not followed, for known reasons, but nevertheless should be followed.

II. Recommendations

We still felt strongly that our data needs should be met by a judicious combination of both our experimental and theoretical capabilities. We should therefore strive in our experimental programs for a proper balance between acquiring data which directly meet the needs and those which enhance our ability to test and improve our theoretical calculations. We emphasize the fact that it seems to us that where model calculations are used as a substitute for experimental data they should not be mere predictions based on some model but by some estimate of what the true cross sections are, including estimated uncertainties. We understand that this may not be easy but is a price which we must necessarily pay when theoretical predictions are mere interpolation of experimental data and their uncertainties.

At the last Symposium we set apart the dosimetry cross sections and think this division should still be made.

A. Nondosimetry Cross Sections

1. Hydrogen, helium, charged-particle production, and transmutation cross sections.

In this area much progress has been made as we heard during the conference. Yet we think that all of the 1977 recommendations are still valid today. They were:

a) The likely improvements to the existing programs of measurements should be carried out.

b) The measurements near 14 MeV and at 50 MeV should cover the materials of both fusion energy and medical interest.

c) These measurements should also be used to validate model codes as well as to improve evaluated data files.

d) Measurements of the charged particle production cross sections, spectra and angular distributions should be made on selected isotopes at a few energies between 15 and 50 MeV. The isotopic data should be used to check nuclear model calculations.

e) For carbon, oxygen and nitrogen, more measurements should be made at more energies in the 15 to 50 MeV range. The nuclear models may not be appropriate for these light elements which are of crucial importance in neutron therapy.

f) The feasibility of and need for measurements of other transmutation cross sections should be assessed.

g) Pulsed white neutron sources between 15 and 40 MeV in the mesurement of the charged particle production cross sections should be considered. These sources would offer the possibility of measuring the cross sections over the entire energy range.

1980 Comments:

A particular area where little progress has been made since 1977 is in the measurement of transmutation cross sections. A broad attack on this problem is difficult and we realize that specific needs are hard to anticipate since they are very "device" dependent.

2. Other cross sections.

In spite of much progress here the needs for data remain great. We endorsed the 1977 recommendations fully which were:

a) Total cross sections should be measured over the complete energy range and be reproduced by model calculations.

b) Elastic scattering measurements be made at selected energies from 15 to 40 MeV to establish the systematics of the optical model parameters used in calculations and obtain reference reaction cross sections which should be reproduced by model calculations. The extensive data base for charged particle scattering should be used with the neutron data to establish the optical model parameters.

c) Multiple particle emission data such as (n,xn) should be obtained, particularly for the specific nuclides of

interest in applications, in order to check the model calculations.

d) Inelastic cross sections, neutron and gamma ray emission spectra should be obtained in order to check the model calculations.

e) Charged particles data should also be used to validate the model calculations.

f) The experimental program should be strongly coordinated with the model calculations and evaluation effort. The CSEWG seems an adequate forum where interaction between measurers, evaluators, and users should take place to have an effective program.

1980 Comments:

a) Total cross sections: The failure of frequently used sets of "global parameters" to reproduce data came as a shock to some people. We thought that it may point out an underestimation of the usefulness of this rather easily acquired kind of data and an overestimation of the ability of models to properly estimate those important cross sections. We think that the matter deserves to be looked upon carefully.

b) We saw at this meeting data obtained via an adaptation of the old "sphere transmission" technique for measuring reaction cross sections. We felt in the workshop that the method should be further investigated and could possibly be developed as a general tool to measure more reaction cross

sections over a broad energy region. If the method could be adapted for use with white neutron sources, it would be very valuable. The failure of some model calculations in predicting total cross sections leaves some doubt as to their ability to predict also the reaction cross sections.

c) Since 1977 much new data on neutron emission spectra, mostly on natural elements at around 15 MeV, have been reported. We saw at this conference that some improved model calculations are now capable of reproducing these data well. This is a recent development which we welcome. We feel that in the past this class of data, which we know how to obtain, has been underexploited from a theoretical point of view and in many evaluations. It was suggested that efforts be made to obtain neutron emission spectra on at least some separated isotopes at the same or very close to the same incident neutron energies where we have charged-particle emission spectra.

d) We saw at this meeting an example of the use of charged-particle data to better understand model calculations relevant to neutron cross sections. It was pointed out that there has been a dramatic reduction in facilities devoted to study light-ion induced reactions in the last few years. There are many data in the literature on charged-particle induced reactions, in particular protons, and they should be exploited as much as possible, but a large fraction may not be accurate

enough to be of much use since they were not acquired with our applications in mind.

e) We thought three years ago that the CSEWG could be an effective place for strong interaction between measurers, evaluators, and users. It was the general impression in the workshop that this strong interaction needed for a very effective experimental program had not occurred. We understand that there are plans to implement our recommendations. The strong national, i.e., U.S.A. character of the CSEWG does not fully meet the needs of the international community in this regard. A suggestion was made and endorsed by the workshop that a newsletter be established to serve the needs of providers and users of data in the range of 10 to 50 MeV. This newsletter could be patterned after similar ones dealing with gamma rays and actinide cross sections. We understand the National Nuclear Data Center is willing to undertake this effort and we welcome it.

B. Dosimetry Cross Sections

We had made in 1977 very extensive and detailed recommendations concerning data for dosimetry. We felt then that such strong and detailed recommendations were needed and should be followed if we were to see any significant progress in this area. We were rather sorry to see that, even though there is an increasing awareness of the great importance of detailed dosimetry for proper interpretation of radiation damage in an

environment, such as provided by FMIT, and an increasing awareness of the importance of the correlations in the data, for adequate unfolding, very little has happened in the data program. Papers were presented at this conference which reemphasize these needs.

We feel in 1980 as strongly as we did in 1977, and possibly even more, that we do understand fairly well the problems of differential data measurements in this area. If little progress has been accomplished in the last three years, it is not, we feel, because of our lack of capabilities in this area but rather because considerable experience has taught us that not doing it right will impose severe limitations. We think that it takes a dedicated and sustained effort of highly trained people at the appropriate facilities, and that the problem must be viewed in its entirety, in order to make significant progress.

We recommend that people interested in seeing that substantial progress be made in this area study our 1977 workshop report dealing with this subject.

THIS PAGE

WAS INTENTIONALLY

LEFT BLANK

FMIT RELATED PROBLEMS: SHIELDING AND MATERIALS DAMAGE STUDIES

F.M. Mann, HEDL - Chairperson

R.G. Alsmiller Jr., ORNL
L.L. Carter, HEDL
D.G. Doran, HEDL
H. Farrar IV, RI
A.N. Goland, BNL
R. Gold, HEDL
L.R. Greenwood, ANL
D. Heikkinen, LLL
D.L. Johnson, HEDL
D.W. Kneff, RI
R.J. LaBauve, LASL
D.C. Larson, ORNL
B. Leonard, BNW
E.P. Lippincott, HEDL
B.A. Magurno, BNL
D.W. Muir, LASL
S.M. Qaim, KFA
M.W. Guinan, LLL
R.E. Schenter, HEDL

I. Introduction

The primary objective of FMIT is to provide a high flux of fusion energy neutrons for the study of radiation effects in fusion reactor materials. In order to apply materials-property data obtained in FMIT to the prediction of radiation effects in a fusion device, two requirements dependent on nuclear data must be met. One is that the neutron environment to which each specimen is exposed be well defined. To accomplish this, a combination of dosimetry measurements and transport calculations will be needed. A second requirement is that the neutron environment must be expressed in terms of energy-dependent damage parameters such as displacement and transmutation rates. Such parameters provide the starting point for damage correlation models needed to relate data obtained in different environments.

Several other areas impacting both FMIT design and utilization are dependent on adequate nuclear data. These include 1) transport calculations of attenuation in shielding materials

and flux-spectra in experimental assemblies, 2) energy deposition in test cell walls and experimental assemblies, 3) activation of facility components and experimental assemblies and specimens.

The FMIT neutron spectra extend to about 50 MeV. In addition, spallation sources such as (LAMPF-NWR, IPNS-I, and SIN) may be used to study radiation effects and their spectra will extend to still higher energies. Hence nuclear data for the above applications are needed well above the 20 MeV limit of the ENDF/B files. In the following section, the status of nuclear data for FMIT applications is briefly described. Recommendations are made for actions that are considered vital for the successful utilization of the FMIT facility.

II. Status and Recommendations

A. Interaction among users and generators of nuclear data

Although there has been informal contact between the users of nuclear data for materials damage studies and for shielding applications and those who generate such data, there must be increased interaction. Generators of nuclear data, whether experimentalists, evaluators, or theorists, must realize that request lists are just indications of user needs. Direct contact must be made so that proper materials, reactions, and energy ranges are investigated.

In order to formalize such interactions the Cross Section Evaluation Working Group (CSEWG) should create a committee designed to insure that nuclear data needs for fusion materials

studies are recognized and met in a timely and acceptable manner. Coordination with the Damage Analysis and Fundamental Studies Task Group of the DOE-OFE/MRE branch would be crucial for success. The shielding subcommittee of CSEWG provides an example of such interaction. Such a new committee would help ensure that user needs are presented to the nuclear data community in a way that the community can understand and respond to. In addition, the committee could oversee the methods, adequacy, and accuracy of files not only in the traditional ENDF/B range of 0.00001 eV to 20 MeV but also for the higher energy of FMIT (50 MeV for dosimetry cross sections and 40 MeV for damage cross sections). The Special Application Files subcommittee is already responsible for dosimetry, activation, and gas production files to 20 MeV.

The creation of nuclear data is not solely an United States effort. Foreign participation has been significant and is expected to remain so.

B. Dosimetry Reactions

Dosimetry plays an essential role in damage studies as it allows the determination of the neutron exposure of the samples. In order to ensure that an adequate data base is available for FMIT operation, support must be maintained for dosimetry development.

Since the last symposium, much success has been achieved. Passive radiometric foils have been irradiated in d+Be neutron fields produced by 40 MeV deuterons. Measured activities agreed well with calculated activities based on extrapolated cross

sections and a time-of-flight measurement of the neutron spectrum (1). In addition mapping of the d+Be neutron field produced by 30 MeV deuterons using both radiometric foils and helium accumulation neutron dosimetry is being performed (2). Solid state track recorders (SSTR) are being investigated for possible use (3). Also, the ENDF/B-V dosimetry file has been released. Although the file extends to only 20 MeV, it does contain uncertainty data.

However, much work remains to be performed. Table I lists the most important reactions for passive in situ dosimetry. Note that Arthur et al., (4) have recently provided evaluations of Co-59 and Fe reactions. Additional reactions which may be used for radiometric studies are given in Reference 5 (Table V) and in Reference 6 (Table VI). Because of the limited space in the region of highest flux in FMIT, materials with several useful reactions should have high priority. For the same reason, consideration should be given to using alloys for dosimetry materials. An important candidate for passive dosimetry is the helium accumulation fluence monitor (HAFM) which requires total helium production cross sections. Because of their possible interference in the interpetation of the active dosimeters, (n,charged particles) cross sections of C, O, and Si will be needed. The measurement of Ra-226 (n,f), (n,2n) and (n,pn) would help extend the usefulness of SSTR's. Further cross section needs may be found in Reference 6.

The supplier of nuclear data must not only supply the needed cross section data, but also the uncertainties in such data. The

modern unfolding codes (FERRET, SAND, and STAYSL) use such information to provide the adjustments. In particular, the presence of cross material covariances in the ENDF/B dosimetry file is necessary in certain cases.

C. Damage Cross Sections

Damage cross sections allow material scientists to correlate damage experienced in one type of facility with that in another type. The most important (although not the only) nuclear data needed for the calculation of damage cross sections are the primary recoil spectra and total helium and hydrogen production. The primary recoil spectrum is the energy spectrum of the heavy atoms recoiling from elastic scattering and nuclear reactions. Although, this spectrum is generated by obtaining the angle-energy emission cross sections of light reactants and then determining the corresponding recoil of the heavy reactant, using kinematics, it should be emphasized, that it is the recoil of the heavy atoms that are desired. Thus the creation of primary recoil files (especially if taken directly from adequate model calculations) is highly desirable. Helium production, it must be remembered, includes not only (n,α) reactions but also such reactions as (n,nα) and (n,αn). Similarly, hydrogen production is not simply described by the (n,p) cross section.

A major impediment for damage cross section application for FMIT is the limitation of ENDF/B to a maximum energy of 20 MeV. Greenwood (7) has extended recoil spectra for several metals up to 44 MeV using approximations to compensate for inadequate data.

The LASL evaluation of Fe (4) to 40 MeV and the ORNL evaluation of Cu (8) to 32 MeV are good examples of work needed to lessen the impact of the ENDF/B limitation.

The acquisition of nuclear data for total helium production by use of helium accumulation (11), charged particle observation (12,13) and activation techniques (14) has been impressive. A recent advance in methodology is the calculation of damage cross sections in multicomponent nonmetals (9,10).

Although many data have been acquired, the nuclear data base is still meager, particularly in a format useful to the damage studies community. The samples most likely to be irradiated in FMIT will contain Fe, Ni, Cr (highest priority), Ti, Al, Cu (next priority) C, Sn, Nb, and W (lowest priority). Evaluated files containing the recoil spectrum and total helium and hydrogen production are needed for these metals for neutron energies to 40 MeV. In addition, elemental transmutation cross sections are needed but with much lower priority and accuracy. Guidance on specific transmutation products of interest must come from metallurgists. Needless to say, uncertainty estimates and proper documentation are extremely important.

D. Shielding

The need for shielding information is of primary concern during FMIT design. Already data have been obtained for the total cross sections of importance: (Fe, O, Si, Ca, and C) by ORNL (15) by UC Davis (16), and by LASL (17). In addition, nonelastic and removal cross sections at 40 and 50 Mev have been determined by UC

Davis for Fe, O, Ca, and C. The new LASL evaluation for Fe which conserves energy will be quite useful in heating calculations.

What is most needed now are evaluations of C, O, and Si. The time scale is short (essentially CY80) and the need is for consistent evaluations. The concept of removal cross sections has been a useful tool and their measurement is encouraged.

Although activation is not strictly a shielding problem, activation cross sections play an important role not only in bulk shielding design but also in the design of experimental assemblies. The creation of activation files at ANL (18) and at HEDL (19) will be helpful. However, because of their importance, some experimental activation determinations would be helpful. Other needed activation cross sections can be found in Reference 19.

E. Sensitivity Studies

As this area is still in its infancy, sensitivity studies will provide ample rewards. The evaluator of the recoil spectrum should provide strong guidance to the experimenter and model code user as to which cross sections are important in each energy range and for each material. For example, the damage energy response for Fe at 15 MeV arises from inelastic (30%), (n,2n) (~30%), elastic (~21%), and (n,charged) particle (~20%) (20).

Sensitivity studies in calculational dosimetry will provide guidance to evaluators, experimentalists, and model code users as to important reaction types and energy ranges. The use of

calculated flux maps will show the response of dosimetry cross sections (6) and damage cross sections (21).

F. Integral Testing

Unlike the situation at fission energies, there does not exist sufficient differential data at higher energies for the important materials to provide complete evaluations. Therefore, the use of integral experiments will provide needed checks on the accuracy of the available experimental data and on the reliability of nuclear model codes. Such checks will not only confirm cross sections but also the methods and data used in the calculational dosimetry.

Progress has already been made. Greenwood (1) has shown the consistency of many of the passive dosimetry reactions. Qaim et al., (14) have used the d+Be neutron sources to integrally test activation cross sections while Kneff et al., (11) have used similar sources for total helium production. Finally, using time-of-flight measurements, Johnson et al., (22) and Saltmarsh et al., (23) have characterized d+Li and d+Be at deuteron energies of 35 and 40 MeV, respectively.

III. Summary

Much progress has been made in the three years since the last symposium. However, much more progress needs to be made. Increased interaction between the user community and the generators of nuclear data will expedite this progress. Measured

and calculated cross section sets must be put into usable form in order to have impact on FMIT utilization.

References

1. L.R. Greewood "Integral Cross Section Testing in a Be-9(d,n) Field At E(deuteron) = 40 MeV". Nuclear Science and Engineering,72,175 (1979)
2. D.W. Kneff et al., "Characterization Of The Be(d,n) Neutron Field By Passive Dosimetry Techniques". Proceedings of this Symposium.
3. F.H. Ruddy et al., "CR-39 Polymer, A Promising New Solid State Track Recorder For High Energy Neutron Applications". Ibid.
4. E.D. Arthur et al., "Evaluation Of Neutron Cross Sections To 40 MeV For Fe-54,56" also, "Calculation Of Co-59 Neutron Cross Sections Between 3 and 50 MeV". Ibid.
5. L.R. Greewood "Review Of Source Characterization For Fusion Materials Irradiations". Ibid.
6. R. Gold et al., "Cross Sections Required For FMIT Dosimetry". Ibid.
7. L.R. Greenwood, Argonne National Laboratory, Private Communication.
8. C.Y. Fu and F.G. Perey, Jour. of Nucl. Materials,61,153(1976)
9. G.F. Dell et al., "Damage Parameters For Non-metals In A High Energy Neutron Environment". Proceedings of this Symposium.
10. D.M. Parkin and C.A. Coulter, Journal of Nuclear Materials, 85 and 86,611(1979), Ibid,88,249(1980)

11. D.W. Kneff et al., "Helium Generation Cross Sections For Fast Neutrons". Proceedings of this Symposium.

12. R.C. Haight and S.M. Grimes "Status Of (n,charged particle) Measurements At LLL"., Ibid.

13. G. Randers-Pehrson et al., "Neutron Induced Charged Particle Reaction Studies At Ohio University". Ibid.

14. S.M. Qaim et al., "Integral Cross Section Measurements On (n,x) Reactions Induced By 30 MeV d(Be) Break-up Neutrons On FRT Wall And Structural Materials". Ibid.

15. D.C. Larson, "ORELA Measurements To Meet Fusion Energy Cross Section Needs". Ibid.

16. C.I. Zanelli et al., "Measurements Of Neutron Total And Total Nonelastic Cross Sections For C, O, Ca And Fe At UC Davis". Ibid.

17. P.W. Lisowski et al., "Neutron Cross Section Measurements At WNR". Ibid.

18. L.R. Greenwood "Extrapolation Of Neutron Activation Cross Sections For Dosimetry to 44 MeV". ANL-FPP-TM-115, Nov 1978.

19. L.L. Carter et al., "Nuclear Data Relevant To Shield Design Of FMIT Facility". Proceedings of this Symposium.

20. D.G. Doran et al., HEDL-TME-76-70(1976)

21. F.M. Mann et al., "Neutron environment In d+ Li Facilities". Proceedings of this Symposium.

22. D.L. Johnson et al., "Thick Target Neutron Yields And Spectra From The Li(d,xn) Reaction At 35 MeV". Ibid.

23. M.J. Saltmarsh et al., Nuclear Inst. and Methods, 145, 81 (1977)

TABLE I

HIGHEST PRIORITY DOSIMETRY REACTIONS

^{59}Co:	(n,p)	(n,2n)	(n,3n)	(n,4n)	(n,He)$^{+}$
^{197}Au:	(n,2n)	(n,3n)	(n,4n)	(n,He)$^{+}$	
^{54}Fe:	(n,p)	(n,t)*	(n,α)	(n,He)$^{+}$	
^{56}Fe:	(n,t)*	(n,He)			
^{58}Ni:	(n,p)	(n,2n)	(n,3n)	(n,He)$^{+}$	
^{60}Ni:	(n,p)	(n,t)*	(n,He)$^{+}$		

* includes (n,t), (n,nd), (n,dn), (n,2np)

\+ includes (n,α), (n,αn), (n,nα), (n,n2α), etc.

THIS PAGE
WAS INTENTIONALLY
LEFT BLANK

NUCLEAR MODEL CODES AND DATA EVALUATION

P.G. Young, LASL - Chairperson

E.D. Arthur, LASL
P.J. Dimbylow, NRPB
M. Divadeenam, BNL
R.W. Finlay, OHIO U.
C.Y. Fu, ORNL
D.G. Gardner, LLL
M.A. Gardner, LLL
H. Gruppelaar, ECN-Petten
L.F. Hansen, LLL
C. Kalbach, TUNL
D. Larson, ORNL
F.M. Mann, HEDL
G.Randers-Pehrson, OHIO U.
C. Philis, BRC
T.W. Phillips, LLL
A. Prince, BNL
A. Smith, ANL
H. Vonach, IRK

I. Introduction

The above group met on May 13, 1980, in conjunction with the Symposium on Neutron Cross Sections from 10-50 MeV, to discuss problems associated with nuclear data evaluation and model code calculations for applied data needs in the 10-50 MeV range. This report follows the form of the previous one from the 1977 meeting and is essentially an update of those findings. The remaining sections describe the present status of evaluations and nuclear models, outline problem areas in model calculations, and give recommendations and conclusions regarding future work.

II. Status of Nuclear Data Evaluation

As was the case three years ago at the last meeting, formal nuclear data evaluations still primarily cover the neutron energy range below 20 MeV, including the newly issued Version V of ENDF/B. Several evaluations have been referred to at this meeting that extend to the 40-50 MeV range. These efforts have been

mainly in conjunction with FMIT facility project and include a number of dosimetry evaluations, a full ENDF-formatted natural iron evaluation with energy-angle data, and several ad hoc multigroup and continuous energy data sets, based on optical model and intranuclear cascade calculations.

A number of new measurements of importance were reported at this symposium, however, that have not been incorporated into evaluations. A frequently expressed concern at the workshop regarded the incorporation of new experimental data into the evaluation process. While such data are useful in themselves, it is only through the evaluation process that the experiments can be fully exploited. In particular, since current experimental techniques are not able to provide all the needed data, it is necessary to use model calculations to fill gaps and to supply much of the energy-angle data that has been requested. The most reliable model calculations are those which simultaneously reproduce in a consistent manner all available experimental data for a nucleus. Such analyses serve to improve the reliability of calculated cross sections in regions where experimental data do not exist, and therefore extend the usefulness of measurements far beyond their original scope. It was the feeling of the group that insufficient emphasis is being given to such analyses.

Another area of concern expressed at this meeting was a desire for better communication between the experimenters, evaluators, and users. Since model calculations will be relied on to provide many of the necessary cross sections, it is important

that the experimenters have input from the evaluators as to which measurements will be most useful to guide model calculations. Frequently one or two carefully chosen measurements will allow determination of parameters sufficient to calculate a number of other required cross sections. As a means to this end, Table I gives the lead evaluator and laboratory for each of the materials contained in ENDF/B-V.

III. Nuclear Model Improvements and Remaining Problems

The primary nuclear models applicable to nuclear data problems in the 10-50 MeV region are the multistep Hauser-Feshbach, precompound, direct reaction, and intranuclear cascade/evaporation models. Several computer codes that implement one or more of these models are described in the symposium proceedings and are summarized in Table II.

While a number of deficiencies remain in nuclear model capabilities, several improvements have occured over the past three years. The sections below summarize some of the developments and list certain of the outstanding problems that remain.

A. Unification of Reaction Models

This topic has been one of substantial interest due largely to the efforts of the Weidenmuller group although implementation of a rigorous theoretical approach appears to be complex. As a first step, parameters used in different models employed to analyse neutron experimental data should be consistent if a

meaningful predictive capability is desired. Efforts are underway to unify preequilibrium and Hauser-Feshbach models to produce a consistent approach through incorporation of angular momentum effects in the preequilibrium model. Such efforts should be encouraged with a desire towards testing these approaches over a wide mass region under various conditions. Deficiencies remaining in existing preequilibrium models such as pairing or shell effects should be addressed as well as treatments used to describe composite particle emission.

B. Angular Distributions for Continuum Emission

Considerable progress appears to have been made based on several papers presented at this Symposium ranging from phenomenological analyses of angular distribution data to fits of large amounts of experimential data using more basic preequilibrium models. Problems remain regarding representation of data at backward angles and the effect of approximations used in these models.

C. Level Densities

Since the 1977 Symposium little advancement has been made in the use of level densities other than the Gilbert-Cameron or back-shifted Fermi-gas models. However such models are applied with more effort towards determination of constant temperature parameters based on recent experimental discrete level data and the use of more realistic systematics for the spin cut-off parameter. The prospects for better level density models as regards energy dependence and parity ratios have perhaps improved

through the recent basic work by Grimes et al.

D. Gamma-Ray Strength Function

Considerable progress towards determination and prediction of gamma-ray strength functions has been achieved through the work of D.G. Gardner and M.A. Gardner. Efforts should be made towards the implementation of such results into multi-step Hauser-Feshbach calculations.

E. Optical Model Parameters

Progress has been made in the determination of neutron optical parmeters valid over a wide energy range from several hundred keV to several tens of MeV. Such parameter sets should be identified for use in applicable mass and energy regions. Little improvement exists, though, in the determination and verification of energy-dependent alpha-particle optical parameters. The subcoulomb barrier behavior of proton optical parameters as discussed recently in the literature may be important for certain proton-production calculations.

IV. Additional Recommendations

A. While progress in acquiring higher energy data has been made through the FMIT project, there is still no systematic effort to develop, validate, document, and disseminate microscopic data libraries in the 10-50 MeV region. We recommend that fusion-related data activities be coordinated with CSEWG and that development of data files for selected materials to 50 MeV be a goal for the next version of ENDF/B. Such development includes

the identification of appropriate formats for representation of energy-angle data at higher energies where many reaction channels are open and for specifying the charged particle and recoil nucleus spectra and angular distributions needed for radiation damage studies. Additionally we recommend that the problem of energy balance, which was noted at this meeting, be brought to the attention of CSEWG and appropriate remedies devised.

B. The time, effort, and requisite skills required to produce reliable data evaluations have expanded significantly with the increased demands and requirements for data evaluations. It should be recognized that carrying out reliable data evaluations spanning the energy region from thermal to 50 MeV require large scale efforts. It is the feeling of the group that evaluation efforts would benefit from closer collaboration among evaluators at different laboratories, both nationally and internationally.

C. The LLL-LASL code comparisons cited in the review talk, which led to agreement of $\leq$ 5% among the independent model codes, are valuable activities that should be expanded. The group recommends that CSEWG continue its code comparison effort and identify problems that test calculations in the 10-50 MeV range. Additionally, consideration should be given to comparisons of equivalent calculations with different models such as the intranuclear cascade and multistep Hauser-Feshbach models.

D. Evaluation methods that combine differential and integral measurements, theoretical calculations, and covariance data files have been developed for other applications. Such techniques

should also be considered for higher energy data evaluations, e.g., in dosimetry data evaluations for the FMIT facility.

E. Considerable effort has been directed at specification of covariance data for ENDF/B evaluations. It is recommended that the question of uncertainties in model calculations at higher energies be addressed by evaluators.

F. In the review paper for this session, Gardner recommended that consideration be given to setting up computer files of data needed in model calculations, e.g., level energies, spins, parities, gamma branching ratios, etc. We recommend that the establishment of such files be investigated by the model codes group in CSEWG. Additionally we recommend that the model codes group look more closely into the question of what experimental data are most important for defining nuclear model parameters in higher energy calculations.

G. Examples were given at this symposium of cases where global optical parameter sets resulted in very poor calculated total cross sections at higher energies. Care should be taken in all model calculations to ensure that the parameters being used are appropriate for the specific nuclei and energy ranges being studied.

H. Nuclear model calculations for light elements are relatively more difficult than for medium mass nuclei. In particular, global parameterizations are not as reliable, and special care should be taken to ensure the appropriateness of models and parameters for nuclei lighter than Al-27. This

conclusion implies, of course, a more extensive measurement program for important light nuclei.

I. The models and techniques discussed here can be validated and parameters obtained from proton-induced measurements as well as from incident-neutron experiments. Therefore, the group recommends that available proton data be carefully utilized in model studies when possible. In addition, we encourage charged-particle experimenters to consider measurements of such quantities as alpha and proton production cross sections, spectra, and angular distributions induced by protons up to 50 MeV, as well as proton elastic scattering and emission spectra.

J. Authors of nuclear model codes are urged to provide documentation of their codes, including updates to reflect later improvements. Documentation should include a theoretical description and, if the code is to be generally available, user instructions.

K. The neutron-induced measurements that are most essential for providing the required data evaluations up to 50 MeV are neutron total cross sections, elastic scattering angular distributions, elastic or nonelastic cross sections, hydrogen and helium production cross sections, and important dosimetry and activation cross sections. While we can provide estimates of these quantities with model codes now, experimental data at a few energies for important materials would greatly improve the overall accuracy of the calculations. Additionally, measurements of secondary neutron and charged-particle emission spectra at a few

angles for a few nuclei are needed at an incident energy where preequilibium effects dominate ($E \geq 20$MeV). These data are needed to verify relative neutron and proton cross sections predicted by preequilibrium theory.

V. Acknowledgments

The chairperson wishes to thank all participants for their help with the workshop. Particular thanks are due to M. Divadeenam, who prepared TABLE II, and to E.D. Arthur and D. Larson, who helped draft the workshop report.

Z EL A	MAT NO.	SPECIFICATION	NO. CARDS	LABORATORY	REFERENCE	DATE	AUTHOR
1-H - 1	1301	Neut. + gamma prod. +error	513	LASL	LA-4574 (1971)	JAN77	L.STEWART, R.J.LABAUVE, P.G.YOUNG
1-H - 2	1302	Neutron + gamma production	909	LASL	LA-3271 (1968)	JAN77	L.STEWART (LASL) A.HORSLEY (AWRE)
1-H - 3	1169	Neutron+decay data	849	LASL	LA-3270 (65) UPDATE67	OCT74	LEONA STEWART
2-He- 3	1146	Neutron cross sections only	405	LASL	NO PUBLICATION	JUN68	LEONA STEWART (LASL)
2-He- 4	1270	Neutron cross sections only	429	LASL	NO PUBLICATION	OCT73	HISLEY, HALE, YOUNG (LASL)
3-Li- 6	1303	Neut. + gamma prod. +error	2584	LASL		SEP77	G.HALE, L.STEWART, P.G.YOUNG
3-Li- 6	6424	Neutron+err.files	199	LASL		DEC78	L.STEWART, G.HALE, P.YOUNG
3-Li- 7	1272	Neutron + gamma production	680	LASL		OCT72	R.J.LABAUVE, L.STEWART, M.BATTAT
4-Be- 9	1304	Neutron + gamma production	2758	LLL		OCT76	HOWERTON, PERKINS
5-B - 10	1305	Neut. + gamma prod. +error	3539	LASL		JAN77	G.HALE, L.STEWART, P.YOUNG
5-B - 10	6425	Neutron+err.files	179	LASL		JAN79	L.STEWART, G.HALE, P.YOUNG
5-B - 11	1160	Neutron cross sections only	1014	CE-BNL		NOV74	C.COWAN
6-C - 0	1306	Neut. + gamma prod. +error	2634	ORNL	INDC(P/R)-7/L	JAN77	C.Y.FU AND F.G.PEREY
7-N - 14	1275	Neut. + gamma prod. +error	6109	LASL	LA-4725 (1972)	JUN75	P.YOUNG, D.FOSTER, JR., G.HALE
7-N - 15	1307	Neutron + gamma production	3813	LASL		MAR77	E.ARTHUR, P.YOUNG, G.HALE
8-O - 16	1276	Neut. + gamma prod. +error	6048	LASL	LA-4780 (1972)	JUN75	P.YOUNG, D.FOSTER, JR., G.HALE
8-O - 17	1317	Neutron cross sections only	829	BNL		JAN78	B.A.MAGURNO
9-F - 19	1309	Neut. + gamma prod. +error	4739	ORNL		DEC76	C.Y.FU, D.C.LARSON, F.G.PEREY
11-Na- 23	1311	Neut.(RP) + gamma prod. +error	4361	ORNL		DEC77	D. C. LARSON
11-Na- 23	6311	Neut.(RP)+err.files	180	ORNL		DEC77	D.C.LARSON
12-Mg- 0	1312	Neutron + gamma production	4601	ORNL		FEB78	D.C.LARSON
13-Al- 27	1313	Neut. + gamma prod. +error	6101	LASL	LA-4726 (1973).	AUG77	P.G. YOUNG, D.G. FOSTER, JR.
13-Al- 27	6313	Neutron+err.files	183	LASL	LA-4726 (1973).	AUG77	P.G. YOUNG, D.G. FOSTER, JR.
14-Si- 0	1314	Neut. + gamma prod. +error	12730	ORNL		DEC76	LARSON, PEREY, DRAKE, YOUNG
15-P - 31	1315	Neutron + gamma production	937	LLL	UCRL 50400 VOL15(B)	OCT77	HOWERTON
16-S - 32	1316	Neutron + gamma production	959	LLL	UCRL 50400 VOL15(B)	OCT77	HOWERTON
17-Cl- 0	1149	Neutron + gamma production	3712	GGA	GA-7829 VOL-4(1967)	FEB67	M.S.ALLEN AND M.K.DRAKE
19-K - 0	1150	Neutron + gamma production	3852	GGA	GA-7829 VOL-5 (1967)	FEB67	M.K.DRAKE
20-Ca- 0	1320	Neutron + gamma production	5912	ORNL	ADNDT 17(1976)127.	OCT76	C.Y.FU AND F.G.PEREY
21-Sc- 45	6426	Neut.(RP)+err.files	279	BNL		JUL79	MAGURNO AND MUGHABGHAB
22-Ti- 0	1322	Neutron + gamma production	5380	BURANLLLL	ANL/NDM-28,1977	AUG77	C.PHILIS, A.SMITH, R.HOWERTON
22-Ti- 46	6427	Neutron+err.files	60	ANL		JAN77	C.PHILIS, O.BERSILLON, D.SMITH, ETC.
22-Ti- 47	6428	Neutron+err.files	87	ANL		JAN77	C.PHILIS, O.BERSILLON, D.SMITH, ETC
22-Ti- 48	6429	Neutron+err.files	86	ANL		JAN77	C.PHILIS, O.BERSILLON, D.SMITH ETC.
23-V - 0	1323	Neutron + gamma production	2335	ANLLLLHEDL	ANL/NDM-24,1977	JAN77	A.SMITH-, H.HOWERTON, F.MANN.
24-Cr- 0	1324	Neut.(RP) + gamma prod. +error	13347	BNL		DEC77	A.PRINCE AND T.W.BURROWS
25-Mn- 55	1325	Neut.(RP) + gamma prod. +error	2836	BNL		MAR77	S.F. MUGHABGHAB
25-Mn- 55	6325	Neutron+err.files	63	BNL		MAR77	S.F. MUGHABGHAB
26-Fe- 0	1326	Neut.(RP) + gamma prod. +error	8861	ORNL	ORNL-4617(1970)	OCT77	C.Y.FU AND F.G.PEREY
26-Fe- 54	6430	Neutron+err.files	79	HEDL		JUN79	R.SCHENTER F.SCHMITTROTH F.MANN
26-Fe- 56	6431	Neutron+err.files	108	ORNL		JUL78	C.Y.FU
26-Fe- 58	6432	Neut.(RP)+err.files	158	HEDL		JUN79	R.SCHENTER F.SCHMITTROTH F.MANN
27-Co- 59	1327	Neutron(RP)+gamma production	3279	BNL		JUN77	S.MUGHABGHAB
27-Co- 59	6327	Neut.(RP)+err.files	363	BNL		JUN77	S.MUGHABGHAB
28-Ni- 0	1328	Neut.(RP) + gamma prod. +error	9171	BNL(NNDC)		MAR77	M.DIVADEENAM
28-Ni- 58	6433	Neutron+err.files	127	BNL		MAR77	M.DIVADEENAM
28-Ni- 60	6434	Neutron+err.files	70	BNL		MAR77	M.DIVADEENAM
29-Cu- 0	1329	Neutron(RP)+gamma production	3681	ORNL,SAI	DNA-3356F(1974)	MAR78	FU, DRAKE, FRICKE
29-Cu- 63	6435	Neut.(RP)+err.files	295	ORNL		JUL78	C.Y.FU
29-Cu- 65	6436	Neutron+err.files	95	ORNL		JUL78	C.Y.FU

Z EL A	MAT NO.	SPECIFICATION	NO. CARDS	LABORATORY	REFERENCE	DATE	AUTHOR
36-Kr- 78	1330	Neutron cross sections only (RP)	1061	BNL		DEC78	A.PRINCE
36-Kr- 80	1331	Neutron cross sections only (RP)	1007	BNL		DEC78	A.PRINCE
36-Kr- 82	1332	Neutron cross sections only (RP)	1039	BNL		DEC78	A.PRINCE
36-Kr- 83	1333	Neutron cross sections only (RP)	1064	BNL		DEC78	A.PRINCE
36-Kr- 84	1334	Neutron cross sections only (RP)	866	BNL		APR78	A.PRINCE
36-Kr- 86	1336	Neutron cross sections only (RP)	867	BNL		JUN75	A.PRINCE
40-Zr- 0	1340	Neutron cross sections only (RP)	1807	SAI	EPRI NP-250	APR76	M.DRAKE D.SARGIS T.MAUNG
40-Zr- 90	1385	Neutron cross sections only (RP)	1103	SAI	EPRI NP-250	APR76	M.DRAKE D.SARGIS T.MAUNG
40-Zr- 91	1386	Neutron cross sections only (RP)	1313	SAI	EPRI NP-250	APR76	M.DRAKE D.SARGIS T.MAUNG
40-Zr- 92	1387	Neutron cross sections only (RP)	1157	SAI	EPRI NP-250	APR76	M.DRAKE D.SARGIS T.MAUNG
40-Zr- 94	1388	Neutron cross sections only (RP)	1228	SAI	EPRI NP-250	APR76	M.DRAKE D.SARGIS T.MAUNG
40-Zr- 96	1389	Neutron cross sections only (RP)	1047	SAI	EPRI NP-250	APR76	M.DRAKE D.SARGIS T.MAUNG
41-Nb- 93	1189	Neutron(RP)+gamma production	2144	ANL,LLL		MAY74	R.HOWERTON(LLL) AND A.SMITH
42-Mo- 0	1321	Neutron(RP)+gamma production	1821	LLL,HEDL		FEB79	HOWERTON,SCHMITTROTH,SCHENTER
43-Tc- 99	1308	Neut.(RP)+decay data	823	HEDL,BAW		NOV78	SCHENTER,LIVOLSI,SCHMITTROTH,ETAL
45-Rh-103	1310	Neutron cross sections only (RP)	955	HEDL,BAW		NOV78	SCHENTER,LIVOLSI,SCHMITTROTH,ETAL
47-Ag-107	1371	Neutron cross sections only (RP)	874	HEDL,BNL		NOV78	SCHENTER,BHAT,PRINCE,JOHNSON,ETAL
47-Ag-109	1373	Neutron cross sections only (RP)	807	HEDL,BNL		NOV78	SCHENTER,BHAT,PRINCE,JOHNSON,ETAL
48-Cd- 0	1281	Neutron cross sections only	2465	BNL		NOV74	S.PEARLSTEIN(TRANS FROM U.K.)
48-Cd-113	1318	Neut.(RP)+decay data	562	BNL,HEDL		NOV78	PEARLSTEIN,MANN,SCHENTER
49-In-115	6437	Neut.(RP)+err.files	302	HEDL/ANL		JAN78	F.SCHMITTROTH/D.L.SMITH
53-I -127	6438	Neutron+err.files	74	STANFORD		AUG72	R.SHEB
54-Xe-124	1335	Neutron cross sections only (RP)	714	BNL		MAR78	M.R.BHAT AND S.F.MUGHABGHAB
54-Xe-126	1339	Neutron cross sections only (RP)	718	BNL		MAR78	M.R.BHAT AND S.F.MUGHABGHAB
54-Xe-128	1348	Neutron cross sections only (RP)	684	BNL		MAR78	M.R.BHAT AND S.F.MUGHABGHAB
54-Xe-129	1349	Neutron cross sections only (RP)	845	BNL		MAR78	M.R.BHAT AND S.F.MUGHABGHAB
54-Xe-130	1350	Neutron cross sections only (RP)	784	BNL		MAR78	M.R.BHAT AND S.F.MUGHABGHAB
54-Xe-131	1351	Neutron cross sections only (RP)	818	BNL		MAR78	M.R.BHAT AND S.F.MUGHABGHAB
54-Xe-132	1352	Neutron cross sections only (RP)	694	BNL		MAR78	M.R.BHAT AND S.F.MUGHABGHAB
54-Xe-134	1354	Neutron cross sections only (RP)	656	BNL		MAR78	M.R.BHAT AND S.F.MUGHABGHAB
54-Xe-135	1294	Neutron+decay data	853	BNW	PRI.COM.JUNE,1967	MAY75	B.R.LEONARD,JR. AND K.B.STEWART
54-Xe-136	1356	Neutron cross sections only	654	BNL		MAR78	M.R.BHAT AND S.F.MUGHABGHAB
55-Cs-133	1355	Neutron cross sections only (RP)	861	HEDL,BNL		NOV78	SCHENTER,BHAT,PRINCE,JOHNSON,ETAL
56-Ba-138	1353	Neutron + gamma production	1098	LLL	UCRL-50400 VOL. 15	AUG78	HOWERTON
62-Sm-149	1319	Neut.(RP)+decay data	1606	HEDL,BNW		NOV78	SCHENTER,LEONARD,STEWART,ET AL.
63-Eu-151	1357	Neutron(RP)+gamma production	1853	BNL		DEC77	S.F. MUGHABGHAB
63-Eu-152	1292	Neut.(RP)+decay data	3211	BNL		JUN75	H.TAKAHASHI
63-Eu-153	1359	Neutron(RP)+gamma production	2036	BNL		FEB78	S.MUGHABGHAB
63-Eu-154	1293	Neut.(RP)+decay data	2428	BNL		JUN75	H.TAKAHASHI
64-Gd-152	1362	Neutron cross sections only (RP)	1405	BNL		JAN77	B.A.MAGURNO
64-Gd-154	1364	Neutron cross sections only (RP)	1459	BNL		JAN77	B.A.MAGURNO
64-Gd-155	1365	Neutron cross sections only (RP)	1554	BNL		JAN77	B.A.MAGURNO
64-Gd-156	1366	Neutron cross sections only (RP)	1447	BNL		JAN77	B.A.MAGURNO
64-Gd-157	1367	Neutron cross sections only (RP)	1488	BNL		JAN77	B.A.MAGURNO
64-Gd-158	1368	Neutron cross sections only (RP)	1476	BNL		JAN77	B.A.MAGURNO
64-Gd-160	1370	Neutron cross sections only (RP)	1223	BNL		JAN77	B.A.MAGURNO
66-Dy-164	1031	Neutron cross sections only (RP)	1271	BNW	PRI.COMM.JUNE,1967	JUN67	B.R.LEONARD,JR. AND K.B.STEWART
71-Lu-175	1032	Neutron cross sections only (RP)	1069	BNW	PRI.COMM.JUNE,1967	JUN67	B.R.LEONARD,JR. AND K.B.STEWART
71-Lu-176	1033	Neutron cross sections only (RP)	1139	BNW	PRI.COMM.JUNE,1967	JUN67	B.R.LEONARD,JR. AND K.B.STEWART
72-Hf- 0	1372	Neutron cross sections only (RP)	1069	SAI	EPRI NP-250	APR76	M.DRAKE D.SARGES T.MAUNG

Z EL A	MAT NO.	SPECIFICATION	NO. CARDS	LABORATORY	REFERENCE	DATE	AUTHOR
72-Hf-174	1374	Neutron cross sections only (RP)	676	SAI	EPRI NP-250	APR76	M.DRAKE D.SARGES T.MAUNG
72-Hf-176	1376	Neutron cross sections only (RP)	681	SAI	EPRI NP-250	APR76	M.DRAKE D.SARGES T.MAUNG
72-Hf-177	1377	Neutron cross sections only (RP)	865	SAI	EPRI NP-250	APR76	M.DRAKE D.SARGES T.MAUNG
72-Hf-178	1378	Neutron cross sections only (RP)	673	SAI	EPRI NP-250	APR76	M.DRAKE D.SARGES T.MAUNG
72-Hf-179	1383	Neutron cross sections only (RP)	714	SAI	EPRI NP-250	APR76	M.DRAKE D.SARGES T.MAUNG
72-Hf-180	1384	Neutron cross sections only (RP)	668	SAI	EPRI NP-250	APR76	M.DRAKE D.SARGES T.MAUNG
73-Ta-181	1285	Neutron(RP)+gamma production	2814	LLL		NOV74	HOWERTON, PERKINS, MACGREGOR
73-Ta-182	1127	Neutron cross sections only (RP)	762	AI	AI-AEC-12990 (1971)	APR71	J.OTTER,C.DUNFORD,AND E.OTTEWITTE
74-W -182	1128	Neutron(RP)+gamma production	3202	AI,LASL		JUN73	OTTER,OTTEWITTE,ROSE,YOUNG
74-W -183	1129	Neutron(RP)+gamma production	3536	AI,LASL		OCT74	OTTER,OTTEWITTE,ROSE,YOUNG
74-W -184	1130	Neutron(RP)+gamma production	3092	AI,LASL		APR74	OTTER,OTTEWITTE,ROSE,YOUNG
74-W -186	1131	Neutron(RP)+gamma production	3074	AI,LASL		JUN73	OTTER,OTTEWITTE,ROSE,YOUNG
75-Re-185	1083	Neutron cross sections only (RP)	1365	CE(NMPO)	GEMP-587	JAN68	W.B.HENDERSON AND J.W.ZWICK
75-Re-187	1084	Neut.(RP)+decay data	1436	CE(NMPO)	GEMP-587	JAN68	W.B.HENDERSON AND J.W.ZWICK
79-Au-197	1379	Neut.(RP)+err.files	1931	BNL		FEB77	S.F.MUGHABGHAB
79-Au-197	6379	Neut.(RP)+err.files	558	BNL		FEB77	S.F.MUGHABGHAB
81-Tl-208	8108	Decay data only	168	INEL		AUG78	REICH
82-Pb- 0	1382	Neut. + gamma prod. +error	3895	ORNL	ADNDT,16(1975)4C9.	AUG76	C.Y.FU AND F.G.PEREY
82-Pb-212	8212	Decay data only	83	INEL		AUG78	REICH
83-Bi-212	8312	Decay data only	168	INEL		NOV78	REICH
84-Po-216	8416	Decay data only	36	INEL		AUG78	REICH
86-Rn-220	8620	Decay data only	32	INEL		AUG78	REICH
88-Ra-224	8824	Decay data only	73	INEL		AUG78	REICH
90-Th-228	8028	Decay data only	79	INEL		AUG78	REICH
90-Th-230	8030	Neut.(RP)+decay data	748	HEDL		NOV77	MANN
90-Th-231	8031	Decay data only	200	INEL		AUG78	REICH
90-Th-232	1390	Neut(RP)+decay+FPY+gam.+err.	7479	BNL		DEC77	BHAT,SMITH,LEONARD,DESAUSSUREETAL
90-Th-232	6390	Neut.(RP)+err.files	862	BNL		DEC77	BHAT,SMITH,LEONARD,DESAUSSUREETAL
90-Th-233	8033	Decay data only	357	INEL		AUG78	REICH
91-Pa-231	8131	Neut.(RP)+decay data	872	HEDL		NOV77	MANN
91-Pa-232	8132	Decay data only	180	INEL		AUG78	REICH
91-Pa-233	1391	Neut.(RP)+decay data	1140	HEDL,INEL		MAY78	MANN,SCHENTER,REICH
92-U -232	8232	Neut.(RP)+decay data	681	HEDL		NOV77	MANN
92-U -233	1393	Neut(RP)+decay+fiss.prod.yld	6708	LASL-ORNL	TANSAO 28, 721. 1978	DEC78	STEWART ET AL, WESTON, MANN,HEDL
92-U -234	1394	Neut.(RP)+decay data	1128	BNL,HEDL,+		JUL78	DIVADEENAM,MANN,DRAKE,REICH,ET.AL
92-U -235	1395	Neut(RP)+decay+FPY+gam.+err.	10161	BNL		NOV77	M.R.BHAT
92-U -235	6395	Neut.(RP)+err.files	1439	BNL		APR77	M.R.BHAT
92-U -236	1396	Neut(RP)+decay+fiss.prod.yld	2814	BNL,HEDL,+		JUL78	DIVADEENAM,MANN,MCCROSSON,REICH,+
92-U -237	8237	Neut.(RP)+decay+gamma prod. data	1752	BNL,SRL,LLL		JUL76	KINSEY-ASSEMBLER(SEE COMMENTS)
92-U -238	1398	Neut(RP)+decay+FPY+gam.+err.	8350	ANL+	ANL/NDM-32	MAR79	E.PENNINGTON,A.SMITH,W.POENITZ
92-U -238	6398	Neut.(RP)+err.files	858	ANL+	ANL/NDM-32	MAR79	E.PENNINGTON,A.SMITH,W.POENITZ
92-U -239	8239	Decay data only	384	INEL		AUG78	REICH
93-Np-236	8336	Decay data only	132	INEL		AUG78	REICH
93-Np-236m	8346	Decay data only	105	INEL		AUG78	REICH
93-Np-237	1337	Neut(RP)+decay+FPY+err.	4150	HEDL,SRL,+	HEDL TME 77-54	APR78	MANN,BENJAMIN,SMITH,STEIN,REICH,+
93-Np-237	6337	Neut.(RP)+err.files	1234	HEDL,SRL,+	HEDL TME 77-54	APR78	MANN,BENJAMIN,SMITH,STEIN,REICH,+
93-Np-238	8338	Neut.(RP)+decay data	593	SRL		AUG75	BENJAMIN AND MCCROSSON
93-Np-239	8339	Decay data only	195	INEL		AUG78	REICH
94-Pu-236	8436	Neut.(RP)+decay data	632	HEDL,SRL	HEDL TME 77-54	APR78	MANN,SCHENTER,BENJAMIN,MCCROSSON
94-Pu-237	8437	Neutron+decay data	694	HEDL	HEDL TME 77-54	APR78	MANN AND SCHENTER (FAST)

Z EL A	MAT NO.	SPECIFICATION	NO. CARDS	LABORATORY	REFERENCE	DATE	AUTHOR
94-Pu-238	1338	Neut.(RP)+decay data	1121	HEDL,AI,+	HEDL TME 77-54	APR78	MANN,SCHENTER,ALTER,DUNFORD,+
94-Pu-239	1399	Neut(RP)+decay+FPY+gam.+err.	9313	GE-FBRD		OCT76	E.KUJAWSKI,L.STEWART(LASL)
94-Pu-239	6399	Neut.(RP)+err.files	916	GE-FBRD		OCT76	E.KUJAWSKI,L.STEWART(LASL)
94-Pu-240	1380	Neut(RP)+decay+FPY+gam.+err.	4025	ORNL		APR77	L.W. WESTON
94-Pu-241	1381	Neut(RP)+decay+FPY+gam.+err.	4546	ORNL		OCT77	L.W. WESTON,R.Q. WRIGHT,HOWERTON
94-Pu-242	1342	Neut(RP)+decay+FPY+gam.+err.	4248	HEDL,SRL,+		OCT78	MANN,BENJAMIN,MADLAND,HOWERTON,+
94-Pu-243	8443	Neut.(RP)+decay+gamma prod. data	2070	BNL,SRL,LLL		JUL76	KINSEY-ASSEMBLER(SEE COMMENTS)
94-Pu-244	8444	Neut.(RP)+decay data	672	HEDL,SRL	HEDL TME 77-54	APR78	MANN,SCHENTER,BENJAMIN,MCCROSSON
95-Am-240	8540	Decay data only	175	INEL		AUG78	REICH
95-Am-241	1361	Neut.(RP)+decay+gamma prod.+err.	2111	HEDL,ORNL		APR78	MANN,SCHENTER, AND WESTON
95-Am-242m	1369	Neut.(RP)+decay+gamma prod. data	231	HEDLSRLLLL	HEDL TME 77-54	APR78	MANN,BENJAMIN,HOWERTON,ET AL.
95-Am-242	8542	Neut.(RP)+decay data	472	SRL		AUG75	BENJAMIN AND MCCROSSON
95-Am-243	1363	Neut.(RP)+decay+gamma prod. data	986	HEDLSRLLLL	HEDL TME 77-54	APR78	MANN,BENJAMIN,HOWERTON,ET AL.
95-Am-244	8544	Decay data only	107	INEL		AUG78	REICH
95-Am-244m	8554	Decay data only	78	INEL		AUG78	REICH
96-Cm-241	8641	Neutron+decay data	683	HEDL	HEDL TME 77-54	APR78	MANN AND SCHENTER
96-Cm-242	8642	Neut.(RP)+decay+gamma prod. data	1185	HEDLSRLLLL	HEDL TME 77-54	APR78	MANN,BENJAMIN,HOWERTON,ET AL.
96-Cm-243	1343	Neut.(RP)+decay+gamma prod. data	1554	HEDLSRLLLL	HEDL TME 77-54	APR78	MANN,BENJAMIN,HOWERTON,ET AL.
96-Cm-244	1344	Neut.(RP)+decay+gamma prod. data	1515	HEDLSRLLLL	HEDL TME 77-54	APR78	MANN,BENJAMIN,HOWERTON,ET AL.
96-Cm-245	1345	Neut.(RP)+decay+gamma prod. data	1796	SRL		SEP75	BENJAMIN AND MCCROSSON
96-Cm-246	1346	Neut.(RP)+decay+gamma prod. data	2041	BNL,SRL,LLL		JUL76	KINSEY-ASSEMBLER(SEE COMMENTS)
96-Cm-247	8647	Neut.(RP)+decay+gamma prod. data	2267	BNL,SRL,LLL		JUL76	KINSEY-ASSEMBLER(SEE COMMENTS)
96-Cm-248	8648	Neut.(RP)+decay+gamma prod. data	1232	HEDLSRLLLL	HEDL TME 77-54	APR78	MANN,BENJAMIN,HOWERTON,ET AL.
96-Cm-249	8649	Decay data only	129	INEL		AUG78	REICH
97-Bk-249	8749	Neut.(RP)+decay+gamma prod. data	2053	BNL,SRL,LLL		JUL76	KINSEY-ASSEMBLER(SEE COMMENTS)
97-Bk-250	8750	Decay data only	233	INEL		AUG78	REICH
98-Cf-249	8849	Neut.(RP)+decay+gamma prod. data	2014	BNL,SRL,LLL		JUL76	KINSEY-ASSEMBLER(SEE COMMENTS)
98-Cf-250	8850	Neut.(RP)+decay+gamma prod. data	1953	BNL,SRL,LLL		JUL76	KINSEY-ASSEMBLER(SEE COMMENTS)
98-Cf-251	8851	Neut.(RP)+decay+gamma prod. data	2021	BNL,SRL,LLL		JUL76	KINSEY-ASSEMBLER(SEE COMMENTS)
98-Cf-252	8852	Neut(RP)+decay+FPY+gam.	2283	BNL,SRL,LLL		JUL76	KINSEY-ASSEMBLER(SEE COMMENTS)
98-Cf-253	8853	Neut.(RP)+decay data	830	SRL		DEC75	BENJAMIN AND MCCROSSON
99-Es-253	8953	Neut.(RP)+decay data	998	BNL,SRL		JUL76	KINSEY,BENJAMIN, AND MCCROSSON

STATUS OF NUCLEAR MODEL CODES FOR THE 10-50 MeV REGION

TABLE II

Program	Authors	Affliation	Formalism†	Ang. Distribution /Spectra	Computer	Document	Availability
ALICE	M. Blanc	LLL, Livermore USA	Evaporation + Exciton Precompound, Fission	No; $\frac{d\sigma}{dE}$	IBM PDP	UR-NSRL-181	Author
AMALTHEE	O. Bersillon L. Faugère	CEBC France	Master Equation Exciton Model (time integration to∞)	No; $\frac{d\sigma}{dE}$	CDC	Yes	Authors
GNASH	E.D. Arthur P. Young	LASL, Los Alamos USA	Multi-step H.F. + Exciton Precompound, (n,γ) and Fission.	No; $\frac{d\sigma}{dE}$	CDC	LA-6947(1977)	Authors or NESC at ANL or RSIC at ORNL
HAUSER*5	F. Mann	HEDL, Hanford USA	Multi-step H.F. + Exciton Precompound, (n,γ) and Fission.	$\frac{d\sigma}{d\Omega}$ and $\frac{d\sigma}{dE}$	IBM CDC UNIVAC	HEDL-TME-78-90	Authors or NESC or RSIC
HAUSER*6	F. Mann	HEDL, Hanford USA	Multi-step H.F. + Exciton Precompound (n,γ) and Fission.	$\frac{d\sigma}{d\Omega}$, $\frac{d^2\sigma}{dEd\Omega}$, $\frac{d\sigma}{dE}$	IBM CDC	-	Under development
JULIAN	M. Hillman Y. Eyal	BNL, Upton, USA *Weizmann Inst. Israel	Monte-Carlo + H.F.	$\frac{d^2\sigma}{dEd\Omega}$ and $\frac{d\sigma}{dE}$	CDC IBM	Yes	Authors
NMTC	R.G. Alsmiller, Jr. T.A. Gabriel	ORNL	Intranuclear Cascade + Evaporation	$\frac{d^2\sigma}{dEd\Omega}$, $\frac{d\sigma}{dE}$ No $\frac{d\sigma}{d\Omega}$ to disc. Levels	IBM CDC	Yes	RSIC at ORNL
ORION	T. Tamura T. Udagawa	Univ. of Texas, Austin USA	Multi-step Direct Reaction and the possibility of linking to H.F. codes	$\frac{d\sigma}{d\Omega}$, $\frac{d^2\sigma}{dEd\Omega}$, $\frac{d\sigma}{dE}$	IBM CDC	-	In progress

STATUS OF NUCLEAR MODEL CODES FOR THE 10-50 MeV REGION (cont.)

TABLE II

Program	Authors	Affliation	Formalism†	Ang. Distribution /Spectra	Computer	Document	Availability
PREANG	J.M. Akkermans H. Gruppelaar F.J. Luider (Revised version of PREEQ by E. Betak)	ECN, Petten The Netherlands	Master Equation Exciton Precompound (time integration to ∞)	$\frac{d^2\sigma}{dEd\Omega}$, $\frac{d\sigma}{dE}$ No $\frac{d\sigma}{d\Omega}$ to disc. levels	CDC	ECN-60(1979)	Authors (Gruppelaar)
PRECO-D	C. Kalbach	TUNL, Durham USA	Griffin Exciton model, semi-empirical direct reactions and Phenomenalogical Ang. Distribution	$\frac{d^2\sigma}{dEd\Omega}$, $\frac{d\sigma}{dE}$ No $\frac{d\sigma}{d\Omega}$ to disc. levels.	IBM Honeywell	In preparation	Author
STAPRE	M. Uhl B. Strohmaier	IRK, Vienna Austria	Multi-step H.F. + Exciton Precompound (n,γ)	No; $\frac{d\sigma}{dE}$	IBM	Yes	NEA CPL-Saclay or Authors
TNG	C.Y. Fu	ORNL, Oak Ridge USA	Multi-step H.F. + Exciton Precompound-Ang. Mom. Conserved for Precompound process also, and (n,γ)	$\frac{d\sigma}{d\Omega}$, $\frac{d^2\sigma}{dEd\Omega}$, $\frac{d\sigma}{dE}$	CDC	No	Author
UHL Code	M. Uhl B. Strohmaier	IRK, Vienna Austria	Multi-step H.F. + Exciton Precompound (n,γ) and Fission.	$\frac{d\sigma}{d\Omega}$, $\frac{d^2\sigma}{dEd\Omega}$, $\frac{d\sigma}{dE}$	IBM	-	Under development

*The Codes are listed alphabetically.

†The term Multi-step H.F. implies higher order corrections, e.g., in DWBA approximation, and is probably not proper: instead the term Multi-Stage H.F. would be more appropriate.

THIS PAGE

WAS INTENTIONALLY

LEFT BLANK

INTRODUCTORY REMARKS

Session Chairman: M.R. Bhat, BNL

THIS PAGE

WAS INTENTIONALLY

LEFT BLANK

10-50 MeV NEUTRON CROSS SECTIONS, AN OVERVIEW OF ACCOMPLISHMENTS IN THE CONTEXT OF THE 1977 SYMPOSIUM*+

Alan Bowen Smith

Argonne National Laboratory
Argonne, Illinois 60439, U.S.A.

ABSTRACT

Some reflections on the status of 10-50 MeV neutron cross sections are given as viewed from an outside perspective. The foundation is the Symposium of 1977 with its conclusions and recommendations. Responsiveness to those recommendations and accomplishments during the intervening three years are assessed.

INTRODUCTORY REMARK

Over the years I have made very minor contributions to neutron cross sections in the present energy range and that continues so today. During these decades age has come upon me. There is some advantage to this generally depressing geriatric fact. From my perspective one develops a longer-range view supported by experience in analogous data contexts. It is from that viewpoint that I look back over the intervening three years upon the 1977 Symposium. How responsive have we been to our recommendations and plans? What goals have been reasonably achieved, where have we fallen short, and where are we in relation to contemporary issues? Such assessments are usually opinionated. I will follow convention remembering that, on good authority, Port Jefferson still maintains a "dunking chair" for those who stray too far from the truth.

---

*Symposium on neutron cross sections from 10 to 40 MeV, Brookhaven National Laboratory, (1977), Proceedings given in BNL-NSC-50681.

+This work supported by the U.S. Department of Energy.

SOURCES, FIELDS, DETECTORS AND STANDARDS

As three years ago, the primary sources of interest are; d-T, d-^{7}Li (E_d=30-50 MeV) and, to a lesser extent, d-^{9}Be and p incident on ^{7}Li and ^{9}Be at energies of tends of MeV. A number of measurements have given new definition to these reactions at incident energies of $\lesssim$50 MeV (e.g. ORNL [1], U-C-Davis [2] and Chalk River [3]). There remain detailed questions, particularly at lower energies (e.g. below 1 MeV). However, it seems likely that the basic parameterization of the d-T and d-^{7}Li source reactions is sufficiently known for the large majority of the engineering applications. In practice, engineering environments may well introduce much larger uncertainties than are inherent to the knowledge of the underlying source reaction.

The trend in thick-target white sources is toward higher energies (200 MeV and above) and the spallation process [4]. The yield per energy input is very good (25 MeV/neutron) and advantage is taken of recent advances in medium and high-energy accelerator technology. There is a potential for very high intensities with particular advantage in the studies of condensed matter and radiation damage [5]. Certainly, such facilities should be employed in high-energy cross section measurements where it is productive to do so [6]. However, as three years ago, most of the high-energy cross section needs are consistent with the capabilities of conventional and operational facilities and there remain extensive data areas that are not compatible with the white-source concept.

It should be pointed out that our knowledge of thick-target-yield data is becoming available from established compilation centers [7]. Similar compilations of thin-target yields are being considered.

It was recommended that standard-reference fields be made available at; 14 MeV (d-T), moderated 14 MeV and based upon the d+^{7}Li (E_d=40 MeV) reaction. The d-T 14 MeV source is very well understood at the relevant energies and standard fluxes are obtained to accuracies of $\lesssim$1% [8]. There appears to be no inherent problem to the provision of moderated 14 MeV fields other than engineering development and validation. The d+^{7}Li field was recommended to a relative accuracy of 3-5% from 0.5-30 MeV. Not surprisingly, that objective has not been approached. It is doubtful that, after 40 years of study, the fission-neutron spectrum is known to such accuracy over a much narrower energy range.

There has been some improvement in the knowledge of standard reference cross sections, notably in the fission cross sections [9]. However, possibly excepting the H(n,p) reaction, standard reference cross sections at high energies are not available to the ultimate desired accuracy. This shortcoming is not now restrictive but it is a long term concern.

Calibrated neutron detectors were sought to phenomenal accuracies; e.g. 2-4% from 0.5-30 MeV. This goal has not been approached and when it is there will be an enormous impact on the entire neutron data field.

TOTAL, SCATTERING AND EMISSION CROSS SECTIONS

For many years energy-averaged neutron-total cross sections have been a problem, primarily at lower energies. Thus it is good to note significant improvements up to energies of 80 MeV largely as the result of the comprehensive measurement program at ORNL, augmented by selected reference measurements elsewhere [10,11]. Much of this accomplishment is the result of the application of an already well developed capability. The total cross section plays a central role in both evaluation and physical analysis and it is in this broader scope that the results are most valued. They are also responsive to project needs. However, we have had a fair knowledge of total cross sections up to at least 30 MeV for more than a decade [12] and one would have thought that if anything could be reasonably extrapolated with calculation it is the energy-averaged total cross section. One wonders if this was systematically attempted in order to meet project needs and how reliable the results proved in the light of the new experimental evidence.

Recently there have been some truly elegant experimental studies of elastic and quasi-elastic neutron scattering at selected energies in the range 10-30 MeV [13,14]. Physical interpretation has been in the context of the optical model with attention to the the details of; energy dependence, direct-reaction mechanisms, charge dependence and the character of the spin-orbit interaction. What has been achieved is a refinement giving confidence to quantitative calculation and a better understanding of the interrelation of charged-particle and neutron processes [15]. However, there have been no real surprises. The potentials may be only "regional" but they are applicable to wide cross section domains. The problem is to put them to use.

Direct applied use of the measured elastic-scattering results is more difficult. One tends to forget that at these energies those distributions are very peaked forward and that all those large-angle details at several orders-of-magnitude reduced intensity are of essentially no applied importance. Indeed, they are not even consistent with the accepted evaluation formats, not to mention the macroscopic calculational systems.

Some recent measurements of the non-elastic cross section are very useful [16]. In a sense, the high-energy field is now where the fission data was 15-20 years ago and at that stage the non-elastic cross section is a particularly valued quantity [17].

Results of measurements of emitted neutron spectra including discrete-inelastic, pre-compound and fusion components are becoming available [13,14]. In the light nuclei there are some notable improvements in our knowledge of discrete excitations, e.g. in the lithium isotopes [13]. The measurement of continuum angle-energy spectra is far more difficult and progress correspondingly slower. Again, the information that is becoming available appears to contain no surprises. It is noteworthy that a large share of our knowledge of emitted spectra comes from abroad--and the east-block

at that [18]. The situation may be a bit deceptive as charged-particle emission involves the same physical processes and there we are in better shape.

PROPAGATION OF THE SPECIES

The essential matter of breeding is of more than a little embarrassment. The matter has long been identified as being of the highest priority and increasingly so as ETF concepts turn to lithium-oxide compounds wth consequent sharp reductions in breeding gains [19]. Integral measurements have suggested alarming reductions in the cross sections of the relevant lithium reactions [20]. This was noted abroad and recent Harwell measurements indicate a more than 25% reduction in the ^{7}Li(n;n',alpha)t cross section [21]. This reduction has a large and detrimental impact on breeding in many blanket concepts. The situation reminds one of the ^{239}Pu-ALPHA "flap" of a few years ago resulting in an analogous detrimental impact on fast-breeder performance. As in that case, the potential for such a problem should not have been a surprise as the underlying data base was both old and uncertain [22]. The ^{7}Li issue will soon be further delineated by the results of comprehensive measurements now nearing completion at ANL and CBNM-Julich [23,24]. However, we should not be complacent. Most breeding concepts depend strongly on tritium production in ^{6}Li and the corresponding cross sections are not all that certain. Despite extensive study of the n+^{6}Li system [25], the basic structure underlying tritium production at even low energies is uncertain and even the qualitative features of the reaction mechanism remain a matter of debate [26]. Confidence is not enhanced by similar questions as to the structure of the mirror ^{7}Be system. There are similar uncertainties in "advanced" fusion concepts where studies of underlying light-charged-particle reactions have been too largely moribund for several decades.

(N, CHARGED-PARTICLE) DATA

The primary focus is on the production of protons, deuterons and alpha-particles (and secondarily, other light particles) at incident energies up to 16 MeV [27]. In the 14-16 MeV region the understanding is remarkably comprehensive largely due to the efforts of the LLL-Group [28]. Cross section and particle-spectra results have been obtained for a wide range of structural materials in the mass range A=40-60 and work is in progress in the A=100 region [29]. The cross sections vary widely but the spectra and the spectrum-averaged energies (and thus relative energy deposition) are very similar and well described by multi-step Hauser-Feshbach and pre-compound calculations [30]. This suggests that a number of future needs can be met by simple activation measurements (where a residual activity is available) as, for example,

pursued at Julich [31]. Below 14 MeV and toward threshold the situation is less satisfactory but work underway at Ohio University promises improvement. Both LLL and Ohio groups use similar Q-pole devices. A simpler solid-state detection system has been productively employed at CBNM where direct-particle measurements have yielded impressive results well into the threshold region [32]. It is unfortunate that such an alternative approach to direct-particle detection has apparently not been implemented in this country. Measurements can be extended above 16 MeV but they will be increasing tedious and difficult and thus should be carefully chosen as calculational benchmarks.

DOSIMETRY CROSS SECTIONS

Despite the importance of high-energy (10-50 MeV) dosimetry at the FMIT and in similar applications, the general data community has shown remarkably little interest in the problem area. The situation is analogous to that existing in fission-reactor dosimetry for many years. The latter has recently improved with the advent of some truly suitable basic results. It is fortunate that some of our friends abroad have not been so casual [33]. Responsiveness is not encouraged by the profusion of "primary" dosimetry reactions. The engineering community has given far more attention to dosimetry matters but their efforts are project oriented and handicapped by the lack of facilities and techniques requisite to establishing a comprehensive microscopic data base. However, they have been very effective in the integral testing of dosimetry data in reference spectra such as that provided by the $^{9}Be(d,n)$ (E_d=40 MeV) reaction [34,35]. Such tests have involved many of the dosimetry reactions recommended at the past meeting. A fragmentary data base was used, partly derived from ENDF/B-IV extrapolated to higher energies either empirically or with the assistance of simple calculations [36]. Beyond the basic data uncertainties, are those inherent in the reference spectra themselves. Given these collective uncertainties, the consistencies between measured and calculated response rates (frequently within 10%) are remarkably good. Indeed, such quality results have only recently been generally achieved in the area of fission reactor dosimetry. Success may be in part due to the fact that the differential response of a number of the reactions in the reference spectra peaks well below 20 MeV.

MODELS AND CALCULATIONS

At the previous meeting the potential of calculations, validated with selected experimental results, was repeatedly stressed. It was implied that primary reliance should be placed upon such an approach. Following this course there have been a few successes [37] usually on the part of a single group fortunate enough

to combine measurement and calculational capability. However, the approach has not been implemented on a comprehensive scale. It seems that the obstacle has been the lack of cooperation between measurement and calculation communities.

To the outside observer, the calculational efforts seem to be of somewhat variable quality. One could have hoped that simple processes, such as (n;p) reactions at relatively low energies, could be predicted with reasonable consistency and assurance. This appears to be so when the data base is reasonably defined by experiment. Without the experiment things are far more uncertain. Calculated results can differ by a factor of two or more and, at least in one case, subsequent measurements suggest that the "wrong" calculational result found its way into the evaluated files [38]. In another case a careful calculation explained the prominent structure in a common (n;p) cross section in terms of quasi-particle states--unfortunately the structure was probably an experimental artifact. Recently there have been extensive comparisons of calculated, measured and evaluated neutron continuum spectra at incident energies of 14 MeV [39]. It was an impressive effort which highlighted areas of both very good and very poor agreement. In some cases the evaluations were very clearly at fault as they gave no attention to pre-compound processes. In other instances the situation is less clear as the calculated results do not seem to be entirely consistent with those obtained in integral tests [40].

Reflecting on the above, it seems that a successful calculational program requires a substantive experimental input. Even with that there appears to be more than a little "artistry" in the use of those models.

I have been called many names but never "theorist". I did, however, get curious about some of those basic questions raised at the previous meeting and sought the views of our resident specialist. One issue is the uncertain knowledge of level densities. Basically it seems we still have to rely on the old formula of Gilbert and Cameron [41] which is anchored only at the neutron binding energy with no other experimental verification reasonably free of other theoretical assumptions. Recent measurements have led to much better definition of the optical potential; the problem appears to be getting this new information into use. On this point, the lethargy tends to suggest that the details of the potential do not have a sharp impact on many calculational results. In any event, I am told that Perey and Perey will continue to maintain an up to date compilation of optical parameters [42]. Gamma-ray strength functions appear to remain a continuing problem and, indeed, strength functions generally are a matter of debate to be discussed at a forthcoming work shop on the methods of evaluation.

EVALUATED DOSIMETRY CROSS SECTIONS

A list of "primary" dosimetry reactions was recommended, all extending well above 20 MeV--some to 40 MeV. It was an extensive list of which less than 25% are available in either ENDF/B-IV or V dosimetry files in any energy range. The quality of the Version-V file is much improved. Indeed, nearly a third of the file has achieved the desired accuracy goals specified in the context of integral fission-related benchmarks [43]. However, the most recent version of the file remains confined to energies of less than 20 MeV and it is little more responsive to those "primary" high-energy dosimetry needs than its predecessor. Thus, after three years, we apparently do not have a nationally recognized dosimetry file responsive to the higher-energy requirements we set forth.

A new initiative with wide potential for the improvement of dosimetry (and other) data applications is the quantitative specification of evaluated data uncertainties [44]. Concurrently, sound statistical methods for the application of these uncertainties in a dosimetry context have been proposed [45]. Taken together there is promise for a very significant improvement in dosimetry applications--a promise that has apparently not yet been realized on a substantive scale.

COMPREHENSIVE EVALUATION

A promise of the previous meeting was the calculational capability to provide comprehensive evaluated files in the complex high-energy region where the measurements are so difficult. Indeed, it was prophecied that two years after a decision to build FMIT comprehensive evaluated files would be available primarily via calculation. It is my understanding that FMIT is under construction. ENDF/B-V has become available and provides an improved calculational base to 20 MeV. Model calculations played a part in its construction; very nicely so in some instances. However, large portions of ENDF/B-V continue to rely on phenomenological perscriptions known to be consistent with microscopic and integral observation [46]. Calculational models have had less impact than one might have hoped. Above 20 MeV the situation is not good. FMIT construction needs were apparently met with multi-group cross-section sets derived under other auspices [47,48]; augmented by selected engineering measurements. Indeed, there seem to be very few comprehensive, high-energy microscopic evaluations in existence. One effort is to be described at this meeting and it appears to be the only above-20 MeV evaluation cited in the last CCDN evaluation newsletter (NNDEN/27) [50]. Recent discussions have given attention to high-energy evaluation formats. It is not a new issue and one that one would have hoped to have in hand by now. Evaluations are complicated by fluid formats not to mention all those problems of incorporating the evaluations into the practical calculational systems.

It is good to note that some of the above issues will be resolved with ENDF/B-VI [49]. It is proposed to extend the energy range to 50 MeV and to incorporate major improvements in the formats. These are very substantive and much needed initiatives.

There is a school of thought that extoles the merit of fusion-fission hybrids and another that envisions the use of lithium-oxide compounds in breeding blankets. In both contexts n-2n multipliers are an important consideration. Be, Pb or Bi are frequently considered and the latter has a particularly large n-2n cross section (a fact that did not escape the Canadian ING project), yet there is no comprehensive bismuth file in the ENDF system.

MATTERS OF TIMING AND COMPETENCE

In the developmental business of fusion energy, long-range projections are speculative. Near-term estimates may be more realistic. FMIT is under construction. The design data needs were met from underlying capability augmented by project motivated efforts. Three years hence data for the use of this facility must be available. With current plans, data impacting on the choice of ETF design must be in hand within the coming four years. These are short time scales that largley preclude major and comprehensive goal-oriented data efforts. Reliance is, and will continue to be, largely placed upon underlying and long term competence. That faith may be misplaced as that general capability, particularly in experimental areas, is being seirously eroded. With present trends, it is doubtful that future needs, yet unspecified, can be met. These concerns have been expressed before [51] but never in such trying circumstances.

REFERENCES

The above remarks are of a broad but qualitative nature that preclude detailed referencing of the large body of relevant literature. Therefore, the following references are only illustrative. In a number of instances there are two review papers which contain comprehensive literature citations.

1. M. Saltmarsh et al., Nucl. Instr. and Methods 145 81(1977).

2. D. Johnson et al., Proc. Conf. on Nucl. Cross Sections and Tech., Knoxville (1979).

3. M. Lone and R. Robertson (see also K. Tsukada), Proc. IAEA Consultant's Mtg. on Neutron Source Properties, Debrecen (1980).

4. Summary of white source working group, C. Bowman Chrm., Proc. IAEA Consultant's Mtg. on Neutron Source Properties, Debrecen (1980).

5. G. Manning, Proc. Conf. on Neutron Phys. and Nucl. Data for Reactors and other Applied Purposes, Harwell (1978).

6. M. Moore et al., Proc. Conf. on Nucl. Cross Sections and Tech., Knoxville (1979).

7. H. Münzel, Nuclear Data for Fusion Reactor Tech., IAEA-TECDOC-203 (1978), IAEA press; also T. Burrows, Private Communication (1980).

8. M. Drosg, Proc. IAEA Consultant's Mtg. on Neutron Source Properties, Debrecen (1980).

9. B. Patrick, Proc. Conf. on Neutron Phys. and Nucl. Data for Reactors and other Applied Purposes, Harwelll (1978).

10. D. Larson, J. Harvey and N. Hill, Oak Ridge Natl. Lab. Status Report to the DOE Nucl. Data Com. (1980).

11. G. Zanelli et al., Bull. Am. Phys. Soc., 24 658(1979).

12. S. Cierjacks et al., Kernforschung Karlsruhe Report, KFK-1000 (1968).

13. R. Walter et al., Triangle Nucl. Lab. Status Report to the DOE Nucl. Data Com. (1980) and references cited therein.

14. J. Rapaport et al., Ohio Univ. Status Report to the DOE Nucl. Data Com. (1980) and references cited therein.

15. S. Grimes et al., Lawrence Livermore Lab. Status Report to the DOE Nucl. Data Com. (1980).

16. P. Urone et al., Bull. Am. Phys. Soc., 24 657(1979).

17. M. Walt, Proc. Conf. on Atoms for Peace, Geneva (1955) Vol.-2.

18. D. Hermsdorf et al., ZFK-277, Zentralinstitute für Kernforschung (1974).

19. M. Abdou, Nucl. Data for Fusion Reactor Technology, IAEA-TECDOC-223, IAEA press (1978), also private communication.

20. H. Bachmann et al., Nucl. Sci. and Eng., 67 74(1978).

21. M. Swinhoe, Proc. Conf. on Nucl. Cross Sections for Tech., Knoxville (1979).

22. Neutron Cross Sections, Brookhaven Natl. Lab. Report, BNL-325, Vol.-2, 3rd Ed., Eds. D. Garber and R. Kinsey (1976).

23. D. L. Smith, Private Communication (1980).

24. H. Liskien, Private Communication (1980).

25. G. Hale, National Bur. of Stds. Pub., NBS-493 (1977).

26. H. Weigmann and P. Manakos, Z. Phys., A289 383(1979).

27. C. R. Head, Nuclear Data for Fusion Reactor Technology, IAEA-TECDOC-223 (1978), IAEA press; Also update submitted to DOE Nucl. Data Com.

28. R. Haight, Lawrence Livermore Lab. Report, UCRL-83127 (1979).

29. R. Haight, Lawrence Livermore Lab. Status Report to the DOE Nucl. Data Com. (1980).

30. E. Arthur and P. Young, Brookhaven National Lab. Report, BNL-NCS-50681 (1977).

31. S. Qaim and R. Wölfle, Proc. NEANDC Topical Discussion on Neutron Data of Structural Materials, Geel (1979).

32. A. Paulsen et al., Proc. Conf. on Nucl. Cross Sections for Tech., Knoxville (1979).

33. See, for example, Proc. 3rd ASTM-EURATOM Sym. on Reactor Dosimetry, Ispra (1979).

34. L. Greenwood et al., Nucl. Sci. and Eng., 72 175(1979).

35. S. Qaim, Proc. Conf. on Neutron Phys. and Nucl. Data for Reactors and other Applications, Harwell (1978).

36. S. Pearlstein, J. Nucl. Energy 27, 81 (1973).

37. L. Vesser, E. Arthur and P. Young, Phys. Rev, C16 1792(1977), also Private Communication.

38. D. L. Smith and J. W. Meadows, to be published.

39. D. Hetrick, D. Larson and C. Fu, Proc. Conf. on Nucl. Cross Sections for Tech., Knoxville (1979).

40. L. Hansen et al., Lawrence Livermore Lab. Status Report to the DOE Nucl. Data Com. (1980), also see this symposium.

41. A. Gilbert and A. Cameron, Can. Jour. of Phys., 43 1446(1965).

42. F. G. Perey, Private Communication (1980).

43. D. L. Smith, Proc. Conf. on Nucl. Cross Sections for Tech., Knoxville (1979).

44. F. G. Perey, Proc. Conf. on Neutron Phys. and Nucl. Data for Reactors and other Applications, Harwell (1978).

45. F. G. Perey, Oak Ridge Natl. Lab. Report, ORNL/TM-6062 (1977).

46. For example, S. Perkins et al., Nucl. Sci. and Eng., 57 1(1975).

47. W. Wilson, Los Alamos Sci. Lab. Report, LA-7159-T (1978).

48. R. Alsmiller and J. Barish, Oak Ridge Natl. Lab. Report, ORNL-TM-6486 (1978).

49. S. Pearlstein, Private Communication (1980).

50. E. Arthur and P. Young, to be reported at this symposium.

51. Report of the Research Panel on Atomic, Molecular and Nuclear Physics in CTR, J. Leiss Chrm., (1974).

THIS PAGE

WAS INTENTIONALLY

LEFT BLANK

INTENSE HIGH ENERGY NEUTRON SOURCES AND THEIR CHARACTERISTICS

Session Chairman: J.S. Fraser, CRNL

THIS PAGE

WAS INTENTIONALLY

LEFT BLANK

REVIEW OF SOURCE CHARACTERIZATION FOR FUSION MATERIALS IRRADIATIONS

L. R. Greenwood

Argonne National Laboratory
Argonne, Illinois 60439, U.S.A.

ABSTRACT

Fusion materials irradiations require accurate knowledge of neutron fluence, spectrum, and derived damage parameters, such as nuclear displacements, transmutations, and gas production. Irradiations are being conducted in diverse facilities including mixed-spectrum and fast reactors, T(d,n) and Be(d,n) accelerator sources, and high-energy spallation neutron sources. The characterization of each type of source is discussed, with emphasis on the principal sources of error and needed improvements in dosimetry techniques and nuclear data needs.

INTRODUCTION

Neutron irradiations designed to study radiation damage in fusion reactor materials are currently being conducted at a wide variety of facilities, including reactors and accelerators. Present generation fusion reactor devices (including TFTR) do not generate enough neutrons to produce significant damage in engineering materials. Thus, the strategy [1] of the U.S. magnetic fusion community is to use existing neutron facilities to study bulk damage effects, even though the neutron spectra are quite different from those expected in commercial fusion reactors. At present, only reactors have both the high neutron flux and large experimental volume required for extensive materials irradiations. Hence, most fusion studies will, by necessity, be conducted in mixed-spectrum and fast reactors. However, since reactor spectra do not include the high 14-MeV neutron peak expected in fusion reactors, accelerators must be used to produce high-energy neutrons. At present, the Rotating Target Neutron Source (RTNS II) [2] at Lawrence Livermore Laboratory produces the highest flux (about 10^{13} n/cm^2-s) of 14-MeV neutrons via the T(d,n) nuclear reaction. However, this flux is not high enough to produce fluences comparable to a fusion

reactor (about 10^{22} n/cm^2-year), and the experimental volume is only about 1 cm^3. Hence, a Fusion Materials Irradiation Test Facility (FMIT) [3] is under construction at Hanford Engineering Development Laboratory and is expected to produce a neutron flux of about 10^{15} n/cm^2-s with an experimental volume of about 10 cm^3. FMIT uses the Li(d,n) reaction to produce a broad neutron spectrum (0-55 MeV), roughly centered near 14 MeV. High-energy spallation neutron sources, such as the Los Alamos Meson Physics Facility (LAMPF) and the Intense Pulsed Neutron Source (IPNS) at ANL, have also been used for materials studies.

Clearly, the challenge in this strategy is to develop techniques to characterize all neutron sources in such a way that materials effects can be readily correlated between facilities and extrapolated to fusion reactors [4]. Present data at low fluence tend to support the strategy [5].

The purpose of this paper is to describe existing techniques to measure the neutron flux and spectra during fusion materials irradiations and to calculate pertinent damage parameters such as nuclear displacements and gas production. Emphasis will be placed on deficiencies in the existing techniques, especially concerning the need for improvements in the nuclear data base. Each type of facility will then be considered separately, followed by a discussion of damage calculations.

NEUTRON DOSIMETRY

The passive, multiple-foil dosimetry technique is being used to measure the neutron flux and energy spectrum during all fusion materials irradiations. In this method, a number of materials are simultaneously irradiated. Activation products, as well as helium gas, are then analyzed. After decay, geometry, and absorption corrections are applied, one has a number of simultaneous integral equations to solve for the most probable flux and spectrum. Each activation integral is solely a product of the flux-spectrum times the appropriate differential cross section. Obviously, the results obtained from this unfolding technique are no better than the nuclear cross sections which concern this conference.

Probably the most well-known computer code used for spectral analysis is SAND II [6]. However, two new codes, STAYSL [7] and FERRET [8], appear to be superior mathematically and include all known covariance errors; cross section covariances are now being published in ENDF/B-V [9]. The following discussion will use STAYSL as an example since it is well-developed for routine applications and is currently used in most fusion dosimetry.

Three types of data are required as input in the spectral adjustment codes, namely, activation integrals, nuclear cross sections, and the best estimate of the flux and spectrum. Errors and covariances are assigned to each type of data. At present, only integral activation data can usually be treated in a straightforward, scientific manner, where all errors and covariances are

rigorously analyzed. In a practical sense, the integral errors are typically very small (≤2%) and covariances are negligible due to comparison with certified standards and inter-laboratory comparisons.

Our knowledge of nuclear cross section errors and covariances has improved considerably over the last few years, especially since this data is now included in ENDF/B-V [9]. Thirty-three reactions are included in the dosimetry file with typical errors of 5-30%. However, the file stops at 20 MeV and covariance files are only available for a very limited set of reactions. For high-energy neutron measurements a cross section file to 44 MeV [10] has been created using available measurements and calculations, as will be discussed later.

Unfortunately, the largest source of uncertainty in spectral analysis is often the input flux and spectrum. Only rarely can a spectrum of practical interest be reasonably well-specified prior to analysis. For reactors, neutronics calculations are generally relied on and errors are estimated from previous experience. At high-energy accelerators, spectra are estimated from time-of-flight measurements made at large distances from the source, averaged for finite geometry effects close to the source where materials irradiations are conducted [11,12]. In practice, errors are assigned to the input spectra either by sensitivity studies or integral testing in a known spectrum, as described later.

Input cross section and flux self-covariances are presently approximated by a Gaussian function on the assumption that closely spaced energy groups must be highly correlated. Widely spaced groups are assumed to be more or less independent, with an arbitrary constant covariance. Cross section self- and cross-covariances are now included in ENDF/B-V [9]; however, the files are not complete and estimates must be made for most reactions. Nevertheless, the recognition and acceptance of covariance effects is an important development in spectral analysis and it is anticipated that more complete files will be available in the near future.

The validity and accuracy of the multiple-foil technique for neutron dosimetry has been integrally tested in known neutron fields, such as ^{235}U, ^{252}Cf, various reactor spectra [13], and accelerator spectra measured by time-of-flight spectrometry [11,12]. Naturally, such tests are principally used to assess the accuracy of nuclear cross sections. However, such sensitivity studies can also be made to better define input and output flux errors and covariances.

FISSION REACTORS

Fusion materials irradiations are currently being conducted primarily in mixed-spectrum (part thermal and part fast) reactors, namely, the Oak Ridge Research Reactor (ORR), the High Flux Isotopes Reactor (HFIR) at Oak Ridge National Laboratory, and the Omega West

Reactor (OWR) at Los Alamos Scientific Laboratory. Fast reactor irradiations are also being done at the Experimental Breeder Reactor (EBR II) at Argonne National Laboratory West.

Whereas fission reactor dosimetry has been conducted for many years, surprisingly little work has been done in mixed-spectrum reactors. This is partly due to the fact that materials irradiations have been concentrated in fast reactors for the breeder development programs. However, it should also be pointed out that the multiple-foil technique is very insensitive in the 1-500 keV energy region which usually has a significant part of the total flux. Figure 1 shows the results of a spectral measurement in ORR using the STAYSL code. The spectrum can be divided into four energy regions, namely, thermal (<0.5 eV), resonance (0.5 eV-1 keV), intermediate (1-500 keV), and fast (>500 keV). Errors in the flux in the thermal and resonance regions can be reduced to less than 10% using a variety of thermal and resonant reactions, with and without cadmium or gadolinium covers. Accurate self-shielding corrections [14] must be included with the cross sections prior to spectral adjustment, especially for the strong resonances in dilute materials. Such corrections can easily be as large as a factor of 2 and constitute another possible source of error in spectral unfolding. Computer codes are not yet available to process the resonance parameter error files in ENDF/B-V, but should be available soon from the Radiation Shielding Information Center at Oak Ridge National Laboratory [15].

Flux errors in the fast neutron energy region can also be reduced to 10-15% due to the large number of threshold reactions available. In fact, the multiple-foil unfolding technique works the best in the fast energy region (including accelerator spectra) since the results are usually limited primarily by the quality of available nuclear cross sections.

The intermediate energy region remains the most difficult to measure due to the lack of threshold reactions. Work is now in progress on reactions such as $^{93}Nb(n,n')^{93m}Nb$ (13.6 y) [16] which may reduce the large errors (about 20-50%) in the intermediate energy region. However, it is evident that we must rely on neutronics calculations to define this part of the energy spectrum and work is needed to further compare calculations and measurements.

The importance of measuring various regions of a mixed-reactor spectrum is summarized in Table I, which lists unfolding results for the ORR spectrum in Figure 1. The last column lists the fraction of displacement damage in nickel caused by each energy region (thermal effects are neglected). It is very important to note that about 27% of the displacements are caused by neutrons below 1 MeV. Inadequate knowledge of the intermediate energy region can thus lead to a significant error in the calculated damage rate. For example, analysis shows that reliance on a single fast reaction such as $^{54}Fe(n,p)$ for damage estimation could underpredict total displacement damage and flux by as much as a factor of two during materials experiments. Hence, accurate dosimetry is a necessity if we are serious about modeling or correlating materials effects.

Improvements in fission reactor dosimetry require more accurate nuclear cross sections as well as refinements in defining input spectra, errors, and covariances used in the adjustment codes. Integral testing [13] has helped to define nuclear data needs. In particular, the $^{93}Nb(n,n')$ and other reactions with long half-lives (>30 days) would be of the most benefit since only limited spectral analysis can be done at present for long irradiations. Typical errors observed in some common dosimetry reactions are shown in Table II for a STAYSL analysis of an irradiation in ORR. Note that overall results are improved with recently tested ENDF/B-V cross sections, but significant differences remain.

T(d,n) NEUTRON SOURCES

Dosimetry at 14-MeV neutron sources, such as RTNS II, is simplified by the nearly monoenergetic and isotropic neutron field. A single reaction, $^{93}Nb(n,2n)^{92m}Nb$ (10 day), is used to routinely measure fluences to ±7% [17], and longer irradiations will use the longer-lived $^{54}Fe(n,p)^{54}Mn$ (312 day) reaction product. However, care must be taken to adequately measure flux gradients in the small experimental volume near the source. Extensive flux maps have been made on a very small scale at RTNS I [18] (see Figure 2) and similar experiments will be conducted shortly at RTNS II.

Experiments are now being planned to measure more complicated spectra farther away from the source, using large masses of material to return low energy neutrons, similar to a fusion reactor spectrum. Concern has been raised about the unfolding of weak, low-energy neutrons in the presence of a dominant 14-MeV peak. However, recent experiments by Kuijpers [19] seem to be quite successful. Actual fusion reactor experiments are also planned when the Tokamak Fusion Test Reactor becomes operational at Princeton.

Be AND Li(d,n) NEUTRON SOURCES

The stripping neutron sources at cyclotrons have been the most difficult to characterize due to steep flux and spectral gradients as well as poorly defined neutron cross sections, especially above 28 MeV. Figure 3 shows the measured dependence of the neutron flux and spectrum at large distances (>1 m) from a Be(d,n) source at ORNL [20]. However, materials irradiations must be conducted very close to the source (about 4-10 mm) to produce any measureable radiation damage in engineering materials. Precision dosimetry with multiple-foils must thus be conducted to adequately measure the damage produced in a sample. Figure 4 shows fluence and calculated damage and helium contours measured at the U.C. Davis cyclotron [Be(d,n), E_d = 30 MeV]. Note that the gradients are very steep off-axis, especially for the damage and helium contours which are more dependent on high-energy neutrons.

Slowly moving the d beam across the target helps to moderate the steep gradients [21] and may in fact increase the total exposure seen by a sample since the beam spot is quite small (about 3-5 mm). The larger size of the FMIT source (about 1 x 3 cm) will also naturally moderate the steep gradients; however, precision dosimetry will still be needed, especially if the beam profile is irregular. In practice, small irregularities are not important to long-term exposure and calculational models of the source can be constructed which fit measured activity or damage rates with high precision, as shown in Figure 4.

Neutron cross sections for dosimetry have been a problem due to a general lack of measurements above 15 MeV. However, some excellent data is available from Bayhurst et al. [22] up to 28 MeV. Extrapolations based on the THRESH computer code [23] and a few available theoretical calculations were then made up to 44 MeV [10]. Integral tests [11,12] have been made in which activations are compared to calculations in a well-defined geometry where the spectrum has been measured by time-of-flight spectrometry. The results have been surprisingly good, as shown in Table III. In fact, the neutron spectrum at a Be or Li(d,n) source can presently be measured with 10-30% flux errors in the 2-30 MeV energy range where 90% of materials damage is produced, as shown in Table IV and Figure 5. Damage rates can be calculated to ±10% for these spectra.

Nevertheless, neutron cross sections are needed to define the flux spectrum above 28 MeV (up to 50 MeV at FMIT) and to reduce the errors in the low threshold reactions above 14 MeV. Table V lists a number of reactions which are most urgently requested for dosimetry. In particular, the material cobalt appears to be an excellent choice since five independent reactions with long half-lives can be easily measured, spanning the entire energy spectrum at FMIT.

SPALLATION NEUTRON SOURCES

High-energy (500-800 MeV) proton beams have been used to create neutrons by spallation at LAMPF [24] and IPNS [25]. Figure 6 shows a spectrum recently measured at a mock-up of IPNS. As can be seen, the spectrum is similar to a fast reactor; however, a weak tail extends up to 500 MeV (not shown). At present, no nuclear data is available for measuring neutrons above 30 MeV. Neutron-induced spallation reactions (e.g., Al) could in principle be used in this region. However, calculations show that less than 1% of materials damage is caused by this part of the neutron spectrum.

A weak flux of high-energy protons and other particles is also produced by the spallation process. However, recent tests [25] show that proton fluxes are too weak (<1% of neutrons) to interfere with either materials damage or neutron dosimetry [e.g., (n,2n) is indistinguishable from (p,d)]. Proton activation measurements are

needed both to monitor the incoming beam and to better define secondary fluxes. Measurements of neutron flux spectra and gradients are in reasonable agreement with neutronics calculations, as will be presented at this conference [26].

HELIUM MEASUREMENTS

The amount of helium produced in a material has proven to be an important parameter needed to understand irradiation effects. Fortunately, a mass-spectrometric technique has been developed for measuring helium quite accurately. Joint experiments [18,27] have been conducted in many types of facilities to simultaneously measure helium production and the flux-spectrum, thereby integrally testing helium production cross sections. Recent results from ORR are listed in Table VI. It is hoped that some of the larger discrepancies will be resolved with the anticipated release of gas production files in ENDF/B-V.

Nickel is a very important element in reactor irradiations since high helium levels can be produced by the thermal neutrons via the $^{58}Ni(n,\gamma)^{59}Ni(n,\alpha)$ reaction, thereby simulating helium-to-damage ratios close to fusion reactor values. The tests reported in Table VI demonstrated that good agreement between helium measurements and calculations can only be obtained with precise knowledge of the neutron spectrum. The appropriate spectral-averaged cross sections for nickel must be obtained by comparison to radiometric measurements, since formulas based on measurements in other reactors [28] were found to be in error by 20-30%.

There are two goals of the work with helium detectors. First, integral testing can be used to refine helium production cross sections, thereby improving calculations used in damage analysis. Secondly, with accurate cross sections, helium detectors can be used to improve flux and spectral measurements. This is especially useful for very long irradiations since helium is a stable product. Total helium cross sections are needed up to 40 MeV primarily for Al, Fe, Cr, Cu, Ti, Ni, W, and Au.

OTHER TECHNIQUES

The gamma field produced by a neutron source is of interest in materials irradiations due to ionization-induced damage in insulators and gamma heating of samples. However, present calculations and a few measurements indicate that neither problem is very significant at accelerator-based neutron sources since the total gamma flux is only about 1% of the total neutron flux [11,12]. There are very few techniques for measuring the gamma flux-spectrum in the presence of a much stronger neutron flux, although a new method using Compton scattering is being developed by R. Gold [29].

Solid state track recorders may also prove useful in source characterizations, especially with new materials like CR-39 which is sensitive to protons up to 18 MeV [30]. Fission cross sections need development in the 14-40 MeV energy range and data are needed for charged particle reactions on emulsion materials including Ag, Br, C, O, and N.

DISPLACEMENT DAMAGE CALCULATIONS

The overall strategy of correlating damage between irradiation facilities crucially depends on the development of suitable theoretical models with clearly definable damage parameters [4]. The best such parameters are thought to be displacements-per-atom (dpa) and gas production (H,He) [31]. Exposure should thus be recorded in dpa and He, as well as neutron flux and spectrum. On the one hand, this is advantageous to dosimetry since such damage parameters are integrals of the neutron spectrum and can be measured more accurately than the flux in various energy regions due to very strong covariances in the output flux spectrum from unfolding codes. In other words, the neutron spectrum can be viewed as representing a mathematical transfer function between two integral quantities, namely, activity integrals and damage parameters. For example, using the full covariance matrix for the output flux from STAYSL, dpa and helium levels can generally be computed to ±10%, in spite of the fact that errors in some flux groups are as large as ±30-50%.

On the other hand, displacement damage cross sections are in themselves difficult to calculate, especially above 14 MeV, since they require an enormous amount of detailed nuclear reaction data, including cross sections and angular distributions for most elements up to 50 MeV. Hence, at present, we are in the strange position of being able to measure spectral uncertainties (about 10%) in dpa calculations at high neutron energies far more accurately than we can calculate displacement cross sections (20-50%).

Obviously, theoretical calculations and selected nuclear measurements are needed to improve damage calculations. Some work has already been done [32,33,34] and evaluated files are now starting to become available [35]. The most important nuclear data (experiment and calculation) needs are differential, angular cross-sections for elastic and inelastic scattering and secondary particle emission data for Al, Fe, Ni, Cr, Cu, W, Sn, Ti, and V, especially from 15-35 MeV. Obviously, the most probable reactions have the highest priority since they produce most of the damage in materials. Transmutation cross sections are an interesting subtopic since they eventually lead to composition changes in alloys. Other papers at this conference will present a more detailed analysis of high-energy fusion materials studies.

CONCLUSIONS

In conclusion the characterization of neutron sources for materials studies at high neutron energies appears to have improved enormously since the last conference in 1977. In particular, integral data testing [11,12] has demonstrated that flux-spectra can now be routinely measured to ±10-30% and integral damage parameters to ±10-15% for most materials irradiations. New computer codes [7,8] have also emerged to include covariances, allowing a more precise statement of measurement errors.

Nevertheless, nuclear data is still needed to improve dosimetry measurements and damage calculations. At present, no activation cross sections are well-known above 28 MeV and displacement calculations have large errors above 14 MeV. Whereas present analyses indicate that high energy neutrons (>30 MeV) may not be crucial to understanding fusion materials damage, it should also be remembered that this basic strategy has not yet been tested at high neutron fluence (10^{22} n/cm^2) and that, as materials programs mature, more demands will be placed on source characterization. Failure to adequately develop the required nuclear data base and techniques will ultimately undermine the entire strategy of predicting the performance of materials in fusion reactors based on experiments in diverse neutron sources.

REFERENCES

1. The Fusion Reactor Materials Program Plan, DOE/ET-0032, July 1978.

2. Experimenter's Guide, Rotating Target Neutron Source II Facility, Lawrence Livermore Laboratory, M-094, July 1978.

3. See papers by L. L. CARTER and F. M. MANN et al., in Session IV of these proceedings.

4. G. R. ODETTE, J. Nucl. Mater. 85, 533 (1979).

5. R. H. JONES, D. L. STYRIS, E. R. BRADLEY, L. R. GREENWOOD, and R. R. HEINRICH, J. Nucl. Mater. 85, 889 (1979).

6. Neutron Flux Spectra Determination by Multiple Foil Activation, AFWL-TR-67-41, Vols. I-IV, Air Force Weapons Laboratory (1967).

7. F. G. PEREY, Least Squares Dosimetry Unfolding: The Program STAYSL, ORNL/TM-6062 (1977); modified by L. R. Greenwood, Argonne National Laboratory (1979).

8. F. SCHMITTROTH, Nucl. Sci. Eng. 72, 19 (1979).

9. ENDF/B-V, National Neutron Cross Section Center, Brookhaven National Laboratory, 1979.

10. L. R. GREENWOOD, Extrapolated Neutron Activation Cross Sections for Dosimetry to 44 MeV, ANL-FPP/TM-115 (1979).

11. L. R. GREENWOOD, R. R. HEINRICH, R. J. KENNERLEY, and R. MEDRZYCHOWSKI, Nucl. Technol. 41, 109 (1978).

12. L. R. GREENWOOD, R. R. HEINRICH, M. J. SALTMARSH, and C. B. FULMER, Nucl. Sci. Eng. 72, 175 (1979).

13. M. F. VLASOV, A. FABRY, and W. N. MCELROY, Status of Neutron Cross Sections for Reactor Dosimetry, IAEA, INDC(NDS)-84/L+M (1977).

14. S. PEARLSTEIN and E. V. WEINSTOCK, Nucl. Sci. Eng. 29, 28 (1967).

15. Radiation Information Shielding Center, Oak Ridge National Laboratory (1980).

16. F. HEGEDUS, Proceedings of the Second ASTM-EURATOM Symposium on Reactor Dosimetry, Palo Alto, California, Vol. II, p. 825 (1977).

17. D. R. NETHAWAY, The ^{93}Nb (n,2n) ^{92m}Nb Cross Section, UCRL-80097 (1977).

18. H. FARRAR IV, D. W. KNEFF, R. A. BRITTEN, and R. R. HEINRICH, Proceedings of Symposium on Neutron Cross-Section from 10-40 MeV, Brookhaven National Laboratory, BNL-NCS-50681, p. 175 (1977).

19. L. J. M. KUIJPERS, Spectrum Unfolding from Activation Measurements in a CTR-Model Blanket Experiment, KFA-1435 (1977).

20. M. J. SALTMARSH, C. A. LUDEMANN, C. B. FULMER, and R. C. STYLES, Characteristics of an Intense Neutron Source Based on the d+Be Reaction, ORNL/TM-5696 (1976); also, Nucl. Instrum. Methods 145, 81 (1977).

21. D. R. NETHAWAY, R. A. VON KONYNENBURG, M. W. GUINAN, and L. R. GREENWOOD, Proc. Symp. Neutron Cross Sections from 10-40 MeV, BNL-NCS-50681, p. 135, Brookhaven National Laboratory (1977).

22. B. P. BAYHURST, J. S. GILMORE, R. J. PRESTWOOD, J. B. WILHELMY, N. JARMIE, B. H. ERKKILA, and R. A. HARDEKOPF, Phys. Rev. C12, 451 (1975).

23. S. PEARLSTEIN, Neutron-Induced Reactions in Medium Mass Nuclei, BNL-16271 (1971).

24. M. L. SIMMONS and D. J. DUDZIAK, Nucl. Technol. 29, 337 (1976).

25. M. A. KIRK, R. C. BIRTCHER, T. H. BLEWITT, L. R. GREENWOOD, R. J. POPEK, and R. R. HEINRICH, Measurements of Neutron Spectra, Fluxes, and Flux Gradients at Tantalum and Depleted Uranium Spallation Neutron Sources and their Application to Radiation Effects Research, to be published.

26. See papers concerning IPNS in Session II of this conference.

27. D. W. KNEFF, H. FARRAR IV, L. R. GREENWOOD, and M. W. GUINAN, Characterization of the Be(d,n) Neutron Field by Passive Dosimetry Techniques, see Session II of this conference.

28. T. A. GABRIEL, B. L. BISHOP, and F. W. WIFFEN, Calculated Irradiation Response of Materials Using Fission Reactor Neutron Spectra, ORNL/TM-6361 (1979).

29. R. GOLD, Overview of Gamma-Ray Energy Deposition and Spectra in Fast Reactor Environments, Proceedings of Second ASTM-EURATOM Symposium on Reactor Dosimetry, NUREG/CP-0004, p. 101 (1977).

30. F. H. RUDDY, C. C. PRESTON, R. GOLD, E. V. BENTON, and J. H. ROBERTS, CR-39, A Promising New Solid State Track Recorder for High Energy Neutron Applications, see proceedings of this conference.

31. Recommendations of IAEA Working Group on Reactor Radiation Measurements, Nucl. Eng. Des. 33, 92 (1975).

32. R. G. ALSMILLER, Jr. and J. BARISH, Neutron-Photon Multigroup Cross Sections for Neutron Energies ≤60 MeV, ORNL/TM-6486 (1978).

33. C. Y. FU and F. G. PEREY, J. Nucl. Mater. 61, 153 (1976).

34. C. KALBACH-WALKER, Calculating Angular Distributions for Pre-equilibrium Particle Emission, HEDL-TC-1544 (1979).

35. E. D. ARTHUR and P. G. YOUNG, Calculation of Neutron Cross Sections for Iron Between 3 and 40 MeV, LA-UR-79-2834 (1979).

TABLE I.

Typical Flux Errors for Spectral Analysis in ORR (E7, 1 MW). Displacement damage in nickel[a] is also listed as a function of neutron energy. The spectrum is shown in Fig. 1.

Energy Range	Integral Flux ($\times 10^{12}$ n/cm^2-s)		Energy Range (MeV)	Damage (%)
		±%		
Total	20.1	15	<.01	0.6
Thermal, <.55 eV	5.4	4	<0.1	3.7
0.55-9.2 eV	1.8	6	0.1-0.4	9.2
9.2 eV-1.3 keV	2.8	7	0.4-1	13.8
1.3-190 kcV	2.8	50	1-2	24.8
190-920 keV	2.9	31	2-4	32.2
0.92-5 MeV	4.1	8	4-6	11.2
5-20 MeV	0.3	7	>6	5.2

[a] σ_D = 28.8 ± 3.0 keV-barns.

TABLE II.

Typical Deviations between Measured and Calculated (ENDF/B) Activation Integrals in ORR (E7, 1 MW) after Spectral Adjustment (STAYSL). +Cd means cadmium covered (20 mil).

Reaction	Deviation, % (Measured-Calculated) IV	V
$^{197}Au(n,\gamma)^{198}Au$	-3	-1
+Cd	-4	+1
$^{45}Sc(n,\gamma)^{46}Sc$	-1	-9
+Cd	-2	+2
$^{59}Co(n,\gamma)^{60}Co$	-5	-7
+Cd	+2	+4
$^{58}Fe(n,\gamma)^{59}Fe$	+3	+3
+Cd	-1	+4
$^{238}U(n,\gamma)^{239}Np$	-4	-2
+Cd	0	+4
$^{237}Np(n,\gamma)^{238}Np$ (+Cd)	+15	+11
$^{235}U(n,f)$	+4	+1
+Cd	-8	-2
$^{237}Np(n,f)$ (+Cd)	-1	+1
$^{238}U(n,f)$ (+Cd)	+8	+2
$^{58}Ni(n,p)^{58}Co$	+6	+3
$^{60}Ni(n,p)^{60}Co$	-14	-13
$^{54}Fe(n,p)^{54}Mn$	+5	+3
$^{54}Fe(n,\alpha)^{51}Cr$	+11	+17
$^{46}Ti(n,p)^{46}Sc$	-3	+1
$^{47}Ti(n,p)^{47}Sc$	-18	-25
$^{48}Ti(n,p)^{48}Sc$	-8	+2
$^{197}Au(n,2n)^{196}Au$	+1	+1

TABLE III.

Integral Cross Section Errors (ENDF/B) Deduced from Activation and Time-of-Flight Measurements in Be(d,n) Fields. Absolute errors are ±10%.

Reaction	E_D = 14-16 MeV IV	V	E_D = 40 MeV IV	V
$^{235}U(n,f)$	+7	+8	+1	+1
$^{238}U(n,f)$	+4	+4	-1	-1
$^{115}In(n,n')^{115m}In$	-1	-2	-3	-2
$Ti(n,p)^{46}Sc$	-7	-1	-89(+14)[a]	(+24)[a]
$Ti(n,p)^{47}Sc$	+2	+6	-798(+15)[a]	(-56)[a]
$^{48}Ti(n,p)^{48}Sc$	-7	-1	+2	+4
$Fe(n,p)^{54}Mn$	+6	-3	-88(+1)[a]	(+4)[a]
$^{56}Fe(n,p)^{56}Mn$	-2	-2	-4	-4
$^{59}Co(n,p)^{59}Fe$	-8	-4	+8	+5
$^{58}Ni(n,p)^{58}Co$	0	-3	+9	+3
$^{60}Ni(n,p)^{60}Co$	+14	-2	+3	+3
$^{27}Al(n,\alpha)^{24}Na$	+3	+6	0	-1
$^{54}Fe(n,\alpha)^{51}Cr$	-4	+1	-36	-20
$^{59}Co(n,\alpha)^{56}Mn$	-4	-2	-4	-5
$^{45}Sc(n,2n)^{44m}Sc$	-14	-15	-1	+3
$^{58}Ni(n,2n)^{57}Ni$	-11	+1	-30(+14)[b]	(+14)[b]
$^{59}Co(n,2n)^{58}Co$	+1	+6	-9	-3
$Zr(n,2n)^{89}Zr$	+13	+9	-4	-1
$^{93}Nb(n,2n)^{92m}Nb$	+7	+6	+6	+7
$^{169}Tm(n,2n)^{168}Tm$	--	--	+7	+10
$^{169}Tm(n,3n)^{167}Tm$	--	--	-9	-8
$^{197}Au(n,2n)^{196}Au$	-9	-8	-1	+1
$^{197}Au(n,3n)^{195}Au$	--	--	+8	+12
$^{197}Au(n,4n)^{194}Au$	--	--	+1	+1
$^{238}U(n,2n)^{237}U$	+4	+1	-11	-11

[a] Values in parenthesis include contributions from higher mass isotopes.

[b] Value in parenthesis modified according to Ref. 22.

TABLE IV.

Typical Flux Errors for Be(d,n) Spectral Analysis at ORNL Cyclotron, E_d = 40 MeV. Displacement damage[a] in nickel is also listed as a function of neutron energy. The spectrum is similar to FMIT.

Energy Range (MeV)	Integral Flux ($\times 10^9$ n/cm^2-μC)		Damage (%)
		±%	
Total	4.66	5	
<0.1	0.08	17	
<1	0.46	19	2
1-5	0.56	15	4
5-10	0.63	13	11
10-15	0.97	13	23
15-20	0.98	16	28
20-25	0.64	17	19
25-30	0.27	21	8
>30	0.15	19	5

[a] σ_D = 273 keV-barns.

TABLE V.

Threshold Activation Reactions Desired for Fusion Dosimetry Listed by Material in Order of Priority. Elements with multiple, long-lived products are favored. Many other reactions could also be used.

Reaction	Energy Range (MeV)	Reaction	Energy Range (MeV)
$^{59}Co(n,p)^{59}Fe$	4-28	$^{90}Zr(n,p)^{90}Y$	5-26
$(n,2n)^{58}Co$	10-30	$Zr(n,x)^{89}Zr$	12-36
$(n,3n)^{57}Co$	20-40	$(n,x)^{88}Zr$	18-45
$(n,4n)^{56}Co$	30-50	$^{89}Y(n,p)^{89}Sr$	4-25
$^{197}Au(n,2n)^{196}Au$	8-25	$(n,2n)^{88}Y$	12-34
$(n,3n)^{195}Au$	15-35	$(n,3n)^{87}Y$	22-50
$(n,4n)^{194}Au$	23-45	$(n,\alpha)^{86}Rb$	8-28
$Fe(n,x)^{54}Mn$	1-40	$^{169}Tm(n,2n)^{168}Tm$	9-28
$^{54}Fe(n,\alpha)^{51}Cr$	7-25	$(n,3n)^{167}Tm$	16-36
$^{54}Fe(n,t)^{52}Mn$	14-35	$(n,5n)^{165}Tm$	25-50
$^{58}Ni(n,p)^{58}Co$	2-25	$^{23}Na(n,2n)^{22}Na$	12-30
$(n,2n)^{57}Ni$	12-36	$^{107}Ag(n,2n)^{106m}Ag$	10-28
$(n,3n)^{56}Ni$	22-40	$(n,3n)^{105}Ag$	16-40
$^{60}Ni(n,p)^{60}Co$	3-30	$^{238}U(n,2n)^{237}U$	6-18
$^{93}Nb(n,n')^{93m}Nb$	0.1-10	(n,f)f.p.	1-50
$(n,2n)^{92m}Nb$	9-28	$^{55}Mn(n,2n)^{54}Mn$	11-28

TABLE VI.

Comparison of Measured[a] and Calculated (ENDF/B-IV) Helium Production in the Oak Ridge Research Reactor

Material	Ratio (Measured/Calculated)
Al	0.95 ± .02
Fe	1.27 ± .07
Cu	1.24 ± .05
Ni	1.00 ± .03
Ti	1.85 ± .07

[a] D. Kneff and H. Farrar IV, Rockwell International, DOE/ET-0065-8 (1980).

[b] $^{58}Ni(n,\gamma)^{59}Ni(n,\alpha)$ process included using spectral-averaged cross sections from dosimetry.

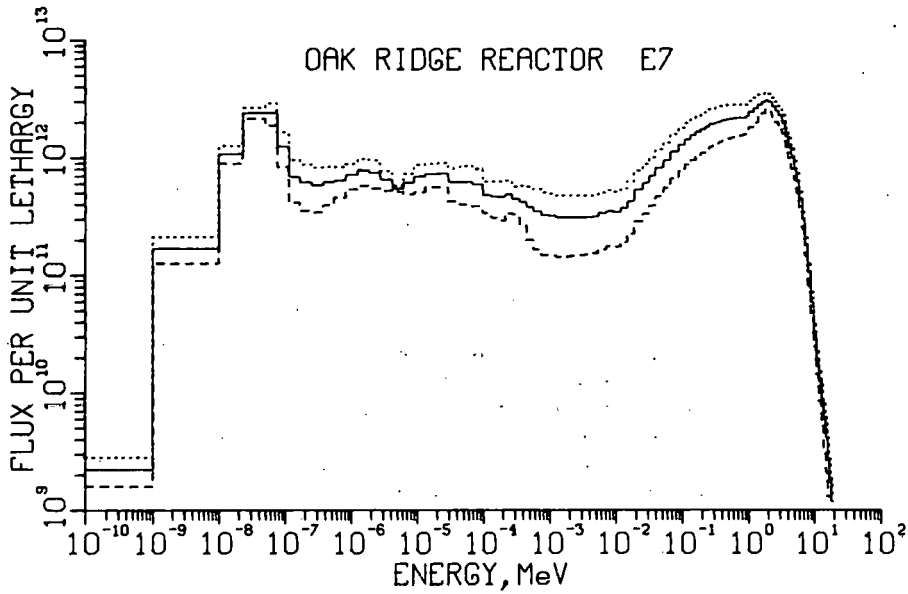

Fig. 1. Neutron Flux Spectrum for the Oak Ridge Reactor (E7,1 MW) Using the STAYSL Computer Code. The reactions are listed in Table II and flux integrals in Table I. The dotted and dashed lines represent one standard deviation error limit.

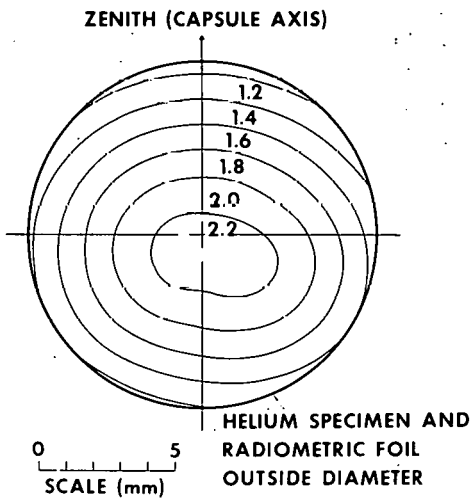

Fig. 2. Constant Flux Contours ($\times 10^{17}$ n/cm^2) Deduced from Helium and Radiometric Dosimetry at RTNS I. Note the asymmetry and small scale. Data from Ref. 18.

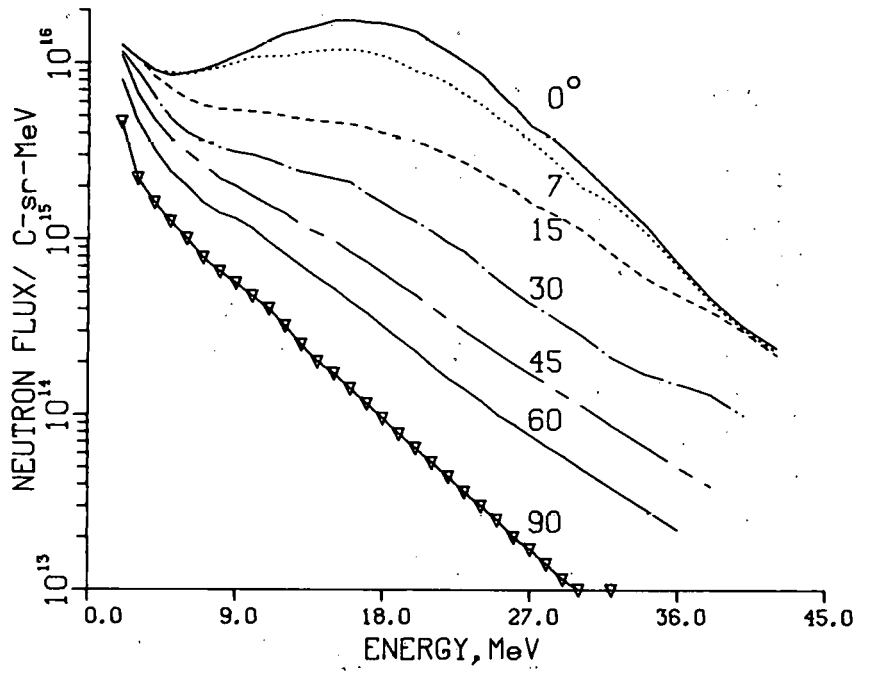

Fig. 3. Neutron Spectra Measured by Time-of-Flight Spectrometry at the Oak Ridge Isochronous Cyclotron [Be(d,n), E_d = 40 MeV]. Data from Ref. 20.

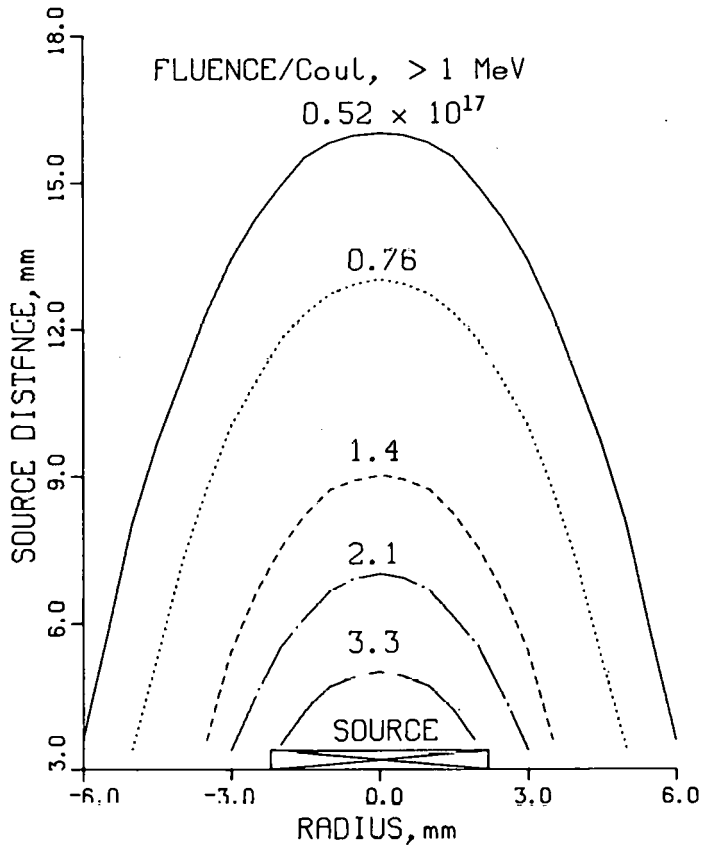

Fig. 4. (a) Fluence. Measured by Radiometric and Helium Dosimetry at the U. of C. Davis Cyclotron [Be(d,n), E_d = 30 MeV]. Note the very steep gradients, especially off-axis, and the very fine scale.

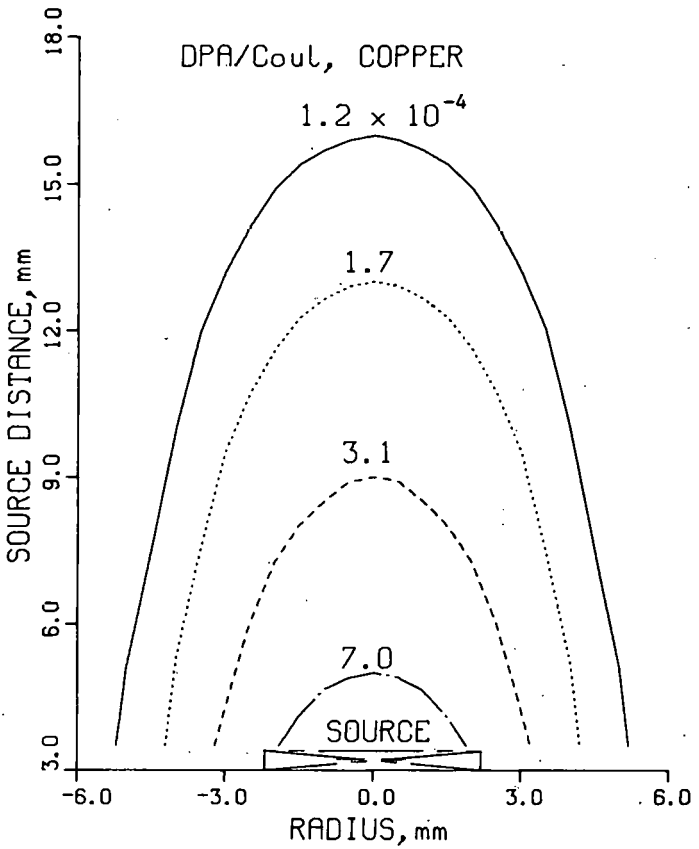

Fig. 4. (b) Displacement Damage. Measured by Radiometric and Helium Dosimetry at the U. of C. Davis Cyclotron [Be(d,n), E_d = 30 MeV]. Note the very steep gradients, especially off-axis, and the very fine scale.

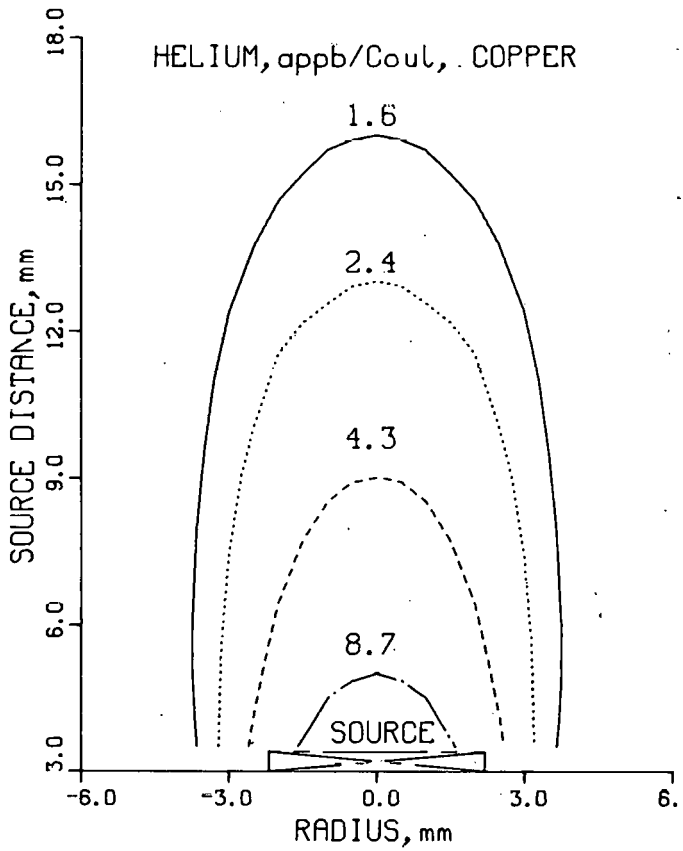

Fig. 4. (c) Helium Contours. Measured by Radiometric and Helium Dosimetry at the U. of C. Davis Cyclotron [^{9}Be(d,n), E_d = 30 MeV]. Note the very steep gradients, especially off-axis, and the very fine scale.

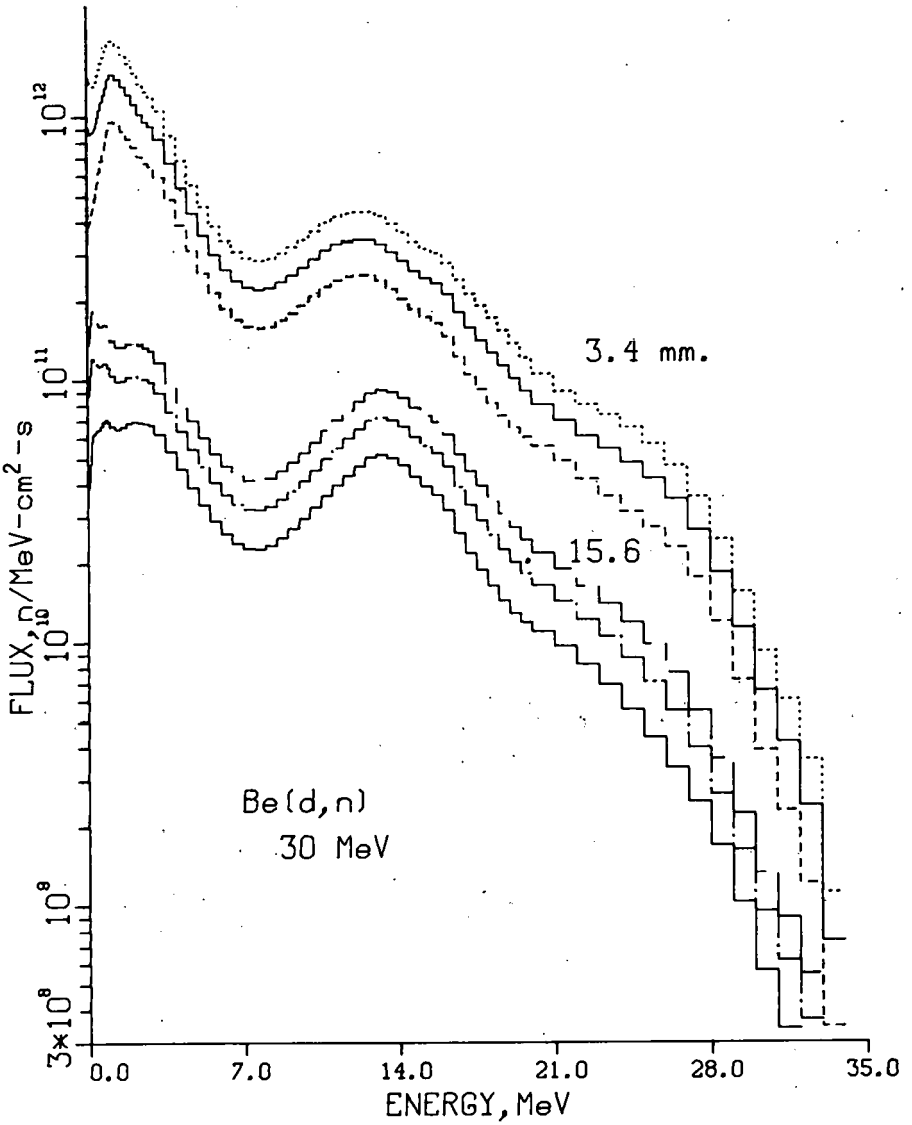

Fig. 5. Spectra Unfolded at Nominally Zero Degrees at Various Distances from a Be(d,n) Source (E_d = 30 MeV) at U. of C. Davis. Note that the spectrum is softer closer to the source. The STAYSL code was used with 21 reactions.

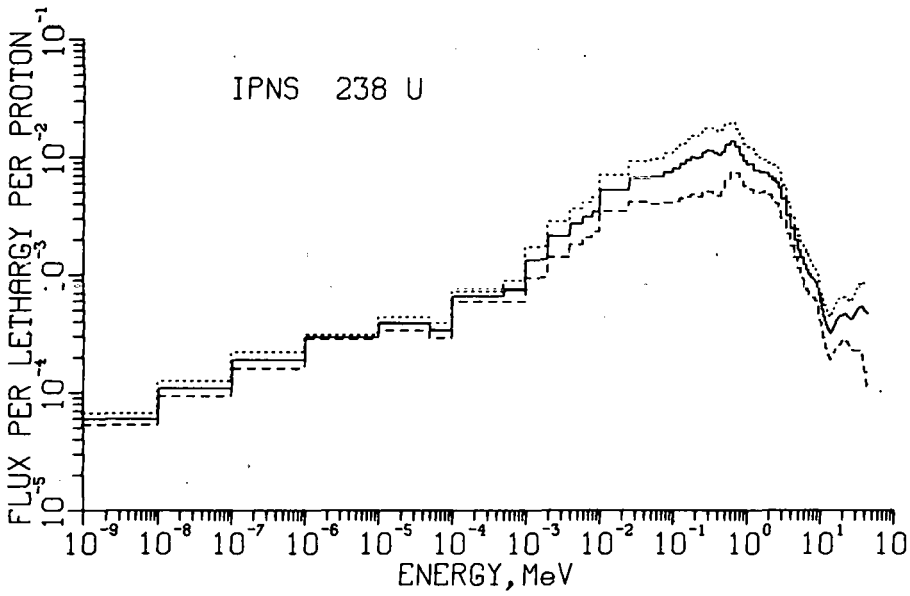

Fig. 6. Spectrum Measured at a Mock-Up of the Intense Pulsed Neutron Source under Construction at Argonne. A 500 MeV proton beam was stopped in a depleted uranium target. The STAYSL code was used with 26 reactions and dotted and dashed lines represent one standard deviation error. The flux above 44 MeV is not shown.

Dup

THICK TARGET NEUTRON YIELDS AND SPECTRA FROM THE Li(d,xn) REACTION AT 35 MeV

D.L.Johnson and F.M.Mann

Hanford Engineering Development Laboratory
Richland, Washington 99352

J.W.Watson,† F.P.Brady, J.L.Ullmann, J.L.Romero,
C.M.Castaneda, C.I.Zanelli, and W.C.Wyckoff*

University of California
Davis, California 95616

ABSTRACT

Accurate knowledge of the neutron source characteristics from 35 MeV deuterons on a target of thick lithium were needed to support design and operation of the Fusion Materials Irradiation Test (FMIT) facility.

To meet this need, measurements were performed using a 35 MeV deuteron beam from the isochronous cyclotron at the University of California at Davis. Data were obtained using the time-of-flight technique with an NE213 liquid scintillator. One set of measurements was used to observe the neutron spectrum from $\sim$ 1 MeV to $\sim$ 50 MeV, the maximum kinematically allowed energy. Observation angles were from 0° to 150° with emphasis on forward angles. Spectral data below $\sim$ 1.5 MeV had poor accuracy. It was felt that a significant fraction of the neutron yield might lie at still lower energies, therefore a second set of measurements was performed to investigate the spectra to as low an energy as possible. Additional measurements were performed with a target enriched in the isotope ^{6}Li replacing the natural lithium target used in previous measurements. The main advantage of a ^{6}Li target is that the maximum kinematically allowed neutron energy is only about 38 MeV, hence reducing shielding requirements. The experiments, preliminary results, and future needs will be described.

INTRODUCTION

The needs for data concerning the neutron source characteristics for 35 MeV deuterons on thick lithium for the FMIT facility arose primarily because there had been few prior measurements with similar goals in mind. Most previous measurements were done with different deuteron energies, and the neutron spectra were observed primarily at or near 0° with respect to the direction of the incident beam. Furthermore, many measurements did not observe the neutron spectrum below $\sim$ 3 - 10 MeV.

The experiments described here were undertaken with the objectives to:

(1) Provide as complete a data set as possible for calculations that make direct use of spectra and yields obtained at a distance from the target. Examples of these calculations are shielding, activation, and radiation heating in walls somewhat distant from the source.

(2) To obtain thick target data of sufficient quantity and quality that it would aid in an evaluation of the thin target differential neutron production cross section as a function of deuteron energy. This was needed for calculations of the neutron flux-spectra at positions very close to the target in the FMIT test cell. The evaluation is described in reference [1].

Measurements Emphasizing Neutron Energies Greater than 1.5 MeV

Measurements of the neutron spectra and yields were made using a beam of 35 MeV deuterons from the isochronous cyclotron at the University of California at Davis. Neutrons were observed with the time-of-flight technique using an NE213 liquid scintillator that was 2" x 2". The experiment has been described elsewhere [2] so only the results will be shown here. Figure 1 shows the spectral results of measurements for neutron emission angles 0°, 4°, 12°, 20°, 30°, 45°, 70°, 105°, and 150° in the lab.

The results of spectral measurements have been binned in 1 MeV steps for energies greater than 1 MeV, as shown in Figure 1. Displaying the data both linearly and logarithmically illustrates different features of the data.

In the linear plot, one sees a strong peak at 0° with a maximum between 13 and 14 MeV and a full width at half maximum of about 14 MeV. The magnitude of the neutrons observed decreases rapidly with increasing angle and the spectral shape changes into one that falls monotonically with increasing neutron energy. Some evidence for a peak or inflection in the vicinity of 14 MeV may be seen in spectra for angles perhaps as large as 45°.

There are very few neutrons emitted at any angle with energies greater than about 30 MeV, although the maximum kinematically allowed neutron energy is as large as about 50 MeV for forward angles. From the observed spectra, one would expect the bulk of

damage in experimental materials in FMIT to be due to neutrons less than about 30 MeV with most of it from neutrons within about ± 10 MeV of the 14 MeV peak.

For the portion of the spectra less than about 30 MeV, the data shown in Figure 1 are quite similar to the 35 MeV data at 0° of Amols, et al,[3] and to the 40 MeV data for 0° to 90° of Saltmarsh, et al, [4]. On the other hand, the 34 MeV data of Goland, et al, [5] for 0° to 20° are only about half the magnitude of these data and their spectra drop sharply below 5 MeV.

The interpretation of the data below about 30 MeV is that it is composed of a component due to the deuteron breakup reaction plus a component resulting from formation of a compound nucleus followed by statistical evaporation.

The breakup contribution results from the breakup of the weakly bound deuteron in the field of a lithium nucleus with the neutron continuing on with essentially the same velocity and direction as the incident deuteron. Neutrons from breakup are very forward peaked and have energies in the forward direction that are about half that of the deuteron which broke up. The breakup reaction can be described by the classical Serber model [6].

There is also evidence, as shown in Figure 1, for another component that can be viewed as the result of statistical evaporation. For this component, one would expect a more isotropic angular distribution and spectra that decrease monotonically with increasing neutron energy, similar to observation at large angles.

In the logarithmic plot in Figure 1, the features of the spectra of neutrons above 30 MeV become apparent. Here one sees a shoulder in forward angle spectra which extends as high as 50 MeV near 0°. This shoulder has not been previously observed for deuterons of similar incident energy. Although there are very few of these high energy neutrons compared to those below about 30 MeV, they are very important for shielding considerations because of their deep penetration in thick walls. The highest energy neutrons in the spectra dominate the dose received through a thick wall of ordinary or high density concrete and the bulk of the neutrons below 20-30 MeV have much less effect. This is described in more detail by Carter and Morford [7].

The shoulder is caused specifically by $^{7}Li(d,n)^{8}Be$ stripping reactions which populate primarily the ground and first excited states of ^{8}Be. The 50 MeV neutrons come only from the $^{7}Li(d,n_{o})^{8}Be$ reaction to the ground state (Q-value about + 15 MeV) with 35 MeV deuterons.

There are several features of the data above 30 MeV that indicate that it can probably be accounted for with well known deuteron stripping theories such as DWBA.

First, in such a view one would expect that transitions to the broad 2+ first excited state at an excitation energy of 2.94 MeV would be about 3 times as strong as transitions to the 0+ ground state. Spectroscopic factors for transitions to each state are known from shell model calculations to be comparable in magni-

tude, but angular momentum considerations would lead to a predominance of transitions to the 2+ state. This predominance probably leads to the roll off in the shoulder that is seen for neutron energies above about 45 MeV.

Another feature is the relatively constant value of the yield at a particular forward angle over a wide range of neutron energies. One would expect such a result for high energy deuterons where direct reactions are dominant and the stripping cross section is proportional to the (constant) spectroscopic factor that is involved. The flat spectrum occurs because one gets contributions from all deuteron energies as they slow down in the lithium.

Finally, the magnitude of the yield of shoulder neutrons peaks somewhere between about 12° and 20°. This is consistent with the angular distribution expected for the stripping of p-wave nucleons. For such a reaction, one expects a small yield at 0°, a large peak in yield at a forward angle, and a small oscillating cross section for larger angles.

The total neutron yield as a function of angle was obtained by integrating each of the spectra in Figure 1 over neutron energy from 1 to 50 MeV. Then, to obtain the total neutron yield for neutrons of all energies, it was assumed at each angle that the unobserved yield from 0 to 1 MeV was equal to the yield measured from 1 to 2 MeV. The total yield is shown as a function of emission angle in Figure 2 and numerical values are shown in Table 1 for yields above 1 MeV and 0 MeV respectively. Also shown in Figure 2 is the product of the yield times $2\pi \sin\Theta$ which is proportional to the element of solid angle for neutrons emitted within an increment $d\Theta$ about the emission angle Θ. The second curve shows the contribution of neutrons emitted in the direction Θ to the total neutron yield.

By integrating the second curve in Figure 2 over angle, the total neutron yield was found to be 3.0 (10^{11}) neutrons/μc. This is an enormous conversion of deuterons to neutrons, which corresponds to 4.8 neutrons emitted for every 100 incident deuterons. In the FMIT target design, only the yield forward of 90° is useful for irradiation experiments. Fortunately, about three-fourths of the neutrons are emitted in the forward hemisphere. The yield of these neutrons corresponds to 2.2 (10^{11}) neutrons/μc or 3.5 neutrons per 100 incident deuterons.

In FMIT, the most important experimental samples will be placed as close as possible to the target in order to experience the maximum neutron flux. Therefore, due to the spread in the beam, they will also be exposed to neutrons emitted at all angles up to about 90° relative to the beam direction. One notes that, although the measured yield in Figure 2 is very strongly forward peaked, the distribution as a function of Θ is very broad with about half the neutrons emitted between about 10° and 70°.

The significance of this broad emission is that samples close to the target in FMIT will be exposed to much softer neutron spectra than might be anticipated. This is because the neutron emission spectra soften quite a bit as a function of angle as seen

in Figure 1. Figure 3 shows the average energy of neutrons emitted above 0 MeV as a function of angle. Numerical values are given in Table 1 for neutrons emitted above 1 MeV and 0 MeV respectively. Using these data, it was found that the average energy of all neutrons emitted above 0 MeV was only about 7.3 MeV. Neutrons emitted in the forward hemisphere have a slightly higher average energy of about 8.1 MeV. Hence one should expect a soft spectrum for positions very close to the target. This effective softening at close positions has been observed experimentally for neutrons from 30 MeV deuterons on thick beryllium by Nethaway, et al,[8].

Another significant point is that the yield of neutrons between 0 and 1 MeV is more important than one would think at first glance in evaluating the total yield of neutrons. It can be seen in Figure 1 and Table 1 that the fractional contribution to the yield at each angle due to neutrons from 0 to 1 MeV increases with angle. For the data here, the contribution varies from $\sim$ 3% at 0° to $\sim$ 27% at 150°. Hence there is a need to better understand the yield and spectra of neutrons emitted at such low energies in order to determine the total number of neutrons emitted with better accuracy. The first set of measurement had a neutron threshold of $\sim$ 0.9 MeV, however, data were of poor quality below $\sim$ 1.5 MeV. A second set of measurements was undertaken to extend the observation to lower energies.

Measurements Emphasizing Neutron Energies Less Than 1.5 MeV

Measurements were repeated with a neutron threshold set at $\sim$ 0.4 MeV and good quality data was obtained down to about 0.7 MeV. All angles between 4° and 70° (where most of the neutrons are emitted) were remeasured. Figure 4 compares preliminary results from the new data at 45° to the previous data. Note the scatter in the older data below about 1.5 MeV, which indicates increasing uncertainties (not shown in Figure 4). The newer data does not start to scatter in a similar fashion until below about 0.7 MeV. Similar gradual trends were noted in the spectra for the other angles.

The significance of these preliminary results is that one can say that the previous estimates of the yield from 0 to 1 MeV were not grossly in error. There are no sharp rises or falls in the spectra as far as we have been able to observe. When analyses of these data are complete, they will be incorporated with the previous data to provide improved values of the yield and spectra as a function of angle. We have not observed a turnover in the spectra at very low energies which we believe should be observable. This must await future experimenters.

Measurements with a ^{6}Li Target

Another aspect of the data shown in Figure 1 was the presence of neutrons up to 50 MeV in the spectra. Although only about 1%

of the neutrons emitted have energies greater than 30 MeV, these are the most penetrating in thick concrete shields and the higher the energy, the greater the penetration.

There was an incentive to use a target of ^{6}Li, since the maximum kinematically allowed neutron energy would be only 38 MeV. The significant question was whether or not there would be a similar number of neutrons emitted from 35 MeV deuterons on ^{6}Li compared to natural lithium ($\sim$ 92.5% ^{7}Li).

Measurements were conducted during the experiment to measure the very low energy neutrons by simply switching targets and keeping everything else the same. Spectral data were obtained for angles of 30° and 45° where one expects large contributions to the total neutron yield as shown in Figure 2. These data have not been completely analyzed; however, preliminary results indicate that at these angles, the neutron yield is $\sim$ 30% less than that from natural lithium. It therefore appears that ^{6}Li will not be a practical target for the FMIT facility.

Future Plans and Needs

There are plans to complete analysis and document these results in the near future.

One area that we are looking into is the calculation of the angular distributions of the $^{7}Li(d,n_0$ and $n_1)^{8}Be$ reactions so that interpolation between angles of the high energy shoulder (as in Figure 1) due to these reactions can be improved.

Another area that is of interest is the measurement of thin target neutron yields and spectra for deuterons up to 35 MeV on lithium. This will improve our ability to predict the neutron flux-spectra at positions very close to the target in the FMIT test cell.

† Present address: Physics Department, Kent State University, Kent, Ohio 44242.

* Present address: Physics Department, Humboldt State University, Arcata, California 95521.

REFERENCES

(1) F.M.Mann and F. Schmittroth, "Neutron Environment in d+Li Facilities," proceedings of this symposium (also HEDL-SA-2123FP).

(2) D.L.Johnson, et al., "Measurements of Neutron Spectra from 35 MeV Deuterons for the FMIT Facility," proceedings of the International Conference on Nuclear Cross Sections for Technology, Knoxville, TN., Oct. 22-26, 1979 (also HEDL-SA-1905FP).
D.L.Johnson, et al., "Measurements and Calculations of Neutron Spectra from 35 MeV Deuterons on Thick Lithium for the FMIT Facility," Jour. of Nuclear Materials 85 & 86 (1979) 467.

(3) H.I.Amols, et al., "Physical Characterization of Neutron Beams Produced by Protons and Deuterons of Various Energies Bombarding Beryllium and Lithium Targets of Several Thicknesses." Medical Physics 4 (1977) 486.

(4) M.J.Saltmarsh, et al., "Characteristics of an Intense Neutron Source Based on the d+Be Reaction," Nucl. Instr. and Meth. 145 (1977) 81 and ORNL/TM-5696.

(5) A.N.Goland, et al., "Use of Li(d,n) Neutrons for Simulation of Radiation Effects in Fusion Reactors," IEEE Trans. Nucl. Sci. NS-22 (1975) 1776.

(6) R. Serber, Physical Review 72 (1947) 1008.

(7) L.L.Carter and R.J.Morford, "Nuclear Data Relevant to Shield Design of FMIT Facility," proceedings of this symposium.

(8) D.R.Nethaway, et al., Proceedings of the Symposium on Neutron Cross Sections from 10 to 40 MeV, May 3-5, 1977, Brookhaven National Laboratory (BNL-NCS-50681, p:135).

Table I

NEUTRON YIELDS AND ENERGY PARAMETERS OBTAINED FROM MEASUREMENTS OF 35 MeV DEUTERONS ON THICK LITHIUM

Angle (Degrees)	E_n > 1 MeV			E_n > 0 MeV		
	Yield (n/μc-Sr)	Tot. Energy (MeV/μc-Sr)	Avg. Energy (MeV/n)	Yield (n/μc-Sr)	Tot. Energy (MeV/μc-Sr)	Avg. Energy (MeV/n)
0	$2.43(10^{11})$	$3.05(10^{12})$	12.56	$2.50(10^{11})$	$3.05(10^{12})$	12.21
4	$2.08(10^{11})$	$2.73(10^{12})$	13.09	$2.14(10^{11})$	$2.73(10^{12})$	12.75
12	$1.20(10^{11})$	$1.48(10^{12})$	12.28	$1.25(10^{11})$	$1.48(10^{12})$	11.74
20	$7.13(10^{10})$	$8.04(10^{11})$	11.27	$7.66(10^{10})$	$8.06(10^{11})$	10.52
30	$5.07(10^{10})$	$4.93(10^{11})$	9.71	$5.51(10^{10})$	$4.95(10^{11})$	8.98
45	$3.11(10^{10})$	$2.48(10^{11})$	7.97	$3.52(10^{10})$	$2.50(10^{11})$	7.10
70	$1.85(10^{10})$	$1.19(10^{11})$	6.42	$2.12(10^{10})$	$1.20(10^{11})$	5.66
105	$1.31(10^{10})$	$7.79(10^{10})$	5.95	$1.51(10^{10})$	$7.89(10^{10})$	5.21
150	$6.45(10^{9})$	$2.85(10^{10})$	4.42	$8.19(10^{9})$	$2.94(10^{10})$	3.59

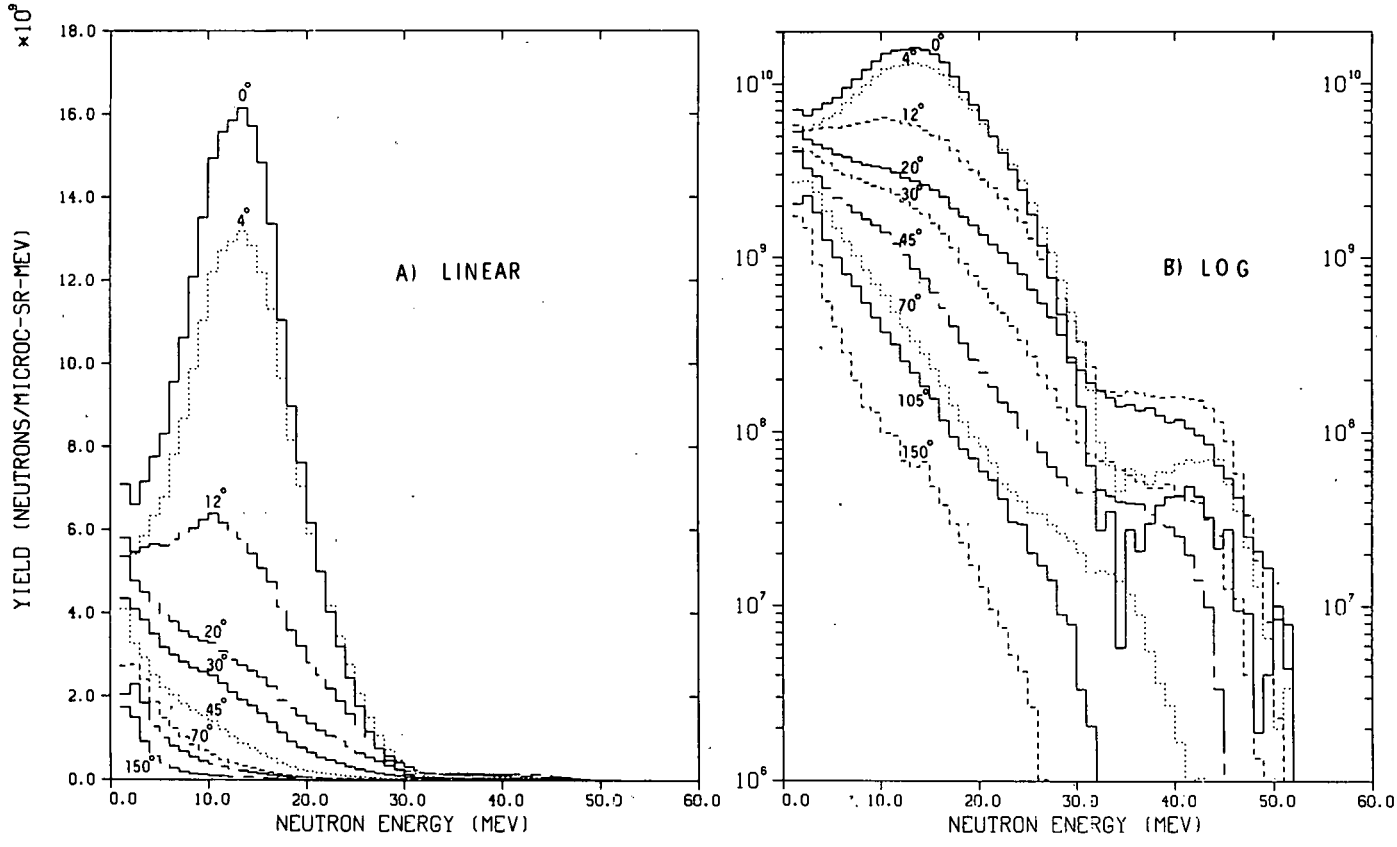

Fig. 1. Measured neutron yield spectra as a function of emission angle in the laboratory for 35 MeV deuterons on thick natural lithium.

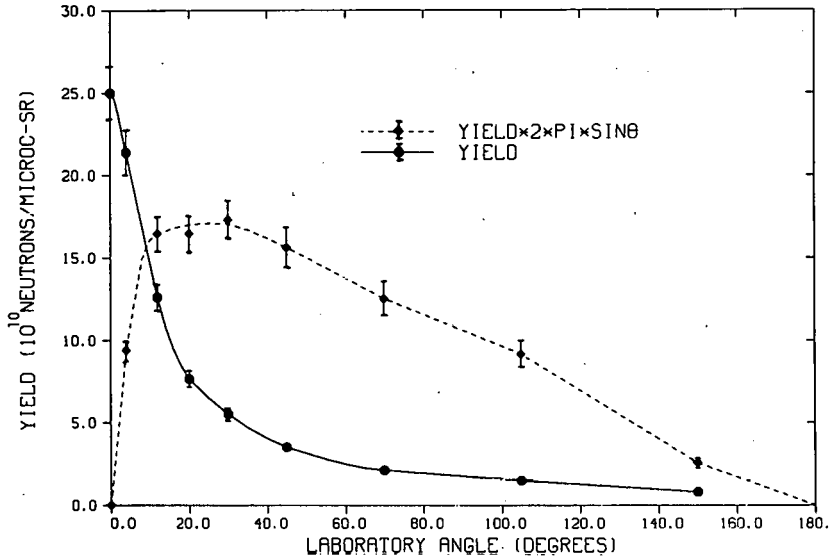

Fig. 2. Yield of neutrons greater than 0 MeV as a function of emission angle in the laboratory for 35 MeV deuterons on thick natural lithium. The curve of the product of yield and 2π Sinθ shows the relative contribution of neutrons emitted at various angles to the total yield.

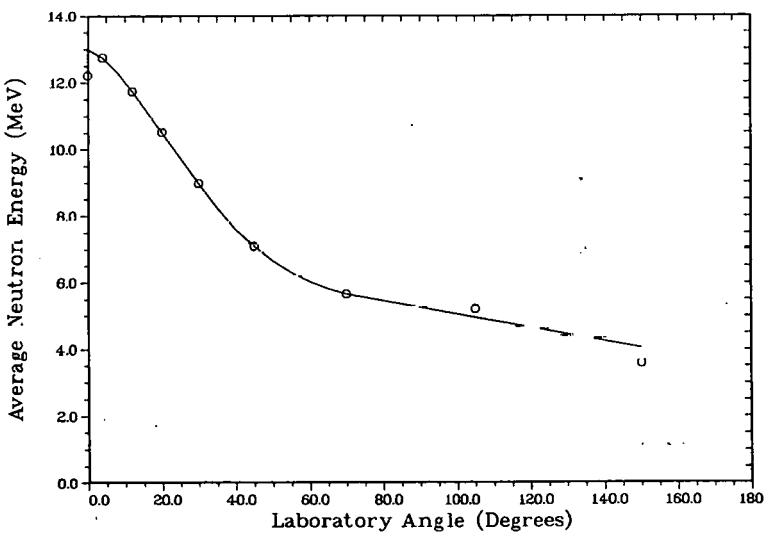

Fig. 3. Average energy of neutrons greater than 0 MeV as a function of emission angle in the laboratory for 35 MeV deuterons on thick natural lithium.

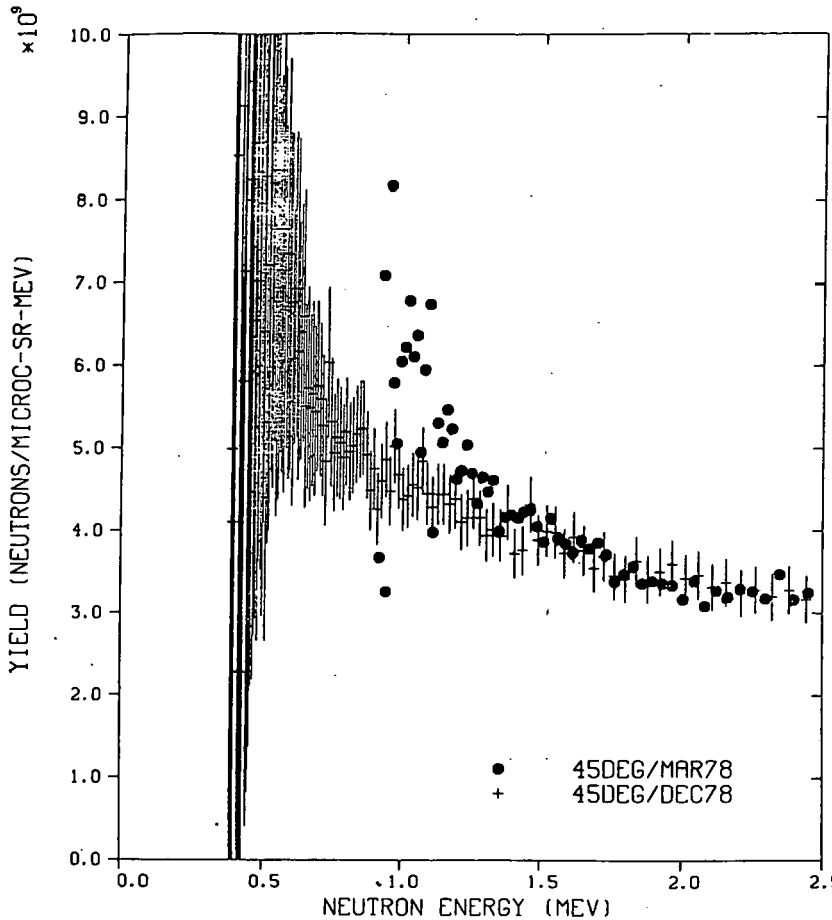

Fig. 4. Measured low energy portion of the neutron yield spectrum at 45° from 35 MeV deuterons on thick natural lithium. Dots (crosses) correspond to measurements with a neutron detector threshold of 0.9 MeV (0.4 MeV). Uncertainties are not shown for the dots but can be inferred from the scatter of nearby data points.

THIS PAGE
WAS INTENTIONALLY
LEFT BLANK

MEASUREMENTS ON THE ZING-P' PULSED SPALLATION NEUTRON SOURCE

Members of the IPNS Group

Paper Presented by
John M. Carpenter

Argonne National Laboratory
Argonne, Illinois 60439, U.S.A.

ABSTRACT

ZING-P' is a prototype of the Intense Pulsed Neutron Source, a pulsed spallation source under construction at Argonne National Laboratory. We have performed measurements in support of the design of Neutron Scattering and fast neutron Radiation Effects Facilities, using 300 and 500 MeV protons. The total power and (indirectly) neutron yields from targets of W and U have been measured. Fast neutron energy spectra, and spatial distributions have been determined for Ta and U targets with Pb reflector. The power density distribution has been determined for the U target. Energy deposited in moderator and reflector materials near the source have been measured. The particulate, dissolved and radioactive materials in the U target cooling stream have been examined.

Since the text of this paper was not available by the final deadline of June 16, 1980, the Editors regret having to omit it from the Proceedings of the Sympsoium.

THIS PAGE

WAS INTENTIONALLY

LEFT BLANK

CHARACTERIZATION OF THE Be(d,n) NEUTRON FIELD BY PASSIVE DOSIMETRY TECHNIQUES

D. W. Kneff and Harry Farrar IV

Rockwell International, Energy Systems Group
Canoga Park, California 91304, U.S.A.

L. R. Greenwood

Argonne National Laboratory
Argonne, Illinois 60439

and

M. W. Guinan

Lawrence Livermore Laboratory
Livermore, California 94550

ABSTRACT

Neutrons from the Be(d,n) reaction are presently being used for fusion reactor materials testing, because of their relatively high available flux, and because of the close similarity of the neutron spectrum to that of the Fusion Materials Irradiation Test Facility (FMIT), now being constructed. However, both irradiation environments have (or will have) steep fluence and energy spectrum gradients in the high-flux regions of their irradiation volumes. Characterization of these neutron environments is thus necessary for the full understanding of any irradiation experiments. This paper describes a characterization of the Be(d,n) neutron field for 30-MeV deuterons, using foil activation and helium accumulation neutron dosimetry. The results show the steep fluence and spectrum gradients, and demonstrate the importance of including comprehensive passive dosimetry in all Be(d,n) and Li(d,n) irradiations where a knowledge of fluence information is required. Relative helium generation cross sections are presented for the helium accumulation dosimetry materials, and some comparisons are made with ENDF/B-IV helium production cross sections.

INTRODUCTION

The Be(d,n) reaction is an important source of neutrons for the fusion reactor materials program, because of its relatively high available flux of high-energy neutrons for materials testing, and because of the close similarity of its neutron spectrum to that of the Fusion Materials Irradiation Test Facility (FMIT). However, the neutron yield in the high flux region contains steep flux and spectral gradients. Characterization of the Be(d,n) neutron field is thus important at this time, both because of the neutron fluence and energy information it provides for ongoing experiments, and because of the opportunity it provides to develop and test dosimetry and energy-dependent cross sections that will be needed for FMIT.

A joint Rockwell International-Argonne National Laboratory (ANL)-Lawrence Livermore Laboratory (LLL) irradiation experiment was undertaken to characterize the Be(d,n) neutron field for 30-MeV deuterons. This experiment included an extensive set of foil activation and helium accumulation neutron dosimetry materials, plus a large number of pure elements and stable isotopes. The objectives of the experiment were to characterize this neutron field in detail, further develop both radiometric and helium accumulation dosimetry in a fast-neutron environment, and measure helium generation cross sections for several pure elements and isotopes. This paper describes the Be(d,n) characterization results, and presents relative integral cross section information for the helium accumulation dosimetry materials.

EXPERIMENT DESCRIPTION

The irradiation assembly used for this experiment is shown schematically in Fig. 1. The basic components of the assembly included three thin stainless steel arcs, concentric about the midpoint of the beryllium target at radial distances of 5, 15, and 30 cm, and a small stainless steel capsule assembly, mounted 1 cm from the front face of the beryllium target assembly and approximately aligned with the deuteron beam axis. Additionally, six thin-walled stainless steel tubes containing multiple helium generation materials were mounted at various distances behind the capsule. Stacks of activation foils were mounted at 0°, 15°, 30°, 45°, and 60° on the three stainless steel arcs, and on the face of the beryllium target assembly. A foil stack typically consisted of thin foils of In, Ti, Fe (including some separated ^{54}Fe and ^{56}Fe), Au, Ni, Nb, Zr, Co, Al, ^{235}U, ^{238}U, Sc_2O_3, Tm_2O_3, and Y_2O_3.

The geometry of the small capsule assembly is shown in Fig. 2. This assembly consisted basically of a 2-cm-diameter by 9-mm-thick capsule, containing three layers of helium generation materials sandwiched between four layers of dosimetry foils. The foil materials were those used for the arc foil sets. The helium generation materials included eleven Al, Fe, Ni, Cu, and Au

pure-element helium accumulation neutron dosimetry wire rings, oriented concentrically with the irradiation capsule axis. The rings for each element were located at different neutron source angles with respect to the source axis. Also included were several smaller helium generation specimens of 22 pure elements, 21 separated isotopes, and 19 alloys and compounds.

The entire irradiation assembly was mounted on the front face of the beryllium target assembly [1]. The beryllium target was bombarded with 30-MeV deuterons from the 76-Inch Isochronous Cyclotron at the University of California at Davis, producing a ~0-32 MeV neutron energy spectrum. The deuteron beam was rastered ~±0.5 mm in a two-dimensional pattern to average out any hot spots in the deuteron beam profile. The total irradiation time was 93 hours, for a total integrated charge of 8.46 C. A few of the dosimetry foils with short-lived activation products were removed for analysis after the first four hours of the irradiation.

Following the irradiation, the capsule foils were cut into (typically) nine segments, following a pre-scribed pattern, and the capsule and arc activation foils were analyzed at ANL and LLL using Ge(Li) detectors. Several foils were counted at both laboratories to insure a common calibration. The analysis techniques and nuclear decay data are given in Refs. 2 and 3. Most of the resulting activity rates are accurate to ±1.5%, based on counting statistics and previous interlaboratory comparisons. The results provided sets of multiple activation reaction yields for several positions within and behind the irradiation capsule.

The helium accumulation dosimetry rings from the irradiated capsule were etched, segmented, weighed, and analyzed for generated helium using a high-sensitivity gas mass spectrometer [4]. The etching removed the effects of helium recoiling into or out of each sample. The helium results provided detailed helium concentration gradients for a number of materials as a function of position within the capsule.

The radiometric and helium accumulation results were subsequently analyzed to produce a detailed description of the Be(d,n) neutron environment for this irradiation. The most detailed calculations were made for the high flux region occupied by the small irradiation capsule. This high-flux region is more difficult to characterize than further source distances, because it is in the region of the steepest fluence and energy spectrum gradients. This is further complicated by the close source geometry, for which the neutron spectrum at any given location is produced by neutrons from a wide range of source angles. This region is of particular interest, because it is reasonably representative of the high fluence region of the FMIT Li(d,n) neutron environment, and because this characterization will later be used to deduce cross sections for the numerous other materials irradiated within the capsule assembly.

IRRADIATION ASSEMBLY OFFSET

The offset of the irradiation assembly from the deuteron beam axis was the first information determined from the dosimetry materials. The presence of this assembly offset was determined by plotting the helium concentrations measured in the segmented rings as a function of polar angle about the irradiation capsule axis, as shown in Fig. 3. The large but smooth sinusoidal variation in helium concentration with angle reflects the different fluence received by each ring segment because of the offset.

The magnitude of the capsule offset was determined by constructing an initial fluence profile map for the capsule irradiation volume, normalizing the measured helium concentrations to this map, and adjusting the map offset to minimize the helium concentration variations. The validity of this procedure was based on the data in Fig. 3, where it can be seen that all of the curves have similar shapes. This indicates that the Al, Fe, Ni, and Cu(n,total helium) cross sections, when integrated over the forward-direction Be(d,n) neutron spectra, have similar energy responses. These integrated responses also appear to be roughly constant as a function of energy, as supported by the limited cross section information available [5]. For this preliminary data analysis, therefore, these four dosimetry materials were assumed to provide an approximately energy-insensitive measure of the total neutron fluence ≥5 MeV.

The initial fluence profile map was based on a least-squares cubic fit to the time-of-flight data of Meulders, et al. [6], multiplied by a linear function approximating the fluence variation with distance from the beryllium target. The linear function was based on the present radiometric counting results. An irradiation assembly offset of 1.27 mm was obtained by combining the helium accumulation dosimetry data with this fluence map. The results also indicate that the neutron fluence profile was generally symmetrical about the deuteron beam axis, as would be expected from the deuteron beam rastering. Later comparisons of this approximate map showed that the fluence profiles were consistent with those produced by the radiometric data (next section) over the region subtended by the helium accumulation rings. This agreement, and later helium data comparisons, confirmed this determination of the capsule offset.

The fact that the assembly was offset by only 1.27 mm, and that this resulted in almost factor-of-two differences in flux for symmetrical locations around the assembly clearly demonstrate the steep fluence gradients present in this neutron environment.

FOIL ACTIVATION SPECTRAL UNFOLDING

The Be(d,n) neutron fluence and energy spectra were unfolded from the radiometric data using the least-squares spectral analysis code STAY'SL [7]. The measured foil activities were first

reduced to saturated activation integrals, using the procedures outlined in Ref. 2, and corrected for gamma absorption and decay during and following irradiation. All integral rates were then corrected to a common geometry for each foil set, assuming a $1/R^2$ distance correction and integrating each activity rate over the finite solid angles of the neutron source and the foil. The source was assumed to be symmetrical and to have a 4.4-mm diameter, as deduced from autoradiographs.

The input spectra used for the STAY'SL analyses were deduced from previous time-of-flight data [6,8] and from previous Be(d,n) irradiations at the University of California at Davis [9]. The spectral unfolding used typically 23 to 26 reactions at each position. These reactions are listed in Table I, along with the energy range containing 90% of the integral activity for each reaction at approximately a 0° neutron source angle. Also given are the percentage deviations between the individual measured and STAY'SL-calculated activation integrals. These deviations should not be viewed as an exact integral test of the dosimetry cross sections, but rather as typical deviations found after spectral adjustment by the code STAY'SL. These results are consistent with the integral testing results from other experiments [3].

The STAY'SL output fluence spectrum was generated in 100 energy groups. Typical results are shown in Fig. 4. Here the calculated Be(d,n) neutron flux is shown as a function of energy for 0°, 30°, and 60°, at a distance of 30 cm from the beryllium target. The solid lines are the calculated spectra, and the dotted lines bracketing the 0° spectrum represent typical one standard deviation uncertainties. It is obvious from Fig. 4 that the change in spectral shape with source angle is very pronounced.

These analyses were then extended to calculate the neutron fluence and energy spectrum profiles in the region occupied by the small irradiation capsule. Here the finite source and foil geometries, plus the capsule offset, were folded in by integrating the calculated angular yields over the foil and source areas. The results are shown in Figs. 5 and 6. Figure 5 shows the calculated two-dimensional fluence contours relative to the beryllium target, for neutron energies above 1 MeV. Contours at source distances less than 6 mm are approximate only, since the effective source thickness was not folded in. Figure 6 shows fluence profiles for several different energy spectrum intervals as a function of radial distance from the source axis, 13.5 mm from the center of the beryllium target. This source distance represents the location of the front face of the irradiation capsule. Both figures demonstrate the rapid change in fluence with position near the source. At these close distances the finite source size also affects the shape of the spectrum. Neutrons from a wide distribution of source angles will intercept any given position, and the neutron energy spectrum at close positions will thus be influenced by the softer (lower energy) neutrons from larger source angles. Because of this a close-up sample can see a softer neutron spectrum near the source than one at the same angle but further away.

The unfolded neutron spectra were also used to calculate displacement damage (in displacements per atom, dpa) and helium generation concentration contours, as shown in Figs. 7 and 8, respectively. These parameters were calculated using the code SPECTER [10]. Comparison of Figs. 7 and 8 with Fig. 5 shows that the dpa and helium gradients are even steeper than the fluence gradients. This follows from the fact that the energy spectrum softens rapidly with angle, as shown in Fig. 4. This is an important consideration when designing an experiment to produce maximum displacement damage or helium generation.

HELIUM GENERATION RESULTS

The helium concentrations measured for the helium accumulation dosimetry ring segments were then used to calculate relative helium generation cross sections. To calculate them, the helium measurements were normalized using the spectrum-integrated fluence profiles, estimated to have ±10% uncertainties. The profiles were integrated over the finite source geometry, for neutron energies above 5 MeV. The results are shown in Fig. 9, where the normalized helium concentrations are plotted as a function of polar angle about the irradiation capsule axis. The ordinate scale is in mb for a spectrum-integrated fluence above 5 MeV. The 5-MeV cutoff was chosen as an approximate energy lower limit for helium generation in these materials. A comparison between the spectrum-integrated fluences for various energy cutoffs is shown in Fig. 6.

Examination of Fig. 9 shows that the normalized helium data for each ring are generally constant with angle, verifying that the capsule offset was determined correctly. The small variations that do exist are attributed to nonuniformities in the assumed circular profile, for example due to the rectangular deuteron beam rastering pattern. Figure 9 also shows that the relative cross sections calculated for each material do vary slightly for the different rings. This is attributed to a softening of the Be(d,n) neutron spectrum with increasing source angle.

The relative cross sections calculated for the different helium dosimetry rings are given in Table II, along with the average source angles subtended by the rings. The range of angles subtended by each ring was due to the small irradiation capsule offset from the source axis. The average values in the last column were calculated ignoring the slight source angle dependence, in order to make a general comparison with relative helium production values determined for other neutron environments. The results, calculated as cross section ratios relative to copper, are shown in Table III.

The Cu, Ni, and Fe helium generation data were also used to compare with cross section information available from the literature. The copper total helium production cross section was taken from ENDF/B-IV [13] and from the calculations of Fu and Perey [14]. The nickel and iron cross sections were estimated from the

calculations of Alsmiller and Barish [15]. These cross sections were used to predict helium production as a function of angle, using the codes STAY'SL and SPECTER, and then integrated over the finite source geometry. The predicted helium generation profiles for Cu, Ni, and Fe are shown in Figs. 10, 11, and 12, respectively, as a function of radial source distance for various capsule sample layers. Also shown in these figures are the measured helium data for the corresponding ring segments. The distribution of points as a function of distance from the source axis for each ring was again produced by the small (1.3 mm) capsule offset. Comparison of the data with the calculated curves shows generally good agreement, considering the incomplete nature of the estimated input cross sections. Figures 10 through 12 demonstrate the potential to integrally test helium generation cross sections for this neutron environment. This will be studied further with updated cross sections.

DISCUSSION

The results described above demonstrate the importance of including comprehensive passive dosimetry in Be(d,n) and Li(d,n) irradiation experiments for which neutron fluence and spectral information is needed. This is very clearly shown by the fact that a capsule offset of only 1.3 mm resulted in a factor of 1.7 variation in fluence ($E_n > 5$ MeV) around the periphery of the irradiation capsule.

It is also recognized that the available irradiation space in Be(d,n) and Li(d,n) test neutron environments will be very limited. Means of reducing the space required by dosimetry materials are thus also being addressed. This is being done by developing a set of dosimetry materials each of which has multiple reactions that are useful for spectral unfolding. In this respect, radiometric dosimetry wires such as Au, Fe, and Ni, with several useful activation cross sections, are also being used for helium accumulation dosimetry measurements following the radiometric counting. The helium accumulation facet is particularly valuable for long irradiations planned for FMIT, because many of the activation reactions have insufficiently long half-lives.

The development and application of passive dosimeters to neutron dosimetry in FMIT will therefore require a knowledge of the energy-dependent cross sections for both the activation and total helium generation reactions for neutrons with energies up to 40-50 MeV.

ACKNOWLEDGEMENTS

The beryllium target used for the Be(d,n) irradiation was supplied by C. M. Logan (LLL). The irradiation was performed with the cooperation of the staff of the Crocker Nuclear Laboratory of

the University of California at Davis, including E. Russell and J. A. Jungerman. The help of J. F. Johnson, M. M. Nakata, B. M. Oliver (Rockwell International), R. R. Heinrich, R. Malewicki, R. Popek (ANL), C. Rowe, S. C. MacLean, and N. Ragaini (LLL) in the preparation and analyses of the irradiation packages is gratefully acknowledged, as are the continued encouragement and support of this work by K. M. Zwilsky, M. M. Cohen, and T. C. Reuther, Jr. (DOE). This work was supported by the U.S. Department of Energy's Materials Irradiation Effects Branch of the Office of Fusion Energy.

REFERENCES

1. C. M. LOGAN, R. BOOTH, and R. A. NICKERSON, "A Compact Beryllium Target for Production of Fast Neutrons," Nucl. Instrum. Methods, 145, 77 (1977).

2. L. R. GREENWOOD, R. R. HEINRICH, R. J. KENNERLEY, and R. MEDRZYCHOWSKI, "Development and Testing of Neutron Dosimetry Techniques for Accelerator-Based Irradiation Facilities," Nucl. Technol., 41, 109 (1978).

3. L. R. GREENWOOD, R. R. HEINRICH, M. J. SALTMARSH, and C. B. FULMER, "Integral Tests of Neutron Activation Cross Sections in a $^{9}Be(d,n)$ Field at E_d = 40 MeV," Nucl. Sci. Eng., 72, 175 (1979).

4. H. FARRAR IV, W. N. McELROY, and E. P. LIPPINCOTT, "Helium Production Cross Section of Boron for Fast-Reactor Neutron Spectra," Nucl. Technol., 25, 305 (1975).

5. See, for example, D. I. GARBER and R. R. KINSEY, "Neutron Cross Sections, Volume II, Curves," BNL 325, Third Edition, Brookhaven National Laboratory (1976).

6. J. P. MEULDERS, P. LELEUX, P. C. MACQ, and C. PIRART, "Fast Neutron Yields and Spectra from Targets of Varying Atomic Number Bombarded with Deuterons from 16 to 50 MeV," Phys. Med. Biol., 20, 235 (1975).

7. F. G. PEREY, "Least Squares Dosimetry Unfolding: The Program STAY'SL," ORNL/TM-6062, Oak Ridge National Laboratory (1977); as modified by L. R. Greenwood, Argonne National Laboratory (1979).

8. M. J. SALTMARSH, C. A. LUDEMAN, C. B. FULMER, and R. C. STYLES, "Characteristics of an Intense Neutron Source Based on the d+Be Reaction," Nucl. Instrum. Methods 145, 81 (1977).

9. D. R. NETHAWAY, R. A. VAN KONYNENBURG, M. W. GUINAN, and L. R. GREENWOOD, "Neutron Spectra from 30-MeV Deuterons on a Thick Beryllium Target," in Symposium on Neutron Cross-Sections from 10 to 40 MeV, BNL-NCS-50681, Brookhaven National Laboratory (1977).

10. L. R. GREENWOOD, Argonne National Laboratory, Private Communication (1979).

11. D. W. KNEFF, B. M. OLIVER, M. M. NAKATA, and H. FARRAR IV, "Helium Generation Cross Sections for Fast Neutrons," this symposium.

12. E. P. LIPPINCOTT, W. N. McELROY, and H. FARRAR IV, "Helium Production in Reactor Materials," in Nuclear Cross Sections and Technology, Vol. I, R. A. Schrack and C. D. Bowman, eds., National Bureau of Standards Special Publication 425, U.S. Department of Commerce, p. 375 (1975).

13. ENDF/B-IV, National Nuclear Data Center, Brookhaven National Laboratory (1974).

14. C. Y. FU and F. G. PEREY, "Calculated Neutron Cross Sections for Cu and Nb Up to 32 MeV for Neutron Damage Analysis," J. Nucl. Mater. 61, 153 (1976).

15. R. G. ALSMILLER, JR., and J. BARISH, "Neutron-Photon Multigroup Cross Sections for Neutron Energies ≤60 MeV," ORNL/TM-6486, Oak Ridge National Laboratory (1978).

TABLE I

Activation Reactions Used for
Be(d,n) Neutron Spectrum Unfolding

Reaction	Energy Range (MeV)	Average Deviation
$^{59}Co(n,\gamma)^{60}Co$	10^{-9} - 1	+4.4%
$^{45}Sc(n,\gamma)^{44m}Sc$	10^{-9} - 1.25	-6.0%
$^{197}Au(n,\gamma)^{198}Au$	10^{-8} - 2.25	+1.6%
$^{235}U(n,f)$	10^{-8} - 21.0	+2.3%
$^{238}U(n,\gamma)^{239}U \rightarrow {}^{239}Nb$	10^{-7} - 3	+0.3%
$^{115}In(n,n')^{115m}In$	1.25 - 16.0	-12.5%
$^{238}U(n,f)$	2.0 - 24.0	+4.3%
$^{58}Ni(n,p)^{58}Co$	3.0 - 18.5	+3.2%
$^{59}Co(n,p)^{59}Fe$	7.0 - 21.0	-4.4%
$^{60}Ni(n,p)^{60}Co$	7.5 - 19.5	+2.9%
$^{238}U(n,2n)^{237}U$	7.5 - 15.0	+17.0%
$^{27}Al(n,\alpha)^{24}Na$	8.5 - 18.5	-2.4%
$^{48}Ti(n,p)^{48}Sc$	9.5 - 22.0	+2.9%
$^{169}Tm(n,2n)^{168}Tm$	10.0 - 19.5	-4.3%
$^{197}Au(n,2n)^{196}Au$	10.0 - 20.0	+4.1%
$^{93}Nb(n,2n)^{92m}Nb$	10.5 - 20.0	-6.6%
$^{59}Co(n,2n)^{58}Co$	12.0 - 23.0	+5.6%
$^{45}Sc(n,2n)^{44m}Sc$	13.0 - 24.0	+0.1%
$^{89}Y(n,2n)^{88}Y$	13.0 - 24.0	+1.3%
$^{90}Zr(n,2n)^{89}Zr$	13.0 - 24.0	-1.3%
$^{58}Ni(n,2n)^{57}Ni$	14.0 - 25.0	-8.6%
$^{197}Au(n,3n)^{195}Au$	17.0 - 26.0	-8.2%
$^{169}Tm(n,3n)^{167}Tm$	17.0 - 26.0	+3.2%
$^{59}Co(n,3n)^{57}Co$	21.0 - 29.0	+0.3%
$^{89}Y(n,3n)^{87}Y$	23.0 - 31.0	+3.8%
$^{197}Au(n,4n)^{194}Au$	25.0 - 32.0	-13.6%

TABLE II

Relative Helium Generation Cross Sections for Be(d,n) Neutrons (E_d = 30 MeV)

Dosimetry Ring	Source Distance (mm)	Source Angle		Relative Cross Section[a]	
		Range	Average	Ring[b]	Average
Al-1	16.5	3.9^o-12.9^o	8.6^o	123 ± 2	
Al-2	17.9	10.1^o-17.1^o	14.2^o	116 ± 3	120
Fe-1	16.5	15.5^o-23.3^o	19.5^o	39.8 ± 1.1	
Fe-2	17.9	3.2^o-11.1^o	7.8^o	43.5 ± 1.2	42
Ni-1	15.1	22.3^o-30.1^o	26.6^o	97 ± 3	
Ni-2	17.9	6.5^o-14.2^o	10.6^o	101 ± 2	99
Cu-1	16.4	19.8^o-27.1^o	23.8^o	39.2 ± 0.8	
Cu-2	17.8	12.5^o-20.0^o	16.6^o	41.4 ± 1.1	
Cu-3	17.8	1.4^o-7.9^o	5.2^o	45.3 ± 0.9	42
Au-1	15.1	5.2^o-15.3^o	10.7^o	1.26 ± 0.08	
Au-2	21.0	17.6^o-23.6^o	21.2^o	1.16 ± 0.08	1.2

[a]Cross section in mb for a spectrum-integrated fluence above 5 MeV.

[b]Quoted uncertainties are relative uncertainties based on source angle variation and data scatter due to helium measurements and map nonuniformities.

TABLE III

Relative Spectrum-Integrated Helium Generation Cross Sections for Pure-Element Helium Accumulation Dosimetry Materials

Element	Cross Section Relative to Copper		
	Be(d,n) E_d = 30 MeV	T(d,n) RTNS-I[a]	EBR-II Core[b]
Cu	1	1	1
Al	2.9	2.84	1.87
Fe	1.0	0.94	0.99
Ni	2.4	1.96	13.2
Au	0.03	0.01	0.04

[a] D. W. KNEFF, B. M. OLIVER, M. M. NAKATA, and H. FARRAR IV, Ref. 11.

[b] E. P. LIPPINCOTT, W. N. McELROY, and H. FARRAR IV, Ref. 12.

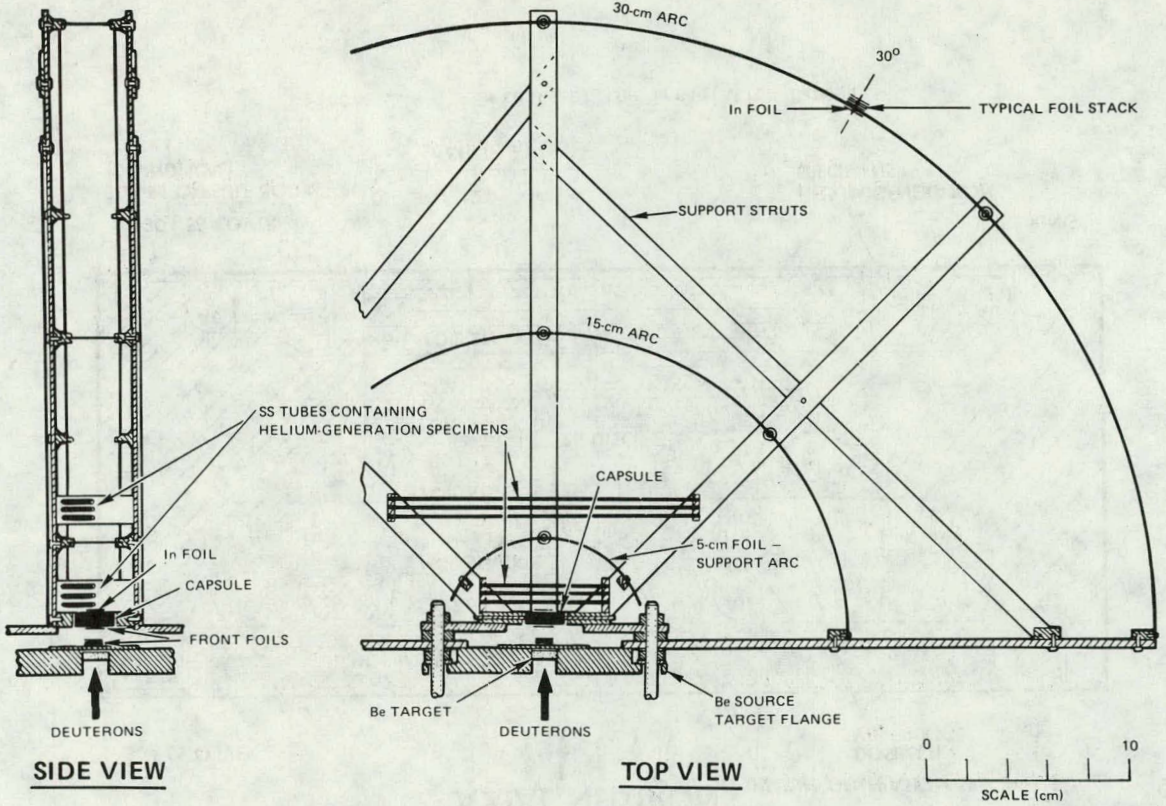

Figure 1. Be(d,n) Irradiation Assembly

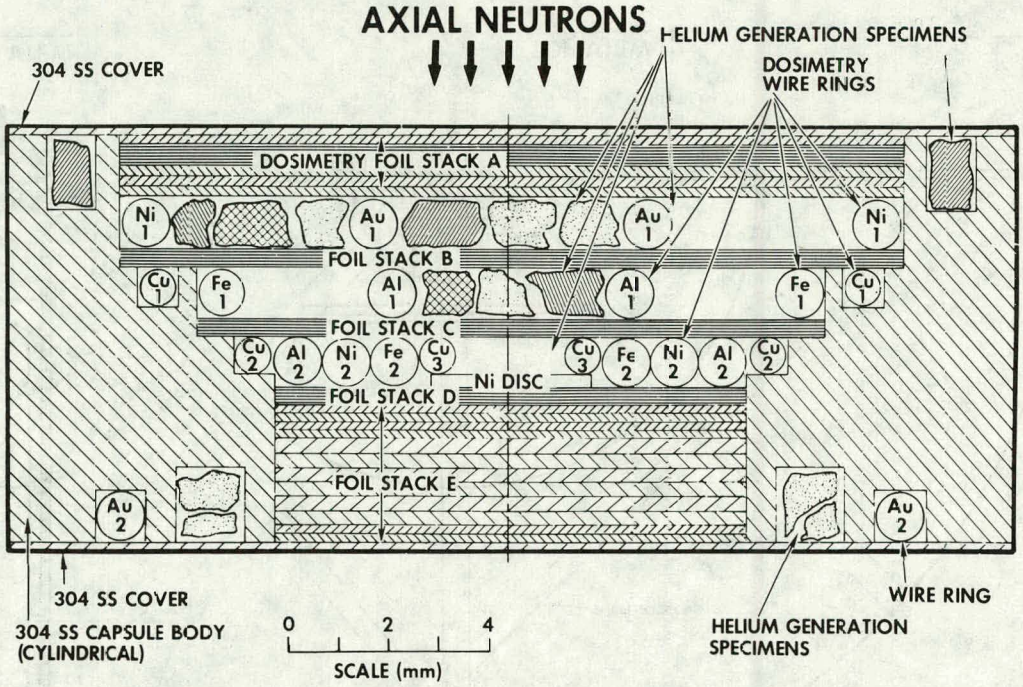

Figure 2. Details of the Irradiation Capsule

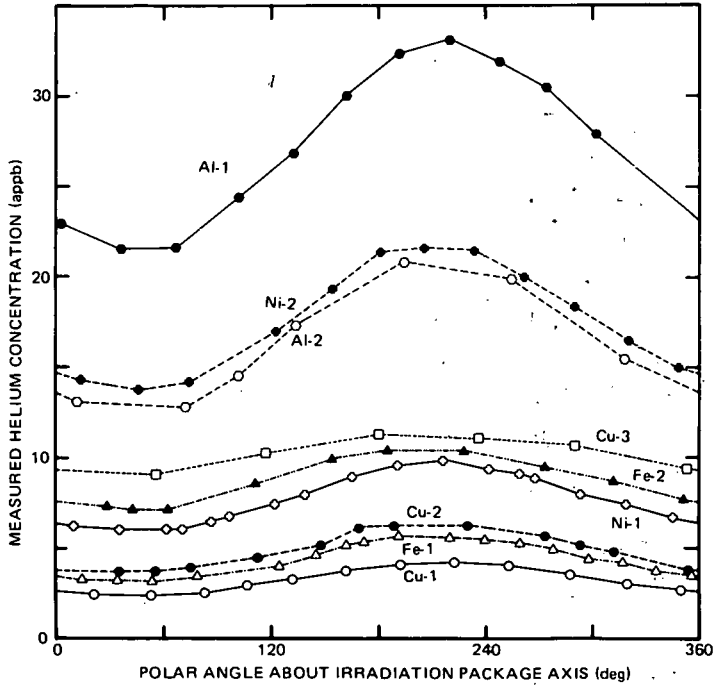

Figure 3. Measured Helium Generation Concentrations in the Irradiation Capsule Pure Element Ring Segments

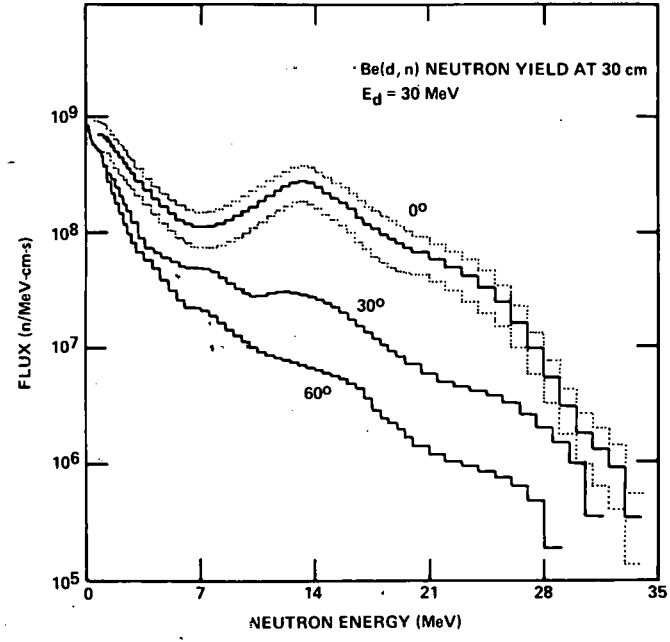

Figure 4. Be(d,n) Neutron Energy Spectra for 0^{o}, 30^{o}, and 60^{o}, 30 cm from the Beryllium Target

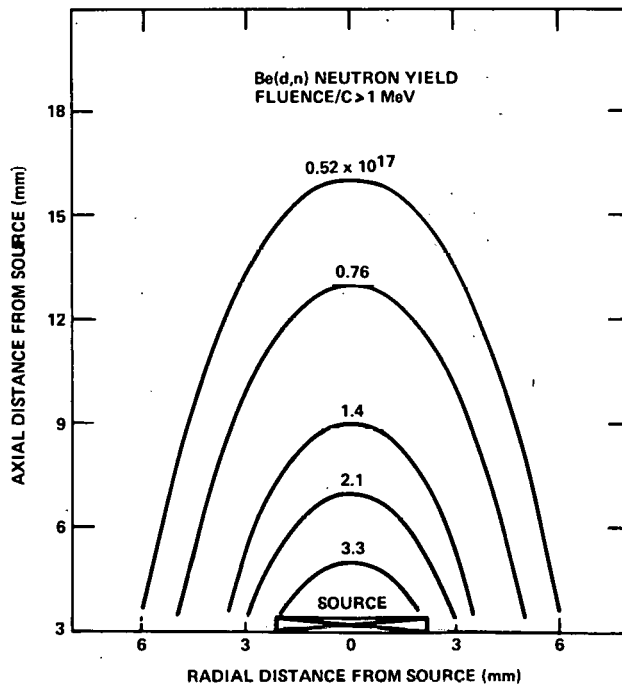

Figure 5. Fluence Contours ($E_n > 1$ MeV) Near the Be(d,n) Neutron Source

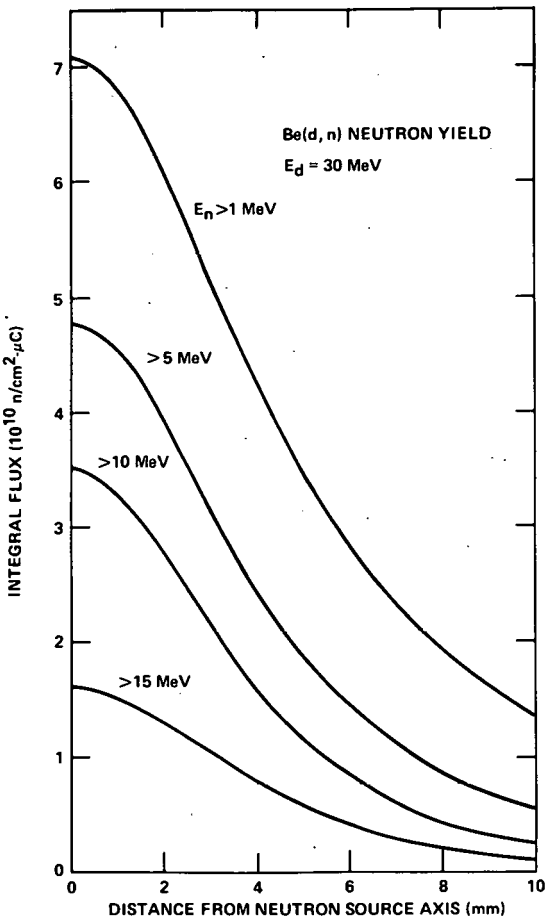

Figure 6. Fluence Profiles as a Function of Radial Distance from the Be(d,n) Source Axis, 13.5 mm from the Source Center

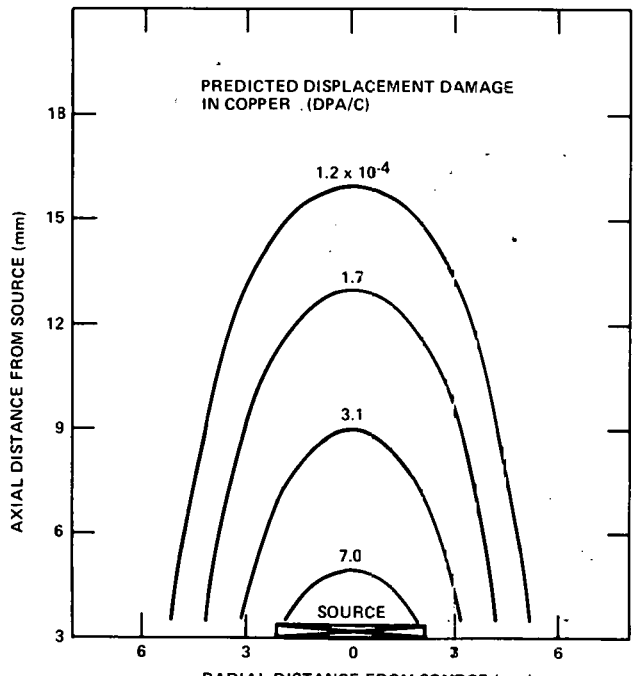

Figure 7. Predicted Displacement-per-Atom Contours for Copper near the Be(d,n) Neutron Source

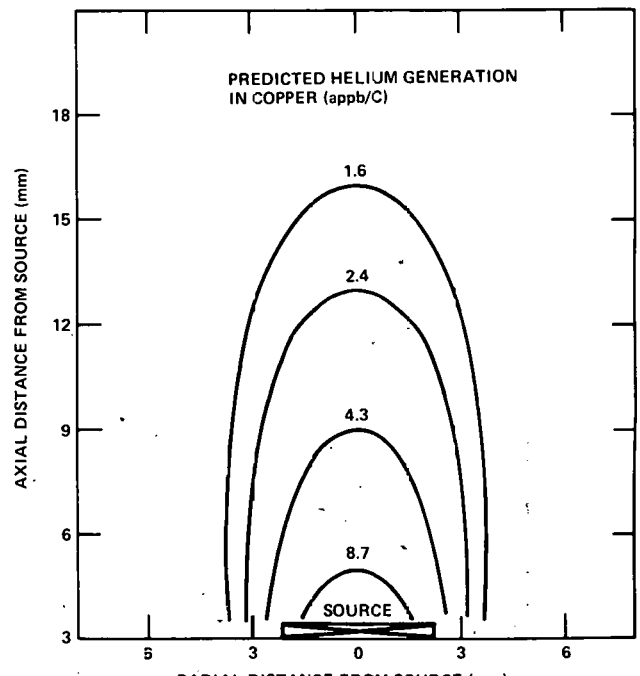

Figure 8. Predicted Helium Production Contours for Copper Near the Be(d,n) Neutron Source

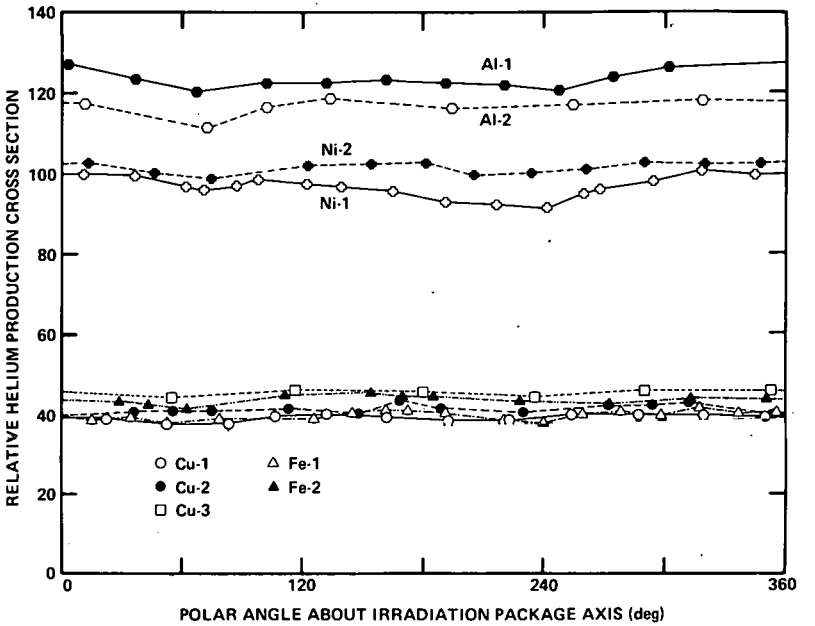

Figure 9. Relative Helium Production Cross Sections for the Irradiation Capsule Pure Element Ring Segments. The Ordinate Is in mb for a Spectrum-Integrated Fluence above 5 MeV

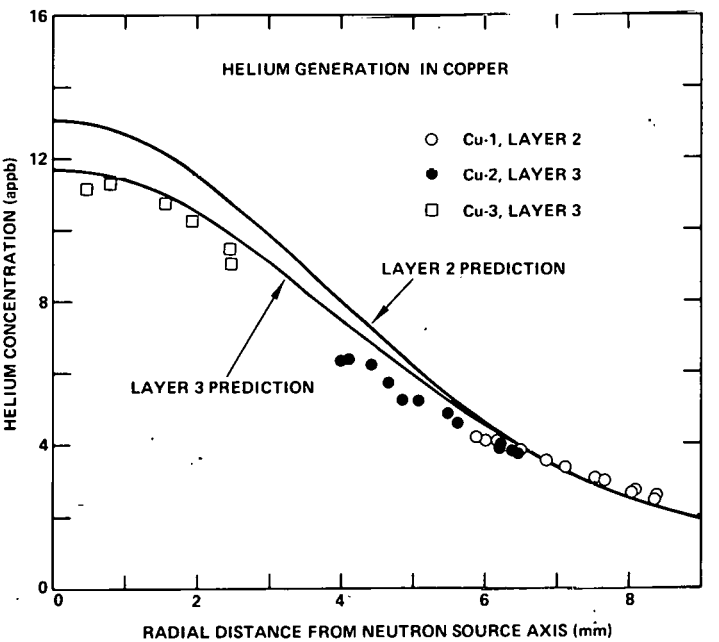

Figure 10. ENDF/B-IV-Predicted and Measured Helium Generation Concentrations in Copper within the Irradiation Capsule

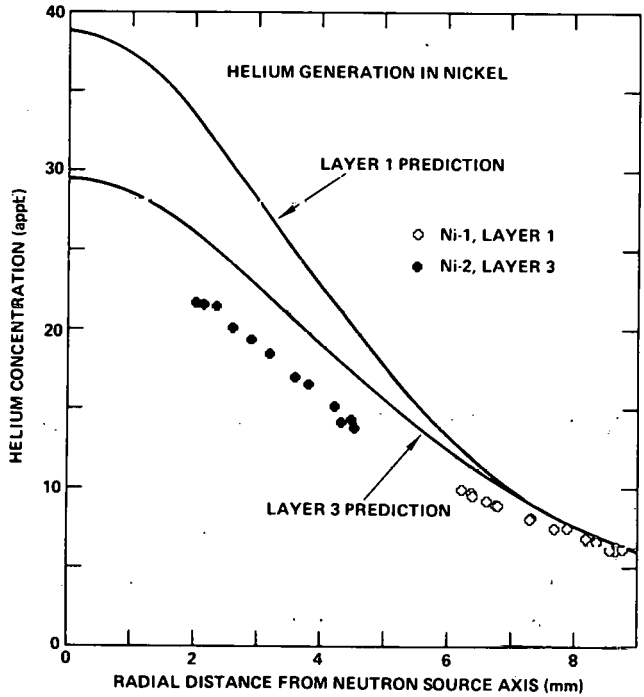

Figure 11. ENDF/B-IV-Predicted and Measured Helium Generation Concentrations in Nickel within the Irradiation Capsule

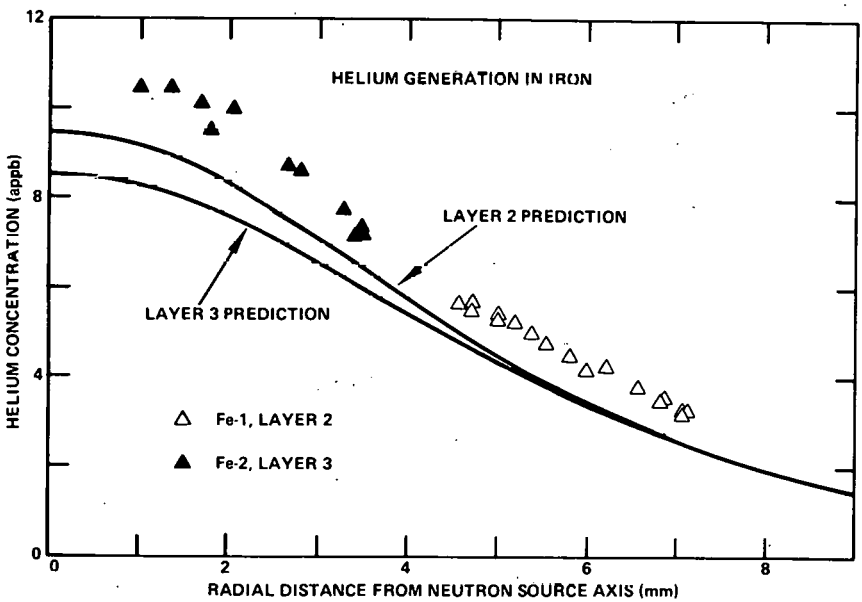

Figure 12. ENDF/B-IV-Predicted and Measured Helium Generation Concentrations in Iron within the Irradiation Capsule

FISSION REACTION IN HIGH ENERGY PROTON CASCADE

H. Takahashi

Brookhaven National Laboratory
Upton, New York 11973, U.S.A.

ABSTRACT

Fission reactions are incorporated in the intranuclear cascade code NMTC to calculate the neutron yield from the high energy nucleon-nucleus collision. It is assumed that the fission reaction occurs in competition with the evaporation reaction after the spallation reaction. The branching ratio of fission reaction to neutron evaporation reaction is calculated by using the Vandenbosch and Huizenga formula and the distribution of fission product nuclei is calculated using Fong's statistical model. Although the most general distribution for fission product nuclei is a function of their excitation energies, mass numbers, charge numbers, kinetic energies, deformation energies and spin states, a simplification of the model using the most probable kinetic energies and deformation energy has been implemented for determination of the mass and charge distributions.

The mass distributions of the post-evaporation nuclei calculated by Fong's mass formula has peaks which are closer to experimental results than the distribution used in Janecke, Garvey and Kelson's (JGK) mass formula. The mass distribution calculated by the mass formula in the NMTC code is very close to the one calculated with the JGK mass formula. In contrast to the flat plateau of mass distribution shown in the experimental results of Stevenson for 300 MeV protons on U^{238} nuclei, the three calculations show the dip between two peaks. The total number of the neutrons emitted by fission products which are calculated by Fong, JGK and NMTC mass formulae are, respectively, 12.25, 12.83 and 12.80 reaction.

INTRODUCTION

For the study of the feasibility of nuclear fuel breeding [1, 2] and in designing a high intensity spallation neutron source [3] using neutrons produced by high energy protons, it is required to calculate the intra-nuclear cascade process for fissionable nuclei. This calculation has been carried out by using the codes NMTC [4] and HETC [5]. However, these codes do not include the fission process in high energy reactions and the neutron yield estimate is smaller than the experimental value.

Incorporation of the fission reaction into the intra-nuclear cascade code was studied by H. Hahn and H. Bertini [6], but they did not calculate particle evaporation following the fission. Thus, their resulting neutron yield is too small. On the other hand, intensive studies on neutron yield from uranium had been performed by V. Barashenkov, D. Toneyev et al. [7,8]. This study resulted in a substantial increase in the calculated neutron yield.

Recently, for design studies of high intensity spallation neutron sources, the incorporation of fission reactions in the intra-nuclear cascade code has been revived by Alsmiller et al. [9], Atchinson [10] and the present author [11]. The methods used are statistical models. Alsmiller et al. put much more reliance on empirically derived constants. The present author's formula is very close to Fong's formula for the statistical fission model [12] and does not rely on the experimental data.

Competition Process of Fission to Evaporation

In the intra-nuclear cascade model, nonelastic collisions of the nucleon and pion with a nucleus are assumed to be composed of a two-step process of spallation followed by an evaporation reaction. In the first step, the cascade nucleon and pion are emitted and leave an excited residual nucleus. In the second step, this excited nucleus loses its energy by evaporating particles. When the excited nucleus has a sufficiently large mass number, the fission process will compete with the evaporation process. This competition process had been studied by I. Dostrovski et al. [13], R. Hahn and H. Bertini [6] and R. Vandenbosch and J. Huizenga [14].

The probability of fission in competition with neutron evaporation is expressed by

$$P_f = \left(1 + \frac{\Gamma_n}{\Gamma_f}\right)^{-1} \tag{1}$$

where Γ_f and Γ_n are, respectively, widths for fission and neutron emission reactions. The probability that the fission event occurs after emitting i neutrons is expressed by

$$(P_n)^i P_f = (1 - P_f)^i P_f \tag{2}$$

In our calculation, the formula obtained by R. Vandenbosch and J. Huizenga for the branching ratio Γ_n/Γ_f is used. This is expressed as follows for the actinide region $z \geq 90$:

$$\log \frac{\Gamma_n}{\Gamma_f} = \phi(z)\, A + \psi(z) \tag{3}$$

where A is the mass number of the fissioning nucleus, and the tabulated values of $\phi(z)$ and $\psi(z)$ [10] as functions of charge number are used in our calculation. For the subactinide region, $z < 90$, F. Atchinson [10] had made a statistical model fit to experimental data and estimated the fission probability given z, A, E* (excitation energy), and the mass difference table. His expression for subactinide fission for nucleus z, A and excitation energy E* is

$$\Gamma_n = 0.3518099(1.68I_o + 1.93A^{1/3}I_1 + A^{2/3}(0.76I_1 - 0.05I_o)) \tag{4}$$

$$I_o = \frac{4.0}{a_n}\left[(S_n - 1.0)\cdot e^{S_n} + 1.0\right] \tag{5}$$

$$I_i = \frac{2.0}{a_n^2}\left[(6.0 - 6.0S_n + 2.0S_n^2)\, e^{S_n} + S_n^2 - 6.0\right] \tag{6}$$

$$S_n = 2.0\sqrt{a_n(E^* - BE')} \tag{7}$$

$$a_n = (A - 1.0)/8.0 \tag{8}$$

BE' = Separation energy - pairing energy

$$\Gamma_f = \left\{(S_f - 1.0)\, e^{S_f} + 1.0\right\}/a_f \tag{9}$$

$$S_f = 2.0\sqrt{a_f(E^* - E_f')} \tag{10}$$

$$E_f' = BE' + 321.175 - 16.70314\frac{Z^2}{A} + 0.2185024\left(\frac{Z^2}{A}\right)^2 \tag{11}$$

$$\frac{a_f}{a_n} = 1.089257 + 0.01097897\cdot\left(\frac{Z^2}{A} - 31.08551\right)^2 \tag{12}$$

Statistical Model for Fission Product Nuclei Distribution

As a calculational model for the distribution function of fission product nuclei, Fong's statistical model [12] is used. In the statistical model, it is assumed that the fission process is so

slow that an instantaneous equilibrium state will be established at every moment of the process. Thus, the relative probability of occurrence of a fission mode is determined from the instantaneous equilibrium at the moment just before the two fragments separate from each other. The probability is calculated from the density of quantum states of the different nuclei configuration at the moment just before scission.

In a fission mode in which fission product fragments (A_1,z_1) and (A_2,z_2) are formed, the probability of this mode to occur with a given set of C (the mutual coulomb energy of a fission pair at the moment just before scission), k (the total translational energy of the same), D (the total deformation of two fission fragments), and E (the total energy available to the compound system G minus k), with a given partition of excitation energy E_1,E_2, and with given angular momenta j_1 and j_2 for the two fragments (assuming j=0 and no orbital angular momentum) is expressed as

$$N(A_1,A_2,Z_1,Z_2,C,D,k,E,E_1,j_1,j_2)$$

$$= c_1c_2(2j_1+1)(2j_2+1)\exp\left[\frac{-(j_1+\frac{1}{2})^2}{2g_1T_1} - \frac{(j_2+\frac{1}{2})^2}{2g_2T_2}\right]$$

$$\cdot \frac{4\pi V}{k^3}\sqrt{2\mu^3 k}\,\exp\left[2\sqrt{a_1E_1} + 2\sqrt{a_2(E-E_1)}\right]dE_1\cdot dk \qquad (13)$$

where c is a parameter which depends on A as

$$c = 0.38\ e^{-0.005A} \qquad (14)$$

g, T and μ are given as

$$g = \frac{2}{5}\frac{MR^2}{\hbar^2} \sim A^{5/3} \qquad (15)$$

(M and R are mass and radius of nucleus, respectively)

$$T = \sqrt{E/a} \qquad (16)$$

$$\mu = \frac{m_1 m_2}{m_1+m_2} \sim \frac{A_1 A_2}{A_1+A_2}\ , \qquad (17)$$

and V is the volume of space in which the translational energy of pair (k) is normalized.

Incorporation of this most general distribution function of fission products into the intra-nuclear cascade code causes the calculation to be very time consuming; thus, a distribution function of a few variables is used to obtain a partition of important variables like mass and charge numbers A and z. The summation of j and the integration of k in Eq. (13) are carried out. The distribution

function of partition masses A_1 and A_2 is obtained by using the most probable value for the other variables as

$$N(A_1,A_2) \sim c_1 c_2 \frac{(a_1\ a_2)^{1/2}}{(a_1+a_2)^{13/4}} \left(\frac{A_1^{5/3}\ A_2^{5/3}}{A_1^{5/3}+A_2^{5/3}}\right)^{3/2} \left(\frac{A_1\ A_2}{A_1+A_2}\right)^{3/2}$$

$$\frac{(z_{p_1}\ z_{p_2})^{1/2}}{(B_{A_1}+B_{A_2}-c_{12})^{1/2}} \cdot E^{11/4} \left(1 - \frac{5}{2}\frac{1}{\sqrt{(a_1+a_2)E}}\right) e^{2\sqrt{(a_1+a_2)E}} \qquad (18)$$

where E is to be calculated for the mode of most probable charge division $z_{p_1} : z_{p_2}$ and most probable kinetic energy release and deformation energy for the given mass division A_1, A_2.

In Eq. (18)

$$z_p = \frac{B_{A_1} z_{A_1} - B_{A_2} z_{A_2} + z(B_{A_2} - \frac{1}{2} c_{12})}{B_{A_1} + B_{A_2} - c_{12}} \qquad (19)$$

$$z_{p_2} = z - z_{p_1} \qquad (20)$$

$$B_A = 0.041505/z_A \qquad (21)$$

$$z_A = A/(1.980670 + 0.0149624A^{2/3}) \qquad (22)$$

c_{12} in Eqs. (18) and (19) is a constant with respect to charge division as follows:

$$K = c_{12}\ z_1\ z_2 \qquad (23)$$

The excitation energy E is expressed by

$$E = M^*(A,z) - M^C(A_1,z_1) - M^C(A_2,z_2) - K - D \qquad (24)$$

and in Fong's formulation, $M^C(A,z)$ is expressed by

$$M^C(A,z) = M_A + \Delta M_A + B_A(z-z_A-\Delta z_A)^2 + 0.036/A^{3/4} \qquad (25)$$

where

$$M_A = 1.0146A + 0.014A^{2/3} - 0.041905z_A \qquad (26)$$

and the correction curves Δz_A and ΔM_A, which are defined, respectively, by $z_A(\text{exp}) - z_A(\text{theo})$ and $\Delta M_A(\text{exp}) - M$ (liquid drop model), are shown in Fong's paper.

The total fission fragment kinetic energy K in Eq. (24) is expressed by

$$K = c + k \tag{27}$$

where c is coulomb repulsion energy of fission fragment at the moment of scission point, and the value of k turns out to be very small (about 0.5 MeV) compared with c, so that it can be neglected in the calculation. The coulomb repulsion energy for fission fragments which have deformation parameters, respectively, of α_{31} and α_{32} is expressed by

$$c(\alpha_{31},\alpha_{32}) = z_1 z_2 e^2 \Big[r_{01}(1 + \alpha_{31}(1 - \tfrac{3}{7}\eta_1^2)) + r_{02}(1 + \alpha_{32}(1 - \tfrac{3}{7}\eta_2^2)) \Big]^{-1} \tag{28}$$

where

$$r_0 = 1.5 \times 10^{-13} A^{1/3} \tag{29}$$

$$\eta_1 = \eta_2 = 0.4 \tag{30}$$

The total deformation energy of the fission fragments is

$$D = D_1(\alpha_{31}) + D_2(\alpha_{32}) \tag{31}$$

where

$$D_i(\alpha_{3i}) = 0.7143\, \alpha_{3i}^2\, E_{si}^0 - 0.2041\, \alpha_{3i}^2\, E_{ci}^0 \qquad i = 1,2 \tag{32}$$

$$E_s^0 = 0.014\, A^{2/3} \text{ (AMU)} \tag{33}$$

$$E_c^0 = 0.000627\, z^2/A^{1/3} \text{ (AMU)} \tag{34}$$

In this calculation, the most probable combination of deformation parameters, α_{31} and α_{32}, is determined by minimizing $D_1(\alpha_{31}) + D_2(\alpha_{32})$. Their values are calculated by minimizing the value of $C(\alpha_{31},\alpha_{32}) + D_1(\alpha_{31}) + D_2(\alpha_{32})$. After determining the partition of mass numbers A_1 and A_2 according to Eq. (18), the partition of charge numbers of z_1 and z_2 is calculated by using the distribution function of

$$N(z_1,z_2) \sim (z_1,z_2)^{1/2}\left(1 - \frac{5}{4}\frac{1}{\sqrt{(a_1+a_2)E}}\right) E^{5/2}\, e^{2\sqrt{(a_1+a_2)E}} \tag{35}$$

The distribution functions for the total fission fragment kinetic energy K and deformation energy D are not taken into account; instead these values are represented by their most probable ones. The total excitation energy is partitioned between the two fission

fragments with the assumption of equal nuclear temperature

$$E_1 : E_2 = (a_1T^2) : (a_2T^2) = a_1 : a_2 = A_1 : A_2 \qquad (36)$$

Thus, the excitation energy of fragments (A_1,z_1) in the state far from scission point is expressed by

$$E_i = \frac{A_i}{A_1+A_2} E + D_i \qquad (37)$$

The nucleus loses its excitation energy by evaporating particles.

By using the formula described above, the mass distribution of the pre- and post-evaporation fission products and the number of neutrons emitted will be calculated after obtaining the distribution of compound excited nuclei which go into the fission reaction. This distribution is calculated by the Monte Carlo intra-nuclear cascade code NMTC [4], and the branching ratio of fission to evaporation reactions. In the calculation of distribution of pre-evaporation fission products, the following three mass formulae are used. The first one is Fong's mass formula [12] based on the liquid drop model and expressed in Eq. (25). The second one is the mass formula used in the NMTC [4] and HETC [5] codes. This is based on A. Wapstra [15], J. Huizenga [16] and J. Mattauch et al.'s formula[17]. The third is the formula obtained by J. Janecke, G. Garvey and I. Kelson (JGK) [18].

Results and Discussion

In Figure 1, the distributions of pre-evaporation nuclei mass from the various excited Pu^{239} compound states calculated are shown. In this calculation, Fong's mass formula is used. The excitation energies of compound states are proton energy (E_p) plus the binding energy (B.E.) of proton in Pu^{239}. As the excitation energy increases, the valley of distribution becomes shallow and the two peaks are lowered. The peak of distribution on the heavy mass side is located at A=141. When the mass formulae of NMTC and JGK are used, the peaks appear at around A=132 instead of 141.

Figure 2 shows the distributions of pre- and post-evaporation fission product nuclei in the Pu^{239} compound states with their excitation energies of proton energy E_p + (B.E.). Cases for E_p=10 MeV and 70 MeV are shown. Since more particles are evaporated from the higher excited state than the lower excited state, the distribution of post-evaporation nuclei in the case of E_p=70 MeV is shifted more than the one of E_p=10 MeV toward the direction of light mass. The fission product nuclei with heavy mass are shifted more than those with light mass.

In Figure 3, the distribution of post-evaporation fission products from 300 MeV protons on U^{238} calculated by three mass formulae (Fong [12], NMTC [4] and JGK [18])are shown with the results of P. Stevenson's experiment [19]. In contrast to the rather flat

plateau of experimental results, all three calculations show the dip between two peaks. The reason for this discrepancy should be clarified in future study. One of the reasons may be due to the fluctuation in excitation energy partition between the two fragments and to not taking into account the distribution functions for the kinetic and deformation energies. The distributions calculated with the mass formula of NMTC and JGK show a shorter distance between the two peaks than the one calculated with Fong's mass formula and the experiment. Recently, M. Prakash et al. [20] stated that this discrepancy can be removed by taking into account the nucleon exchange process which occurs during the fission process, similar to what is observed in heavy ion reaction.

Figure 4 shows the distribution of the number of neutrons emitted by fission product nuclei as a function of mass number. These results are calculated by the mass formulae of Fong and of JGK. Since the mass formula for nuclei of light mass is not obtained from Fong's mass formula, the JGK mass formula is used for the mass, which is required to calculate the energy difference between pre- and post-evaporation nuclei in the case of Fong's mass formula. Thus, only the effect of different distributions of pre-evaporation fission product nuclei on the neutron yield is studied. The difference between the two distributions is smaller in the light mass region than in the heavy mass region, and the number of neutrons calculated with Fong's mass formula is slightly smaller than that calculated with the JGK mass formula.

As seen in the figure, the heavy mass fission product nuclei emit more neutrons than those of light mass, causing a larger shift in the distribution of heavy mass nuclei than those of light mass. This is due to the larger excitation energy of the heavy mass nuclei than of the light mass nuclei, as shown in Eq. (37). The experimental data of E. Chiefetz et al. [21] for 155 MeV protons on U^{238} show the same tendency. The central peak appearing in the calculation is due to the fact that some even mass number nuclei are split into equal mass fission products, and they contribute to the increase of this peak.

The total number of neutrons emitted by fission products with distributions calculated by Fong, JGK and NMTC mass formulae are 12.25, 12.83 and 12.80, respectively. The differences between the total number calculated by the JGK and the NMTC mass formulae and that calculated by Fong's mass formula are not very large in spite of the large difference in distributions of fission product nuclei mass. Thus, the total neutron yield seems to be insensitive to the mass distribution.

The difference between all the results obtained by NMTC and JGK mass formulae is very small, since the mass values calculated by two formulae are very close to each other.

In Figure 5, the distributions of the number of neutrons emitted multiplied by the yield of pre-evaporation fission product nuclei are shown for the two mass formulae of Fong and JGK. The heavy mass peak is higher than the light mass peak because more neutrons are emitted from the heavy mass fission product nuclei

than from the light mass nuclei.

Although the total neutron yield from the fission reaction is insensitive to the distribution of pre-evaporation fission product nuclei mass, the discrepancy between the calculated and experimental mass distributions for the post-evaporation fission product nuclei should be clarified in future study. More experimental data are needed to improve the model.

ACKNOWLEDGMENTS

The author would like to express his appreciation to Drs. F. Atchinson, F. Alsmiller and Y. Nakahara for their valuable discussions. This work was performed under the auspices of the U.S. Department of Energy.

REFERENCES

1. Proceedings of an Information Meeting on Accelerator Breeding, Brookhaven National Laboratory, June 18-19, 1977, NTIS CONF-770107.

2. H. TAKAHASHI et al., "Nuclear Fuel Breeding by Using Spallation and Muon Catalysis Fusion Reaction," 2nd Int. Conf. on Emerging Nuclear Energy, Lausanne, Switzerland, April 8-11, 1980.

3. J. M. CARPENTER, Nucl. Instr. Methods, 145, 133 (1977).

4. Radiation Shielding Information Center, ORNL, "NMTC Monte Carlo Nucleon Meson Transport Code System," CCC-161.

5. Radiation Shielding Information Center, ORNL, "Monte Carlo High-Energy Nucleon Meson Transport Code," CCC-178.

6. R. L. HAHN and H. W. BERTINI, Phys. Rev. C 6, 660 (1972).

7. V. S. BARASHENKOV and V. D. TONEYEV, Atomnaya Energiya 35, 163 (1973).

8. V. S. BARASHENKOV and S. E. CHIGRINOV, Atomnaya Energiya 37, 480 (1974).

9. F. ALSMILLER et al., Bull. of Amer. Phys. Soc., 24, 874 (1974).

10. F. ATCHINSON, "High Energy Fission in HETC", Private Communication.

11. H. TAKAHASHI and Y. NAKAHARA, Bull. of Amer. Phys. Soc., 24, 874 (1979).

12. P. FONG, Statistical Theory of Nuclear Fission, Gordon and Breach Science Publisher, New York, N. Y. (1969).

13. I. DOSTROVSKY, Z. FRAENKEL and P. RABINOWITZ, "A Monte Carlo Calculation of Fission-Spallation Competition," Proc. 2nd UN Inter. Conf., P/1615, 15, 301 (1958).

14. R. VANDENBOSCH and J. R. HUIZENGA, "Nuclear Fission Process," Proc. 2nd UN Inter. Conf., P/688, 15, 284 (1958).

15. A. M. WAPSTRA, Physica 21, 367, 385 (1955).

16. J. R. HUIZENGA, Physica 21, 410 (1955).

17. J.H.E. MATTAUCH, W. THIELE and A. M. WAPSTRA, Nucl. Phys. 67, 1 (1965).

18. J. JANECKE, Atomic Data and Nuclear Data Table 17, 455 (1976).

19. P. C. STEVENSON et al., Phys. Rev. 111, 886 (1958).

20. M. PRAKASH, V. S. RAMAMURTHY and S. S. KAPOOR, "Studies in the Statistical Theory of Nuclear Fission and Explanation of Fragment Mass Symmetry in Terms of Nuclear Exchange Mechanism," Int. Symp. on Phys. & Chem. of Fission, Jülich, FRG, May 14-18, 1979, IAEA-SM-241/F-19.

21. E. CHIEFETZ et al., Phys. Rev. C 2, 256 (1970).

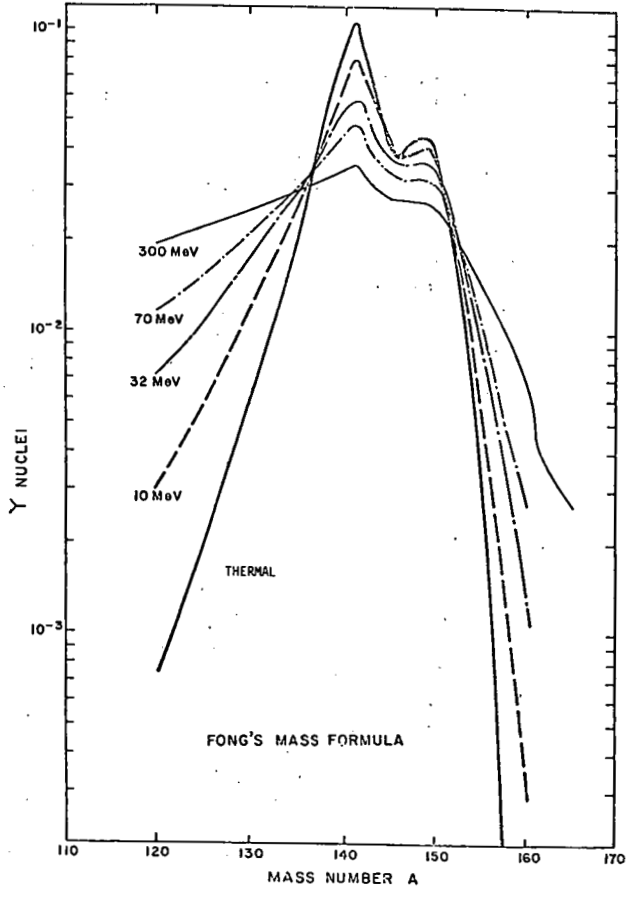

FIGURE 1. Pre-Evaporation Nuclei Distribution from the Highly Excited Pu^{239} Compound State

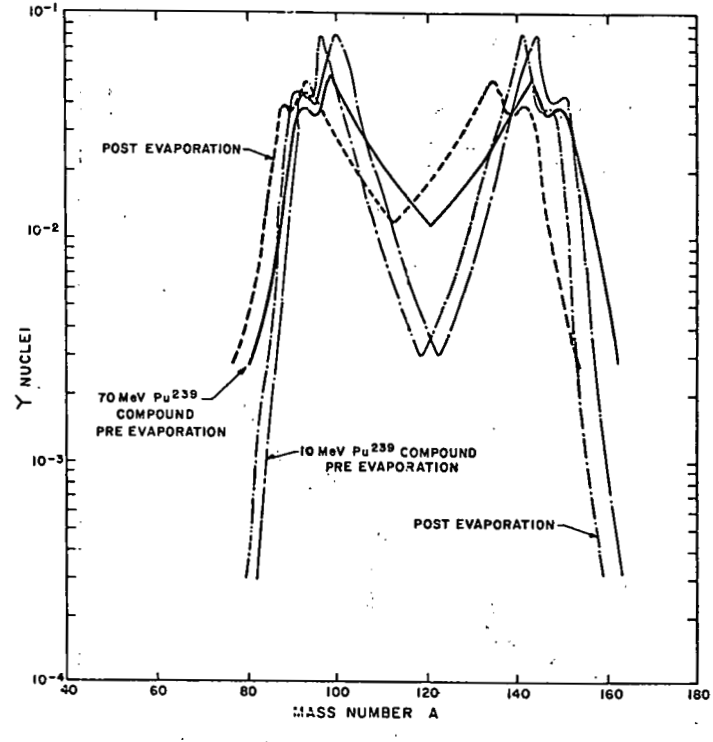

FIGURE 2. Pre- and Post-Evaporation Nuclei Distribution from the Highly Excited Pu^{239} Compound State

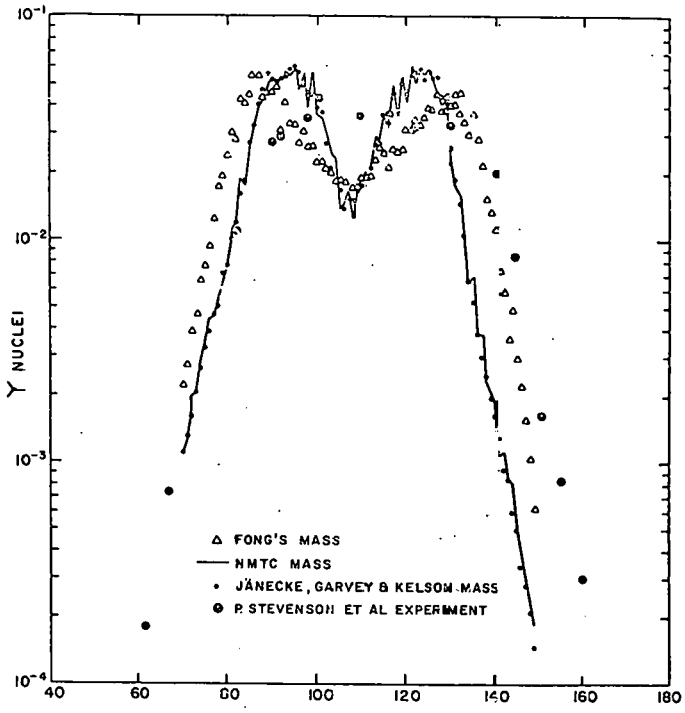

FIGURE 3. Post-Evaporation Nuclei Distribution from 300 Proton on U^{238}

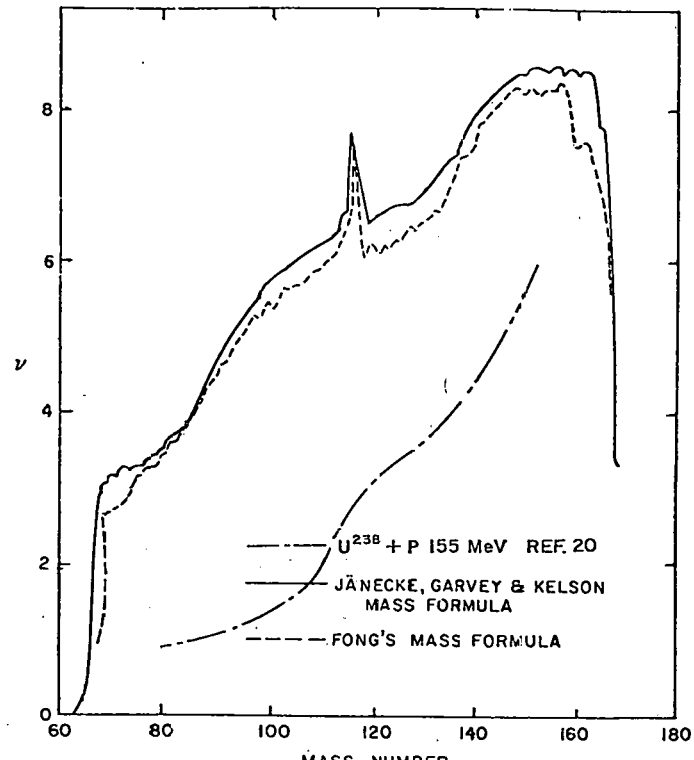

FIGURE 4. Number of Neutrons Emitted from Fission Product Nuclei 300 MeV Proton on U^{238}

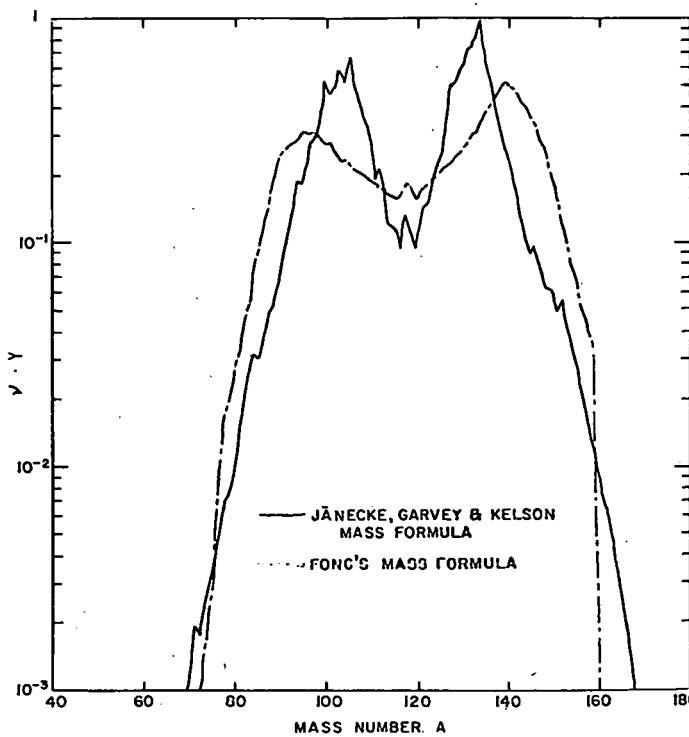

FIGURE 5. Distribution for Number of Neutron Multiplied by Yield of Pre-Evaporation Fission Product Nuclei

THIS PAGE
WAS INTENTIONALLY
LEFT BLANK

LOW ENERGY NEUTRON EMISSION FROM ^{9}Be(d,n) AND ^{9}Be(p,n) REACTIONS

M.A. Lone
Atomic Energy of Canada Limited
Chalk River Nuclear Laboratories
Chalk River, Ontario, Canada K0J 1J0

AND

B.C. Robertson
Queen's University, Kingston, Ontario, Canada

ABSTRACT

Neutron sources based on Be+d reactions at $E_d \geq 16$ MeV and Be+p reactions at $E_p \geq 30$ MeV are commonly used for cancer therapy. The neutron spectral distributions from these reactions show significant yield at neutron energies below 2 MeV. The relative proportion of these low energy neutrons at E =10, 15, 20 and 25 MeV is 33, 28, 21 and 15% for deuterons and 70, 62, 52 and 40% for protons respectively. Several nuclear reaction mechanisms, e.g. compound nucleus decay and multi-body breakup have been discussed as possible sources of the low-energy neutron component. The systematic studies carried out by us indicate that the neutron decay of states in Be excited by direct inelastic reactions also plays a significant role in producing low energy neutrons particularly from the Be+p reaction.

INTRODUCTION

Nuclear reactions Be(p,x)n and Be(d,x)n are used for production of intense beams of neutrons for cancer therapy and for irradiations in material damage studies. These applications often require knowledge of thick target neutron yields under various geometrical conditions. An understanding of the neutron-producing mechanism in these reactions is useful for calculation[1] of the relevant neutron fluences.

OBSERVATIONS

At proton energies above 20 MeV the neutron production from the Be(p,n) reaction is dominated by direct charge exchange, and at $\theta_n=0°$ the ground state transition is the strongest[2]. In thick targets, energy loss of the protons results in a broad distribution of neutron energies[3]. In the Be(d,n) reaction the majority of the neutrons are produced by the deuteron stripping reaction[4] which gives rise to gaussian-like neutron spectral distributions[3,5]. In addition reaction channels such as compound nucleus formation, multi-body breakup and coulomb excitations of states in ^{9}Be lead to the emission of lower energy neutrons, $E \leqslant 2$ MeV.

A theoretical estimate of the magnitude and angular distribution of the low energy component of the neutron spectrum is difficult at present because of uncertainty in the relative cross sections of the various reaction channels mentioned earlier.

Table 1 gives the fraction of the neutron yield at $E \leqslant 2$ MeV for $\theta_n=0°$ from proton- and deuteron-induced reactions in Be at various energies. The magnitude of this fraction increases at higher neutron emission angles, as manifested by the decrease in the average neutron energy of the observed spectra[3]. Figure 1 shows the dependence of the proportion of the low energy neutrons on the projectile energy. For comparison, data for a ^{7}Li target are also shown. It is interesting to note that the ^{9}Be target produces more lower energy neutrons than the ^{7}Li target. A similar trend is observed with thin targets and the differences between the yields for ^{9}Be and ^{7}Li targets cannot be explained on the basis of secondary reactions such as ^{9}Be(n,2n).

DISCUSSION

Figure 2 provides a possible clue to the mechanism giving rise to the enhancement of low energy neutron emission from ^{9}Be targets. As shown in Figure 2, there are several neutron-unbound states above 1.6 MeV in ^{9}Be whereas in ^{7}Li the neutron-unbound states lie above 7.3 MeV. This suggests that the differences in the low energy neutron yields is due to the excitation and decay of these neutron-unbound states. With this assumption we find from Figure 2 that at 15 MeV projectile energy the inelastic excitations contribute $\sim$30% to the low energy neutron yield from Be+p reactions and $\sim$4% from the Be+d reactions.

Figure 3 shows neutron spectral distributions from Be(d,n) at $E_d=12$ MeV, $\theta_n=0°$. In this and other spectra at $E_d > 5$ MeV, there is a well resolved neutron peak at $E_n \sim 700$ keV. This resolved peak is not observed in any of the neutron spectra from ^{9}Be+p, ^{9}Be+α, ^{7}Li+p, ^{7}Li+d or ^{7}Li+α reactions which were studied under identical conditions[3].

The observation of this unexpected well-resolved peak in neutron spectra measured at $\theta_n=0°$ following deuteron bombardment of thin and thick Be targets for beam energies above 5 MeV has led to an extended effort to identify the reaction mechanism responsible for its production.

Detailed sequential decay kinematics of the type $^9Be(proj, proj')\ ^9Be^*(2.43\ MeV) \rightarrow\ ^8Be+n$ were carried out to ascertain whether the production is consistent with neutron emission from $^9Be(2.43\ MeV)$ in its decay to the ^8Be ground state. Such a process would account for the independence of the observed neutron energy $\sim$700 keV from the incident deuteron energy. The calculations confirm that the kinematic restrictions concentrate $\sim$30% of the total neutron decay to a single spike at approximately the observed neutron energy for the (d,d') reaction.

However a comparison of corresponding kinematic factors for protons, deuterons and α-beams shows little difference between them so that the known relative cross sections to the 2.43 MeV state[6] would require comparable production for all three projectiles, whereas experimentally only the deuteron beams produce the well-resolved neutron peak at $E_n \sim 700$ keV.

The known (d,d') inelastic excitation cross-section as a function of bombarding energy[6] can be satisfactorily approximated with a constant value of $\sim$40 mb for $3\ MeV \leq E_d < 30\ MeV$. This value of the cross section predicts for thick Be targets an energy dependence of the excitation function for the $\sim$700 keV neutron peak that is in good agreement with the experimentally observed excitation function, see Figure 4, but the predicted absolute yield is a factor of 65 smaller than the experimental value.

CONCLUSIONS

The above discrepancy makes it impossible to identify the neutron spike with a simple (d,d') excitation of the 2.43 MeV state in ^9Be. A novel inelastic process has been suggested by Goldhaber[7]. If inelastic deuteron excitation of the 2.43 MeV state (M1 transition from the ground state) is accompanied by a high probability of concurrent deuteron breakup (M1 excitation) then the ensuing excitation of the 2.43 MeV state by coherent proton and neutron inelastic scattering could account for the excess in the yield while retaining many of the usual features of neutron decay from an excited ^9Be state, e.g. independence of the neutron energy from incident deuteron energy. The angular distributions of the low energy neutrons from such a reaction would be different than those from other reaction channels.

REFERENCES

1. D. CHRISTENSON, W.M. McNAUGHTON and J.A. JUNGERMAN, "Monte Carlo Calculation of d-Be Neutron Yields", Nucl. Inst. & Meth. 160, 499 (1979).

2. J.D. ANDERSON et al., "Fast-Neutron Spectroscopy of the Reaction $^{9}Be(p,n)^{9}B$ at 20 MeV", Phys. Rev. C2, 319 (1970).

3. M.A. LONE et al., "Thick Target Neutron Yields and Spectral Distributions from the $^{7}Li(\frac{d}{p},n)$ and $^{9}Be(\frac{d}{p},n)$ Reactions", Nucl. Inst. & Meth. 143, 331 (1977).

4. R. SERBER, "The Production of High Energy Neutrons by Stripping", Phys. Rev. 72, 1008 (1947).

5. M.A. LONE, "Intense Fast Neutron Source Reactions", Int. Proc. Symposium on Neutron Cross-Sections from 10 to 40 MeV. National Nuclear Data Center, Brookhaven National Laboratory (1977), p.79.

6. A. AJZENBERG-SELOVE AND T. LAURITSEN, "Energy Levels of Light A=5-10", Nucl. Phys. A227, 1 (1974).

7. M. GOLDHABER, Brookhaven National Laboratory, private communication (1978).

TABLE 1

Yield of Low Energy (0.4-2 MeV) Neutrons from Thick ^{9}Be Targets

E (MeV)	Projectile	
	Deuteron	Proton
10	33%	70%
15	28	62
20	21	52
25	15	49

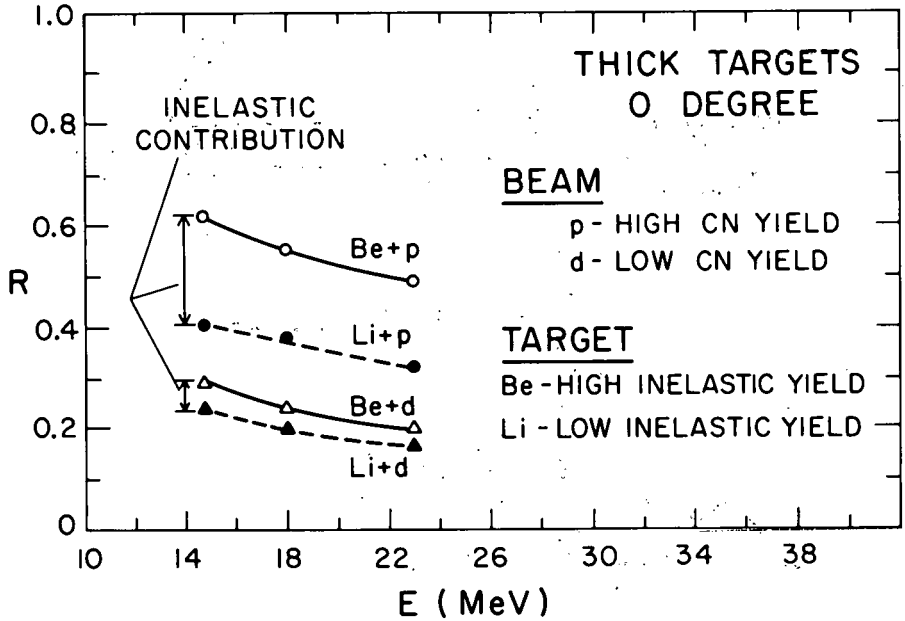

Figure 1 Variation of the low energy neutron fraction $R = \sum_{0.3}^{2.3} (\text{neutron yield}) \Big/ \sum_{0.3}^{E_{max}} (\text{neutron yield})$ with the projectile energy.

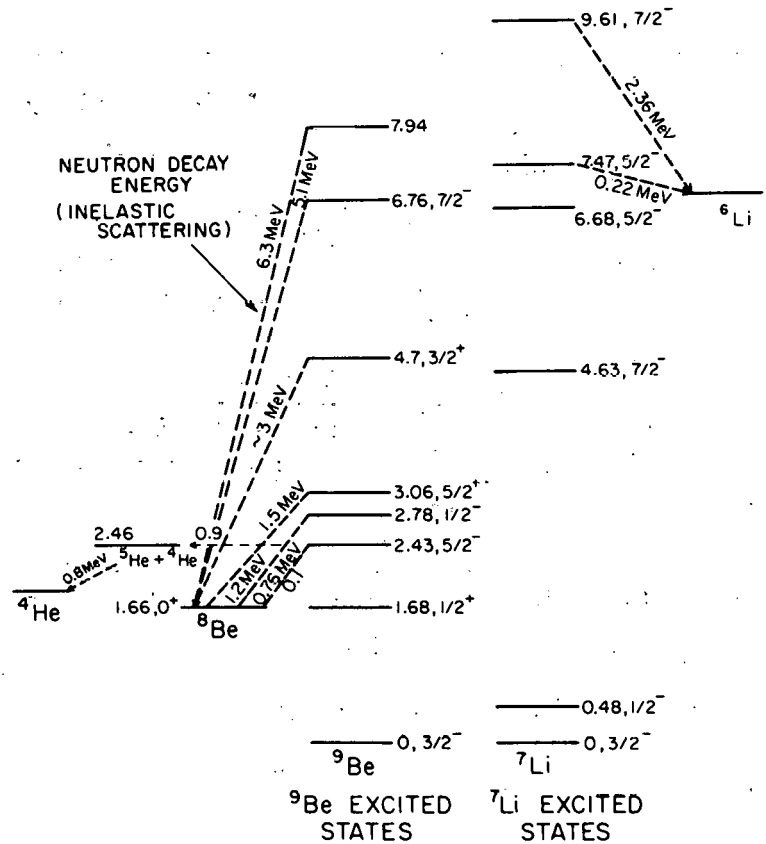

Figure 2 Partial level scheme of Be and Li isotopes.

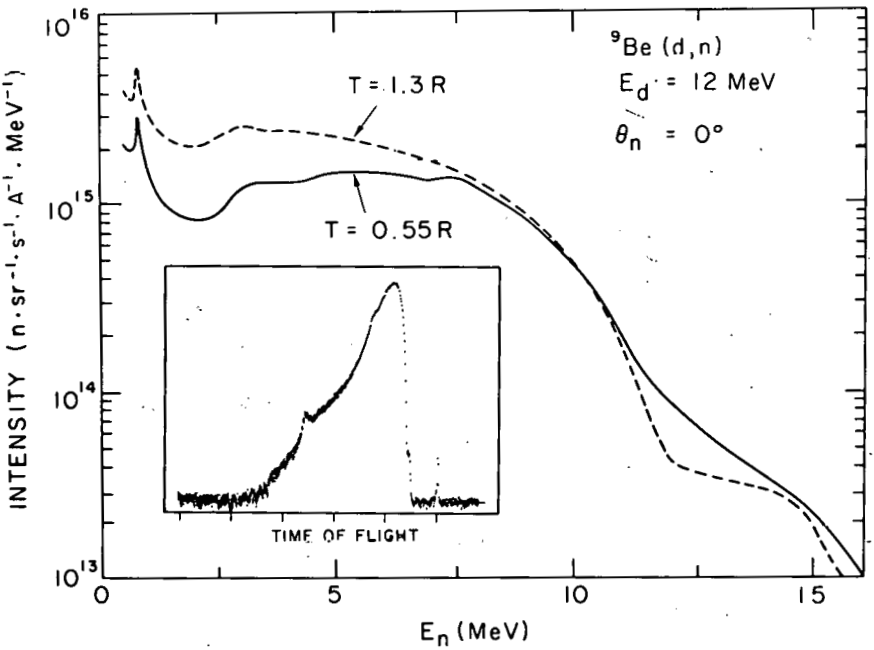

Figure 3 Neutron spectral distributions from Be targets of thickness T=1.3 and 0.55 times the range of 12 MeV deuteron in Be. The inset shows the neutron T.O.F. spectrum for T=1.3 R. Arrow indicates the 700 keV peak.

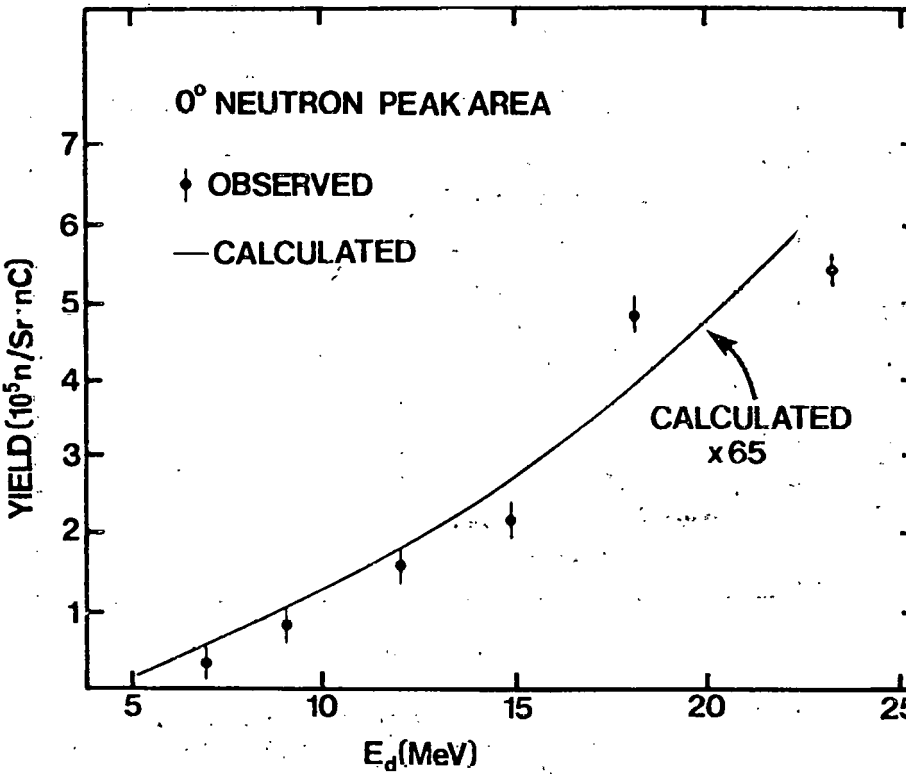

Figure 4 Excitation function for the $E_n \sim 700$ keV neutron peak.

NEUTRON PRODUCTION IN THICK TARGETS OF LEAD, THORIUM AND URANIUM BOMBARDED BY 480 MeV PROTONS

J.S. Fraser, P.M. Garvey and J.C.D. Milton

Chalk River Nuclear Laboratories
Atomic Energy of Canada Ltd., Chalk River, Ontario, Canada K0J 1J0

and

F.M. Kiely and I.M. Thorson

Simon Fraser University, Burnaby, B.C., Canada V5A 1S6

and

B.D. Pate

TRIUMF, Vancouver, B.C., Canada V6T 2A3

ABSTRACT

Neutron capture rates in a water bath surrounding thick, heavy-element targets bombarded by 480 MeV protons have been measured by foil activation. The proton beams impinged on the central element of hexagonal arrays of cylindrical target elements of metallic Pb, Th and depleted U and of natural UO_2. The experimental data are presented as a function of effective radius. The effects of indenting the central element and of substituting central elements of Pb in place of Th or depleted U have been studied. The data are compared with the results of intranuclear cascade and neutron transport calculations and with the results of analyses of earlier measurement.

INTRODUCTION

Charged particle accelerators were proposed many years ago as a means of producing fissile material for use in power reactors [1,2]. The idea of converting fertile material to fissile grew out of the observation [3,4] of copious neutron production in the bombardment of heavy elements by medium energy protons, deuterons or alpha particles. In recent years there has been a resurgence of interest in the accelerator breeder as a system capable of extending nuclear

resources in a large and expanding nuclear power industry. This paper describes the first results from an experimental program intended to provide some of the basic target information needed for the design of an accelerator breeder.

THE BNL-COSMOTRON EXPERIMENTS

In part, the FERFICON (Fertile-to-Fissile Conversion) series of experiments was patterned after measurements made here at the Cosmotron in 1965 by a joint Chalk River-ORNL team [5,6,7]. The set-up is shown schematically in Fig. 1. The system consisted of a large tank filled with H_2O in which targets, of variable forms and sizes, were placed in the centre. Uranium, lead, tin and beryllium, basically in the form of cylinders of 5 cm radius and 60 cm length, were used. The lead targets were also of 10 cm radius. Next to this target an array of 55-Cu or Au-foils was placed in the H_2O. From the measurement of the activity on these foils one could deduce the total capture rate in the H_2O and relate this to the yield of neutrons from the targets. The proton beam was 1 cm radius and was measured by the production of ^{11}C in a polyethylene foil placed in front of the target. In Table I the parameters of the uranium and lead targets are summarized. The proton energies used were 0.54, 0.72, 0.96 and 1.47 GeV. The depleted uranium contained 0.22 w/o ^{235}U.

Before describing the experimental results and comparing them with calculated ones, I would like to review the method of calculation. The methods we used are probably typical of those used by other laboratories although the codes may be somewhat different. The Chalk River system is shown in Fig. 2. We first started off with MC 74 which was written by Milton and Fraser at CRNL [8]. It was a parametric program, treating spallation by a Monte Carlo method. The intranuclear part was parametrized data from Bertini[9]. About two years ago we replaced this by a Los Alamos version of the NMTC-code [10] adapted to the CDC 6600 computer. The output of this code feeds either the one-dimensional S_N-transport code ANISN [11] or the three-dimensional Monte Carlo code MORSE [12]. These two codes basically treat the transport of the evaporation neutron component, using various interfacing programs to pass data from one code to another. The data libraries for these codes (which treat neutron transport below 15 MeV) were originally derived from ENDF/B-III. Subsequently we have produced our own data libraries using SUPERTOG [13] which has (n,3n)-effects built into it. It produces a 99-group library which can be collapsed in various ways through ANISN or through a derived spectrum into a 23-group cross section library for either ANISN or MORSE. Most of the calculations I will describe are based upon the MORSE-code.

The results of these experiments are summarized in Fig. 3. H_2O captures have been plotted rather than the total neutron yield usually quotes as it is quite difficult to derive the total neutron yield from a uranium target due to the large neutron absorption in the uranium. Therefore, it seems preferable for a comparison

between theory and experiment to compare the total number of neutron captures in the water. From Fig. 3 one can see that, for the uranium case, the experimental values are somewhat higher than the calculated values. For the Pb the reverse is true, the experimental results being below the calculated data. This effect varies with energy, the discrepancy being of the order of 20 to 30%. The yield which is normally reported in the literature is basically the H_2O-captures plus a deduced thermal neutron capture rate in the uranium target. The difficulty that arises is that in the actual measurement the flux has a very strong gradient into the target. This may have resulted in an over-estimation of the total neutron yield.

THE FERFICON EXPERIMENTS

The basic method used in the Cosmotron experiments was repeated in the FERFICON series. The arrangement is shown in Fig. 4. The target is placed in a can of fixed dimensions so that there is a gap between the target and the can for the small target diameters. Because of the low proton energy, the target length is only 31.75 cm. The array of Au-foils is somewhat larger than in the Cosmotron experiments and is in the horizontal plane. The proton beam in this case is measured by the ^{24}Na activity produced in the Al-foils. The size of the tank is sufficient to absorb basically all the neutrons that are slowed down by the H_2O.

The target itself is made up of a close-packed array of rods of various sizes as indicated in Fig. 5. The target may consist of a single rod or of seven rods, etc., up to 27. A composite target can also be built with, say, a Pb rod in the centre and surrounded by U rods. A description of the set of targets used is given in Table II. A brief summary of the experimental methods of analysis used in the BNL Cosmotron and in the FERFICON experiments is given in Table III. Whereas in the Cosmotron experiments polynomials were fitted to the measured flux distribution for the integration, spline functions are now used for that purpose.

The measured thermal flux distribution around a 37-rod target is shown in Fig. 6. One can see that there is a strong variation with radius. As the radius of 9.6 cm is smaller than the radius of the target can, there is no continuous flux curve. The radius of the proton beam was again about 1 cm.

A comparison between experimental and calculated results for the pure uranium and the thorium targets of various effective radii is given in Fig. 7. The data are still somewhat preliminary because some uncertainties still exist in the calibration of the absolute counting efficiencies.

Even allowing for the possibility that the experimental results are somewhat high, the calculations still yield significantly lower values, with the difference depending on the target diameter. So far, no conclusive explanation for this effect has been found.

Results for the full range of targets, also somewhat preliminary for the reasons mentioned above, are compiled in Table IV. The agreement is quite good for lead and relatively poor

for uranium. No calculations have so far been performed for UO_2 and the composite targets Pb-Th.

DISCUSSION OF RESULTS

A comparison of the NMTC evaporation spectrum and the fission spectrum of ^{235}U in Fig. 8, shows the harder spectrum arising from evaporation. Also included are the fission cross section for ^{238}U and the (n,2n) cross section. Obviously the secondary processes depend very critically on the hardness of the spectrum. Therefore, one of the possible causes for the discrepancy between experimental and calculated results might be that the evaporation spectrum as calculated by NMTC is too soft. This type of conclusion could help to improve the agreement not only for the uranium target but also for the lead target, because a harder spectrum would give a lower total yield as there is no further multiplication in the lead. (The (n,2n) cross section is quite small.)

A summary of possible contributions to the observed discrepancies is given in Table V. Of course, such questions as accuracy of the proton beam monitoring in the BNL experiments cannot be checked now. We tried to obtain a harder evaporation spectrum by varying the level density constant. However, this did not give a real improvement for if the level density constant is changed in order to harden the spectrum, a smaller number of neutrons is produced at the evaporation stage, which almost completely matches the extra neutrons from subsequent fission. Fission is neglected in our version of NMTC.

So far, we have not been using ENDF/B-V data, but we found very little change in going from ENDF/B-III to ENDF/B-IV. There is some possible change due to reduced inelastic cross sections for ^{238}U in ENDF/B-V.

ACKNOWLEDGMENTS

This work was performed under contract between Atomic Energy of Canada Ltd. and Simon Fraser University.

REFERENCES

1. "The MTA Process", Livermore Research Laboratory Report No. LRL-102 (1954).

2. W.B. LEWIS, "The Significance of the Yield of Neutrons from Heavy Nuclides Excited to High Energies", Atomic Energy of Canada Limited, Report AECL-968 (1952).

3. R.H. GOECKERMAN and I. PERLMAN, "Characteristics of Bismuth Fission with High Energy Particles", Phys. Rev. 73, 1127 (1948).

4. P.R. O'CONNOR and G.T. SEABORG, "High Energy Spallation and Fission Products of Uranium", Phys. Rev. 74, 1189 (1948).

5. J.S. FRASER, R.E. GREEN, J.W. HILBORN, J.C.D. MILTON (AECL), W.A. GIBSON, E.E. GROSS, and A. ZUCHER (ORNL), "Neutron Production in Thick Targets Bombarded by High Energy Protons", Phys. in Canada 21 (2), 17 (1965).

6. G.A. BARTHOLOMEW and P.R. TUNNICLIFFE, Eds., "The AECL Study for an Intense Neutron Generator", Atomic Energy of Canada Limited, Report AECL-2600, p. VII-11 (1966).

7. T.G. CHURCH, Ed., "The AECL Study for an Intense Neutron Generator, ING Status Report, July 1967", Atomic Energy of Canada Limited, Report AECL-2750 (1967).

8. J.C.D. MILTON and J.S. FRASER, "A Monte Carlo Calculation of Neutron Production in Heavy Element Targets by Protons in the Range 0.3 - 1 BeV", Atomic Energy of Canada Limited, Report AECL-2259 (1965).

9. H.W. BERTINI, "Low Energy Intranuclear Cascade Calculation", Phys. Rev. 131, 1801 (1963) and erratum in Phys. Rev. 138, AB2 (1965).

10. W.E. KINNEY, "A Nucleon Transport Code", Oak Ridge National Laboratory Report ORNL-3610 (1964).

11. W.W. ENGLE, JR., "A Users Manual for ANISN, A One-Dimencional Discrete Ordinates Transport Code with Anisotropic Scattering", Union Carbide Corporation Tech. Report K-1693 (1967).

12. E.A. STRAKER et al., "The MORSE Code - A Multigroup Neutron and Gamma Ray Monte Carlo Transport Code", Oak Ridge National Laboratory Report ORNL-4585.

13. R.Q. WRIGHT et al., "SUPERTOG: A Program to Generate Fine Group Constants and P_n Scattering Matrices from ENDF/B", Oak Ridge National Laboratory Report ORNL-TM-2679.

TABLE I

Description of Pb and U-targets for the BNL Cosmotron Experiments

Target	Density	Length	Radius
U[a]	18.94	609.6	50.8
Pb-1	11.34	609.6	50.8
Pb-2	11.34	609.6	101.6

[a]Depleted uranium - 0.22 wt% ^{235}U.

TABLE II

Description of Target Assemblies for the FERFICON Experiments

Target	Length (mm)	Radius (mm)		Density ($g \cdot cm^{-3}$)
		Rod	Array[a]	
U-1[b]	304.8	16.26	16.26	18.94
U-7[b]			43.02	
U-19[b]			70.88	
U-37[b]			98.91	
Th-1		20.96	20.96	11.30
Th-7			55.45	
Th-19			91.36	
Pb-1		50.80	50.80	11.34
Pb-7		19.18	50.75	
UO_2-37[c]	247.7	11.94	72.63	10.20
Pb-1/U-6	304.8	16.26	16.26	11.34/18.94
Pb-1/U-36			43.02	
Pb-7/U-30			70.88	
Pb-1/Th-6		20.96	20.96	11.34/11.30
Pb-1/Th-18			55.45	
Pb-7/Th-12			91.36	

[a]Effective radius $R = r\sqrt{n}$.

[b]Depleted uranium - 0.26 wt% ^{235}U.

[c]Natural UO_2 clad in aluminum.

TABLE III

Summary of Experimental Methods of Analysis

1. BNL Cosmotron Experiments

Proton Intensity:	$^{12}C(p,pn)^{11}C$ reaction
H_2O Capture Rate:	Irradiation of Cu(bare) and Au(bare and sub Cd) to derive Westcott flux (ϕ_o), polynominals fitted to ln $\phi_o(r,z)$ and integrated to determine total capture rate in H_2O tank.

2. FERFICON Experiments

Proton Intensity:	$^{27}Al(p,3pn)^{24}Na$ reaction
H_2O Capture Rate:	Irradiation of Au(bare and sub Cd) to derive Westcott flux (ϕ_o).
	Integration via fitted Spline Functions to obtain total capture rate in H_2O tank.

TABLE IV

Compilation of FERFICON Results -
H_2O Captures per Proton of 480 MeV

Target	Experiment	Calculation
U-1	9.6 ± 0.7	10.1 ± 0.4
U-7	14.1 ± 0.9	10.9 ± 0.4
U-19	15.2 ± 1.0	12.4 ± 0.4
U-37	17.1 ± 1.0	12.3 ± 0.4
U-37[a]	17.2 ± 1.0	-
Th-1	8.1 ± 0.6	9.1 ± 0.5
Th-7	9.2 ± 0.6	8.7 ± 0.5
Th-19	9.6 ± 0.7	8.3 ± 0.5
Pb-1	8.3 ± 0.5	8.2 ± 0.3
Pb-7	8.0 ± 0.4	
UO_2-37	10.0 ± 0.6	-
Pb-1/U-6	-	-
Pb-1/U-36	12.7 ± 0.7	9.5 ± 0.5
Pb-7/U-30	11.0 ± 0.7	9.0 ± 0.5
Pb-1/Th-6	7.4 ± 0.9	-
Pb-1/Th-18	6.6 ± 0.8	-
Pb-7/Th-12	8.0 ± 0.6	-

[a]Central rod indented by 150 mm.

TABLE V

Summary of Discussion

1. BNL Cosmotron experiments give approx. 25% lower n/p ratio than Ferficon Experiments (BNL experiments extrapolated to 480 MeV).

	BNL	FERFICON	Ratio
Pb (50.8 mm)	6.6	9.0	0.73
U (50.8 mm)	12.7	17.0	0.75

POSSIBLE REASONS

I) Proton Beam Monitoring:

$^{12}C(p,pn)^{11}C$ vs $^{27}Al(p,3p)^{24}Na$.

II) Different Geometry

Target length 610 mm (BNL); 305 mm (FERFICON)
H_2O in contact with BNL target; separated from FERFICON target by fixed target can.

Calculation absorption ratio (U/H_2O)

BNL	0.40	(0.13)
FERFICON (interpolated)	0.35	(0.12)

Other reaction rates similar.

2. Spectrum of Evaporation Source

Calculation gives too many neutrons with too soft a spectrum - to be confirmed by thin target spectrum measurements.

Effect of level density constant
Pre-equilibrium evaporation model
Fission channel effect

Lead targets - n/p ratio over-predicted

Uranium targets - n/p ratio under-predicted

Harder spectrum would lead to an increase in fast fission and (n,2n) reactions.

3. Nuclear Data

Reduced inelastic cross-section for ^{238}U in ENDF/B-V would lead to further fast fission, etc.

4. Resonance Absorption

Indefinitely dilute cross sections
Small effect (approx. 5%)

5. H_2O Thermal Constants - Small effect.

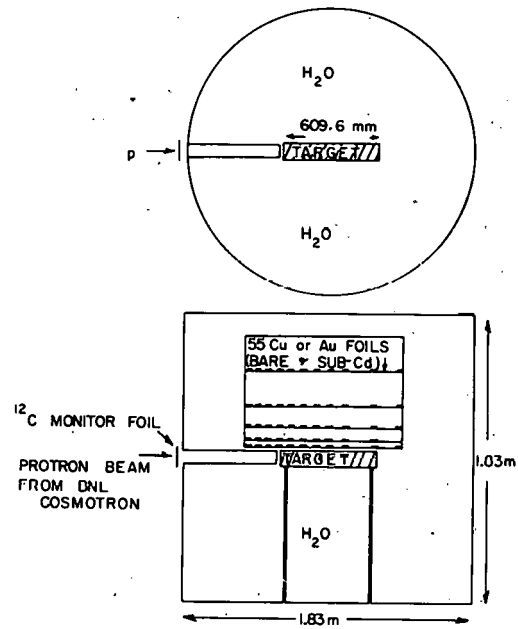

Fig. 1: H_2O tank and target assembly for the BNL Cosmotron experiments.

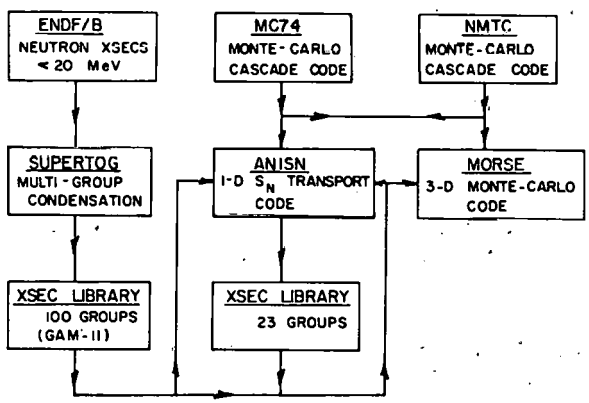

Fig. 2: Program group for target neutronics calculations.

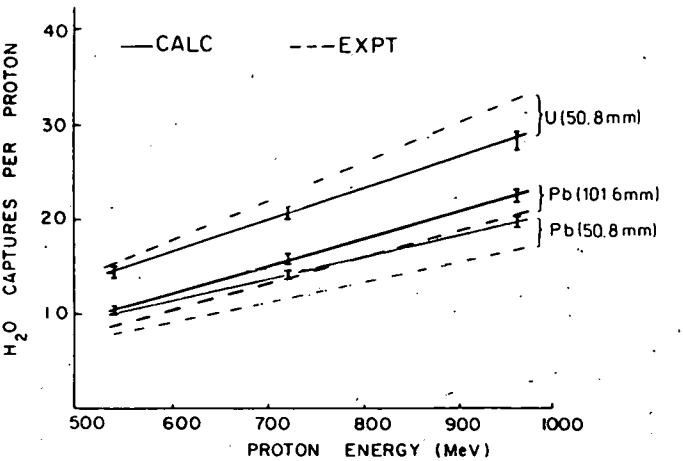

Fig. 3: H_2O captures per incident proton as measured in the BNL Cosmotron experiments and calculated at CRNL. Error bars on the calculated data are statistical errors in the Monte Carlo calculation. Experimental errors are not available.

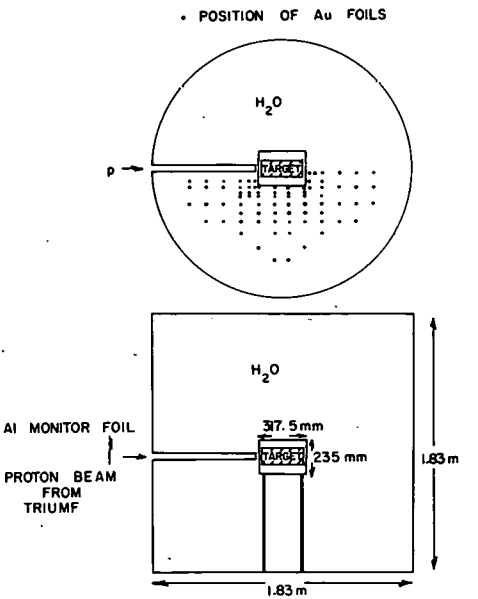

Fig. 4: H_2O tank and target assembly for FERFICON experiments.

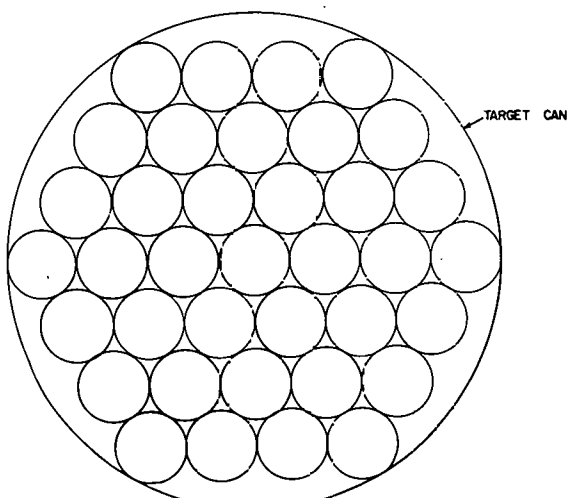

Fig. 5: Array of rods in target canister for the FERFICON experiments. Canister inside diameter is 235 mm. A 37-rod assembly is shown.

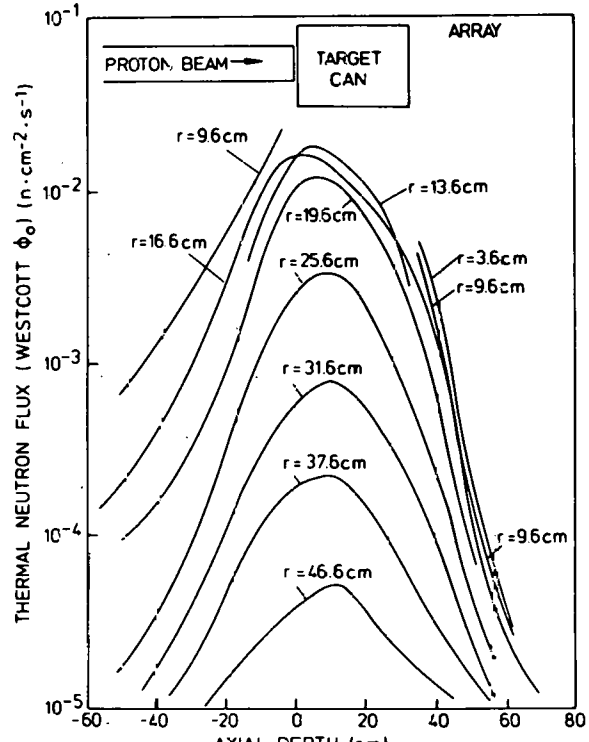

Fig. 6: Distribution of thermal neutron flux around a 37-rod uranium target assembly as measured in the FERFICON experiments.

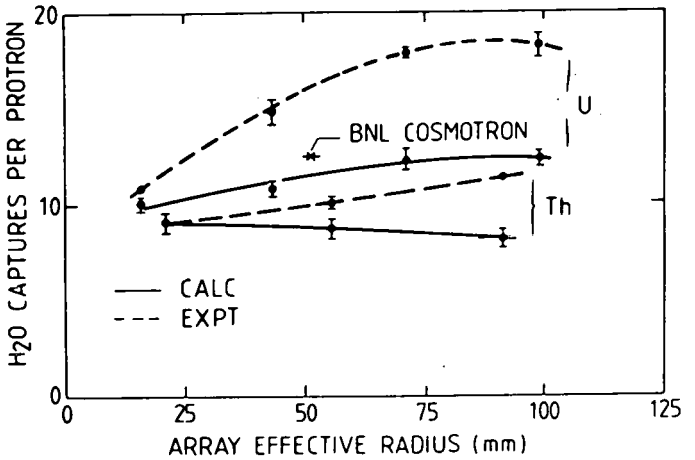

Fig. 7: H_2O captures per incident proton obtained in the FERFICON experiments compared to calculated results.

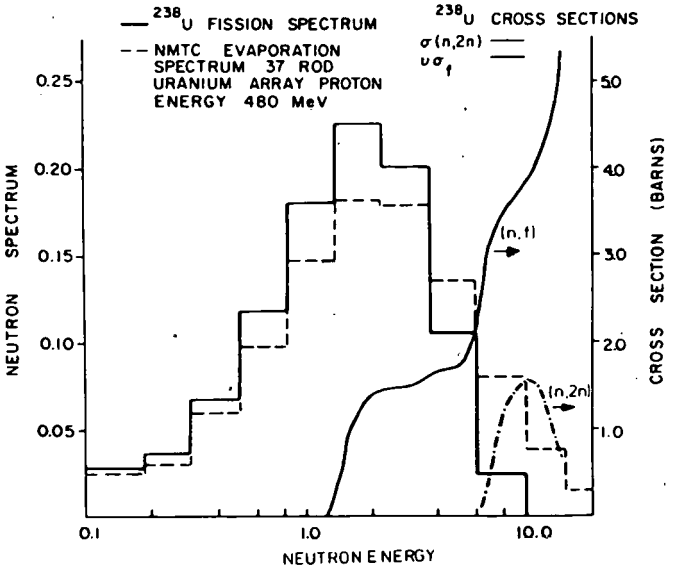

Fig. 8: Comparison of neutron source spectrum (evaporation and fission) and the ^{238}U cross sections.

THIS PAGE
WAS INTENTIONALLY
LEFT BLANK

Dup

SPALLATION TARGET-MODERATOR-REFLECTOR STUDIES AT THE WEAPONS NEUTRON RESEARCH FACILITY

G. J. Russell, J. S. Gilmore,
R. E. Prael, and H. Robinson

Los Alamos Scientific Laboratory
Los Alamos, New Mexico 87545, U.S.A.

S. D. Howe
Kansas State University
Manhattan, Kansas 66506, U.S.A.

ABSTRACT

Basic neutronics data, initiated by 800-MeV proton spallation reactions, are important to spallation neutron source development and electronuclear fuel production. We are measuring angular-dependent and energy-dependent neutron production cross sections, energy-dependent and total neutron yields, thermal and epithermal neutron surface and beam fluxes, and fertile-to-fissile conversion ratios. The measurements are being done at the Weapons Neutron Research facility on a variety of targets and target-moderator-reflector configurations. The experiments are relevant to the above applications and provide data to validate computer codes. Preliminary results are presented and compared to calculated predictions.

INTRODUCTION

Several laboratories throughout the world are building and designing intense thermal and epithermal spallation neutron sources, both pulsed and steady state [1-5]. There is a cooperative effort among some nine laboratories to share pertinent information; this cooperative endeavor is called the International Collaboration on Advanced Neutron Sources (ICANS). There is also some interest in utilizing high-energy particle accelerators for converting fertile material to fissile material [6]. At the Los Alamos Scientific Laboratory (LASL), we have a self-consistent experimental program (using 800-MeV protons) relevant to the above applications.

The 800-MeV proton source is the Clinton P. Anderson Meson Physics Facility (LAMPF). We conduct the experiments at the Weapons Neutron Research facility (WNR)--see Fig. 1. The present experimental program consists of the following measurements:

- angular-dependent neutron production cross sections from 0.5-800 MeV for targets of Aℓ, Cu, In, Pb, and depleted U,
- neutron yields (at 90°) from 0.5-400 MeV for Ta and W targets,
- total neutron yields from targets of W, Pb, Th, and depleted U,
- fertile-to-fissile conversion yields inside Th and depleted U targets,
- thermal and epithermal neutron surface and beam fluxes from moderators, and
- thermal neutron leakage spectra from moderators.

The differential measurements provide data to test the fundamental processes and assumptions used in the Monte Carlo computer codes. The integral measurements inherently provide more complicated data because they include the effects of transport and secondary processes. We describe here our experimental program and show some preliminary results. Ultimately, we will compare all experimental data with calculated predictions. The Monte Carlo computer codes used in the calculations are the Oak Ridge National Laboratory code HETC [7] for particle transport $\gtrsim$20 MeV, and the LASL code MCNP [8] for neutron transport $\lesssim$ 20 MeV.

TOTAL NEUTRON YIELDS AND CONVERSION MEASUREMENTS

The LASL Fertile-to-Fissile Conversion (FERFICON) program is a cooperative effort with the Canadians at the Chalk River Nuclear Laboratory. The LASL experiments provide an extension to 800 MeV of similar measurements (but more exhaustive in numbers) being conducted using the TRIUMF-cyclotron in Vancouver, B.C. The Canadian measurements are being done at proton energies of 350 and 480 MeV. The LASL FERFICON program consists of two parts: a) determination of total neutron yields from stopping-length targets, and b) measurement of fertile-to-fissile conversion efficiencies inside stopping-length targets.

Total Neutron Yields

To determine a target neutron yield, we place the target inside a 2-m-diam by 2-m-high water-bath, and measure, using an array of bare and cadmium-covered gold foils, the axial and radial neutron flux distributions in the water. We beta count the 0.0025-cm-thick foils (without chemical separation) to determine the $^{197}Au(n,\gamma)^{198}Au$ reactions, and use the cadmium ratio to correct the gold activation for resonance neutron capture. We integrate the measured flux distribution over the water-bath volume and calculate the total neutron captures in the water.

The number of protons striking the target are found by passing them through a three-foil alumimum packet located just upstream of the target. We count the central 0.025-cm-thick foil with a Ge-Li detector system and determine the number of $^{27}Al(p,3pn)^{24}Na$, $^{27}Al(p,x)^{22}Na$, and $^{27}Al(p,x)^{7}Be$ reactions. Measured spatial distributions of protons striking the targets are shown in Fig. 2. In general, the proton distributions are strongly peaked at the center and have 'wings' which do not fall off as rapidly as a circular bivariate (Gaussian-type) distribution.

The characteristics of the targets used in the measurements are shown in Table I, and the targets are depicted in Fig. 3. All targets were stopping-length targets (long enough to range-out 800-MeV protons). The thorium and (larger) uranium targets were stopping targets since essentially no protons leaked from them.

In an applied sense, the most useful quantity is the neutron yield from the target per proton, and not the total neutron captures in the water-bath per proton. Therefore, we need to remove the effects of the water-bath on the neutron yield. The water-bath affects the neutron yield in several ways:

- There is an energy above which neutrons from the target are lost from the water-bath.
- Spallation reactions with oxygen nuclei by high-energy neutrons and protons escaping from the target produce a distributed neutron source throughout the water-bath.
- The water-bath reflects neutrons back into the target to be captured, that is, the target can act as a neutron sink.
- The water-bath reflects neutrons back into the target which can cause "secondary" (n,f) and (n,xn) source-type reactions, that is, the target can act as a "secondary" neutron source. These latter neutrons supplement the "primary" spallation neutrons and attendant "primary" (n,f) and (n,xn) source-type reactions which occur in the absence of the water-bath.

The first two items in the above list tend to compensate each other and are not too dependent on target material and size; the last two items can compensate each other, however, the net effect is somewhat more complicated and depends on target material and size. We also need to correct the experimental data for the effects of structural material surrounding the target.

Preliminary Monte Carlo calculations of bare-target neutronics for the LASL FERFICON targets are shown in Table II. The low-energy (<20 MeV) neutron-enhancement (ratio of low-energy leakage neutrons to low-energy spallation neutrons) is about 3% for tungsten, lead, and thorium, and about 21% for uranium. Note the low-energy neutron captures and fissions in the thorium and uranium targets.

Table III shows a comparison of the initial LASL data with BNL Cosmotron data (interpolated at 800 MeV)--Refs. [9,10]. For comparable targets, there is excellent agreement between our experimental data and the BNL Cosmotron results. For the lead target, where water-bath effects are minimal, the two calculations agree, but are high relative to the measured values. The LASL calculations do not have water-bath effects included. Zeroth-order comparisons of our calculated low-energy (<20 MeV) neutron leakage with our measured neutron captures in the water show the calculations to be $\sim$30% high for the tungsten, lead, and thorium targets, and $\sim$3% high (on-the-average) for the uranium targets. Such comparisons may indicate that the measured uranium data are artificially high because of water-bath effects, and (or) the uranium predictions are too low because fission competition with evaporation is presently not included in the HETC portion of the computation. Further data reduction and analysis are in progress. We will compare measured and calculated neutron captures per proton in the H_2O, and then attempt to convert the experimental data to neutron yield and compare with calculated predictions.

Conversion Measurements

We will measure the radial and axial distributions of fertile-to-fissile conversion yields (^{232}Th to ^{233}U and ^{238}U to ^{239}Pu) inside the 19-rod thorium and 37-rod depleted uranium targets. We plan to determine the fissile nuclei production with a Ge-Li detection system by observing the ^{233}Pa activity for the thorium target and the ^{239}Np activity for the depleted uranium target. Both the spatial and integrated measured conversion yields will be compared with calculated predictions.

ENERGY-DEPENDENT NEUTRON YIELDS AND PRODUCTION CROSS SECTIONS

We have measured, at 90° to the proton beam, the energy-dependent (0.5-400 MeV) neutron yields (spectra) from the tantalum

and tungsten production targets used in the WNR high-current target area. We have also measured angular- and energy-dependent (0.5-800 MeV) neutron production cross sections for aluminum, copper, indium, lead, and depleted uranium targets. These latter measurements were made at 0°, 30°, 45°, and 112° to the proton beam. The production cross section measurements are part of the Ph.D. thesis research of S. D. Howe; he is preparing the data for publication. We report here preliminary results of the tantalum and tungsten neutron spectra measurements.

The tantalum (2.54-cm diam by 15.24-cm long) production target is water cooled and inside an aluminum canister. The tungsten (4.45-cm diam by 24.13-cm long) production target is water cooled and inside a stainless steel canister. The first 5 cm of the tungsten has a tapered reentrant hole (2.54-cm diam to 1.42-cm diam).

The experimental setup used in the spectra measurements is shown in Fig. 4. The proton beam consisted of micropulses ($\sim$0.2-ns wide) separated by 11 μs and occuring over 640 μs. This beam pattern was repeated at 12 Hz.

We used a 5.1-cm-diam by 2.5-cm-thick NE-213 liquid scintillator located 29.37 m from the target. The detector bias was set using the 60 keV gamma-ray from a ^{241}Am source. This established the neutron energy bias at $\sim$425 keV. The efficiency of the detector at this bias was measured up to 31 MeV at the LASL Tandem Van de Graaff accelerator. Above 31 MeV, the detector was cross calibrated to previous work using our 0° neutron production cross section data. The electronics and data reduction techniques are described in Ref. [11].

Our preliminary experimental results are shown in Figs. 5 and 6; the experimental data have been arbitrarily normalized to the calculations at 10 MeV. This initial normalization criteria is not too unreasonable since previous comparisons [11,12] between measurements and calculations show fair agreement at 10 MeV.

The underprediction of the calculations above $\sim$20 MeV is consistent with other results obtained using 740-MeV protons [13], but disagrees with 450-MeV proton data [14,15]. Since calculations are generally used to predict the neutron source incident on a shield, the underprediction of the neutron yield above $\sim$50 MeV is relevant to shield design problems for spallation neutron sources.

MODERATED NEUTRON YIELDS

Research programs utilizing the WNR high-current target area require thermal ($E \leqslant 0.5$ eV), epithermal (0.5 eV $\leqslant E \leqslant 100$ keV), and fast (100 keV $\leqslant E \leqslant$ 400 MeV) neutrons. We use the water-cooled tantalum target by itself for fast neutron production, and polyethylene moderators around the tantalum target, in a hybrid slab geometry, for epithermal neutron production. We are now

producing thermal neutrons using the tungsten target and a hybrid slab geometry (see Fig. 7). The water moderator is heterogeneously poisoned with cadmium and backed with polyethylene to shorten the thermal neutron pulses.

For a pulsed spallation neutron source, a beryllium reflected moderator can increase thermal neutron production by a factor of 2-4 over a bare moderator. We are going to install a reflected target-moderator geometry in the WNR high-current target area for thermal neutron production. The changeover is being done to: a) increase thermal neutron production, b) increase the number of simultaneous thermal neutron experiments, and c) reduce neutron background problems associated with center-looking (where the field-of-view looks at the target) flight paths by going to offset geometry (where the target is not viewed directly).

Total neutron production from a target is not necessarily a definitive indicator of thermal neutron beam fluxes. The particular target-moderator-reflector configuration needs to be assessed as an integral unit relative to thermal neutron generation. We have a measurement program (using the WNR low-current target area) underway at LASL to ascertain thermal neutron production from a variety of target–moderator–reflector configurations.

In addition to the unreflected hybrid slab-moderator, we are studying several reflected target-moderator configurations; these reflected geometries are shown in Figs. 8-10. We measure, using bare and cadmium-covered gold foils, the spatial distribution of the neutron surface flux, and the thermal and epithermal neutron beam fluxes. Preliminary neutron beam fluxes were measured using the experimental layout shown in Fig. 11. Data from these measurements are being analyzed; we present here some preliminary results for the reflected wing-moderator shown in Fig. 9.

The target was a cylinder of depleted uranium (10.0-cm diam by 40.7-cm long) placed in a stainless steel canister. There was an air gap (~1 cm) between the uranium and the outside of the stainless steel canister. The polyethylene premoderator was 5.0-cm thick, poisoned with 0.076-cm of cadmium, and backed with a 1.27-cm-thick polyethylene moderator. The beryllium reflector was essentially a cube with sides 66-cm long, and was decoupled from the polyethylene by 0.076-cm of cadmium. The wing-moderator was located 2 cm from the front surface of the target.

We define the 2200 m/s neutron flux, φ_0, to be the activations in a gold foil by neutrons with energies < 0.5 eV divided by the 2200 m/s gold cross section. The Maxwellian thermal neutron flux, φ_m, is related to φ_0 by Eq. (1) -- Ref. [17].

$$\varphi_m = \frac{1}{g(T)} \frac{2}{\sqrt{\pi}} \left(\frac{T}{T_0}\right)^{\frac{1}{2}} \varphi_0 \ , \qquad (1)$$

where g(T) is the non-1/v factor, T is the absolute temperature of the neutrons, and T_0 = 293.6 °K. Some preliminary spatial distributions of φ_0 at the moderator surface are shown in Figs. 12 and 13. Note the rapid falloff of the neutron flux with distance from the target; the neutron flux in the direction of the targets axis is fairly symmetric. An average $\bar{\varphi}_0$ (over ~78 cm^2 of moderator surface) is $\bar{\varphi}_0 \sim 1.8 \times 10^{-3}$ $n/cm^2 \cdot p$. Preliminary values of the Maxwellian, φ_m, and epithermal, φ(1eV), neutron beam fluxes are $\varphi_m \sim 2.4 \times 10^{-2}$ $n/sr \cdot p$ and $\varphi(1eV) \sim 1.2 \times 10^{-2}$ $n/sr \cdot eV \cdot p$, respectively. The value for φ_m assumes a Maxwellian temperature of 400 °K which is about what we measured for an unreflected moderator [1]. The neutron beam fluxes are for a moderator field-of-view of ~65 cm^2 centered on the moderator. The moderating ratio, φ_m/φ(1eV), is ~2.0; this ratio is in reasonable agreement with other work [3].

FUTURE PLANS

We plan to continue our measurements of total neutron yields and neutron production cross sections using other materials and angles. The fertile-to-fissile conversion measurement will be made this year. We will measure thermal neutron spectra, pulse widths, and beam fluxes in a continuing study of target-moderator-reflector configurations; these studies will include the effects of decoupler materials used between the moderator and reflector. We will measure thin-target total neutron yields using bath techniques, and neutron spectra from bare, stopping-length targets. We plan to measure cold moderator neutron yields, spectra, and pulse widths. We also would like to measure total neutron yields and fertile-to-fissile conversion yields for massive (~2000 kg) thorium and uranium targets. Energy deposition in spallation targets is another area where we could make relevant measurements.

ACKNOWLEDGEMENTS

This work was performed under the auspices of the U.S. Department of Energy. We would like to acknowledge the support and encouragement of R. Woods, and useful discussions with J. L. Yarnell, P. W. Lisowski, and J. S. Fraser. We appreciate the help of J. R. Baldonado and K. J. Hughes in setting up the experiments. We acknowledge the cooperation of the WNR operations crew of R. D. Ryder, H. M. Howard, R. A. Johnson, and T. L. Bogart, and the help of the CNC-11 counting room personnel.

REFERENCES

1. G. J. Russell, P. W. Lisowski, and N.S.P. King, "The WNR Facility--A Pulsed Spallation Neutron Source at the Los Alamos Scientific Laboratory," Intl. Conf. on Neutron Physics and Nucl. Data for Reactors and Other Appl. Purposes, Harwell, England (1978).

2. L.C.W. Hobbis, G. H. Rees, and G. C. Stirling, eds., "A Pulsed Neutron Facility for Condensed Matter Research," Rutherford Laboratory report RL-77-064/C (1977).

3. J. M. Carpenter, D. L. Price, and N. J. Swanson, eds., "IPNS--A National Facility for Condensed Matter Research," Argonne National Laboratory report ANL-78-88 (1978).

4. Y. Ishikawa and N. Watanabe, "KEK Neutron Source and Neutron Scattering Research Facility," National Laboratory for High Energy Physics report KEK-78-19 (1978).

5. G. S. Bauer, ed., "Targets for Neutron Beam Spallation Sources," Jül-Conf-34, ISSN 0344-5798, Jülich (1980).

6. H.J.C. Kouts and M. Steinberg, eds., "Proceedings of an Information Meeting on Accelerator-Breeding," ERDA Conf-770107, Brookhaven National Laboratory (1977).

7. K. C. Chandler and T. W. Armstrong, "Operating Instructions for the High Energy Nucleon Meson Transport Code HETC," Oak Ridge National Laboratory report ORNL-4744 (1972).

8. W. L. Thompson, ed., "MCNP - A General Monte Carlo Code for Neutron and Photon Transport," Los Alamos Scientific Laboratory report LA-7396-M (1979).

9. J. S. Fraser, et al., "Neutron Production by Thick Targets Bombarded by High-Energy Protons," Physics in Canada, Vol. 21, No. 2, 17-18 (1965).

10. P. M. Garvey, "Neutron Production by Spallation in Heavy Metal Targets," Proc. of Meeting on Targets for Neutron Beam Spallation Neutron Sources, Jül-Conf-34, ISSN 0344-5798, Jülich (1980).

11. S. D. Howe, et al., "Neutron Spectrum at 90° from 800-MeV (p,n) Reactions on a Ta Target," Proc. Conf. on Nuclear Cross Sections for Technology, Knoxville (1979) - to be published.

12. L. R. Veeser, et al., "Neutrons Produced by 740-MeV Protons on Uranium," Nucl. Inst. Meth., Vol 17, 509-912 (1974).

13. R. Madey and F. M. Waterman, "High-Energy Neutrons Produced by 740-MeV Protons on Uranium," Phys. Rev. C, Vol. 8, No. 6, 2412-2418 (1973).

14. J. W. Wachter, W. A. Gibson, and W. R. Burrus, "Neutron and Proton Spectra from Targets Bombarded by 450-MeV Protons," Phys. Rev. C, Vol. 6 No. 5, 1496-1508 (1972).

15. R. G. Alsmiller, Jr., "Calculation of the Neutron and Proton Spectra from Thick Targets Bombarded by 450-MeV Protons and Comparison with Experiment," Nucl. Sci. Engr., 36, 291-294 (1969).

16. K. H. Beckurts and K. Wirtz, Neutron Physics, Springler-Verlag, New York, Inc. (1964).

TABLE I
PHYSICAL CHARACTERISTICS OF FERFICON TARGETS

TARGET MATERIAL	DENSITY (g/cm^3)	DIAMETER (cm)	LENGTH (cm)	U ENRICHMENT (wt%)
W[a]	18.26	4.45	24.13	----
Pb	11.31	9.85	40.65	----
U	18.4	10.01	40.65	0.19802
Th	11.38	18.28[b]	40.65	----
U	19.04	20.09[c]	40.65	0.25051

[a]The first 5 cm of the target had a tapered reentrant hole (2.54-cm diam to 1.42-cm diam).

[b]Effective diameter ($D = d\sqrt{n}$) for a 19 rod array with an individual rod diameter of 4.1928 cm.

[c]Effective diameter ($D = d\sqrt{n}$) for a 37 rod array with an individual rod diameter of 3.3035 cm.

TABLE II

BARE-TARGET CALCULATED NEUTRONICS FOR FERFICON TARGETS[a]

	W 4.45-cm diam (n/p)	Pb 9.85-cm diam (n/p)	U 10.01-cm diam (n/p)	Th 18.28-cm diam[b] (n/p)	U 20.09-cm diam[b] (n/p)
LOW-ENERGY (< 20 MeV) SPALLATION NEUTRON PRODUCTION[c]	13.15±0.16	16.12±0.20	21.37±0.27	21.39±0.27	25.06±0.33
NEUTRON LEAKAGE (< 20 MeV)[d]	13.47±0.17	16.55±0.20	25.84±0.32	22.05±0.26	30.42±0.38
NEUTRON LEAKAGE (> 20 MeV)	1.18±0.02	1.17±0.02	1.05±0.02	0.97±0.02	0.71±0.02
TOTAL NEUTRON LEAKAGE	14.65±0.17	17.72±0.20	26.89±0.32	23.02±0.26	31.13±0.38
NEUTRON CAPTURE (< 20 MeV)[e]	0.155±0.002	0.009±0.0002	1.05±0.02	1.51±0.02	4.44±0.06
TOTAL NEUTRON PRODUCTION	14.81±0.17	17.73±0.20	27.94±0.32	24.53±0.26	35.57±0.39
NEUTRON INDUCED FISSIONS [< 20 MeV] (fiss/p)	———	———	2.34±0.04	0.60±0.01	4.43±0.07

[a]Proton energy is 800 MeV; the W target was 24.13-cm long, and the first 5 cm had a tapered reentrant hole (2.54-cm diam to 1.42-cm diam); all other targets were 40.65-cm long.

[b]Effective diameter $D = d\sqrt{n}$; d is the individual rod diameter and n is the number of rods.

[c]Evaporation neutrons produced inside the target; fission competition with evaporation is not included in HETC.

[d]Includes net effects of (n,f)- and (n,xn)-type reactions occuring during transport of low-energy spallation neutrons.

[e]Neutron capture occuring in target during transport of the low-energy spallation neutrons.

TABLE III

PRELIMINARY LASL FERFICON RESULTS COMPARED TO BNL COSMOTRON DATA (INTERPOLATED AT 800 MeV)

TARGET MATERIAL	LASL TARGET SIZE diam x length (cm x cm)	LASL FERFICON		BNL COSMOTRON		BNL COSMOTRON TARGET SIZE diam x length (cm x cm)
		CALCULATED NEUTRON LEAKAGE PER PROTON[b]	MEASURED H_2O NEUTRON CAPTURES PER PROTON	CALCULATED H_2O NEUTRON CAPTURES PER PROTON[c]	MEASURED H_2O NEUTRON CAPTURES PER PROTON[c]	
W	4.45 x 24.13[a]	13.5 – 14.7	10.2	---	---	----
Pb	9.85 x 40.65	16.6 – 17.7	13.0	16.4	13.4	10.2 x 61.0
U	10.01 x 40.65	25.8 – 26.9	25.3	23.3	26.3	10.2 x 61.0
Th	18.28[d] x 40.65	22.1 – 23.0	17.1	---	---	----
U	20.09[d] x 40.65	30.4 – 31.1	28.8	---	---	---

[a] The first 5 cm of the target had a tapered reentrant hole (2.54-cm diam to 1.42-cm diam).

[b] Neutron leakage from a bare target; the smaller number is for neutrons with energies $\leq$ 20 MeV, and the larger number is for neutrons with energies $\leq$ 800 MeV.

[c] Ref. [10].

[d] Effective diameter $D = d\sqrt{n}$; d is the individual target diameter and n is the number of rods.

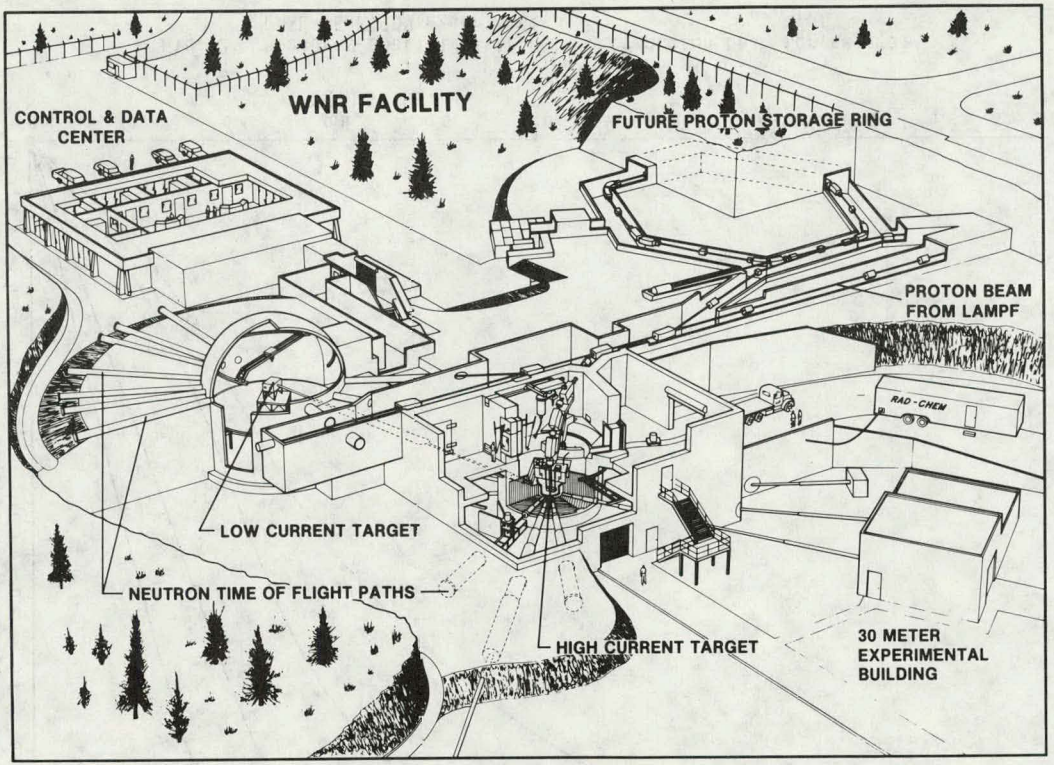

Fig. 1 General layout of the WNR showing the two target areas. The high-current target is located in a vertical proton beam and is viewed by 11 horizontal flight paths. The low-current target is located in a horizontal proton beam and viewed by 12 flight paths.

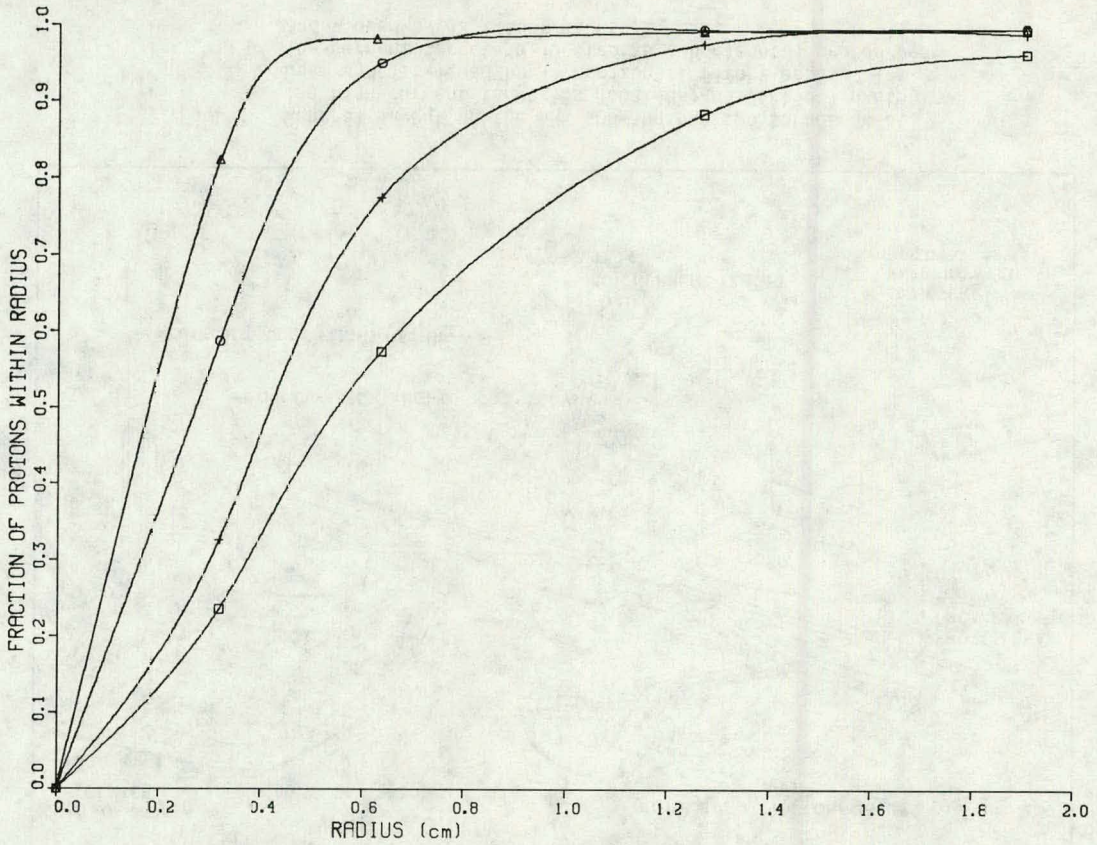

Fig. 2 Measured spatial distribution of proton beam for several LASL FERFICON experiments.

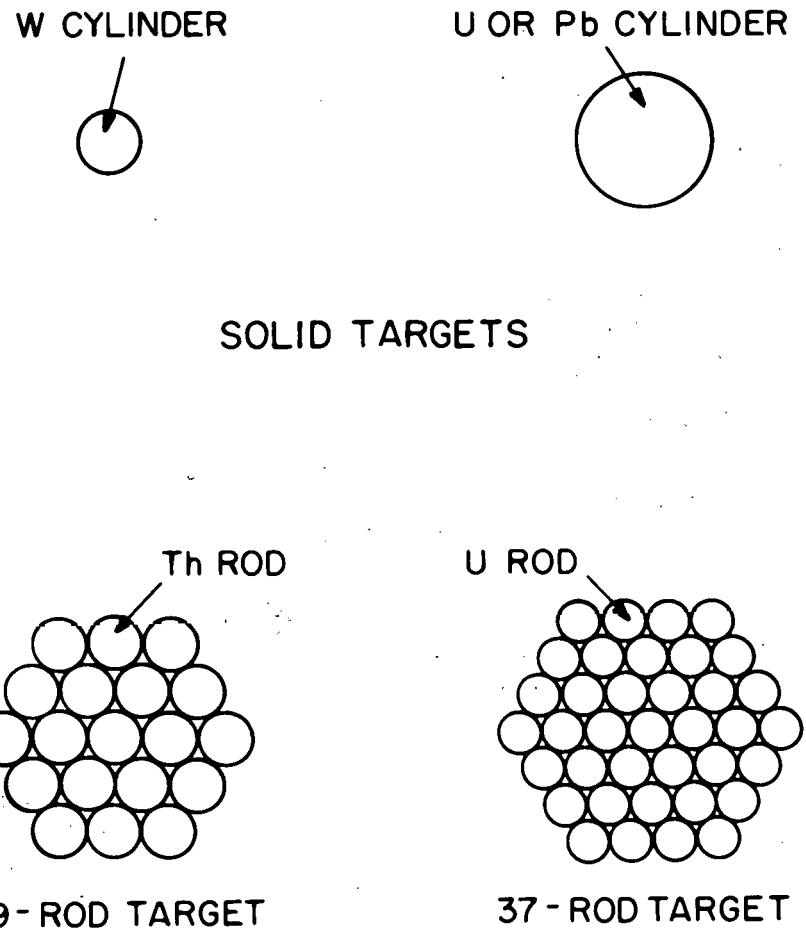

Fig. 3 Targets used in the LASL FERFICON experiments (relative sizes are as indicated).

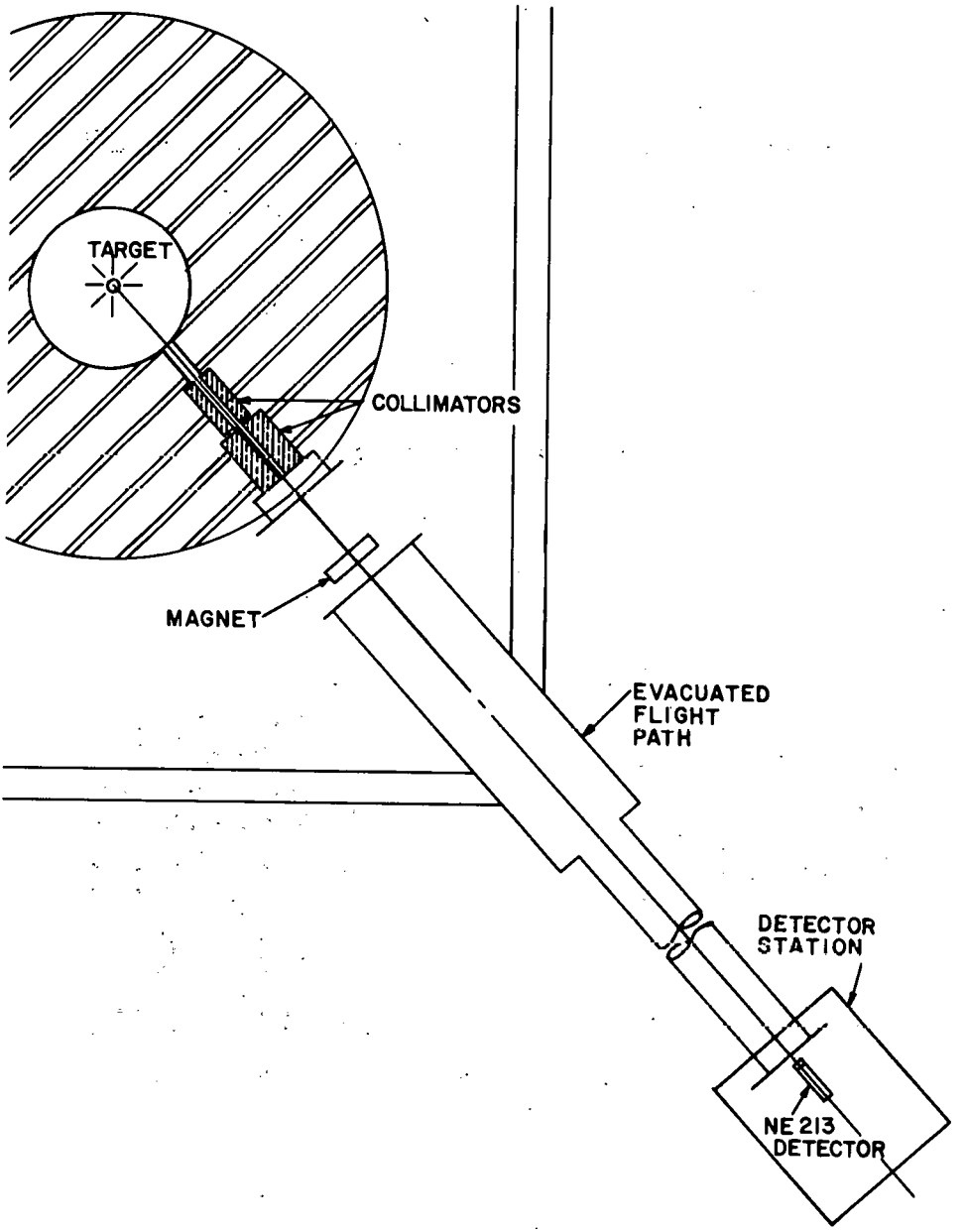

Fig. 4 Experimental setup to measure the neutron yield from WNR high-current production targets.

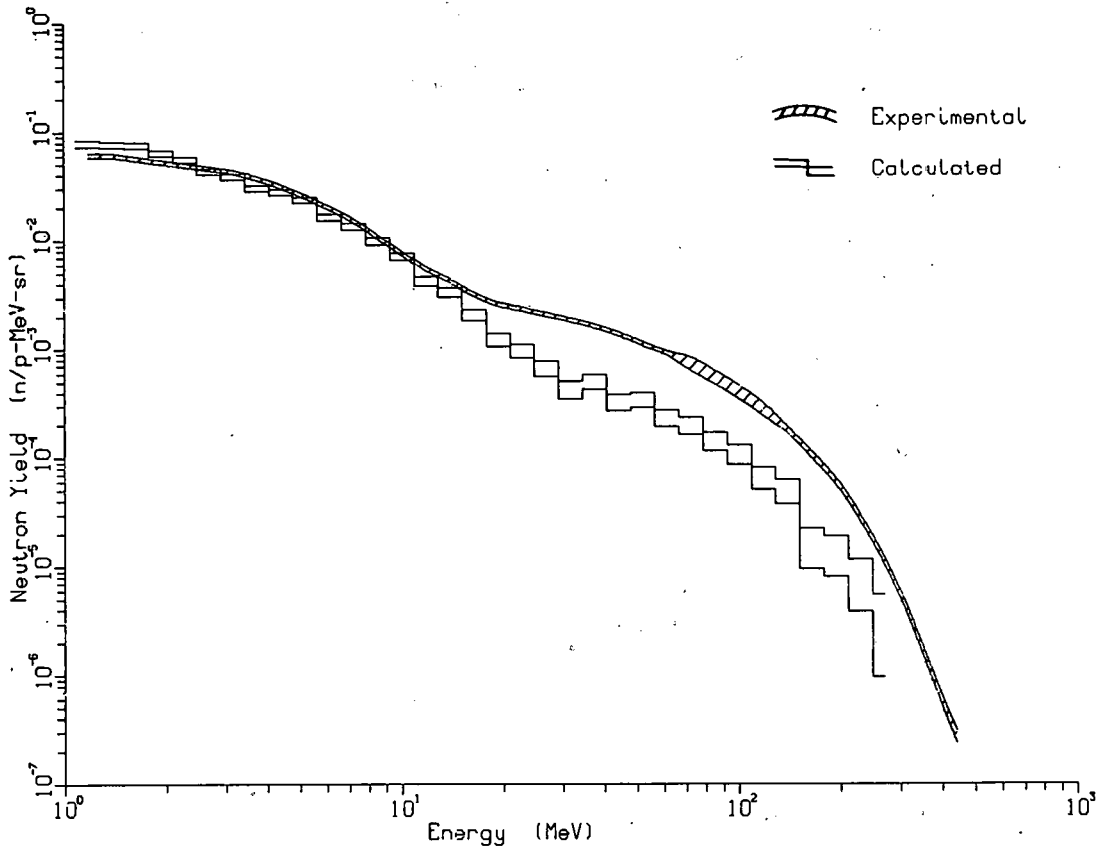

Fig. 5 Neutron yield at 90° to the axis of the WNR tantalum production target. We viewed the full target diameter, and limited the vertical "field-of-view" to ± 2.2 cm centered 3.8 cm from the target top. The experimental data are arbitrarily normalized to the calculation at 10 MeV.

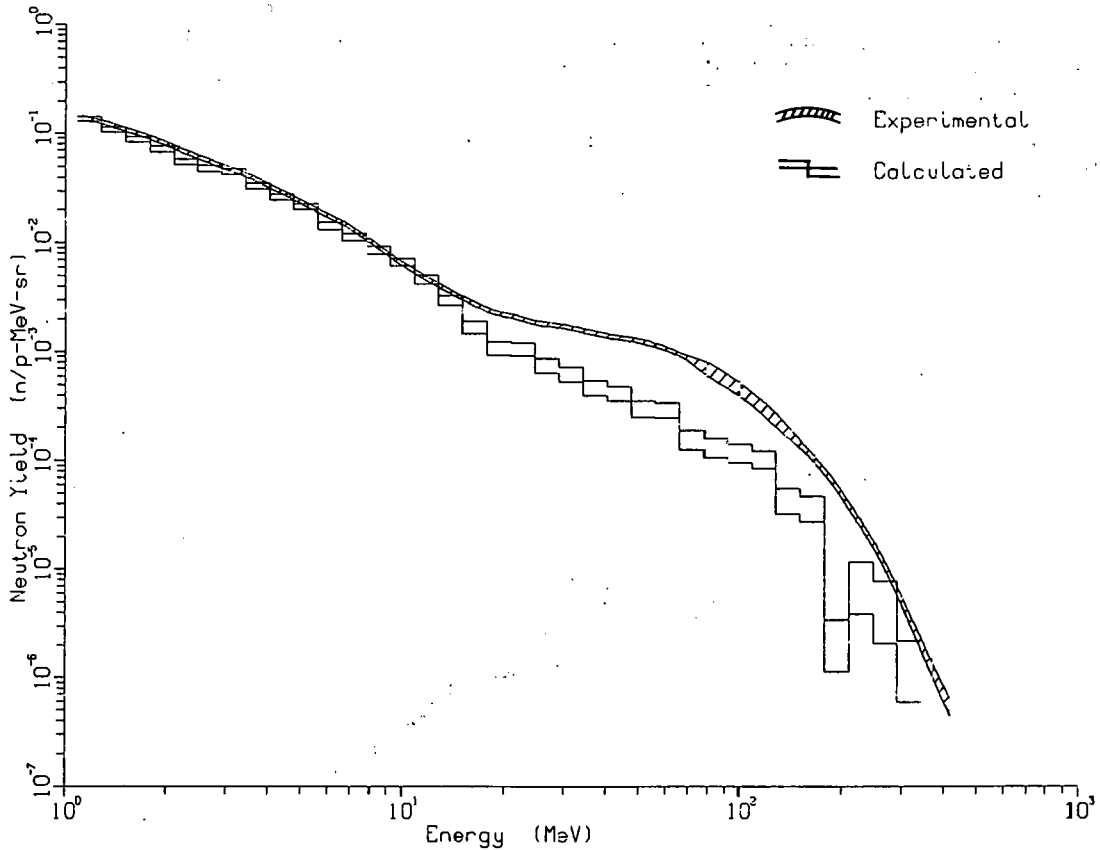

Fig. 6 Neutron yield at 90° to the axis of the WNR tungsten production target. We viewed the full target diameter, and limited the vertical "field-of-view" to ± 2.2 cm centered 3.8 cm from the top of the solid tungsten rod. The experimental data are arbitrarily normalized to the calculation at 10 MeV.

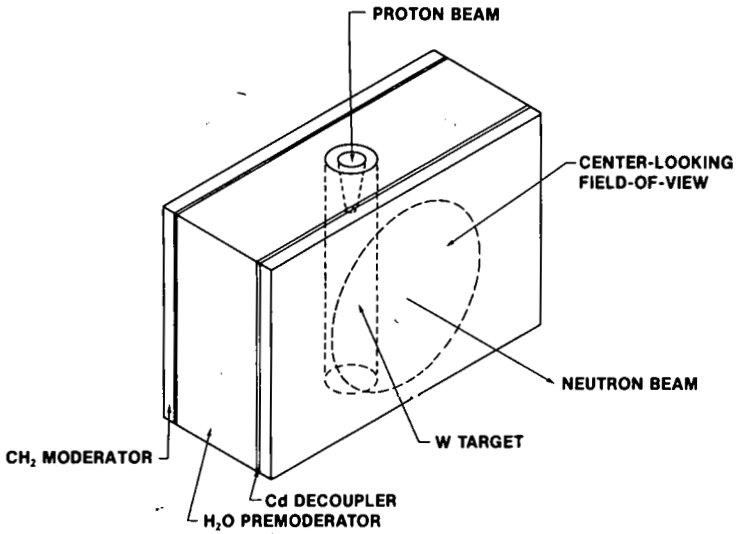

Fig. 7 Unreflected hybrid slab-moderator which is presently used at the WNR for thermal neutron production. An unpoisoned CH_2 moderator is used with the tantalum production target for epithermal neutron generation.

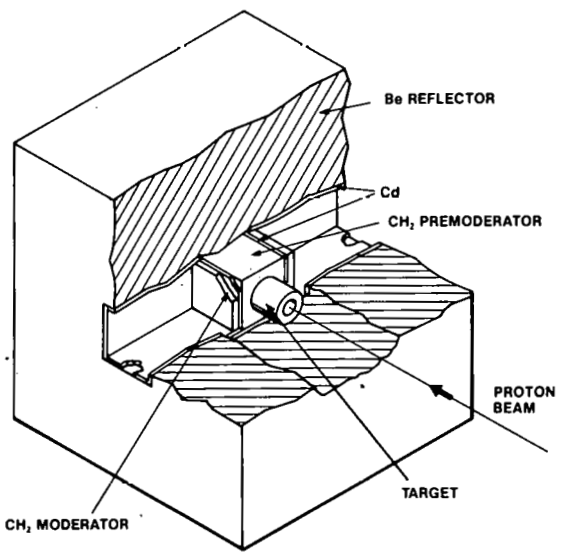

Fig. 8 This figure depicts a reflected hybrid slab-moderator. Such a configuration is neutronically efficient.

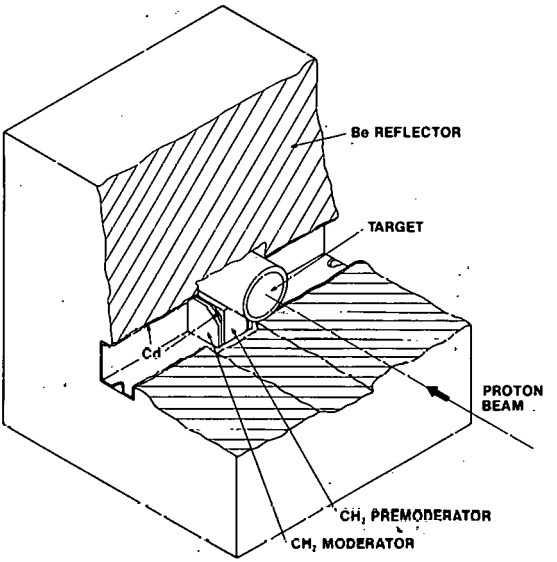

Fig. 9 This figure depicts a reflected wing-moderator. A variation of this configuration is being adopted at several pulsed spallation neutron sources.

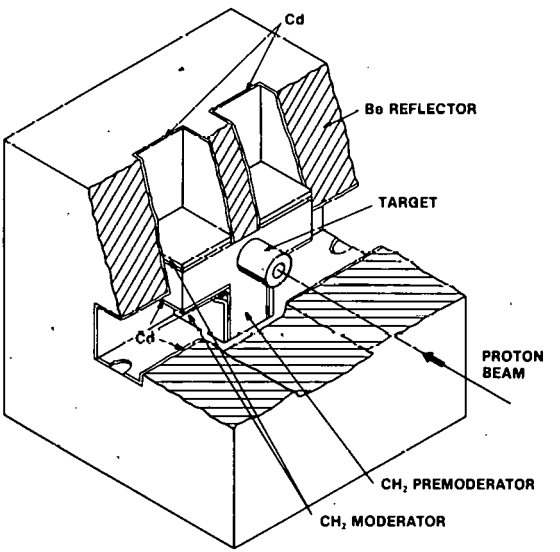

Fig. 10 This figure depicts a reflected T-shaped-moderator. The WNR target-moderator geometry is being reconfigured in this manner for thermal neutron production.

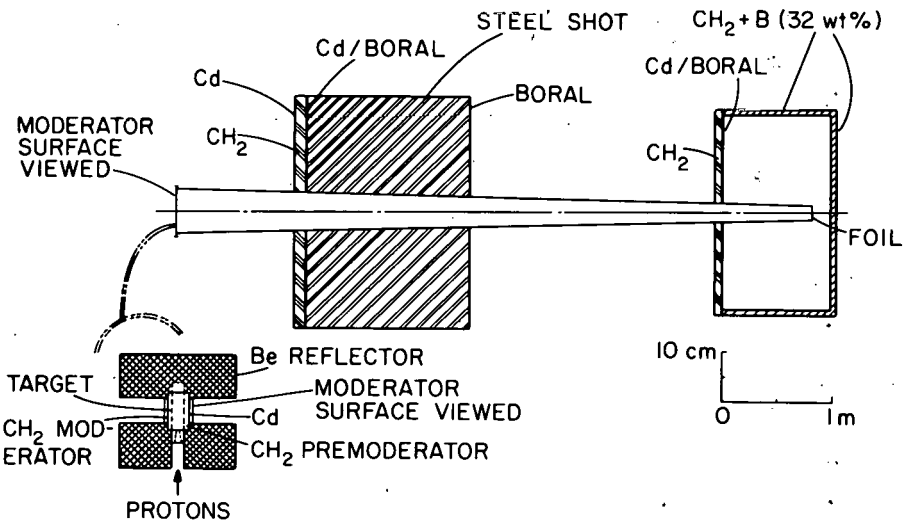

Fig. 11 Experimental setup used in preliminary measurements of thermal and epithermal neutron beam fluxes.

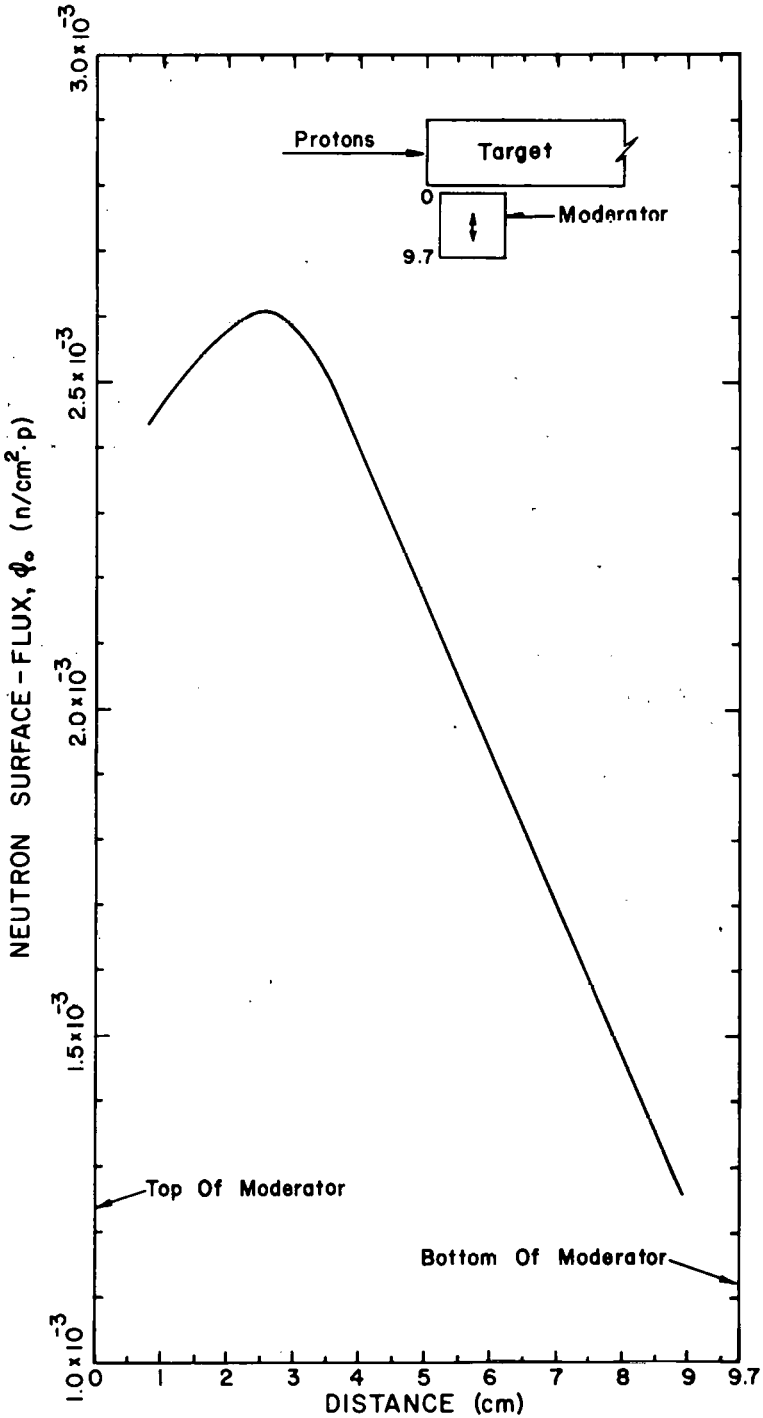

Fig. 12 Preliminary 2200 m/s neutron surface flux distribution from a reflected wing-moderator (see Fig. 9). The distribution shown lies along the vertical center of the 9.7-cm by 9.7-cm moderator surface.

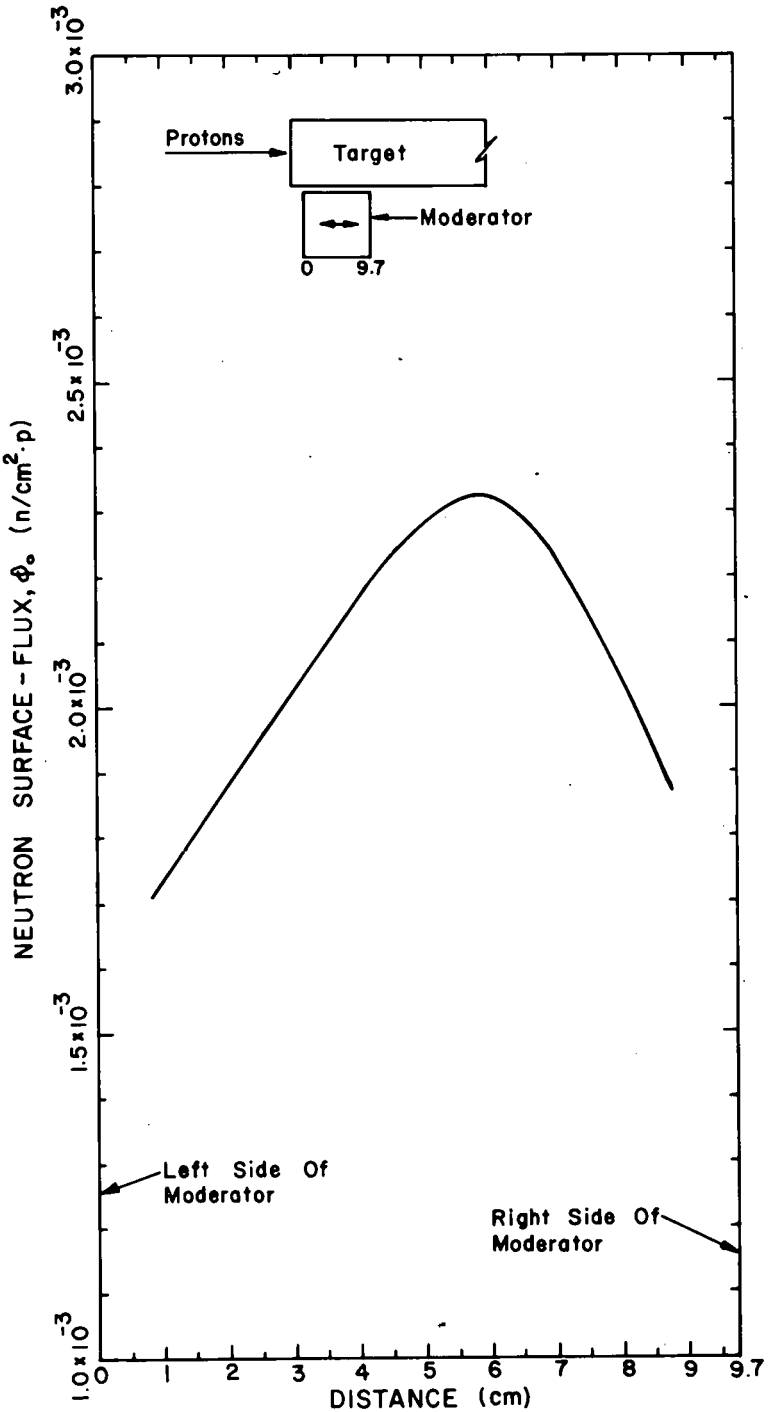

Fig. 13 Preliminary 2200 m/s neutron surface flux distribution from a reflected wing-moderator (see Fig. 9). The distribution shown lies along the horizontal center of the 9.7-cm by 9.7-cm moderator surface.

THIS PAGE
WAS INTENTIONALLY
LEFT BLANK

PRODUCTION OF 14 MeV NEUTRONS WITH THERMAL NEUTRONS ON ^{6}LiD

M.A. Lone, D.C. Santry and W.M. Inglis

Atomic Energy of Canada Limited
Chalk River Nuclear Laboratories
Chalk River, Ontario, Canada K0J 1J0

ABSTRACT

Production of fast neutrons from capture of thermal neutrons in ^{6}LiD and LiD is measured and calculated. The thick target fast neutron yield measured from a ^{6}LiD converter is 156×10^{-6} per thermal neutron of which ∿67% is from neutrons with $E_n > 12$ MeV. The corresponding numbers for LiD are 318×10^{-6} and ∿35%.

INTRODUCTION

There is increasing interest in intense source of fast neutrons particularly 14 MeV for materials radiation damage studies for fusion related programs. The bombardment of light nuclei with tritons yields very energetic neutrons owing to the large positive Q value of (t,n) reactions [1,2]. The principal disadvantage of these reactions is the need for using radioactive tritium either as a target or projectile. The reaction $T(d,n)^{4}He$ has been commonly used for production of 14 MeV neutrons and even at low deuteron bombarding energies this reaction has a prolific yield [3,4]. The maximum neutron flux attainable at present, with solid TiT targets, is $\leq 10^{12}$ $n \cdot s^{-1} \cdot sr^{-1}$ [3]. This limitation is partly due to the target heating which results in thermal dissociation and release of tritium.

Another means of producing 14 MeV neutrons is to irradiate a ^{6}LiD converter with thermal neutrons [5]. Tritons of energy 2.73 MeV are produced in the primary reaction $^{6}Li(n,t)^{4}He$ for which the thermal neutron cross section is 940 b (1 b = 10^{-28} m^2). Subsequent interactions of these tritons with deuterium and isotopes of Li produce high energy neutrons by the following reactions:

$$D + t \rightarrow {}^{4}He + n + 17.586 \text{ (MeV)}$$

$$^{6}Li + t \rightarrow {}^{8}Be + n + 16.02 \text{ (MeV)}$$
$$\rightarrow 2\,{}^{4}He + n + 16.115$$
$$\rightarrow {}^{5}He + {}^{4}He + 15.15$$

$$^{7}Li + t \rightarrow {}^{9}De + n + 10.435 \text{ (MeV)}$$
$$\rightarrow {}^{8}Be + 2n + 8.768$$
$$\rightarrow 2\,{}^{4}He + 2n + 8.85$$
$$\rightarrow {}^{5}He + {}^{4}He + n + 7.905$$

Although these reactions produce neutrons with a broad energy distribution, there is a dominant high energy component with $E_n > 12$ MeV due to the D(t,n) reaction and the ground state transition in the $^{6}Li(t,n)$ reaction. Here we call these components the 14 MeV neutrons.

In this paper we report on our measured and calculated thick target fast neutron yields from ^{6}LiD and LiD following bombardment with thermal neutrons.

EXPERIMENTAL PROCEDURE

Thick target fast neutron yields from thermal neutron capture in several Li and B compounds were measured at the N4 external thermal neutron facility at the CRNL NRU reactor. The experimental set up is shown in Fig. 1. It provides an extremely clean thermal neutron beam with a Cd ratio of $\sim 10^{6}$ at the target location.

Fast neutron yields were measured at 90° to the beam with a long counter of high efficiency and relatively flat response. The targets studied were powders contained in thin polyethylene bags. The overall uncertainty in the measured yields is less than 30%. Further experimental details are given in ref. 2.

CALCULATION OF FAST NEUTRON YIELDS

The neutron yields expected from ^{6}LiD and LiD compounds were calculated [2] using known (t,n) cross sections and the stopping powers of tritons in lithium and deuterium.

For a thick compound target the neutron yield per incident triton can be calculated from the expression

$$Y_n = \int_{o}^{2.7} \sum_{i} [e^{-\sigma X} N_i S_i^{-1}(E)\, \sigma_{t,n}^{i}(E)\, \delta E_i]\, dE$$

where $e^{-\sigma x}$ = the transmission of the triton ≈ 1,

N_i = the number of atoms of the isotope i per cm^3,

S_i = the stopping power of the isotope i for tritons,

$\sigma^i_{t,n}$ = the neutron production cross section,

and

E_i = the fraction of the dE energy loss of tritons due to the isotope i.

In a thick target the number of tritons interacting with the target will be less than the number of incident thermal neutrons since there is a competition between Li(n,t) and other reaction channels, i.e. (n,γ) and (n,n) reactions. In addition, due to the isotropic angular distributions of the tritons, some tritons will escape from the surface of the target. An accurate evaluation of the fraction of tritons available for interaction within the target per incident thermal neutron would require detailed Monte Carlo calculations. This fraction will be between 0.5 and 1 depending on the target composition, packing density and the geometrical shape.

RESULTS

The calculated thick target yields from ^{6}LiD and LiD compounds are given in Table 1. In ^{6}LiD target the D(t,n) reaction contributes 60% to the neutron yield, all of which is at neutron energies above ∿12 MeV. The neutron spectral distribution from ^{6}Li(t,n) reaction at E_t = 1.1 MeV is shown in Fig. 2. From this we estimate that for E_t = 2.73 MeV ∿20% of the neutrons from thick targets have energies above 12 MeV. Thus the relative magnitude of the yield with E_n > 12 MeV from ^{6}LiD is ∿67%.

In a LiD target with natural abundance of lithium isotopes the ^{7}Li(t,n) reaction accounts for 66% of the neutron production, most of which is at E_n < 12 MeV. Thus the percentage of high energy neutrons from this target is only ∿35%.

Our measured yield from ^{6}LiD is 156×10^{-6} per thermal neutron, of which 104×10^{-6} would be high energy neutrons. The ratio between the observed yield per incident thermal neutron and the calculated yield per triton is 0.6. This is quite reasonable in light of the isotropic angular distributions of tritons from the ^{6}Li(n,t) reaction as discussed earlier. Assuming the same reduction factor for LiD, the corresponding numbers would be 318×10^{-6} and 112×10^{-6} respectively. The 15 MeV neutron yield values for ^{6}LiD and LiD reported by Frigerio [6] are 170×10^{-6} and 110×10^{-6}, respectively.

DISCUSSION

The above results indicate that a ^{6}LiD converter can be effectively used to produce an almost homogeneous flux of neutrons with energies 12 to 18 MeV at an efficiency of 10^{-4} per thermal neutron. Assuming a factor of 2 for flux depression, a thermal neutron flux of 2×10^{15} $cm^{-2} \cdot s^{-1}$ will give a fast neutron flux of $\sim 10^{11} cm^{-2} \cdot s^{-1}$ and neutron fluence of $3 \times 10^{18} cm^{-2}$ over a period of one year.

The practical usefulness of a ^{6}LiD converter can be assessed by comparing its conversion efficiency ($\sim 10^{-4}$) with the fast neutron fraction available from a neutron irradiation position in a reactor core [7]. For applications where only neutrons with $E_n > 12$ MeV are effective (e.g. for reactions involving (n,2n) thresholds) the ^{6}LiD converter would provide little improvement because, as one can estimate from the Watt expression [8], in such locations the fraction of neutrons with $E_n > 12$ MeV is about 3×10^{-4}. However, for applications of neutrons with $E_n > 12$ MeV and for which the background of neutrons of lower energy is important, the use of a ^{6}LiD converter in an irradiation location with good cadmium ratio could provide a source with almost 67% of the neutrons with $E_n > 12$ MeV.

TABLE 1

Calculated thick target fast neutron yields per 10^6 tritons

Target	^{6}Li abundance %	Relative Contribution %			Yield per 10^6 triton	
		^{6}Li	^{7}Li	D	All E_n	$E_n > 12$ MeV
^{6}LiD	95.5	34	6	60	283	190
LiD	7.5	2	66	32	531	187

ACKNOWLEDGMENTS

We greatly appreciate the help of Mr. R.D. Werner and Mr. J. Gallant for preparation of targets and in the foil activation analysis for thermal beam monitoring.

REFERENCES

1. C. MAPLES, G.W. GOTH and J. CERNY, "Nuclear Reactions Q-Values", Nuclear Data Tables 2A, 429 (1966).

2. M.A. LONE, D.C. SANTRY and W.M. INGLIS, "MeV Neutron Production from Thermal Neutron Capture in Li and B Compound". Accepted for publication in Nucl. Instr. & Methods, 1980.

3. H.H. BARSCHALL, "Intense Sources of Fast Neutrons", Ann. Rev. Nucl. Part. Sci. 28, 207 (1978).

4. M.A. LONE, "Intense Fast Neutron Source Reactions", Int. Proc. Symp. on Neutron Cross-Sections from 10-40 MeV. National Nuclear Data Centre, Brookhaven National Laboratory (1977), p.79.

5. E. ALMQVIST, "Fast Neutrons from the T+D and T+Li Reactions", Can. J. Research, A28, 433 (1950).

6. N.A. FRIGERIO, "Conversion of Reactor Neutrons to 15 MeV with LiD", Argonne National Laboratory Report ANL-7870 (1971), p.10.

7. C.M. WYSOCKI and H.C. GRIFFIN, "On the Utility of an In-Core Fast Neutron Generator", Nucl. Instr. & Meth. 156, 605 (1978).

8. B.E. WATT, "Energy Spectrum of Neutrons from Thermal Fission of ^{235}U", Phys. Rev. 87, 1037 (1952).

9. V.I. SEROV and B. YA. GUZHOUSKII, "Investigation of the Reactions $^{6}Li(t,n)$, $^{7}Li(t,n)$, $^{7}Li(^{3}He,n)$, $^{9}Be(t,n)$ and $^{9}Be(^{3}He,n)$", Atomnaya Energiya 12, 11 (1962).

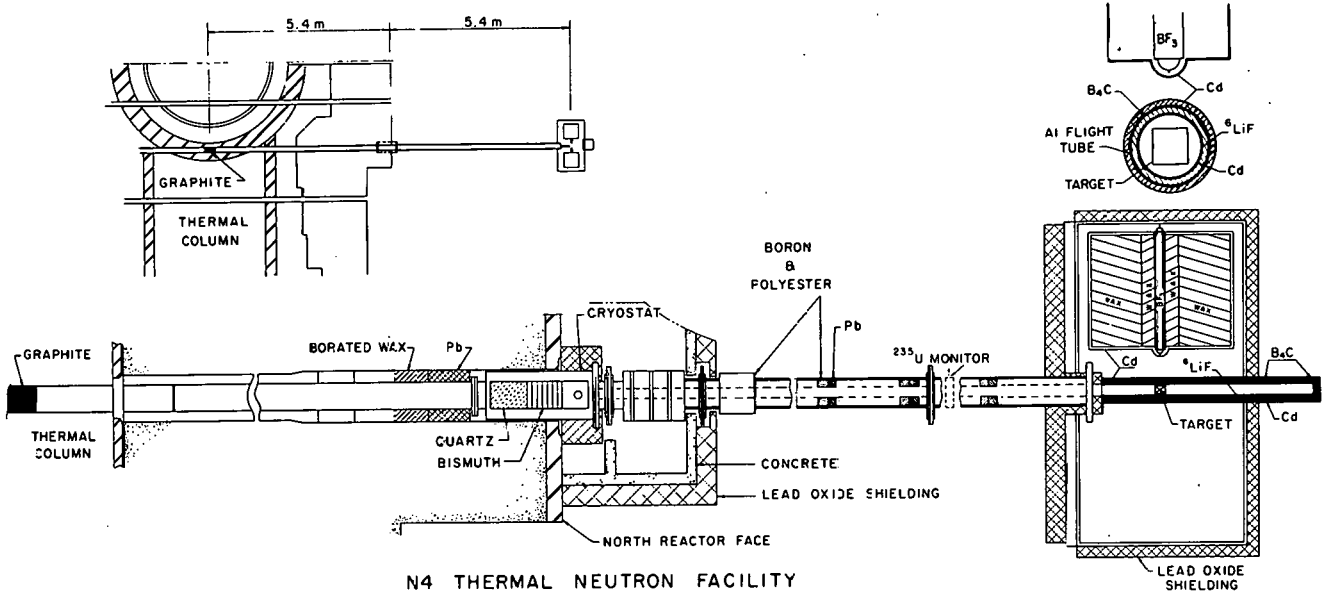

N4 THERMAL NEUTRON FACILITY

Fig. 1. Arrangement of the N4 external thermal facility at NRU. The target tube was lined with Cd for the fast neutron measurements [Ref. 2]. Thermal neutron flux at the target was 4×10^7 $cm^{-2} \cdot s^{-1}$ and the Cd ratio was $\sim 10^6$.

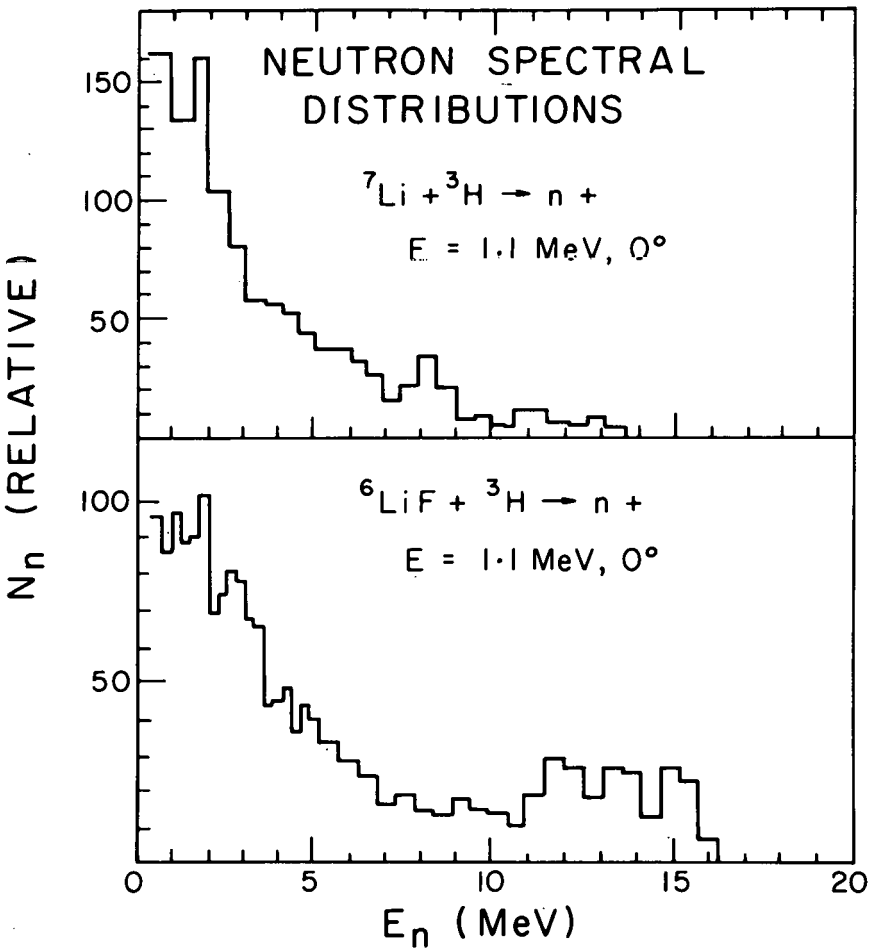

Fig. 2. Spectral distributions of neutrons from triton interactions with ^{7}Li and ^{6}LiF. The group above 12 MeV in ^{6}LiF is due to the $^{6}Li(t,n)^{8}Be$ reaction [Ref. 9].

THIS PAGE

WAS INTENTIONALLY

LEFT BLANK

NEUTRON YIELDS AND SPECTRA FROM 590 MeV (p,n) REACTIONS ON LEAD TARGETS

S. Cierjacks, M.T. Rainbow,[x] M.T. Swinhoe[+] and L. Buth

Kernforschungszentrum Karlsruhe
Institut für Kernphysik II
Postfach 3640
7500 Karlsruhe
Federal Republic of Germany

ABSTRACT

Time-of-flight measurements of neutrons and protons produced by bombardment of thick lead targets with 590 MeV protons have been carried out at the SIN cyclotron. Measurements were made at angles of 30°, 90° and 150° for different penetration depths of protons in a 10 cm diam x 60 cm long target. The detector was an NE 213 liquid scintillator. Differential neutron data are presented and compared with intranuclear-cascade-evaporation model calculations. First results of the secondary proton yield and spectra are also presented.

1. INTRODUCTION

In the last few years the interest in medium energy proton reactions has considerably increased, mainly because of the growing interest in spallation neutron sources and the continuing interest in accelerator breeding. In order to predict the important quantities such as neutron or secondary proton yields and spectra, several theoretical models have been developed during the last two decades. Nevertheless, the accuracy of such predictions, particularly for detailed differential data, is often not well enough known. This is mainly due to the lack of experimental information in this area. Apart from various total yield determinations, only a few differential measurements of absolute particle emission spectra from bare metal targets have been made in the past. Comparisons of existing measurements with model predictions have shown good

[x] On leave from A.A.E.C. Research Establishment, Sydney, Australia

[+] On leave from University of Birmingham, England.

agreement as well as significant differences. The latter is mainly true for the high energy tails of angular dependent neutron spectra, which are often underestimated by theoretical models. Therefore we have carried out new absolute measurements of angular dependent particle emission spectra as a function of proton penetration into a thick lead target. These data, at 600 MeV, provide additional experimental information to test theoretical predictions in the previously not well covered intermediate energy range. The measurements give neutron and proton emission spectra at 30°, 90° and 150° at seven distances into the target between 0 and 35 cm.

In section 2 of this paper the experimental set-up and electronic circuitry are described. Section 3 gives a brief summary of the method used in the data analysis. Typical results of neutron and secondary proton spectra are presented in section 4 and compared to theoretical calculations. Prospects of the future KfK experimental programme at SIN and SATURN are outlined in section 5.

2. EXPERIMENTAL DETAILS

The measurements were performed at the Swiss Institute for Nuclear Research (SIN) using the 590 MeV proton beam from the ring cyclotron. A schematic diagram of the experimental arrangement is presented in Figure 1. The proton beam, which was pulsed at 16.9 MHz with a $\sim$0.2 ns pulse width, was focussed to 2 cm diameter onto a cylindrical lead target. The target was composed of twelve cylindrical blocks, each 5 cm long and 10 cm in diameter, to give an overall length of 60 cm.

Measurements of secondary particle emission from the target were made at 30°, 90° and 150° via an iron collimator which was $\sim$1m thick. Measurements of particle emission corresponding to different distances into the target were made by moving the target along the beam axis so that individual blocks were opposite the collimator entrance.

The principal detector used was a 2.5 cm thick, 5 cm diameter NE 213 liquid scintillator; used for its pulse shape (particle) discrimination properties. A 0.5 cm thick plastic scintillator was located immediately in front of the liquid scintillator to provide further assistance with particle identification. The passage of charged particles causes both detectors to generate signals, whereas neutral particles, in general, give a pulse in only one. Charged particle spectra (for protons) were accumulated by operating the two detectors in coincidence. Neutral particle spectra (for neutrons) were accumulated by operating the plastic scintillator as a veto detector. Background measurements were performed with the target block opposite the collimator entrance removed.

A block diagram of the electronics is presented in Figure 2. The pulse height signals from the liquid scintillator were fed

through two amplifier channels, one with ten times the gain of the other, to cover the required dynamic range. The timing signal from the liquid scintillator was involved in three functions:

(i) In conjunction with the timing signal from the plastic scintillator, it was used to operate a coincidence unit, in coincidence or veto mode, to generate a master trigger signal which notified the computer that an event of interest had occurred and the gates to the ADCs should be opened.

(ii) It was analysed by a pulse shape discrimination unit. The result of this analysis appeared as a 'pulse shape discrimination time' signal from the TAC, the output of which went to ADC3.

(iii) It started the TAC which provided time-of-flight information via ADC4. This TAC was stopped by a timing signal derived from the cyclotron high frequency.

The contents of the four ADCs were stored event by event on magnetic tape to allow subsequent 2-parameter particle discrimination and time-of-flight analysis.

The charge deposited in the target was monitored by recording the output of the proton beam monitor (see Figure 1). This system consists of a carbon scatterer located in the beam and a pair of plastic scintillators which operated in coincidence to detect scattered protons. It was calibrated by determining the ratio of the count rate of the monitor to that of another plastic scintillator placed in the direct proton beam at reduced current.

The number of master triggers applied to the computer was recorded and used, in conjunction with the number of accepted events, to evaluate the dead time correction.

3. DATA ANALYSIS

The analysis of the neutron data (neutral particle spectra) began with the separation of events into neutron and non-neutron (gamma) by a consideration of pulse height versus 'pulse shape discrimination time'. The neutron events from the corresponding background run were then subtracted. The data were subsequently sorted into suitable time-of-flight bins. The corresponding neutron energies were calculated relativistically according to the time of occurence of the γ-flash and the flight path length.

The beam pulse frequency (16.9 MHz) and flight path lengths (e.g. 1.17 m at 90°) resulted in the production of a single overlap in part of each time-of-flight spectrum. For example, 1.74 MeV neutrons appear to have the same flight time as 500 MeV neutrons for measurements at the 90° position. Separation of the response due to high energy neutrons from that due to low energy neutrons, was achieved by linear extrapolation of the high energy pulse height response down to the bias level. The error associated with this procedure is small due to the shape of the distributions.

The contents of each time-of-flight bin were integrated and the results divided by the detection efficiency of the NE 213 liquid scintillator. The Monte Carlo code of Cecil et al. [1] was used to calculate the required efficiency. The shape of the pulse height spectra produced by the code are in good agreement with the measured spectra in individual time bins. This is the case even when the ranges of the charged particles produced in the detector are greater than the detector dimensions. This gives some confidence in the operation of the code. The bias level used in the calculations was determined by locating the upper edges of the pulse height spectra in various time-of-flight bins and extrapolating to find the proton energy corresponding to the pulse height threshold.

The data were finally scaled by the solid angle subtended by the detector, the dead-time correction factor and the number of incident protons to produce the absolute neutron yield as neutrons per steradian per MeV per proton incident on the target per 5 cm of target length. Finally the results for various distances into the target were added to produce the absolute neutron yield from the whole target.

The analysis of the proton data (charged particle spectra) is much simpler. The response of the liquid scintillator to protons of a particular energy appears as a Gaussian peak in the pulse height spectrum. The data were sorted into time bins as for the neutron case. The peaks in the pulse height spectra in the various time-of-flight bins were located and the area under the peaks above the background was evaluated. The measured spectrum only extends down to 27 MeV due to absorption in the plastic scintillator, which stops protons of lower energy. The absolute secondary proton yield was evaluated in the same manner as the neutron yield.

A correction was made to both the neutron and proton spectra for the measured time resolution of the system. This was done by the second derivative method [2].

4. RESULTS

Figure 3 shows the spectrum of neutrons emitted from the first lead block in the target (0 to 5 cm) at 90° to the incident proton beam. This is compared to the results of measurements made at Los Alamos [3] at an angle of 112° for 800 MeV protons incident on a thin (0.45 cm) lead target. The Los Alamos spectrum has been normalized to give an integral number of neutrons per incident proton (n/p) which is consistent with the data of Fraser et al. [4]. Despite the fact that the two spectra are not directly comparable there is an obvious similarity in shape.

The neutron yield above 1.5 MeV is shown in Figure 4 as a function of distance into the target. These results show that the yield from distances greater than 30 cm is less than 1 per cent

of the total yield. The experimental results suggest that the neutron yield decreases monotonically through the target. However, there is calculational evidence which indicates that the yield actually peaks at small distance from the front surface. This feature is indicated by the solid line drawn through the experimental results.

The sum of the 90° differential spectra for the whole target is presented in Figure 5. It is a reasonable approximation to take this spectrum as representing the average spectrum for all angles of emission with respect to the incident proton beam. On this basis 12.2 neutrons with a mean energy of 22.2 MeV are emitted from the whole target into all angles per incident proton.

The target integrated 90° spectrum from Figure 5 is compared to a recent calculation performed at KFA, Jülich /5/ in Figure 6. The calculational method is based on the 3-dimensional 'High Energy Nuclear-Meson Transport Code, HETC ' [6]. The results presented are from a preliminary calculation of the energy spectrum of neutrons emitted from the whole target (15 cm diam., 80 cm long) at all angles. Also included for comparison are the Los Alamos experimental results [3] already presented in Figure 3 and some calculational results from the same laboratory reported by Fullwood et al. [7]. This latter calculation gives the neutron emission from a lead target (15cm diam., 30 cm long) for an incident proton energy of 800 MeV. The spectra are presented on a relative lethargy scale so that the fraction of neutrons below or above a certain energy is represented by areas under the curves. They have been normalized to the respective n/p values [4]. It is clear, despite the fact that the spectra are not directly comparable, that at the present time calculations are producing spectra which are much softer than those measured.

The differential spectrum of secondary protons emitted from the first block (0 to 5 cm) in the target at 90° is shown in Figure 7. This result shows that the contribution from elastic scattering in lead is small. The bulk of the spectrum is the result of inelastic and nuclear reactions. From our experimental data we have made an estimate of the secondary proton yield. Our preliminary value is 0.11 secondary protons per incident proton.

5. PROSPECTS

Analysis is proceeding on data already collected. In the near future similar measurements will be performed with a uranium target using the 590 MeV proton beam at SIN. Later this year the proton beam from SATURN (Saclay, France) will be used to measure neutron and proton yields from lead and uranium targets for an incident proton energy of 1.1 GeV.

REFERENCES

1. R.A. Cecil, B.D. Anderson and R. Madey, Nucl. Instrum. Methods 161, 439 (1979)

2. H.W. Schmitt, W.E. Kiker and C.W. Williams, Phys. Rev. B 137, 837 (1965)

3. S.D. Howe, N.S.P. King, P.W. Lisowski and G.J. Russell, Contr. Int. Conf. on Nuclear Cross Sections for Technology, Knoxville, Oct. 1979

4. J.S. Fraser, R.E. Green, J.W. Hilborn, J.C.D. Milton, W.A. Gibson, E.E. Gross and A. Zucker, Phys. Canada 21 (2), 17 (1965); G.A. Bartholomew and P.R. Tunnicliffe (Eds.) AECL-2600 (Chalk River) (1966) p. VII, 12

5. D. Filges, P. Cloth, R.D. Neef and G. Sterzenbach, Contr. to Spallation Source Meeting, Bad Königstein, FRG, 18-20 March, 1980

6. HETC - ORNL-4744 (Oak Ridge National Laboratory)

7. R.R. Fullwood, J.D. Cramer, R.A. Haarman, R.P. Forrest, Jr. and R.G. Schrandt, LA-4789 (Los Alamos Scientific Laboratory) (1972)

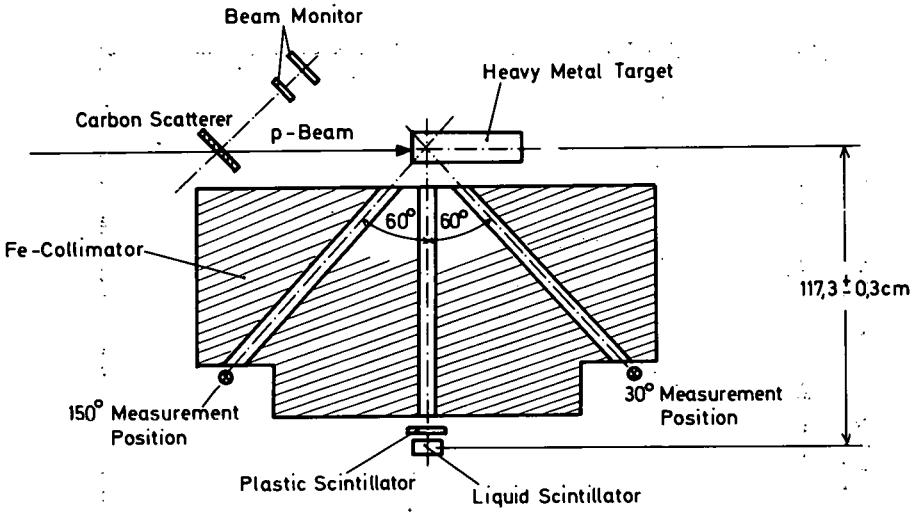

Figure 1 - Schematic diagram of the experimental arrangement for the SIN time-of-flight experiments

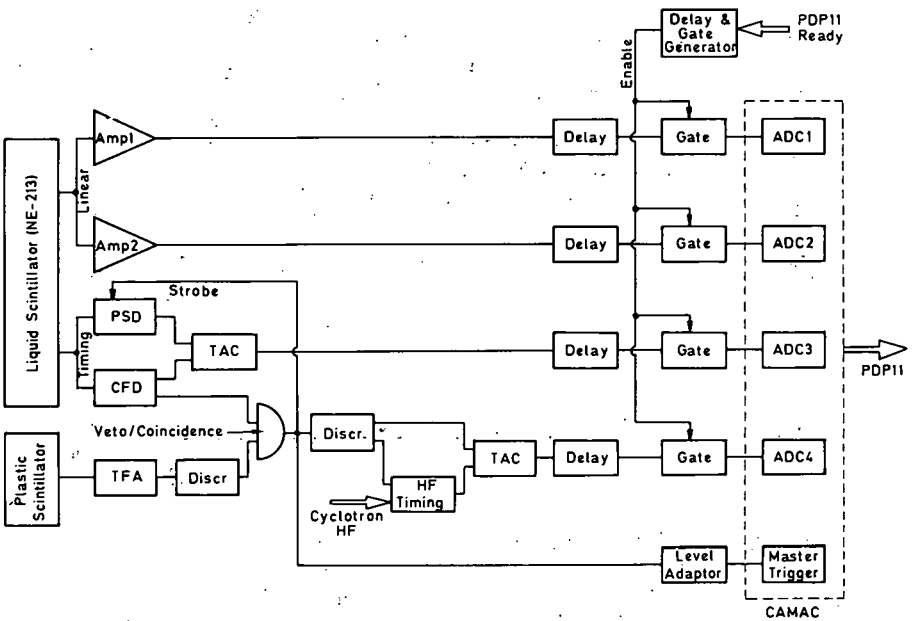

Figure 2 - Block diagram of the electronic system for the SIN time-of-flight experiments

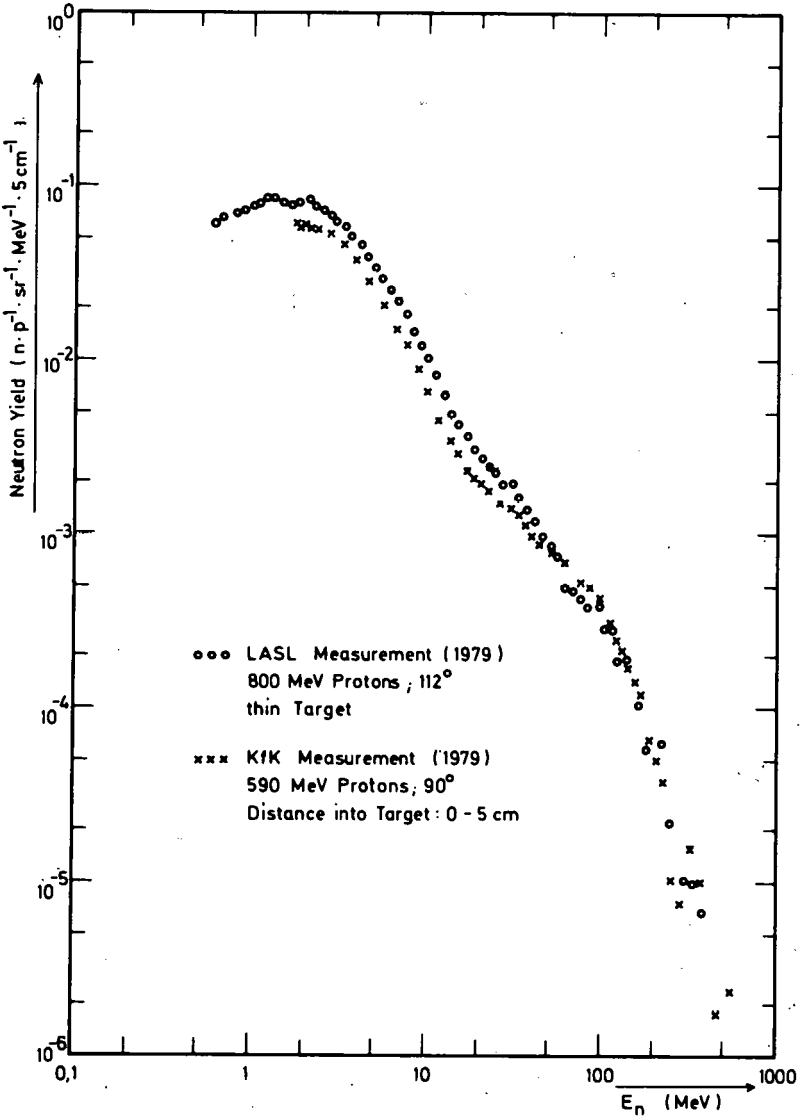

Figure 3 - Differential spectrum of neutrons emitted at 90° from the first 5 cm of the 10 cm diam. lead target for an incident proton energy of 590 MeV. The LASL spectrum was obtained at 112° for 800 MeV protons incident upon a thin lead target

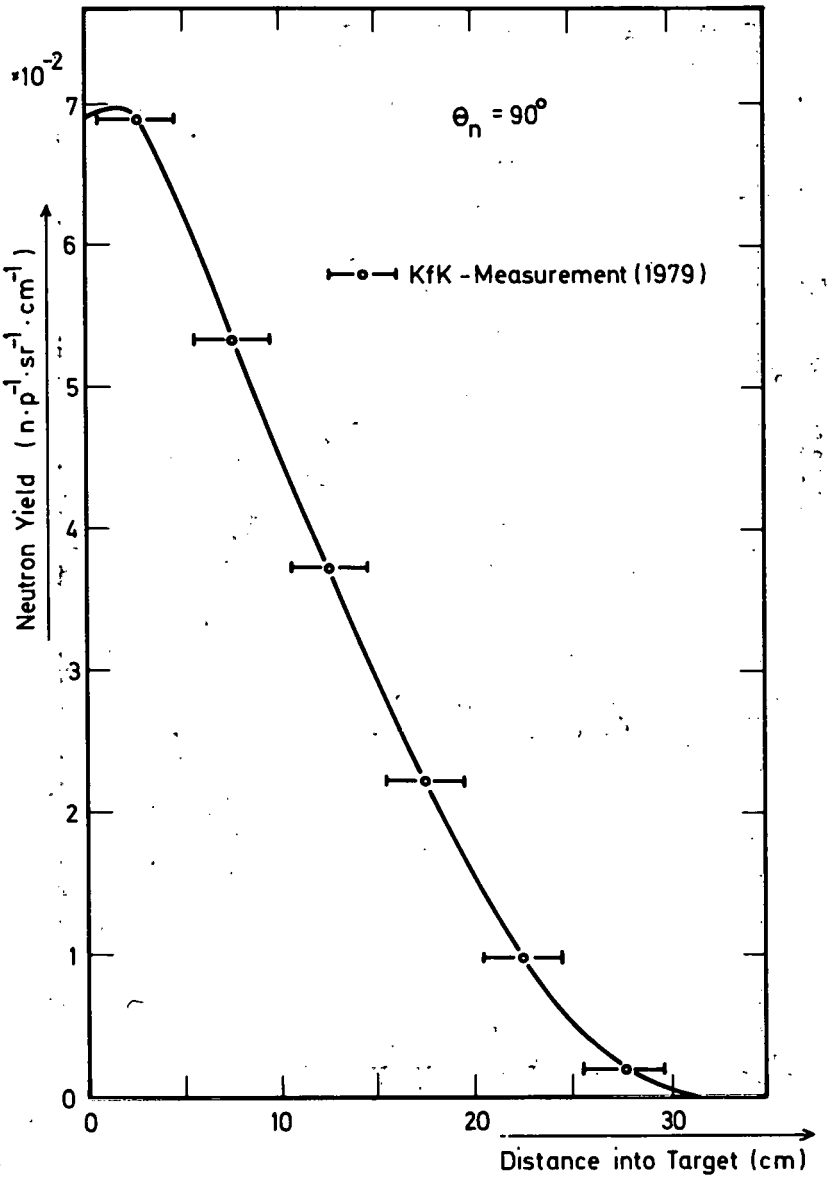

Figure 4 - Total neutron yield at 90° (En ≥ 1.5 MeV) as a function of proton penetration into the 10 cm diam. lead target

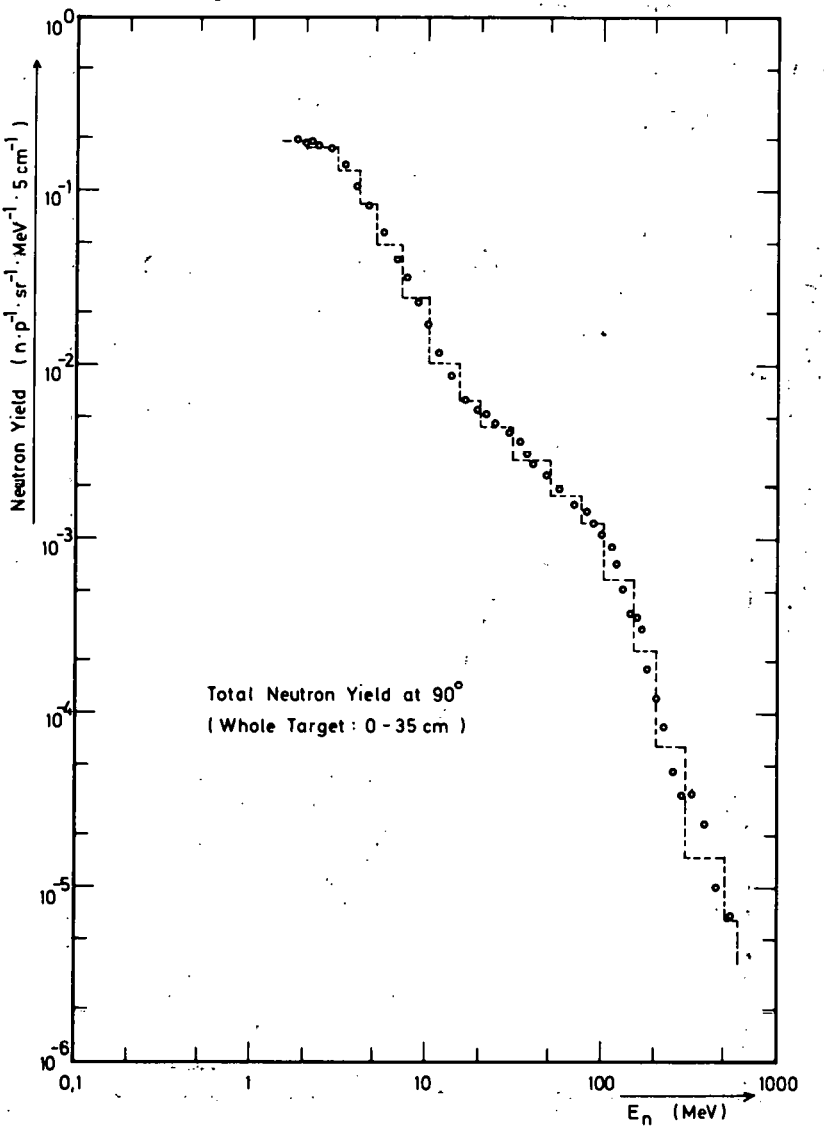

Figure 5 – Differential spectrum of neutrons emitted at 90° integrated over the first 30 cm of the 10 cm diam. lead target. The histogram is a possible energy grouping for numerical calculations

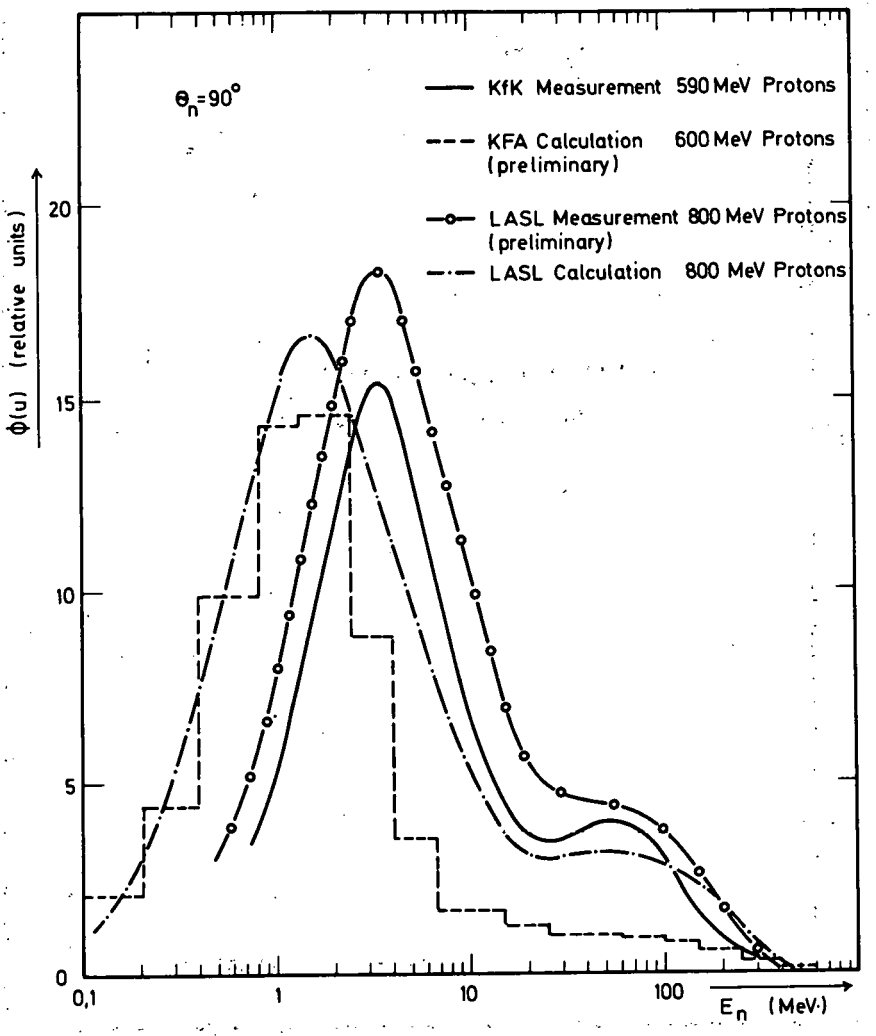

Figure 6 - Measured and calculated neutron spectra for lead targets normalised to respective n/p values

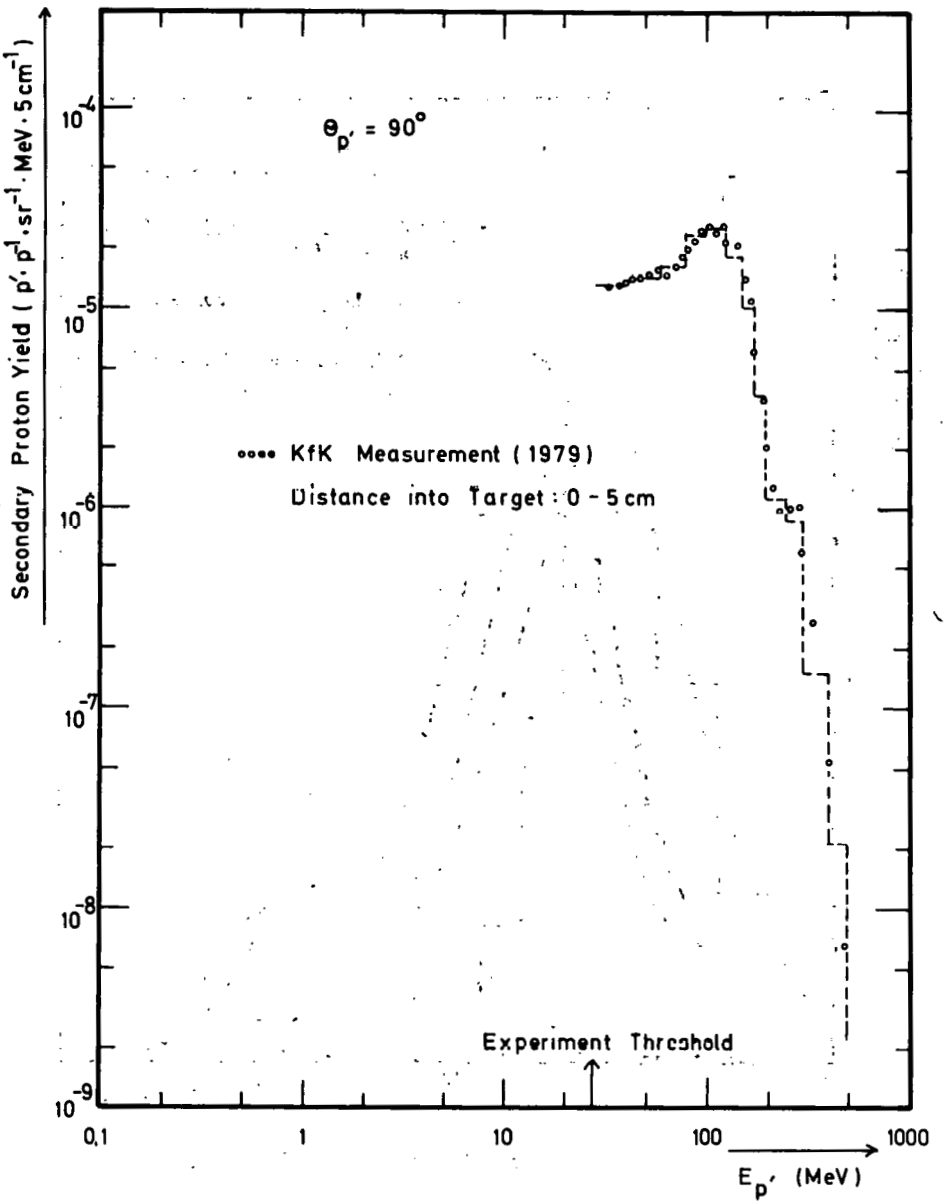

Figure 7 - Differential spectrum of secondary protons emitted at 90° from the first 5 cm of the 10 cm diam. lead target for an incident proton energy of 590 MeV

DIFFERENTIAL DATA INCLUDING DOSIMETRY REACTIONS

Session Chairman: R.C. Haight, LLL

THIS PAGE

WAS INTENTIONALLY

LEFT BLANK

STATUS OF HIGH ENERGY NEUTRON CROSS SECTIONS

J. C. Browne and P. W. Lisowski

Los Alamos Scientific Laboratory
Los Alamos, New Mexico 87545, U.S.A.

ABSTRACT

This paper is a review of the current status of neutron-induced reactions of interest to the fusion community in the 10- to 50-MeV neutron energy range. Although there has been significant activity in this area since the 1977 BNL Symposium on Neutron Cross Sections from 10 to 40 MeV, this review concludes that there are many areas which require more experimentation to obtain the requested accuracy. Examples of various neutron data obtained since 1977 are presented and compared to determine the extent of agreement. An attempt is made to determine what the prospects are for satisfying the fusion data needs defined by the USDOE based upon progress to date.

INTRODUCTION

The nuclear data needs of the fusion-energy program have become more defined as a result of the technical progress in the various fusion concepts (i.e., Tokomaks, magnetic mirrors, ICF, etc.). In particular, system studies of reactor designs have provided direction for material selection and hence cross sections of importance. In addition, the construction of the RTNS-II and the advent of the FMIT facility have provided great stimulus for providing nuclear data needs for radiation-damage studies.

The purpose of this paper is to review the field of high energy neutron differential cross sections in the 10- to 50-MeV energy range since the 1977 BNL symposium on this topic. The review will not be comprehensive but will concentrate on progress to date on the specific requests of the U. S. Department of Energy Fusion Program. The reader is referred to a recent article

by Haight [1] which not only discusses many of the neutron cross sections covered in this paper but also lists previous reviews on neutron data for fusion.

NEUTRON DATA REQUESTS

The neutron data will be discussed according to the requests of the U. S. fusion energy program as delineated by C. R. Head at the IAEA Conference on Nuclear Data for Fusion Reactor Technology [2] held in Vienna in 1978 along with subsequent revisions [3] to that request list. The data will be separated into the needs of the following areas:

1. Data for the Fusion Materials Development Program;
2. Data for the Next Generation of D-T Reactor Designs;
3. Data for D-T Fusion Engineering Prototype and Demonstration Power Plant Designs.

It is difficult to cover every reaction for each element that is of interest. We will concentrate, instead, on providing an overview which should allow the reader to determine the state of the field at this time.

1. DATA FOR THE FUSION MATERIALS DEVELOPMENT PROGRAM

a. Data for FMIT

The main needs pertain to the shielding design for this materials test facility. In particular, total cross section, angular-dependent elastic scattering, and total nonelastic cross section data for Fe, O, Si, Ca, and C are presently required to an accuracy of 10-15% with a longer term (1983) requirement of 5%.

There are several laboratories which have addressed these needs. Both the University of California at Davis [4] and ORELA [5] have recently obtained total cross section (σ_T) data in the 10- to 50-MeV range of the required accuracy for all these elements. In addition, σ_T measurements have been made recently [6] at the WNR facility for carbon and oxygen. Although the quoted accuracy for all these measurements is better than 5%, the agreement is not always so good. Figure 1 shows the case for Fe where a significant discrepancy exists between the Davis and ORELA data. As Fig. 2 shows, including all the σ_T data for Fe clouds the picture even more. The only reasonable assessment at this time is that the short term requirement for 10-15% accuracy has been met, but additional work is necessary to satisfy the longer term need for 5%.

For elastic scattering (σ_{el}) in the 20- to 50-MeV

range, only Ohio University has published any results [7]. Their data are in the 20- to 26-MeV range for Fe, O, Si, and Ca. The quality of the data meets the 10-15% short term need. Recently, U. C. Davis has done some preliminary σ_{el} measurements [4] for carbon at 40 MeV to develop a technique that can be used for satisfying some of these data requirements.

For the total non-elastic cross section, σ_{non}, U. C. Davis developed a technique [4] for obtaining these data which is schematically represented in Fig. 3. Basically, the technique works if σ_T is well known, and if a significant fraction of the elastic cross section is contained within the forward solid angle of the detector. Then σ_{non} is determined from

$$\sigma_{non} = \sigma_T - \eta\sigma_{el}^{OM}$$

using an optical-model (OM) calculation. The result for σ_{non} is not extremely sensitive to the choice of OM parameters. Data have been obtained at 40 and 50 MeV for C, O, Fe, and Ca which meet the 10-15% accuracy requirement in some cases; the most notable exception being C at 40 MeV. This technique is capable of being extended to energies below 40 MeV, particularly if reasonable optical-model parameters exist.

b. Dosimetry Data

Dosimetry cross sections are needed in the 1- to 50-MeV range for a variety of materials to improve the accuracy of flux-spectral measurements and for material-damage-rate calculations. It is unreasonable to discuss the current situation for all thirteen isotopes listed by the USDOE for dosimetry use. Instead, we shall concentrate on cobalt since it appears to be a most promising material.

Cobalt has four reactions of interest to dosimetry, i.e., (n,p), (n,2n), (n,3n), and (n,4n). For the ^{59}Co(n,p) reaction, D. L. Smith of ANL has obtained [8,9] data that cover the 2.6- to 10-MeV energy range and whose accuracy (3-6%) is sufficient for present needs. Near 14 MeV, there is a plethora of data, all of which is not consistent. Table I lists a variety of measurements from 1960 to 1978 which vary over an order of magnitude. If one ignores the result of Jeronymo et al. [14], then the picture is not quite so bad although still unacceptable. The most recent measurement of Fukuda et al. [10] agrees well with Vonach and Munro, [13] Allan, [16] Alvar et al., [11] and Hassler et al. [15] Above the 14- to 15-MeV region, only the suspect data of Jeronymo et al. [14] exist. Clearly there is a need for more accurate data.

For the (n,2n) cross section, Frehaut et al. [18] have data from threshold to 15 MeV, which meet the accuracy requirements of 10-20%. From 16 to 24 MeV, Veeser et al. [19] also have reported data that meet this accuracy. For the (n,3n) reaction, only

Veeser et al. [19] report any data. Their measurements extend from the threshold to 24 MeV with an accuracy of 40% near the threshold and 25% near 25 MeV, neither of which meet the requested accuracy of 10-20%. There are no data reported for the (n,4n) reaction.

It is clear that there is not sufficient data for cobalt to meet these dosimetry needs. Techniques exist for obtaining the (n,xn) data particularly near threshold where the breakup neutrons from the various source reactions do not cause a problem. Such (n,xn) data near threshold are a great aid to model calculations in extending the region of interest above which data cannot be obtained easily. The ^{59}Co(n,p) reaction requires a monoenergetic source, hence its extension to higher energies will require source characterization and unfolding.

The situation for the entire list of requested dosimetry cross sections is not satisfactory. A very comprehensive review of dosimetry data was reported in 1978 by A. B. Smith et al. [20] The conclusions of that review were that only 15% of the primary dosimetry reactions were adequately known with another 35% known with marginal certainty. This has not changed in the intervening two years. There are virtually no data above 28 MeV, and it will be difficult to provide experimental data for all reactions in this energy region. Nuclear-model calculations will have to supply some of the needs. If accurate data are provided at a few energies, calculations should be able to extrapolate with sufficient accuracy. This will be considered more in the Discussion section.

Total helium-production cross sections are also required to complement the radiometric measurements in obtaining flux spectral information. Requirements are for Al, Fe, Cu, Ti, Ni, W, and Au in the 0- to 40-MeV range. Since there is an overlap of this request with that for material damage calculations, this discussion will be covered in Section 1(c).

In addition, fission-fragment track recorders are being developed for dosimetry at FMIT. Fission cross sections, σ_f, in the 14- to 40-MeV range are requested. There are very few data points for σ_f above 20 MeV, and the accuracy and energy resolution are not very good. This is an area where data could be obtained easily for several elements, such as ^{238}U, ^{232}Th, and ^{237}Np, relative to ^{235}U at a variety of white sources (e.g., ORELA, LLL, WNR) or at a quasi-monoenergetic source such as U. C. Davis. Unfortunately, the ^{235}U fission cross section itself is not known so that a measurement relative to the (n,p) cross section probably would be necessary to provide absolute cross section values.

c. Material-Damage Calculations

Differential-angular cross sections for elastic scattering and all nonelastic reactions for Fe, Ni, Cr, Al, Cu, W, Sn, Ti,

and V are needed at a few neutron energies between 15 and 35 MeV for material-damage experiments and calculations.

Elastic-scattering data exist for several of the requested elements in the energy range from 15 to 26 MeV. However, no data exist above 26 MeV. Ohio University has performed measurements on Al [7], Fe [7], Ni [21], and Si [22] between 20 and 26 MeV. Winkler et al. [23] (IRK, Vienna) have measured elastic scattering for Cr at 15 MeV. Galloway et al. [24] (Edinburgh) have made differential-elastic measurements for Cu and W. The requested accuracy is 10% for neutron energies below 25 MeV decreasing to 40% at 35 MeV. The Ohio University measurements are accurate to 5-10%; the results of Winkler have a 15% uncertainty; the Galloway results appear to be within the 10% request.

The request for angular and energy distributions for all emitted particles in nonelastic reactions is, of course, quite comprehensive. Since it is not possible to discuss all pertinent reactions, we shall concentrate on discussing neutron-inelastic scattering and charged particle spectra from neutron reactions.

For differential inelastic scattering, Corcalciuc et al. (Studsvik) have reported results [24a] for ^{56}Fe(n,n') from 16 to 22 MeV. Ohio University has obtained inelastic-scattering data for ^{58,60}Ni [21] at 24 MeV, for Si [22] at 20 and 26 MeV, and for ^{116}Sn [25] at 24 MeV. Winkler et al. [23] (IRK, Vienna) report new inelastic-scattering measurements for Cr at 15 MeV.

For (n, charged particle) measurements involving a determination of the energy spectra and angular distributions of emitted particles, there have been several active groups, most notably that of Haight and Grimes at LLL. Their data cover energy and angular distributions for Al [26], Fe [27], Ni [27], Cr [27], V [28], Ti [26], Cu [27], and Nb [28] for an incident-neutron energy near 15 MeV using a quadrupole spectrometer. A spectrum of emitted protons from Ni for an angle of 90 degrees is shown in Fig. 4. The data were taken at seven angles between 22^{o} and 135^{o}. Examples of angle-integrated α-particle emission spectra for Cr, Fe, Ni, and Cu isotopes are shown in Fig. 5.

Measurements of the ^{50}Cr(n,α) and ^{93}Nb(n,α) energy and angular distributions have been performed by Vonach et al. [29] at 14 MeV using a multitelescope proportional-counter-scintillator system. A multi-angle reaction chamber has been developed at Geel [30] to measure (n,α) energy and angular distributions at 5 angles. Initial measurements [31] on Cr, Fe, and Ni have been in the 5- to 10-MeV range but are capable of being extended to higher energies. Cookson and Wise [32] have developed a proportional-counter-scintillator at Harwell. Initial measurements are planned for Fe, Ni, and Cr near 15 Mev.

All of the above facilities have been developed for use at neutron energies near 15 MeV. Several laboratories have been active above 15 MeV. A facility has been developed at U. C. Davis [4] for neutron-induced charged particle measurements in

the 20- to 60-MeV region. The initial measurements have been for the $^{12}C(n,x\alpha)$ reaction at E_n = 40 MeV. Plans are to extend such measurements to other materials of interest.

Ohio University has constructed a quadrupole spectrometer for differential charged particle spectral measurements. Experiments on $^{58}Ni(n,p)$ at 20 MeV and $^{12}C(n,3\alpha)$ to 25 MeV are planned. [33]

Total differential helium and hydrogen production cross sections are needed at a few points in the 15- to 35-MeV range to allow unfolding of integral helium and hydrogen production data. Virtually all the data on these cross sections exist near 15 MeV although there are plans to measure helium production cross sections at IRK (Vienna) for ^{63}Cu in the 12- to 20-MeV range [34]. Paulsen et al. [35] (Geel) also report data for $^{54}Fe(n,p)$, $^{54}Fe(n,\alpha)$ and $^{56}Fe(n,\alpha)$ in the 12- to 17-MeV region using activation methods. The measurements at 15 MeV have been performed by several laboratories using a variety of techniques. Table II compares the results obtained by LLL [26-28] at 15 MeV for a series of elements using a quadrupole spectrometer, by Rockwell International [36] using the helium-accumulation technique and by Qaim [37] (Julich) using activation methods. The agreement in all cases is quite good. Table III compares results for isotopes of Cu and Ti in which both the activation technique and the quadrupole spectrometer were employed. The results of Qaim et al. [38] for ^{65}Cu agree well with the results of Grimes et al. [26,27] (LLL) while the results of Winkler [39] for ^{63}Cu do not agree well with the LLL results. The Winkler data have a small (2.5%) uncertainty compared to the LLL results (17%). However, a comparison made by Winkler in Ref. 39 of all the data to date indicates that the activation results tend to yield smaller $^{63}Cu(n,\alpha)$ cross sections than the direct alpha-particle measurements. The source of this discrepancy is not known. Preliminary results [10] from Kyushu University for $^{63}Cu(n,\alpha)$ using activation techniques, however, agree well with the LLL results.

The data needs for material-damage calculations are being addressed in a fairly comprehensive manner. There is a need for data at a few energies above 15 MeV to check calculations, however. Adequate techniques exist for providing the required data.

2. DATA FOR THE NEXT GENERATION OF D-T REACTOR DESIGNS

a. Neutron Emission Spectra

The spectra of neutrons as a function of secondary angle and energy are required for selected neutron energies in the 9- to 15-MeV range for the elements listed in Table IV. The required accuracy is 10%.

This area has been addressed with significant experimental

activity. Table IV indicates the incident neutron energies for which data have been obtained, and the laboratories at which the experiments have been performed. Fig. 6 shows the LASL results for ^{6}Li and ^{7}Li at an incident energy near 10 MeV. Fig. 7 shows the preliminary TUNL results for emission spectra from a variety of elements including angular spectra for Fe at an incident neutron energy of 10 MeV. Iwasaki et al. [40] (Tohoku University) have obtained neutron emission spectra for Al at 12 scattering angles for an incident neutron energy near 15 MeV. Morgan and Perey [41] have measured neutron-emission spectra at ORELA for Al and Cu at incident energies between 1 and 20 MeV. Their technique yields data at one secondary angle near 130° (lab). Chalupka et al. [45] (IRK, Vienna) have completed measurements of angle-integrated secondary neutron spectra for elements listed in Table IV. Some of these results will be presented at this conference.

The accuracies obtained in the measurements discussed above all meet the 10% accuracy requirement except for those of Iwasaki et al. who quote a 7-17% uncertainty in their data.

b. Helium and Hydrogen Production

Helium and hydrogen production cross sections are requested in the 9- to 15-MeV range for the same elements listed in Table IV. As mentioned in Section 1(c), most of data exist near 15 MeV where a considerable variety of techniques have been used. Measurements at 15 MeV on Al, Ni, Cu, Fe, and Cr were discussed in Section 1(c). Data for the remaining elements in Table IV will be discussed below.

For carbon, Farrar and Kneff [46] (Rockwell International) report data at 15 MeV using the helium accumulation method. They plan similar measurements on $^{6,7}Li$, $^{10,11}B$, Pb, and Si. Ohio University has obtained preliminary data [47] for $^{12}C(n,\alpha_0)$ at 9 MeV. LLL plans both helium and hydrogen production cross section measurements at 15 MeV on ^{7}Li, ^{11}B, and Si using their quadrupole spectrometer [48].

The measurements made or planned at 15 MeV appear to address the needs adequately. However there is clearly a need for more data at a few energies below 15 MeV.

c. Breeding Reactions in ^{7}Li

Data on the $^{7}Li(n,n't)$ reaction are required for incident-neutron energies between 11 and 14 MeV. The requested accuracy is 5% although 10% would be valuable. Data have been obtained by measurement of tritium accumulation by Brown et al. [49], Osborn and Wilson [50], and Wyman and Thorpe [51]. A direct measurement was performed by Rosen and Stewart [52] in which the triton tracks were observed in photographic emulsions. In addition, this cross section was extracted from neutron emission

spectral measurements. All of these data are compared in Fig. 8. It was stated in Haight's review article [1] on fusion data that the $^{7}Li(n,n't)$ cross section is uncertain to 25% which is consistent with Fig. 8. A measurement of this cross section by β counting the tritium produced is being conducted at Harwell by Uttley and Swinhoe [53]. A collaborative measurement is also being planned by Julich and Geel in this energy region[54].

3. DATA FOR D-T ENGINEERING PROTOTYPES AND DEMONSTRATION POWER PLANT DESIGNS

a. Neutron Emission Spectra

Similar to the request of 2(a) above, neutron spectra as a function of secondary angle and energy are required for selected energies between 9 and 15 MeV. The elements requested are listed in Table V. along with the laboratories which have made recent measurements. The data from Morgan et al. [55] at ORELA for Nb and Ti span the entire incident neutron energy range of interest but are for a single secondary angle. The data from IRK [45] (Vienna) are angle-integrated spectra at 14 MeV incident neutron energy. The most complete data are those from LASL for ^{9}Be and ^{11}B for incident-neutron energies of 10 and 14 MeV. The data of Tohoku University for Nb at 15.4 MeV incident-neutron energy cover 12 angles from 25° to 155°. The accuracy of all these measurements is better than the requested 10% except for the Tohoku measurements which vary from 7% to 17%.

b. Secondary Gamma Production Cross Sections

This request is for $(n,x\gamma)$ data from the inelastic threshold to 15 MeV for ^{10}B, ^{11}B, and Ti with a 10% accuracy. The most complete results are the data of Morgan et al. [55] for Ti (Fig. 9) which cover the entire range of interest with an accuracy of a few percent or better. For ^{10}B, Nellis et al. [57] have obtained $(n,x\gamma)$ data for incident-neutron energies between 0.5 and 5 MeV and at 14 MeV. Haouat et al. [58] measured $(n,x\gamma)$ cross sections from 7 to 10 MeV for ^{11}B. Bezotosnyi et al. [59] have measured secondary gamma production at 14 MeV for both ^{10}B and ^{11}B.

DISCUSSION

It is clear from the preceding sections and from the number of contributed papers to this session that there has been considerable activity in certain areas of data needs for the 10- to 50-MeV region. It is interesting to compare what has actually been measured in the interim since the 1977 BNL Symposium on this

topic with the recommendations of the Working Group on Differential Data at that meeting. Their report was divided into two parts: (i) transmutation and specific damage cross sections; (ii) dosimetry cross sections.

For charged particle production, one of the main recommendations was for measurements at selected energies between 15 and 50 MeV for selected isotopes to check nuclear model calculations. Above 15 MeV, the only differential data published are those of Paulsen et al. [35] for the $^{54}Fe(n,\alpha)$ reaction using activation technique. However, there are measurements planned [33] at Ohio University for $^{58}Ni(n,p)$ near 20 MeV and $^{12}C(n,3\alpha)$ up to 25 MeV. Also, a collaborative measurement is planned [54] for the $^{63}Cu(n,\alpha)^{60}Co$ reaction in the 12- to 20-MeV region by Geel and IRK (Vienna) using the activation technique.

Although there are not many new data above 15 MeV at this point, there have been significant developments in experimental techniques. These include an (n, charged particle) facility at U. C. Davis [4], a new multitelescope proportional counter - CsI scintillator system at IRK (Vienna) [29], a multi-angle reaction chamber (charged-particle telescopes) at CBNM Geel [30], a proportional counter - CsI scintillator system at Harwell [32], and new quadrupole spectrometers at Ohio University [33] and LLL [48]. Such developments will stimulate new measurements above 15 MeV. Indeed, U. C. Davis has already reported some preliminary $^{12}C(n,x\alpha)$ data for E_n = 39 MeV. Such developments will stimulate new measurements above 15 MeV. The report also recommended feasibility studies into the use of white sources for (n, charged particle) measurements since there is a possibility of obtaining data over the entire energy range. There has been some development at ORELA in this direction with no data to date. Feasibility studies are planned for WNR by N. King of LASL [60].

For total cross sections, the Working Group recommended that measurements be performed over the entire 15- to 50-MeV range. As has been seen, this is one area that has received considerable attention. The total cross section measurements at U. C. Davis, ORELA, WNR, and NBS all provide valuable data with which calculations can be compared for all elements of interest to the fusion program. However, the ability to provide 1% statistical data does not guarantee equal systematic errors as can be seen in the comparison of σ_T data for Fe in Fig. 2. It is important to have several laboratories provide data that agree to within statistical errors so that the model calculations are useful. These discrepancies should disappear as the experimentalists learn more about how to do such measurements in this energy range.

Most of the data for elastic scattering come from the Ohio University group for the energy range between 20 and 26 MeV. U. C. Davis is considering elastic-scattering measurements in the 30- to 50-MeV range but have only preliminary data for carbon at 40 MeV. It may be difficult to obtain a significant set of data

above 30 MeV since the number of facilities capable of doing the measurements are small. The use of calculations will have to be extensive and charged-particle scattering data should be very useful in this regard.

For the elements of interest, data for (n,xn) reactions above 20 MeV are limited. Direct measurements are possible but require care in understanding of the breakup neutron spectrum above 30 MeV. There are no new measurements planned at the present time. Data from (p, xn) reactions could be valuable for comparison with model calculations.

Data in the 9- to 15-MeV range is becoming more plentiful as various laboratories have begun to publish neutron-emission spectra, (n, charged particle) data, tritium-breeding data, elastic and inelastic-scattering cross sections. There should not be any difficulty in meeting the needs of the fusion program as was pointed out by the Working Group in 1977. In 1980, the picture looks even better.

In the area of dosimetry cross sections, the Working Group on Differential Cross Sections defined an appropriate program necessary to provide these needs in a short time scale. The recommendations included formation of a study group of measurers - users - evaluators/theorists to define 10 to 15 critical reaction types. The request list now includes 30 reaction types for 13 elements. The review of Smith et al. [20] stated that such a list is too long and probably redundant in certain areas. We would agree with this assessment. It will be difficult to obtain adequate experimental data for all the reactions over the 1- to 50-MeV range. Initially it would be better to specify fewer cases which have the possibility of achieving satisfactory accuracies by both experimentation and calculation. Another recommendation of the Working Group regarding dosimetry cross sections was that secondary reference standards were to be determined to 3% accuracy relative to H(n,n) for use in these dosimetry measurements. It is not clear that this point has received adequate attention. Measurements above 30 MeV are difficult because the characterization of the source is vital in understanding the activation results. The region above 30 MeV has received very little effort in the past 3 years, and no measurements are planned. Below 30 MeV, there is activity because the measurements are easier to perform and the neutron sources easier to use. Although more data are required, this lower energy region should be addressed adequately in the future. In particular, measurements at Geel in collaboration with IRK (Vienna) should be valuable. Measurements by Qaim et al. in Julich should also provide important data.

CONCLUSIONS

Haight concluded his review of this subject in 1977 with the

observation that the picture for the future was bright even though there were very few data because of the arsenal of new experimental techniques. Three years later, it is easy to remark that the picture is even brighter. There are even more techniques, and there are more laboratories contributing to the field. The data in the 9- to 15-MeV range appear to be of very high quality. Although the data above 15 MeV are still limited, there are new programs planned or in progress to address many of the areas.

The main recommendation of the 1977 Working Group on differential data was that the bulk of the data required for applications should come from model calculations verified by some experimental data. Good theoretical tools for such calculations are certainly available to provide evaluated data sets for many of the fusion data needs. This is evidenced by the eleven contributed talks on this subject later in the conference. It would be very appropriate for the theorist/evaluator community to provide more guidance to the experimentalist now that more experimental programs are underway. Rather than obtaining data for every request, it would be better to first make the best calculations possible to determine which cross sections are sensitive and require the most emphasis in a particular problem.

ACKNOWLEDGMENTS

We would like to thank all the laboratories who graciously sent us information regarding their current and future programs on this subject. The assistance provided by P. Young and E. Arthur was also greatly appreciated

REFERENCES

1. R. C. HAIGHT, "Neutron Cross Sections for Fusion," Proc. Conf. Nuclear Data for Technology, Knoxville, 1979 - to be published; also R. C. HAIGHT, "Review of Neutron Data: 10 to 40 MeV," Proc. Symposium on Neutron Cross Sections 10 to 40 MeV, Brookhaven National Laboratory, 1977, p. 201.

2. C. R. HEAD, "Nuclear Data Requirements of the Magnetic Fusion Power Program of the United States of America," Proc. Conf. On Nuclear Data for Fusion Reactor Technology, IAEA, Vienna, 1978, p. 1.

3. R. N. NG, "Magnetic Fusion Energy Program Nuclear Data Needs - Revision," letter to S. L. Whetstone, April, 1980.

4. U. C. DAVIS Progress Report to NSF, July 1, 1977 to June 30, 1979, Report No. UCD-CNL 192.

5. D. C. LARSON, J. A. HARVEY, and N. W. HILL, "Neutron Total Cross Sections of Hydrogen, Carbon, Oxygen, and Iron from 500 keV to 60 MeV," Proc. Conf. on Nuclear Data for Technology, Knoxville, TN, 1979 - to be published.

6. P. W. LISOWSKI et al., "Neutron Total Cross section Measurements at WNR," these proceedings.

7. J. A. RAPAPORT et al., "Neutron Scattering Measurements at Ohio University in the Energy Range 7-26 MeV," Proc. Symposium on Neutron Cross Sections 10-40 MeV, Brookhaven National Laboratory, 1977, p. 247.

8. D. L. SMITH and J. W. MEADOWS, "Cross Section Measurements of (n,p) Reactions for al, Ti, Fe, Co, and Zn from Near Threshold to 10 MeV," Nucl. Sci. Eng., 58, 314 (1975).

9. D. L. SMITH and J. W. MEADOWS, "Measurement of Cross Sections for the ^{59}Co(n,p) Reaction Near Threshold," Nucl. Sci. Eng., 60, 187 (1976).

10. K. FUKUDA et al., "Activation Cross Sections for Co for 14.6-MeV Neutrons," Report No. NEANDC (J)-56U, 1978, p.44; also see NEANDC(J)-61U, 1979, p. 94.

11. K. ALVAR, "Proton Energy and Angular Distributions from (n,p) and (n,np) Reactions," Nucl. Phys. A195, 289 (1972).

12. L. LEVKOVSKI et al., Sov. Nucl. Phys., 8, 4 (1969).

13. H. VONACH and J. MUNRO, "^{59}Co(n,p) Cross Section at 14.8 MeV," Nucl. Phys., 68, 445 (1965).

14. J. JERONYMO et al., "Absolute Cross Sections for Some (n,p), (n,α), and (n,2n) Reactions," Nucl. Phys., 47, 157 (1963).

15. F. HASSLER and R. PECK, "Neutron-Induced Reactions in Third and Fourth Shell Nuclei," Phys. Rev., 125, 1011.

16. D. L. ALLAN, "An Experimental Test of the Statistical Theory of Nuclear Reactions," Nucl. Phys., 24, 274 (1961).

17. I. PREISS and R. FINK, "New Isotopes of Cobalt; Activation Cross Sections of Nickel, Cobalt, and Zinc for 14.8 MeV Neutron," Nucl. Phys., 15, 326 (1960).

18. J. FREHAUT, Proc. 3rd All-Union Conf. Neutron Physics, Kiev, 1975, Vol. 4, p. 303.

19. L. VEESER, E. ARTHUR, and P. YOUNG, "Cross Sections for (n,2n) and (n,3n) Reactions above 14 MeV," Phys. Rev., C16, 1792 (1977).

20. A. B. SMITH et al., "Nuclear Data for High-Energy Neutron-Damage Studies," NEANDC Meeting, Oak Ridge, Tn, 3-7 April, 1978.

21. Y. YAMANOUTI et al., "Elastic and Inelastic Scattering of 24 MeV Neutrons From Even Isotopes of Ni," Proc. Conf. Nuclear Data for Technology, Knoxville, 1979 - to be published.

22. J. RAPAPORT et al., "Neutron Elastic Scattering on T = 0 Nuclei," Nucl. Phys., A286, 232 (19 7).

23. G. WINKLER, K. HANSJAKOB, and G. STAFFEL, "Measurement of Differential Elastic and Inelastic Scattering Cross Sections with 14-MeV Neutrons on Barium and Chronium," Proc. Conf. Nuclear Data for Technology, Knoxville, 1974 - to be published.

24. R. GALLOWAY and F. WATSON, "Polarization and Differential Cross Sections for Elastic Scattering of 16-MeV Neutrons," Report No. NEANDC(E) - 192U, Vol 8, 1978, p. 121.

24a. V. CORCALCIUC et al., "A Study of the Neutron Induced Reactions for ^{19}F, ^{56}Fe, and ^{59}Co in the Energy Interval 16 to 22 MeV," Nucl. Phys., A307, 445 (1978).

25. R. W. FINLAY et al., "Isospin Effects in Nucleon Inelastic Scattering from Closed Shell Nuclei," Nucl. Phys. - to be published, 1980.

26. S. GRIMES, R. HAIGHT, and J. ANDERSON, "Measurement of Sub-Coulomb-Barrier Charged Particles Emitted from Aluminum and Titanium Bombarded by 15-MeV Neutrons," Nucl. Sci. Eng., 62, 187 (1977).

27. S. GRIMES et al., "Charged-Particle Emission in Reactions of 15-Mev Neutrons with Isotopes of Chromium, Nickel, and Copper," Phys. Rev., C19, 2127 (1979).

28. S. GRIMES, R. HAIGHT, and J. ANDERSON, "Charged-Particle-Producing Reactions on ^{51}V and ^{93}Nb," Phys. Rev. C17, 508 (1978).

29. H. VONACH et al., "Investigation of the Energy and Angular Distributions of Protons and Alpha Particles from (n,p) and (n,α) Reactions," Proc. Int. Symp. on the Interaction of Fast Neutrons with Nuclei, Gaussig, 1978., p. 161.

30. H. LISKIEN et al., "Recent Development of Special Detection Systems at the Van de Graaff of CBNM," Proc. Int. Conf. on the Interaction of Fast Neutrons with Nuclei, Gaussig, 1979.

31. A PAULSEN et al., "Measurement of (n,α) Cross Sections on Cr, Fe, and Ni in the 5- to 10-MeV Range," Proc. Conf. Nuclear Data for Technology, Knoxville, 1979 - to be published.

32. J. COOKSON and C. WISE, "(n, α) Cross Sections," Report No. NEANDC(E) - 192U, Vol. 8, 1978, p. 61.

33. G. RANDERS-PHERSON, Ohio University - private communication (1980).

34. H. VONACH, Institut fur Radiumforschung und Kernphysik, Vienna - private communication (1980).

35. A. PAULSEN et al., "Cross Sections for the Reactions $^{54}Fe(n,\alpha)$, $^{54}Fe(n,p)$," Nucl. Sci. Eng., 72, 113 (1979).

36. H. FARRAR and D. KNEFF, "Helium Generation in Twelve Pure Elements by 14.8-MeV Neutrons," Trans. Am. Nucl. Soc., 28, 197 (1978).

37. S. QAIM et al., 9th Symp. on Fusion Technology, Garmisch, 1976, p. 589.

38. S. QAIM and G. STOCKLIN, "Measurement and Systematics of Fast Neutron Induced Hydrogen and Helium Producing Reaction Cross Sections for FRT - Related Structural Materials," Proc. Specialist Meeting, CBNM, 1977, p. 327.

39. G. WINKLER, "Precise Measurement of the $^{63}Cu(n,\alpha)$ Cross Section with 14-MeV Neutrons," Nucl. Sci. Eng., 67, 260 (1978).

40. S. IWASAKI et al., "Neutron Energy Spectra and Angular Distributions for Al and Nb(n,xn) Reactions at 15.4 MeV," Proc. Conf. Nuclear Data for Technology, Knoxville, 1974 - to be published.

41. G. L. MORGAN, "Cross Sections for Cu(n,xn) and Cu(n,xγ) Reactions Between 1 and 20 MeV," Report No. ORNL-5499 (1979); G. L. MORGAN and F. G. PEREY, "Cross Sections for Al(n,xn) and Al(n,xγ) Reactions Between 1 and 20 MeV," Report No. ORNL/TM-5241 (1976).

42. P. LISOWSKI et al., "Cross Sections for Neutron-Induced, Neutron-Producing Reactions in ^{6}Li and ^{7}Li at 5.96 and 9.83 MeV," Report No. LA-83-42 (1980).

43. P. LISOWSKI, Los Alamos Scientific Laboratory - private communication (1980).

44. A. BEYERLE et al., "Double-Differential Neutron Scattering Cross Sections for Fe, Cu, Ni, and Pb between 8 and 12 MeV," Proc. Conf. Nuclear Data for Technology, Knoxville, 1979 - to be published.

45. A. CHALUPKA et al., "Measurement of Angle-Integrated Secondary Neutron Spectra from Interaction of 14-MeV Neutrons with Medium and Heavy Nuclei," Proc. Int. Symp. on the Interaction of Fast Neutrons with Nuclei, Gaussig, 1979.

46. D. KNEFF and H. FARRAR, "Helium Generation in Fusion Materials," Damage Analysis and Fundamental Studies Quarterly Status Report, Jan.-Mar., 1979; also see Ref. 36.

47. R. FINLAY, Ohio University - private communication (1980).

48. R. HAIGHT, Lawrence Livermore Laboratory - private communication (1980).

49. F. BROWN et al., J. Nucl. Energy, A/B17, 137 (1963).

50. A. OSBORN and H. WILSON, AWRE (1961) - private communication in Ref. 1.

51. M. WYMAN and M. THORPE, Los Alamos Scientific Laboratory Report No. LA-2235 (1958).

52. L. ROSEN and L. STEWART, "Neutron-Induced Disintegration of ^{6}Li and ^{7}Li," Phys. Rev., 126, 1150 (1962).

53. C. UTTLEY and M. SWINHOE, "The $^{7}Li(n,n'\alpha t)$ Reaction," Report No. NEANDC(E)-192U, Vol. 8, 1978, p. 60.

54. S. QAIM, Der Kernforschungsanlage Julich - private communication (1980).

55. G. L. MORGAN, "Cross Sections for the Ti(n,xn) and Ti(n,xγ) Reactions between 1 and 26 MeV," Report No. ORNL-5563, 1979; G. L. MORGAN and F. G. PEREY, "Cross Sections for the Nb(n,xn) and Nb(n,xγ) Reactions between 1 and 20 MeV," Report No. ORNL/TM-5829, 1977.

56. D. L. DRAKE et al., "Double-Differential Beryllium Neutron Cross Sections at Incident Neutron Energies of 5.9, 10.1, and 14.2 MeV," Nucl. Sci. Eng., 63, 401 (1977).

57. D. NELLIS, W. TUCKER, and I. MORGAN, "Gamma-Ray Yield from Neutron Interactions with ^{10}B," Phys. Rev. C1, 847 (1970).

58. G. HAOUAT et al., Jour. de Phys. Suppl., S31, 148 (1970).

59. S. BEZOTOSNYJ et al., Proc. All-Union Conf. on Neutron Physics, Kiev, 1975, Vol. 4, p. 133.

60. N. S. P. KING, Los Alamos Scientific Laboratory - private communication (1980).

61. Y. YU and D. G. GARDNER, "Cross Sections of Some Reactions of Ar, Ti, Ni, Cd, and Pb with 14.1-MeV Neutrons, Nucl. Phys., A98, 451 (1967).

62. P. YOUNG, Los Alamos Scientific Laboratory - private communication (1980).

TABLE I

^{59}Co(n,p) Cross Sections Near 14 MeV

Measurement	Reference	E_n(MeV)	Cross Section(mb)
Fukuda et al.	10	15	53.1 ± 4.5
Alvar et al.	11	14	73 ± 22
Levkovski et al.	12	15	37 ± 6
Vonach and Munro	13	14.8	53 ± 12
Jeronymo et al.	14	14.9	428 ± 70
Hassler et al.	15	14	48 ± 5
Allan	16	14	61 ± 10
Preiss and Fink	17	14.8	83 ± 8

TABLE II

Helium Production Cross Sections Near 15 MeV for Material-Damage Calculations

Laboratory	Technique	Al (mb)	Fe (mb)	Ni (mb)	V (mb)	Nb (mb)	Ti (mb)
LLL[a]	Spectrometer	121 ± 25	43 ± 7	97 ± 16	17 ± 3	14 ± 3	(d)
Rockwell Int.[b]	Helium Accumulation	143 ± 7	48 ± 3	98 ± 6	18 ± 2	17 ± 5	38 ± 3
Julich[c]	Activation				16 ± 1		

[a]Ref. 26, 27, 28

[b]Ref. 36

[c]Ref. 37

[d]Isotopic Data for ^{46,48}Ti in Ref. 26

TABLE III

Helium Production Cross Sections Near 15 MeV for Cu and Ti Isotopes

Laboratory	Technique	^{63}Cu (mb)	^{65}Cu (mb)	^{46}Ti (mb)	^{48}Ti (mb)
LLL[a]	Spectrometer	56 ± 10	13.5 ± 2.6	94 ± 18	28 ± 6
Julich[b]	Activation		17.7 ± 4.3		
IRK, Vienna[c]	Activation	40.7 ± 1			
Ill. Inst. Tech.[d]	Activation				39 ± 6
Kyushu Univ.[e]	Activation	50.4 ± 5.7			

[a]Ref. 26, 27

[b]Ref. 38

[c]Ref. 39

[d]Ref. 61

[e]Ref. 10

TABLE IV

List of Elements for which Neutron Emission Spectra are requested in the 9- to 15-MeV region for the next generation of D-T reactor designs along with laboratories performing recent measurements.

Element	Laboratory	Incident Neutron Energy(MeV)
Al	Tohoku Univ.[a]	15.6
	ORELA[b]	1 - 20
^{7}Li	LASL[c]	10, 14
C	LASL[d]	14
Ni	TUNL[e]	10, 12
	IRK, Vienna[f]	14
Cu	TUNL[e]	10, 12
	IRK, Vienna[f]	14
^{10}B	LASL[c]	10, 14
Fe	TUNL[e]	10, 12
	IRK, Vienna[f]	14
Cr	IRK, Vienna[f]	14
Pb	TUNL[e]	10, 12
Si		
W	IRK, Vienna[f]	14
O		
N		

[a]Ref. 40
[b]Ref. 41
[c]Ref. 42
[d]Ref. 43
[e]Ref. 44
[f]Ref. 45

TABLE V

List of Elements for which Neutron Emission Spectra are requested in the 9- to 15MeV range for D-T fusion engineering prototype and demonstration power plant designs. Included are the laboratories performing recent measurements.

Element	Laboratory	Incident Neutron Energy (MeV)
Be	LASL[a]	10, 14
Ti	IRK, Vienna[b]	14
	ORELA[c]	1 - 20
Nb	Tohoku Univ.[d]	15.6
	ORELA[c]	1 - 20
	IRK, Vienna[b]	14
Sn	IRK, Vienna[b]	14
Mo	IRK, Vienna[b]	14
V		
^{11}B	LASL[e]	10, 14
F		

[a]Ref. 56
[b]Ref. 45
[c]Ref. 55
[d]Ref. 40
[e]Ref. 42

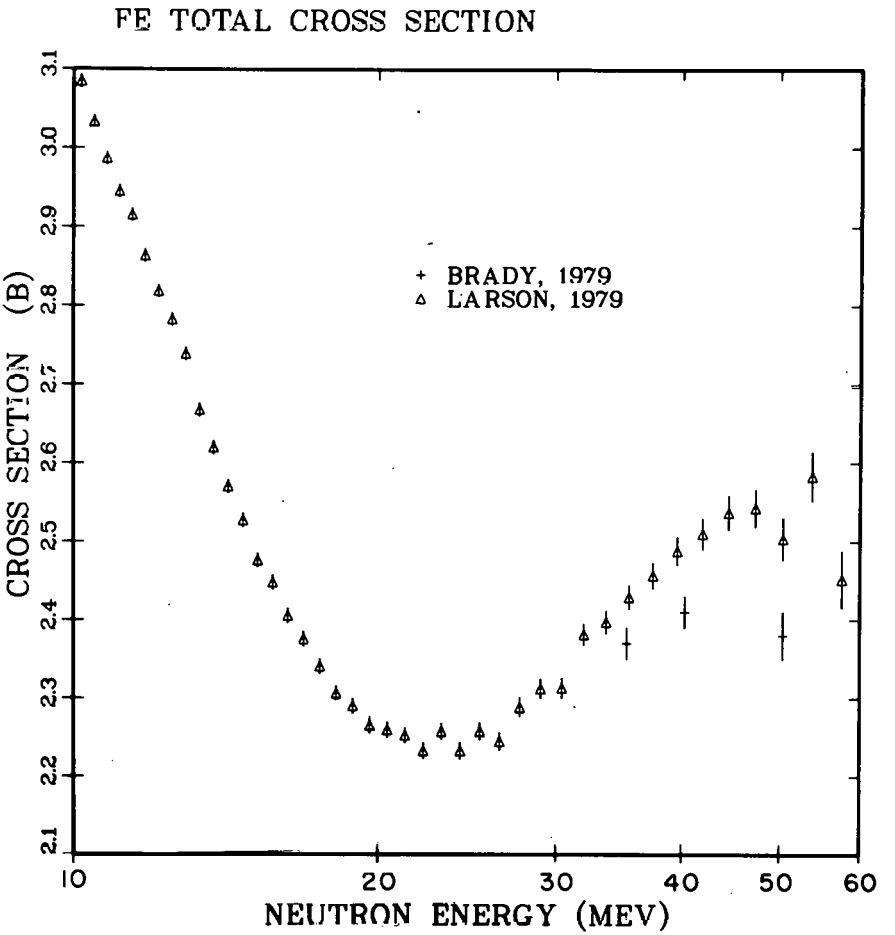

Fig. 1. A comparison of total cross-section results for Fe obtained at U. C. Davis (Brady - Ref. 4) and at ORELA in 1979 (Larson - Ref. 5). The ORELA results are plotted in 5-point averages.

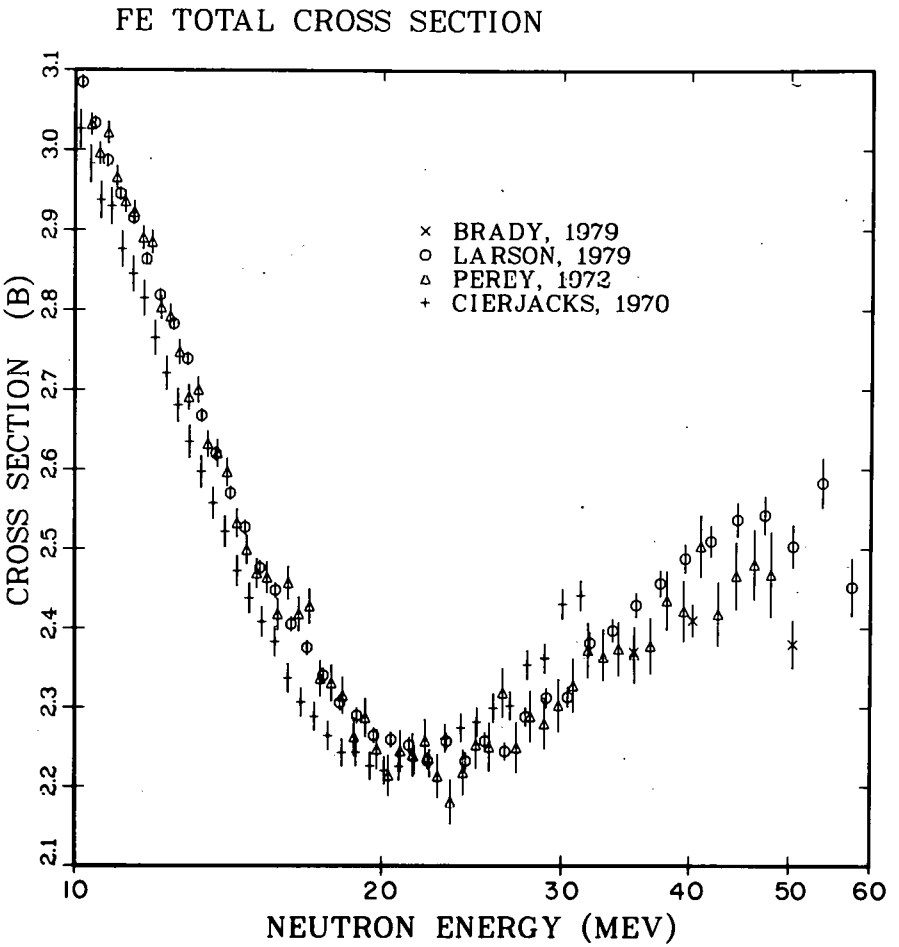

Fig. 2. A comparison of total cross section results for Fe obtained at U. C. Davis (Ref. 4) at ORELA in 1979 (Ref.5), at Karlsruhe (Cierjacks - Ref. 62), and at ORELA in 1972 (Perey - Ref. 62). All ORELA results are plotted as 5-point averages; the Karlsruhe data are plotted as 15-point averages.

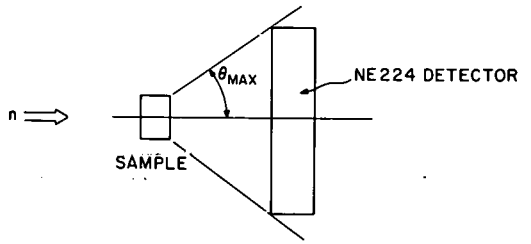

$$\sigma_{NON} = \sigma_{TOT} - \eta \sigma_{EL}^{OM}$$

Fig. 3. A schematic representation of the experimental arrangement used by U. C. Davis (Ref. 4) to obtain non-elastic cross-section data.

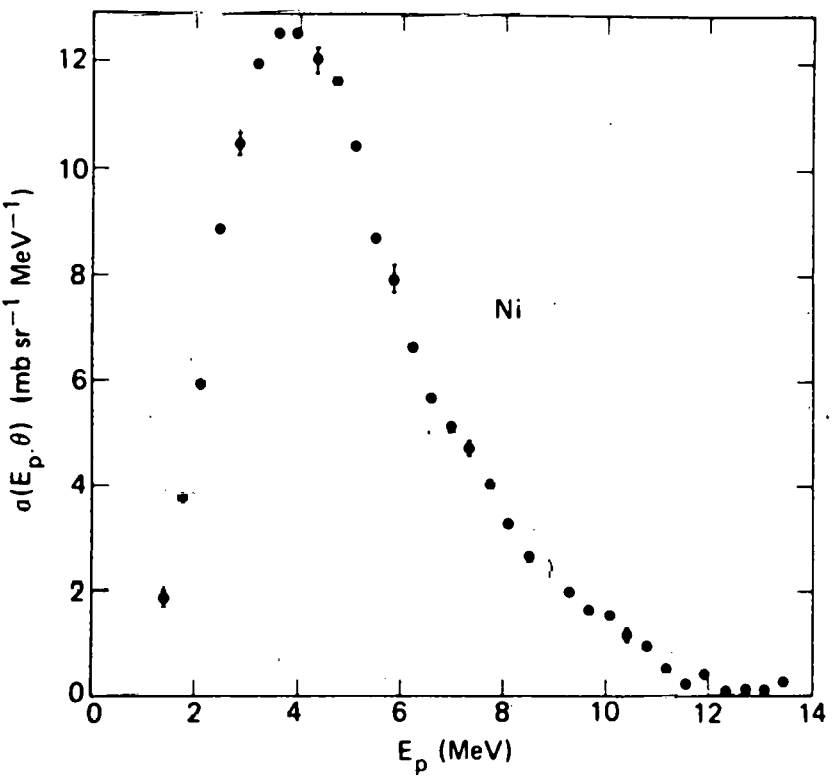

Fig. 4. Proton-emission cross section at 90° for Ni obtained by Grimes et al. (Ref. 27) at LLL using a quadrupole spectrometer.

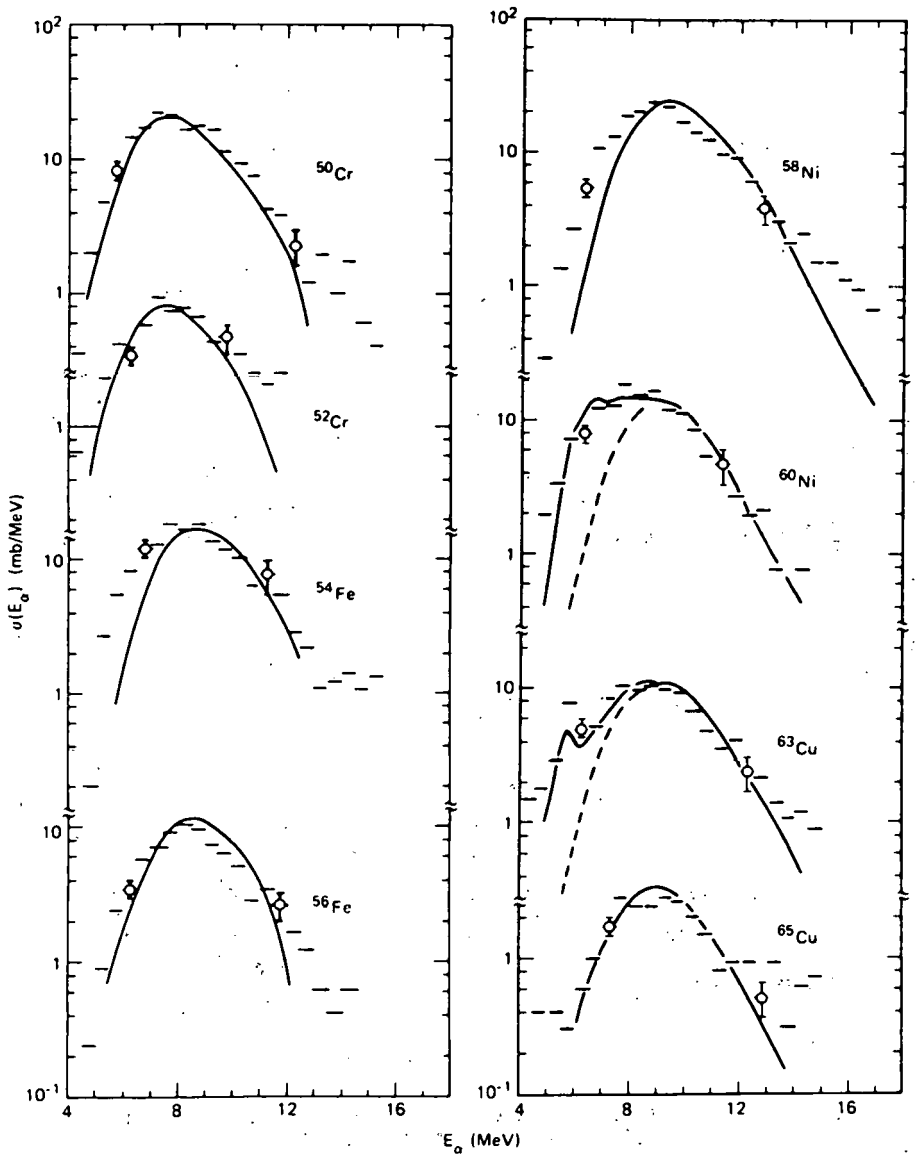

Fig. 5. Angle-integrated alpha-particle-emission cross sections (n,xα) for Cr, Fe, Ni, and Cu isotopes obtained by Grimes et al. (Ref. 27). The data are averaged into 500 keV bins; the solid line is a Hauser - Feshbach calculation; the dashed line represents alphas emitted from the first compound nucleus.

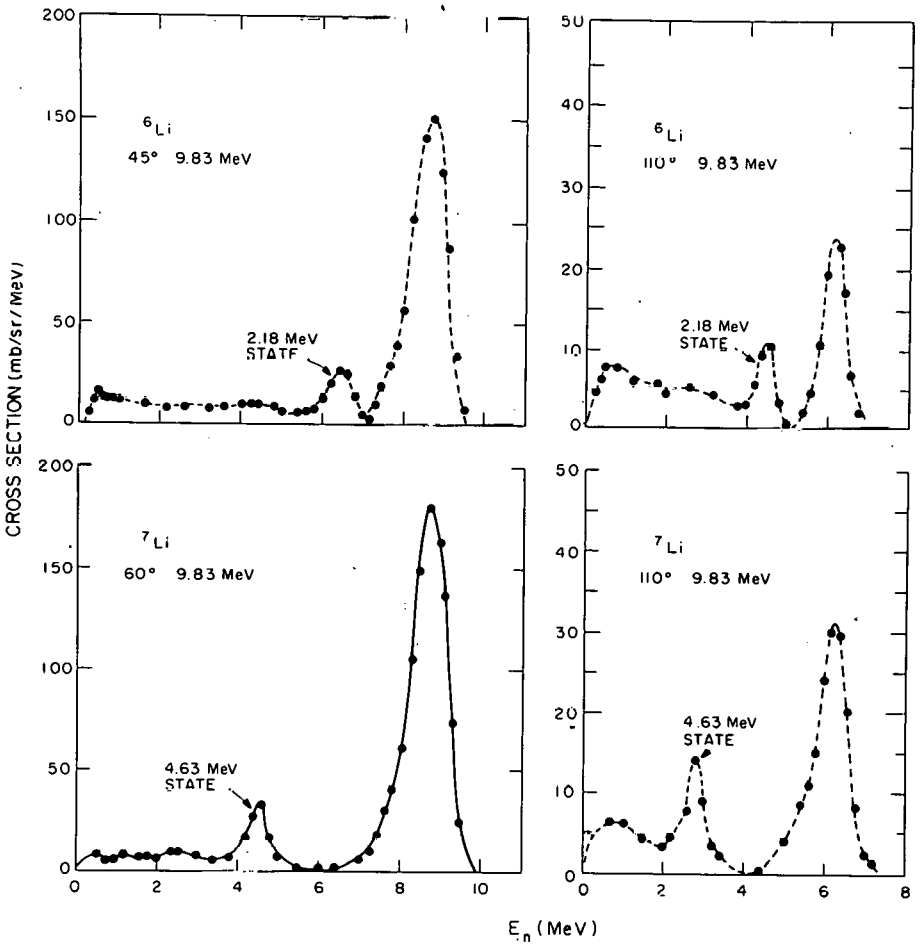

Fig. 6. Neutron emission spectra for ^{6}Li and ^{7}Li at 2 angles for 10-MeV incident neutrons obtained as LASL (Ref. 42).

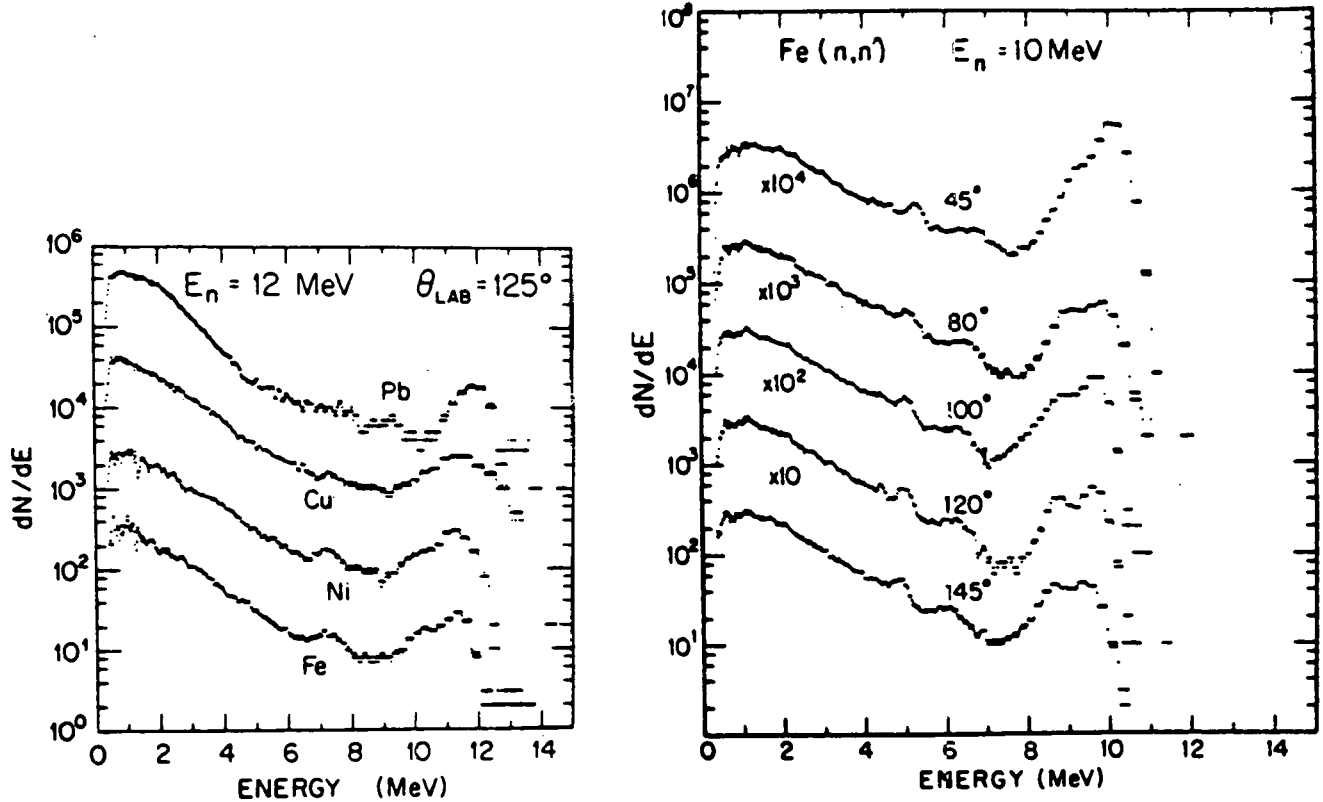

Fig. 7. Preliminary neutron-emission spectra obtained at TUNL (Ref. 44) for Fe, Ni, Cu, and Pb at 12-MeV incident-neutron energy and lab angle of 125° (left plot); neutron emission spectra for Fe at 5 angles for an incident-neutron energy of 10 MeV (right plot.)

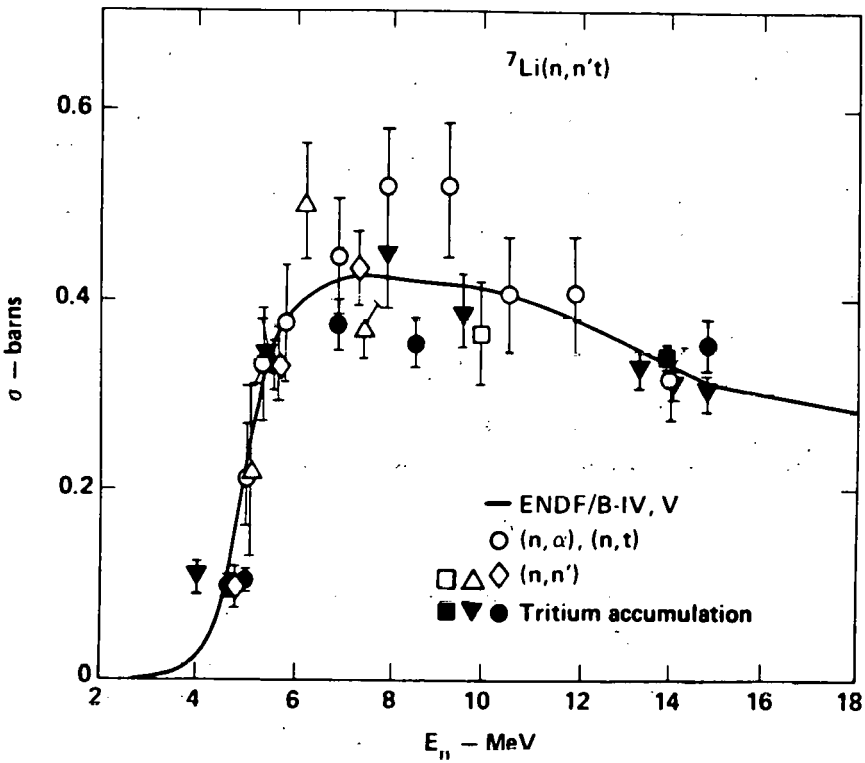

Fig. 8. Cross-section data for the ^{7}Li(n,n'αt) reaction. Tritium accumulation results are Ref. 49 solid circles, Ref. 50 solid square, Ref. 51 solid inverted triangles. The open circles are from photographic emulsions (Ref. 52). The remaining data are deduced from neutron-emission spectra. This figure is from Haight (Ref. 1).

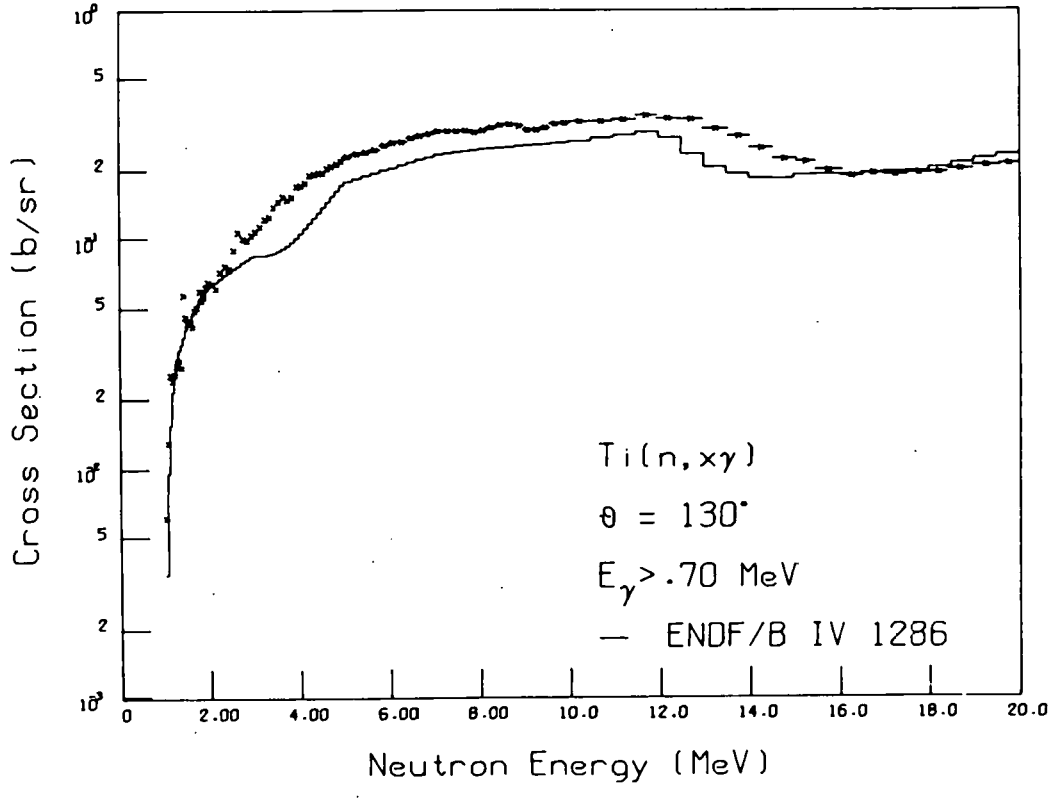

Fig. 9. Integrated yield of secondary gamma rays with $E_\gamma > 0.3$ MeV as a function of incident-neutron energy for Ti. The solid line is the ENDF/B-IV evaluation.

THIS PAGE

WAS INTENTIONALLY

LEFT BLANK

Dup

STATUS OF (N, CHARGED PARTICLE) MEASUREMENTS AT LLL*

Robert C. Haight and Steven M. Grimes†

Lawrence Livermore Laboratory
Livermore, California 94550 U.S.A.

ABSTRACT

Using a charged-particle magnetic-quadrupole spectrometer, we have studied (n, charged particle) reactions on materials bombarded with 14- to 15 MeV neutrons. Charged-particle production cross sections, angular distributions and spectra are measured. The materials investigated to date include most of those proposed for fusion reactor structures, Al, Ti, Cr, V, Fe, Ni, Cu, Nb and stainless steels 304 and 316. Isotopic data on $^{46,48}Ti$, $^{50,52}Cr$, $^{54,56}Fe$, $^{58,60}Ni$ and $^{63,65}Cu$ and on the monoisotopic elements ^{27}Al, ^{51}V and ^{93}Nb have provided stringent tests of reaction model calculations. Equilibrium and pre-equilibrium reaction mechanisms have been identified and quantified. Preliminary data on $^{92,94,95,96}Mo$ and on light nuclides including ^{12}C and ^{7}Li have been obtained recently.

INTRODUCTION

Charged-particle producing reactions of neutrons with materials are of great importance in the development of fusion power. These reactions lead to the production of hydrogen and helium which can alter significantly the properties of materials. These reactions are responsible for a large part of the energy deposited locally in many materials by the neutrons. Nuclear transmutation results from these reactions since the product nucleus is always that of a different element than the target. Finally, cross sections of interest in neutron transport and in displacement damage can be obtained from the study of these reactions.

For the past four years a study of (n, charged particle) reactions has been underway at Livermore with a magnetic quadrupole

---

†Work performed with J. D. Anderson (LLL) and K. R. Alvar, H. H. Barschall and R. R. Borchers (Univ. of Wisconsin).

spectrometer. An earlier report on the development of this spectrometer was given in the preceeding symposium [1]. The spectrometer has undergone further development since then and a wide range of measurements has been completed while others are currently in progress. This report is of the present status of the program.

EXPERIMENTAL DEVELOPMENTS

The magnetic quadrupole spectrometer has previously been described [1,2]. Briefly, the spectrometer consists of a reaction chamber containing the samples which are irradiated with an intense 14-MeV neutron flux, a magnetic quadrupole triplet lens to transport the charged particles, and a ΔE-E detector system. The magnetic lens, which focusses the particles from the target foil onto the detectors, allows the detectors to be moved several meters (typically 2.5 m in our experiments) from the neutron source. The source at the same time can be quite close (5 to 10 cm) to the target foil. The result is a high neutron flux at the foil and a low background at the detectors because of the $1/r^2$ factor and the additional shielding that can be used. The solid angles for detecting charged particles does vary with charged-particle energy at a given magnet setting and several magnet settings must be used to cover the entire spectral range (Fig. 1).

Developments since the last symposium include larger detectors to increase the solid angle, thin-window proportional counters for use as a ΔE detectors for lower energy particles, a helium gas cell for normalization of the low energy alpha spectra, and a specially shaped neutron-production target to allow study of the reactions at 14 MeV. These developments were spurred by the desires to increase the sensitivity of the spectrometer, to be able to investigate more thoroughly low energy charged particles from light nuclei, and to eliminate the variation of neutron energy with reaction angle.

The typical E detector used now is a 300 mm^2 1500 μm silicon surface barrier detector. This thickness is chosen to stop the most energetic protons, 15 MeV, that we expect to produce with 14-15 MeV neutrons. It should be noted that intrinsic Ge detectors of larger area have recently been used at Ohio University [3].

The ΔE detector now in use is a two-element proportional counter filled with 96% Ar-4% CO_2. Its entrance window is several layers ($\approx$ 5) of formvar supported by .025 mm tungsten wires spaced .13 mm apart. This combination can sustain a pressure of at least 8 kPa (60 mm of Hg) over a 1" active diameter. The design of the window is similar to that of ref. 4. Alpha particles to 700 keV have been detected with the ΔE_1-ΔE_2-E coincidence at 9 mm gas pressure.

The high pressure helium gas cell [5] was required to normalize the low energy alpha-particle production cross sections where the detector efficiency is not easily determined from the measured efficiencies for protons or deuterons. A "known" spectrum of

alpha particles is produced by n-α elastic scattering in the helium which is thick enough to stop the alpha particles that would traverse the length of the cell. We calculate the known spectrum from the stopping powers and then deduce the system efficiency by comparing the calculation with the measured spectrum at each magnet setting.

To produce 14-MeV neutrons with our facility, a neutron production angle of 90° is required. Previously this angle was not accessible with the rotating target since the 90° direction was tangential to the locally spherical surface and the neutrons needed to pass through several centimeters of copper before reaching the target. A truncated, conically-shaped rotating target now allows the samples to be placed in the 90° neutron production plane so that measurements can be done at the fusion neutron energy of 14 MeV.

UPDATED RESULTS

A spectrum of protons emitted at 90° from 15-MeV bombardment of ^{58}Ni [6] is shown in Figure 2 to illustrate the range and quality of the data. By integrating such spectra over energy and angle, we arrive at the total proton, deuteron and alpha-particle production cross sections of Table I [6-9]. Average charged-particle energies are also given in the table.

The total hydrogen and helium production cross sections, depicted in Figure 3, show large variations from element to element. It must be remembered however that the responses of materials to the hydrogen and helium produced will certainly be different. With these data and those from other sources, the assessment of materials for fusion application can now be based on a cross section set that is reliable at the 14-MeV fusion neutron energy.

MODEL INTERPRETATION

Model calculations are essential to provide much of the neutron cross section data base, in particular where experimental data are not sufficient. The extrapolation of the cross sections to energies not yet investigated is an example of where a calculational model is necessary.

The spectral and angular distribution data, as well as the cross sections, obtained with the magnetic quadrupole spectrometer provide especially stringent tests of the models. From our results we are able to test the validity of equilibrium and pre-equilibrium particle emission models.

Equilibrium Particle Emission

At 14-MeV incident neutron energy, the open reaction channels usually include (n,p), (n,n'p), (n,pn), (n,d), (n,α), (n,n'α) and other one or two light-particle-emission modes. For nearly all of

the nuclei listed in Table I, the preponderance of proton and alpha-particle emission is well described by emission from an excited nucleus at thermodynamic equilibrium in the first as well as successive stages. Both the spectral shapes (Fig. 4) and angular distributions (Fig. 5) give evidence for this reaction mechanism.

The importance of second-chance proton emission from (n,n'p) can vary widely with isotope as illustrated in Fig. 6 for ^{46}Ti and ^{48}Ti. Because of the relationship between neutron and proton separation energies, there is a region of excitation of ^{46}Ti that can decay by proton emission with no competition to neutron emission. This region accounts for the large, wide peak in the proton emission spectrum just above 2 MeV. A comparable region in ^{48}Ti does not exist and the second chance proton emission peak is nearly absent. This effect is explained also quantitatively [7].

Pre-Equilibrium Particle Emission

Evidence for pre-equilibrium proton and alpha-particle emission is also clear from the spectra (Fig. 7) and angular distributions (Fig. 5). The model used is the hybrid model of Blann [10] and reasonable agreements with the angle-integrated data are found. An interpretation of the angular distributions is qualitative so far in that the pre-equilibrium particles are expected to go mostly in forward directions. A more quantitative analysis remains a challenge.

From the present data, we can conclude generally that the fractional contribution of pre-equilibrium processes increases with a decreasing equilibrium component. Within an element, the pre-equilibrium component is usually more significant for the heavier isotopes.

PRESENT AND FUTURE WORK

Recent preliminary data have been obtained for ^{92,94,95,96}Mo, C and ^{7}Li. A spectrum of protons emitted at 90° from ^{94}Mo bombarded with 15-MeV neutrons is shown in Figure 8 for example.

Measuring the complete spectrum of charged particles from light isotopes poses experimental difficulties because particles of very low energy must be detected. For ^{12}C for example the (n,n'3α) reaction yields most of the alpha particles but with an average energy of only about 2 MeV. We have preliminary data showing that at many angles, the alpha particle spectrum is significant even below 1 MeV. This situation is expected also in the ^{7}Li (n,n'αt) and ^{16}O(n,n'4α) reactions, both of which are of importance for fusion applications.

In the future we plan to complete the measurements on the light nuclides, ^{7}Li, ^{9}Be, ^{11}B, ^{12}C, ^{14}N, ^{16}O and ^{19}F at E_n = 14 MeV; to extend the measurements on structural materials to Zr and others; and, using the LLL cyclograaff facility as a neutron source, to investigate the energy dependence of the cross sections.

ACKNOWLEDGMENTS

*Work performed under the auspices of the U.S. Department of Energy by Lawrence Livermore Laboratory under contract no. W-7405-ENG-48.

REFERENCES

1. S. M. Grimes, R. C. Haight, J. D. Anderson, K. R. Alvar, and R. R. Borchers, Symposium on Neutron Cross Sections from 10 to 40 MeV, ed. M. R. Bhat and S. Pearlstein, Brookhaven National Laboratory report BNL-NCS-50681 (1977), pp 297-304.

2. K. R. Alvar, H. H. Barschall, R. R. Borchers, S. M. Grimes and R. C. Haight, Nucl. Instr. and Meth. 148, 303 (1978).

3. G. Randers-Pehrson, R. W. Finlay, P. Grabmayer, V. Kulkarni, R. O. Lane, and J. Rapaport, this Symposium.

4. R. G. Markham, S. M. Austin, and H. Laumer, Nucl. Instr. and Meth. 129, 141 (1975).

5. R. C. Haight, C. Rambo, J. Cormier and J. Garibaldi, Nucl. Instr. and Meth. 164, 613 (1979).

6. S. M. Grimes, R. C. Haight, K. R. Alvar, H. H. Barschall, and R. R. Borchers, Phys. Rev. C19, 2127 (1979).

7. S. M. Grimes, R. C. Haight, and J. D. Anderson, Nucl. Sci. Eng. 62, 187 (1977).

8. R. C. Haight, S. M. Grimes, and J. D. Anderson, Nucl. Sci. Eng. 63, 200 (1977).

9. S. M. Grimes, R. C. Haight, and J. D. Anderson, Phys. Rev. C17, 508 (1978).

10. M. Blann, Phys. Rev. Lett. 27, 337 (1971); Nucl. Phys. A213, 570 (1973).

TABLE I

Proton, deuteron and alpha-particle emission cross sections and average charged-particle energy

Target	Particle Emitted	Cross Section (mb)	Spectrum-Averaged Charged-Particle Energy (MeV)
^{50}Cr	p	830 ± 100	4.5 ± 0.2
^{50}Cr	d	12 ± 4	5.6 ± 0.6
^{50}Cr	α	94 ± 15	8.4 ± 0.3
^{52}Cr	p	180 ± 25	4.7 ± 0.2
^{52}Cr	d	8 ± 3	4.9 ± 0.7
^{52}Cr	α	36 ± 6	8.4 ± 0.4
Cr	p	180 ± 25	4.7 ± 0.2
Cr	d	10 ± 3	5.7 ± 0.7
Cr	α	38 ± 6	8.6 ± 0.4
^{54}Fe	p	900 ± 110	4.8 ± 0.2
^{54}Fe	d	10 ± 4	5.6 ± 0.6
^{54}Fe	α	79 ± 13	8.7 ± 0.4
^{56}Fe	p	190 ± 22	5.1 ± 0.2
^{56}Fe	d	8 ± 3	5.5 ± 0.7
^{56}Fe	α	41 ± 7	8.8 ± 0.6
Fe	p	230 ± 30	5.0 ± 0.2
Fe	d	8 ± 3	5.4 ± 0.8
Fe	α	43 ± 7	8.8 ± 0.4

TABLE I (Cont'd)

Target	Particle Emitted	Cross Section (mb)	Spectrum-Averaged Charged-Particle Energy (MeV)
^{58}Ni	p	1000 ± 120	5.1 ± 0.2
^{58}Ni	d	14 ± 6	6.5 ± 0.7
^{58}Ni	α	106 ± 17	9.5 ± 0.3
^{60}Ni	p	325 ± 40	5.0 ± 0.2
^{60}Ni	d	11 ± 4	6.0 ± 0.8
^{60}Ni	α	76 ± 12	9.0 ± 0.3
Ni	p	790 ± 100	4.9 ± 0.2
Ni	d	13 ± 5	6.3 ± 0.6
Ni	α	97 ± 16	9.2 ± 0.4
^{63}Cu	p	320 ± 45	4.4 ± 0.2
^{63}Cu	d	9 ± 4	6.4 ± 0.7
^{63}Cu	α	56 ± 10	8.9 ± 0.3
^{65}Cu	p	44 ± 5	6.2 ± 0.3
^{65}Cu	d	10 ± 4	6.6 ± 0.8
^{65}Cu	α	13 ± 3	9.5 ± 0.7
Cu	p	237 ± 28[a]	5.0 ± 0.3[a]
Cu	d	10 ± 4[a]	6.5 ± 0.8[a]
Cu	α	42 ± 7[a]	9.1 ± 0.4[a]

[a]Inferred from isotopic data.

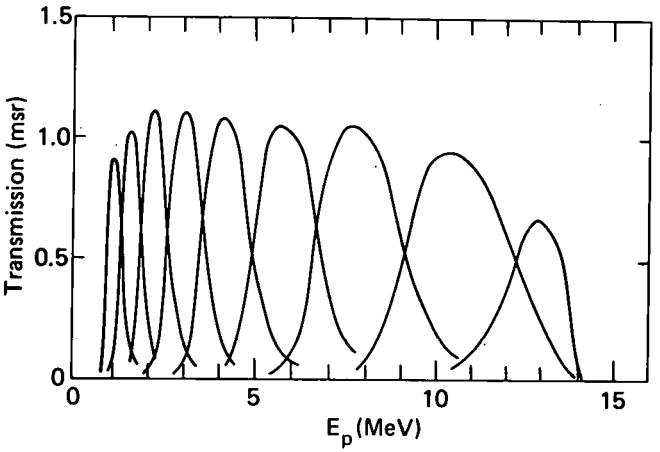

Figure 1. Measured transmissions of protons for nine magnet current settings with 50 mm^2 ΔE and E detectors. The transmissions are expressed as effective solid angles for detecting protons emitted from the target foil. Approximately nine settings are required to cover the proton energy spectra for the structural elements, Al to Nb.

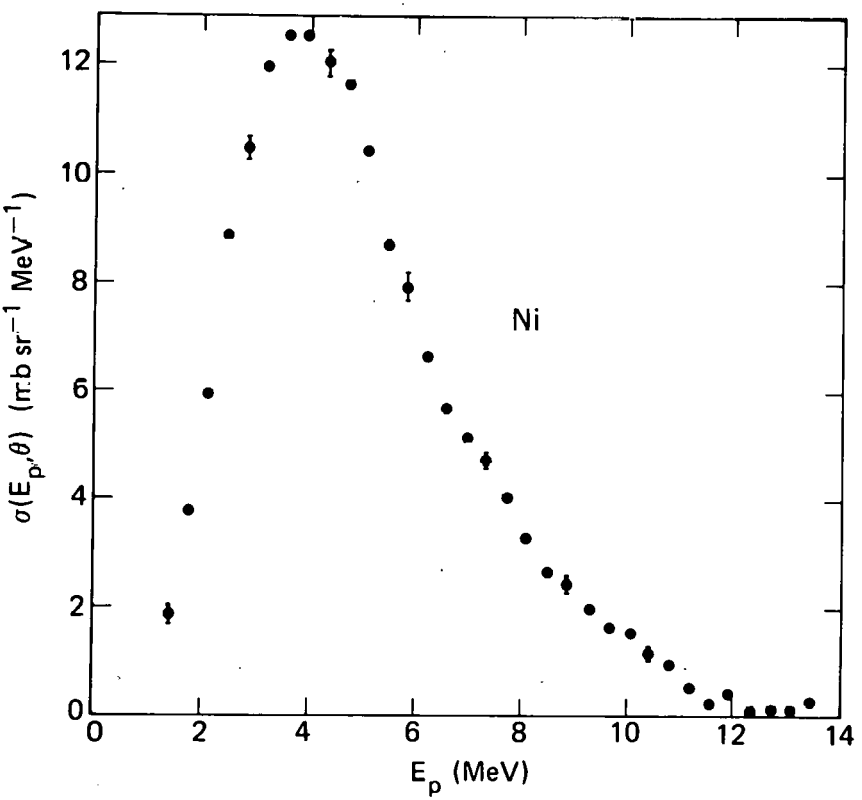

Figure 2. Proton emission cross sections at 90° for natural nickel bombarded with 15-MeV neutrons.

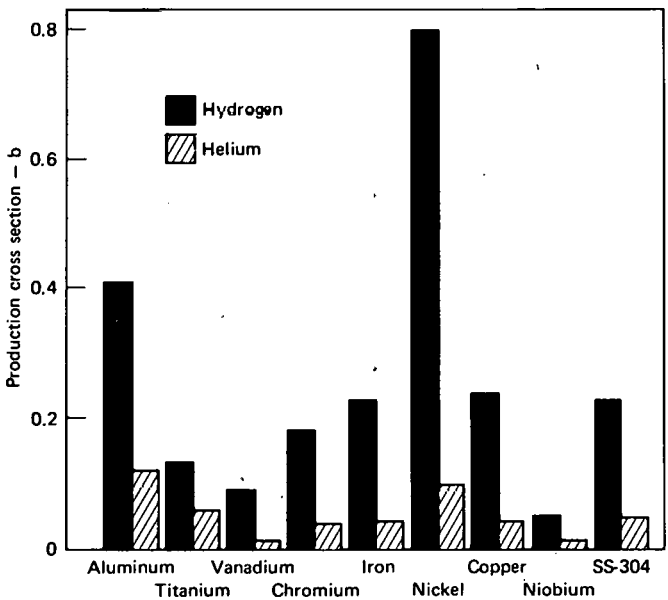

Figure 3. Hydrogen and helium production cross sections at 15 MeV measured with the magnetic-quadrupole charged-particle spectrometer.

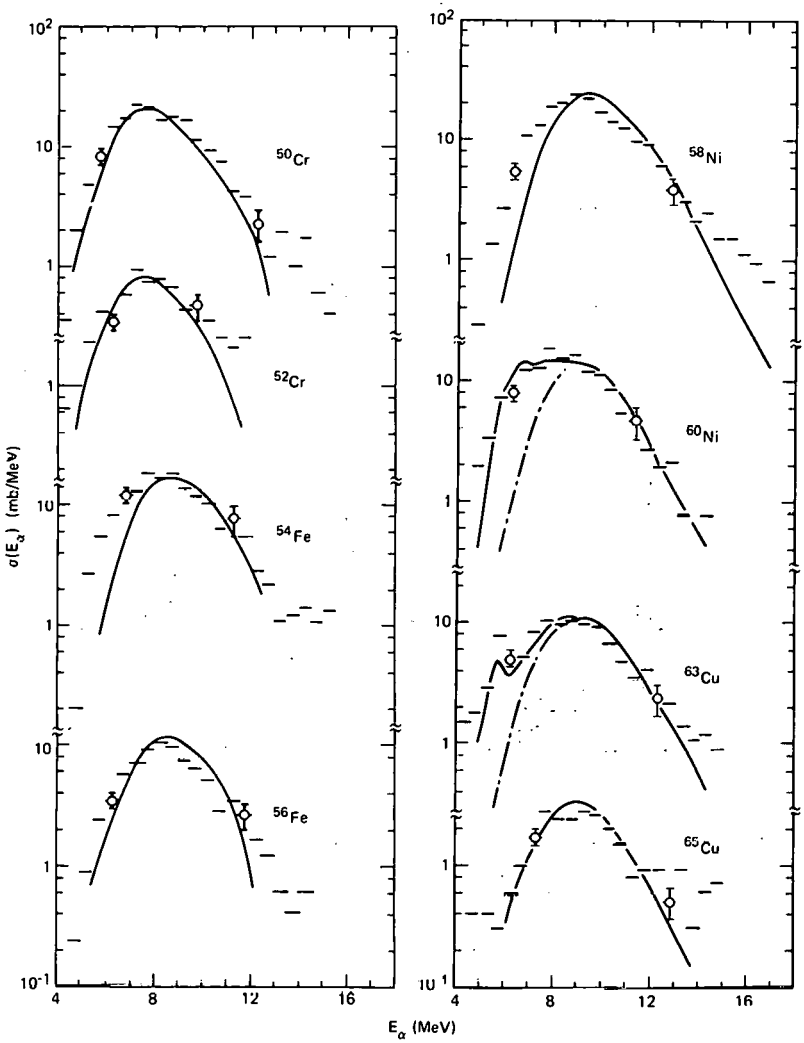

Figure 4. Spectrum of alpha particles from ^{50,52}Cr, ^{54,56}Fe, ^{58,60}Ni and ^{63,65}Cu bombarded with 15-MeV neutrons. The solid curves are Hauser-Feshbach calculations. The dashed curves indicate the alpha spectrum from the first stage of the reactions.

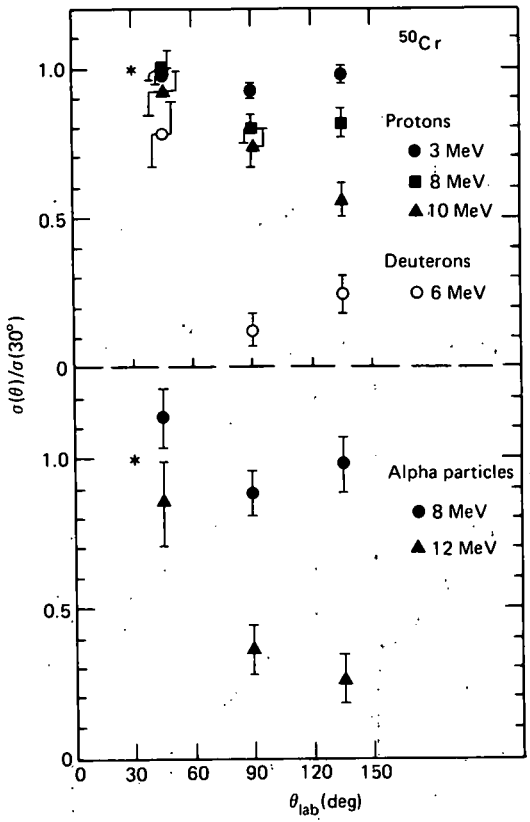

Figure 5. Variation with angle of the cross sections for emission of protons, deuterons, and alpha particles from the bombardment of ^{50}Cr with 14.8 MeV neutrons. The cross sections are normalized to unity at 30°.

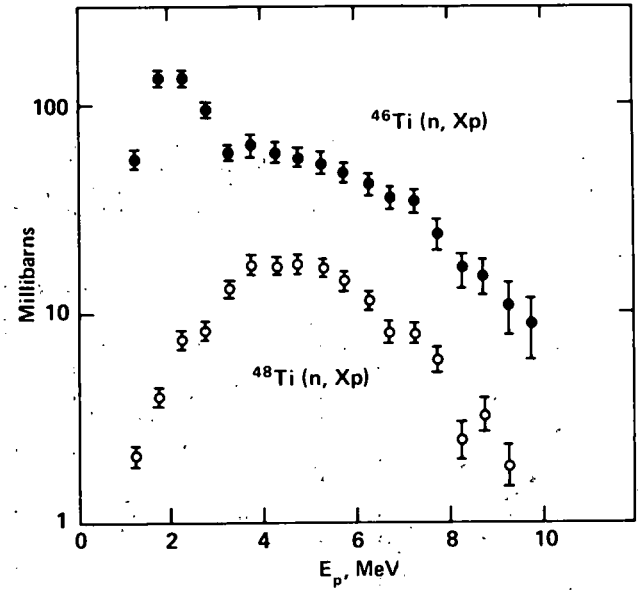

Figure 6. Proton-emission spectra from ^{46}Ti and ^{48}Ti bombarded with 15-MeV neutrons. The large bump in the spectrum for ^{46}Ti near 2 MeV is due to protons from (n,n'p) reactions which are favored for this isotope but not for ^{48}Ti. This effect originates in the relationship of neutron to proton separation energies and has been called "proton trapping" or "second chance proton emission."

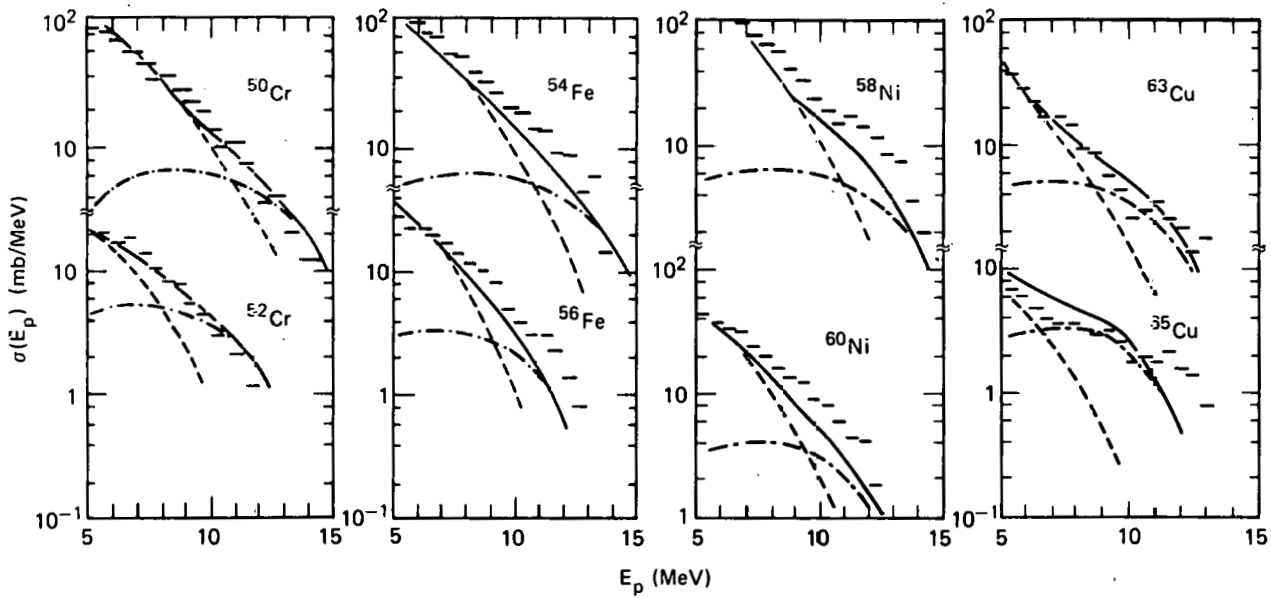

Figure 7. High energy portions of the proton emission cross sections are compared with hybrid model calculations (dot-dashed line), multistep Hauser-Feshbach calculations (dashed line) and the sum of these contributions (solid line).

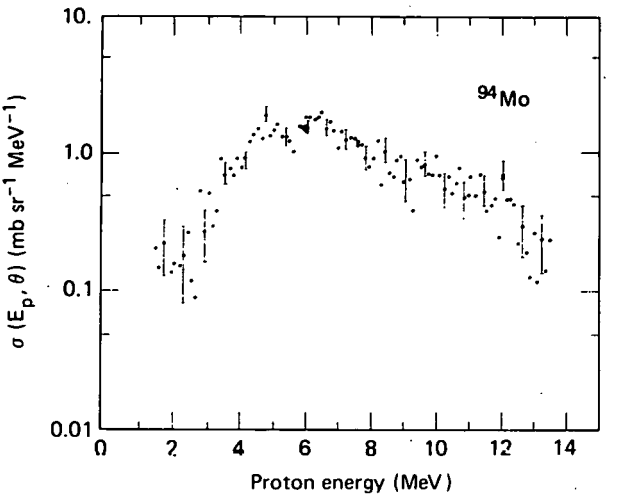

Figure 8. Preliminary data for protons emitted at 90° from ^{94}Mo bombarded with 15-MeV neutrons.

THIS PAGE

WAS INTENTIONALLY

LEFT BLANK

NEUTRON PHYSICS RESEARCH AT TRIANGLE UNIVERSITIES NUCLEAR LABORATORY

Richard L. Walter

Department of Physics, Duke University
and Triangle Universities Nuclear Laboratory
Duke Station, North Carolina 27706, USA

Christopher R. Gould

Department of Physics, North Carolina State University
and Triangle Universities Nuclear Laboratory

ABSTRACT

A review of the neutron physics research related to cross-section determinations or parametrizations is given. Six topics are described: i) Neutron scattering from light nuclei; ii) Elastic and discrete inelastic scattering from medium-weight and heavy nuclei; iii) Highly inelastic neutron scattering; iv) Lane optical-model analyses of complete data sets; v) Neutron polarization and the spin-orbit term; vi) Radiative capture reactions.

INTRODUCTION

The neutron physics aspect of the program at Triangle Universities Nuclear Laboratory is multi-faceted. The research is centered primarily around a tandem Van de Graaff capable of delivering 16 MeV pulsed proton or deuteron beams, both polarized and unpolarized. These beams are utilized in (p,n) and (d,n) reaction studies as well as providing monoenergetic sources of polarized and unpolarized neutrons via the $^{2}H(d,n)$ and $^{3}H(p,n)$ reactions. Most of our neutron measurements and their interpretation relate to cross-section parametrizations, the topic of this conference, so we will take this opportunity to briefly outline most of the TUNL program which involves neutron research.

For technical reasons, neutron experiments at TUNL will be subdivided into six categories in the present paper: i) Elastic and discrete inelastic scattering cross-sections for light nuclei; ii) Elastic and discrete inelastic scattering cross sections for medium-weight and heavy nuclei; iii) Cross sections

for highly inelastic scattering from continuum states; iv) Lane-model studies of (p,p), (p,n), and (n,n) reactions for the same target nuclei; v) Polarization measurements for neutron elastic scattering from selected targets ranging from ^{1}H to ^{208}Pb, vi) Radiative capture reactions induced with polarized and unpolarized neutron beams. We will describe below some of the aspects in each project, focussing particularly on the relation to cross-section determinations or parametrizations.

ELASTIC AND DISCRETE INELASTIC SCATTERING FROM LIGHT NUCLEI

The original emphasis of the neutron time-of-flight program at TUNL was to obtain cross sections in the 7-15 MeV energy range for isotopes of light nuclei. Except for the nuclei ^{13}C and $^{14,15}N$, measurements have been completed in approximately 1 MeV steps for every stable 1-p shell nucleus. The latest data were reported along with optical model calculations at the American Physical Society Meeting at Knoxville [1]. Attempts to describe the smoothly varying 8- to 14-MeV data for $^{10}B(n,n)$ and $^{10}B(p,p)$ with a single spherical optical model were reported there. The results are shown in Fig. 1 where the only difference in the optical model for the two reactions is a Coulomb correction term with magnitude of 1.5 MeV. As can be seen from the fits in Fig. 1, the optical model description is quite good at most energies. The $^{10}B(p,p)$ data is from Watson et al. [2]

The TUNL data for $^{11}B(n,n_0)$ and $^{11}B(n,n_2)$ were studied between 9 and 13 MeV with the coupled-channel code JUPITOR of T. Tamura. The magnitudes of the calculated cross sections agreed with the data but the shapes of the distributions for the two reactions were not well reproduced. The $^{11}B(n,n)$ data were also used in a second "global" spherical optical model search which included the ^{10}B data as well. The results of this search, which contained an energy dependence in the V_o and W_D terms, are shown in Fig. 2. Since this calculation the code GENOA of F. Perey has been transferred to the new DEC VAX 11/780 computer in our laboratory, and the search will be repeated in a more methodical fashion. In addition, new data obtained at 13 and 14 MeV for $^{11}B(n,n)$ will be incorporated and this should aid in limiting the range of acceptable values for these fits.

NEUTRON ELASTIC SCATTERING FROM MEDIUM WEIGHT NUCLEI

Until recently the energy range from 8 to 17 MeV has not been investigated for many medium weight nuclei as far as differential cross sections are concerned. This energy region is readily available to us through the neutron source reaction $^{2}H(d,n)^{3}He$. We have completed measurements on the elastic scattering cross sections for $^{54,56}Fe$ and $^{63,65}Cu$ between 8 and 14 MeV, for $^{58,60}Ni$ at 8 and 10 MeV and for ^{208}Pb at 10 MeV. The Ni isotopes will be studied

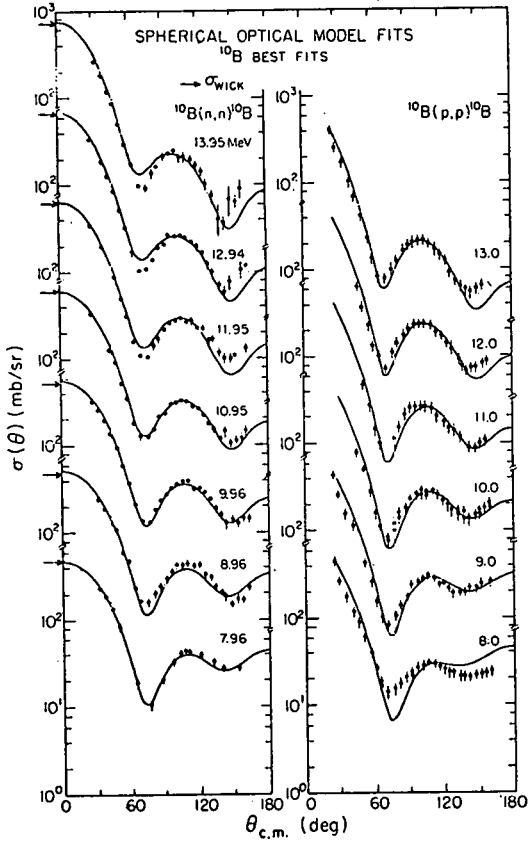

Fig.1. Nucleon scattering from ^{10}B.

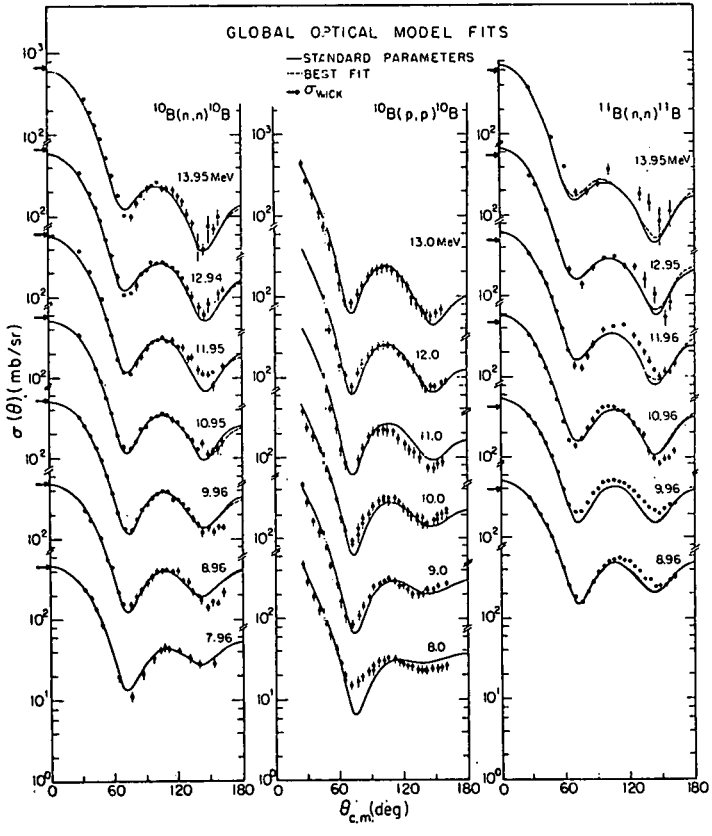

Fig.2. Nucleon scattering from ^{10}B and ^{11}B.

at 12 and 14 MeV as well. Inelastic scattering cross sections for the first excited-state group were also obtained in some cases. The elastic data are just now being incorporated into energy dependent optical model searches using the code GENOA. Upon completion of the searches, the parameters for the different elements will be compared to one another and to available optical model sets, the goal being to obtain the best set for describing the respective regions of the periodic table for the 8 to 14 MeV energy range.

An example of the quality of the data [3] is shown in Fig. 3. The relative uncertainties in the data vary from 2% at forward angles to about 20% in the minimum near 55° where uncertainties in the multiple scattering correction dominate. The optical model predictions using the global parameters of Rapaport et al. [4] are compared to the data for ^{56}Fe and ^{63}Cu at 8, 10, and 12 MeV. The features in the data are quite well predicted except for ^{56}Fe at 8 MeV. In order to get a better characterization of the A and E dependence of the parameters single-energy searches were made for each distribution. The starting parameters were those of Rapaport and a specific strategy was followed. Eventually all the O.M. parameters were permitted to vary. Results of the single-energy searches at 10 MeV are given in Fig. 4. The data are well reproduced by the calculation. Although all the data can be quite well described in single-energy searches, at the present time we will not report the parameters obtained because the whole search project is in its infancy. However, as expressed above, we will pursue a global approach to these data.

Until now the searches in this phase of our program do not include any neutron polarization data as we intend to investigate how well cross-section data can be represented when one allows the strength and geometry of a spin-orbit term of the Thomas type to be relatively free of polarization constraints. This term is discussed in more detail below.

INELASTIC NEUTRON SCATTERING-CONTINUUM SPECTRA

A major effort of the neutron cross-section group has been to obtain data for several nuclei in order to test cross-section calculations for highly inelastic scattering. The experiments are performed with incident neutrons of 7.5, 10 and 12 MeV. The detector cut-off bias is about 300 keV permitting us to know our detector efficiency to within about 6% for neutron energies as low as 1 MeV.

The data at 7.5 MeV is obtained with $^{2}H(d,n)$ neutrons. For this energy the neutron source reaction is monoenergetic and the measurement is straightforward. Four spectra are obtained (gas in, sample in; gas in, sample out; gas out, sample in; gas out, sample out) and subtraction gives the proper spectrum for inelastic scattering of monoenergetic neutrons. The data at 10 and 12 MeV are obtained using $^{3}H(p,n)$ neutrons. Although this reaction is

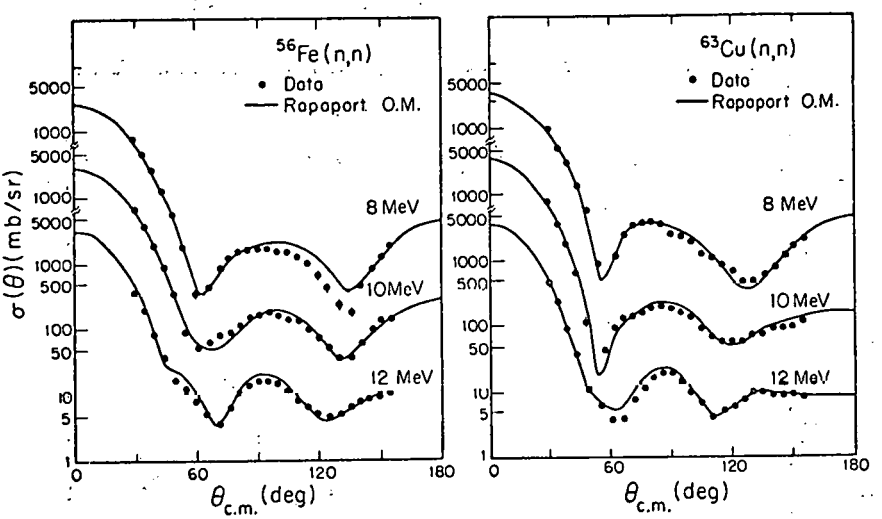

Fig.3. Comparison of data to optical-model predictions for the nuclei ^{56}Fe and ^{63}Cu.

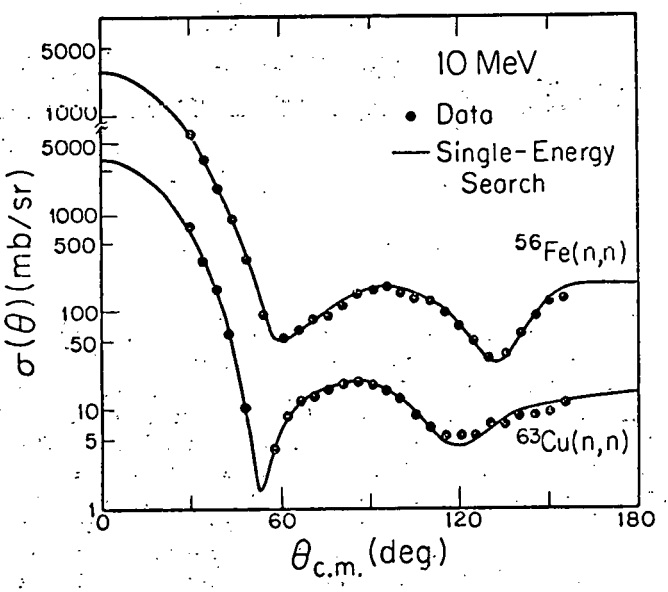

Fig.4. Comparison of 10 MeV data to results of single-energy searches.

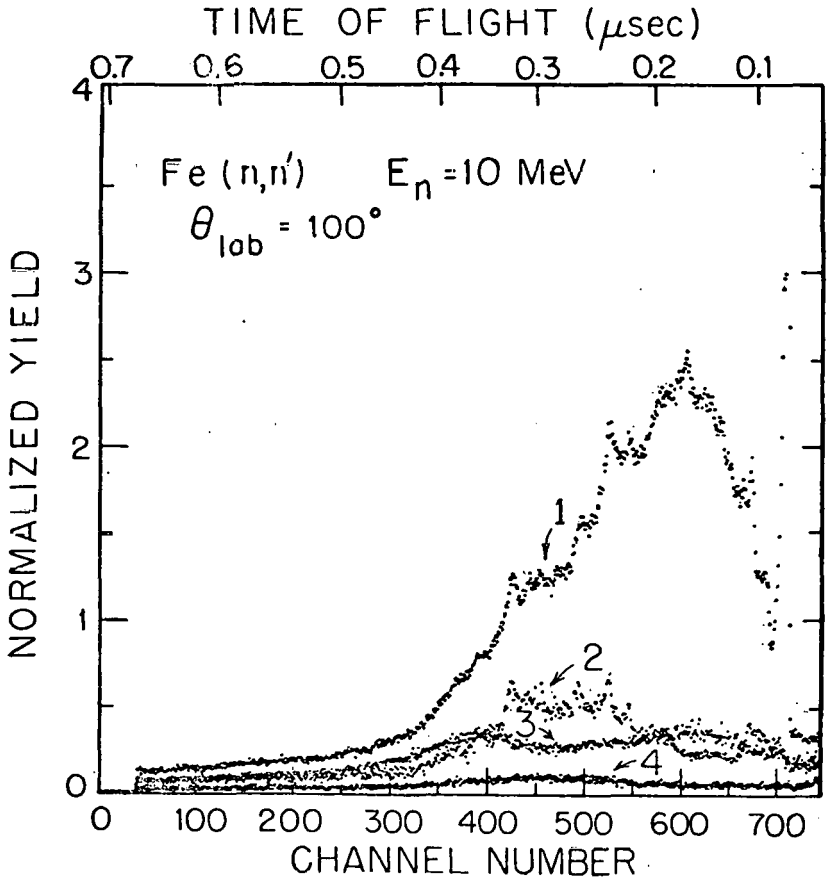

Fig.5. Time-of-flight spectra for 10 MeV neutrons.

the "cleanest" neutron source available, it is known [5] that there are low energy contaminant neutrons from three-body breakup reactions such as $^{3}H(p,n)pd$. These cross sections are known to about 20% accuracy and are not negligible in comparison to the cross section for the main source reaction $^{3}H(p,n)^{3}He$. The contaminant neutrons make the analysis of inelastic scattering data difficult, as a measure of the four-spectra set above does not eliminate the effect of elastic and inelastic scattering of these contaminant neutrons. Therefore, to obtain correct cross-section data, the contribution from gas-breakup neutrons must be carefully calculated and properly subtracted from the final spectrum which is obtained from the set of four spectra.

The evaluation of this cross section, of course, requires a massive calculation because one must account for multiple

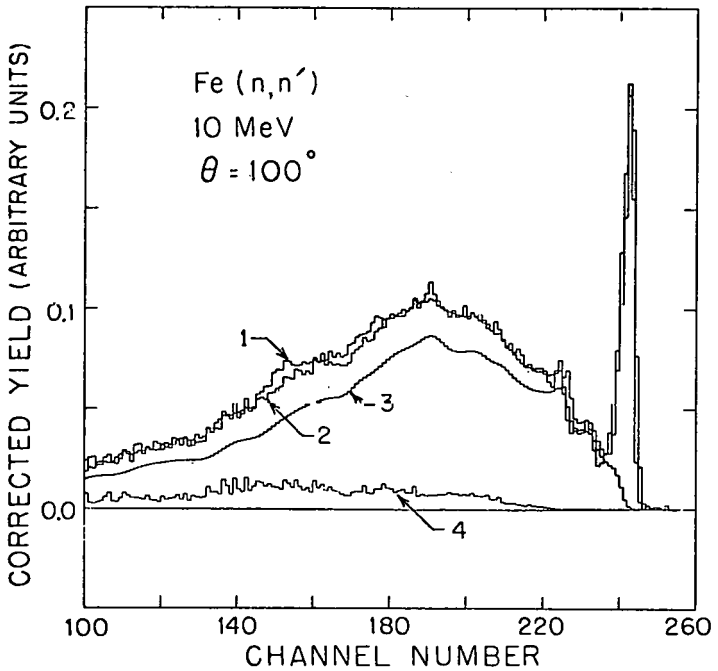

Fig.6. Corrected time-of-flight spectra: spectrum 1 is data and 2,3, and 4 are computer generated.

scattering, attenuation, source anisotropy, finite geometries of the source, scatterer, and detector, and detector efficiency. In addition, the calculation must involve the ENDF library for elastic and inelastic scattering for all neutron energies present in the source spectrum. A code EFFIGY-C has been written at our laboratory to handle this problem [6] . The code has been debugged just recently, and the only calculations that have been made to date are for the Fe scatterer.

In Fig. 5, taken from reference [7] we illustrate the relative strengths of the contributions from the four neutron source conditions. These are time-of-flight spectra and the narrow peak near channel 700 is from elastic scattering. The neutron energy is 10 MeV and the source reaction is $^{3}H+p$. The spectra are: 1) ^{3}H gas in cell, Fe scatterer in place; 2) ^{3}H gas removed, Fe in place; 3) ^{3}H gas in cell, Fe sample removed; 4) ^{3}H gas removed, Fe removed. At 12 MeV the relative strength of spectrum 2) is much greater, even though ^{28}Si collimators and a ^{58}Ni beam stop are employed. Because the 12 MeV measurements require a long time for a set of samples, the ^{3}H gas-out run can follow the gas-in run by as much as 24 hours. Therefore, the 12-MeV data are subject to greater experimental errors than the 10-MeV data. Furthermore, data

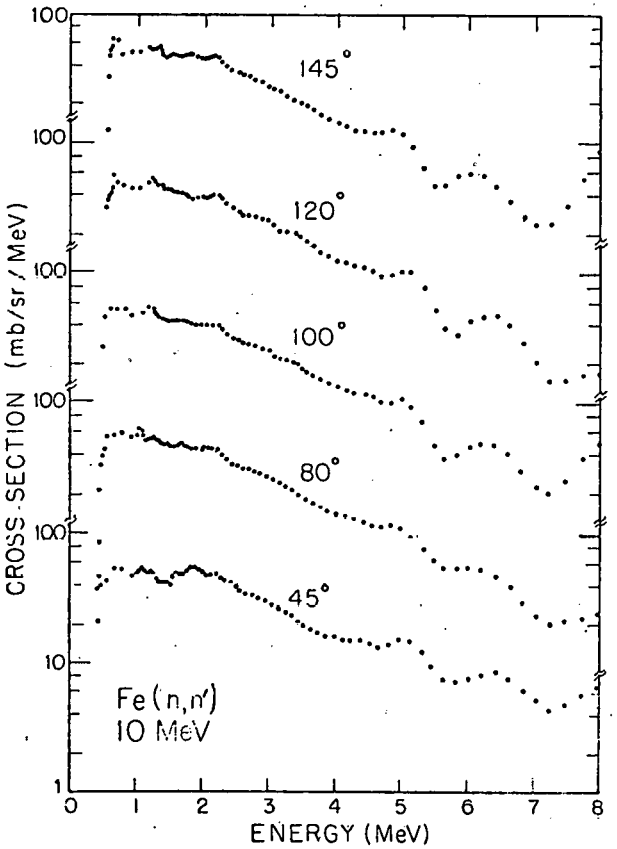

Fig.7. Extracted cross sections for Fe at 10 MeV.

obtained at other laboratories at 14 MeV using the truly monoenergetic $^{3}H(d,n)^{4}He$ reaction induced with very low energy deuterons is not plagued by neutrons produced by deuterons breaking up in the target gas or the target backing. Thus, the intrinsic quality of the 14-MeV data is likely to be superior to 12-MeV measurements that use the $^{3}H(p,n)$ source.

After the data of Fig. 5 are properly combined one gets a time-of-flight spectrum for the scattering of neutrons that were produced in the ^{3}H gas only. Such a compressed spectrum is shown as curve 1 in Fig. 6. The result for the contribution of scattered breakup neutrons as calculated with the Monte Carlo code EFFIGY-C is shown as curve 4. Curve 3 represents the calculated yield for scattering monoenergetic 10 MeV neutrons and curve 2 is the spectrum obtained by combining 3 and 4. The code iterates to a final yield or cross section for the range from about 300 keV to the incident neutron energy. The results shown here correspond to the

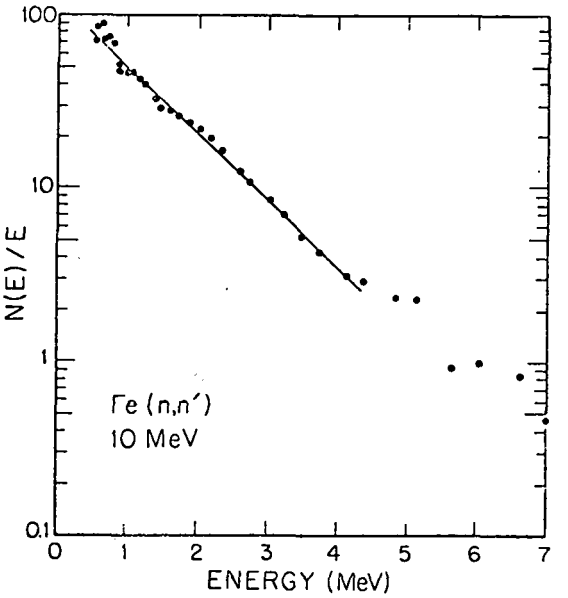

Fig.8. Cross section replotted as N(E)/E.

solution after the third iteration.

Continuum emission data were obtained for the naturally occurring elements of Fe, Ni, Cu and Pb, all materials of significance in the design of fusion energy reactors. We will measure similar spectra for Si, W, Cr, Nb and Sn in the immediate future using the same technique. Preliminary cross-section data for 10 MeV are shown in Fig. 7 for Fe at five scattering angles. For Fe at 10 MeV some structure from discrete inelastic scattering is clearly noticeable down to 5 MeV. To compare to evaporation models, the data for 100° is replotted in Fig. 8. This illustration shows N(E)/E vs. E where E is the energy of the emitted neutron and N(E)/E is the number of neutrons detected in an energy bin divided by the width of the bin. The curve is a straight line which corresponds to a nuclear temperature (kT) of about 1.15 MeV, a slightly higher value than is typically obtained.

Comparing the data to the evaporation theory in this way, i.e., a straight line fit, provides a way to look for systematic trends above the continuum theory. The good agreement suggests that the experimental system is properly calibrated and that the pre-equilibrium contribution is quite small. Lastly, the measurements did show anisotropy about 90°, with the forward angles as well as the back angles showing deviations of about 15% in the low-energy region of the spectra and 25% in the high-energy region.

LANE OPTICAL MODEL STUDIES TO COMPLETE DATA SETS

During the past few years, one group at TUNL has been pursuing the analysis of (p,n) reactions on light nuclei and a variety of related polarization measurements. In order to obtain an insight into the significance of the data, an optical model analysis using Lane's isospin approach [8] to nucleon-nucleus scattering was initiated. The main emphasis has been on interpreting the ^{9}Be(p,p), ^{9}Be(n,n) and ^{9}Be(p,n) data [9]. Recently the approach has been extended to the targets ^{13}C and ^{15}N, but with less success than for ^{9}Be because one must work around the considerable resonance structure present in these cases. The novel aspect in the Lane model analyses at TUNL is the inclusion of polarization data in the search and the insertion of the isospin spin-orbit term into an optical model search code. This term has never been satisfactorily investigated, and its strength is an unknown quantity.

In the Lane approach, one considers the neutron and proton merely to be different isospin projections of a nucleon. Then, by introducing isospin dependent terms one can calculate both (p,p) and (n,n) scattering, as well as the quasi-elastic (p,n) reaction, from a single potential.

The latest analyses incorporated cross-section and analyzing power data for ^{9}Be(p,p), ^{9}Be(p,n) and cross-section data for ^{9}Be(n,n) between 11 and 15 MeV. The quality of the fits are illustrated in Fig. 9 where $A(\theta)$ is the analyzing power for the reactions induced with polarized protons. The trends of all the data are reproduced with the model. The optical model parameters were permitted to vary with energy, but the variation was restricted to be nearly linear.

At the time of this analysis, no ^{9}Be(n,n) polarization data existed. At TUNL we have recently obtained this data set for this energy range [10] and it will be incorporated into an extension of the Lane analysis. At the present time the parameters do not predict the ^{9}Be(n,n) polarization function exactly. It is hoped that the model will eventually describe this data also, and that in the process of doing so, the strength or even the need for the isospin ($\ell \cdot s$) interaction will be established. It is also intended to obtain data on heavier nuclei to permit comparable studies of other complete sets of data for nucleon-nucleus scattering.

ANALYZING POWER MEASUREMENTS FOR NEUTRON SCATTERING

Over the last few years the neutron polarization group has been involved in accurately measuring the analyzing power $A_y(\theta)$ for the hydrogen and helium isotopes in order to provide an exact understanding of these scattering processes. A careful measurement for the n-p system gave analyzing powers with an accuracy to ±0.002, the best ever achieved with neutron beams in any analyzing power measurement [11]. This data complements high accuracy cross-section data, and the combination suggests that the n-p phase

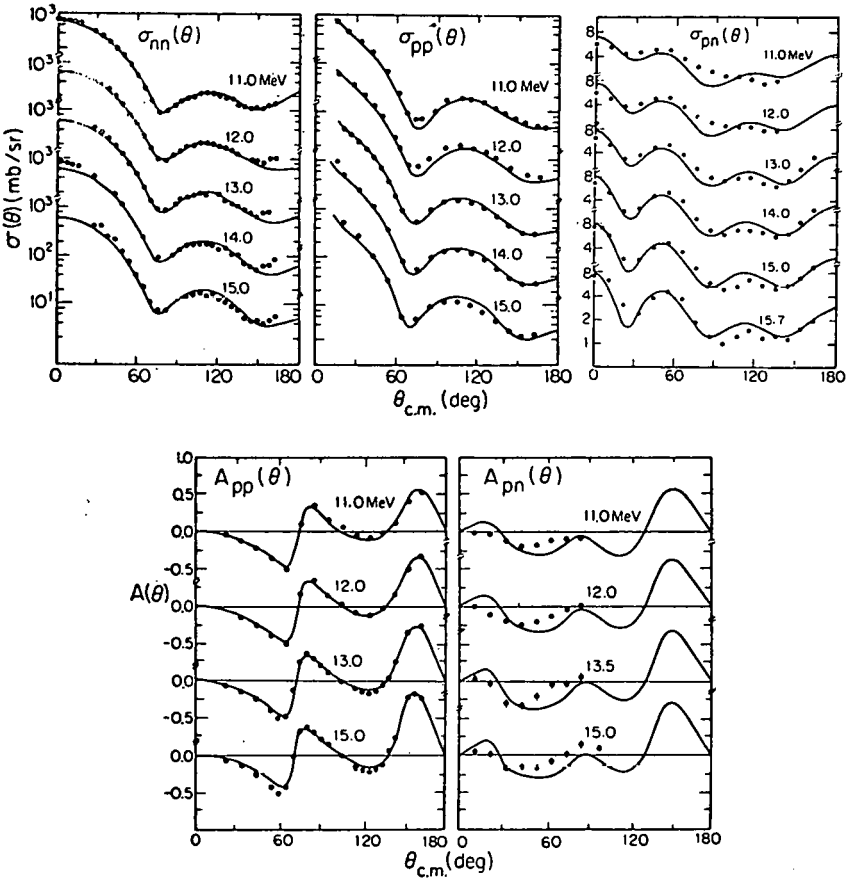

Fig.9. Results of Lane model calculations for ^{9}Be.

shifts need some readjusting in the region around 15 MeV. A re-analysis should help limit the n-p cross-section uncertainties, and this in turn should provide better calibrated neutron detectors and monitors.

The arrangement for the n-p and n-He polarization measurements involved scatterers that were also scintillators. This permitted the use of coincidence requirements to reduce neutron backgrounds which are a problem in double-scattering and triple-scattering experiments. The technique also used the ^{2}H+d reaction induced by a polarized deuteron beam to give a highly polarized neutron beam at 0° reaction angle where the cross section is strongly peaked. The deuteron beam was not pulsed however and so normal time-of-flight scattering techniques could not be employed to study other targets.

However, during the past year we have had a major breakthrough with the polarized deuteron beam. By a clever method [12] of

ramping and double-bunching the polarized deuteron beam before injection into the tandem, about 75% of the DC beam can be compressed into 2 ns wide bursts at the target. These deuterons, which are about 70% polarized, then produce 2 ns bursts of 63% polarized neutrons at the 0° $^{2}H(d,n)$ reaction angle. This system permits us to measure analyzing powers using standard neutron time-of-flight cross-section techniques. (Recall that the analyzing power is the ratio of the difference $\sigma_{\uparrow}-\sigma_{\downarrow}$ to the sum $\sigma_{\uparrow}+\sigma_{\downarrow}$ where $\sigma_{\uparrow}$ is the scattering cross section for spin-up neutrons and $\sigma_{\downarrow}$ is the cross section for spin-down neutrons.)

The significance of this development becomes apparent when one recognizes that very little accurate polarization data exist for neutron energies above a few MeV. Because the compound nucleus contributions are quite large at low energies, it has not been possible in the past to make a good determination of the spin-orbit interaction for neutrons, a term that is present in all optical models today. At the present time, one usually just carries over the $(\ell \cdot s)$ term from (p,p) scattering into the neutron optical model.

Our technique has been used for the targets ^{9}Be, ^{12}C, ^{40}Ca, ^{54}Fe, ^{58}Ni, ^{65}Cu, and ^{208}Pb. More experiments are planned in order to complete the data set. Three to ten analyzing power distributions in the range 7 to 17 MeV have been obtained for the first three nuclei listed. The nuclei ^{54}Fe and ^{65}Cu have been studied at 10 and 14 MeV, and ^{58}Ni and ^{208}Pb at 10 MeV. Much of the data have been corrected for multiple scattering already. This contribution can account for 80% of the detected neutrons in the cross-section minima. Large statistical uncertainties on the data cannot be avoided at these angles. Examples of the data for the medium-weight nuclei are shown in Figs. 10 and 11 [13] . The analyzing powers are seen to exhibit considerable structure and large magnitudes at some angles.

We intend to combine the neutron polarization data with cross-section data to provide a better determination of optical-model parameters. In the more distant future we will incorporate proton polarization and cross-section data into the search also. Presently, we are just beginning to look at some optical-model sensitivities. Some interesting aspects are beginning to surface already.

In Figs. 10 and 11 we compare the data to calculations using the global parameters of Rapaport et al. [4] . The model includes a Bechetti-Greenlees spin-orbit term [14] . The main structures in the analyzing power function $A(\theta)$ are reproduced with the calculation. Cursory single-energy searches on the cross-section and $A(\theta)$ simultaneously gave the results shown in Figs. 10 and 11. The optical model parameters did not change a great deal to obtain these fits, but the chi-square for the fits are still very large and improvements must be possible. Preliminary conclusions are that the spin-orbit potential depth for neutrons is near to that of protons, that is, 6 MeV, and adding an imaginary spin-orbit term makes a sizeable improvement in the

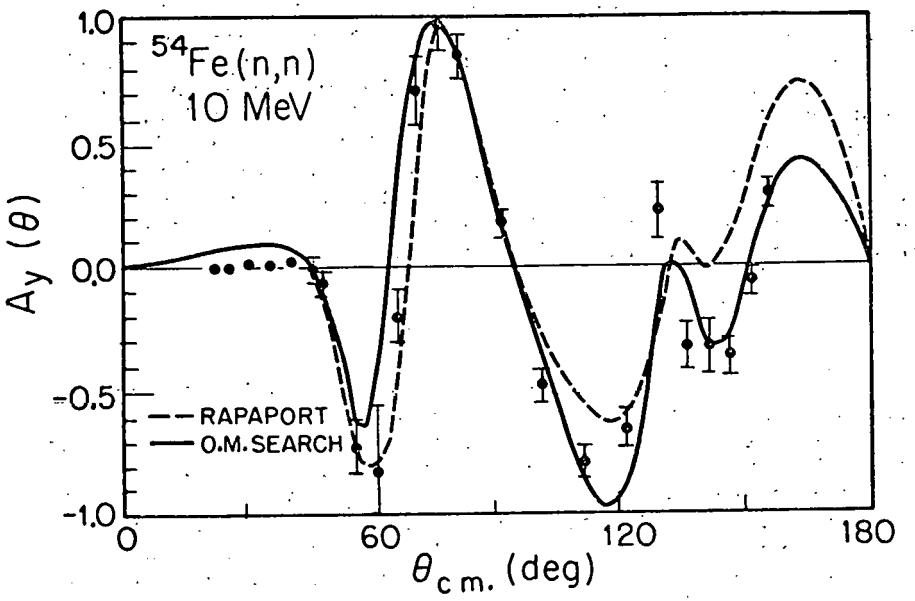

Fig.10. Analyzing power measurements for ^{54}Fe.

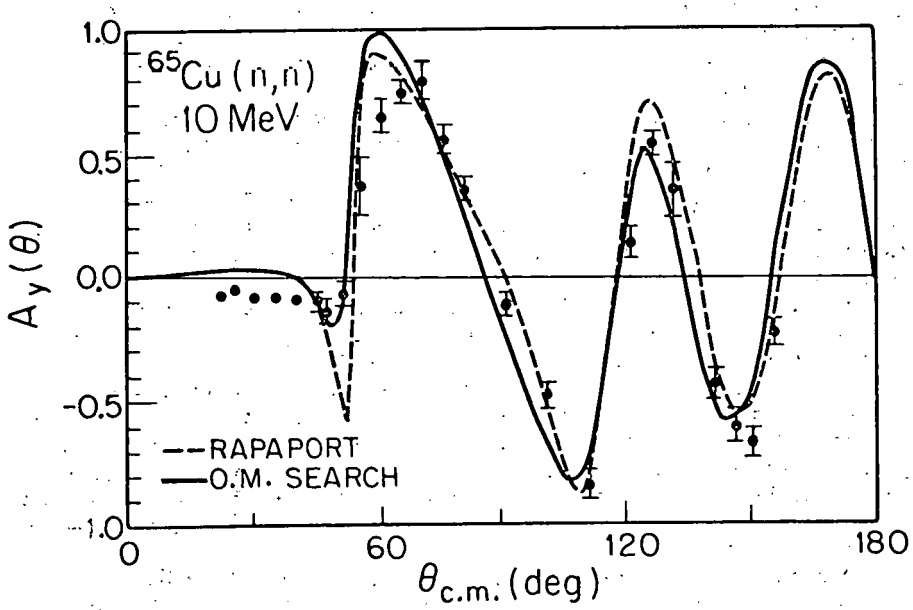

Fig.11. Analyzing power measurements for ^{65}Cu.

quality of the fit. Lastly, none of the searches this far have given us a good fit to our forward angle data. These data have been measured to an accuracy of about ±0.003 and there is little chance of experimental error in the method we employ in these measurements. We are aware of the large A(θ) produced in Mott-Schwinger scattering at forward angles, but it is not of sufficient importance to affect our calculations in the 20° to 40° region [15]. To reproduce the effect that we observed with a calculation may require a departure from the standard Thomas-type interaction for the spin-orbit real term.

RADIATIVE CAPTURE REACTIONS

A major effort of the research program at TUNL involves (n,γ) and (p,γ) capture reaction studies. The program utilizes a high resolution 25 cm long x 25 cm diameter NaI detector with an anti-coincidence annular detector for suppression of Compton scattered gamma rays. A unique aspect of the research involves the study of the analyzing power function A(θ) for the capture of polarized neutrons. As in the previous section, the ^{2}H(d,n) reaction induced with polarized deuterons provides the polarized neutron beam.

The neutron studies focus on giant dipole and quadrupole resonances, and the structures therein. In comparison to protons, neutrons are a particularly beautiful probe for separating the GQR effects from the GDR. In proton capture direct E2 radiative capture is normally quite large. However, the (uncharged) neutron has a small E2 effective charge and the direct E2 cross sections are diminished.

In the (n,γ) studies excitation functions at 90° are usually taken in about 200 keV steps for neutron energies between 6 and 14 MeV. This corresponds to resonances between 15 to 30 MeV in the residual nuclei. Studies until now have involved the nuclei ^{3}He, ^{13}C, ^{14}N, ^{40}Ca, and ^{208}Pb. For several of the nuclei angular distributions of the γ-rays have been obtained at five to eight energies.

To illustrate the quality of the data and the structure in the cross section, we show the recent results [16] for the reaction ^{13}C(n,γ)^{14}C in Fig. 12. The curve is a guide to the eye. The cross-section data and analyzing power data around 10 MeV have been compared to a direct-semidirect calculation and the agreement is quite good. Preliminary analyses also use a T-matrix approach which permits one to determine the relative amplitudes that contribute to the resonance structures. In this reaction the $d_{3/2}$ amplitude was found to account for almost all of the E1 cross section at 10 MeV.

One can obtain cross sections for (n,γ) reactions by using (γ,n) measurements and the detailed balance principle. However, the nature of (γ,n) experiments make accurate measurements very difficult. One of the recent TUNL (n,γ) measurements,

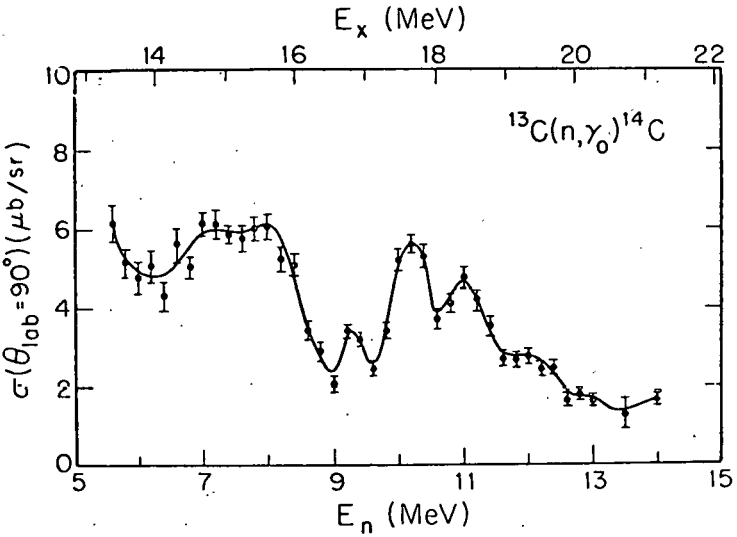

Fig.12. Cross section measurements for $^{13}C(n,\gamma)$.

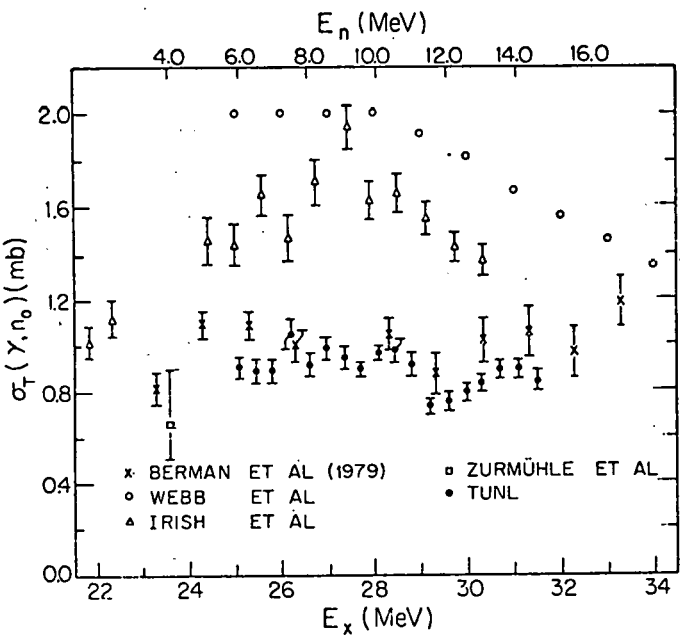

Fig.13. Cross section measurements for $^{4}He(\gamma,n)^{3}He$.

$^{3}He(n,\gamma)^{4}He$, indicate another significant aspect of the use of the system. Shown in Fig. 13 are the results of five separate experiments for the total cross section for the photodisintegration of ^{4}He, i.e., $^{4}He(\gamma,n_0)^{3}He$. The TUNL data have been included through detailed balance methods [17]. Clearly, the (calibrated) TUNL data help resolve the confusion existing in this puzzling set of data. The significance of the new data, which confirms a lower cross-section value, lies in the fact that the (γ,p) cross section appears to be twice as large at the (γ,n) cross section. This suggests that there is significant isospin mixing present in ^{4}He. Analyzing power measurements should provide additional clues on the nature of this effect.

SUMMARY AND ACKNOWLEDGEMENTS

In summary, there is a diverse neutron program actively being pursued at TUNL. Many of the measurements only affect small details related to cross-section magnitudes. But most of the work will permit a better understanding of nuclear parameters, and thereby will permit more accurate predictions of cross sections, some which have not been measured yet and some which are impossible to measure in the laboratory.

We are happy to acknowledge the cooperation of the groups at TUNL in preparing this manuscript. About 30 research staff, students and visitors were involved in the data shown here.

Triangle Universities Nuclear Laboratory is partially supported by the U. S. Department of Energy.

REFERENCES

1. S. G. GLENDINNING, F. O. PURSER, and C. R. GOULD, "Optical Model Fits to Nucleon Scattering from ^{10}B, ^{11}B," Bull. Am. Phys. Soc. 24, 830 (1979).

2. B. WATSON, "The Elastic and Inelastic Scattering of Protons from ^{10}B Between 5 and 16 MeV", Argonne National Laboratory Informal Report PHY-1968B (1968).

3. S. EL-KADI et al., "Neutron Elastic and Inelastic Scattering from $^{63,65}Cu$ and $^{54,56}Fe$ Between 8 and 14 MeV", Bull. Am. Phys. Soc. 24, 866 (1979).

4. J. RAPAPORT, V. KULKARNI and R. W. FINLAY, "A Global Optical-Model Analysis of Neutron Elastic Scattering Data", Nucl. Phys. A330, 15 (1979).

5. M. DROSG, G. F. AUCHAMPAUGH and F. GURULE, "Neutron Background Spectra and Signal-to-Background Ratio for Neutron Production Between 10 and 14 MeV by the Reactions $^{3}H(p,n)^{3}He$,

$^{1}H(t,n)^{4}He$, and $^{2}H(d,n)^{3}He$", Los Alamos Scientific Laboratory Report No. LA-6459-MS (1976).

6. H. HOGUE and A. BEYERLE, "Finite Geometry and Multiple Scattering Cross Sections for Neutron Cross-Section Measurements", Bull. Am. Phys. Soc. 24, 877 (1979).

7. A. BEYERLE et al., "Double-Differential Neutron Scattering Cross Sections for Fe, Cu, Ni and Pb Between 8 and 12 MeV", Bull. Am. Phys. Soc. 24, 866 (1979) and 25, 543 (1980).

8. A. M. LANE, "Isobaric Spin Dependence of the Optical Potential and Quasi-Elastic (p,n) Reactions", Nucl. Phys. 35, 676, (1962).

9. R. C. BYRD, "Isospin in (p,n) Reactions between Mirror Nuclei: The Lane Model and Comparisons between Polarizations and Analyzing Powers", Ph.D. Thesis, Duke University (1978); R. C. BYRD, R. L. WALTER, and S. R. COTANCH, "Detailed Study of the Lane Potential: Multichannel and Polarization Constraints", Phys. Rev. Letters 43, 260 (1979).

10. C. E. FLOYD et al., "Scattering of Polarized Neutrons from ^{9}Be", Bull. Am. Phys. Soc. 24, 837 (1979).

11. W. TORNOW et al., "Discrepancies Between Global Nucleon-Nucleon Phase Shifts and New Data for n-p Scattering at 16.9 MeV", Phys. Rev. Letters 39, 915 (1977); "Analyzing Power Measurements for n-p Scattering Between 13.5 and 16.9 MeV", Nucl. Phys. (in press).

12. S. A. WENDER et al., "A High Efficiency Bunching System for Polarized Beam", Nucl. Instr. and Methods (in press).

13. C. E. FLOYD et al., "Polarization for Neutron Elastic Scattering from ^{54}Fe, ^{65}Cu, and Pb at 10 and 14 MeV", Bull. Am. Phys. Soc. 25, 542 (1980).

14. F. D. BECHETTI, JR. and G. W. GREENLEES, "Nucleon-Nucleus Optical-Model Parameters, A>40, E<50 MeV", Phys. Rev. 182, 1190 (1969).

15. W. S. HOGAN and R. G. SEYLER, "Influence of Electromagnetic Interaction on Neutron Scattering from Nuclei," Phys. Rev. 177, 1706 (1969).

16. M. J. JENSEN et al., "Radiative Capture of Polarized Neutrons by ^{13}C", Bull. Am. Phys. Soc. 25, 603 (1980).

17. L. WARD et al., "Radiative Capture of Neutrons by ^{3}He", Bull. Am. Phys. Soc. 25, 576 (1980).

THIS PAGE
WAS INTENTIONALLY
LEFT BLANK

Dup

ORELA MEASUREMENTS TO MEET FUSION ENERGY NEUTRON CROSS SECTION NEEDS

D. C. Larson

Oak Ridge National Laboratory
Oak Ridge, Tennessee 37830, U.S.A.

ABSTRACT

Major neutron cross section measurements made at the Oak Ridge Electron Linear Accelerator (ORELA) that are useful to the fusion energy program are reviewed. Cross sections for production of gamma rays with energies $0.3 < E_\gamma < 10.5$ MeV have been measured as a function of neutron energy over the range $0.1 < E_n < 20.0$ MeV for Li, C, N, O, F, Na, Mg, Al, Si, Ca, Ti, V, Cr, Mn, Fe, Ni, Cu, Zn, Nb, Mo, Ag, Sn, Ta, W, Au, Pb and Th. Neutron emission cross sections have been measured for ^{7}Li, Al, Ti, Cu and Nb for $1 < E_n < 20$ MeV. Some results of recent neutron total cross section measurements from 2-80 MeV for eleven materials (C, O, Al, Si, Ca, Cr, Fe, Ni, Cu, Au and Pb) of interest to the FMIT project will be presented. Finally, future directions of the ORELA program will be outlined.

INTRODUCTION

During the past four years a number of programs at the Oak Ridge Electron Linear Accelerator (ORELA) have provided data which are of use in the design of fusion energy devices. The purpose of this paper is to review these measurements, and to collect in one place a list of references which document these measurements. In addition, results are presented for some neutron total cross section measurements recently completed from 2-80 MeV. Finally the future directions of the ORELA fusion energy program are outlined. Besides the larger measurement programs discussed below, other measurements of importance made at ORELA include cross sections for the reactions ^{14}N(n,charged particle) [1], ^{6}Li(n,α) [2] and ^{7}Li(n,n'γ) [3].

(n,xγ) MEASUREMENTS

One major area in which ORELA has provided the bulk of the available cross section data is the production of gamma rays resulting from neutron-induced interactions. Cross sections for the production of gamma rays with energies of $0.3 < E_\gamma < 10.5$ MeV were measured as a function of neutron energy over the range $0.1 < E_n < 20.0$ MeV. Details of the experimental method are given in refs. 4 and 5. The measurements were made using a heavily shielded NaI detector in conjunction with the white neutron spectrum from ORELA. Incident neutron energies were determined by the time-of-flight technique over a 47-m flight path, while the gamma-ray energy distributions were obtained from pulse-height unfolding techniques using the code FERD [6]. The data have poor energy resolution compared to results using Ge(Li) detectors; however, they have the advantage of including the numerous weak transitions which appear as a continuum, a feature especially important for the heavier nuclei. Since the data span the neutron energy region of interest to ENDF/B, the data have frequently been used directly in evaluations. In addition, since they often provide cross section information for energy regions where few data exist, they are used to guide nuclear model calculations. Table 1 lists the elements on which data have been taken, the angle(s) at which data were acquired, whether or not the data have been utilized in the ENDF/B-V evaluation for the material, and the ORNL report number in which the measurement is described and numerical values of the data are given. Much of the earlier data was obtained under research sponsored by the Defense Nuclear Agency, with the more recent measurements made for the Basic Energy Sciences program to provide data useful for fusion energy problems. This series of measurements was carried out by G. L. Morgan, J. K. Dickens, G. T. Chapman, T. A. Love, E. Newman, D. C. Larson and F. G. Perey.

(n,xn) AND (n,xγ) MEASUREMENTS

The second major measurement program which is underway is the simultaneous measurement of (n,xn) and (n,xγ) cross sections produced by neutron interactions with materials of interest to the fusion community. Details of the experimental technique are documented in refs. 7 and 8. Using ORELA as the neutron source, annular scattering samples located 47 m from the neutron source are viewed by a NE-213 scintillation detector. The average scattering angle is determined by the position of the detector along the axis perpendicular to the plane of the sample. Neutron-gamma discrimination is used to classify a given event, which is then stored in one of two pulse-height versus time-of-flight two parameter arrays (one for neutrons, one for gamma rays). Secondary neutron and gamma-ray spectra are determined by unfolding the pulse-height distributions with the code FERD [6]. These measurements provide data that have the global testing power of integral

experiments while retaining enough differential character to localize the source of discrepancies with evaluated data. They are useful in providing a means of checking evaluated cross sections over wide ranges of incident and secondary energies, in addition to aiding in the development of advanced nuclear model codes. The gamma-ray-production cross sections obtained from these measurements are in good agreement with the sodium iodide results discussed previously. Results of these measurements are available for five elements to date and are listed in Table II along with the ORNL report number. G. L. Morgan and F. G. Perey initiated and carried out the measurements listed in Table II.

HIGH ENERGY TOTAL CROSS SECTION MEASUREMENTS

The final set of experiments to be discussed are the recent high energy transmission measurements done at ORELA to help meet shielding design data needs for the FMIT project. Table III lists the elements which have been measured, the sample thicknesses, and the sample transmission in percent at 40 MeV. Two sets of measurements were done; the first set included data for H, C, O and Fe from 0.5 to 60 MeV and is documented in ref. 9. The second set of measurements cover the energy range from 2 to 80 MeV and will be discussed briefly here. The flight path was 80 m, with a NE-110 scintillator used to detect the neutrons. Corrections were made for deadtime and background effects. Samples of CH_2, C and Fe were rerun as checks for the H, C and Fe cross sections, and were found to be in good agreement with results from the first measurement [9]. The repetition rate was dropped from 1000/sec to 800/sec for this run, since more peak power could then be applied to the klystrons, which resulted in higher energy electrons, thus increasing the number of high energy neutrons above $\sim$50 MeV. Since ample data are available up to 2 MeV for the materials measured in this run, the bias cutoff was raised to $\lesssim$ 2 MeV neutron energy to further reduce any low energy gamma-ray backgrounds which may be present. The average run time for each material was 27 hours. Integrating the area under our data from 2-20 MeV and comparing with the integral obtained from the ENDF/B-V evaluations for these materials yielded agreement to better than 1% for all elements except Al (1.2%) and Au (1.8%). A similar comparison for hydrogen from 2-80 MeV compared with the latest results of Arndt [10] from his nucleon-nucleon phase shift analysis shows agreement to better than 1%.

Figure 1 shows a comparison of our hydrogen total cross section data from both runs, compared with the results of Arndt [10] from 2-80 MeV. Figure 2 compares our data for chromium from 15-80 MeV with all data currently available from the CSISRS data repository at BNL. The data have been suitably averaged to reduce the number of points for comparison purposes. The four data points of Peterson *et al.* [11] from 18 to 29 MeV are in good agreement with the present results. The data of Perey *et al.* [12] were also

taken at ORELA using the same sample, but a different flight path, detector, data acquisition method and neutron target. These data extend to 29 MeV and are generally in good agreement with our results. The data of Cierjacks *et al.* [13] extend to 32 MeV, and are systematically lower than our data near 21 MeV by ~4%.

In the absence of experimental data, total cross sections have often been obtained from the optical model. Two of the more common optical model parameter sets used are those of Wilmore and Hodgson [14], and Becchetti and Greenlees [15]. We have compared the predictions of these parameter sets with our data [16], and a typical result is shown in Fig. 2 for chromium. In general, we found that cross sections predicted by the Wilmore-Hodgson set are better at lower energies, while the Becchetti-Greenlees parameters are somewhat better for higher energies.

Figure 3 compares our data for iron with data available from CSISRS from 15 to 80 MeV, along with the recent data of Zanelli *et al.* [17] from the University of California at Davis. Again the various data sets have been averaged. The data of Perey *et al.* [18], Peterson *et al.* [11] and Hildebrand and Leith [19] are generally in good agreement with our present results. The data of Cierjacks *et al.* [13] are systematically low near 21 MeV and high above 24 MeV. The data point of Deconninck *et al.* [20] lies above our averaged data while the data of Ragent [21] are generally low with the exception of the two points near 36 MeV.

Figure 4 shows a comparison of our data for nickel with other results available from CSISRS. The data of Perey *et al.* [12] and Peterson *et al.* [11] are in good agreement with our results. The data of Cierjacks *et al.* [13] appear to be slightly larger than the general trend of our data above 20 MeV, and the data point of Hildebrand and Leith [19] is slightly smaller than the trend of our data.

The data for the elements listed in Table III provide a consistent extension of the data base to higher energies where very few data are presently available. A complete report describing the measurement and results for all the elements will be published elsewhere. The total cross section work was done by D. C. Larson, J. A. Harvey, D. M. Hetrick and N. W. Hill.

FUTURE DIRECTIONS

Current plans for future experimental work at ORELA include more simultaneous measurements of (n,xn) and (n,xγ) on materials of interest to the fusion energy program, a continuation of the high energy total cross section measurements and an exploratory program to determine the feasibility of measuring (n,charged particle) reactions over a wide range of incident neutron energies and secondary charged particle energies to complement the work going on at Livermore and Ohio University.

ACKNOWLEDGEMENT

Research sponsored by the Division of Basic Energy Sciences, U. S. Department of Energy, under contract W-7405-eng-26 with the Union Carbide Corporation.

REFERENCES

1. G. L. Morgan, ORNL Report TM-6528/R1 (November 1978).

2. C. Renner, J. A. Harvey, N. W. Hill, G. L. Morgan, and K. Rush, Bull. Am. Phys. Soc. 23, 526 (1978).

3. D. K. Olsen, G. L. Morgan and J. W. McConnell, to be published in Nucl. Sci. Eng.

4. J. K. Dickens, G. L. Morgan and F. G. Perey, Nucl. Sci. Eng. 50, 311 (1973).

5. J. K. Dickens, G. L. Morgan, G. T. Chapman, T. A. Love, E. Newman and F. G. Perey, Nucl. Sci. Eng. 62, 515 (1977).

6. W. R. Burrus and V. V. Verbinski, Nucl. Instrum. Methods 67, 181 (1969), and W. R. Burrus, B. W. Rust and J. E. Cope, Proceedings of the Second Annual Workshop on the Information Linkage Between Applied Mathematics and Industry, Monterrey, Academic Press (in press).

7. G. L. Morgan, T. A. Love and F. G. Perey, Nucl. Instrum. Methods 128, 125 (1975).

8. G. L. Morgan and F. G. Perey, Nucl. Sci. Eng. 61, 337 (1976).

9. D. C. Larson, J. A. Harvey and N. W. Hill, to be published in Proceedings of the International Conference on Nuclear Cross Sections for Technology, Knoxville (1979).

10. Private communication from R. A. Arndt, Virginia Polytechnic Institute, December 1979, Solution Set CD79.

11. J. M. Peterson, A. Bratenahl and J. P. Stoering, Phys. Rev. 120, 521 (1960).

12. F. G. Perey, T. A. Love and W. E. Kinney, extension of work reported in Report ORNL-4823 (1973).

13. S. Cierjacks, P. Forti, D. Kopsch, L. Kropp, J. Neve and H. Unseld, Karlsruhe Report KFK-1000 (June 1978) and Supplement 1 to this report.

14. D. Wilmore and P. E. Hodgson, Nucl. Phys. 55, 673 (1964).

15. F. D. Becchetti, Jr. and G. W. Greenlees, Phys. Rev. 182, 1190 (1969).

16. D. C. Larson, D. M. Hetrick and J. A. Harvey, Bull. Am. Phys. Soc. 25, 543 (1980).

17. C. I. Zanelli, F. P. Brady, J. L. Romero, C. M. Castaneda and D. L. Johnson, Bull. Am. Phys. Soc. 24, 658 (1979) and private communication from F. P. Brady.

18. F. G. Perey, T. A. Love and W. E. Kinney, Report ORNL-4823 (December 1972).

19. R. H. Hildebrand and C. E. Leith, Phys. Rev. 80, 842 (1950).

20. G. Deconninck, A. Gonze, P. Macq and J. P. Meulders, J. Phys. Rad. 22, 652 (1961).

21. B. Ragent, Report UCRL-2337 (1953).

TABLE I

ORNL (n,xγ) Measurements

Element	90°	125°	Used in ENDF/B-V	ORNL Report
Li		X	N	TM-4538
C	X	X	Y	TM-3702
N	X	X	Y	ORNL-4864
O		X	N	ORNL-5575
F		X	Y	TM-4538
Na		X	Y	TM-6281
Mg	X	X	Y	TM-4544
Al	X	X	Y	TM-4232
Si	X	X	Y	TM-4389
Ca		X	Y	TM-4252
Ti		X	N	TM-6323
V		X	Y	TM-5299
Cr		X	Y	TM-5098
Mn		X	Y	TM-5531
Fe		X	Y	TM-5416
Ni		X	Y	TM-4379
Cu		X	Y	ORNL-4846
Zn		X	N	TM-4464
Nb	X		N	TM-4972
Mo		X	N	TM-5097
Ag		X	N	TM-5081
Sn		X	N	TM-4406
Ta	X	X	Y	TM-3702
W		X	Y	ORNL-4847
Au		X	N	TM-4973
Pb		X	Y	TM-4822
Th		X	N	TM-6758

TABLE II

ORNL (n,xn) Measurements

Element	Angle	ORNL Report
^{7}Li	50°,126°	TM-6247
Al	127°	TM-5241
Ti	130°	ORNL-5563
Cu	130°	ORNL-5499
Nb	129°	TM-5829

TABLE III

ORNL Total Cross Section Measurements

Element	Energy Range (MeV)	Sample Thickness (at/b)	Transmission at 40 MeV (%)
H	0.5-60	0.8224	83
H	2.0-80	0.8224	83
C	0.5-60	0.4115	64
C	2.0-00	0.4115	64
O	0.5-60	0.5485	46
Al	2.0-80	0.4134	48
Si	2.0-80	0.3472	54
Ca	2.0-80	0.3512	45
Cr	2.0-80	0.2106	59
Fe	0.5-60	0.4296	34
Fe	2.0-80	0.4296	34
Ni	2.0-80	0.2304	56
Cu	2.0-80	0.2149	57
Au	2.0-80	0.1139	63
Pb	2.0-80	0.1653	48

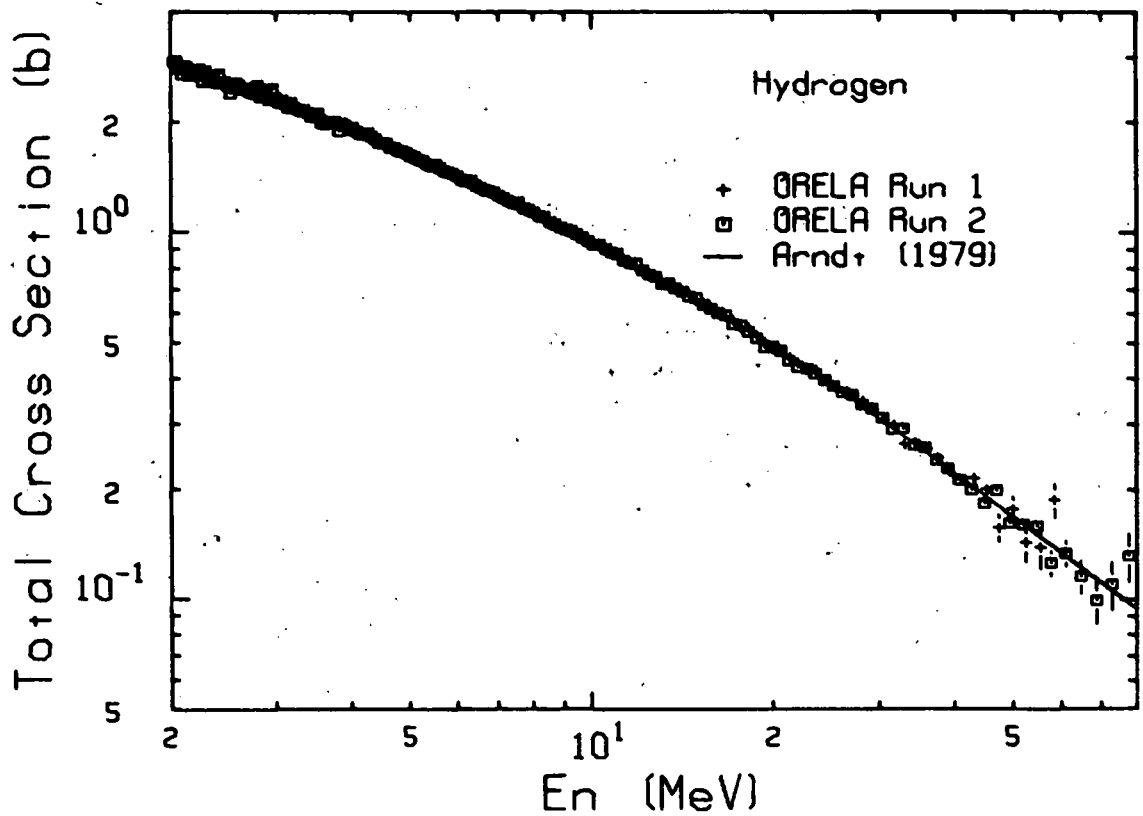

Figure 1. Comparison of hydrogen total cross section data for Run 1 (2-60 MeV) and Run 2 (2-80 MeV) with results of a nucleon-nucleon phase-shift analysis of ref. 10.

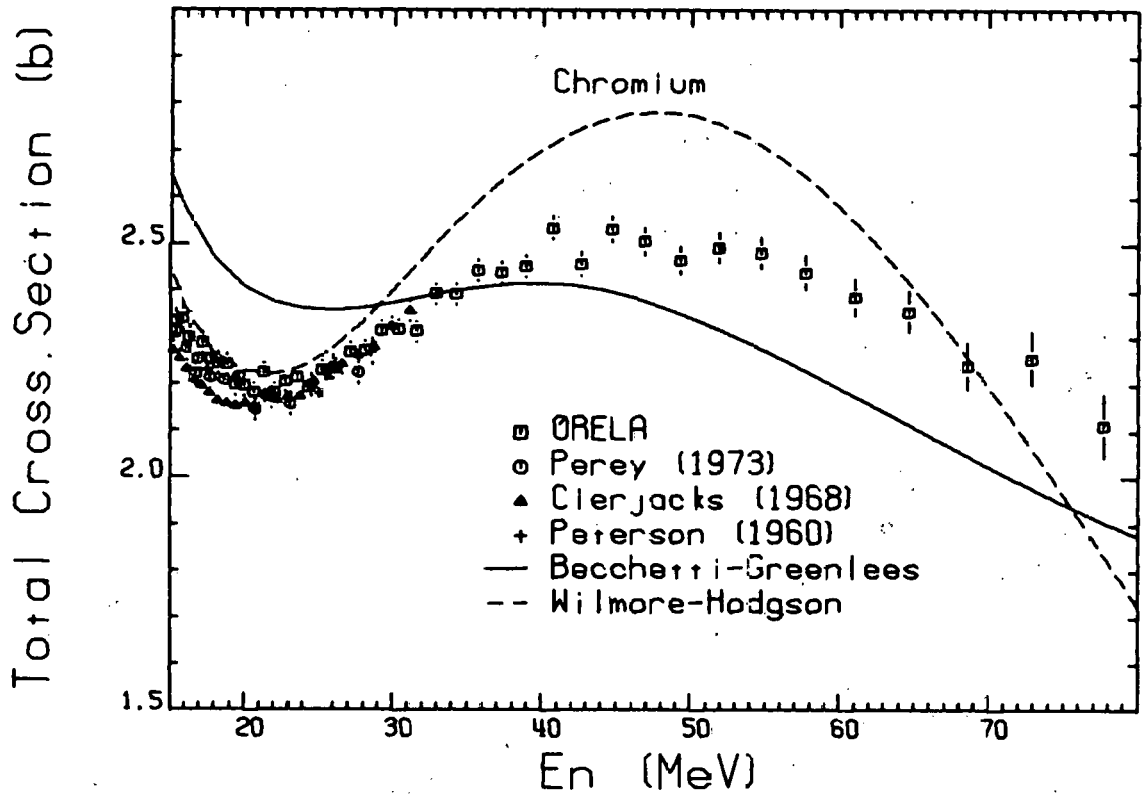

Figure 2. Comparison of present total cross section data for chromium with results of refs. 11-13, and predicted total cross sections from the optical model parameter sets of refs. 14 and 15.

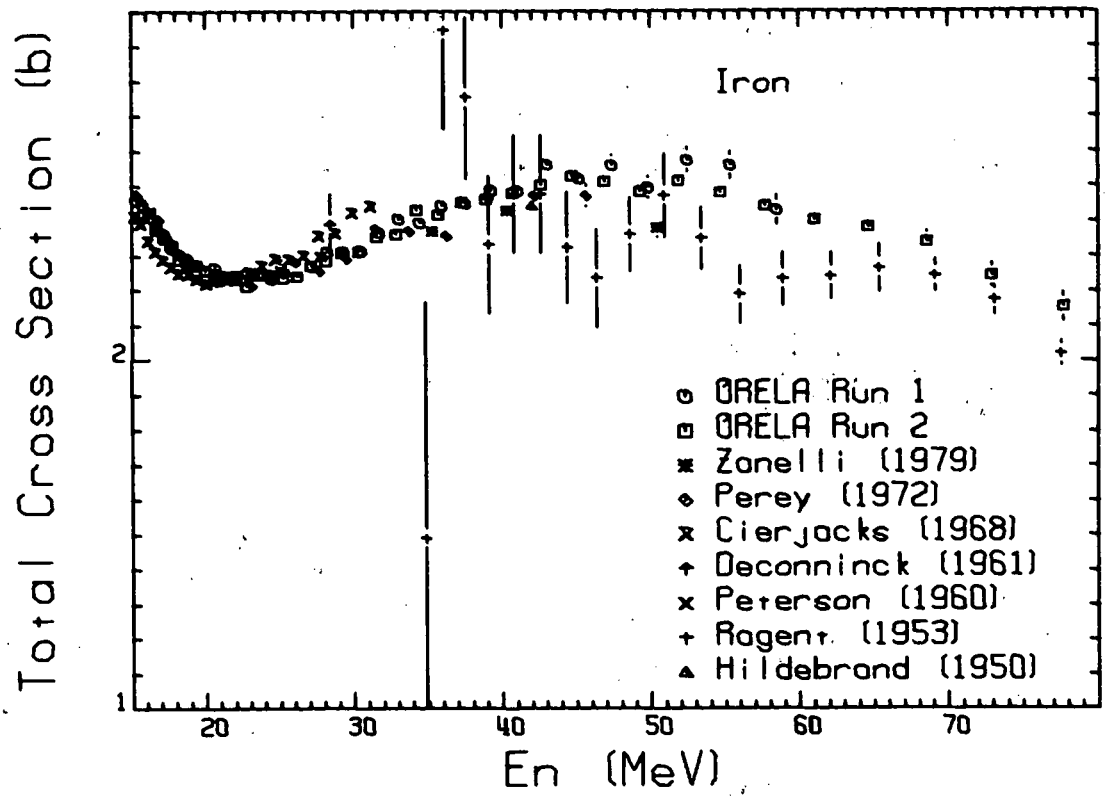

Figure 3. Comparison of present total cross section data for iron with results of refs. 11, 13, 17-21.

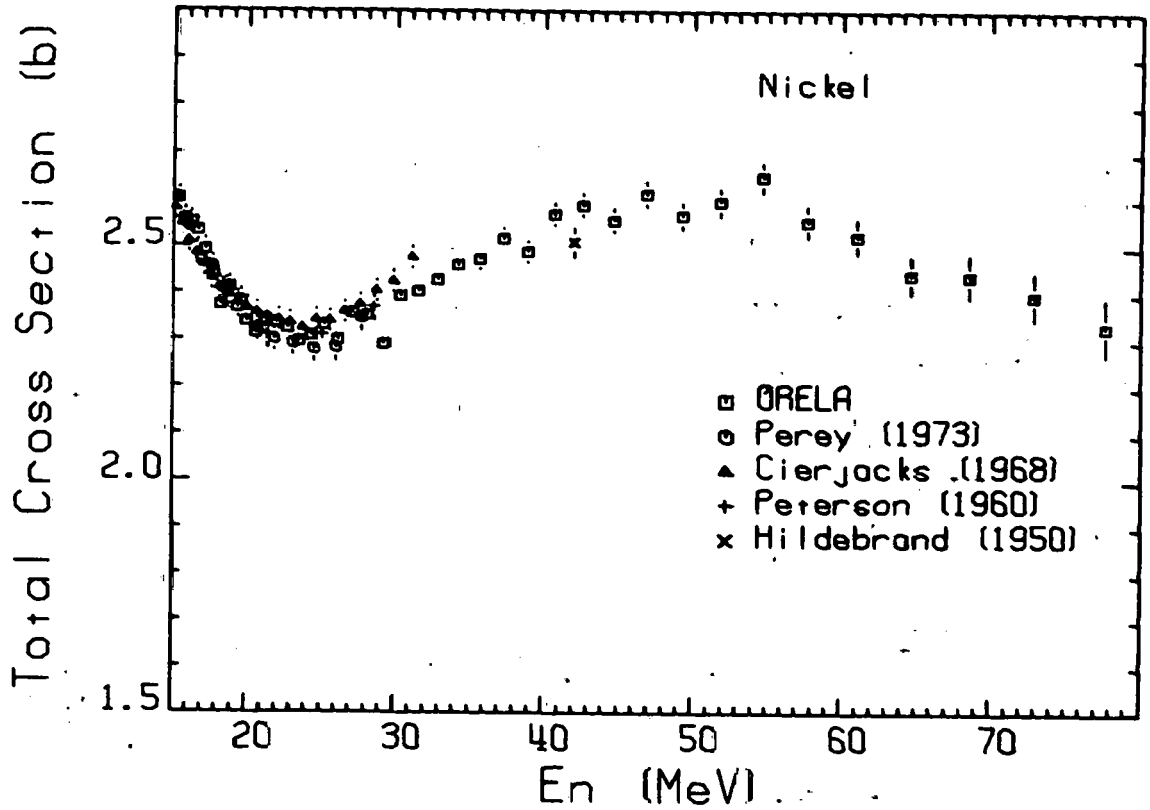

Figure 4. Comparison of present total cross section data for nickel with results of refs. 11-13, 19.

HELIUM GENERATION CROSS SECTIONS FOR FAST NEUTRONS

D. W. Kneff, B. M. Oliver, M. M. Nakata, and Harry Farrar IV

Rockwell International, Energy Systems Group
Canoga Park, California 91304, U.S.A.

ABSTRACT

Fast-neutron-induced total helium production cross sections are an important source of information for the development of materials for fusion reactors. These cross sections are presently being measured at Rockwell International, with the measurements based on high-sensitivity gas mass spectrometry. Cross sections are given for helium production in Al, Ti, Cr, Fe, Ni, Cu, Au, and the separated isotopes of Ni and Cu, for ~14.8-MeV neutrons from the T(d,n) reaction. A detailed fluence mapping of the irradiation volume was required to relate helium generation measurements to cross sections, emphasizing the importance of comprehensive passive dosimetry in all fast-neutron irradiation experiments.

INTRODUCTION

Helium produced by fast neutrons is a major consideration in the development of materials for fusion reactors. This helium, combined with neutron damage and transmutation, will affect the mechanical and physical properties of the reactor components. It is thus important to measure the neutron-induced total helium generation cross sections of a broad range of pure elements and their isotopes. These measurements have direct application to the design and assessment of candidate fusion reactor materials, and provide important comparisons with theoretical helium generation cross section predictions.

The fast-neutron-induced helium generation cross sections of several pure elements and isotopes are presently being measured at Rockwell International for neutron environments produced by the T(d,n) and Be(d,n) reactions. These measurements are made by irradiating a capsule containing a large number of samples in the neutron environment of interest, and subsequently analyzing, by high-sensitivity gas mass spectrometry, the total amount of helium

generated in each sample [1]. A comprehensive set of foil activation and helium accumulation neutron dosimeters is also included, to characterize the neutron irradiation environment over the capsule volume. The helium generation measurements are then combined with the neutron fluence data to deduce cross sections. These cross sections are total integral helium generation cross sections for the incident neutron energy spectrum, including helium produced from all neutron-induced reactions.

This paper presents the results of the recent helium production cross section measurements made for the pure elements Al, Ti, Cr, Fe, Ni, Cu, and Au, and the separated isotopes of nickel and copper, for ~14.8-MeV neutrons from the T(d,n) reaction. The detailed fluence mapping of the irradiation volume is also described, because it played an important role in the accurate cross section determinations. The status of cross section measurements in the Be(d,n) neutron environment is reviewed in another paper in this symposium [2].

EXPERIMENT DESCRIPTION

The T(d,n) helium production cross section measurements were made using the Rotating Target Neutron Source-I (RTNS-I) facility at Lawrence Livermore Laboratory (LLL). The irradiation assembly is shown in Fig. 1. This assembly was similar to, but more extensive than, that used in a previous RTNS-I irradiation [3]. The assembly consisted of a small stainless steel capsule containing two layers of pure elements, separated isotopes, and pure element helium accumulation dosimetry rings, sandwiched between layers of thin radiometric dosimetry foils. The radiometric foils, provided by Argonne National Laboratory (ANL), included thin discs of Nb, Au, Co, Fe, Ni, and Zr.

The assembly was mounted on the fixed outside cover of the RTNS-I rotating tritium target assembly, and irradiated for 76.7 h. The measured total neutron fluence received by the assembly ranged from 0.3 to 2.6 x 10^{17} neutrons/cm^2. The assembly was approximately centered on the deuteron beam axis by using autoradiographs taken immediately before the irradiation. The average energy of the neutrons incident upon the helium generation materials was calculated to be 14.8 ± 0.1 MeV, based on reaction kinematics for 400-keV deuterons slowing down in the tritiated titanium target [4], and based on approximate numerical integrations performed over the large target solid angle. The spectrum full-width-at-half-maximum was determined to be ~0.6 MeV.

Three days after the end of the irradiation, the experimental capsule was disassembled, and the radiometric foils were cut into segments for counting at ANL and LLL. The helium generation samples and rings were subsequently etched, segmented, weighed, and analyzed for helium using the high-sensitivity gas mass spectrometer system [1]. Etching removed the effects of helium recoiling into or out of each sample.

NEUTRON FLUENCE DETERMINATION

A detailed three-dimensional neutron fluence map was required for the capsule irradiation volume, because of the steep fluence gradients present. This mapping was particularly important, because the fluence determination is the largest source of uncertainty in the cross section measurements, and irregularities in the fluence profile can cause significant cross section errors. The fluence mapping for this irradiation is presented here in some detail, to emphasize the importance of comprehensive passive dosimetry in fast-neutron irradiation experiments.

The mapping procedures used were similar to those used for a previous RTNS-I irradiation experiment [3,5]. An average map was first constructed using the foil activation counting results. Detailed adjustments were then made to the map using the results from the helium accumulation neutron dosimetry rings. The absolute fluence normalization for this map was based on the niobium radiometric foil results, for which the $^{93}Nb(n,2n)^{92m}Nb$ cross section was assumed to be 463 ± 19 mb [6].

The mapping was initiated by estimating the irradiation assembly offset from the neutron source axis, using the radiometric foil data and autoradiographs of an unsegmented foil. A series of least-squares fits was made to the measured foil segment average fluences, for several diagonals across each of several foils, to determine the coordinates of the fluence maximum. These calculations yielded an assembly offset of 1.6 mm from the neutron source axis. The autoradiographs gave a similar result, but displayed limited fluence sensitivity.

The average radial neutron fluence profile for each radiometric foil (i) was then assumed to be of the form:

$$\Phi_i(R) = C_{io} + C_{i2}R^2 + C_{i3}R^3, \qquad (1)$$

where R is the radial distance from the neutron source axis. The constants were evaluated for each foil by numerically integrating $\Phi(R)$ over the area of each foil segment, with offset corrections, and performing a multiple regression analysis.

A single three-dimensional expression was then constructed that reproduced the fluence profiles of the individual Nb and Au dosimetry foils:

$$\Phi(R, \Delta Z) = \alpha\left[C_o + C_2(\beta R)^2 + C_3(\beta R)^3\right]. \qquad (2)$$

Here ΔZ is the axial distance from the front face of the capsule, α is the normalization of the radial profile as a function of ΔZ, and β is a correction factor for the changing radial shape of the fluence curve as a function of ΔZ. The normalization factor $\alpha = [A/(A + \Delta Z)]^2$, where A = constant, was determined by a least-squares fit to the axial fluences calculated for the niobium and gold foils [from Eq. (1)]. Figure 2 shows a contour map of the fluence profile calculated for the midplane of the upper (upstream)

specimen layer of the irradiation capsule, as generated from the average fluence map defined by Eq. (2).

This initial fluence map was then combined with 91 individual helium measurements for the nine finely-segmented Al, Ti, Fe, Ni, and Cu helium accumulation dosimetry rings. Variations in the normalized helium concentration results with position in the capsule for each element provided a very sensitive measure of the irregularities in the neutron fluence profile. The sensitivity of these latter measurements follows from the fact that the helium generated in each segment was measured with an absolute uncertainty of ±1-2%. Additionally, because the rings were approximately concentric about the neutron source axis, and the average neutron energy was nearly constant over the sample irradiation volume, the helium generation cross sections were also effectively constant over this volume. Combining the helium data with the initial map revealed large variations, reflecting a nonsymmetric fluence profile about the neutron source axis, and an irradiation assembly offset (3.27 mm) significantly larger than that determined from the radiometric data alone.

The revised assembly offset was used to re-evaluate the constants in Eqs. (1) and (2). Further adjusting the map with the helium data produced a neutron profile with an elongated shape and a steep gradient on one side. This shape, not readily discernable from the less detailed radiometric data, appears to have produced the initial underestimate of the assembly offset. It appears that this irregular shape resulted from attenuation of one edge of the time-averaged deuteron beam by a beam-line collimator. Equation (2) was modified to incorporate this irregular shape, producing the following three-dimensional fluence profile:

$$\Phi(R,\theta_c,\Delta Z)=\alpha\left[C_0+C_2(\beta R)^2+C_3(\beta R)^3\right]\left[1+K\left(\frac{R_c-4.5}{15}\right)\sin(\theta_c-60)\right]. \quad (3)$$

Here θ_c is the polar angle about the irradiation assembly axis, R_c is the radial distance from this axis, and K = 1 ($R_c > 4.5$) or 0 ($R_c \leq 4.5$).

Figure 3 is the final contour plot of the fluence profile map, represented by Eq. (3), for the midplane of the irradiation capsule's upper specimen layer. Comparison of Fig. 3 with Fig. 2 shows that the deuteron beam profile irregularities produced fluences significantly different from those calculated by initially assuming a symmetric fluence profile. For example, the radiometrically determined average profile (Eq. (2) and Fig. 2) gave a fluence maximum 9% lower than that obtained with the final map (Eq. (3) and Fig. 3). Although the final map had nonsymmetric details that were obtained from the helium accumulation dosimetry data, this map was also found to be more consistent with the radiometric dosimetry results. This all demonstrates the importance of including this sort of comprehensive passive dosimetry in neutron irradiation experiments. A further demonstration is

provided by the factor-of-four variation in fluence over the 2-cm^2 area represented by Fig. 3.

Information on the relative cross sections of the radiometric dosimetry reactions can also be obtained from the fluence mapping. Figure 4 shows the calculated neutron source axis fluences [C_{io}, Eq. (1)] for most of the segmented radiometric foils, plotted as a function of the foil distances from the front face of the irradiation capsule. The solid curve is α, as defined in Eq. (2). Examination of the data shows that a number of inconsistencies exist between these reaction cross sections. The assumed cross section for the $^{197}Au(n,2n)^{196}Au$ reaction (2110 mb) is in excellent agreement with the $^{93}Nb(n,2n)^{92m}Nb$ cross section used for normalization (as previously demonstrated in Ref. 3), but the assumed $^{59}Co(n,2n)^{58}Co$ cross section (692 mb) is about 12% low relative to $^{93}Nb(n,2n)$, and that for $^{90}Zr(n,2n)^{89}Zr$ (760 mb) is about 5% low. The assumed cross sections for $^{54}Fe(n,\alpha)^{51}Cr$ (95 mb) and $^{54}Fe(n,p)^{54}Mn$ (306 mb) both appear to be high relative to niobium, but each of the two iron foils analyzed was cut into only five segments, giving insufficient information for accurate fluence profile calculations. The data for iron in Fig. 4 are thus estimates only.

The absolute fluence uncertainty for the final profile map of the irradiation capsule volume, given by Eq. (3), is estimated to be ±7%. This includes an estimated ±5% relative uncertainty from the map itself, due in part to small irregularities not incorporated in the map, and ±2% and ±4% absolute uncertainties from the radiometric counting results and from the $^{93}Nb(n,2n)$ cross section, respectively.

HELIUM PRODUCTION CROSS SECTIONS

The ^4He generated in the irradiated samples measured to date from this experiment ranged from 3×10^{11} atoms (from ~0.5-mg samples) to 1.2×10^9 atoms (from ~5-mg samples). This corresponds to ^4He concentrations ranging from 25.7 appb (atomic parts per billion, 10^{-9} atom fraction) in aluminum, to 0.072 appb in gold. Absolute 1σ uncertainties for most of the ^4He measurements were $\lesssim$±2%. The particularly low helium concentrations in the gold samples were measured to average uncertainties of ~±3%-10%. ^3He measurements were also made for several samples, including all of the separated isotopes, but none was detected in each case. The ^3He concentration upper limit for the nickel and copper isotopes was 0.05 appb.

The total helium production cross sections determined for these materials are presented in Table I. They were obtained by combining the measured helium concentrations with the neutron fluences obtained from the map. The cross sections for the individual isotopes were determined by first evaluating the cross sections for the available isotope enrichments, and then solving a matrix of equations for each isotopic material to correct for the

small concentrations of each of the other isotopes in the material. The cross section values obtained for each material from samples at different locations within the irradiation capsule were generally in very close agreement ($\lesssim \pm 4\%$). This reflects the reproducibility of the helium measurements ($\lesssim \pm 2\%$), and also demonstrates the validity of the final fluence map.

Table I also compares the present cross section determinations with those made for the same materials in a previous RTNS-I irradiation [7,8]. The values for the pure elements Al, Ti, Fe, Ni, and Cu are in excellent agreement with those determined previously. The exception is gold, for which the high helium concentrations measured previously are attributed almost entirely to α recoils into the thin foils from nearby materials. Also shown in Table I are the corresponding charged-particle measurements of Grimes, et al. [9,10]. Comparison of these measurements with the helium generation results shows that the cross section measurements of Grimes et al. are generally lower, but agree within the quoted uncertainties.

A comparison between the helium production cross sections for the individual isotopes and their associated pure elements provides a good consistency check of the measurements. The sums of the isotopic cross sections for nickel and copper, respectively, weighted by the natural isotopic abundances, are 102 ± 7 mb and 52 ± 4 mb. These values are in excellent agreement with the 100 ± 7 mb and 51 ± 3 mb pure element cross sections, respectively.

It is also of interest to compare the previously-measured helium production cross section of Type 316 stainless steel, a primary candidate structural material for first-generation fusion reactors, with the weighted sum of the cross sections of the component elements. The measured stainless steel cross section is 57 ± 4 mb [7]. The weighted sum of the constituent elements Fe, Cr, Ni, Mo, and C (Mo and C from a previous experiment [7]) is 52 ± 3 mb. The small difference is greater than expected from the various uncertainties, and may be due in part to a minor stainless steel component with a relatively high helium production cross section.

FUTURE WORK

Several materials other than those listed in Table I were also irradiated in this experiment, and will be analyzed shortly to determine their helium generation cross sections. These include C, V, Zr, Nb, Mo, and the separated isotopes of B, Fe, and Mo. A third T(d,n) experiment, now being prepared for irradiation at the Rotating Target Neutron Source-II (RTNS-II) facility at LLL, will expand this measurement set further to include Be, O, F, Si, Mn, Co, Sn, W, Pb, and most of the separated isotopes of Ti, Cr, Sn, W, and Pb.

The present T(d,n) experiment also provides cross section information relevant to activation reactions and foil activation

dosimetry. An example is the comparison between the radiometric dosimetry cross sections illustrated in Fig. 4. In addition, a number of the Fe, Cu, Ti, Ni, and Mo pure element and separated isotope helium generation specimens were radiometrically counted at ANL before helium analysis. The cross section data obtainable by combining this information with the irradiation fluence profile map will be evaluated jointly with ANL and LLL personnel.

ACKNOWLEDGEMENTS

The irradiation was a joint experiment with M. W. Guinan (LLL) and L. R. Greenwood (ANL), who provided the radiometric foils and the counting. The help of the staff of the RTNS-I facility in performing the irradiation and of J. F. Johnson (Rockwell International) in the preparation of the irradiation package is gratefully acknowledged, as are the continued encouragement and support of this work by K. M. Zwilsky, M. M. Cohen, T. C. Reuther, Jr., and S. L. Whetstone (DOE). This work was supported by the U.S. Department of Energy's Office of Fusion Energy and Office of Basic Energy Sciences, under Contract Nos. DE-AT03-76ET52015 and DE-AT03-79ER10388, respectively.

REFERENCES

1. H. FARRAR IV, W. N. McELROY, and E. P. LIPPINCOTT, "Helium Production Cross Section of Boron for Fast-Reactor Neutron Spectra," Nucl. Technol., 25, 305 (1975).

2. D. W. KNEFF, H. FARRAR IV, L. R. GREENWOOD, and M. W. GUINAN, "Characterization of the Be(d,n) Neutron Field by Passive Dosimetry Techniques," this Symposium.

3. H. FARRAR IV, D. W. KNEFF, R. A. BRITTEN, and R. R. HEINRICH, "Fluence Mapping of RTNS-I by Helium Accumulation and Foil Activation Methods," in Symposium on Neutron Cross-Sections from 10 to 40 MeV, BNL-NCS-50681, Brookhaven National Laboratory (1977), p. 175.

4. J. D. SEAGRAVE, "D(d,n)He^3 and T(d,n)He^4 Neutron Source Handbook," LAMS-2162, Los Alamos Scientific Laboratory (1958).

5. D. W. KNEFF and H. FARRAR IV, "Helium Accumulation Fluence Dosimetry for Fusion Reactor Materials Irradiations," J. Nucl. Mater., 85 and 86, 479 (1979).

6. D. R. NETHAWAY, "The $^{93}Nb(n,2n)^{92m}Nb$ Cross Section," J. Inorg. Nucl. Chem., 40, 1285 (1978).

7. H. FARRAR IV and D. W. KNEFF, "Helium Generation in Twelve Pure Elements by 14.8-MeV Neutrons," Trans. Am. Nucl. Soc., 28, 197 (1978).

8. D. W. KNEFF, H. FARRAR IV, F. M. MANN, and R. E. SCHENTER, "Experimental and Theoretical Determination of Helium Production in Copper and Aluminum by 14.8-MeV Neutrons," Nucl. Technol. (to be published).

9. S. M. GRIMES, R. C. HAIGHT, K. R. ALVAR, H. H. BARSCHALL, and R. R. BORCHERS, "Charged-Particle Emissions in Reactions of 15-MeV Neutrons with Isotopes of Chromium, Iron, Nickel, and Copper," Phys. Rev. C, 19, 2127 (1979).

10. R. C. HAIGHT and S. M. GRIMES, "Experimental Studies of (n, charged particle) Cross Sections, Angular Distributions and Spectra with a Magnetic Quadruple Spectrometer," UCRL-80235, Lawrence Livermore Laboratory (1977).

TABLE I

Total Helium Generation Cross Sections for ~14.8-MeV Neutrons

Material	Cross Section (mb)		
	Present Work	Previous Experiment[a]	Charged-Particle Measurements[b]
Al	145 ± 10	143 ± 7	121 ± 25
Ti	37 ± 3	38 ± 3	34 ± 7
Cr	34 ± 4	-	38 ± 6
Fe	48 ± 3	48 ± 3	43 ± 7
Ni	100 ± 7	98 ± 6	97 ± 16
^{58}Ni	116 ± 8	-	106 ± 17
^{60}Ni	79 ± 6	-	76 ± 12
^{61}Ni	53 ± 4	-	-
^{62}Ni	18 ± 6	-	-
^{64}Ni	61 ± 4	-	-
Cu	51 ± 3	51 ± 3	42 ± 7
^{63}Cu	67 ± 5	-	56 ± 10
^{65}Cu	17 ± 2	-	13 ± 3
Au	0.72 ± 0.09	24 ± 12[c]	-

[a]Farrar and Kneff, Ref. 7.

[b]Grimes, et al., Ref. 9, 10.

[c]High value attributed to helium recoil into the thin Au samples available for analysis.

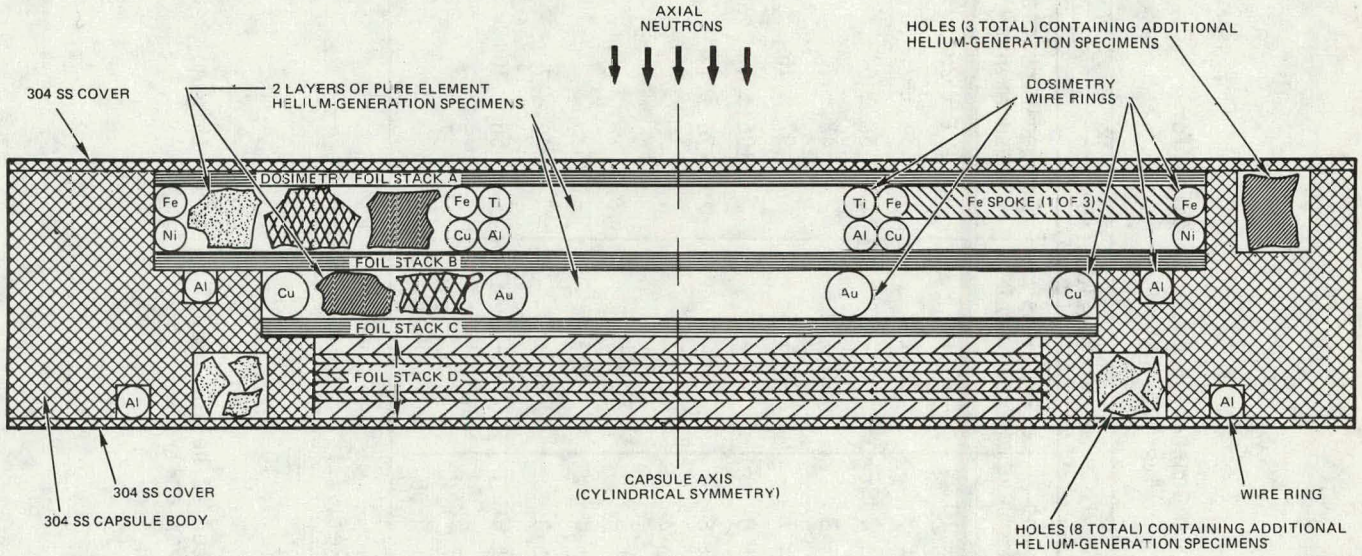

CAPSULE THICKNESS = 4 mm
OUTSIDE DIAMETER = 2 cm
TOTAL MASS = 8.89 g

0 2 4
SCALE (mm)

9077-4017

Figure 1. Cross Sectional View of the Irradiation Capsule

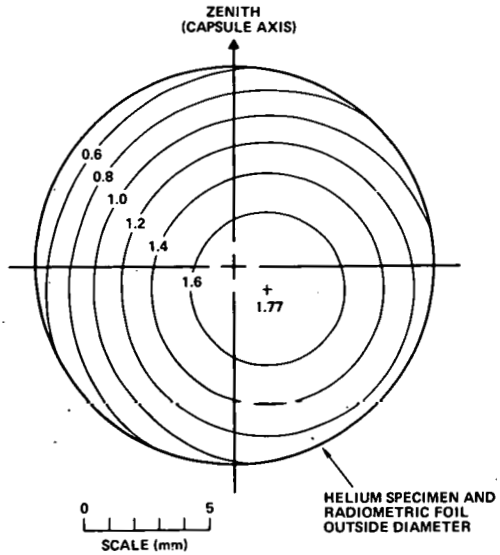

Figure 2. Contours of Constant Neutron Fluence for the Midplane of the Irradiated Capsule's Upper Helium Specimen Layer, Based on the Radiometric Dosimetry and Assuming a Symmetric Profile (Eq. (2); Units of 10^{17} n/cm^2)

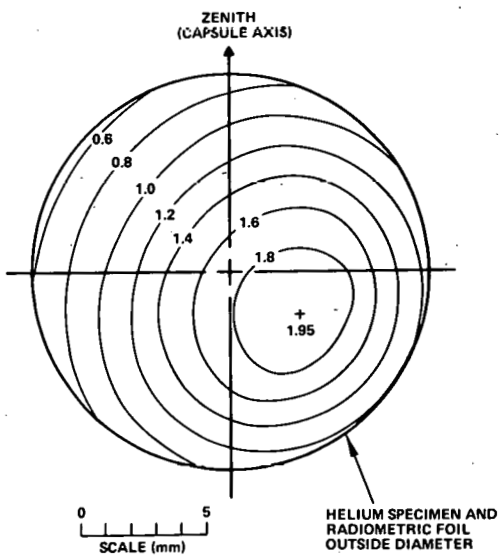

Figure 3. Contours of Constant Neutron Fluence for the Midplane of the Irradiated Capsule's Upper Helium Specimen Layer, Based on Radiometric Plus Helium Accumulation Dosimetry (Eq. (3); Units of 10^{17} n/cm^2)

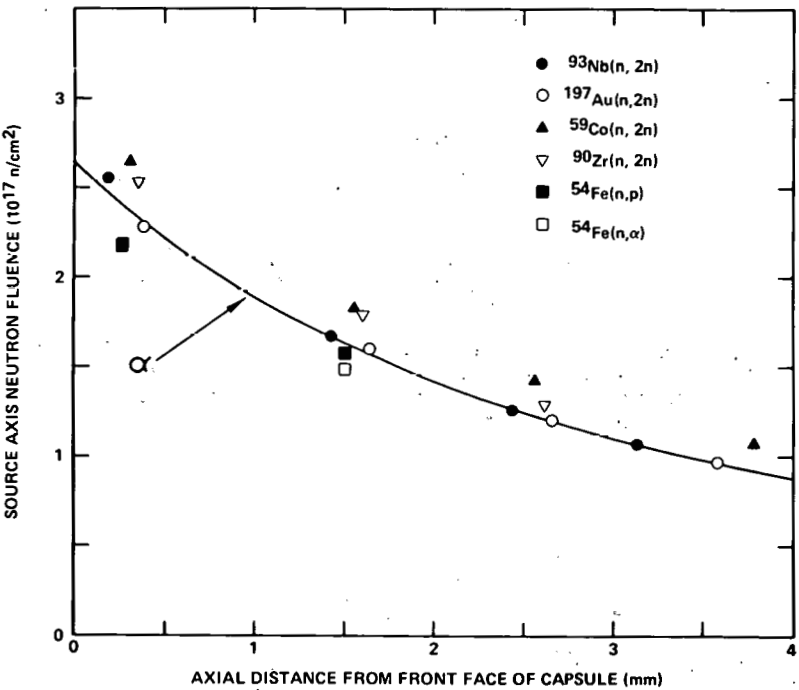

Figure 4. Comparison of Fluences Obtained from the Various Radiometric Dosimetry Foils

Dup

NEUTRON CROSS SECTION MEASUREMENTS AT WNR

P. W. Lisowski, G. F. Auchampaugh,
M. S. Moore, G. L. Morgan. amd R. E. Shamu*

Los Alamos Scientific Laboratory
Los Alamos, New Mexico 87545, U.S.A.

ABSTRACT

The Weapons Neutron Research Facility has been used to obtain moderate-resolution total neutron cross section data for H, C, ^{208}Pb, ^{232}Th, ^{238}U, and ^{242}Pu over the energy range 5 to 200 MeV. Neutrons were produced by bombarding a 2.5-cm diam by 15-cm long Ta target with an 800 MeV pulsed proton beam from LAMPF. A 10.2-cm diam by 15.2-cm thick NE110 proton recoil detector was used at a flight path of 32 meters, giving a time-of-flight resolution of 60 ps/m. The total cross section results are compared to ENDF/BV evaluations and to previous data where possible.

INTRODUCTION

The Weapons Neutron Research Facility (WNR) has recently become operational as a pulsed white-neutron source [1]. At WNR, a portion of the 800-MeV proton beam from the Los Alamos Meson Physics Facility (LAMPF) is used to produce neutrons by spallation reactions on various heavy-metal targets. Proton pulses of variable width may be provided along with suitable targets and moderators to give a time-of-flight capability covering the energy range from a few meV to several hundred MeV.

Of interest to this conference is the fact that the neutron flux at WNR is particularly suited for measurements in the 10- to 50-MeV energy range. This is because there is significantly more neutron intensity at WNR in that energy range than at any other white-source facility and because the γ-ray burst is many orders of magnitude smaller than at an electron machine, permitting data to be obtained nearly up to time t = 0.

We give here a description of the technique used in total cross section measurements and the results for H, C, ^{208}Pb, ^{232}Th, ^{238}U, and ^{242}Pu for energies from 5 to 200 Mev.

EXPERIMENTAL PROCEDURE

Neutrons were produced by spallation reactions using an 800-MeV proton beam incident on a water-cooled aluminum-clad tantalum target (2.5-cm diam. by 15-cm high). The proton beam was pulsed at an average rate of about 1500 sec^{-1} and had a time spread less than 0.5 ns. For the fast-neutron measurements reported here, no moderator was used.

A fiducial signal (t_0) was obtained from a capacitive pick-off located upstream of the target in the proton beam line. This signal provided both a start pulse for the time-of-flight electronics, and a measure of the relative proton intensity and intensity variation using an integrating analog-to-digital converter.

The total cross section measurements were performed on a 31.78-m flight path. About 30-m of the flight path was evacuated to minimize any structure in the neutron flux caused by resonances in air.

A main collimator located approximately 16-m from the WNR target was used to define the neutron beam at the sample[a]. This collimator was composed of sections of brass, iron and lead with a length of 80 cm. A brass scraper collimator 29-cm long with a 3-cm-diam opening was placed after the samples to remove neutrons which penetrated the aluminum aligning sleeve around the main collimator.

A neutron flux monitor was placed in the neutron beam after the main collimator. Because there are a significant number of charged particles in the neutron beam, a two-detector veto-monitor system was used. This technique eliminated the charged-particle contribution which was actually greater than the neutron contribution due to the much higher efficiency for detecting charged particles.

The transmission samples were placed in a motorized changer located about 0.5-m downstream of the main collimator. This sample changer was controlled by the data collection computer using a CAMAC interface and stepping motors. Optical encoding was used to provide positioning accuracy to about 0.03 mm.

The continuous distribution of charged particles was removed from the neutron beam using a sweep magnet after the sample changer. Tests using a thin fast-plastic detector placed at the

a) The ^{242}Pu measurement used a setup which varied somewhat from that described here due to the small (6-mm diam) sample size. Reference 2 provides more detail.

main detector location demonstrated that the charged particles were completely removed by the magnet.

Two different neutron detectors were used. For the ^{242}Pu data, a 10.2-cm diam by 3.1-cm thick cylinder of NE110, viewed by an RCA 8854 photomultiplier was used. For the other measurements, the detection efficiency for high energy neutrons was increased by replacing the scintillator by one 15.2-cm thick.

The neutron beam was stopped beyond the main detector in a beam dump located at the end of an evacuated pipe approximately 30-m long.

The electronics consisted of a complete TOF system for the main detector and a fast-scaler system for the neutron-flux monitor. Time-of-flight spectra from the main detector were collected using an EG&G TDC-100 digital clock operated in single-stop-per-start mode. The proton t_0 signal was used to start the clock. An Ortec 934 constant-fraction discriminator provided the stop signal. Data were stored at four bias settings ranging from ~ 2 MeV to ~ 10 MeV at a time-channel width of 0.5 ns. Main detector dead-time corrections were less than about 30% for all the data.

The output of the neutron-flux monitor system was time-gated to only count neutron events occuring after the γ-burst. The resulting pulses were counted by a fast scaler. Dead-time losses for this system were negligible as the rate from the gated monitor detector was only about 0.1 counts/burst.

Backgrounds were measured by replacing the sample with a 1.9-cm diam by 46-cm long tungsten rod. These spectra were measured several times and had a shape approximately that expected for the transmission of high-energy neutrons through the collimating system. The backgrounds were less than 0.6% below 60 MeV, 0.8% below 100 MeV, and 2% at 200 MeV.

A Modcomp/IV computer and CAMAC interface were used to accumulate the data. Time-of-flight spectra of 4096 channels were recorded for each bias along with various scaler readings for diagnostic purposes. The computer also controlled the sample changer, moving various samples in and out of the beam at intervals of about 15 minutes, based on a preset monitor-detector count. A typical counting time for each sample was 20 hours.

The data were reduced using the central computing facility at Los Alamos Scientific Laboratory. After correcting all spectra for dead-time losses, a normalized background spectrum was subtracted from both sample-in and sample-out data. A small residual time-uncorrelated background, typically less than 1%, was also subtracted.

For data below 60 MeV, the lowest bias data were used. Above 60 MeV only the highest bias data were used both to avoid any contribution from time slewing of the prompt γ-ray peak produced when the beam struck the target and to lower the time-uncorrelated background.

Data for individual time channels were combined into bins of constant energy resolution and then converted to total cross section as a function of neutron energy.

SAMPLES

All of the samples were right circular cylinders approximately 2.1-cm in diameter. Measurements of the mass and diameter of each sample were used to obtain thicknesses. Polyethylene and carbon samples matched to better than 0.1% were used to obtain the hydrogen cross section data. Where possible, the samples were analyzed for impurities. Only the thorium sample was found to contain an appreciable contaminant material (0.36 wt.% oxygen). The ^{208}Pb, ^{238}U, and ^{242}Pu samples were isotopically enriched to 99.8% or greater. Table I gives a summary of the sample thicknesses.

RESULTS AND DISCUSSION

With the exception of ^{242}Pu, total cross section data in the MeV region for each of the materials investigated here have been presented before. Below about 15 MeV there are considerable data as well as the ENDF evaluation, which extends to 20 MeV. Between 15 and 200 MeV data are sparse, but there are several results from different laboratories for comparison.

The hydrogen total cross section is used as a standard for measurements up to about 20 MeV. Above that energy, measurements by several groups show differences of nearly 3%. Our data generally agree to within 1% with the ENDF/B-V evaluation and with data of Brady et al. [3] (25 to 60 MeV), Groce and Sowerby [4], (20 to 80 MeV), and Measday and Palmieri [5] (90 to 150 MeV). The data of Bowen et al. [6] are 2-3% below our values from 30 to about 100 MeV. Fig. 1 shows our data compared to the semi-empirical fit of Gammel [7], chosen because it extends to 40 MeV and agrees with our results nearly as well as ENDF/B-V.

The carbon total cross section shown in Fig. 2 agrees with the ENDF/B-V evaluation to better than 0.6% below 8.5 MeV in the relatively smooth regions between resonances where energy resolution is unimportant. Above 8.5 MeV, our data agree better with the data of Heaton et al. [8] and Auchampaugh et al. [9] than with the ENDF/B-V evaluation. At higher energies, our results tend to agree with the data of Auman et al. [10] (24 to 60 MeV) to better than 1%, and with Meadsday et al. [11] (80 to 150 MeV) to about 2%. Data of Bubb et al. [12] (20 to 45 MeV) are systematically higher than our results; the data of Bowen et al. (15 to 120 MeV) are consistently lower than our data below about 90 MeV. Above 150 MeV, there exist no recent data; however,

Dejuren and Moyer [13], and Mott et al. [14] have results which compare well with our data between 156 and 220 MeV.

Of the remaining sets of cross section data, only ^{238}U and ^{232}Th can conveniently be compared with other data since all other Pb data were obtained with a natural sample and no other fast-neutron data at all exists for ^{242}Pu.

The present results for ^{208}Pb, ^{232}Th, and ^{238}U are compared to the ENDF/B-V results in Fig. 3. Although the ENDF/B-V evaluation was for natural lead, the agreement with the present ^{208}Pb data is remarkably good, except at the ENDF/B-V dip near 16 MeV.

The ^{232}Th data were corrected for an oxygen contaminant using data measured at WNR in a separate experiment. Agreement with ENDF/B-V and with the data of Foster and Glasgow [15] is reasonable below ~ 14 MeV, the upper end of the available data. Above 10 MeV, however, the evaluated data is systematically too low, disagreeing by as much as 4% at 20 MeV.

The ^{238}U data agree with the ENDF/B-V evaluation to within about 1%. with the greatest differences being near 4 MeV and 19 MeV. The most recent ^{238}U data of Schwartz et al. [16] (0.5 to 15 MeV) and Hayes et al. [17] (0.8 to 30 MeV) agree with our data within the quoted errors, except for the data of Hayes near 30 MeV where the errors are quite large. The data of Schneider and McCormack [18] (100 to 150 MeV) provide the only high energy ^{238}U data for comparison, and again, agreement is generally better than 1.5%.

The ^{242}Pu total cross section values are shown in Fig. 4, compared to a recent evaluation by Madland and Young [19]. As was pointed out earlier, the ^{242}Pu data were obtained using the same flight path but with a different geometry due to the very limited amount of sample material available. These data were, in fact, obtained using a neutron beam collimated to 5 mm at the sample.

CONCLUSIONS

The technique used to obtain neutron total cross section data from 5 to 200 MeV at the WNR has been described and demonstrated to yield accurate results with hydrogen and carbon as test cases. In addition, high energy data for ^{208}Pb, ^{232}Th, ^{238}U, and ^{242}Pu have been provided.

REFERENCES

1. G. F. AUCHAMPAUGH, "Status and Comparison of New, Planned, and Upgraded Pulsed 'White' Neutron Source Facilities Since 1970," International Conference on Nuclear Cross Sections for Technology, Knoxville (1979).

2. M. S. MOORE, P. W. LISOWSKI, G. L. MORGAN, and G. F. AUCHAMPAUGH, "Total Cross Section of ^{242}Pu Between 0.7 and 170 MeV," International Conference on Nuclear Cross Sections for Technology, Knoxville (1979).

3. F. P. BRADY, W. J. KNOX, J. A. JUNGERMAN, M. R. McGIE, and R. L. WALRAVEN, "Precise Measurement of Neutron-Proton Total Cross Section from 25 to 60 Mev," Phys. Rev. Lett., 25, 1628 (1970).

4. D. R. GROCE and B. D. SOWERBY, "Neutron-Proton Cross Sections Near 20, 24, and 28 MeV," Nucl. Phys., 83, 199 (1966).

5. MEASDAY and PALMIERI "Neutron Total Cross Sections for Neutrons, Protons, and Deuterons in the Energy Range of 90 to 150 Mev," Nucl. Phys., 85, 142 (1966).

6. P. H. BOWEN, J. P. SCANLON, G. H. STAFFORD, J. J. THRESHER, "Neutron Total Cross Sections iin the Energy Range 15 to 120 Mev," Nucl. Phys., 640, 22 (1961).

7. J. L. GAMMEL, "The n-p Total and Differential Cross Sections in the Energy Range 0-40 MeV," Fast Neutron Physics, Part II, Chap. VI, p. 2185, Interscience Pub., Inc., New York (1960).

8. H. T. HEATON, II, J. L. MENKE, R. A. SCHRACK, and R. B. SCHWARTZ, "Total Neutron Cross Section of Carbon from 1 keV to 15 MeV," Nucl. Sci. Eng., 56, 27 (1975).

9. G. F. AUCHAMPAUGH, S. PLATTARD, and N. W. HILL, "Neutron Total Cross-Section Measurements of ^{9}Be, ^{10,11}B, and ^{12,13}C from 1.0 to 14 MeV Using the ^{9}Be(d,n) ^{10}B Reaction as a 'White' Neutron Source," Nucl. Sci. Eng., 69, 30 (1979).

10. M. AUMAN, F. P. BRADY, J. A. JUNGERMAN, W. J. KNOX, M. R. McGIE, and T. C. MONTGOMERY, "Neutron Total Cross Sections of the Light Elements in the Energy Range 24-60 MeV," Phys. Rev., C5, 1 (1972).

11. D. F. MEASDAY and J. N. PALMIERI, "Neutron Total Cross Sections for Neutrons, Protons and Deuterons in the Energy Range 90 to 150 MeV," Nucl. Phys., 85, 142 (1966).

12. I. F. BUBB, S. N. BUNKER, M. JAIN, J. W. LEONARD, A. MCILWAIN, K. I. ROULSTON, K. G. STANDING, D. O. WELLS, and B. G. WHITMORE," Can. J. Phys., 52, 648 (1974).

13. J. DEJUREN and B. J. MOYER, " Variation with Energy of Nuclear Collision Cross Sections for High Energy Neutrons," Phys. Rev., 81, 919 (1951).

14. G. R. MOTT, G. L. GUERNSEY, and B. K. NELSON, "Total cross Sections of Carbon and Hydrogen for High Energy Neutrons," 88, 9 (1951).

15. D. G. FOSTER and D. W. GLASGOW, "Neutron Total Cross Sections, 2.5-15 MeV. I. Experimental," Phys. Rev., 3, 576 (1971).

16. R. B. SCHWARTZ, R. A. SCHRACK, and H. T. HEATON, II, "Total Neutron Cross Sections of Uranium-235, Uranium-238, and Plutonium-239 from 0.5 to 15 MeV," Nucl. Sci. Eng., 54, 322 (1974).

17. S. H. HAYES, P. STOLER, J. M. CLEMENT, and C. A. GOULDING, "The Total Neutron Cross Section of Uranium--238 from 0.8 to 30 MeV," Nucl. Sci. Eng., 50, 243 (1973).

18. R. J. SCHNEIDER and A. M. MCCORMACK, "Neutron Total Cross sections in the Energy Range 100 to 150 MeV," Nucl. Phys., A119, 197 (1968).

19. D. G. MADLAND and P. G. YOUNG, "Evaluation of n + ^{242}Pu Reactions from 10 keV to 20 MeV," LA-7533-MS (1978); see also Trans. Am. Nuc. Soc., 32, 745 (1975).

TABLE I

Sample Thickness

Sample	Atoms (Barn)
H	2.10280 (a)
C	1.05191 (a)
C	1.3682
^{208}Pb	0.3218
^{232}Th	0.2135
^{238}U	0.3254
^{242}Pu	0.0760

(a) matched polyethylene and carbon

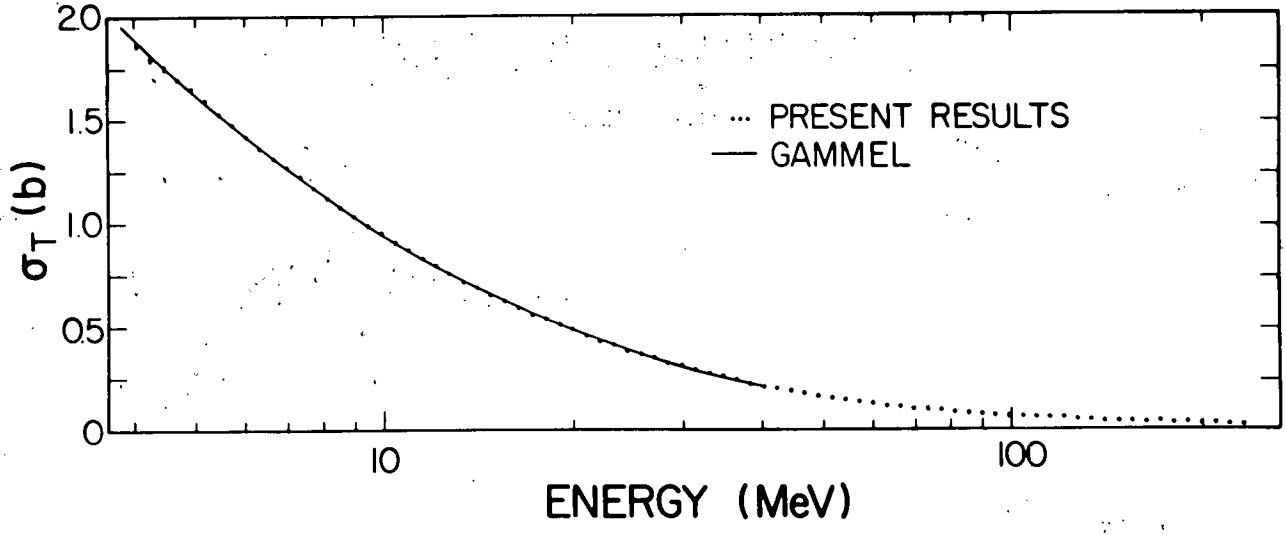

Fig. 1. Present results for the hydrogen total cross section. The solid curve was calculated from a fit to previous data by Gammel.

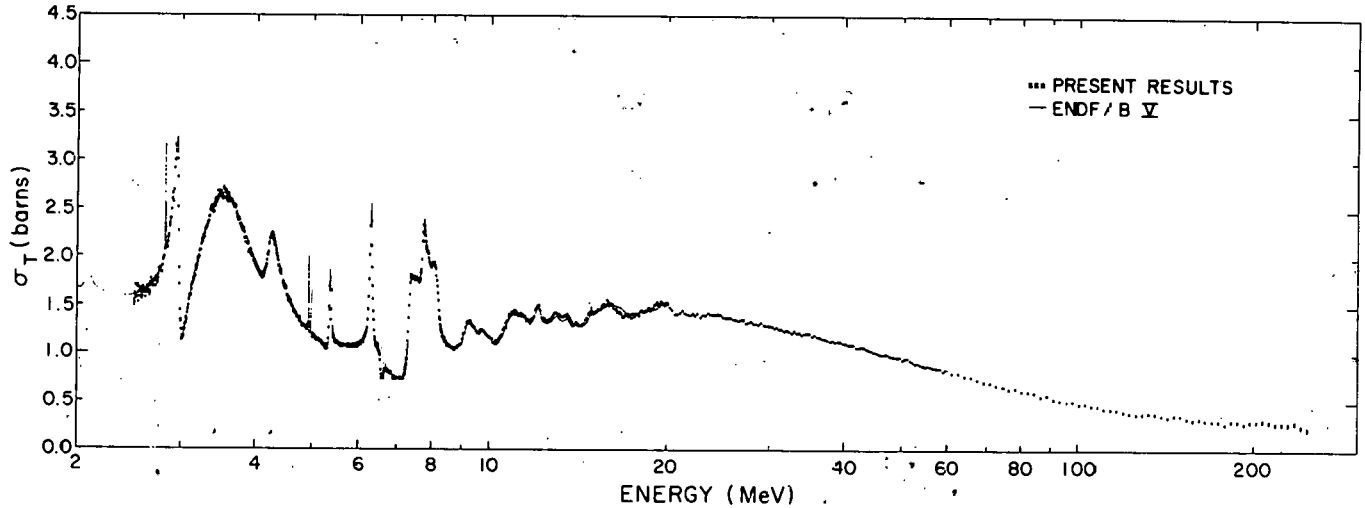

Fig. 2. Present results for the carbon total cross section. The solid curve is from the ENDF/B-V evaluation.

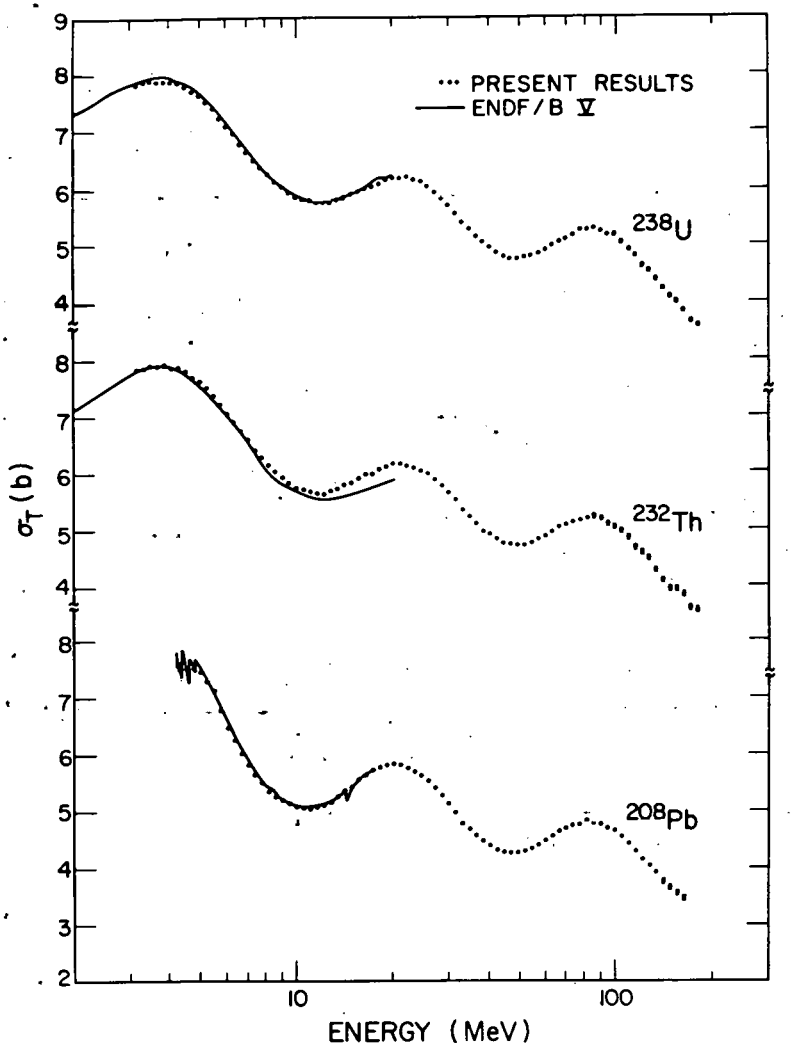

Fig. 3. The total cross section for ^{208}Pb, ^{232}Th, and ^{238}U. The solid curve represents the ENDF/B-V evaluation.

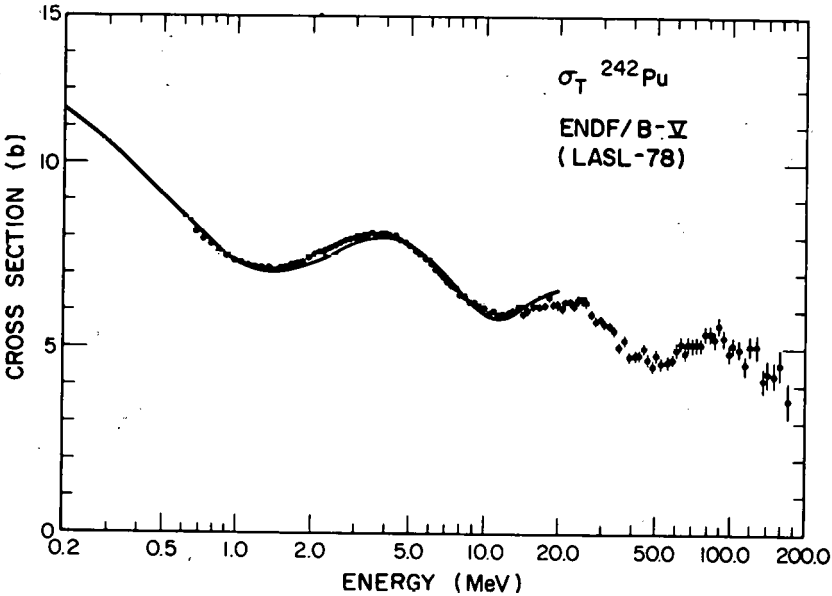

Fig. 4. The total cross section for ^{242}Pu from 0.7 to 170 MeV. The solid curve represents an ENDF/B-V evaluation by Madland and Young.

MEASUREMENTS OF NEUTRON TOTAL AND TOTAL NONELASTIC CROSS SECTIONS FOR C, O, Ca, AND Fe AT UC DAVIS

C.I. Zanelli, F.P. Brady, J.L. Romero, C.M. Castaneda *
M.L. Johnson, G.A. Needham, J.L. Ullmann, and P.P. Urone

Crocker Nuclear Laboratory and Department of Physics
University of California, Davis, California

and

D.L. Johnson

Hanford Engineering Development Laboratory
Richmond, Washington 99352

ABSTRACT

Neutron total cross sections for Ca and Fe at 35.3, 40.3, and 50.4, and for C at 50.4 MeV have been measured using nearly mono-energetic neutron beams. The overall total cross section uncertainties are <3%. Total non-elastic cross sections for C, O, Ca, and Fe were measured for incident neutrons of 40.3 and 50.4 MeV using a transmission technique with a nearly mono-energetic beam. The overall uncertainties average about 8% for the non-elastic cross sections.

INTRODUCTION

Neutron cross section data are not abundant at energies above 14 MeV and this is particularly true above 25 MeV. This is in marked contrast to the situation for proton data. As a consequence, most theoretical and applied needs for neutron cross sections at energies higher than 25 MeV must be met with estimates based on proton data or extrapolations of lower energy neutron cross sections at energies above 25 MeV for both theoretical and applied purposes.

Neutron total and total non-elastic cross sections are important as basic measurements which can be related to other

*Permanent address: California State University, Sacramento, CA 95819

nuclear measurements and to nuclear models. In particular, the optical model (OM) predicts both total shape elastic and total reaction cross sections, whose sum is the total cross section. At these higher energies the compound-elastic cross section is small so these OM predictions are very closely the total elastic and non-elastic cross sections.

One of the original motivations for these measurements was to fill the need for accurate neutron cross sections for elements which form major constituents of shielding. In particular accurate cross sections allow shielding thickness to be optimized for facilities which produce copious energetic neutrons. The Fusion Materials Irradiation Test facility under construction at Hanford, will use the d + ^{6}Li reaction to produce neutrons having energies up to 50 MeV, even though the peak intensity will be near 14 MeV. Neutron cross sections are also important in calculating neutron dosimetry, as in neutron cancer therapy, and form the basis of neutron detector efficiency codes.

In our method of measuring total non-elastic cross sections it is important to have good values for the total cross sections. For light elements such measurements are available [1] in the 30-60 MeV range. However, for Ca and Fe there existed large uncertainties in available data in this energy range. Only at lower energies are good data available.[2-5] Hence the total cross sections for Ca and Fe measured here were necessary for the use in the non-elastic analyses.

We present here measurements of the neutron total cross sections for Ca and Fe at 35.3, 40.3, and 50.4 MeV, and measurements of the total non-elastic cross sections for C, O, Ca, and Fe at 40.3 and 50.4 MeV.

EXPERIMENTAL METHODS

Total Cross Sections

Neutron beams of energy width ~1 MeV were produced via the ^{7}Li(p,n) reaction utilizing the U.C. Davis cyclotron. Protons were swept into a faraday cup by a clearing magnet and the neutrons were then collimated into a 15 mm x 15 mm beam spot by a 1.5 meter long iron channel.[6]

The experimental configuration for total cross section measurements is shown in Fig. 1. The shadow bar was used for background determinations and was normally out of the beam. The collimated neutron beam passes in sequence through a front (incident-flux) detector telescope, the sample, and back (transmitted-flux) detector telescope. Each telescope contained a ≅1 mm thick veto NE102 scintillator, a CH_2 converter, and two more thin (≅1 mm) NE102 scintillators separated by a copper absorber. The CH_2 converter was 1.5 mm thick for the front detector telescope and 3.0 mm for the back one. The discriminator thresholds of the last

two scintillators in each detector telescope were set in the middle of the coincidence count-rate plateaus produced by the recoil protons from the CH_2. This rendered the telescopes insensitive to gain or threshold shifts in the individual detectors. The thresholds were such that the telescopes were insensitive to γ-rays and electrons. Their neutron detection efficiency is about 1%.

Roughly, 60% of the neutrons produced in the reaction $^7Li(p,n)^7Be$ fall within a well-defined high energy peak, determined by the ^7Li target thickness to be ≅1 MeV wide [10], corresponding to transitions principally to the ground state of ^7Be. The remaining neutrons are spread over a broad, lower-energy tail. Only neutrons in the narrow, high-energy peak - selected by time-of-flight - were used in the transmission measurements. The 0.15 mm copper absorber in the back detector telescope eliminated recoil protons due to lower-energy neutrons from earlier bursts.

Total Non-Elastic Cross Sections

The total non-elastic measurements were carried out with neutron beams similar to those used for σ_{tot}. The back detector telescope is replaced by a large, 8" diameter by 3" thick, NE213 plastic scintillator. See Fig. 2. As shown, the detector is placed close to the target subtending a large angle, 22°-38°, and intercepting the paths of ≅85% of the elastic flux. Time-of-flight (TOF), neutron pulse height (NPH), and pulse shape (PSD) signals are recorded for each event in the scintillator. For most of the analysis a fairly high threshold (8 MeV electron energy) is set on the NPH so that events from the low-energy tail wrapping around from earlier proton beam bursts (period of ≅50 ns) are eliminated.

For both total and non-elastic measurements natural targets were used with H_2O serving as the O target. The effects of H were removed using the known H cross sections.[7] The target thicknesses were such that transmissions averaged about 75%. In some non-elastic measurements different target thicknesses and different distances from the NE213 were used.

ANALYSES AND RESULTS

Total Cross Sections

Time-of-flight spectra for both the front (incident-flux) and back (transmitted-flux) detector telescopes were recorded over periods of about 10 minutes for both target-in and target-out arrangements. (This was also done with the shadow bar in the beam, and the backgrounds were essentially negligible.) About a dozen cycles of target in and target out were recorded for each target-energy combination. For each one the integrated TOF peak

yield for the incident (I) and transmitted (T) intensity is calculated. The transmission ratio R is defined as T/I for the target-out case divided by T/I for the target-in. Then

$$\sigma_{tot} = \ell n\ R/N \qquad (1)$$

where N is the number of target nuclei per cm^2.

Corrections due to impurities, air displacement, and hardening were essentially negligible. The correction due to the finite solid angle of the transmitted flux detector is

$$\Delta\sigma_{tot} = \Delta\Omega\ d\sigma(0°)/d\Omega \qquad (2)$$

and for the worst case, 50.4 MeV, amounted to 10, 7, and 2 mb for Fe, Ca, and C.

Figure 3a and b shows the resulting values of σ_{tot} plotted vs energy, along with previous measurements of σ_{tot} in this energy range, and shows the significant improvement in the knowledge of σ_{tot} in this energy range. The present measurements give for carbon $\sigma_{tot}(C) = 922 \pm 24$ mb. Extrapolation of previous measurements[1] gives $\sigma_{tot}(C) = 938 \pm 4$ mb at 50.4 MeV, in agreement with the present measurement.

Total Non-elastic Cross Sections

The first stages of analysis are similar to the case of σ_{tot}. The yield of neutron counts in the TOF peak of the neutron detector is normalized to the incident flux and denoted Y_{in} and Y_{out} for the cases of target-in and -out. A measured cross section is defined:

$$\sigma_{meas} = \ell n\ (Y_{out}/Y_{in})/N_i \qquad (3)$$

σ_{meas} depends on σ_{tot} and on the elastic differential cross section, $\sigma_{el}(\theta)$, as well as on target thickness (via attenuation and multiple-scattering effects). It also depends on the variation of detector efficiency with detector radius and angle of incidence of the neutrons relative to the detector axis.

The approach used in our analysis is to obtain an expression relating σ_{meas} to σ_{tot} and $\sigma_{el}(\theta)$. The optical model is used to provide the relative elastic differential cross section. The experimental measurements, yielding σ_{meas}, determine the average absolute normalization, η, of the optical model predictions, $\sigma_{el}^{OM}(\theta)$, for the elastic cross section. The total elastic cross

section for a given nucleus is determined from

$$\sigma_{el} = \eta \int \sigma_{el}^{OM}(\theta)\, d\Omega. \qquad (4)$$

Then the total non-elastic cross section can be calculated from

$$\sigma_{tot} = \sigma_{el} + \sigma_{non}. \qquad (5)$$

The results for σ_{el} and σ_{non} are not very sensitive to the optical model used. The variation in σ_{el} is typically a few percent, while the variation in the values of η as determined here ranges up to 40% for the different potentials of a given nucleus.

The experimental technique and method of analysis are detailed elsewhere.[8] The most difficult part of the analysis is dealing with multiple-scattering effects, and incorporating them into the target-in yield, Y_{in}. The contributions to Y_{in} form a series of terms Y_0, Y_1, Y_2, etc., where Y_n is the term containing n scatterings in the target. Using a forward scattering approximation we have shown [8] that the magnitude of Y_n falls off rapidly, approximately as $Y_{n+1}/Y_n \cong N\,\sigma_{el}/(n+1)$ for $n > 0$ and that the contribution to σ_{meas} of the term Y_2 is $\leqq 10\%$ and of terms beyond Y_2 is $\sim 1\%$. Here $N\sigma \cong 0.2$. Instead of doing the lengthy and tedious five-fold integration which the calculation of Y_2 entails, we include the effects of Y_2 and higher-order terms through the choice of σ_{meas} as the attenuation cross section in Y_1. The physical reason for this choice is discussed in ref. 8 and there it is also shown that the results of the forward scattering approximation support the choice of σ_{meas} in Y_1. The calculation and parameterization of the detector efficiency is also discussed and illustrated in ref. 8.

The resulting values of σ_{non} are given in Fig. 4, which also illustrates the accuracy of the method. Values of σ_{non} together with their estimated uncertainties are plotted for thick and thin targets, "close" and "far" geometries, and for various OM parameter sets. In no case are the variations in σ_{non} larger than the statistical uncertainties. The lack of dependence on target thickness indicates that our estimate of the target attenuation is good. The lack of dependence on "close" or "far" geometry and on OM parameters indicates that this method is OM independent as long as most of the elastic scattering cross section lies within the angle subtended by the neutron detector. Our largest source of uncertainty was in fact the statistical uncertainty in the number of monitor counts in the incident-flux detector telescope.

Insufficient time resolution plus the kinematic shift of elastic neutrons prevent us from eliminating all inelastic scattering contributions to $\eta\sigma_{el}^{OM}$. But based on (p,p')[13] and (n,n')[14] data we estimate the inelastic cross section contributions to be less than 2% of the elastic cross section integrated out to the largest angles subtended. This correction is considerably less than our statistical uncertainties and was not included.

The experimental values for σ_{non} and their uncertainties are given in Table I. They are weighted averages of the data in Fig. 4. Uncertainties shown are primarily statistical. In addition to these there are estimated uncertainties of 2-4% in the method due largely to the approximations used in relating σ_{meas} to σ_{tot} and σ_{el}.

At these particular energies there are no neutron data to compare to. A measurement[15] of σ_{non} on C at 55 MeV, yielded σ_{non} = 278 ± 26 mb, and at lower energies values of 450 ± 40 for C and 1210 ± 70 mb for Fe at 29.2 MeV have been published.[16] All these appear to be consistent with our values.

Comparison with OM Calculations

The literature on OM potentials for single nucleon scattering is extensive[17]. Many single nucleon OM potentials have been obtained from global fits to large numbers of proton elastic scattering angular distributions, polarizations, total cross sections, (p,n) data, and a more limited body of neutron elastic scattering data[11,12,18]. The resulting parameter sets are semi-empirical in that energy and isospin dependencies of the parameters are incorporated. The present data allow us to judge how well various single-nucleon OM parametrizations apply to 40 and 50 MeV neutron data. Comparison can be made in two ways: via the normalization, η, of the forward angle elastic scattering[19], and through the total non-elastic cross sections, σ_{non}.

Table 2 gives values of the normalization, η, for various OM sets[20]. If an OM set correctly predicts $\sigma_{el}(\theta)$, η should be close to 1. It can be seen that η can vary considerably from one OM potential set to another. However the renormalized total elastic cross sections, $\eta\sigma_{el}^{OM}$, are not very dependent on the OM set.

Figure 5 shows the present σ_{non} data (closed circles) compared with OM calculations (solid lines) based on various OM sets. Also shown are proton non-elastic cross sections and proton OM calculations. Within errors σ_{non} is the same for protons and neutrons on the same nucleus and at or near the same energy.

(a) Parameters of WSS [9]

Watson, Singh, and Segel[9] obtained their parameters from fitting proton elastic scattering and polarization data on light elements at energies up to 50 MeV and neutron elastic scattering at 14 MeV. Calculations of σ_{non} based on WSS are shown for C and O are seen not to describe either neutron or proton data as well as calculations based on other parameter sets, WSS being systematically high. Our data indicates that $\eta > 1$ for their fits to C and O. This has been verified by examining their plots of OM predictions vs elastic proton data.

(b) Parameters of BH[10]

Bassel and Herling [10] obtained their parameters by fitting proton and neutron elastic and, when available, inelastic data on ^{12}C and ^{16}O specifically. The available neutron data were at energies less than 20 MeV. It is not surprising that the BH parameters predict both neutron and proton cross sections more accurately than the other sets since the BH parameters are not global, nor do they use the same parametrization for C and O.

(c) Parameters of BG [12]

Becchetti and Greenlees [12] proton "best fit" and neutron parameters sets are used here to produce the values of σ_{non} which are compared to measured values for Ca and Fe in Fig. 3. BG [12] obtained their parameters by fitting proton and neutron elastic scattering and σ_{non} data for $A \geq 40$. With the exception of our 40 MeV neutron data for Fe, the BG parameters predict the values of σ_{non} rather well and better on the average than the others. An isospin dependence was observed by BG in both the real and imaginary well depths and in the imaginary diffuseness.

(d) Parameters of M [11]

Menet et al. [11] obtained their parameters by fitting a large body of data for $12 \leq A \leq 208$ and proton energies of 30 to 61 MeV. Included in their fits were proton and neutron elastic scattering angular distributions and a large number of non-elastic cross sections. Menet et al. [11] were looking specifically to improve upon the BG parameter sets and to firm up the "true" isospin dependence of the OM parameter. By "true" isospin dependence one generally means that the sign of any $\varepsilon = (N-Z)/A$ term in the potentials will be positive when treating protons and negative when neutrons. Menet et al.[11] observed a "true" isospin dependence in the real and imaginary well depths, as did Becchetti and Greenlees [12]. They also examined the ε-dependence of the imaginary diffuseness previously observed by Becchetti and Greenlees [6] and found the sign of the ε term in the imaginary diffuseness to work best when it is the same for proton and neutron scattering.

Our results using the parameter set M tend to confirm the observations of Menet et al[11] and can be seen in Fig. 5 for Fe.

The solid and dashed lines labeled M^+ and M^- respectively are for a positive ε term and a negative ε term in the imaginary diffuseness. As was also observed by Menet et al. [11] use of the minus sign produces smaller and less satisfactory results than a positve sign.

(e) Parameters of P [18]

Patterson et al. [18] obtained their parameters by fitting proton and neutron elastic scattering data and (p,n) reaction data. The resulting parameters do an equally good, though not superior job of predicting σ_{non} for Ca and Fe as do those of BG [6]. Patterson et al. [18] started their searches using the parameter sets of BG.

(f) General Observations

In all cases, except for parameter set M for Fe, the OM predicts lower values of σ_{non}^{OM} for protons than neutrons. It should be pointed out that, in general, proton and neutron data should be compared at slightly different energies since the Coulomb force slows the proton and it therefore has less energy when interacting with the nucleus than does the neutron. However, this cannot be the source of difference in OM calculations since using a higher energy for the protons by the amount of the Coulomb barrier would further decrease the calculated values of σ_{non}^{OM} for protons. Because of the size of the error bars of the present neutron data we cannot judge whether the lower values of σ_{non}^{OM} for protons are correct or an artifact of the available OM parametrizations.

Although some OM parameters sets predict σ_{non} more accurately than others, no obvious correlation of the depth, shape or volume integral of the imaginary potential to σ_{non} predictions is apparent.

CONCLUSIONS

Improved values of total neutron cross sections for Ca and Fe have been obtained at 35.3, 40.3, and 50.4 MeV. A method for measuring total non-elastic cross sections, σ_{non}, has been developed [8] and used to obtain values of σ_{non} for neutrons on C, O, Ca, and Fe at 40.3 and 50.4 MeV. The experimental values of σ_{non} for neutrons are the same, within experimental uncertainties, as those for protons.

The OM set BH [10] best predicts σ_{non} for C and O while the sets of BG [12], M [11], and P [18] work about equally well for Ca and Fe.

ACKNOWLEDGEMENTS

We are indebted to Eugene Dines, Tim Ford, and Walt Kemmler for assistance and helpful discussions. We also thank E. Russell, J. McCurdy, and the cyclotron crew.

This work was partially supported by US NSF grant PHY77-05301 and US DOE Cont. No. DE-AC14 76FF02170, and this support is gratefully acknowledged.

REFERENCES

1. M. Auman, F.P. Brady, J.A. Jungerman, W.J. Knox, M.R. McGie, and T.C. Montgomery, Phys. Rev. C5, 1 (1972).

2. S. Cierjacks, P. Forti, D. Kopsch, L. Kropp, J. Nebbe, and J. Unseld, Institut für Angewandte Kernphysik, Karlsruhe, W. Germany KFK-1000, EUR 3963-e EANDC(E)-11 "U" (1968).

3. J.M. Peterson, A. Bratenahl, an J.P. Stoering, Phys. Rev. 120, 521 (1960).

4. G. Deconnick, A. Gonze, P. Macq, and J.P. Meulders, J. Physique Rad 22, 652 (1961).

5. G.J. McCallum, G.S. Mani, and A.T.G. Ferguson, Nucl. Phys. 16, 313 (1960).

6. J.A. Jungerman and F.P. Brady, Nucl. Instr. Methods 89, 167 (1970).

7. F.P. Brady, W.J. Knox, J.A. Jungerman, M.R. McGie, and R.L. Walraven, Phys. Rev. Lett. 25, 1629 (1970). T.C. Montgomery, F.P. Brady, W. Bonner, W. Broste, M. McNaughton, Phys. Rev. 31, 640 (1973) and Phys. Rev. C16, 499 (1977).

8. F.P. Brady, C.I. Zanelli, J.L. Romero, M.L. Johnson, G.A. Needham, J.L. Ullmann, P.P. Urone, and D.L. Jonhson, to be published.

9. B.A. Watson, P.P. Singh, and R.E. Segel, Phys. Rev. 182, 977 (1969).

10. R. Bassel and G. Herling, private communication.

11. J.J. Menet, E.E. Gross, J.M. Malanify and A. Zucker, Phys. Rev. C4, 1114 (1971).

12. F.D. Becchetti, Jr. and G.W. Greenlees, Phys. Rev. 182, 1190 (1969).

13. e.g. B. Zweiglinski, G.M. Crawley, H. Nan, and A.J. Nolen,Jr. Phys. Rev. C17, 872 (1978).

14. e.g. Y. Yamanouti, Nucl. Phys. A283, 23 (1977) and M. Hyakutake, M. Matoba, T. Tonai, J. Niidome, and S. Nakamura, J. Phys. Soc. Japan 38, 606 (1975).

15. R.G.P. Voss and R. Wilson, Proc. Phil. Soc. (London) A236, 41 (1956).

16. M.H. Mac Gregor, W.P. Ball, and R. Booth, Phys. Rev. 111, 1155 (1958).

17. C.M. Perey and F.G. Perey, Atomic Data and Nuclear Tables 17, 1 (1976).

18. D.M. Patterson, R.R. Doering, and A. Galonsky, Nucl. Phys. A263, 261 (1976).

19. The assumption has been made that η is angle-independent, while in general η will be a function of θ. Thus the values of η derived from the experimental data are average values weighted according to integrals given in ref. 8; that is, essentially weighted by $\sin\theta$ over the forward angles containing $\cong$85% of σ_{el}.

20. C.I. Zanelli, P.P. Urone, J.L. Romero, F.P. Brady, M.L. Johnson, G.A. Needham, J.L. Ullmann (U.C. Davis) and D.L. Johnson (Westinghouse Hanford) (CNL - UCD 192 and to be published).

21. R.H. Hildebrand and C.E. Leith, Phys. Rev. 80, 842 (1950).

22. B. Ragent, UCRL-2337, 1953 (unpublished).

23. R.F. Carlson, A.J. Cox, J.R. Nimmo, N.E. Davison, S.A. Elbahr, J.L. Horton, A. Hoadeyer, A.M. Sourkes, W.T.H. Van Oers, and D.J. Margaziotis, Phys. Rev. C12, 1167 (1975).

TABLE I

Experimental Values for σ_{tot} and σ_{non} in Millibarns

		σ_{tot}	σ_{non}
40.3 MeV			
	C	1118 ± 1.3[a]	356 ± 28
	O	1398 ± 6.6[a]	416 ± 35
	Ca	2284 ± 59[b]	930 ± 53
	Fe	2461 ± 24[b]	909 ± 39
50.4 MeV			
	C	938 ± 3.0[a]	344 ± 28
	O	1208 ± 5.6[a]	387 ± 45
	Ca	2250 ± 70[b]	849 ± 112
	Fe	2431 ± 57[b]	899 ± 42

a. Ref. 1.

b. This work.

TABLE II

OM Normalization Factors η and Normalized Total Elastic Cross Sections in Millibarns. Parameters set are WSS[9], BH[10], M[11], and BG[12].

40.3 MeV

	OM set	η	$\eta\,\sigma_{el}^{OM}$	σ_{el} (average)
C	WSS	1.17 ± .04	764	
	HB	.96 ± .04	768	
	M	.87 ± .03	754	
				762 ± 28
O	WSS	1.36 ± .05	994	
	BH	1.04 ± .04	972	
	M	.97 ± .03	982	
				982 ± 35
Ca	BG	1.08 ± .04	1322	
	M	.97 ± .03	1387	
				1354 ± 53
Fe	BG	1.13 ± .03	1523	
	M	.98 ± .02	1583	
				1552 ± 39

50.4 MeV

C	WSS	1.05 ± .05	582	
	BH	.86 ± .04	585	
	M	.78 ± .04	619	
				594 ± 28
O	WSS	1.25 ± .07	819	
	BH	1.20 ± .06	832	
	M	.91 ± .05	812	
				821 ± 45
Ca	BG	1.08 ± .09	1400	
	M	.99 ± .08	1401	
				1401 ± 112
Fe	BG	1.05 ± .03	1525	
	M	.94 ± .02	1540	
				1532 ± 42

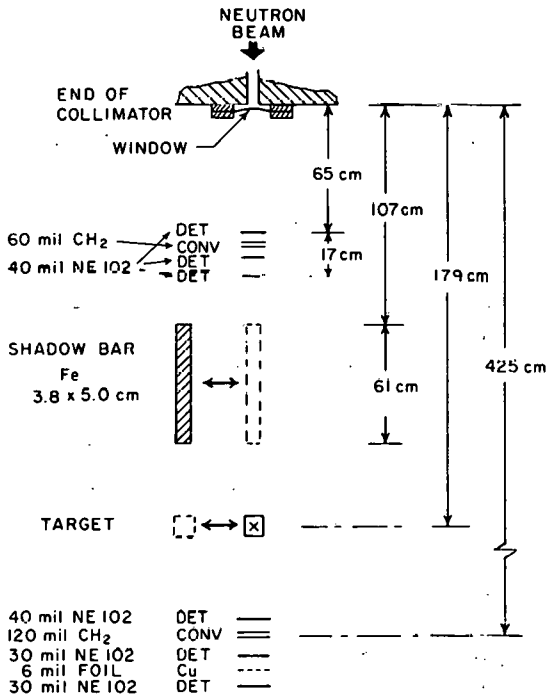

Fig. 1. Experimental set-up for total cross section measurements. Both target and shadow bar could be remotely moved in and our of the beam.

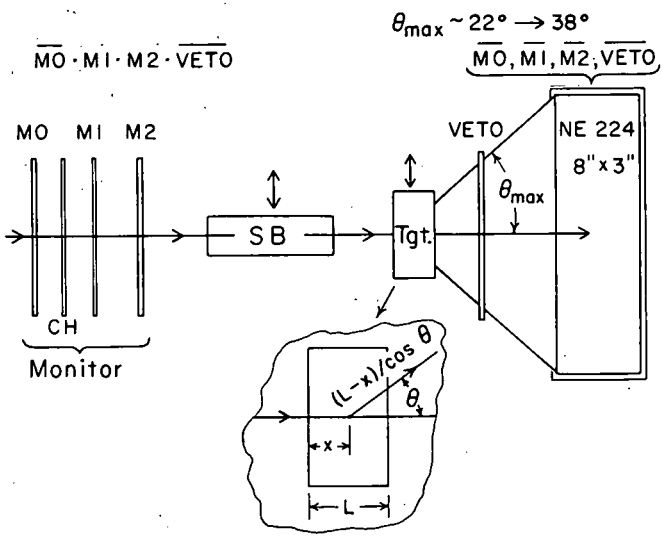

Fig. 2. The experimental configuration for the non-elastic measurements with an expanded view of the target.

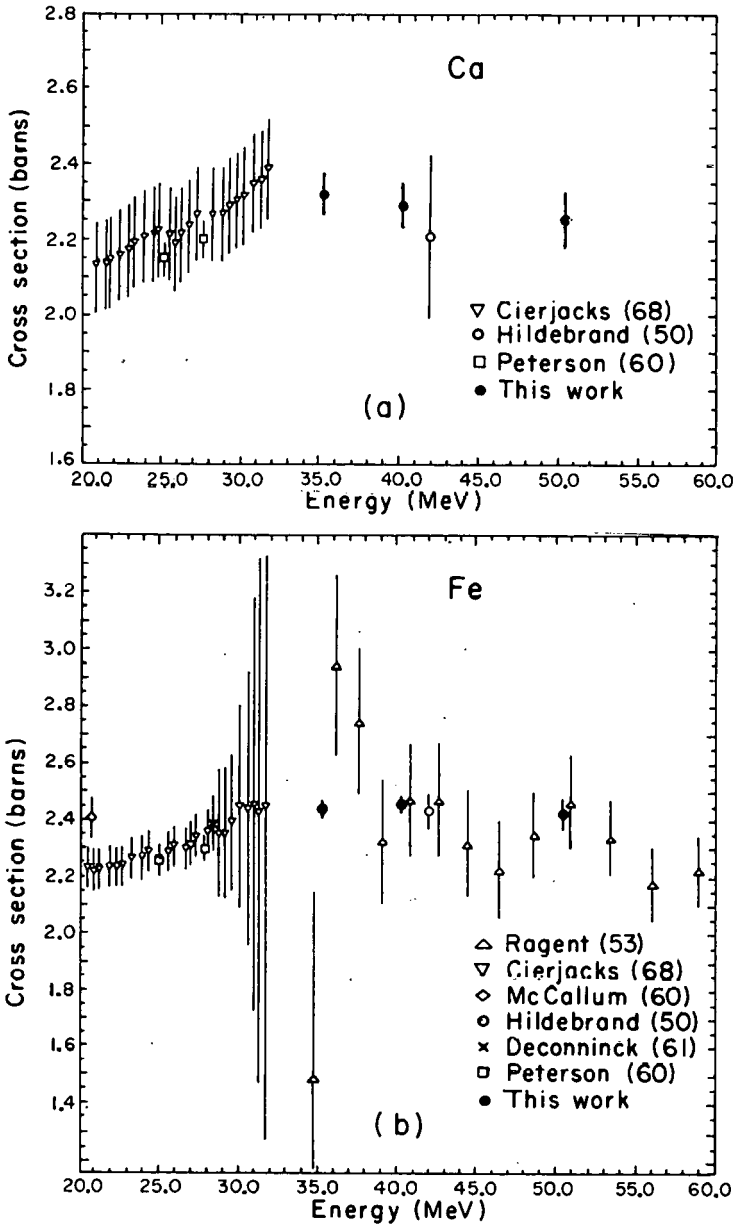

Fig. 3. Available total cross sections for calcium (a) and iron (b) in the energy region 20 to 60 MeV, showing data from this experiment. Data source is identified in the figure by the first author's name and year (refs. 2, 3, 4, 5, 21, 22).

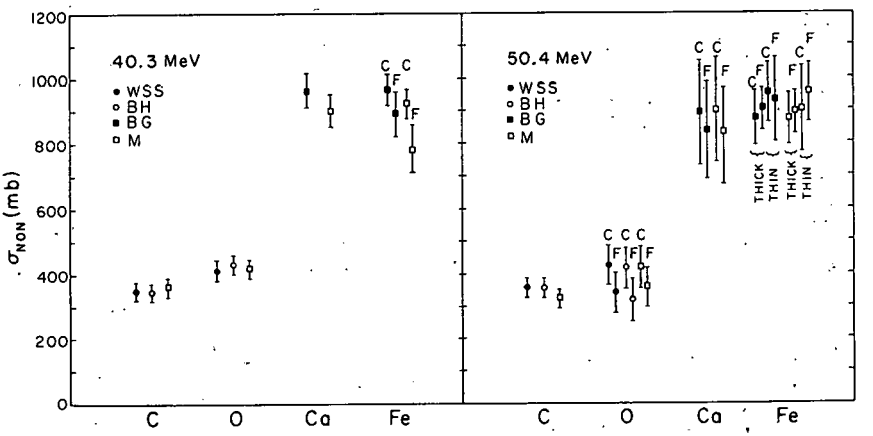

Fig. 4. Experimental values of σ_{non} for thick and thin targets, close and far geometries, and various OM parameter sets showing the model and geometry independence of the analysis technique. OM sets are WSS [9], BH [10], M [11], and BG [12]. C stands for close geometry, F for far geometry.

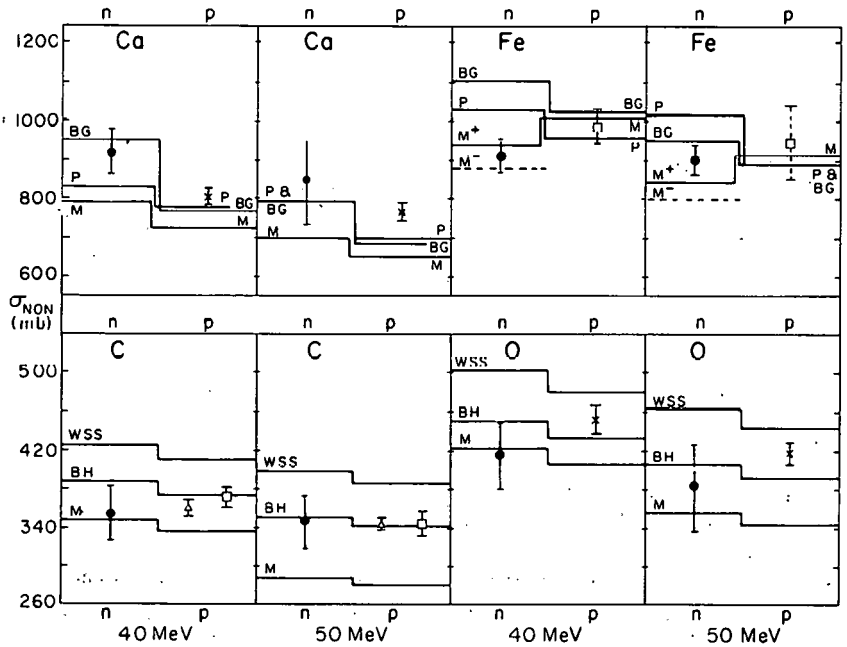

Fig. 5. Comparison of σ_{non} data and OM calculations. Filled circles are present neutron data. For proton data, Δ is Ref. 14, □ is Ref. 11, × is Ref. 23. The proton data points labeled 50 MeV on O and Ca were taken at 48 MeV rather than 50 MeV and the proton data point labeled 50 MeV on Fe is an interpolation between data at 40 and 60 MeV, hence the larger error bar which includes interpolation uncertainties. OM sets are WSS [9], BH [10], M [11], BG [12], and P [18].

NEUTRON-INDUCED CHARGED PARTICLE MEASUREMENTS FROM CARBON, NITROGEN, AND OXYGEN AT U.C., DAVIS

T.S. Subramanian*, J.L. Romero, and F.P. Brady

Crocker Nuclear Laboratory and Department of Physics
University of California, Davis, California

ABSTRACT

Continuum differential cross sections for neutron-induced reactions on light elements have been measured at the Crocker Nuclear Laboratory of the University of California at Davis. The neutrons are produced via the $^{7}Li(p,n)$ reaction and the beam is collimated at 0° to deliver a flux of $\sim 10^{5}/cm^{2}/sec$ at the experimental area. Charged particles ranging from protons through alphas are detected with three-element charged-particle-detection telescopes. The measurements were made at incident neutron energies of 27.4 MeV, 39.7 Mev, and 60.7 MeV and for wide angular range covering 15° through 150°. Some of these continuum cross sections obtained for Carbon, Oxygen, and Nitrogen are presented. Where possible, comparisons are made for both differential and angle integrated cross sections, with corresponding charge-symmetric reaction cross sections from data published from ORNL with protons as projectiles. Model predictions are also presented for comparison with angle-integrated spectra.

INTRODUCTION

Differential cross-section measurements for charged particles arising from neutron-induced reactions at neutron energies above the d-t generator energies are virtually nonexistent. These higher energy ranges (up to about 50 MeV) have recently drawn a closer attention because neutrons of these energies are realized in configurations such as the d-Li irradiation facilities and the d-Be medical therapy facilities. These cross sections, where available, help to evaluate the performance of a given element as

*Present address: Lawrence Berkeley Laboratory, Berkeley, California

a constituent of a reactor structure or human tissue. In addition the charged-particle cross sections for carbon for instance, are relevant to the evaluation of neutron detection efficiencies of plastic scintillators, or for use in neutron spectrum tailoring. Similarly, the cross sections for oxygen are relevant to reactor-shielding calculations. Combining the cross sections for hydrogen (elastic proton), oxygen, carbon and nitrogen, one can obtain quantities relevant to neutron dosimetry, such as KERMA in tissue. Some of these cross sections, particularly limited to the light elements, carbon, nitrogen, and oxygen, have been measured at the Crocker Nuclear Laboratory in Davis.

EXPERIMENTAL FACILITY

The unpolarized neutron beam line at the Crocker Nuclear Laboratory is designed to provide nearly monoenergetic neutron beams in the 20-60 MeV range via the $^{7}Li(p,n)^{7}Be$ reaction [1-3] (Fig. 1). The neutron spectrum consists of a monochromatic peak containing 60% of the neutrons; the remaining 40% spread out in the flat low energy tail region. For a typical 40 MeV, 10 μA proton beam incident on a Li target, the neutron flux at 3 m is 5×10^{5} (cm ^{2} sec) in a 1 MeV FWHM peak. A scattering chamber housing the target and the triple-element, charged-particle detector telescopes under vacuum has been incorporated in the beam line. This facility has been used to measure the differential cross sections for neutron-induced charged particles from light elements, such as carbon, nitrogen, and oxygen [4-6].

Target Selection and Normalization

Polysteyrene (CH) was chosen as a target for carbon instead of pure carbon sheets. The overwhelming reason for such a choice is the ease of direct normalization to the concurrently measured n-p elastic scattering, whose cross section is well known. Since solid targets help minimize low energy cut-offs in the measured charged-particle spectra, particularly those of alphas, foils containing N and O were used for their respective targets: Melamine ($C_3H_6N_6$) for nitrogen and Kodacel plastic ($C_3H_4O_2$) for oxygen. The N and O cross sections were obtained by subtracting out the contributions from carbon in the respective targets. Again, the absolute normalization was obtained by referring to the concurrently measured n-p elastic peaks. The targets so used were typically 5 mg/cm^{2} thick. The cross sections presented here have been corrected for (alpha) particle and energy loss in targets [7].

Differential Cross Sections

Typical spectra of deuterons, tritons, ^{3}He and alphas measured from oxygen for an incident neutron beam of 60.7 MeV are

shown in Fig. 2. Charge symmetric proton-induced neutron cross sections of Bertrand and Peelle [8] have been compared as histograms in the same figure. The error bars in our data do not include normalization errors; they are only indicative of the statistics. Figure 3 presents such a comparison for carbon at 39.7 MeV, and the data for nitrogen obtained at 27.4 MeV is presented in Fig. 4.

Angle Integrated Spectra

The differential cross sections have been obtained at nine different angles in the range between 15° and 150°. For those sets of data with all nine angles covered, the integration is obtained via Gaussian quadrature by assuming that the cross-section levels off on either end of the measured angular range. For sets of data deficient in larger angles, an extrapolation is done first to obtain cross sections for the next missing angle, and then the integration is performed. The errors shown in the plot are purely statistical. The additional uncertainties associated with the angle integrals are estimated to be 5% for the cases where 9 angles were measured and 20% when only 6 angles were measured. Such angle-integrated spectra are presented in the bottom row of each of the figures 2-4. Again, charge symmetric (p, xz) cross sections of Bertrand, et al. are compared as histograms where available.

Model Predictions

Predictions from calculations, using the code TNG with pre-equilibrium effects included, have been compared for protons and alphas [9]. Predictions for Oxygen at 60.7 MeV, for Carbon at 39.7 MeV and for Nitrogen at 27.4 MeV have been presented as solid curves in Figures 5, 6, and 7 respectively.

SUMMARY

Differential cross sections for charged particle continua arising from neutron induced reactions on C, N, and O have been measured at CNL at neutron energies of 27.4, 39.7, and 60.7 MeV. The selection of neutron beam energies for this study was guided by the proton-induced reaction measurements of Bertrand and Peelle at Oak Ridge. Since the elements chosen are all self conjugate, it is immensely reassuring to see the similarity in charge symmetric cross sections as expected. The model predictions presented here for comparison are the outcome of an effort expressly undertaken to interpret our data. These calculations are absolute; they have not been normalized to experiment. The predictions for protons have a scope for improvement at the high energy end by the inclusion of transitions to analogs of giant

resonances. As for the alphas, the major hurdle seems to be the handling of kinematics for the multi-particle exit channels.

ACNOWLEDGEMENTS

This work was supported by Grant PHS CA-16261 from NCI, DHEW and by U.S. NSF Grant PHY 71-03400 and PHY 77-05301. Experimental and technical assistance from W. Cline, C. Castaneda R. Garrett, D. Fitzgerald, G. Needham, J. Ullmann, J. Watson, C. Zanelli, and the cyclotron crew is gratefully acknowledged.

REFERENCES

1. J.A. Jungerman and F.P. Brady, Nucl. Inst. and Meth. 89, 167 (1970).

2. J.A. Jungerman, F.P. Brady, W.J. Knox, T. Montgomery, M.R. McGie, J.L. Romero, and Y. Ishizaki, Nucl. Inst. and Meth. 94, 421 (1971).

3. F.P. Brady, W.J. Knox, and S.W. Johnsen, Nucl. Inst. and Meth. 89, 309 (1970).

4. J.L. Romero, T.S. Subramanian, F.P. Brady, N.S.P. King, and J.F. Harrison, BNL-NCS-50681, 247 (1977).

5. T.S. Subramanian, J.L. Romero, and F.P. Brady, Accepted for publication in Nuclear Instruments and Methods.

6. T.S. Subramanian, Ph.D. Dissertation, University of California, Davis, 1979. Unpublished.

7. M.L. Johnson, J.L. Romero, T.S. Subramanian, and F.P. Brady. Nucl. Inst. and Meth. 169, 179 (1980).

8. F.E. Bertrand and R.W. Peelle. ORNL Report No. 4799 (1973) unpublished.

9. G.H. Herling and R.H. Bassel. Private communication.

9.a. Code TNG: C.Y. Fu, BNL-NCS-50681, 453, (1977).

9.b. Code PRECO: C. Kalbach, Report interne, DPH-N/BE/74/3. C.E.N., Saclay; 91190 Gif-Sur-Yvette (1974).

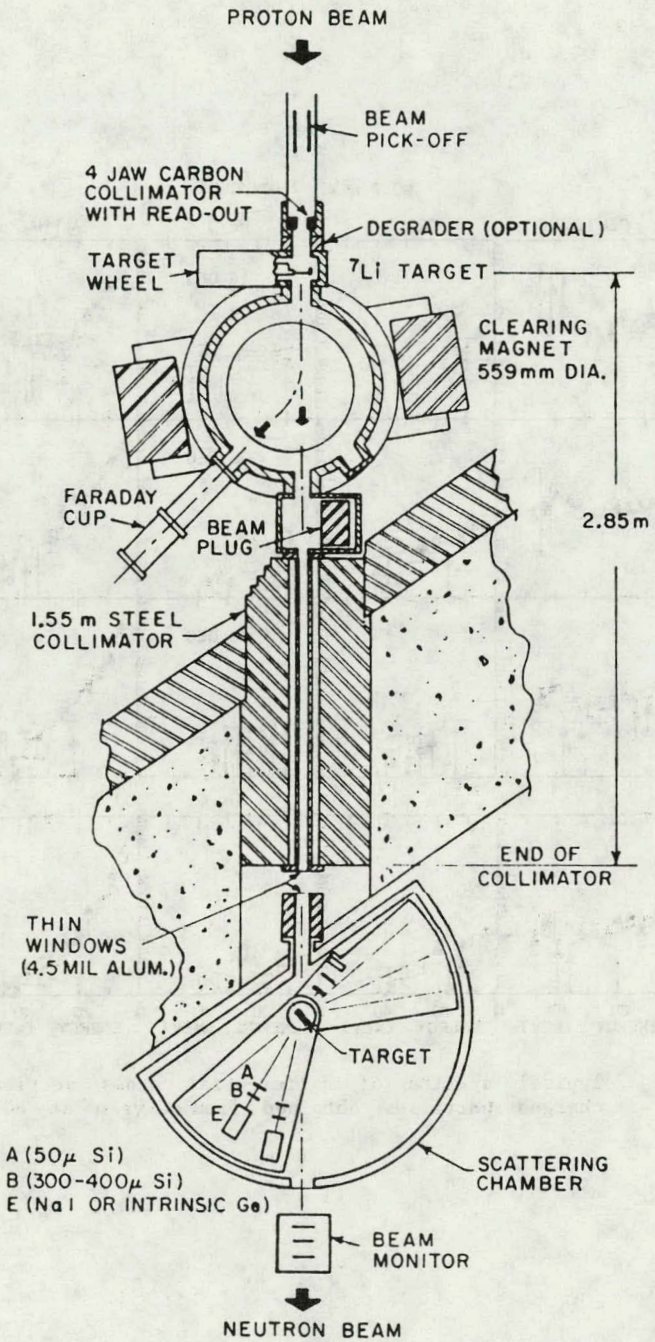

Fig. 1 The unpolarized neutron beam line and the associated scattering chamber at the Crocker Nuclear Laboratory.

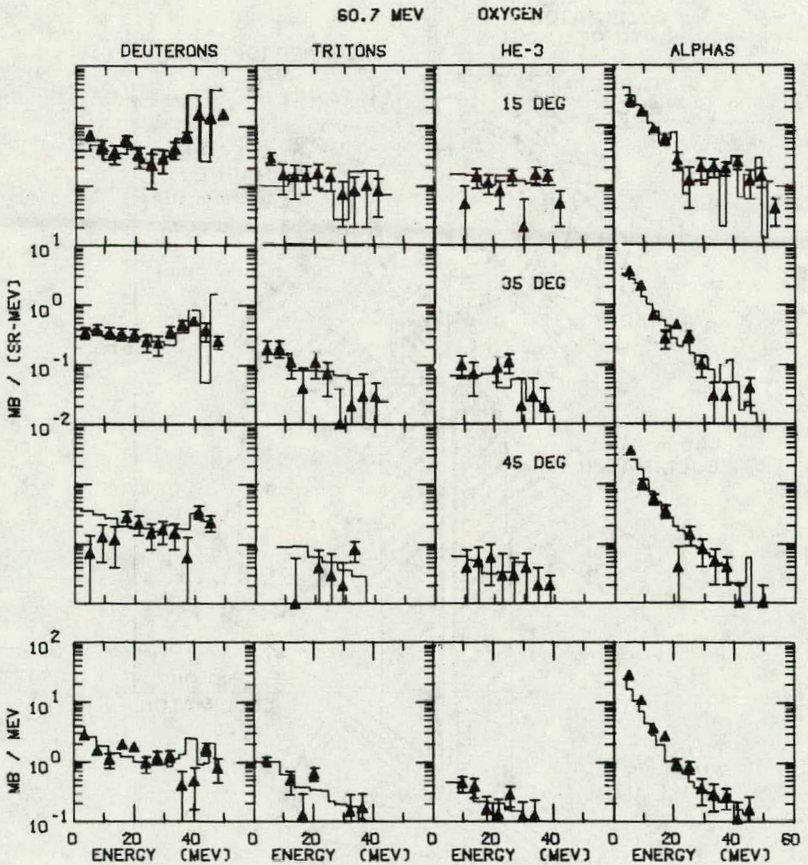

Fig. 2 Typical spectra of differential cross sections for charged particles obtained from Oxygen at 60.7 MeV.

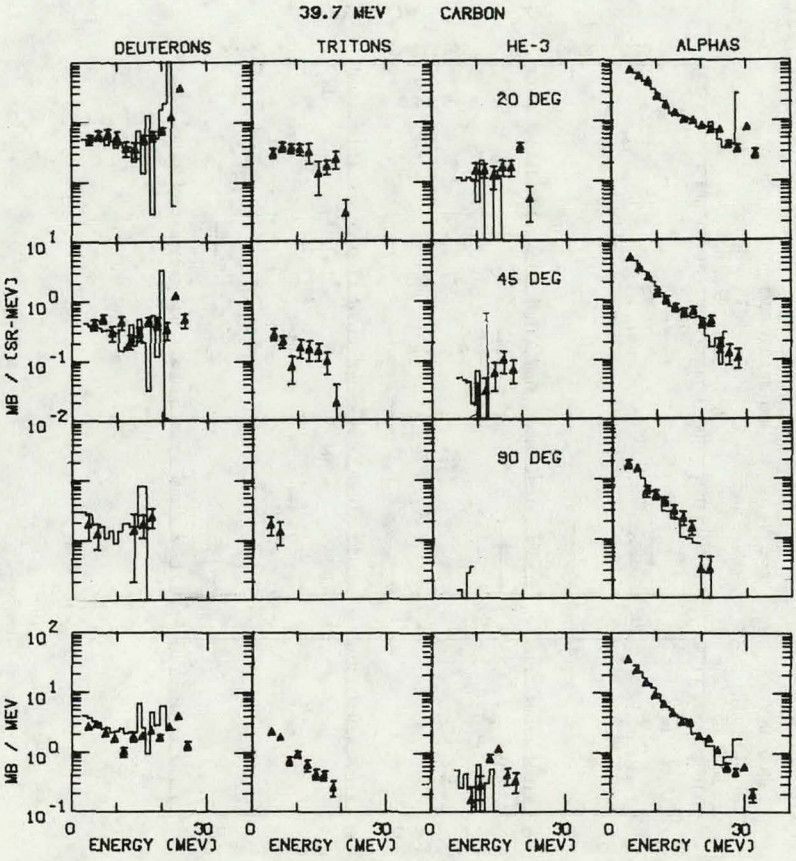

Fig. 3 Typical spectra of differential cross sections for charged particles obtained from Carbon at 39.7 MeV.

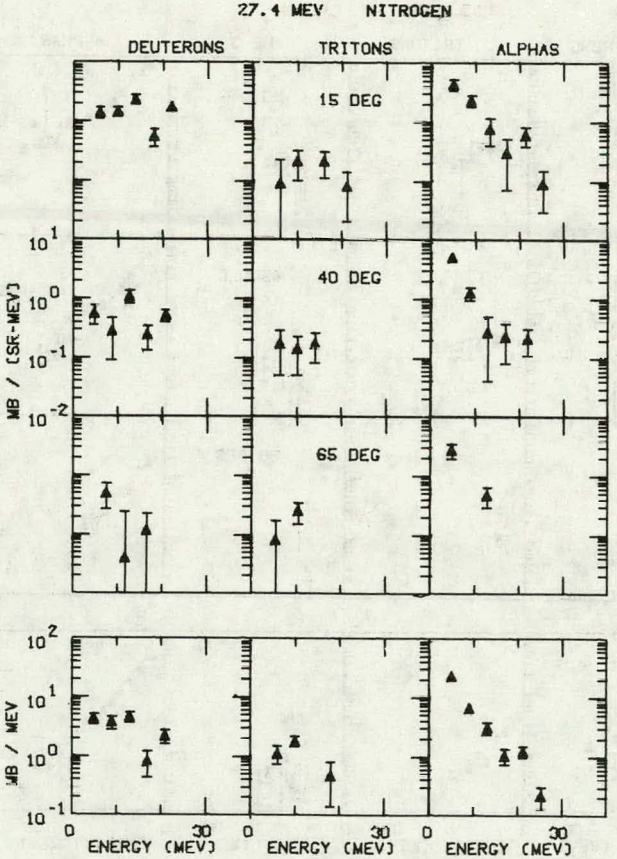

Fig. 4 Typical spectra of differential cross sections for charged particles obtained from Nitrogen at 27.4 MeV.

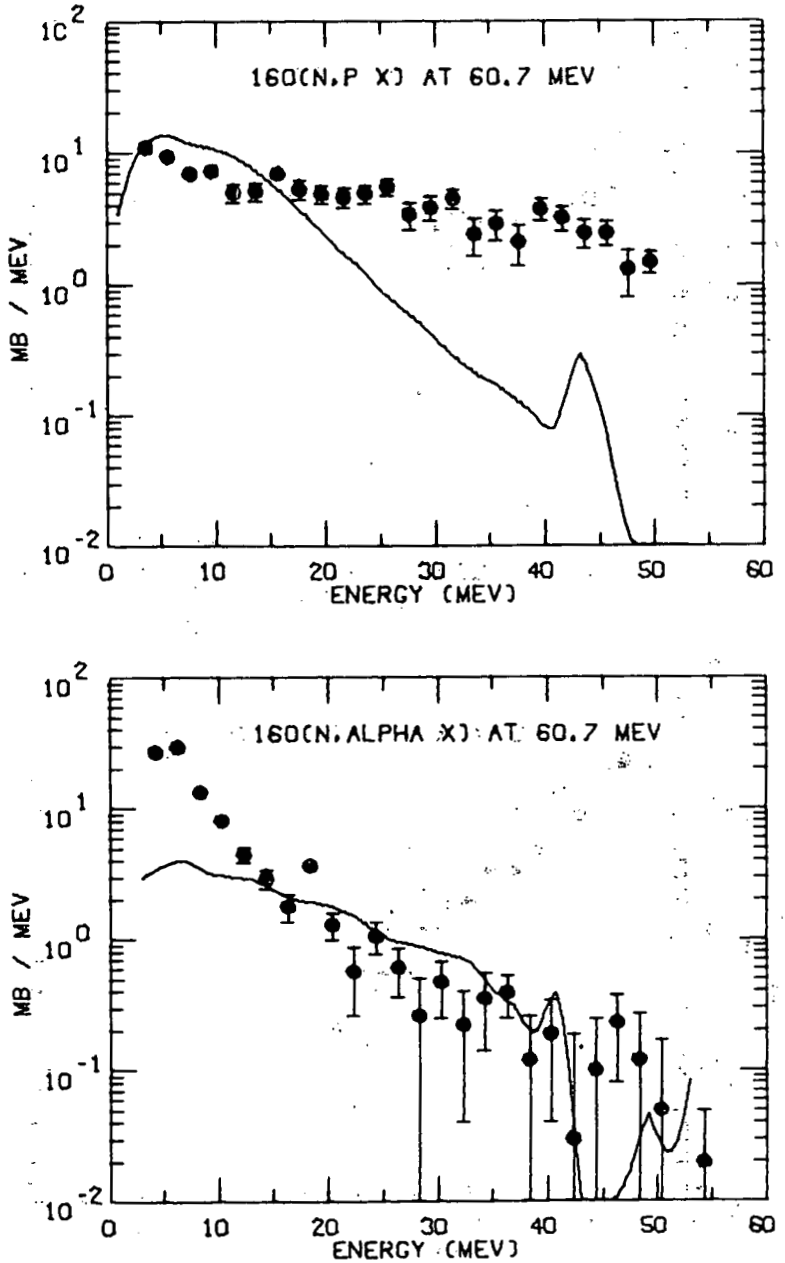

Fig. 5 Comparison with model predictions for angle integrated cross sections for protons and alphas from Oxygen at E_n = 60.7 MeV.

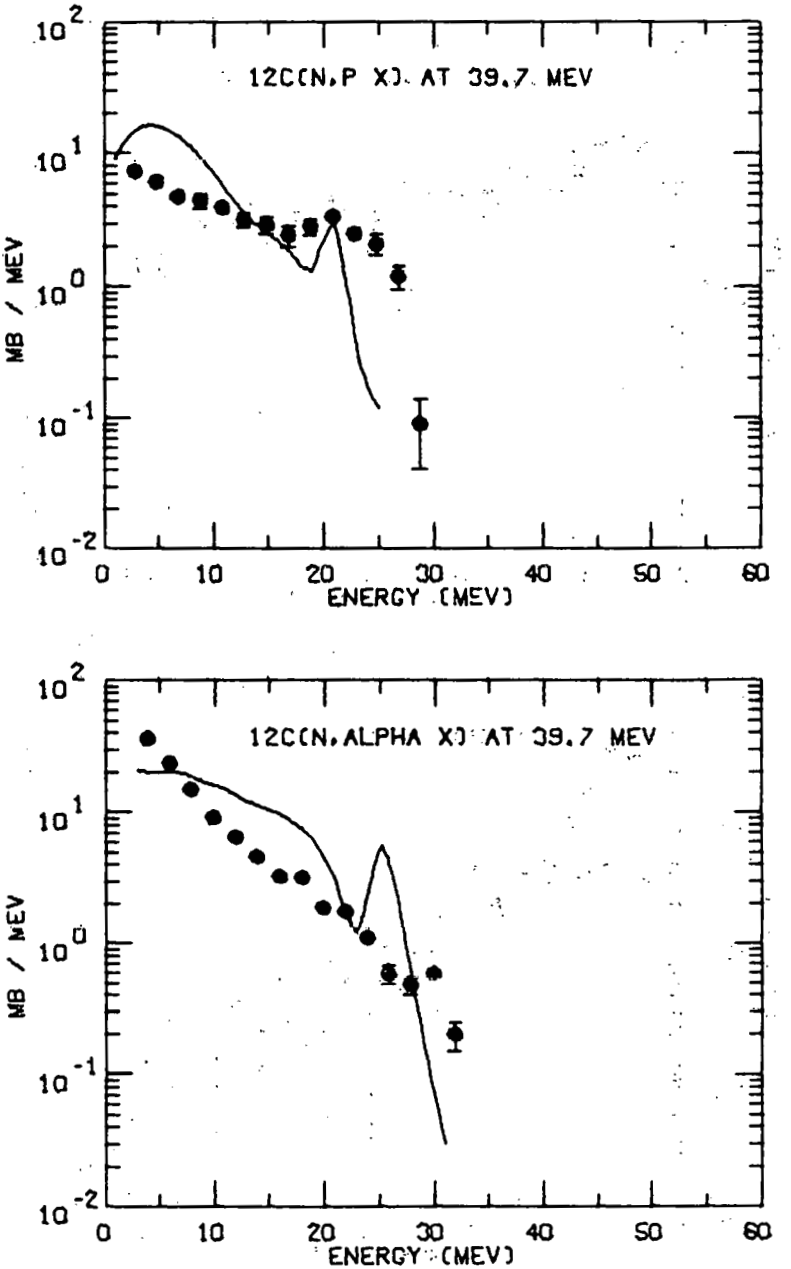

Fig. 6 Comparison with model predictions for angle integrated cross sections for protons and alphas from Carbon at E_n = 39.7 MeV.

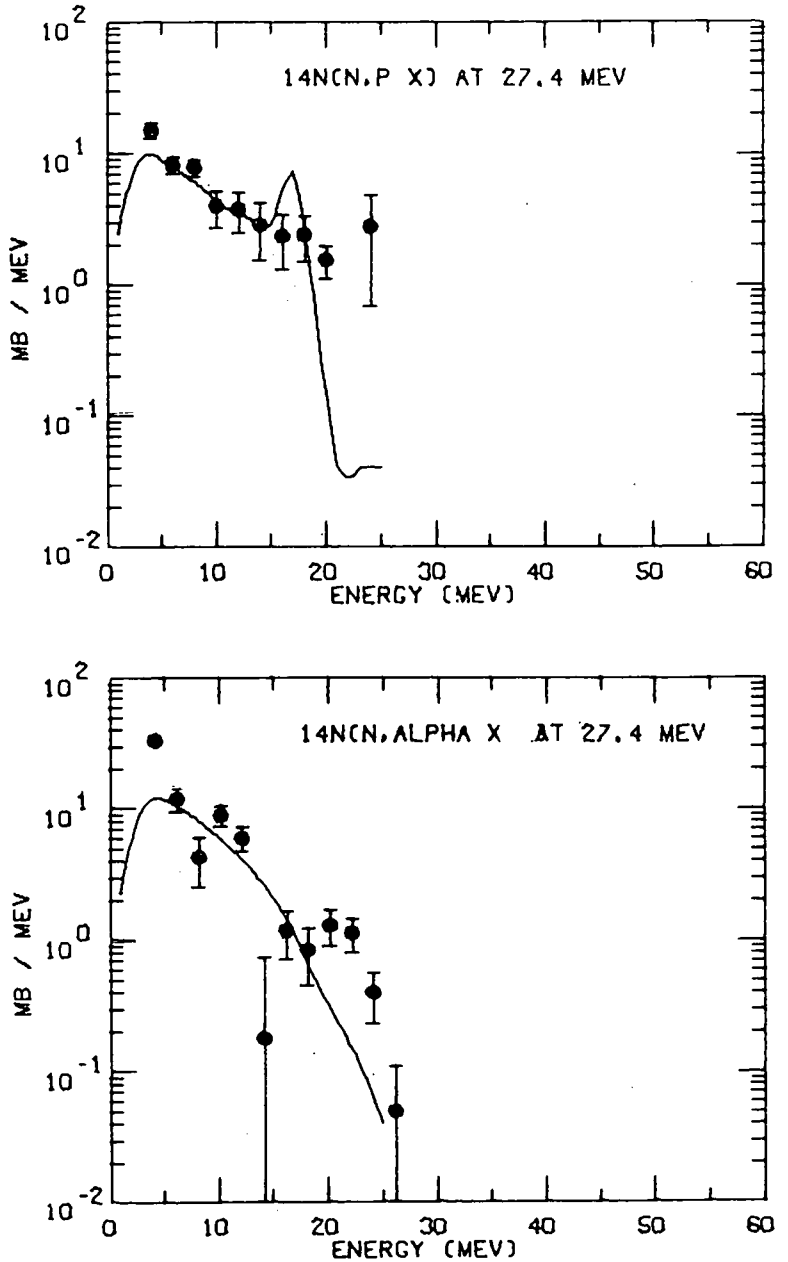

Fig. 7 Comparison with model predictions for angle integrated cross sections for protons and alphas for Nitrogen at E_n = 27.4 MeV.

THIS PAGE

WAS INTENTIONALLY

LEFT BLANK

MEASUREMENT OF THE ANGLE-INTEGRATED SECONDARY NEUTRON SPECTRA FROM INTERACTION OF 14 MEV NEUTRONS WITH MEDIUM AND HEAVY NUCLEI

H. Vonach, A. Chalupka, F. Wenninger, G. Staffel

Institut für Radiumforschung und Kernphysik der Österr. Akademie der Wissenschaften, Wien, Austria.

ABSTRACT

The angle-integrated secondary neutron spectra from interactions of 14.1 MeV neutrons with 17 elements in the range Ti to Bi were measured over the secondary neutron energy range 0.25 - 6 MeV with special emphasis on obtaining reliable and accurate neutron production cross-sections in the low energy region (0.25 - 1 MeV). An overall accuracy of 5 - 7% was obtained over most of the investigated energy ranges. The results are in good agreement with the predictions of statistical model calculations and in the neutron energy range above 1.5 MeV also with most other recent measurements; in the low energy range there are still large discrepancies between the results of different measurements.

INTRODUCTION

Secondary neutron spectra from the interactions of 14 MeV neutrons with nuclei have been investigated in a considerable number of experiments (1 - 7) and reasonable agreement on both the form of the spectra and the absolute neutron emission cross-sections have been obtained in the neutron energy range above about 1.5 MeV. The low energy parts of the secondary spectra, however, are rather poorly known in most cases due to experimental difficulties especially with n-γ-discrimination, background and multiple scattering at low secondary neutron energies. An excess of low energy neutrons compared with the theoretical predictions has been observed by a number of authors [1 - 4] whereas

Salnikov and co-workers [6] found much smaller neutron production cross-sections and also a measurement on iron at our institute [7] did not show any indication for abnormally high low-energy neutron-production cross-sections. Therefore new measurements have been performed at our institute to determine those spectra for a large number of elements.

EXPERIMENTAL PROCEDURE

Fig. 1 shows the experimental set-up. Pulsed neutrons are produced by means of the 250 keV Cockroft Walton accelerator of the institute [7] in an extremely small low-mass TiT target construction. The scattering samples (hollow cylinders of about 6 cm^3) surrounded the target and the neutron time-of-flight spectrum is measured at a distance of 1 m by means of a NE213 (1.5"x 0.5") scintillator coupled to a low dark current 56 DVP multiplier. The scintillator is operated at a very low threshold (equivalent to about 135 keV proton recoil energy) and a pulse-shape (PSD) method is used to discriminate between neutrons and photons. As reported earlier [8] the application of the PSD method is possible down to this very low threshold. Time of flight, recoil proton energy and pulse-shape detector output for each event is recorded on disc in order to enable optimal off-line analysis with respect to n-γ-discrimination and background reduction.

In order to save disc space the count-rate in the region of the 14.7 MeV peak from direct source neutrons was reduced by a factor of ten by means of a gate system. Accordingly the time spectra show a corresponding discontinuity at about channel 680. The stability of the whole electronic system was checked continuously by means of pulser peaks both in the time of flight spectra and especially in the low-energy part of the proton recoil spectrum and continuous monitoring of all important single count-rates.

The time resolution was about 1.5 nsec (FWHM) for the 14.7 MeV neutron peak in spite of the very large dynamic range (1:200) of pulses admitted for the proton recoil energy (s. Fig. 4 - 5). Apertures needed to collimate the deuteron beam onto the 3 mm Ø TiT-targets were positioned in such a way that DD neutrons produced there arrived at the detector at times outside the time range actually used for the measurements (s. Fig. 4 and 5).

3 to 4 separate measurements were performed for each element and background measurements after each

sequence of 3 sample-in measurements.

The efficiency of the neutron detector for the secondary neutrons (0.25 - 6 MeV) and for the primary 14.7 MeV neutrons was determined in two additional experiments.

The detector calibration for 0.25 - 6 MeV neutrons was done by replacing the target assembly by a fast low-mass ionisation chamber containing a ^{252}Cf source [9]. Using the fission product pulses of the ionisation chamber (which detects the fragments with an efficiency of about 98% and time resolution of better than 1 nsec) as start signals the ^{252}Cf neutron time-of-flight spectrum is measured in exactly the same way as described above. In this way the problem of absolute measurement of the secondary neutron spectra induced by 14 MeV neutrons is essentially reduced to a measurement relative to the known ^{252}Cf spectrum, which in addition has a form quite similar to evaporation spectra produced by the scattering samples and thus systematic errors e.g. because of room scattering and others will tend to cancel to a large extent in this calibration method.

The efficiency for the primary 14.7 MeV neutrons was determined by an experiment in which the target assembly was surrounded by an aluminum sample identical in shape to the scattering samples and observing both the intensity of the 14.7 MeV peak in the time of flight spectrum and the amount of ^{24}Na formed in the aluminum sample by means of the $^{27}Al(n,\alpha)$ reaction, the cross-section of which is known very accurately.

DATA ANALYSIS

The raw 3 parameter data were analyzed and transformed to energy differential neutron production spectra in the following way:

A) Derivation of the net (background subtracted) time-of-flight spectra.

1) The effect of small electronic drifts (1-2 channels) was eliminated by address-shifting of every data set deviating by at least one channel in the positions of either the pulser peak in the proton recoil spectrum, the γ-peak in the pulse shape (PSD) spectrum or the 14.7 MeV neutron peak in the time-of-flight (TOF) spectrum from the average values. In this way it is assured that the time scales of all measurements agree within ± 0.15 nsec, the recoil energy thresholds within ± 4 keV, and the

positions of the γ- and neutron peaks in the PSD spectra within a few % of the peak separation.

2) TOF-spectra were generated from the data using the following criteria for acceptance of events:
   a) γ-induced events were eliminated with minimum loss of neutron events by admitting only pulses from an appropriate region of the E_{recoil}-PSD plane. All spectra including the ^{252}Cf calibration spectra were treated in exactly the same way. Thus the efficiency determined with the ^{252}Cf measurement takes care of any neutron loss resulting from the γ-rejection procedure. As on the other hand inclusion of γ-induced events constitutes a source of systematic error which is difficult to correct for, considerable loss of neutrons was admitted in the low-energy region in order to get sufficient γ-rejection down to the lowest recoil pulse heights included. The quality of n-γ discrimination obtained in this way is shown in fig. 2 and 3 which show the PSD spectra for a pure γ-spectrum (^{60}Co source) and an almost pure neutron spectrum (neutron part of ^{252}Cf time spectrum see fig. 7) for different pulse-height bins in the region between 50 and 100% of the 59 keV Americium γ-peak; also shown are PSD thresholds used for the various pulse-height bins. As apparent from the figures it was possible to measure the neutron spectra with very little γ-contamination even at the lowest proton recoil energies. In addition it has to be kept in mind that the net (background subtracted) spectra contain only a very small γ-contamination in the interesting time range. Thus the residual γ-contribution to the net spectra can be completely neglected.
   b) Only pulses from that region of the E_{recoil}-TOF plane were admitted which is physically allowed for neutrons originating from target and scattering sample. Especially in the low neutron energy region a background reduction of about a factor of 2 could be obtained in this way.

Time-of-flight spectra were generated for all events admissible according to criteria a) and b) with proton recoil pulse heights larger than the chosen threshold of 0.5 of the pulse height of the 59 keV Am γ-peak (corresponding to approx. $E_{recoil} \sim 135$ keV). The threshold was chosen as the lowest possible value compatible with the conditions of n-γ discrimination and negligible loss of pulses in the constant fraction

trigger.

3) Background subtraction:
After execution of step 1 and 2 on all measured (sample-in and sample-out) spectra background subtraction is performed by subtracting from each sample-in spectrum an average of the background spectra measured before and after the respective measurement. In this way the effect of build-up of DD neutrons in the target is essentially eliminated. Background spectra are normalized relative to the sample-in spectra by means of the intensity in the 14 MeV time of flight peak taking into account the small (1 - 3%) contribution of elastically scattered neutrons to the 14 MeV peaks in the sample-in spectra. The above procedure assumes that the background can be obtained from sample-out measurements; this is certainly not exactly true as neutron interactions with the sample will to some extent modify the neutron spectrum hitting the walls of the target-room and thus also the general room background. However, it could be checked experimentally that the possible change of the background by the sample amounts to only a few percent. In the time range beyond the time of flight of the slowest detectable neutron (channel 100 - 200 in Fig. 4 and 5) one expects only background in both sample-in and sample-out spectra. Thus these parts of the spectra were used to check the possible dependence of the background on the presence of the scattering samples and in all cases this change was found to be less than 3%. Therefore actually an average of the two possible background normalizations (by means of the 14.7 MeV neutron peaks and by means of the intensity in the pure background region) was used and an error of 1.5% was assigned to the normalization factors obtained in this way.

As an example of the effects of the procedures described above Figures 4a and 5a show the raw TOF-spectra for both a sample-in (Fe) and a background measurement, Fig. 4b and 5b show the same spectra after elimination of the γ-induced and kinematically forbidden events and Fig. 6 shows the net Fe-TOF spectrum derived from the spectra of Fig. 4b and 5b. The s-shaped structure in Fig. 6 at the positions of the 14.7 MeV primary neutron peak is due to a small shift of a few tenth of a channel in the peak positions in the sample-in and sample-out spectra.

B) Efficiency determination of the neutron detector

1) Low energy range (0.25 - 6 MeV)
As already mentioned, in the low energy range (0.25-6 MeV) the detector efficiency was calibrated by means of a ^{252}Cf source. For this purpose the TOF-spectrum measured with the neutron detector and the ^{252}Cf ionisation chamber was treated in exactly the same way as described in A) in order to ensure identical efficiency in the calibration experiment and the rest of the measurements. The ^{252}Cf TOF-spectrum obtained in this way is shown in Fig. 7. Then the known ^{252}Cf neutron spectrum (segment-adjusted Maxwellian according to [10]) was transformed into a TOF-spectrum and the efficiency of the detector was calculated directly as the ratio of the measured to the calculated spectrum. The absolute neutron emission rate of the source was obtained from the fission product count-rate, the known efficiency of the ionisation chamber (98.2%) and the average neutron multiplicity $\bar{\nu}$ = 3.736±0.01 [11] of ^{252}Cf.

2) Efficiency for the 14.7 MeV source neutrons.
This efficiency was determined by simultaneous measurement of the TOF-spectrum with the NE213 detector and activation of an aluminum sample at the position of the scatterer and subsequent measurement of the ^{24}Na activity produced in the sample. From the measured ^{24}Na activity, the source sample-geometry, the known angular distribution of the DT source neutrons and the accurately known $^{27}Al(n,\alpha)^{24}Na$ cross-sections [12] we could derive the total neutron source strength with an accuracy of about 3% and therefrom and from the number of counts in the 14 MeV TOF peak accumulated during the Al-irradiation the efficiency of the detector for 14 MeV neutrons was determined as 4.41%±0.15% .

C) Calculation of the absolute neutron emission cross-sections $\sigma_{nM}(E_n')$ from the net time of flight spectra.

The net time of flight spectra n(t) were first transformed into energy spectra $N(E_n')$ and therefrom the $\sigma_{nM}(E_n')$ values were obtained for our geometry (s. Fig. 1) by means of the relation

$$\sigma_{nM}(E_n') = \frac{N(E_n')}{N(14.7)} \cdot \frac{\varepsilon(14.7)}{\varepsilon(E_n')} \cdot$$

$$\cdot \frac{\left(\frac{d\omega}{d\omega'}\right)(0^o)\,(1+f_{elast})}{n \cdot f_{abs}(E_n')\, f_{mult}(E_n') \int \frac{\exp[-\sigma_{non}(14) d_{abs}]}{4\pi r^2}\, dV} \qquad (1)$$

with $N(E_n')\Delta E_n'$ = total number of counts between E_n' and $E_n'+\Delta E_n'$

$N(14.7)$ = total number of counts in 14.7 MeV peak

$\varepsilon(14.7), \varepsilon(E_n')$ = detector efficiencies for neutrons of 14.7 MeV and E_n' resp.

n = atomic density of sample

The integration has to extend over the whole volume of the scattering sample.

$\left(\frac{d\omega}{d\omega'}\right)(0^o)$ = ratio of zero degree to average neutron emission rate for DT source neutrons

$f_{abs}(E_n')$ = average attenation factor for secondary neutrons in the scattering sample

$f_{mult}(E_n')$ = correction factor for contribution of double scattered neutrons in measured spectrum

f_{elast} = relative contribution of neutrons elastically scattered in sample to 14.7 MeV peak.

dV = volume element in scattering sample

r = distance from source to dV

d_{abs} = distance from source to dV traversed in sample

The absorption correction factor $f_{abs}(E_n')$ was calculated assuming absorption by nonelastic events only and an average path length of one half of the sample height (1 cm) for the scattered neutrons as

$$f_{abs}(E_n') = \exp\left[-\frac{1}{2}\,\sigma_{non}(E_n').h\right] \qquad (2)$$

values range from 0.9 - 1.0.

The elastic scattering fraction to the 14 MeV peak was calculated by integration over all value elements of the sample using elastic scattering cross-

sections derived by optical model calculations using the Perey-Buck [13] potential;values range from 0.9 to 4%.

The multiple scattering corrections were calculated approximately by means of the following relation considering only double scattering.

$$f_{mult}(E_n') = 1 + \frac{N_{double}}{N_{single}}(E_n') \qquad (3)$$

and

$$\frac{N_{double}}{N_{single}} = \frac{\int_{E_n'}^{14} \sigma_{nM}(14 \rightarrow E_n'') \, \sigma_{nM}(E_n'' \rightarrow E_n') \, n \, \bar{d} \, dE_n''}{\sigma_{nM}(14 \rightarrow E_n')} \qquad (4)$$

with $\bar{d}$ = average path length of single-scattered neutrons in the sample = 8.4-8.6 mm as derived by numerical averaging over all points of origin in sample and all emission directions

and $\sigma_{nM}(E_n'' \rightarrow E_n')$ = cross-sections of neutrons with energy E_n'' for emission of neutrons with E_n'. Values of $\sigma_{nM}(E_n'' \rightarrow E_n')$ as function of both E_n'' and E_n' were calculated by means of the statistical model of nuclear reactions as described in the Appendix values of N_{double}/N_{single} range from 0.5 to 11%.

RESULTS AND DISCUSSION

The results, that is the angle-integrated neutron emission spectra $\sigma_{nM}(E_n')$ for all elements investigated, are listed in Table 1. The neutron emission spectra are averages over the incident neutron energy range 13.5 - 14.7 MeV because of the angle-dependence of the DT source neutrons and the chosen scattering geometry (see Fig. 1). However, due to the rather weak dependence of the secondary spectra on the primary neutron energy the cross-sections correspond to good approximation to a neutron energy of 14.1 MeV.

The errors given were obtained by quadratic addition of the statistical errors estimated 1σ errors for all identified sources of systematic errors

and thus correspond to effective 1σ errors. The following contributions are included in our error estimates.

1) The total statistical error including the error of the ^{252}Cf calibration measurement
2) The uncertainty in the form of the ^{252}Cf spectrum according to [10]
3) The error in the absorption correction factor f_{abs} for the secondary neutrons. According to the general status of non-elastic cross-sections an uncertainty of 15% in $\sigma_{non}(E_n')$ was assumed for the error estimate.
4) The error for the multiple scattering correction was calculated assuming errors of 30% for the neutron emission cross-sections $\sigma_{nM}(E_n'' \rightarrow E_n')$ from the statistical model calculations.
5) An uncertainty of 1.5% was assumed for the normalization factors used in the background subtraction as already discussed in section two.
6) The efficiency error for the 14.7 MeV source neutrons (3%).

Errors due to weight, dimensions and possible impurities of the samples, time calibration and residual electronic shifts (see section 3) were estimated to be small compared to the total errors due to 1 - 6 and were neglected.

Fig. 9 shows the size of the various error contributions and the total errors for the case of iron which is typical for most of the elements investigated.

In Fig. 10 - 13 the present results are compared to existing measurements and statistical model calculations for 4 of the elements studied, and in Fig.14 the ratio between our measured and calculated cross-sections is given for all elements investigated.

All calculations were performed by means of the code STAPRE [14] using global parameter sets. Thus the calculations did not involve adjustments of any parameter to the individual elements.

Numerical data for the results of Hermsdorf et al. [5] and Salnikov et al. [6] were taken from the EXFOR file *), the data of Schectman and Anderson [1] were read from the figures in their publication.

Although the figures for the different elements do show some differences with respect to the comparison of the various data the following general statements can be made:

---

*) for Hermsdorf's data revised values are used, obtained by private communication from the authors

1) Above about 1.5 MeV there is reasonable agreement between all measurements.
2) Below 1.5 MeV our data do not confirm the high neutron production cross-sections found in ref. [1] - [4], but show in all cases that the spectra do have the theoretically expected form; in general they are in fair agreement with the results of Salnikov et al. [6] although for some elements (not shown in fig. 10 - 13) the data of ref. [6] seem to be somewhat too low at the lowest energies.
3) Our data for Fe are in excellent agreement with the results measured previously at our institute [7] using a quite different experimental set-up and all of our spectra do show a very smooth behaviour as function of A resp. Z, confirming the consistency of our measurements.
4) As shown in fig. 14 there is a good overall agreement between our measured neutron production cross-sections and the results of the STAPRE calculations using no free parameters for all elements investigated indicating that such calculations may be used to predict unmeasured neutron production cross-sections with an accuracy of better than 20%. In detail it can be noted that there is almost perfect agreement between calculated and measured cross-sections in the range Ti - Ni, whereas for heavier elements our measured production cross-sections for low energy neutrons are consistently by about 10 - 20% higher than the calculated values.

ACKNOWLEDGEMENTS

The authors gratefully acknowledge the help of Dr. G. Stengl in the development of the electronics and of Dr. K. Hansjakob for doing most of the STAPRE calculations, the valuable discussion with Dr.B.Strohmaier and Doz.M. Uhl and the financial support by the Jubiläumsfond der Österr. Nationalbank.

APPENDIX

Statistical model calculations

The calculations were performed by means of the computer code STAPRE [14]. This code is designed to calculate cross-sections for reactions with multiple particle and γ-ray emission. Conservation of angular momentum and parity is taken into account. At low excitation energies all levels of the relevant residual

nuclei are considered; when, with increasing excitation energy, the information about the levels is no longer complete the density of levels is calculated by means of the backshifted Fermi gas model. For emission of the first particle of a given evaporation sequence a preequilibrium decay contribution - calculated in the framework of the exciton model - is included.

Transmission coefficients for neutrons, protons and α-particles were calculated by means of global potentials by Perey and Buck [13], Becchetti et al. [15] and Huizenga and Igo [16], respectively.

The γ-ray transmission coefficients $T_{XL}(\varepsilon)$ for multipole-type XL and transition energy ε are related to the γ-ray strength function $f_{XL}(\varepsilon)$ [17] by $T_{XL} = 2\pi\varepsilon^{2L+1} f_{XL}(\varepsilon)$. For the energy dependence of the strength function $f_{E1}(\varepsilon)$ for the dominant E1 radiation the Brink-Axel model [18] was employed while $f_{M1}(\varepsilon)$, $f_{E2}(\varepsilon)$, ... $f_{M3}(\varepsilon)$ were assumed to be constant and normalized to $f_{E1}(\varepsilon = B_n)$ by Weisskopf's estimate, where B_n represents the neutron binding energy. The normalization of $f_{E1}(\varepsilon)$ is achieved by the demand that the calculated total average radiation width agrees with neutron resonance data [19].

The level density parameters a and Δ were taken from the compilation of Dilg et al. [20], either directly or if necessary by interpolation.

The preequilibrium emission rates for nucleons were corrected for charge conservation as described in refs. [21] and [22]. The exciton state densities were calculated by means of the formula of Williams [23] with single particle state densities $g = (6/\pi^2)A/8$ and no pairing corrections.
For the internal transition rates the expressions of Williams [24] were employed with a matrix element M which depends on excitation energy E of the composite system, as proposed by Kalbach-Cline [25] : $|M|^2 = FMA^{-3}E^{-1}$ and the matrix elements FM chosen in such a way that the $\Delta_n = 2$ decay rates for the three exciton configuration $\lambda^+(3)$ at E = 19 MeV amounts 5.10^{21} sec^{-1} for all nuclides.
Calculations were performed for all isotopes of each element with abundances of more than a few percent and elemental cross-sections obtained therefrom.

n-,p-,α- and γ-decay was considered for the elements up to Ba, whereas p- and α-decay was neglected for the heavier elements. For the nuclides ^{58}Ni, ^{63}Cu and ^{64}Zn the contribution to σ_{nM} from the (n,pn) reaction is also included, for the other nuclides only the (n,nx) and (n,2n) contributions were taken into account.

REFERENCES

[1] R. M. SCHECTMAN and J. D. ANDERSON, Nucl. Phys., 77, 241 (1966)

[2] C. S. MATHUR et al., Phys. Rev., 186, 1038 (1969) NDL-TR 86 (1967)

[3] J. L. KAMMERDIENER, UCRL 51232 (1972)

[4] G. CLAYEUX and J. VOIGNIER, CEA R 4279 (1972)

[5] D. HERMSDORF et al., Kernenergie, 17, 76 (1974), 17, 259 (1974), 18, 83 (1975), 19, 241 (1976) and Bericht ZfK 277U (1975)

[6] O. A. SALNIKOV et al., Sov. J. Nucl. Phys., 122, 620 (1971), YK 7, 102 (1972)

[7] G. STENGL et al., Nucl. Phys., A290, 109 (1977)

[8] A. CHALUPKA et al., Nucl. Instr. and Meth., 150, 209 (1978)

[9] A. CHALUPKA, Nucl. Instr. and Meth., 164, 105 (1979)

[10] J. M. GRUNDL and C. EISENHOWER, IAEA-208 (1978), Vol.I, 64

[11] J. W. BOLDEMANN, Proc. Int. Spec. Symp. on Neutron Standards and Appl., Gaithersburg 1977, NBS Special Publ., 493, 182 (1977)

[12] H. VONACH et al., Z. f. Physik, 237, 155 (1970)

[13] F. PEREY and B. BUCK, Nucl. Phys., 32, 350 (1962)

[14] B. STROHMAIER and M. UHL, Proc. Winter Course on Nuclear Physics and Reactors, Trieste, 16 Jan - 10 Feb. 1978

[15] F. D. BECCHETTI and G. W. GREENLEES, Phys. Rev., 182, 1190 (1968)

[16] J. R. HUIZENGA and G. I. IGO, ANL-6373 (1961)

[17] G. A. BARTHOLOMEW et al., Advances in Nucl. Phys, Vol. 7 (Plenum Press, NY, 1973) ch. 4

[18] P. AXEL, Phys. Rev., 83, 1073 (1951)

[19] S. F. MUGHABGHAB and D. J. GARBER, BNL-325 (1973)

[20] W. DILG et al., Nucl. Phys., A217, 269 (1973)

[21] G. M. BRAGA-MARCAZZAN et al., Phys. Rev., C6, 1398 (1972)

[22] E. GADIOLI et al., Nucl. Phys., A217, 589 (1973)
[23] F. C. WILLIAMS, JR., Nucl. Phys., A166, 231 (1971)
[24] F. C. WILLIAMS, JR., Phys. Lett., 31B, 184 (1970)
[25] C. KALBACH-CLINE, Nucl. Phys., A210, 590 (1973)

Table 1. Angle integrated secondary neutron-production cross-sections $\frac{d\sigma}{dE_n}$ for 14.1 MeV neutrons.

E_n' (MeV)	σ_{nM} (mb/MeV)				
	Ti	Cr	Fe	Ni	Cu
0.25-0.50	399±28	415±21	420±20	319±16	604±26
0.50-0.75	465±22	491±22	523±25	378±16	730±34
0.75-1.00	499±23	473±22	502±24	381±16	699±34
1.00-1.25	454±21	433±20	466±23	346±15	619±30
1.25-1.50	410±19	379±18	394±19	297±13	531±26
1.50-1.75	359±16	340±15	349±17	257±11	445±21
1.75-2.00	321±14	303±14	305±15	224± 9	378±19
2.00-2.25	292±13	285±13	281±14	202± 9	335±17
2.25-2.50	253±12	243±12	237±12	168± 8	285±15
2.50-2.75	222±11	225±12	228±12	169± 8	256±14
2.75-3.00	202±11	191±10	190±10	140± 7	221±14
3.00-3.25	171± 9	169± 9	175± 9	120± 6	180±11
3.25-3.50	148± 8	159± 9	158± 9	119± 6	163±10
3.50-3.75	149± 8	149± 8	150± 8	110± 6	151±10
3.75-4.00	129± 8	134± 8	130± 7	100± 5	140± 9
4.00-4.50	117± 7	109± 6	113± 6	89± 4	110± 7
4.50-5.00	91± 6	91± 6	102± 6	80± 4	95± 7
5.00-5.50	73± 5	70± 5	82± 5	63± 4	73± 6
5.50-6.00	60± 5	55± 5	66± 5	52± 3	53± 6
	Zn	Zr	Nb	Mo	Ag
0.25-0.50	422±10	1208±36	1256±66	1185±39	1669±96
0.50-0.75	519±23	1256±53	1360±60	1418±64	1689±83
0.75-1.00	510±23	1136±49	1252±57	1243±58	1450±74
1.00-1.25	448±20	960±42	1043±49	1030±49	1146±60
1.25-1.50	376±17	815±36	895±42	848±41	923±49
1.50-1.75	324±14	681±29	782±36	710±33	786±41
1.75-2.00	286±13	538±24	655±31	585±28	617±33
2.00-2.25	254±12	462±21	568±27	506±24	545±30
2.25-2.50	224±11	362±19	459±24	415±22	406±24
2.50-2.75	199±10	291±17	380±21	361±19	380±22
2.75-3.00	175± 9	230±15	317±18	293±16	289±20
3.00-3.25	146± 8	173±13	257±15	237±13	224±15
3.25-3.50	131± 7	150±12	212±14	202±12	199±14
3.50-3.75	122± 7	139±12	196±13	168±11	177±13
3.75-4.00	105± 7	114±11	161±12	141±10	145±12
4.00-4.50	85± 5	84± 9	109± 8	115± 7	108± 9
4.50-5.00	74± 5	61± 9	87± 8	87± 7	91± 9
5.00-5.50	60± 4	31± 9	65± 8	70± 6	73± 9
5.50-6.00	46± 4	31± 9	68± 8	50± 6	66± 9

Table 1. cont.

E_n' (MeV)	σ_{nM}(mb/MeV)				
	Sn	Ba	Ta	W	Au
0.25-0.50	1495±44	1500±62	2151±118	2123± 70	1958± 72
0.50-0.75	1675±69	1443±72	2458±123	2508±115	2364±118
0.75-1.00	1566±67	1465±70	2186±113	2347±111	2243±116
1.00-1.25	1305±56	1292±62	1750± 92	1844± 89	1922±101
1.25-1.50	1062±46	1051±52	1360± 72	1469± 72	1586± 84
1.50-1.75	878±37	834±43	1069± 56	1139± 55	1346± 70
1.75-2.00	700±30	688±38	833± 45	887± 44	1120± 59
2.00-2.25	608±27	561±35	671± 37	704± 36	870± 47
2.25-2.50	463±22	420±32	505± 30	527± 30	685± 39
2.50-2.75	362±19	365±33	403± 23	425± 26	619± 33
2.75-3.00	300±17	287±33	278± 18	289± 25	484± 28
3.00-3.25	233±14	262±28	230± 15	243± 19	369± 22
3.25-3.50	180±13	215±28	193± 13	207± 17	289± 18
3.50-3.75	177±13	174±28	154± 12	161± 17	249± 17
3.75-4.00	145±12	202±28	142± 11	126± 15	213± 15
4.00-4.50	109± 9	165±21	93± 8	102± 12	147± 11
4.50-5.00	88± 9	97±22	82± 2	53± 12	114± 11
5.00-5.50	66± 9	57±20	59± 8	50± 13	82± 10
5.50-6.00	30± 8	26±12	55± 8	54± 12	40± 10
	Pb	Bi			
0.25-0.50	1447±62	1701±58			
0.50-0.75	1809±79	1873±80			
0.75-1.00	1885±83	1932±84			
1.00-1.25	1705±76	1845±80			
1.25-1.50	1595±71	1691±73			
1.50-1.75	1422±61	1520±63			
1.75-2.00	1244±54	1346±56			
2.00-2.25	1121±49	1189±51			
2.25-2.50	899±43	999±46			
2.50-2.75	741±38	817±40			
2.75-3.00	526±31	648±34			
3.00-3.25	424±26	514±28			
3.25-3.50	380±24	409±24			
3.50-3.75	304±22	324±21			
3.75-4.00	232±20	277±20			
4.00-4.50	183±15	219±15			
4.50-5.00	136±15	161±14			
5.00-5.50	83±14	97±13			
5.50-6.00	65±15	75±14			

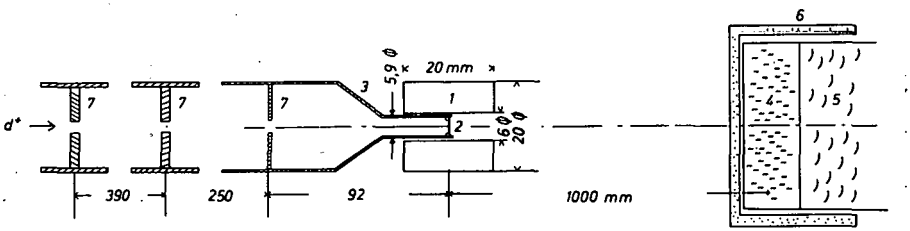

Fig. 1. Experimental set-up for measurement of the angle integrated low-energy part of the secondary neutron spectra from interaction of 14 MeV neutrons with nuclei (schematic, 1: scattering sample, 2: Ti-Target on 0.1 mm Cu-backing, 3: target assembly (0.2 mm Al), 4: Ne 213 scintillator (1.5"Ø x 0.5"), 5: 56 DVP photomultiplier , 6: 2 mm leadshield, 7: Apertures for d^+ beam

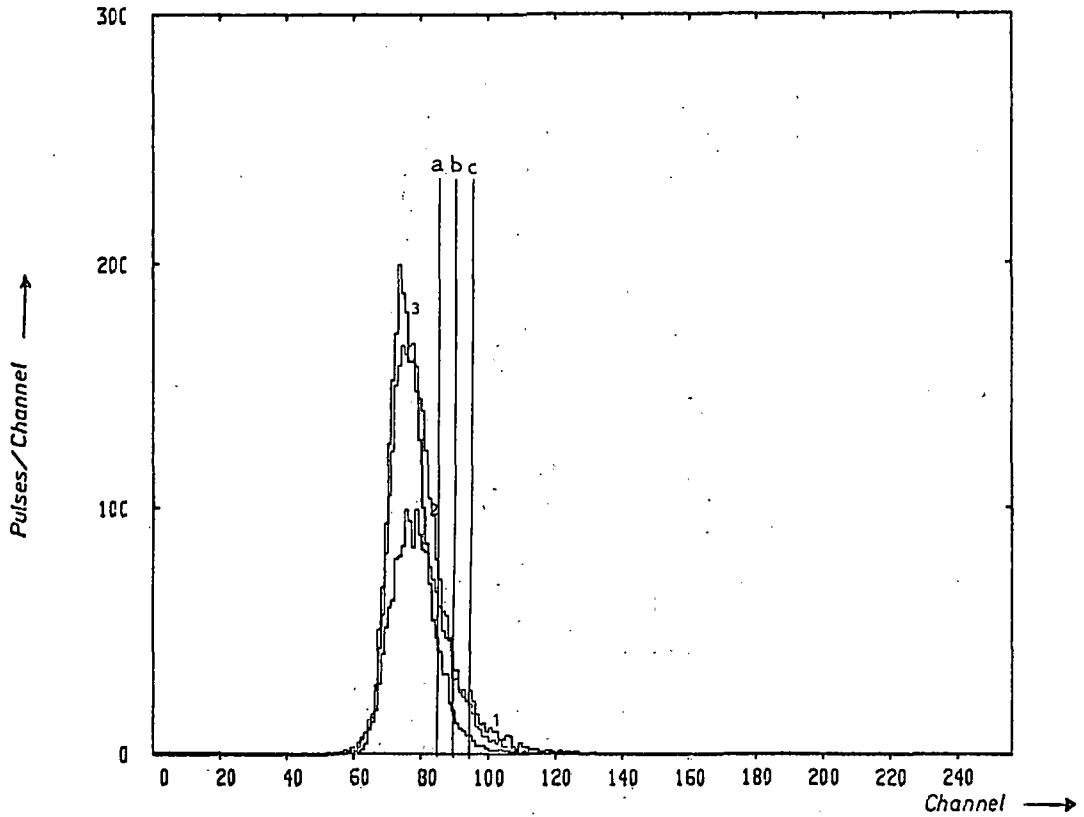

Fig. 2. Pulse-shape spectra of the NE 213 detector for ^{60}Co source. Spectra 1 - 3 correspond to different pulse heigth bins as indicated in the figure. Also indicated are the thresholds a, b, c used for those energy bins in the analysis of all neutron spectra.

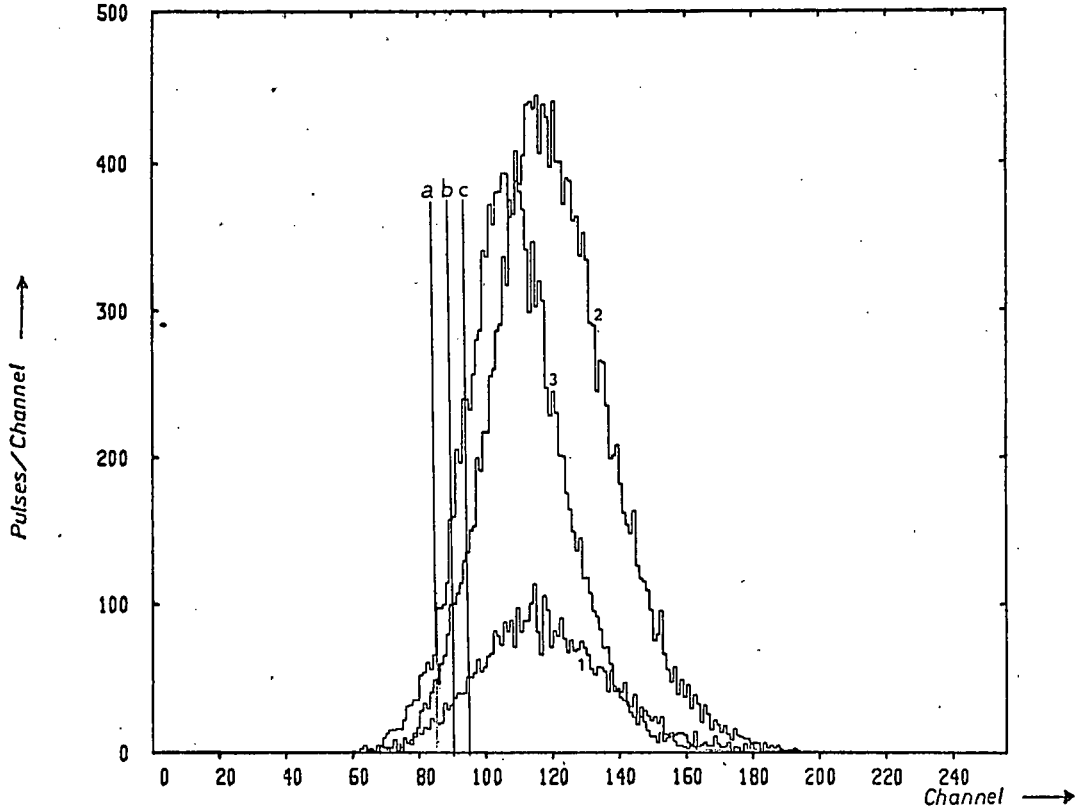

Fig. 3. Pulse-shape spectra of the NE 213 detector for the neutron part of the ^{252}Cf time spectrum (channels 200 - 700 in Figure 7) and the same pulse height bins as in Fig. 2. Also indicated are the thresholds a, b, c used for those energy bins in the analysis of all neutron spectra.

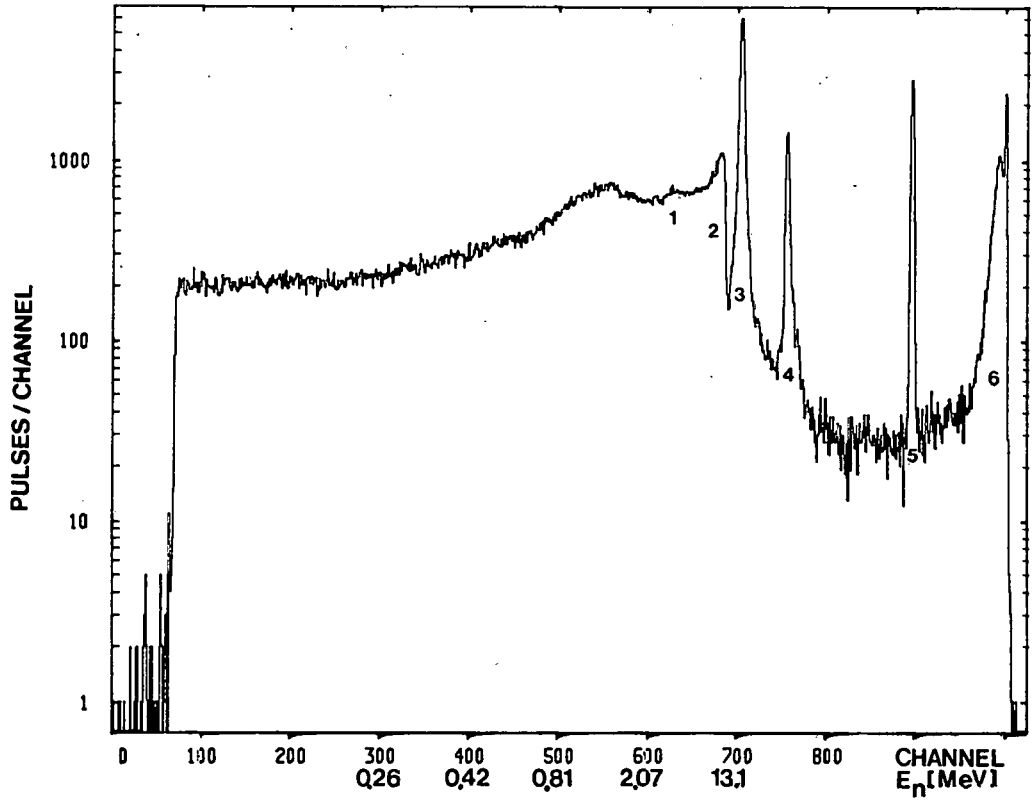

Fig. 4. Time spectra observed with Fe scatterer around TiT target:

a) raw time spectrum: 1: DD-neutrons from target, 2: only every tenth pulse was recorded in region above edge (s. sect.2), 3: DT-neutrons, 4: prompt γ-peak, 5: pulser peak, 6: DD-neutrons from aperture upstream of target (see Fig. 1)

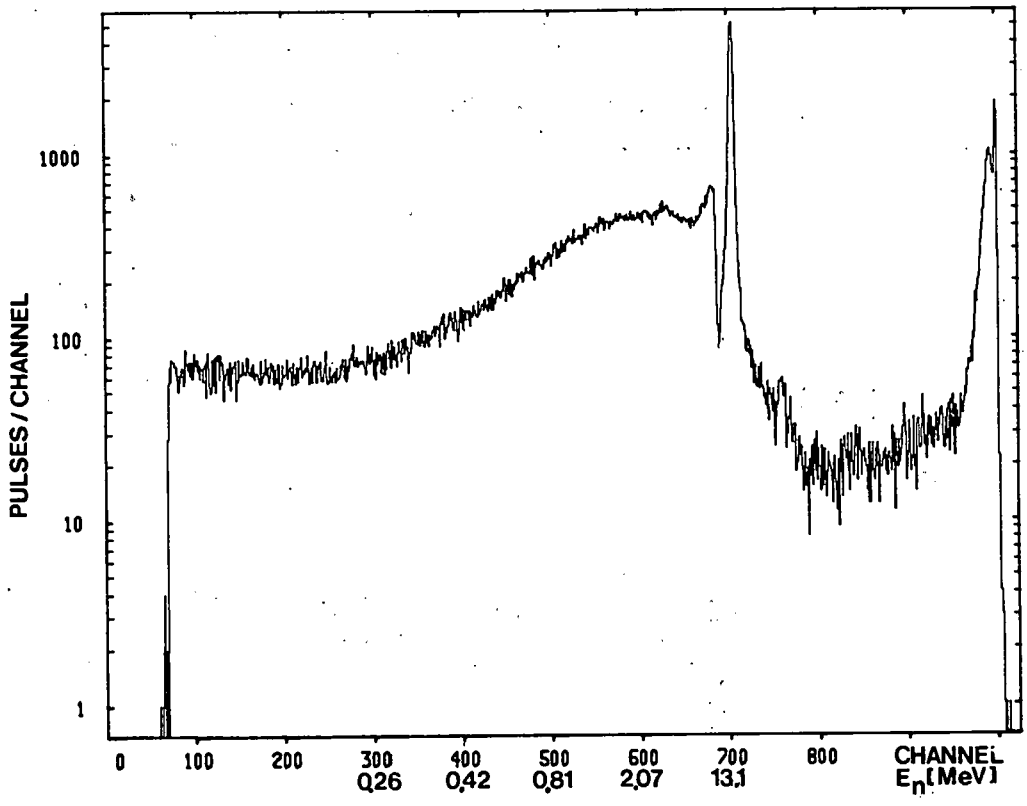

Fig. 4. Time spectra observed with Fe scatterer around TiT target:
b) same spectrum after elimination of γ-induced and kinematically forbidden events.

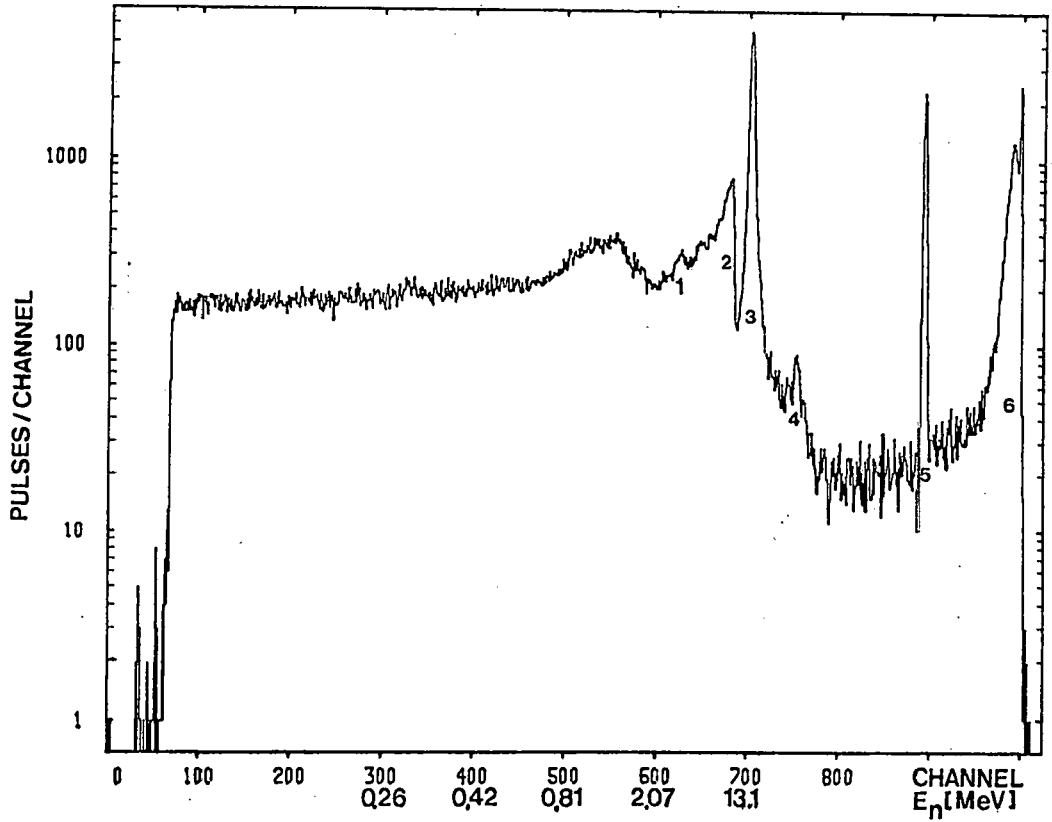

Fig. 5. Background time spectra:
a) raw time spectrum, peaks 1 - 6 as in Fig. 4a

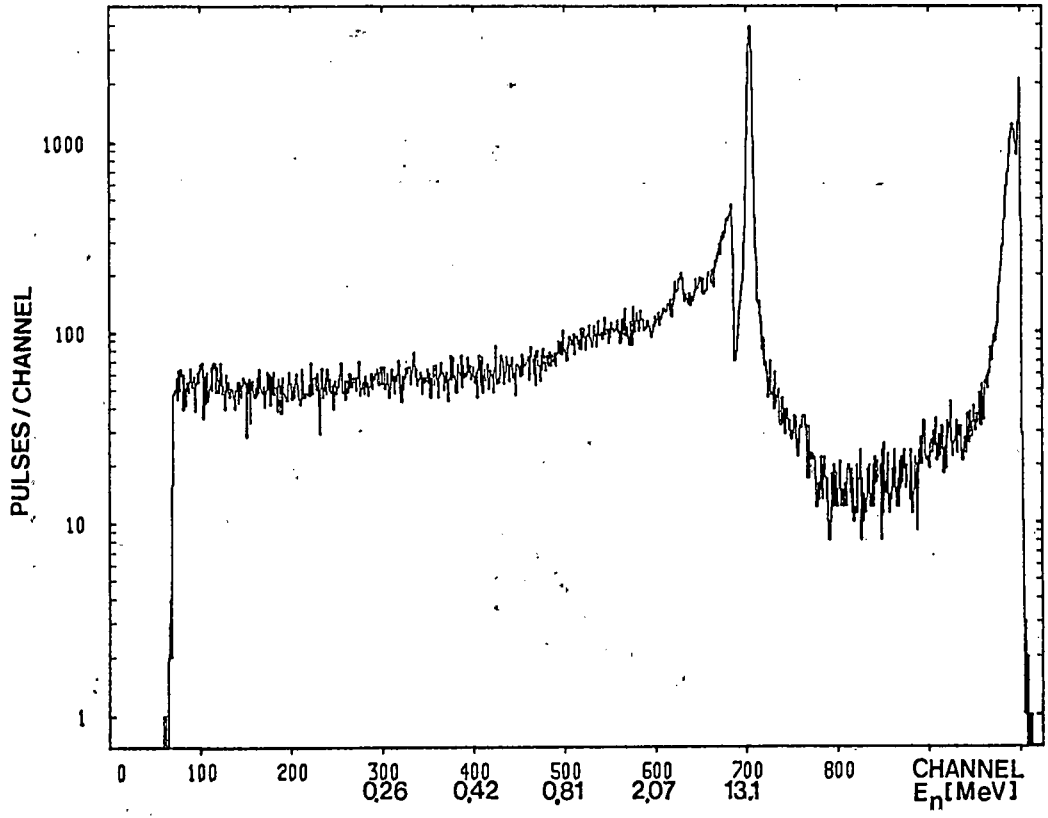

Fig. 5. Background time spectra:

b) same spectrum after elimination of γ-induced and kinematically forbidden events.

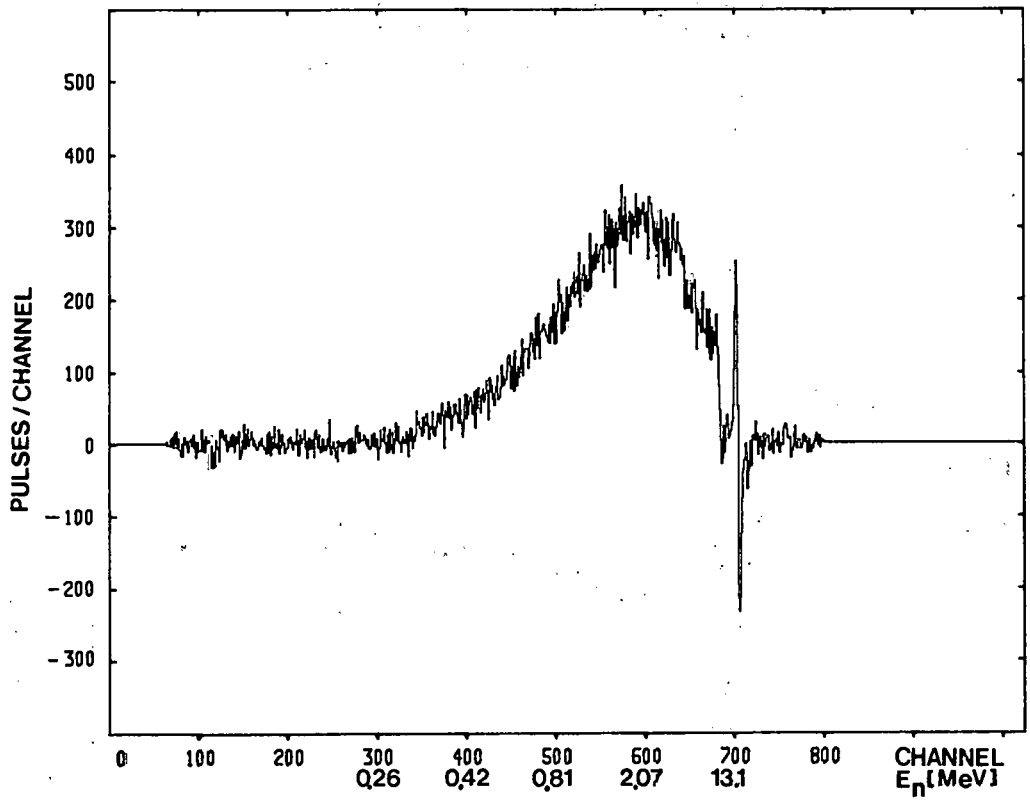

Fig. 6. Background-subtracted neutron time-of-flight spectrum from iron scatterer (difference of spectra 2b and 3b)

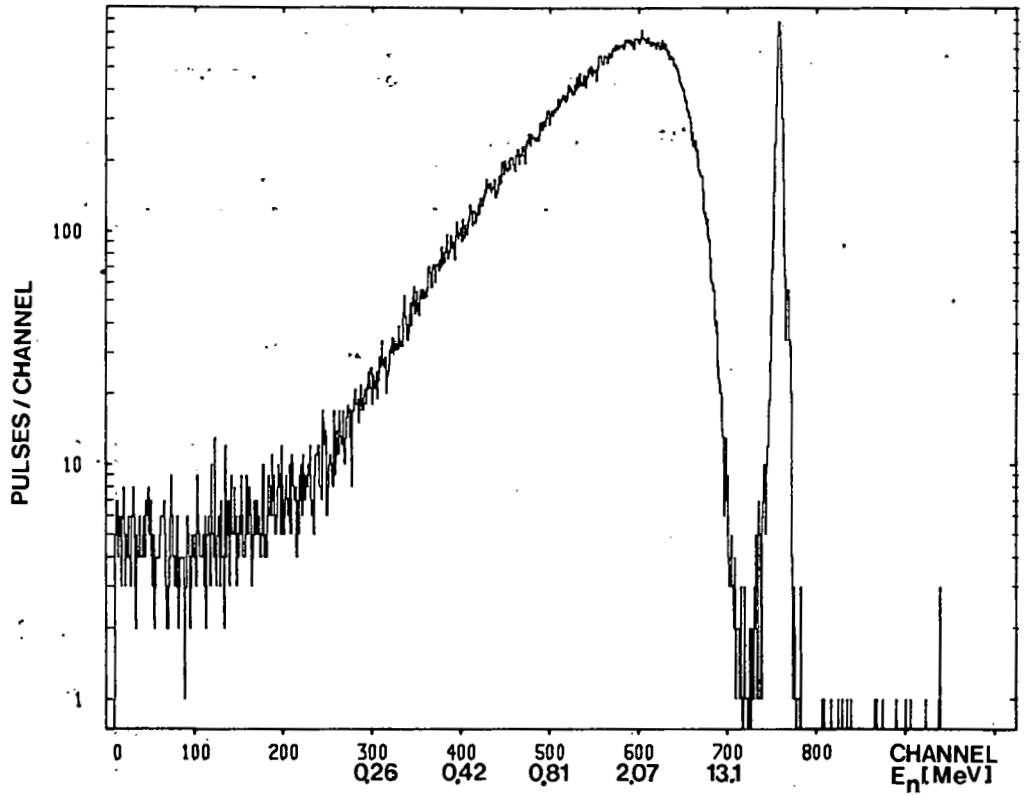

Fig. 7. Time-of-flight spectrum of the ^{252}Cf source (with standard sorting conditions in TOF-E_{recoil} and E_{recoil}-PSD planes (see section 3A)

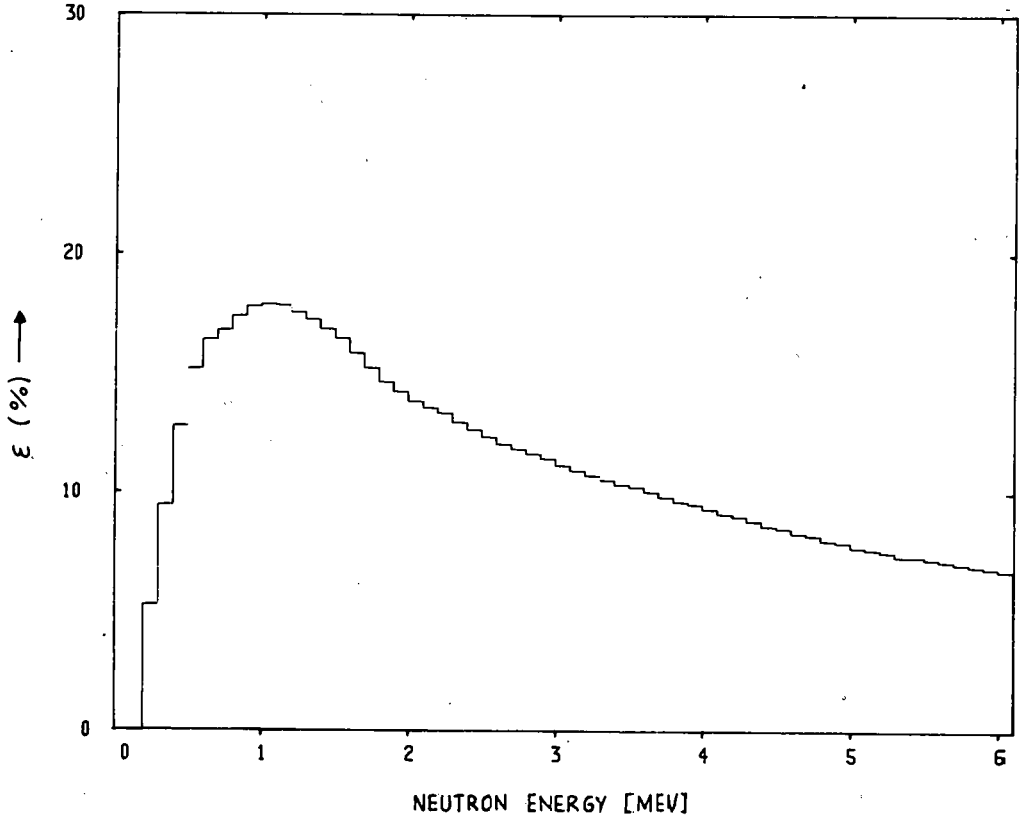

Fig. 8. Efficiency of neutron detector derived from ^{252}Cf spectrum of Fig. 6. (with E_{th} = 0.5 Americium $\hat{=}$ 135 keV E_{prot})

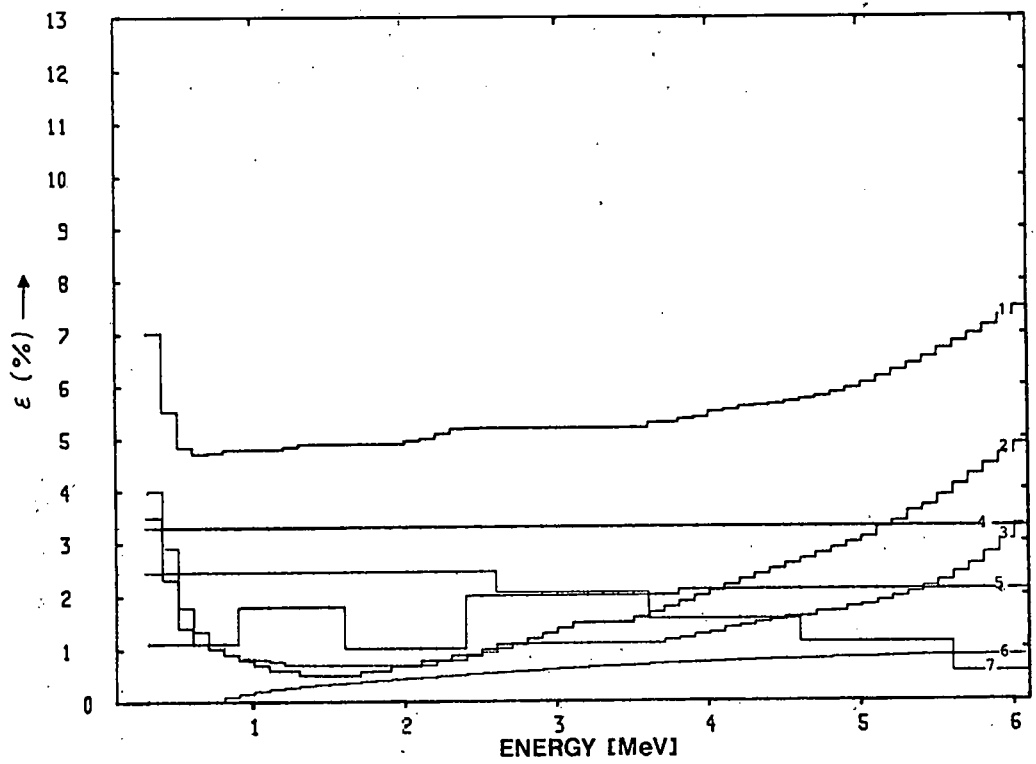

Fig. 9. Error contributions and total error in the determination of the neutron emission cross-sections of iron for 14.1 MeV neutrons. 1: total error, 2: statistical error, 3: error due to uncertainty in background normalization factor, 4: error in 14.7 MeV efficiency, 5: error of form of ^{252}Cf spectrum, 6: error of absorbtion correction, 7: error of multiple scattering correction.

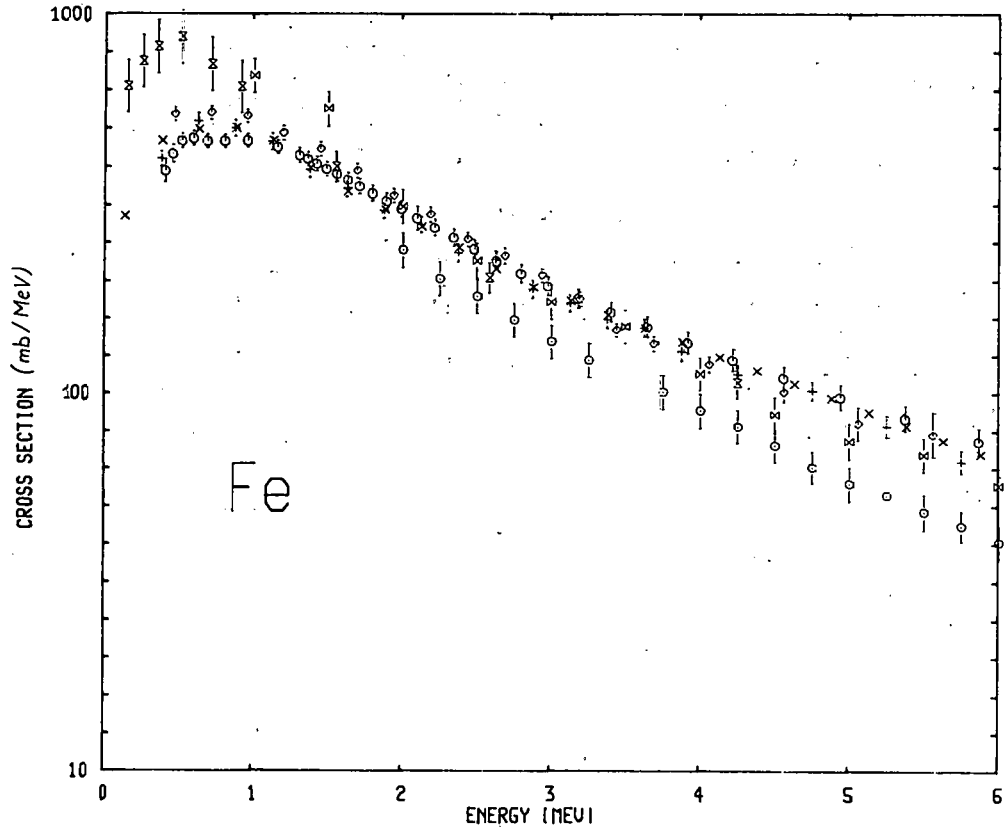

Fig. 10. Angle-integrated secondary neutron spectrum from interactions of 14.1 MeV neutrons with iron: + present result; ⊙ Hermsdorf et al. [5]; ⊙ Salnikov et al. [6]; ⧗ Clayeux [4]; x Schectman [1]; ◇ Stengl et al. [7]; x statistical model calculation.

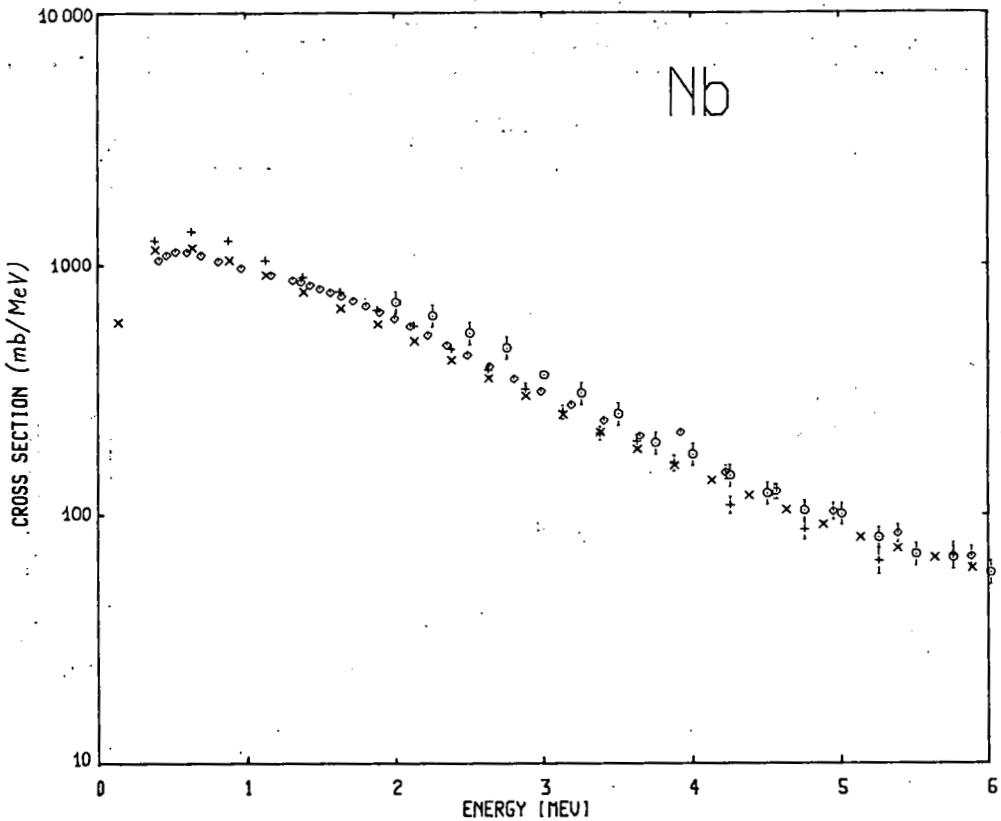

Fig. 11. Angle-integrated secondary neutron spectrum from interactions of 14.1 MeV neutrons with niobium: + present result; ⊙ Hermsdorf et al. [5] ⊙ Salnikov et al. [6]; x statistical model calculation.

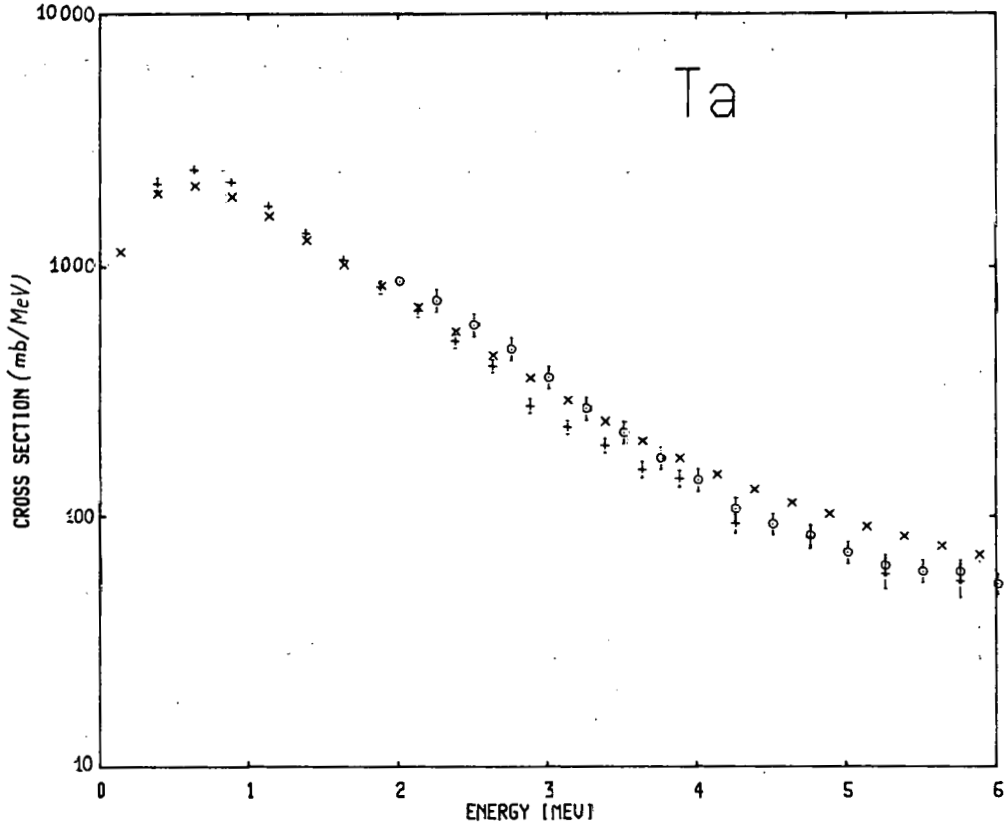

Fig. 12. Angle-integrated secondary neutron spectrum from interaction of 14.1 MeV neutrons with tantalum: + present result; ⊙ Hermsdorf et al. [5]; x statistical model calculation.

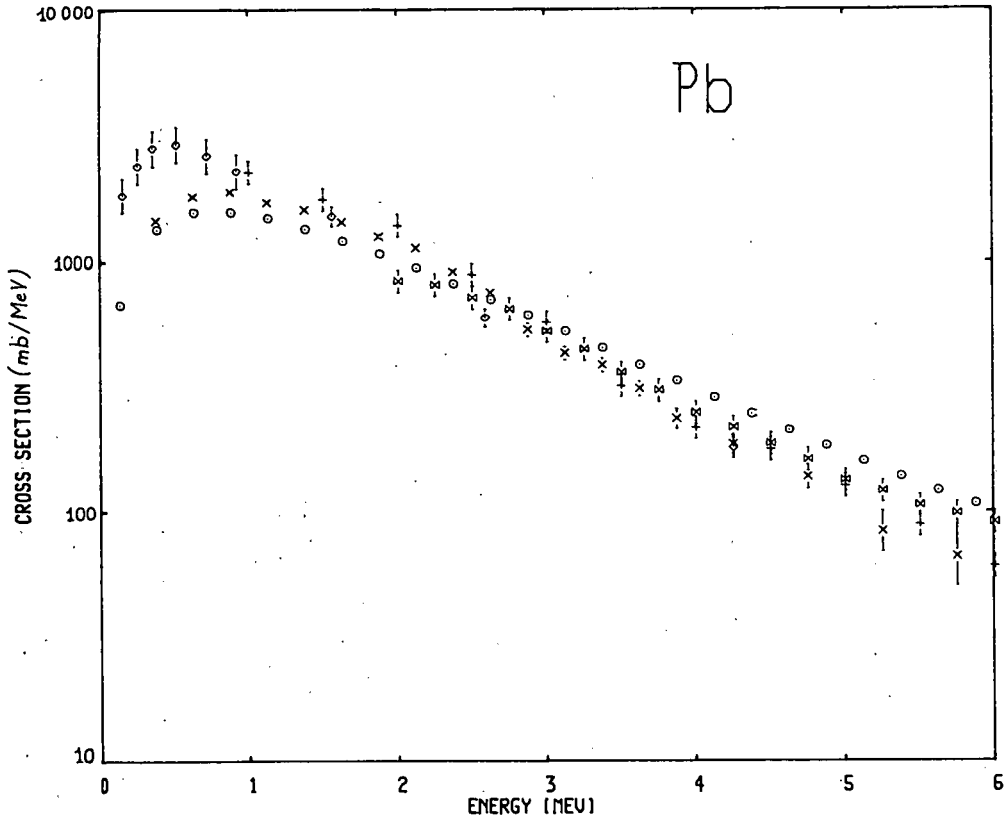

Fig. 13. Angle-integrated secondary neutron spectrum from interactions of 14.1 MeV neutrons with lead x present result; + Schectman [1]; ◇ Clayeux [4]; ⊠ Hermsdorf et al. [5]; ⊂ statistical model calculation.

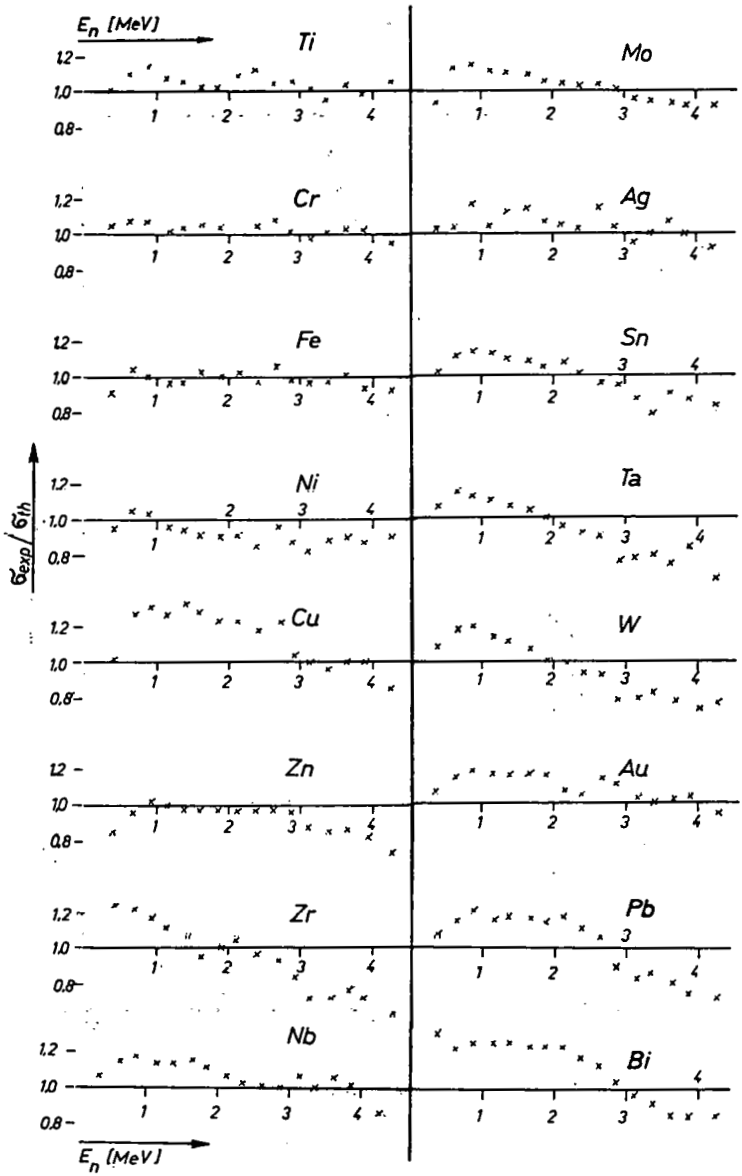

Fig. 14. Ratio of measured to calculated neutron emission cross-sections for all elements investigated.

DIFFERENTIAL SCATTERING CROSS SECTION MEASUREMENTS ABOVE 20 MeV*

R.W. Finlay and J. Rapaport

Ohio University
Athens, Ohio 45701 U.S.A.

ABSTRACT

The status of differential elastic and inelastic neutron scattering data is reviewed in the energy region above 20 MeV from the time of the May 1977 Brookhaven Conference to the present. Substantial progress has been made in this area, and new information about the optical-model description of the nucleon-nucleus interaction has been obtained. Quantitative information about isovector effects in the optical model and in nuclear transition amplitudes is beginning to emerge. Technical limitations in the areas of source intensity, resolution and sample quality have restricted the domain of the measurements to nuclei with widely separated excited states and large natural abundances. Although several of these easily-measured cases remain to be studied, many of the nuclei that are most important to the fusion energy program remain inaccessible to present-day techniques.

INTRODUCTION

In May 1977, R.C. Haight [1] reviewed the status of differential elastic and inelastic neutron scattering data and concluded that, for En > 15 MeV and Z > 6, the field has only recently been attacked and much remains to be done. While it is still true that much remains to be done, it is encouraging to report that considerable progress has already been made. The total number of differential scattering cross section measurements for En > 20 MeV has increased by about one order of magnitude since that time.

*Supported by a grant from the National Science Foundation

In Table I we present a survey of new information on differential scattering [2-12]. The survey is not intended to be exhaustive. It was obtained by consulting the two supplements to CINDA-A (up to October 1979), the proceedings of the Knoxville conferences (November 1979), the Washington meeting of the American Physical Society, and recent issues of Physical Review and Nuclear Physics. We have also added two previously unreported measurements from our own laboratory. The survey included 29 differential elastic scattering angular distributions and 22 inelastic scattering angular distributions to resolved or nearly-resolved final states. In about one half of these cases the measurements have appeared in the literature in final published form and the cross section values have been deposited at the National Nuclear Data Center. Some very recent results are reported in Table II in the form of angle-integrated cross sections.

ELASTIC SCATTERING MEASUREMENTS

The measurement of elastic neutron scattering at energies well above the region of compound nucleus formation provides extremely valuable information toward the understanding of the nucleon-nucleus interaction in terms of an optical model potential. At the 1977 Brookhaven symposium, Rapaport et al. [13] outlined the goals of the program. Scattering from $T = 0$ nuclei is used to evaluate the real part Coulomb correction term in the optical potential [4]. Comparison of neutron and proton scattering from nuclei with $T \neq 0$ leads to an evaluation of the isovector potential strength [14]. Energy dependence of the potential parameters--in particular the energy dependent form of the imaginary potential--can be inferred from neutron elastic scattering over a wide range of energy [8,11]. A global set of optical model parameters has been developed for singly- and doubly-closed shell nuclei [15], and the extension of such a potential into regions of strong nuclear deformation has been investigated [4,8]. The usually-accepted $A^{1/3}$ dependence of the geometrical parameters in the model has been studied by measuring elastic scattering over a long isotopic sequence [10].

Recent measurements from Michigan State University at En = 30 and 40 MeV [2,16] have generally confirmed and extended the energy dependence of the potential parameters reported by earlier investigators. Moreover, the variation of the volume integral of the imaginary potential for ^{40}Ca gives empirical evidence of the predicted [17] but elusive imaginary part of the Coulomb correction term [18].

In general, the recent work on elastic neutron scattering at En > 20 MeV can be well described in terms of an optical model potential with parameters which vary smoothly with energy, isospin and mass number. However, there are several major gaps

in the data. The odd-A nuclei have not been studied, and the deformed nuclei have not received adequate attention in this energy region. Furthermore, the light nuclei need to be examined in much greater detail. In Fig. 1 we present some recent measurements of elastic scattering from ^{16}O and ^{18}O at 24 MeV [3]. The solid lines are optical model fits to the data which are reasonably good except in the backward direction. When this potential model is used to fit 14 MeV data from each isotope, the energy dependence of the best-fit parameters is considerably faster than we have observed with heavier nuclei.

Finally, it should be mentioned that little or no polarization data exists for En > 20 MeV. Consequently, parameters for the spin-orbit potential are borrowed from proton scattering. A few well-selected polarization measurements would be needed to establish the correctness of this practice.

INELASTIC SCATTERING

Inelastic scattering of nucleons from nuclei tends to populate selectively those final states which have strong collective properties. For closed shell nuclei, the collective states are most simply described as vibrations of the nuclear density about the spherical equilibrium shape, and the transition strengths are characterized in terms of deformation parameters. A microscopic description of these transitions would seek to unfold the separate contributions of the target neutrons and target protons to the collective vibration. These contributions can be parameterized in terms of isoscalar and isovector deformation parameters, β_0 and β_1, or in terms of the reduced proton and neutron matrix elements, Mp and Mn. A complete description of the process must take into account the competing effects of shell closure and core polarization.

Information about isovector deformations has been difficult to obtain, but a careful comparison of the differences between proton and neutron scattering to the first 2^+ states in single-closed-shell nuclei has yielded a consistent picture of the process [19]. In Fig. 2 we compare neutron [3] and proton [20] inelastic scattering to the 2^+ state at 1.98 MeV in ^{18}O. Both sets of data are described in terms of an isospin-consistent optical model potential which fits the elastic scattering data of Fig. 1. In Fig. 3 we show inelastic scattering cross sections to the first 2^+ and 3^- states in ^{58}Ni and ^{60}Ni [7]. The corresponding elastic scattering is shown in Fig. 4. For the nucleus ^{18}O as well as for the Ni isotopes the deformation parameters are large enough that the coupled-channel Born Approximation (CCBA) should be considered as well as the Distorted Wave Born Approximation in calculating the direct reaction cross section. Both calculations fit the data rather well in all cases, but slightly different parameters are required for the different calculations.

Comparisons of the type shown in Fig. 2 have been carried out for quadrupole-vibrational states in seven closed-proton-shell nuclei (Z = 8,28,50) with the general result that the isovector deformation parameter is substantially larger than the isoscalar parameter: $2\beta_0 \lesssim \beta_1 \lesssim 6\beta_0$. For closed-neutron shell nuclei [21] the isovector parameter is smaller than the isoscalar parameter and of opposite sign ($\beta_1 \simeq -0.6\beta_0$). Both of these results are in good accord with theoretical expectations [19,22].

While these results indicate that neutron inelastic scattering cross sections cannot be accurately predicted from proton scattering data alone, the effect is not large in some cases. For example, within the accuracy of presently-available measurements, no significant difference between the deformation parameters derived from neutron and proton scattering has been found for 3^- states for either the N = 50 or Z = 50 nuclei [23]. Of course, for T = 0 nuclei (^{16}O, ^{40}Ca), and perhaps also for doubly-closed-shell nuclei, neutron- and proton-induced deformation should be the same; as far as we now know, they are [12].

Not all of the spectroscopic information discussed above was obtained at En > 20 MeV. In fact there are excellent reasons [9] for studying neutron inelastic scattering at En < 15 MeV not the least of which is the better energy resolution of a time-of-flight spectrometer. For light nuclei, however, freedom from the compound-nucleus reaction mechanism is not obtained at lower energies. For ^{16}O the neutron inelastic scattering measurements at 24 MeV shown in Fig. 5 are probably a more reliable source of deformation parameters than any of the published (p,p') measurements which were performed at energies at which compound nuclear resonances are prominent.

PROBLEMS AND PROSPECTS

Examination of Table I indicates that experimental studies of neutron scattering at En > 20 MeV has been sharply focussed on those few target nuclei that are not too difficult to study. The Ohio University Tandem Van de Graaff produces an excellent pulsed beam with burst duration of about 600 picoseconds FWHM, yet it is difficult to obtain an overall spectrometer resolution of much better than 700-800 keV (FWHM) for 26 MeV neutrons. Since the first inelastic peak in the spectrum is rarely more than a foothill next to the elastic scattering peak, a statement of ΔE ($FW\frac{1}{10}M$) might be more appropriate. In practice, the measurement of inelastic scattering to the strong 2^+ state at 1.33 MeV in ^{60}Ni is close to the limit of our present technology.

For nuclear spectroscopy of the heavy nuclei it makes good sense to lower the neutron energy to 10-11 MeV and enjoy an energy resolution of 200-300 keV. For the data needs of the fusion energy program and the neutron radiotherapy program and for the spectroscopy of light nuclei, this solution is unacceptable. The nuclei of many important structural materials

(^{27}Al, ^{46,48}Ti, ^{56}Fe, ^{63,65}Cu) have excited states too close to the ground state to be studied by presently available techniques.

A new time-of-flight spectrometer is being developed at Ohio University which should provide a workable solution to the energy-resolution limitation. The system is based on the Michigan State University Beam Swinger Magnet which was used to obtain the 30 to 40 MeV data cited in Table I. A single, well-shielded neutron detector can be located at flight paths between 4 and 30 meters. Differential cross sections are measured by varying the direction of the incident beam while leaving the position of the detector fixed. Resolution should improve by a factor of three to five, and new detector designs should help to keep the data rate close to present values. Nonetheless, an experiment such as ^{63}Cu(n,n') will require about 300 hours of data acquisition time. It is, therefore, very important that a clear statement of priorities emerge from meetings such as these.

ACKNOWLEDGMENTS

The authors wish to thank R.P. DeVito and S.M. Austin for communicating some of their data prior to publications. They also wish to thank the large group of graduate students and colleagues whose hard work made possible the results presented and referred to here.

REFERENCES

1. R.C. Haight, "Review of Neutron Data: 10 to 40 MeV," in Proc. Symp. on Neutron Cross Sections from 10 to 40 MeV, BNL-NSC 50681, Brookhaven National Laboratory (1977), p 201.

2. R.J. DeVito, "Determination of the Coulomb Correction and Isovector Terms of the Nucleon-Nucleus Optical Model Potential from Neutron Elastic Scattering at 30.3 and 40 MeV," Dissertation, Michigan State University (1979).

3. P. Grabmayr, J. Rapaport and R.W. Finlay, "Elastic and Inelastic Scattering of 24 MeV Nucleons from Oxygen Isotopes," Nucl, Phys. (submitted for publication).

4. J. Rapaport et al., "Neutron Elastic Scattering on T = 0 Nuclei," Nucl. Phys. A286, 232 (1977).

5. Present work. See Table II.

6. Y. Yamanouti, "Elastic and Inelastic Scattering of 21.5 MeV Neutrons from ^{32}S," Nucl. Phys. A283, 23 (1977).

7. Y. Yamanouti et al., "Elastic and Inelastic Scattering of 24 MeV Neutrons from Even Isotope of Ni," in Proc. Int. Conf. on Neutron Cross Sections for Technology, Knoxville, 1979 (to be published).

8. J. Rapaport et al., "Neutron Elastic Scattering from ^{92,96,98,100}Mo between En = 7 and 26 MeV," Nucl. Phys. A313, 1 (1979).

9. R.W. Finlay et al., "Isospin Effects in Nucleon Inelastic Scattering from Single-Closed Shell Nuclei," Nucl. Phys. A338, 45 (1980).

10. J. Rapaport et al., "Neutron Elastic Scattering from ^{116,118,120,122,124}Sn," Nucl. Phys. (to be published).

11. J. Rapaport et al., "Neutron Scattering from ^{208}Pb," Nucl. Phys. A296, 95 (1978).

12. D.E. Bainum et al., "Excitation of Low-Lying Collective States in ^{40}Ca and ^{208}Pb by Inelastic Neutron Scattering," Phys. Rev. C16, 1377 (1977).

13. J. Rapaport et al., "Neutron Scattering Measurements at Ohio University in the Energy Range from 7 - 26 MeV," in Proc. Symp. on Neutron Cross Sections from 10 to 40 MeV, BNL-NCS 50681, Brookhaven National Laboratory (1977), p 257.

14. J. Rapaport, "Determination of the Macroscopic Isovector Potential from Nucleon-Nucleus Scattering," in Proc. Conf. on the (p,n) Reaction and the Nucleon-Nucleon Force, Telluride, Colorado, Plenum Press, New York (1980).

15. J. Rapaport, V. Kulkarni and R.W. Finlay, "A Global Optical Model Analysis of Neutron Elastic Scattering Data," Nucl. Phys. A330, 15 (1979).

16. S.M. Austin, private communication.

17. J.-P. Jeukenne, A Lejeune and C. Mahaux, "Microscopic Calculation of the Symmetry and Coulomb Components of the Complex Optical-Model Potential," Phys. Rev. C15, 10 (1977).

18. J. Rapaport, "The Coulomb Correction Term in Proton Absorbing Optical Potentials," Phys. Lett. (to be published).

19. R.W. Finlay et al., "Isovector Deformation Parameters and Core Polarization," Phys. Lett. 84B, 169 (1979).

20. J.L. Escudie et al., "Macroscopic and Microscopic Model Analysis of Polarized Protons Scattering on ^{18}O," Phys. Rev. C10, 1645 (1974). See also Phys. Rev. C11, 639 (1975).

21. D.E. Bainum et al., "Isospin Effects in Nucleon Inelastic Scattering from Single-Closed-Shell Nuclei," Nucl. Phys. A311, 492 (1978).

22. V.A. Madsen, V.R. Brown and J.D. Anderson, "Differences of Deformation Parameters β for Different Transition Mechanisms," Phys. Rev. C12, 1205 (1975).

23. R.W. Finlay et al., "Neutron Inelastic Scattering to Octupole States in Single-Closed-Shell Nuclei," Nucl. Phys. (submitted for publication).

TABLE I

Partial Survey of New Differential Scattering Measurements Since 1977

Nuclide	En (MeV)	Final States (J^π)	Lab	Ref.
^{12}C	40.0	0^+	MSU	2
^{16}O	24.0	$0^+,3^-,2^+$	Ohio	3
^{18}O	24.0	$0^+,2_1^+,2_2^+,3^-$	Ohio	3
^{28}Si	20	$0^+,2^+$	Ohio	4
	26	0^+	Ohio	4
	26	2^+	Ohio	5
	30.3	0^+	MSU	2
	40	0^+	MSU	2
^{32}S	20	$0^+,2_1^+$	Ohio	4
	21.5	$0^+,2_1^+,3^-$	JAERI	6
	26	0^+	Ohio	4
	26	$2_1^+,2_2^+,3^-$	Ohio	5
	30.3	0^+	MSU	2
	40	0^+	MSU	2
^{40}Ca	20	$0^+,3^-$	Ohio	4
	26	0^+	Ohio	4
	30.3	0^+	MSU	2
	40	0^+	MSU	2
^{58}Ni	24	$0^+,2^+,3^-$	Ohio	7
^{60}Ni	24	$0^+,2^+,3^-$	Ohio	7
$^{92,96,98,100}Mo$	26	0^+	Ohio	8
^{116}Sn	24	$0^+,2^+,3^-$	Ohio	9
^{118}Sn	24	0^+	Ohio	10
^{124}Sn	24	0^+	Ohio	10
^{208}Pb	20	0^+	Ohio	11
	26	$0^+,3^-,5^-$	Ohio	11,12
	30.3	0^+	MSU	2
	40	0^+	MSU	2

TABLE II

Angle-Integrated Scattering Cross Sections
for Resolved Final States

Nuclide	En	J^{π}	Excitation Energy (MeV)	$2\pi \int \sigma(\theta) \sin\theta \, d\theta$ (mb)	Uncertainty
^{16}O	24	0^+	0	1080	<5%
		3^-	6.13	57	20%
		2^+	6.92	36	20%
^{18}O	24	0^+	0	1110	<5%
		2_1^+	1.98	43	10%
		2_2^+	3.92	9	50%
		3^-	5.09	37	12%
^{28}Si	26	0^+	0	1040	<5%
		2^+	1.78	56	30%
^{32}S	26	0^+	0	983	<5%
		2^+	2.24	32	30%
		2_2^+	4.29	16	30%
		3^-	5.01	26	40%
^{58}Ni	24	0^+	0	1010	<5%
		2^+	1.45	28	12%
		3^-	4.47	14	18%
^{60}Ni	24	0^+	0	1067	<5%
		2^+	1.33	33.3	16%
		3^-	4.05	14.4	12%

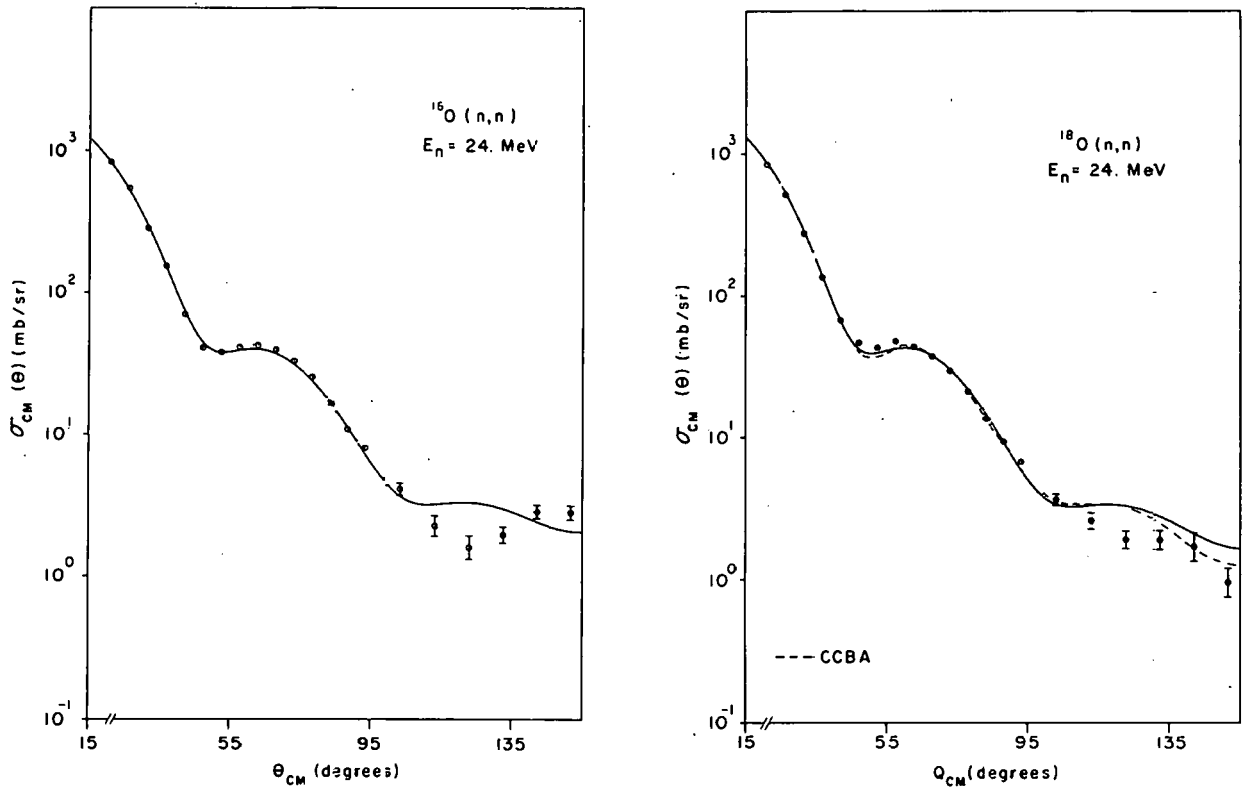

Fig. 1 Elastic scattering of 24 MeV neutron from ^{16}O and ^{18}O. The solid lines are optical model calculations. The dashed line for ^{18}O shows the effect of coupling the first inelastic scattering channel.

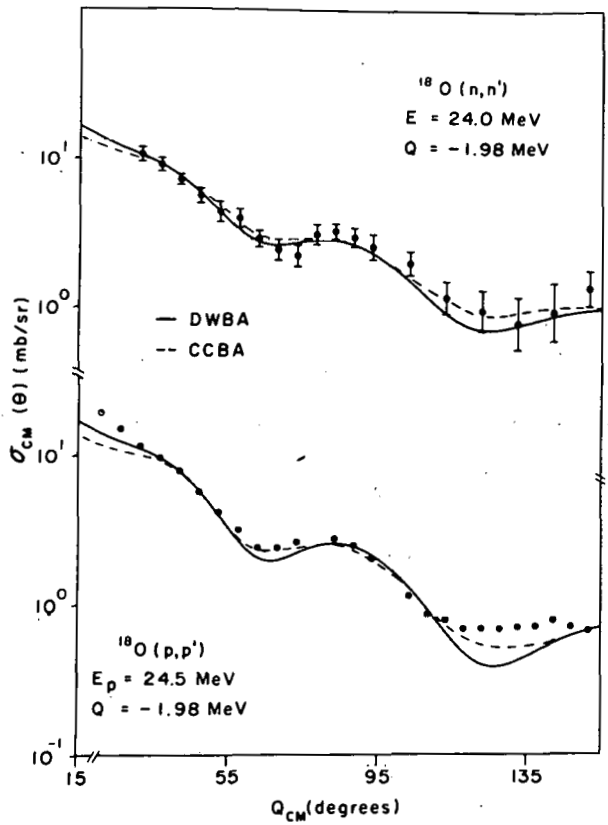

Fig. 2 Inelastic scattering of 24 MeV neutrons and 24.5 MeV protons from the 2^+ state at 1.98 MeV in ^{18}O. Solid lines are DWBA calculations and dashed lines are CCBA calculations. Proton and neutron optical model potentials are identical apart from the Coulomb correction term and the sign of the isovector term.

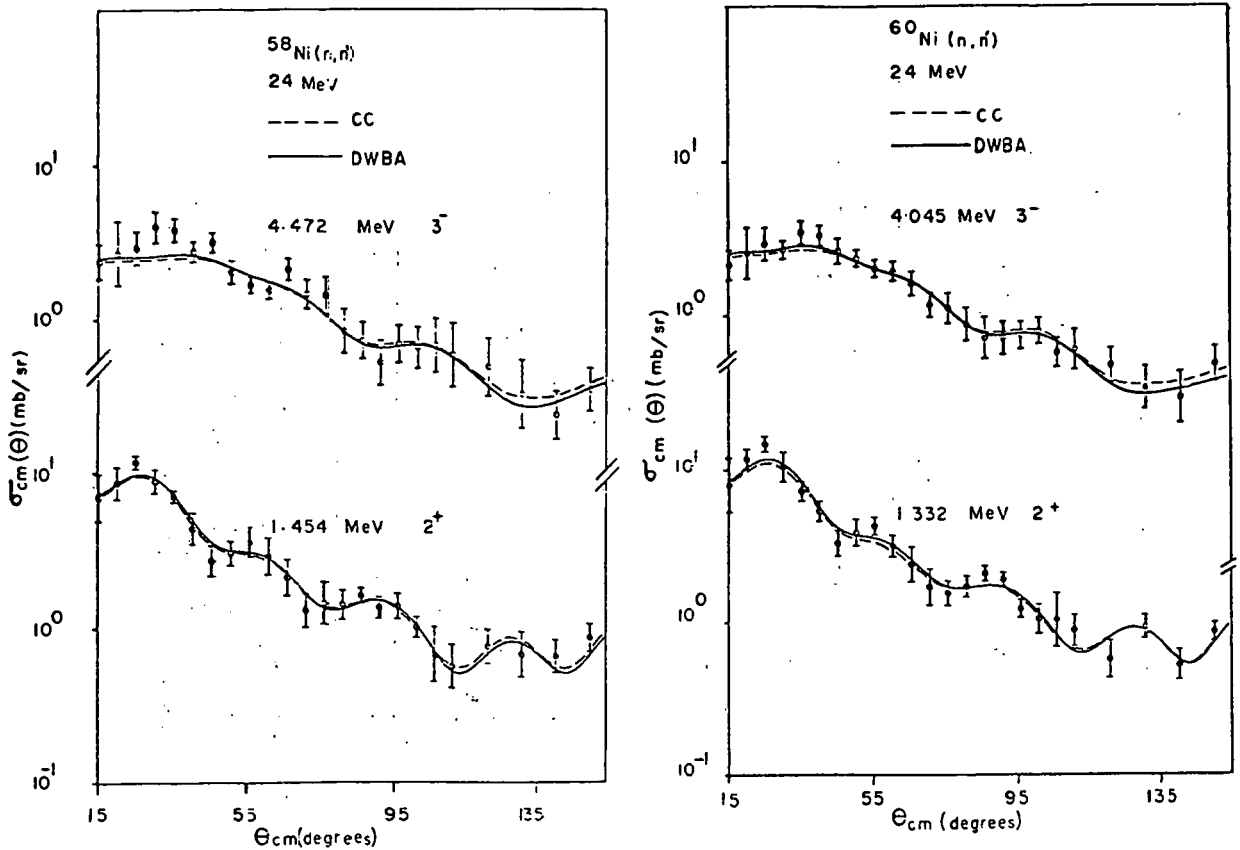

Fig. 3 Inelastic scattering of 24 MeV neutrons to the first 2^+ and 3^- states in ^{58}Ni and ^{60}Ni. Lines indicate the results of DWBA and CCBA calculations.

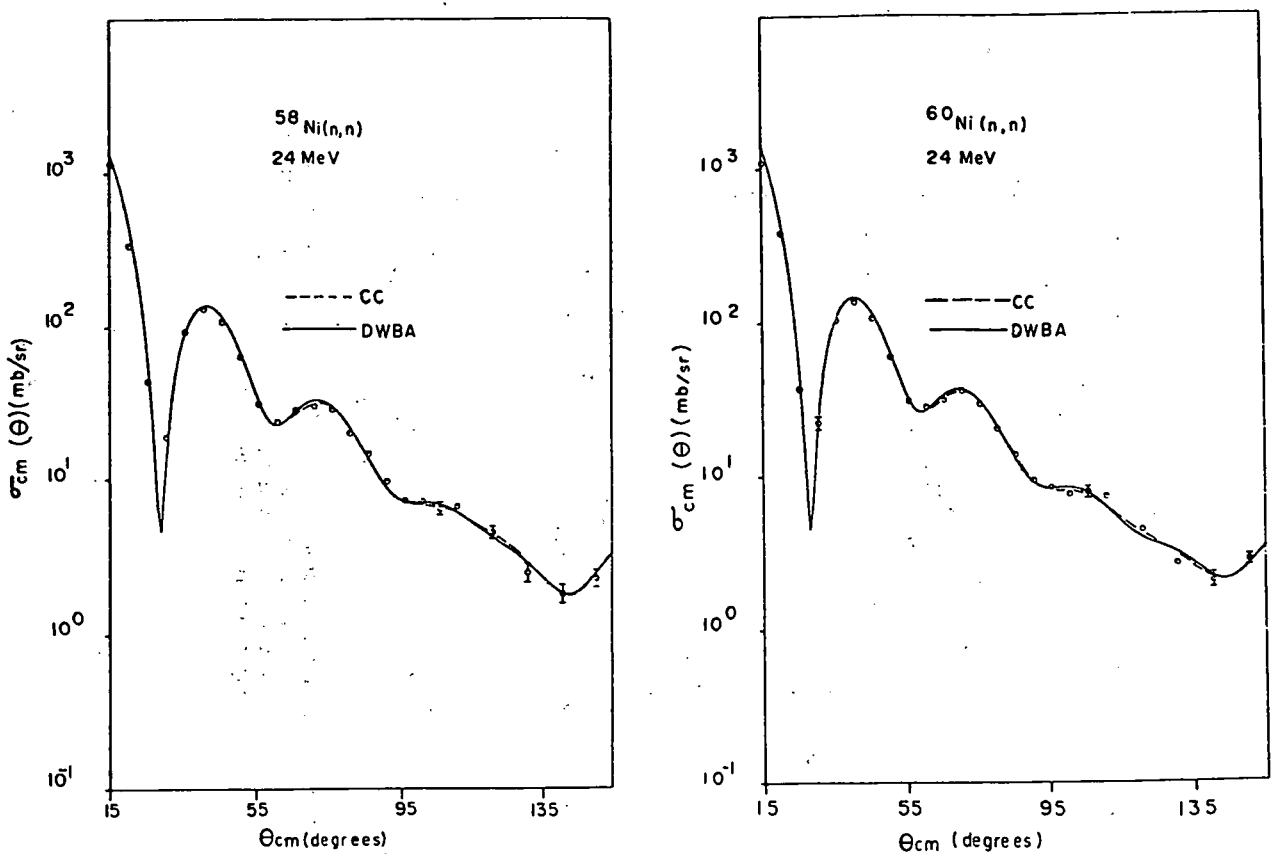

Fig. 4 Elastic scattering of 24 MeV neutrons from ^{58}Ni and ^{60}Ni. The solid lines are optical model calculations with the potentials which were used in Fig. 3.

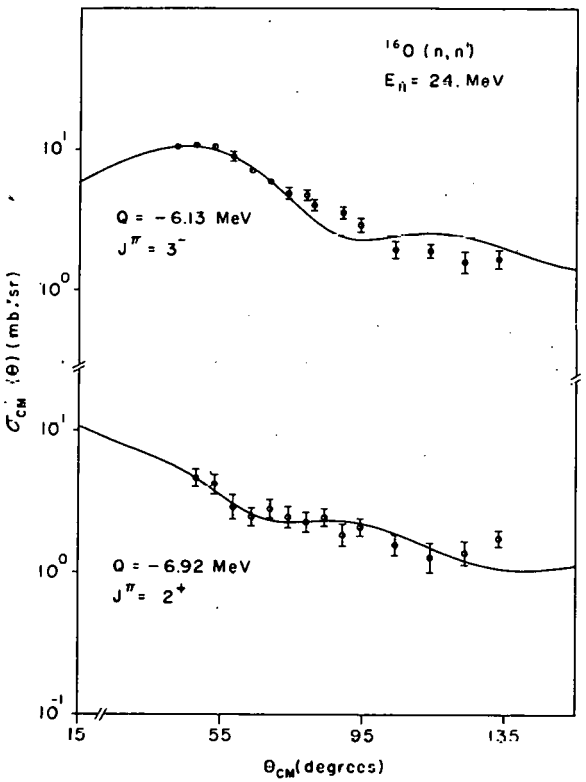

Fig. 5 Inelastic scattering of 24 MeV neutrons from the first and second excited states in ^{16}O. The angular range of the data is limited because of the presence of hydrogen scattering in the H_2O sample.

NEUTRON INDUCED CHARGED PARTICLE REACTION STUDIES AT OHIO UNIVERSITY

G. Randers-Pehrson, R.W. Finlay, P. Grabmayr, V. Kulkarni, R.O. Lane and J. Rapaport

Ohio University
Athens, Ohio 45701

ABSTRACT

We describe the Triplet Quadrupole Spectrometer now in use at Ohio University, emphasizing particularly those features which distinguish it from the similar device at Lawrence Livermore Laboratory. We also review the (n, charged particle) reactions presently under investigation.

INTRODUCTION

A large solid angle Triplet Quadrupole Spectrometer (TQS) is now in service at Ohio University. Combined with the pulsed beam from our tandem Van de Graaff, it provides a means to study charged particles emitted from materials under neutron bombardment. The two major projects under way at present are the study of biologically important elements for the National Cancer Institute and the study of structural materials for fusion reactors with support from the U.S. Department of Energy. We are also considering ways to use the TQS in more fundamental studies of nuclear structure and reaction mechanisms.

APPARATUS

The design of our spectrometer was inspired by the successful operation of a similar instrument at the RTNS facility at Lawrence Livermore Laboratory [1]. The general properties of these devices and their experimental uses have been recently reviewed by Laurent and Schapira [2]. The essential purpose of our TQS is to transport charged particles emitted from a target bombarded by neutrons to a detector telescope located at the focal point 3.4 meters away.

We are presently using telescopes with either two or three elements. A three element telescope is shown in Fig. 1. The second and third elements comprise a traditional ΔE + E telescope; typically a 30 μm silicon detector followed by a 1000 μm stopping detector. The first element is an electron-emitting foil and microchannel plate device more familiar to heavy ion research [3]. The foil is a 6 μg/cm^2 Formvar film [4] supported on a 97 percent transmission tungsten grid which is mounted over an aperture in a cylindrical segment electrode. The foil is held at -4 kV and a second cylindrical grid 0.5 cm away is biased to -2 kV. The 2 kV accelerating voltage directs the electrons emitted from the foil radially inward to a chevron channel electron multiplier (Galileo Electro Optics Model 3025).

Signals from the telescope are amplified by standard NIM electronics and then analyzed by the OUAL minicomputer [5]. Electronic logic requires that signals be present in the ΔE detector AND in either the channel plate or the stopping detector. This logic allows an automatic switch-over of the gating detector depending on whether the particle has long or short range. Gating signals are generated with essentially 100 percent efficiency for long range particles, whereas those particles which stop in the ΔE detector can still be detected but at a lower efficiency. The efficiency is limited by the small number of electrons kinematically emitted by light ions. A beryllium-copper alloy salvaged from the dynodes of a damaged phototube was evaporated on the inside surface of the foil to enhance electron emission. No improvement in efficiency was obtained for several other surface treatment beyond the use of about 12 μg/cm^2 of the Be-Cu alloy.

For each event, the minicomputer calculates a number proportional to the particle mass using the energy signals and time of flight measured relative to a capactive beam pick off in the formula:

$$M = (E + \Delta E) * (TOF - T_0)^2$$

where T_0 is the time corresponding to the arrival of neutrons at the sample. An example of the mass identification spectrum for a thick target of enriched ^{6}Li metal is shown in Fig. 2. The peaks shift less than 0.5 channels as the spectrometer bandpass for the protons is varied from 1.0 to 23 MeV. The excellent mass resolution is not needed to separate real events from each other but to reduce the background from neutron events for which the energy in the detectors is not equal to the neutron energy. Digital gates are set on each peak and separate spectra are simultaneously accumulated for each mass number.

The energy dependence of the spectrometer solid angle is measured together with the neutron flux using the thick-target yield from polyethylene. The proton stopping power and H(n,p) cross section are unfolded from the polyethylene measurement to

obtain an acceptance function which is used to analyze spectra from the targets of interest.

MEASUREMENTS

The first measurements completed on the TQS were for reactions from neutron bombarding deuterium [6]. Elastic scattering angular distributions were measured at 9 and 11 MeV by observing the recoiling deutrons. Protons from deuterium breakup by 11 and 25 MeV neutrons were also measured in the region of enhancement by the final state interaction of the (unobserved) neutrons. Analysis of the proton spectra using three-body Faddeev equations is nearly complete.

Measurements for DOE sponsored study of structural materials for fusion reactors are in progress. One of the interesting results from the Livermore TQS was the observation of large cross sections for the production of low energy protons from nuclei which have a neutron separation energy greater than that for protons [7,1]. For these nuclei it is possible for inelastic scattering to excite states for which proton emission competes only with gamma-ray emission. We are presently studying one of those nuclei, namely ^{58}Ni, in the region where the (n,np) channel is just opening. Preliminary spectra of protons and alpha particles observed at 120° from 11 MeV neutrons on ^{58}Ni are shown in Fig. 3. Spectra have also been obtained at 8 MeV and at 0°, 60° and 120°. At 8 MeV, which is below the threshold for (n,np), the excess of low energy protons observed at 14 MeV is not seen. At 11 MeV, which is above the threshold, low energy protons are present but are strongly forward peaked--a surprising result if the particles result from two steps of nuclear evaporation. It is possible that the low energy protons result from ^{58}Ni (n,p) induced by low energy neutrons from deutron breakup in D(d,n) source reaction. Alternatively, they are due to quasi-elastic (n,p) scattering or another direct process. These possibilities will be examined in our next run using a dummy gas to produce a breakup spectrum without the monoenergetic peak [8].

Another project which is ongoing is the study of charged particles emitted from biologically important materials under the sponsorship of the National Cancer Institute. The angular distribution of the $^{12}C(n,\alpha_0)^9Be$ has been measured at 9.3 MeV to compare with the inverse reaction. We have also observed the continuum from $^{12}C(n,n'3\alpha)$ from outgoing alpha particle energies down to 1 MeV as shown for example from 10.5 MeV neutrons in Fig. 4.

We are presently attempting to extend both the ^{58}Ni and ^{12}C measurements above 20 MeV. We will refine our low energy measurements and extend them to other nuclei of interest to DOE and NCI.

ACKNOWLEDGMENTS

We wish to acknowledge the contributions to this project by Steve Grimes who visited Ohio University from Lawrence Livermore Laboratory last year. We thank also D. Carter, whose design, construction and programming of the minicomputer have been essential to this work.

REFERENCES

1. K.R. Alvar, H.H. Barshall, R.R. Borchers, S.M. Grimes and R.C. Haight. "Detection System for Charged Particles Produced by Neutrons." Nucl. Inst. and Meth. 148, 303 (1978)

S.M. Grimes, R.C. Haight, J.D. Anderson, K.R. Alvar and R.R. Borchers, "Development of a Spectrometer for the Measurement of (n,xp), (n,xd) and (n,xα) Cross Sections, Angular Distributions and Spectra at En = 15 MeV," Proc. Symposium of Neutron Cross Sections 10-40 MeV, May 1977, Brookhaven, New York, BNL-NCS 50681

S.M. Grimes, R.C. Haight, K.R. Alvar, H.H. Barshall and R.R. Borchers, "Charged-particle Emission in Reactions of 15-MeV Neutrons with Isotopes of Chromium, Iron, Nickel and Copper," Phys. Rev. C19, 2127 (1979)

R.C. Haight and S.M. Grimes, "Status of (n, charged particle) Measurements at LLL," Proc. Symposium on Neutron Cross Sections from 10-50 MeV, May 1980, Brookhaven, New York

2. H. Laurent and J.P. Schapira, "Magnetic Quadrupole and Solenoidal Spectrometers," Nucl. Inst. and Meth. 162, 181 (1979)

3. J.L. Wiza, "Microchannel Plate Detectors," Nucl. Inst. and Meth. 162, 587 (1979)

4. R.J. Grader, R.W. Hill, C.W. McGoff, D.S. Salmi and J.P. Stoering, "The Preparation of Large Plastic Films for Proportional Counter Windows," Rev. Sci. Inst. 42, 465 (1971)

5. D.E. Carter, "A High-Speed, Economical Minicomputer," Nucl. Inst. and Meth. 160, 165 (1979)

6. V. Kulkarni, S.M. Grimes, P. Grabmayr, G. Randers-Pehrson, R. Finlay and J. Rapaport, "Study of Neutron-Induced Charged Particle Reactions on Deutrium Using a Quadrupole Triplet Spectrometer," Proc. Int. Conf. on Nuclear Cross Sections for Technology, Knoxville, 1979, to be published

7. S.M. Grimes, R.C. Haight and J.D. Anderson, "Measurement of Sub-Coulomb-Barrier Charged Particles Emitted from Aluminum and Titanium Bombarded by 15-MeV Neutrons," Nucl. Sci. and Eng. 62, 187 (1977)

8. P. Grabmayr, J. Rapaport, R.W. Finlay, V. Kulkarni and S.M. Grimes, "A Study of Neutron Source Reactions," Proc. Int. Conf. on Nuclear Cross Sections for Technology, Knoxville, 1979, to be published

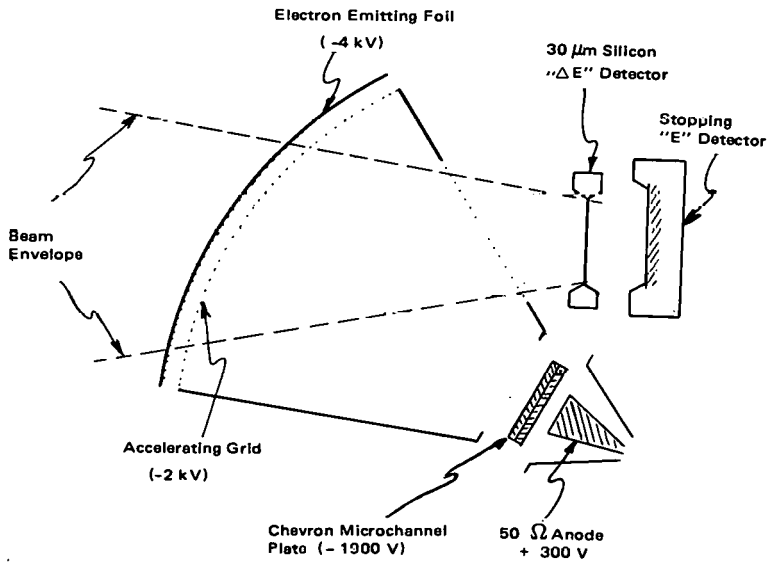

Figure 1 Three element detector telescope used at the focal point of the spectrometer.

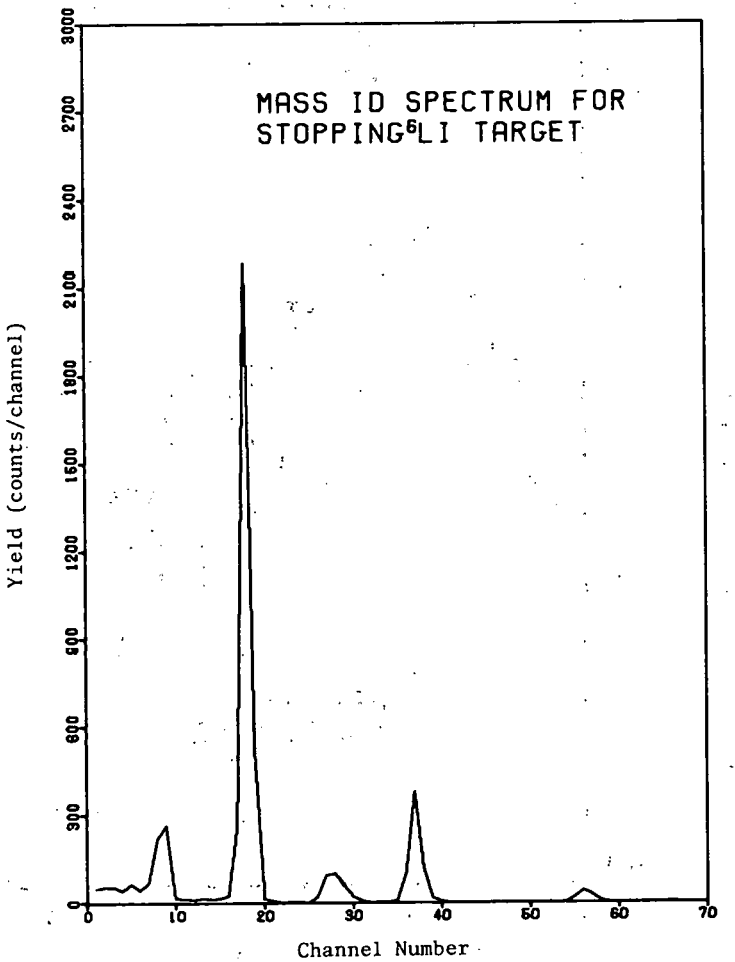

Figure 2 Mass identification spectrum for stopping ^{6}Li met target.

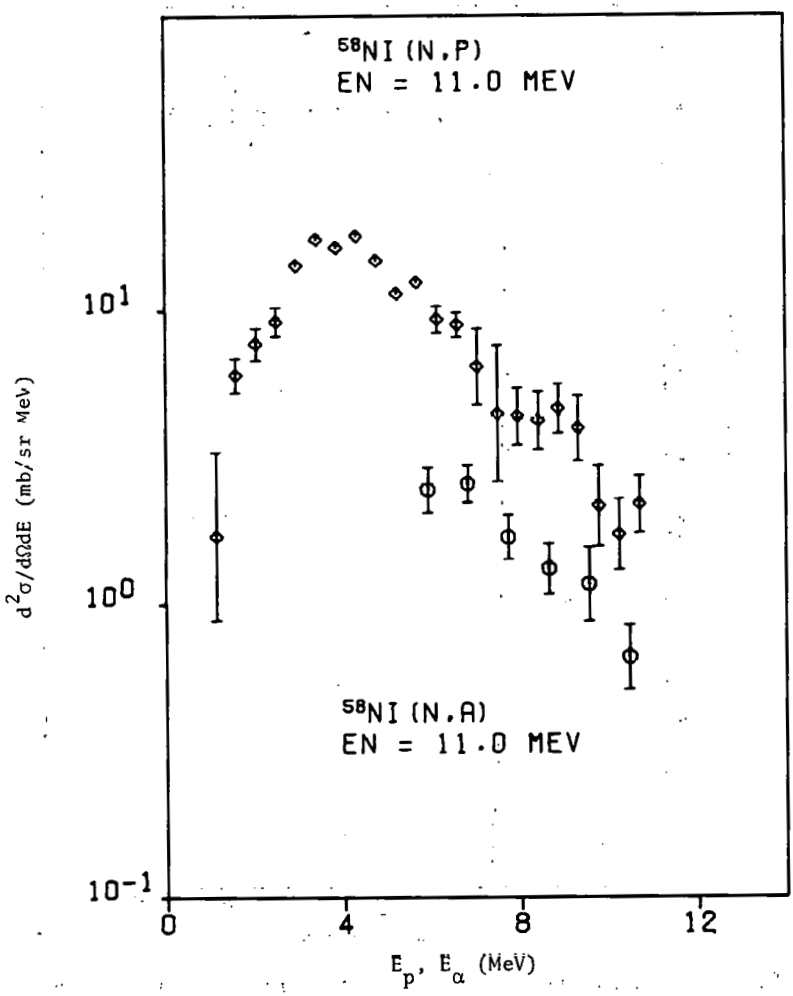

Figure 3 Doubly differential cross section for ^{58}Ni(n,xp) observed at 11 MeV and 120°.

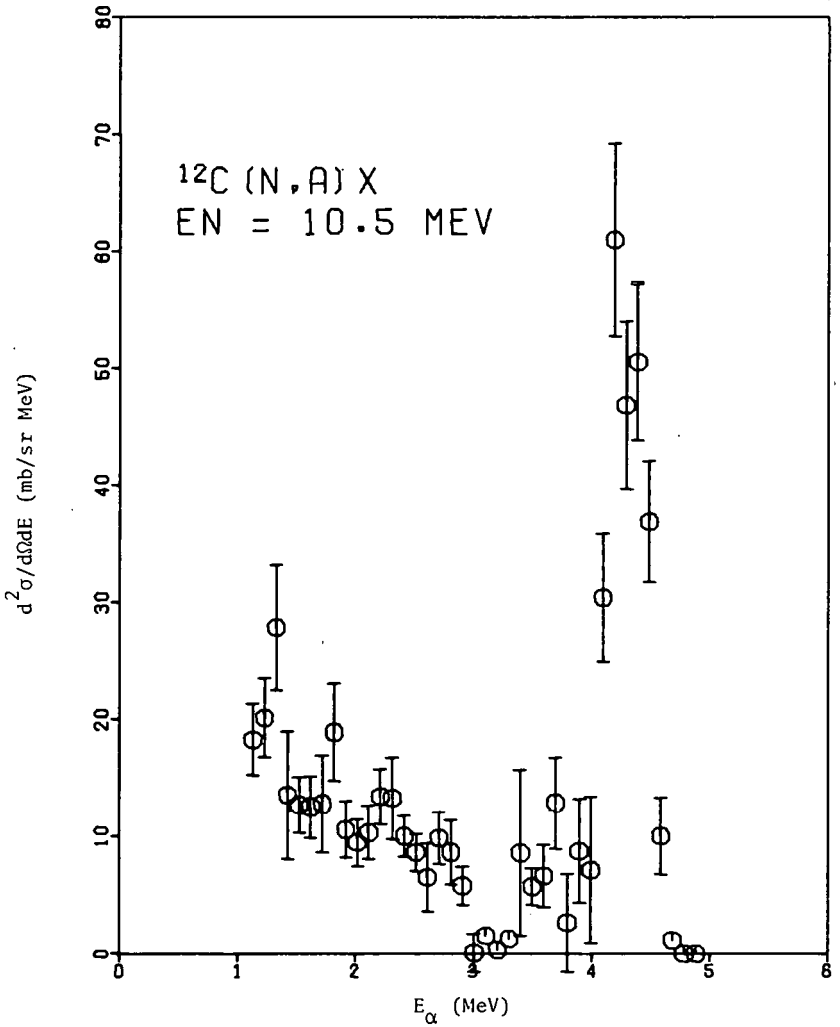

Figure 4 Doubly differential cross section for $^{12}C(n,\alpha)$ observed at 10.5 MeV and 0°.

THIS PAGE
WAS INTENTIONALLY
LEFT BLANK

STATUS OF (n,2n) CROSS SECTION MEASUREMENTS AT BRUYERES-LE-CHATEL

J.FREHAUT, A.BERTIN, R.BOIS and J.JARY

Service de Physique Neutronique et Nucléaire
Centre d'Etudes de Bruyères-le-Châtel
B.P. 561
92542 MONTROUGE CEDEX, France

ABSTRACT

Cross sections for the (n,2n) reactions have been measured between threshold and 15 MeV for about 50 elements and separated isotopes using the large gadolinium-loaded liquid scintillator method and the 7 MV tandem Van de Graaff accelerator of Bruyères-le-Châtel as a pulsed neutron source. The (n,2n) cross sections have been normalized to the fission cross section of ^{238}U ; they are obtained with a relative accuracy of 4% to 10%.

The systematic trends of the data obtained on series of separated isotopes are discussed, and some comparisons with statistical model calculations are presented.

INTRODUCTION

The large gadolinium-loaded liquid scintillator method has been used for several years at Bruyères-le-Châtel to measure the (n,2n) cross sections in the energy range from threshold to 15 MeV. It relies on the direct detection of the emitted neutrons, and therefore it can be used for any natural element or separated isotope, whereas the more common activation method is limited to nuclides which leave a suitably active residual isotope.

The aim of this paper is to give a general outline of the experimental method and to present a comprehensive view of the data obtained for more than 50 natural elements or separated isotopes.

EXPERIMENT

The method used to make the measurements is described in detail in ref. [1]. A schematic of the experiment is shown in fig. 1. A pulsed beam of neutrons was collimated and allowed to irradiate

a sample placed at the center of a large gadolinium-loaded liquid scintillator. A (n,2n) event occuring during a pulse was identified by two separate delayed pulses from the liquid scintillator.

Incident neutrons in the energy range from 6 to 15 MeV were produced by the D(d,n)^{3}He reaction in a 10 cm long gaseous target containing deuterium at a pressure of 1 atm. The deuteron beam was provided by the 7 MV Van de Graaff tandem at Centre d'Etudes de Bruyères-le-Châtel. The neutron beam was collimated onto the sample placed at the center of the detector, a distance of 2.5 m from the neutron source.

The neutron detector is a large spherical tank containing 250 liters of a gadolinium-loaded liquid scintillator and surrounded by 12 photomultiplier tubes. Neutrons emitted by the sample enter the liquid where they are moderated and then captured by the gadolinium nuclei. The neutrons spend an average time of 11 μs in the scintillator before capture, and 95% of the captures occur within 30 μs. The scintillations caused by the resulting capture γ-rays are viewed by the photomultiplier tubes. The dead time of the electronics was 120 ns, so that the captures could be counted individually. A (n,2n) event occuring during a neutron pulse was identified by the presence of two capture pulses within the following 30 μs.

In the particular case of fissionable materials, fissions can also be induced during the neutron pulses, yielding a number of neutrons from 1 to about 10, which cannot be experimentally distinguished from those of (n,2n) or (n,3n) reactions.

However, events with more than 3 neutrons can only result from fission in the incident neutron energy range below 15 MeV considered here. The total number of fissions can thus be calculated from the distributions of events with more than 3 neutrons, by using the fission neutron multiplicity distributions previously measured [2]. The number of fissions giving 2 or 3 neutrons can then be determined and subtracted from the observed rate, to give the true number of (n,2n) and (n,3n) events.

The principle of the measurement limits the repetition period of the neutron beam pulsing to 60 μs in order to avoid problems with overlaps. This requirement was met by chopping the deuteron beam already pulsed conventionally at a repetition rate of 2.5 MHz in such a way as to keep 3 bursts 2 ns wide 400 ns apart every 60 μs. This fine structure allows one to measure the incident neutron energy spectrum, and at the same time to maintain a sufficiently high neutron flux.

The incident neutron energy spectrum measurement is necessary to separate the monoenergetic neutrons from the D(d,n)^{3}He reaction which induces the (n,2n) events from the low energy neutrons resulting from the deuteron break up or (d,n) reactions on target materials. In the case of fissionable materials, fission events are also induced by the non-monoenergetic neutrons, and the apparent fission neutron multiplicity distributions as well as the apparent fission cross sections are determined using the measured energy spectrum.

The spectrum was measured by the time-of-flight technique (fig.1), using a small liquid scintillator associated with a fast photomultiplier tube located 1 m behind the large liquid scintillator tank (4 m from the neutron target). The relative detection efficiency was measured between 0.4 and 8 MeV relative to the ^{252}Cf spontaneous-fission energy spectrum and extrapolated to 15 MeV using a Monte Carlo code calculation.

No attempt was made to measure absolutely the incident neutron flux. In the case of fissionable materials, the method employed gave directly the ratio of the (n,2n) or (n,3n) cross section to the fission cross section. For the other nuclei, a run with a ^{238}U sample was included in every sequence, and the data were normalized to the ^{238}U fission cross section using the relative flux measurement.

DATA REDUCTION

Details on the corrections and cross section derivation are given in ref. [1]. The experimental data recorded for each run consisted of the distribution of the number of events as a function of the number of pulses counted. Five corrections were applied to obtain the multiplicities of neutrons emitted by the sample :

- Subtraction of the detector background, measured with the accelerator beam off.
- Correction for the detection dead time losses (dead time 120 ns).
- Multiple event correction : in some cases, the number of scattered neutrons was large enough that the probability of two single neutron events produced by the same incident neutron burst was not negligible compared to the number of (n,2n) events.
- Efficiency correction. The detection efficiency ($\sim$ 75%) was measured relative to the average number of prompt neutrons for the spontaneous fission of ^{252}Cf ($\bar{\nu}_p$ = 3.732 [3]). The measured efficiency was corrected for the difference in energy spectra between the fission neutrons and the neutrons from the (n,2n) reactions.
- Correction for events not induced in the sample, obtained from a run with the sample out.

For ^{238}U the resulting multiplicity distribution was used to determine the number of fissions and of (n,2n) events as discussed previously. For other nuclei, events with a multiplicity of 2 corresponded to the number of (n,2n) events and the cross section was determined relative to the ^{238}U fission cross section using the relative incident neutron flux measurement.

UNCERTAINTIES

Two sources of uncertainties have been considered. The first

one results from the statistical uncertainty in the measured distributions, which has been transmitted at each step of the corrections. The statistical uncertainty in measuring the efficiency has been included, but not the uncertainty in $\bar{\nu}_p$ for the ^{252}Cf standard. An uncertainty of 10% has been assumed in the correction for the difference in energy spectra for ^{252}Cf fission neutrons and those for (n,2n) reactions.

The second source of uncertainty is connected to the normalization procedure and results mainly from the uncertainties in the fission neutron multiplicities for the neutron induced fission of ^{238}U used to determine the number of fission events. This part represents about 60% of the quoted uncertainties below 13 MeV incident neutron energy, and up to 80% at 15 MeV, and therefore introduces strong correlations between the measured cross sections. The uncertainty in the reference ^{238}U fission cross section [4] has not been included.

RESULTS AND DISCUSSION

More than 50 nuclei have been measured in the energy range between threshold and 15 MeV since the first measurements in 1973. Partial results have been published [5-8]. The whole data have now been reanalysed on a common basis for corrections and normalization. Complementary measurements were made on several nuclei. The resulting (n,2n) and (n,3n) cross sections, normalized to the ^{238}U fission cross section as evaluated by SOWERBY et al. [4], are presented in tables I to XI.

The (n,2n) data on the natural elements Ti, V, Cr, Fe, Cu, Ga, Zr, Mo, W, Pt and Pb are given in tables I and II. For such direct measurements on non monoisotopic elements, it is necessary to use a method based on the direct detection of the emitted neutrons, such as the large liquid scintillator method. As far as we know, the only published data are from LASL and were obtained for Ti, V, Cr, Fe, Ni and Cu in the energy range from 14.7 to 21 MeV using a technique very similar to the one presented here [9].

The (n,2n) data on the natural monoisotopic elements ^{45}Sc, ^{59}Co, ^{89}Y, ^{93}Nb, ^{103}Rh, ^{169}Tm, ^{175}Lu, ^{181}Ta, ^{197}Au and ^{209}Bi are given in tables III and IV. ^{175}Lu and ^{181}Ta are only the major components of the natural elements. The measurements were made on natural elements and slightly corrected for the contribution of the other isotopes. The (n,2n) and (n,3n) cross sections for these nuclei have now been measured on the wide energy range from threshold to 24 MeV (28 MeV in several cases), using both the liquid scintillator and the activation method. All the data tend to agree quite well. A comparison of the most recent measurements is given in ref. [10].

The (n,2n) data for the even isotopes of Se, Nd, Sm, for ^{151}Eu, for the main isotopes of Gd, W, Tl and Pb, and for ^{238}U are given in tables V to X. These measurements were made on separated isotopes and bring appreciable information on the multiple neutron

emission mechanism. The data obtained for the Nd, Sm, Gd, W, Tℓ and Pb isotopes and for ^{209}Bi are plotted as a function of the mass number A for different values of the excess energy U_R above threshold in fig. 2.

For a given value of U_R, $\sigma(n,2n)$ is on the average an increasing function of A for each series of isotopes. For these nuclei, which have generally an excess of neutrons relative to the valley of stability, the binding energy of the last neutron decreases with increasing N-Z. Thus for constant U_R, the relative fraction of phase space available for the primary neutron emission leading to unbound states of the residual nucleus (secondary emission allowed) versus that leading to bound states (secondary emission not allowed) increases with N-Z, which qualitatively can explain the observed behaviour. However this behaviour seems to be also strongly influenced by the level density distributions.

In fig. 2 are also plotted the results of a statistical model calculation for the Nd and Sm isotopes [8]. The level density formalism from GILBERT and CAMERON [11] was adopted for the Nd isotopes, giving a satisfactory overall fit to the experimental data. However the same formalism failed in reproducing the experimental data for the Sm isotopes, and in that case the formalism of IGNATYUK et al. [12] seems to be more appropriate (fig. 2). Thus the (n,2n) cross sections on series of isotopes appear to be very sensitive to the local behaviour of the level density distributions.

For a given value of U_R, the cross sections measured for the isotopes having an odd number of neutrons (^{155}Gd, ^{157}Gd, ^{183}W and ^{207}Pb) are generally lower than those measured for the neighbouring even isotopes (fig. 2). A similar behaviour was obtained in the calculations on Nd and Sm isotopes [8].

Strong shell effects are also observed for the Tℓ and Pb isotopes, and to a lesser extent for ^{209}Bi, at excess energies lower than 5 MeV.

REFERENCES

1. J. FREHAUT, "Use of the Large-Gadolinium-Loaded Liquid Scintillator Technique for (n,2n) and (n,3n) Cross Section Measurements", Nucl. Inst. Meth. 135, 511 (1976).

2. M. SOLEILHAC, J. FREHAUT and J. GAURIAU, "Energy Dependence of $\bar{\nu}_p$ for Neutron Induced Fission of ^{235}U, ^{238}U and ^{239}Pu from 1.3 to 15 MeV", J. Nucl. Energy 23, 257 (1969).

3. E. J. AXTON, Panel on Standard Reference Data, I.A.E.A., Vienna (1972).

4. M. G. SOWERBY, B. H. PATRICK and D. S. MATHER, "A Detailed Report on the Simultaneous Evaluation of the Fission Cross Section of ^{235}U, ^{239}Pu and ^{238}U and the ^{238}U Capture Cross Section in the Energy Range 100 eV to 20 MeV" AERE-R-72/73, U.K. Atomic Energy Authority, Harwell (1973).

5. J. FREHAUT and G. MOSINSKI, "Mesure des sections efficaces (n,2n) des noyaux ^{56}Fe, ^{59}Co, ^{89}Y, ^{169}Tm, ^{175}Lu, ^{181}Ta, ^{197}Au, ^{209}Bi, ^{238}U et (n,3n) de ^{238}U du seuil à 15 MeV", Rapport CEA-R-4627 (1974).

6. J. FREHAUT and G. MOSINSKI, "Measurement of (n,2n) and (n,3n) Cross Sections for Incident Energies between 6 and 15 MeV", Proc. Conf. Nuclear Cross Section and Technology, Washington, D.C., March 1975, CONF-750303, Vol. 2, p. 897, U.S. National Bureau of Standards (1975).

7. J. FREHAUT, E. HOLUB, M. CATES and G. MOSINSKI, "Mesure de la section efficace (n,2n) des isotopes ^{203}Tl et ^{205}Tl du seuil à 15 MeV", Note CEA-N-1998 (1977).

8. J. FREHAUT and J. JARY, "Systématique des sections efficaces de réaction (n,2n) pour des séries d'isotopes séparés", Proc. Conf. Neutron Physics and Nuclear Data for Reactors and Other Applied Purposes, Harwell, Spt. 1978, CONF-780925 430, p. 1038 U.K.A.E.A. (1978).

9. G. F. AUCHAMPAUGH, D. M. DRAKE and L. R. VEESER, "Neutron Cross Section Programs in the Energy Region from 1 to 24 MeV at the LASL Van de Graaff Facilities", Proc. Symposium on Neutron Cross Sections from 10 to 40 MeV, Upton, N.Y., May 1977, BNL-NCS-50681, p. 231, Brookhaven National Laboratory (1977).

10. L. R. VEESER, E. D. ARTHUR and P. G. YOUNG, "Cross Sections for (n,2n) and (n,3n) Reactions above 14 MeV", Phys. Rev. C16, 1792 (1977).

11. A. GILBERT and A. G. W. CAMERON, "A composite Nuclear Level Density Formula with Shell Corrections", Can. J. Physics 43, 1446 (1965).

12. A. V. IGNATYUK, G. N. SMIRENKIN and A. S. TISHIN, "Phenomenological Description of the Energy Dependence of the Level Density Parameter", Sov. J. Nucl. Phys. 21, 255 (1975).

TABLE I

Experimental (n,2n) cross sections for the natural elements Ti, V, Cr, Fe, Cu and Ga.

E_n (MeV)	Ti(mb)	V(mb)	Cr (mb)	Fe (mb)	Cu (mb)	Ga (mb)
9.93 ± 0.110						17 ± 7
10.19 ± 0.105	11 ± 1		26 ± 2		9 ± 2	
10.42 ± 0.100						27 ± 12
10.74 ± 0.095	18 ± 4		31 ± 3		19 ± 5	
10.91 ± 0.095						83 ± 9
11.40 ± 0.090	35 ± 3	15 ± 2	51 ± 3		76 ± 5	180 ± 12
11.88 ± 0.085	48 ± 4	70 ± 7	65 ± 5	48 ± 6	145 ± 11	303 ± 19
12.12 ± 0.085	60 ± 5					
12.36 ± 0.085	89 ± 7	145 ± 12	68 ± 6	100 ± 9	228 ± 18	431 ± 34
12.60 ± 0.080	129 ± 10		100 ± 8			
12.85 ± 0.080	163 ± 13	242 ± 19	128 ± 10	188 ± 14	336 ± 26	546 ± 42
13.33 ± 0.075	239 ± 19	345 ± 28	201 ± 16	271 ± 20	436 ± 33	672 ± 52
13.80 ± 0.075	316 ± 26	433 ± 36	273 ± 22	342 ± 23	502 ± 40	743 ± 56
14.28 ± 0.070	366 ± 28	499 ± 35	344 ± 25	392 ± 32	550 ± 40	829 ± 63
14.76 ± 0.065	440 ± 35	558 ± 44	406 ± 32	470 ± 36	628 ± 48	854 ± 65

TABLE II

Experimental (n,2n) cross sections for the natural elements Zr, Mo, W, Pt and Pb.

E_n (MeV)	Zr (mb)	Mo (mb)	W (mb)	Pt (mb)	Pb (mb)
7.41 ± 0.165					42 ± 31
7.93 ± 0.150	18 ± 10	18 ± 7	208 ± 27	183 ± 26	104 ± 15
8.18 ± 0.145			385 ± 22	±	
8.44 ± 0.135	65 ± 9	41 ± 7	588 ± 46	359 ± 36	299 ± 23
8.69 ± 0.130			758 ± 41		
8.94 ± 0.125	92 ± 11	104 ± 11	911 ± 55	533 ± 47	530 ± 36
9.44 ± 0.115	177 ± 14	165 ± 10	1214 ± 89	858 ± 67	835 ± 44
9.93 ± 0.110	259 ± 14	305 ± 17	1417 ± 93	1102 ± 93	1044 ± 54
10.19 ± 0.105	287 ± 15	382 ± 21			1148 ± 59
10.42 ± 0.100			1479 ± 93	1274 ± 83	
10.74 ± 0.095	347 ± 19	530 ± 30			1386 ± 72
10.91 ± 0.095			1618 ± 94	1458 ± 85	
11.40 ± 0.090	441 ± 24	677 ± 39	1750 ± 109	1562 ± 97	1566 ± 83
11.88 ± 0.085	495 ± 26	796 ± 61	1787 ± 112	1738 ± 109	1707 ± 85
12.36 ± 0.085	558 ± 40	885 ± 68	1831 ± 108	1782 ± 104	1782 ± 129
12.85 ± 0.080	658 ± 47	970 ± 74	1867 ± 114	1830 ± 110	1869 ± 136
13.33 ± 0.075	793 ± 58	1024 ± 79	1899 ± 100	1780 ± 102	1924 ± 143
13.80 ± 0.075	880 ± 68	1043 ± 85	1868 ± 101	1831 ± 110	1961 ± 154
14.28 ± 0.070	946 ± 67	1091 ± 80	1943 ± 157	1888 ± 152	1953 ± 142
14.76 ± 0.065	988 ± 74	1109 ± 88	1950 ± 169	1941 ± 164	2006 ± 156

TABLE III

Experimental (n,2n) cross sections for ^{45}Sc, ^{59}Co, ^{75}As, ^{89}Y, ^{93}Nb, and ^{103}Rh.

E_n (MeV)	^{45}Sc (mb)	^{59}Co (mb)	^{75}As (mb)	^{89}Y (mb)	^{93}Nb (mb)	^{103}Rh (mb)
9.44 ± 0.115					44 ± 17	
9.93 ± 0.110					319 ± 25	82 ± 12
10.42 ± 0.100					493 ± 37	293 ± 23
10.91 ± 0.095		16 ± 6	59 ± 13		694 ± 45	513 ± 31
11.40 ± 0.090		110 ± 10	191 ± 17		794 ± 52	703 ± 46
11.88 ± 0.085		216 ± 17	356 ± 25	49 ± 8	976 ± 64	871 ± 57
12.36 ± 0.085	53 ± 7	326 ± 24	554 ± 45	188 ± 13	1042 ± 63	1022 ± 62
12.85 ± 0.080	90 ± 10	453 ± 30	707 ± 55	395 ± 21	1122 ± 69	1094 ± 67
13.33 ± 0.075	149 ± 14	539 ± 36	839 ± 65	585 ± 41	1195 ± 69	1187 ± 65
13.80 ± 0.075	211 ± 17	640 ± 41	909 ± 70	748 ± 36	1168 ± 70	1223 ± 72
14.28 ± 0.070	250 ± 21	-	997 ± 77	829 ± 43	1270 ± 98	1311 ± 99
14.76 ± 0.065	309 ± 25	734 ± 50	1091 ± 83	914 ± 73	1313 ± 99	1340 ± 99

TABLE IV

Experimental (n,2n) cross sections for ^{169}Tm, ^{175}Lu, ^{181}Ta, ^{197}Au, and ^{209}Bi.

E_n (MeV)	^{169}Tm (mb)	^{175}Lu (mb)	^{181}Ta (mb)	^{197}Au (mb)	^{209}Bi (mb)
7.93 ± 0.150					113 ± 13
8.44 ± 0.135	60 ± 31	192 ± 32	271 ± 28	39 ± 20	342 ± 36
8.94 ± 0.125	335 ± 27	623 ± 48	709 ± 47	254 ± 20	730 ± 51
9.44 ± 0.115	875 ± 87	1092 ± 108	1217 ± 112	651 ± 65	1078 ± 98
9.93 ± 0.110	1102 ± 69	1309 ± 83	1372 ± 83	905 ± 57	1415 ± 86
10.42 ± 0.110	1348 ± 83	1447 ± 91	1518 ± 93	1138 ± 72	1598 ± 96
10.91 ± 0.095	1443 ± 103	1596 ± 120	1581 ± 110	1360 ± 97	1710 ± 119
11.40 ± 0.090	1557 ± 79	1598 ± 104	1653 ± 102	1511 ± 76	1768 ± 108
11.88 ± 0.085	1739 ± 101	1777 ± 108	1778 ± 101	1726 ± 99	1884 ± 106
12.36 ± 0.085	1799 ± 84	1854 ± 119	1845 ± 111	1818 ± 83	1970 ± 117
12.85 ± 0.080	1938 ± 86	1898 ± 124	1935 ± 117	1949 ± 87	2035 ± 121
13.33 ± 0.075	1939 ± 123	1892 ± 124	1891 ± 119	1967 ± 123	1964 ± 122
13.80 ± 0.075	1961 ± 89	1905 ± 122	1920 ± 118	2039 ± 91	2088 ± 129
14.28 ± 0.070	1845 ± 95	1932 ± 159	1900 ± 153	1936 ± 97	2014 ± 163
14.76 ± 0.065	1926 ± 155	1891 ± 162	1856 ± 159	1935 ± 155	2018 ± 170

TABLE V

Experimental (n,2n) cross sections for the selenium isotopes.

E_n (MeV)	^{76}Se (mb)	^{78}Se (mb)	^{80}Se (mb)	^{82}Se (mb)
9.93 ± 0.110				94 ± 6
10.42 ± 0.100			56 ± 5	281 ± 16
10.91 ± 0.095		15 ± 5	219 ± 14	451 ± 26
11.40 ± 0.090		130 ± 9	391 ± 24	605 ± 36
11.88 ± 0.085	98 ± 12	309 ± 21	547 ± 36	721 ± 44
12.36 ± 0.085	213 ± 24	461 ± 38	734 ± 61	868 ± 68
12.85 ± 0.080	368 ± 36	618 ± 50	823 ± 67	944 ± 73
13.33 ± 0.075	520 ± 48	747 ± 60	922 ± 73	1048 ± 80
13.80 ± 0.075	644 ± 56	886 ± 69	1023 ± 81	1044 ± 80
14.28 ± 0.070	699 ± 60	897 ± 70	1008 ± 79	1057 ± 81
14.76 ± 0.065	774 ± 65	951 ± 74	1043 ± 82	1101 ± 84

TABLE VI

Experimental (n,2n) cross sections for the neodynium isotopes.

E_n (MeV)	^{142}Nd (mb)	^{144}Nd (mb)	^{146}Nd (mb)	^{148}Nd (mb)	^{150}Nd (mb)
8.03 ± 0.145			151 ± 14	304 ± 20	213 ± 17
8.18 ± 0.145		127 ± 14			
8.44 ± 0.135			416 ± 24	590 ± 32	533 ± 30
8.59 ± 0.130		291 ± 21			
8.94 ± 0.125		566 ± 31	748 ± 41	985 ± 50	874 ± 47
9.44 ± 0.115		786 ± 43	1008 ± 54	1139 ± 59	1119 ± 59
9.93 ± 0.110		1048 ± 56	1203 ± 65	1311 ± 68	1235 ± 69
10.42 ± 0.110	194 ± 17	1135 ± 61	1303 ± 70	1365 ± 71	1388 ± 73
10.91 ± 0.095	411 ± 26	1264 ± 68	1458 ± 80	1469 ± 78	1479 ± 79
11.88 ± 0.085	862 ± 66	1410 ± 102	1601 ± 116	1548 ± 111	1650 ± 118
12.85 ± 0.080	1318 ± 98	1576 ± 120	1741 ± 128	1654 ± 121	1791 ± 130
13.80 ± 0.075	1564 ± 118	1588 ± 121	1832 ± 137	1755 ± 134	1861 ± 139
14.28 ± 0.070		1619 ± 127		1668 ± 133	
14.76 ± 0.065	1907 ± 146	1713 ± 137	1876 ± 153	1700 ± 142	1652 ± 138

TABLE VII

Experimental (n,2n) cross sections for the samarium isotopes and for ^{151}Eu.

E_n (MeV)	^{148}Sm (mb)	^{150}Sm (mb)	^{152}Sm (mb)	^{154}Sm (mb)	^{151}Eu (mb)
8.44 ± 0.135				122 ± 44	22 ± 14
8.59 ± 0.130	143 ± 14	158 ± 15	31 ± 14		
8.94 ± 0.125	318 ± 20	373 ± 24	278 ± 17	492 ± 29	206 ± 17
9.44 ± 0.115	600 ± 34	637 ± 37	567 ± 31	843 ± 46	483 ± 33
9.93 ± 0.110	916 ± 49	990 ± 57	933 ± 49	1070 ± 61	725 ± 48
10.42 ± 0.100	1052 ± 57	1086 ± 60	1093 ± 58	1259 ± 68	1007 ± 59
10.91 ± 0.095	1236 ± 67	1243 ± 69	1271 ± 68	1414 ± 78	1176 ± 74
11.40 ± 0.090					1340 ± 78
11.88 ± 0.085	1510 ± 110	1418 ± 104	1458 ± 104	1619 ± 118	1476 ± 86
12.36 ± 0.085					1585 ± 120
12.85 ± 0.080	1587 ± 116	1600 ± 119	1613 ± 118	1755 ± 129	1623 ± 122
13.33 ± 0.075					1665 ± 125
13.80 ± 0.075	1697 ± 128	1756 ± 134	1751 ± 132	1888 ± 143	1777 ± 140
14.28 ± 0.070					1702 ± 138
14.76 ± 0.065	1783 ± 139	1876 ± 148	1840 ± 143	1958 ± 156	1752 ± 145

TABLE VIII

Experimental (n,2n) cross sections for the gadolinium isotopes.

E_n (MeV)	^{155}Gd (mb)	^{156}Gd (mb)	^{157}Gd (mb)	^{158}Gd (mb)	^{160}Gd (mb)
6.89 ± 0.185	30 ± 19		104 ± 19		
7.41 ± 0.165	209 ± 22		344 ± 26		
7.93 ± 0.150	513 ± 33		681 ± 43		109 ± 14
8.44 ± 0.135	736 ± 48	16 ± 13	976 ± 60	89 ± 14	502 ± 36
8.94 ± 0.125	920 ± 64	37 ± 12	1133 ± 81	418 ± 34	857 ± 66
9.44 ± 0.115	1103 ± 66	299 ± 25	1300 ± 80	775 ± 52	1146 ± 74
9.93 ± 0.110	1257 ± 87	649 ± 53	1434 ± 100	1079 ± 80	1363 ± 99
10.42 ± 0.100	1410 ± 81	915 ± 59	1524 ± 90	1233 ± 76	1431 ± 88
10.91 ± 0.095	1514 ± 89	1138 ± 72	1594 ± 95	1380 ± 99	1509 ± 108
11.40 ± 0.090	1563 ± 98	1309 ± 87	1672 ± 106	1504 ± 98	1624 ± 105
11.88 ± 0.085	1622 ± 90	1428 ± 83	1668 ± 93	1557 ± 130	1651 ± 138
12.36 ± 0.085	1684 ± 102	1530 ± 96	1718 ± 106	1610 ± 100	1735 ± 107
12.85 ± 0.080	1704 ± 145	1592 ± 136	1754 ± 151	1689 ± 143	1739 ± 147
13.33 ± 0.075	1747 ± 125	1659 ± 119	1752 ± 128	1735 ± 121	1758 ± 127
13.80 ± 0.075	1768 ± 146	1661 ± 134	1830 ± 154	1771 ± 143	1779 ± 147
14.28 ± 0.070	1808 ± 155	1766 ± 143	1817 ± 161	1801 ± 148	1817 ± 155
14.76 ± 0.065	1843 ± 163	1730 ± 143	1820 ± 169	1794 ± 150	1712 ± 151

TABLE IX

Experimental (n,2n) cross sections for the tungsten isotopes and for ^{238}U.

E_n (MeV)	^{182}W (mb)	^{183}W (mb)	^{184}W (mb)	^{186}W (mb)	^{238}U (mb)
6.89 ± 0.185					233 ± 39
7.41 ± 0.165		597 ± 30		50 ± 29	604 ± 54
7.67 ± 0.160			76 ± 24	134 ± 17	811 ± 62
7.93 ± 0.150		944 ± 44	148 ± 15	285 ± 20	879 ± 48
8.18 ± 0.145	15 ± 12	1086 ± 54	318 ± 22	514 ± 29	999 ± 41
8.44 ± 0.135	61 ± 12	1241 ± 56	509 ± 28	691 ± 37	1072 ± 52
8.69 ± 0.130	209 ± 27		725 ± 40	914 ± 48	1029 ± 60
8.94 ± 0.125	342 ± 21	1432 ± 63	913 ± 46	1112 ± 56	1156 ± 42
9.44 ± 0.115	687 ± 40	1535 ± 76	1241 ± 66	1321 ± 69	1171 ± 46
9.93 ± 0.110	1085 ± 58	1671 ± 82	1439 ± 73	1549 ± 78	1232 ± 44
10.42 ± 0.100	1293 ± 67				1258 ± 48
10.91 ± 0.095	1503 ± 77	1788 ± 80	1699 ± 85	1722 ± 86	1260 ± 44
11.40 ± 0.090					1300 ± 52
11.88 ± 0.085	1750 ± 124	1855 ± 132	1837 ± 129	1830 ± 128	1324 ± 48
12.36 ± 0.085					1313 ± 66
12.85 ± 0.080	1869 ± 136	1867 ± 140	1905 ± 138	1927 ± 138	1272 ± 56
13.33 ± 0.075	1887 ± 136	1863 ± 135	1889 ± 135	1925 ± 135	1134 ± 58
13.80 ± 0.075	1912 ± 141	1870 ± 140	1921 ± 135	1897 ± 144	925 ± 54
14.28 ± 0.070	2030 ± 157	1855 ± 170	1950 ± 158	1880 ± 153	790 ± 66
14.76 ± 0.065	2017 ± 150	1855 ± 170	1851 ± 152	1785 ± 149	642 ± 64

TABLE X

Experimental (n,2n) cross sections for the thallium and lead isotopes.

E_n (MeV)	^{203}Tl (mb)	^{205}Tl (mb)	^{206}Pb (mb)	^{207}Pb (mb)	^{208}Pb (mb)
7.41 ± 0.165				21 ± 18	
7.93 ± 0.150				198 ± 18	80 ± 10
8.18 ± 0.145				301 ± 24	162 ± 13
8.44 ± 0.135	39 ± 10	109 ± 22	62 ± 13	396 ± 28	299 ± 21
8.94 ± 0.125	211 ± 26	474 ± 39	225 ± 20	670 ± 45	578 ± 39
9.44 ± 0.115	435 ± 37	738 ± 53	476 ± 33	976 ± 63	897 ± 59
9.93 ± 0.110	714 ± 56	979 ± 50	758 ± 50	1161 ± 74	1122 ± 72
10.42 ± 0.100	1037 ± 80	1312 ± 93	1056 ± 62	1373 ± 80	1356 ± 80
10.91 ± 0.095	1216 ± 71	1421 ± 81	1273 ± 80	1533 ± 95	1493 ± 94
11.40 ± 0.090	1489 ± 90	1576 ± 95	1464 ± 85	1623 ± 93	1637 ± 95
11.88 ± 0.085	1578 ± 121	1660 ± 117	1655 ± 96	1740 ± 100	1772 ± 103
12.36 ± 0.085	1655 ± 121	1748 ± 127	1756 ± 132	1811 ± 137	1776 ± 135
12.85 ± 0.080	1750 ± 128	1811 ± 132	1825 ± 137	1858 ± 140	1865 ± 142
13.33 ± 0.075	1817 ± 142	1841 ± 146	1866 ± 147	1866 ± 147	1877 ± 148
13.80 ± 0.075	1930 ± 151	1878 ± 147	1864 ± 147	1971 ± 161	1961 ± 159
14.28 ± 0.070			1977 ± 159	1888 ± 160	1937 ± 162
14.76 ± 0.065	1927 ± 155	1841 ± 148	1971 ± 160	1920 ± 166	1971 ± 168

TABLE XI

Experimental (n,3n) cross sections

E_n (MeV)	^{146}Nd (mb)	^{148}Nd (mb)	^{150}Nd (mb)	^{160}Gd (mb)	^{184}W (mb)	^{186}W (mb)	^{238}U (mb)
11.88							30 ± 9
12.36							69 ± 13
12.85			9 ± 3				172 ± 24
13.33							295 ± 32
13.80		26 ± 4	47 ± 5			9 ± 3	389 ± 36
14.28		64 ± 6		10 ± 4		58 ± 5	500 ± 46
14.76	29 ± 5	132 ± 11	248 ± 18	53 ± 6	22 ± 4	145 ± 12	568 ± 50

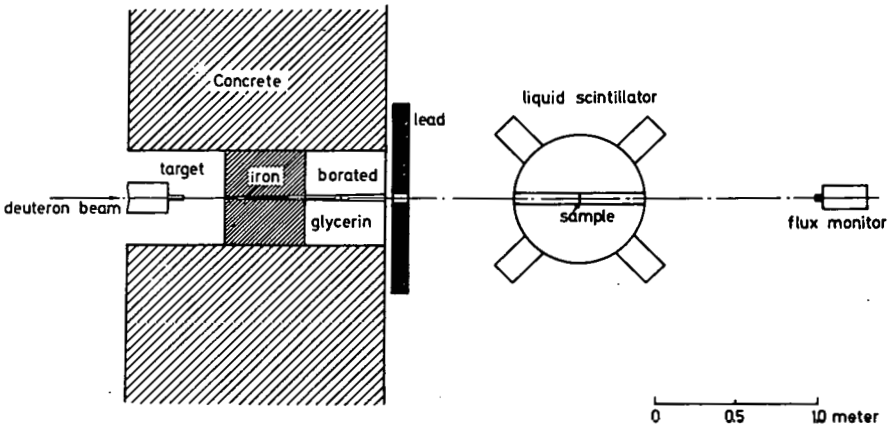

Fig. 1 - Experimental set-up.

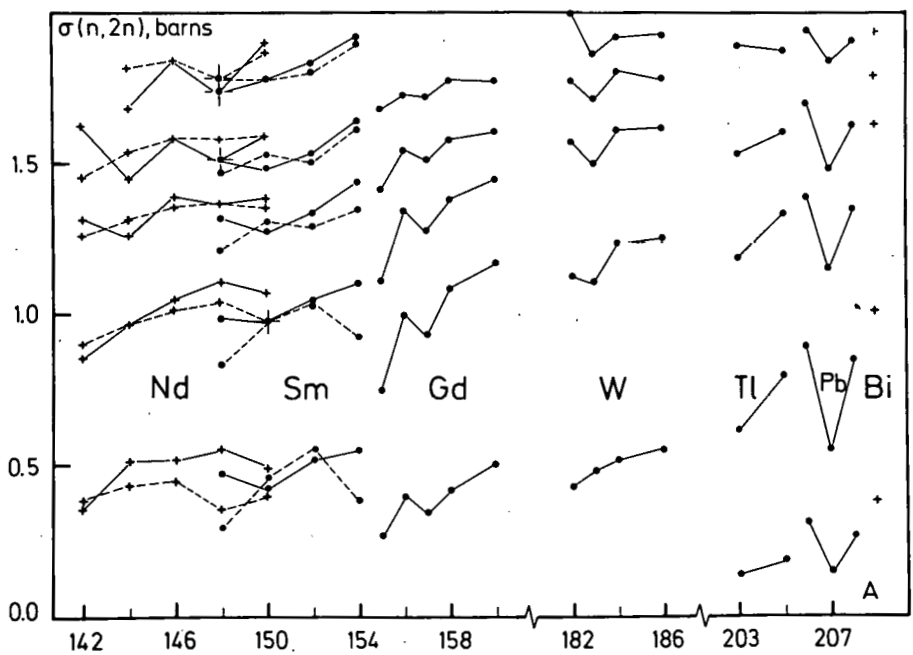

Fig. 2 - Experimental (n,2n) cross sections for the Nd, Sm, Gd, W, Tℓ and Pb isotopes and for ^{209}Bi as a function of the mass number A, for values of the excess energy U_R above threshold of 1,2,3,4 and 6 MeV, respectively from bottom to top for each series of isotopes. The curves with short dashes for Nd and Sm isotopes were calculated using a statistical model.

THIS PAGE

WAS INTENTIONALLY

LEFT BLANK

CROSS SECTIONS FOR THE REACTIONS OF $^{9}Be(n,t_1\gamma)$ AND $^{12}C(n,n'\gamma)$ BETWEEN 13.0 AND 15.0 MeV

Y. Hino, S. Itagaki and K. Sugiyama

Department of Nuclear Engineering
Tohoku University
Aoba, Aramaki, Sendai, Japan 980

ABSTRACT

The neutron induced cross sections of γ-rays have been measured for 0.478 MeV from beryllium and 4.43 MeV from carbon in the region of neutron energies 13.0 to 15.0 MeV. The γ-rays are observed with a Ge(Li) detector placed at an angle of 90°. In order to produce neutrons, the T + d reaction has been used. The 0.478 MeV γ-rays from beryllium follows the emission of triton leading to the first excited state of ^{7}Li. It is concluded that the cross section of $^{9}Be(n,t_1\gamma)$ reaction shows a flat behavior over the neutron energies rather than the large resonance near 13 MeV. The result for the 4.43 MeV γ-ray from carbon is in good agreement with previous data.

INTRODUCTION

The cross sections for the $^{9}Be(n,t)^{7}Li$ reaction is important to estimate the tritium breeding rate in the blanket of fusion reactors, but the detection of produced triton is very difficult because of the large negative Q-value. The portion of this cross section, which is expressed as $^{9}Be(n,t_1\gamma)$, can be measured by detecting 0.478 MeV γ-rays from the first excited state of ^{7}Li. The previously published data for this reaction have shown a large discrepancy in the region of 14 MeV neutron energy. A pronounced dip down to 10 mb near 14 MeV and a resonance peak of 21 mb at 13.5 MeV have been reported by Benveniste et al. [1]. On the other hand, Dietrich et al. [2] have shown rather small and slight change of the cross sections from 7.3 to 4.8 mb for the neutron energies of 13.3 to 15.0 MeV. Drake et al. [3] and Perroud et al. [4] have reported 8.8 mb at 14.2 MeV and 5.52 mb at 13.99 MeV, respectively. The present measurement has been carried out to solve this discrepancy using a Ge(Li) detector with well defined geometry.

The result for the 4.43 MeV γ-ray production cross section from carbon is also given for the sake of confirmation of present measurements.

EXPERIMENTAL PROCEDURES

Monoenergetic neutrons from 13.0 to 15.0 MeV were produced from the T(d,n)He reaction with accelerators of Tohoku University. The 4.5 MV Dynamitron accelerator was used to obtain 13.0 and 13.5 MeV neutrons, and the 600 kV Cockcroft-Walton was used to generate 13.5, 14.0, 14.5 and 15.0 MeV neutrons. The neutron flux at the sample position was monitored by a NE-213 liquid scintillation detector with time-of-flight electronics at the Dynamitron, and was also monitored by detecting associated alpha particles with a silicon surface barrier detector at the Cockcroft-Walton. Further details of these systems have been reported elsewhere [5,6].

The sample of high purity beryllium metal or reactor grade graphite was 5 cm in height and 5 cm in dia. of right cylinder, and was held with fine string. The γ-rays due to the interactions of the neutrons were measured with a 70 cm^3 Ge(Li) detector placed at an angle of 90° in respect to the beam axis. The Ge(Li) detector was housed in a carefully designed shielding assembly consisting of lead, iron, lithium-carbonate and water as shown in Fig. 1.

RESULTS AND DISCUSSION

The typical γ-ray spectra for beryllium and carbon samples of interest energy regions are shown in Figs. 2 and 3. The peaks of 0.478 and 4.43 MeV γ-rays are broadened by Doppler effect. Each sample produces a single line of γ-ray, then γ-ray spectra of the another sample give good estimations of background levels as shown in Figs. 2 and 3.

Differential cross sections at 90° for the $^9Be(n,t_1\gamma)$ and $^{12}C(n,n'\gamma)$ reactions have been obtained and listed in Table I. The details of the data analysis and error estimations have been presented elsewhere [5,6]. The 0.478 MeV γ-ray from the first excited state of ^7Li is emitted isotropically [1], so that the total cross section for the $^9Be(n,t_1\gamma)$ reaction is obtained by multiplying 4π to the above value. The total cross section is shown in Fig. 4 together with the previous results. The present results from two accelerators are connected smoothly at 13.5 MeV. The values of Dietrich et al. [2] and Perroud et al. [4] are in good agreement with the present data. The result of Benveniste et al. [1] is considerably large, and that of Drake et al. [3] is somewhat large in comparison with the present result. The cause of these discrepancies among previous data may be due to the inability to resolve the 0.511 MeV undesired background with NaI(Tl) detectors, which have been used by Benveniste et al. and Drake et al.. It is reasonable that the result of Perroud et al., which is obtained by

detecting tritons with high resolution telescope counter, is in good agreement with those of the present and Dietrich obtained with Ge(Li) detectors.

The present measurement covers the excitation energy region from 18.5 to 20.3 MeV in ^{10}Be. It has been repoted [7] that a 350-keV-wide broad excitation level is located at 18.55 MeV corresponding to the incident neutron energy of 13.04 MeV. The effect of this level appears clearly in the result of Benveniste et al., but is not clear in that of Dietrich et al.. The present result shows that the cross section for this reaction is uninfluenced by this level. This fact reveals that the effect of this level is weak, and the cross section curve would be decreased monotonously to the threshold energy of 12.13 MeV.

The differential cross sections of γ-ray production for the $^{12}C(n,n'\gamma)$ reaction at 90° are shown in Fig. 5. The present result is in good agreement with the previous data [3, 8, 9] except for those of Dickens et al. [10] which has been obtained with white neutrons from an electron linac.

As a conclusion, present result for the $^{9}Be(n,t_1\gamma)$ reaction shows a gently rising cross section curve with neutron energy, and is in good agreement with those of Dietrich et al. and Perroud et al.. The absolute value of the present result is confirmed by the measurement of $^{12}C(n,n'\gamma)$ reaction cross section, which is in good agreement with those of previous.

ACKNOWLEDGMENT

The authors are grateful to crew of the Dynamitron and the Cockcroft-Walton accelerators for the beam time.

REFERENCES

1. J. Benveniste et al., "Gamma Rays from the Interaction of 14-MeV Neutrons with Beryllium," Nucl. Phys., 19, 52 (1960).

2. F. S. Dietrich et al., "Cross Sections for the $^{9}Be(n,t_1\gamma)^{7}Li$ Reaction between 13.3 and 15.0 MeV," Nucl. Sci. Eng., 61, 267 (1976).

3. D. M. Drake et al., "More 14-MeV, Neutron Induced Gamma-Ray Production Cross Sections," LASL Rep. LA-5983-MS (1975).

4. J. P. Perroud and Ch. Sellem, "(n,t) and (n,α) Reactions on ^{9}Be," Nucl. Phys., A227, 330 (1975).

5. Y. Hino et al., "Gamma-Ray Production Cross Sections for Aluminum and Copper at 5.3 MeV Neutron Energy," Jour. Nucl. Sci. Tech., 15, 85 (1978)

6. T. Yamamoto et al., "Gamma-Ray Production Cross Sections for Interactions of 14.8 MeV Neutrons with O, Na, Al, Cl, Cr, Fe, Ni, Cu and Pb," Jour. Nucl. Sci. Tech., 15, 797 (1978).

7. F. Ajzenberg-Selove and T. Lauritsen, "Energy Levels of Light Nuclei A = 5 - 10," Nucl. Phys., A227, 140 (1974).

8. F. C. Engesser and W. E. Thompson, "Gamma Rays Resulting from Interactions of 14.7 MeV Neutrons with Various Elements," Jour. Nucl. Energy, 21, 487 (1967).

9. D. T. Stewart and P. W. Martin, "Gamma Rays from the Interaction of 14 MeV Neutrons with ^{12}C and ^{24}Mg," Nucl. Phys., 60, 349 (1964).

10. J. K. Dickens et al., "Cross Sections for Gamma-Ray Production by Fast Neutrons for 22 Elements Between Z=3 and Z=82," Nucl. Sci. Eng., 62, 515 (1977).

TABLE I

Differential γ-ray production cross sections for the $^{9}Be(n,t_1\gamma)$ and $^{12}C(n,n'\gamma)$ reactions at 90°.

Reaction / Neutron Energy	$^{9}Be(n,t_1\gamma)$	$^{12}C(n,n'\gamma)$
13.0 ± 0.2 MeV [a]	0.40 ± 0.08 mb/sr	12.1 ± 1.9 mb/sr
13.5 ± 0.2 [a]	0.47 ± 0.09	11.8 ± 1.8
13.5 ± 0.2 [b]	0.38 ± 0.06	12.4 ± 1.5
14.0 ± 0.2 [b]	0.49 ± 0.06	12.5 ± 1.5
14.5 ± 0.2 [b]	0.50 ± 0.06	12.4 ± 1.5
15.0 ± 0.2 [b]	0.57 ± 0.08	11.0 ± 1.3

[a] Measured with the 4.5 MV Dynamitron accelerator

[b] Measured with the 600 kV Cockcroft-Walton accelerator

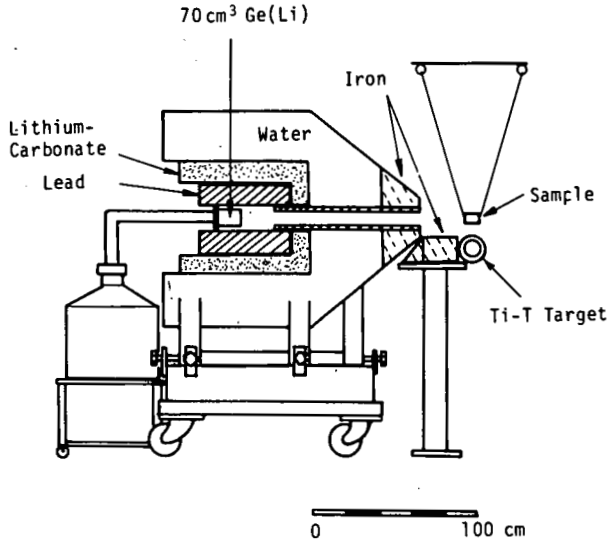

Fig. 1 Experimental arrangement. The cylindrical sample is held with fine string as its axis coordinate with that of the shielding collimator, which is located perpendicular to the plane defined by the deuteron beam axis and the sample direction.

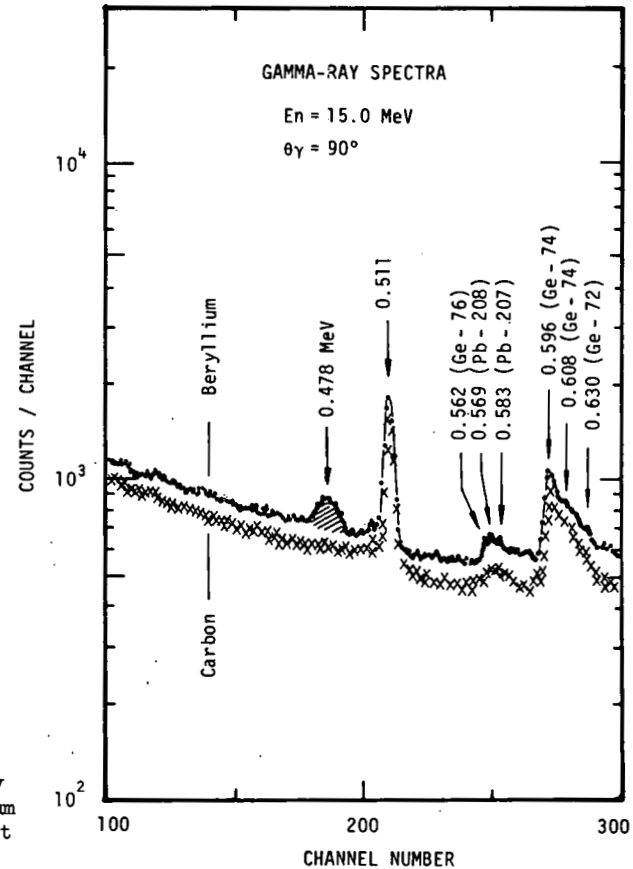

Fig. 2 γ-ray spectra of lower energy region. The 0.478 MeV γ-ray line is observed for the beryllium sample, and the spectrum from the carbon indicates that line structures do not exist in the background under 0.478 MeV peak.

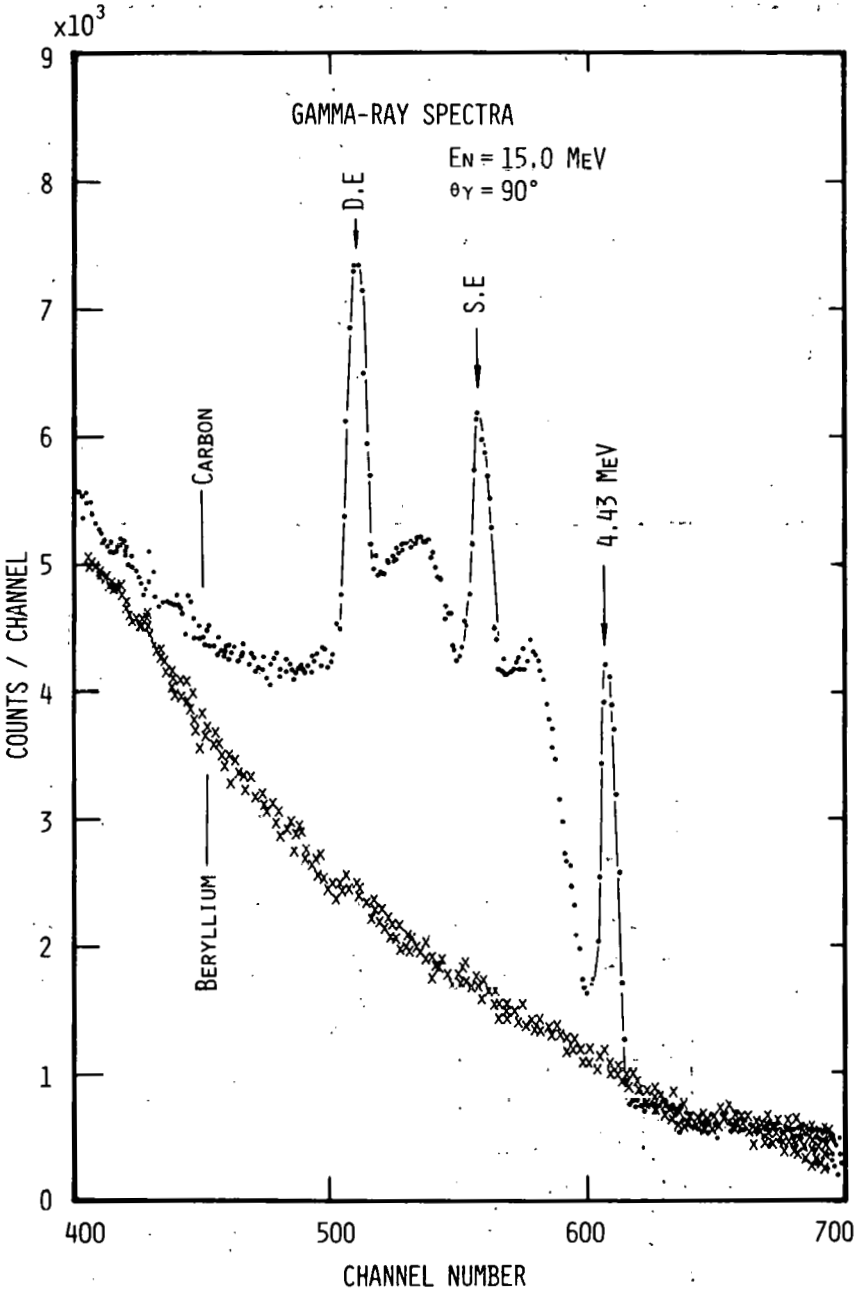

Fig. 3 γ-ray spectra of higher energy region. The 4.43 MeV γ-ray line and escape peaks are observed. Peaks are also broadened by Doppler effect.

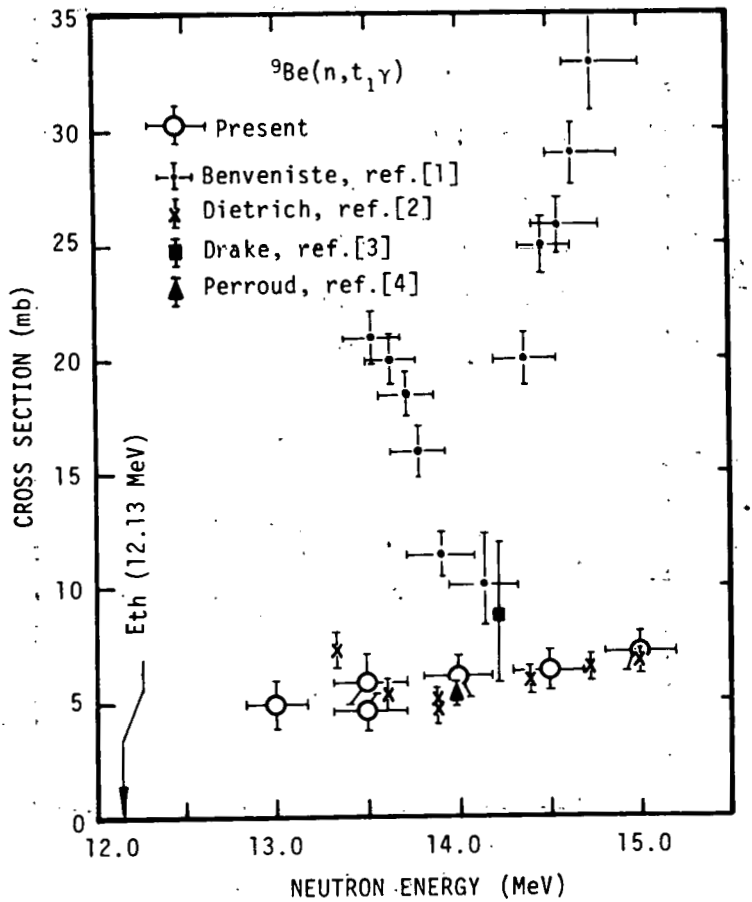

Fig. 4 Cross sections for the $^{9}Be(n,t_1\gamma)$ reaction. The present result shows a gently rising curve, and a dip near 14 MeV or a resonance near 13 MeV is not found out.

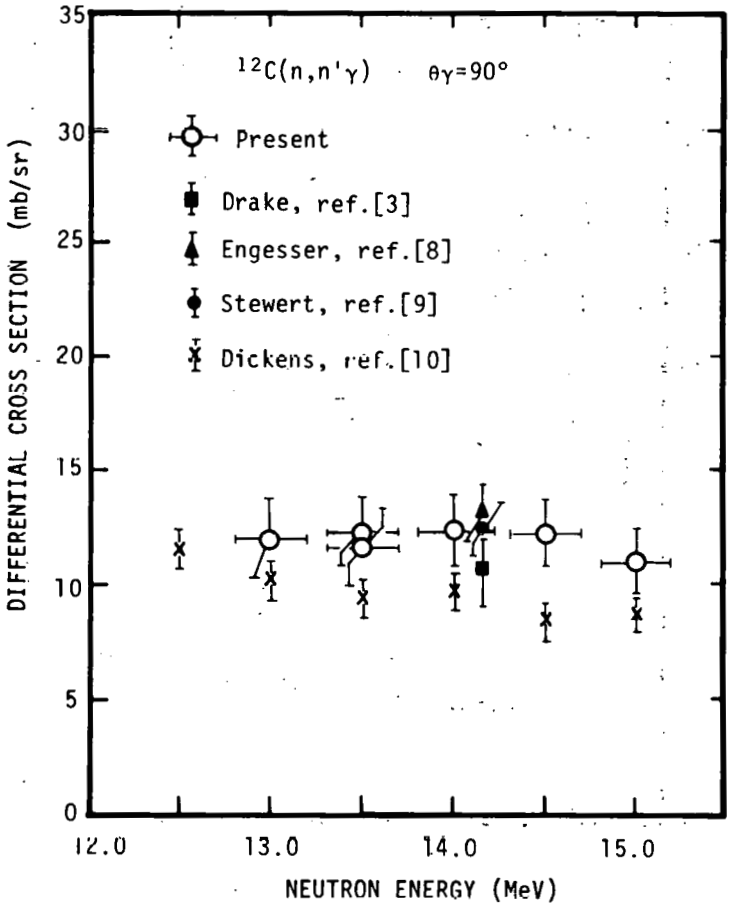

Fig. 5 Differential γ-ray production cross sections at 90° for the $^{12}C(n,n'\gamma)$ reaction. The present result is in good agreement with those of previous which obtained with monoenergetic neutrons.

SCATTERING OF 10 MEV NEUTRONS BY SILICON

W. Pilz, D. Schmidt, D. Seeliger and T. Streil

Technische Universitat Dresden, Sekt. Physik, Dresden, GDR

ABSTRACT

Angular distributions for several neutron groups of the 28-Si(n,n') reaction are measured at 10 MeV bombarding energy. The experimental data are analyzed by a combined statistical and direct reaction model. The theoretical description gives information about excitation modes and strengths.

INTRODUCTION

All investigations of the $^{28}Si(n,n')$ reaction done until now were restricted to a narrow energy region between the energies 3 and 14 MeV. These experiments differ from each other with respect to both the measuring technique and the model parameters of the theoretical analysis used.

The present work has been started with the aim of analyzing on a uniform theoretical basis, the reaction mentioned above in the evergy range from 7 to 14 MeV. This reaction is known to be described by an incoherent superposition of compound nucleus contribution calculated by the Hauser-Feshbach formalism and a direct reaction part (1). It is well known that a good agreement between experimental points and theoretical curves can be obtained easily for one incident energy by a convenient choice of model parameters. But the theoretical description of experimental data, obtained under the same conditions with a consistent set of parameters in a wide energy range, is more attractive because this allows one to get more information about the reaction mechanism. Furthermore, such measurements are important for nuclear data collection and evaluation.

The objectives of the present work are the measurement and its theoretical description at 10 MeV bombarding energy only. A more complex interpretation for the proposed energy range will be reported later.

EXPERIMENTAL PROCEDURE

The elastic and inelastic differential neutron scattering cross sections were measured with the tandem facility in the ZFK Rossendorf. A deuterium gas target (2) using the D(d,n) reaction was employed. The measurements were carried out with a computer-coupled multi-angle TOF-detector system consisting of eight detectors. The experiment is characterized by measuring angles between 15 and 160 degrees, an energy spread of 120 keV, average flight paths of 3 meters and the angle uncertainty of $\pm$ 3 degrees. Fig. 1 shows the complete system, a more detailed description is given in Ref. 3.

As monitor, a ninth TOF-detector was included in the system to reduce the dead time correction. Because the efficiency ratio of monitoring and measuring detectors can be found with sufficient accuracy (error less than 2%), for determination of the absolute cross sections, only the relative efficiency function is necessary. The angular distributions were measured in two independent runs at 15, 30, 50...150 and 20, 40, 60...160 degrees. The absolute cross sections for each run were determined independently and are shown in Fig. 2

The scattering sample consists of natural silicon with a cylindrical shape (3 x 3 cm^2) and a weight of 43.53 g. The measured cross sections were corrected for finite geometry and multiple scattering, which are rather low for the chosen sample size. The background from elastically scattered non-monoenergetic neutrons of the source (2) have been taken into account for the calculation of the cross sections of higher inelastic neutron groups using a special computer code.

ANALYSIS OF THE EXPERIMENTAL DATA

The elastic scattering is described as a sum of shape and compound elastic parts (see also Fig. 2). The calculation of the shape elastic contribution was performed with the spherical optical model (SOM) using parameters from Ref. 1 with a slightly different spin-orbit term. The parameters were chosen to describe all experimental cross sections in the full energy range as well as possible. An optical parameter fit to our data at 10 MeV bombarding energy agrees satisfactorily with the parameter values of Ref. 1.

The calculation of the compound reaction contribution for both the elastic and inelastic scattering are based on the statistical model code ELIESE (4) which includes p- and alpha-channels. In this code, transmission coefficients are calculated with the same parameters as those used for the SOM. This code takes into account discrete levels only. For higher energies, normalization with results from statistical model code STAPRE (5) is necessary. The code STAPRE gives angle-integrated cross sections only, but it takes into account level densities for the unknown higher excited

levels. The parameters used in the code STAPRE were adjusted to reproduce the total cross sections.

Almost the same parameters were used for calculations of the direct reaction part with the coupled channels method (CC) in the code CHUCK (6). Table I gives the parameters used for the SOM and CC calculations.

The elastic scattering is described in the CC analysis also. In this case the influence of the channel coupling on the elastic channel is taken into consideration.

In order to describe the inelastic scattering, an incoherent superposition of compound and direct reaction contribution was carried out, where the second one is obtained from the collective model with the coupled channels method.

Table II gives the excitation modes and their parameters used in the CC-calculation with notation: β_0 - monopole vibration, β_2 - quadrupole vibration etc. These parameters result from the CC-calculation to reproduce the shape and absolute magnitude of the angular distributions as seen in Fig. 2, and they are in good agreement with results from other investigations.

The Hauser-Feshbach contribution is seen to be high for the higher excited levels (3^+ and higher). The reason for this overestimation could be fluctuations in the compound level density of ^{29}Si (1).

Some details of these coupled channels calculations are of interest:

(1) The direct excitation of the 4_1^+ state from ground state is rather small (order of 20%), i.e. multi-step processes must be taken into account.

(2) The excitation of the 3^+ non-normal parity state can be understood as spin-flip process, the $\ell = 2$ transition contributes mainly to the cross section (order of 90%).

(3) The contribution of the 2_3^+ state in the second rotational band to the cross section is small, this level is coupled only to its 0_3^+ "ground" state.

The ground state rotational band has oblate deformation as compared to the second rotational band which has a prolate ("cigar" shape) deformation.

Finally, it should be noted that by an extension of our investigations into the energy range between 7 and 14 MeV, on a uniform basis, more information about the behaviour of the reaction mechanism can be expected.

REFERENCES

1. A.W. Obst, J.L. Weil, Phys. Rev. C7 (1973) 1076.

2. S. Mittag, W. Pilz, D. Schmidt, D. Seeliger, T. Streil, Kernenergie 7 (1979) 237.

3. P. Eckstein, H. Helfer, D. Katzmer, J. Kayser, R. Krause, D. Lehmann, W. Meiling, W. Pilz, J. Rumpf, D. Schmidt D. Seeliger, T. Streil, Nucl. Instr. Meth. (1980), in print.

4. G. Kiessig, Thesis, Technische Universitat Dresden (1974).

5. M. Uhl, B. Strohmaier, report IRK 76/01, Vienna (1976).

6. P.D. Kunz, University of Colorado, code CHUCK, unpublished.

7. H. W. Barz, report ZFK-185, Rossendorf (1969).

TABLE I

Optical Model Parameters

	V_V (MeV)	r_V (fm)	a_V (fm)	W_s (MeV)	r_s (fm)	a_s (fm)	V_{so} (MeV)
SOM	52.0	1.15	0.78	12.1	1.25	0.47	9.0
CC	"	"	"	6.0	"	"	0.0

$a_{so} = a_s$; $r_{so} = r_s$

TABLE II

Excitation mode and parameters of the first low-lying states in ^{28}Si (the group denotes those levels which are coupled to the ground state and/or together in 3 different calculation runs)

level	group	J^π	excit. mode	parameters
g.s.	- - -	0_1^+	-	$\beta_2 = -.48$, $\beta_{2+2} = -0.15$
1		2_1^+	rot	" "
2	I	4_1^+	"	" "
3	- - -	3	vibr	$\beta_2 = +0.3$
4		0_2^+	"	$\beta_o = +0.25$
5	II	3^-	"	$\beta_3 = +0.3$
6	- - -	4_2^+	"	$\beta_4 = +0.6$
7		0_3^+	rot	$\beta_2 = +0.5$
8	III	2_2^+	vibr	$\beta_2 = +0.6$
9		2_3^+	rot	$\beta_2 = +0.5$

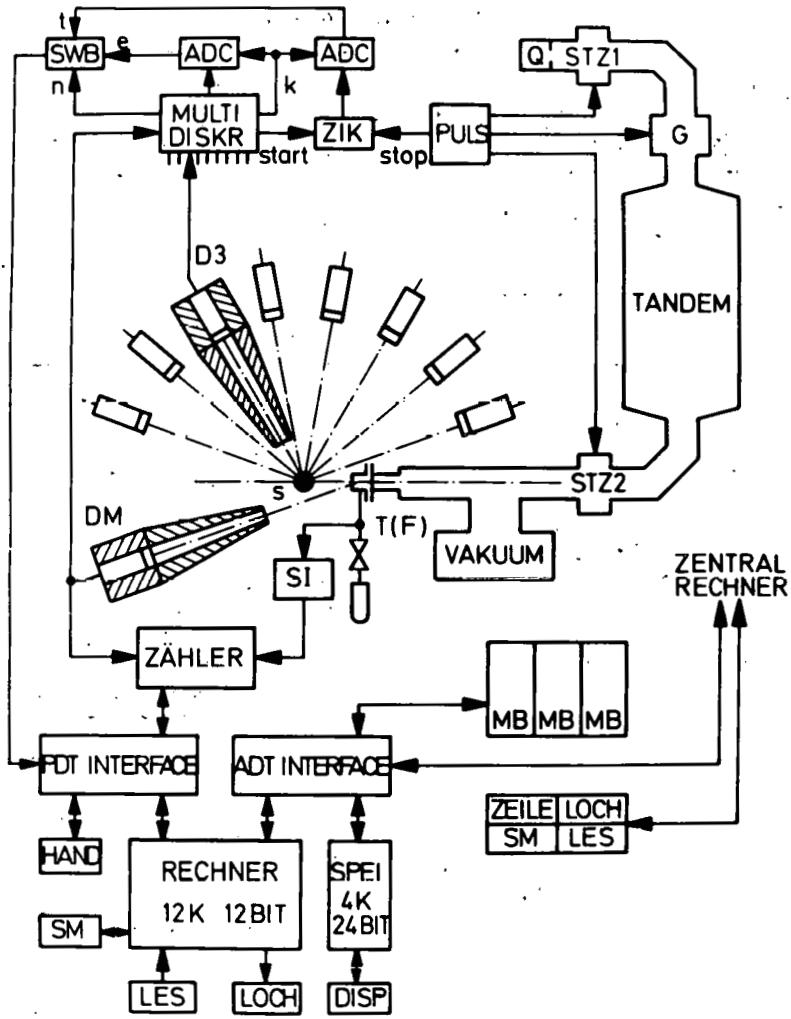

Figure 1. The Computer-controlled Multi-angle TOF-detector System (3).

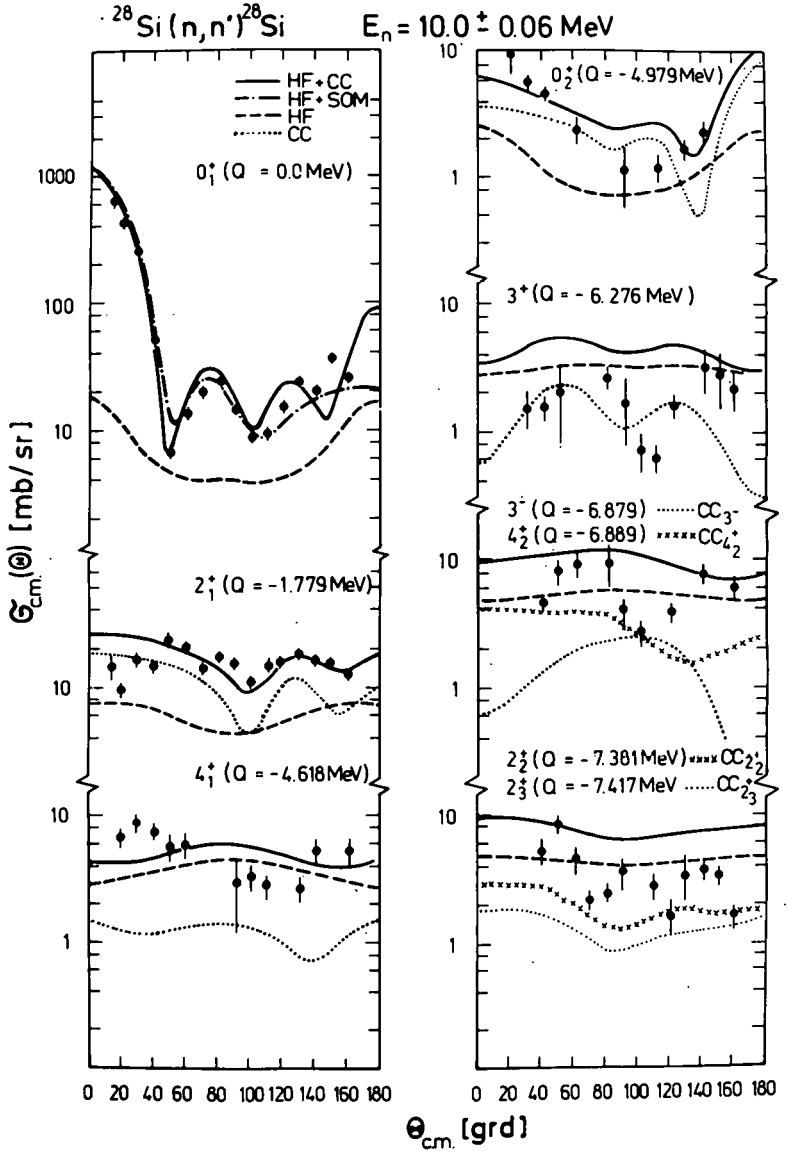

Figure 2. Angular Distributions of Elastic and Inelastic Neutron with 10 MeV Incident Neutrons. The Experimental Cross Sections (•) are shown with their Absolute Errors. (SOM-Spherical Optical Model, CC-Coupled Channel, HF-Hauser-Feshbach contribution).

U.S. GOVERNMENT PRINTING OFFICE: 614-090-#27